

**A PARAMETRIC STUDY INVESTIGATING THE INERTIAL
SOIL-STRUCTURE INTERACTION EFFECTS ON GLOBAL AND LOCAL
DEFORMATION DEMANDS OF MULTISTORY STEEL MRF
STRUCTURES RESTING ON SURFACE RIGID MAT FOUNDATIONS**

**A THESIS SUBMITTED TO
THE GRADUATE SCHOOL OF NATURAL AND APPLIED SCIENCES
OF
MIDDLE EAST TECHNICAL UNIVERSITY**

BY

DENİZ UTKUTUĞ

**IN PARTIAL FULFILLMENT OF THE REQUIREMENTS
FOR
THE DEGREE OF DOCTOR OF PHILOSOPHY
IN
CIVIL ENGINEERING**

MARCH 2009

Approval of the thesis:

**A PARAMETRIC STUDY INVESTIGATING THE INERTIAL SOIL-
STRUCTURE INTERACTION EFFECTS ON GLOBAL AND LOCAL
DEFORMATION DEMANDS OF MULTISTORY STEEL MRF
STRUCTURES RESTING ON SURFACE RIGID MAT FOUNDATIONS**

submitted by **DENİZ UTKUTUĞ** in partial fulfillment of the requirements for the degree of **Doctor of Philosophy in Civil Engineering Department, Middle East Technical University** by,

Prof. Dr. Canan Özgen
Director, Graduate School of **Natural and Applied Sciences**

Prof. Dr. Güney Özcebe,
Head of Department, **Civil Engineering Department, METU**

Prof. Dr. Polat Gülkan
Supervisor, **Civil Engineering Department, METU**

Examining Committee Members:

Prof. Dr. Polat Gülkan
Supervisor, Civil Engineering Department, METU

Assoc. Prof. Dr. Ahmet Yakut
Civil Engineering Department, METU

Assoc. Prof. Dr. Sadık Bakır
Civil Engineering Department, METU

Assoc. Prof. Dr. Kurtuluş Soyluk
Civil Engineering Department, Gazi University

Asst. Prof. Dr. Eray Baran
Civil Engineering Department, Atılım University

Date: 05/03/2009

I hereby declare that all information in this document has been obtained and presented in accordance with academic rules and ethical conduct. I also declare that, as required by these rules and conduct, I have fully cited and referenced all material and results that are not original to this work.

Name, Last Name : Deniz Utkuğ

Signature : _____

ABSTRACT

A PARAMETRIC STUDY INVESTIGATING THE INERTIAL SOIL- STRUCTURE INTERACTION EFFECTS ON GLOBAL AND LOCAL DEFORMATION DEMANDS OF MULTISTORY STEEL MRF STRUCTURES RESTING ON SURFACE RIGID MAT FOUNDATIONS

Utkutuğ, Deniz
Ph.D., Department of Civil Engineering
Supervisor: Prof. Dr. Polat Gülkan

March 2009, 264 pages

In reality, dynamic response of a structure supported on a compliant soil may vary significantly from the response of same structure when supported on a rigid base. A parametric study is conducted for the analysis of the variation in the global and the local deformation demands caused by the inertial soil-structure interaction effects. For the purposes of the study, nonlinear dynamic analyses are performed on 7 steel moment-resisting frame models, which are prepared by the virtue of fixed-base and flexible-base (interacting) conditions. Foundation is modeled with the Truncated Cone Model (Wolf, 1994) with the frequency independent coefficients. Free-field earthquake acceleration records are selected to conform to NEHRP equivalent Site Classes C and D. The study is limited to the structures founded on surface rigid mat foundations subjected to vertically propagating horizontally polarized coherent shear waves. Statistical analysis based on multiple linear regression procedure is performed to represent the variation in the response. Within the scope of the study, the wave parameter and the aspect ratio are observed to be directly proportional to the variation in the response, as a general trend. Maximum beneficial contribution of the SSI is found to be 6% in both global and local deformation demands. In addition, the contribution of inertial interaction effects is found to be in a decreasing trend for the increasing levels of ductility demands. Finally, upper limits of wave parameter for

H/R=0.5, 1, 2 and 3 are calculated where the variation in the demands are capped at 1.0.

Keywords: Inertial Soil-structure Interaction, Coherent Shear Waves, Truncated Cone Model, Surface Foundation, Nonlinear Time-history Analysis, Free-field Acceleration Record, Deformation Demands.

ÖZ

YÜZEYSEL RIJID RADYE TEMELE OTURMUŞ ÇOK KATLI ÇELİK ÇERÇEVE YAPILARDA ATALETE DAYALI YAPI-ZEMİN ETKİLEŞİMİ SONUCU DEFORMASYON TALEPLERİNDE OLUŞAN DEĞİŞİKLİKLERİN İNCELENMESİNE YÖNELİK PARAMETRİK ÇALIŞMA

Utkutuğ, Deniz
Doktora, İnşaat Mühendisliği Bölümü
Tez Yöneticisi: Prof. Dr. Polat Gülkan

Mart 2009, 264 sayfa

Pratikte, yumuşak zemine oturan yapıların dinamik özellikleri rijid zemine oturan yapılardan önemli seviye farklılık gösterebilir. Atalete dayalı yapı-zemin etkileşiminin yapının genel ve yerel seviyesinde meydana gelen şekil değiştirmesine olan etkisinin incelenmesi için parametric bir çalışma yapılmıştır. Bu tezde anlatılan çalışmalar kapsamında rijit-temele ve yapı zemin etkileşimine olanak tanıyan esnek-temele oturan 7 çelik çerçeve türü yapının doğrusal olmayan dinamik analizleri yapılmıştır. Zemin, parametreleri frekans uzayından bağımsız katsayılarla tanımlanan Truncated Cone Model (Wolf, 1994) ile idealleştirilmiştir. Deprem ivme kayıtları NEHRP Zemin Sınıfı C ve D'ye uyacak şekilde seçilmiştir. Bu çalışma, yüzeye doğru dik ilerleyen ve yatay polarizasyona sahip uyumlu kesme deprem dalgalarına maruz kalan yüzeysel, rijit, radye temele oturmuş yapılar için sınırlandırılmıştır. Yapının davranışındaki değişimler istatistiksel olarak analiz edilmiş ve deformasyonlar doğrusal regresyon denklemleri ile temsil edilmeye çalışılmıştır. Çalışma kapsamında incelenen dalga parametresi ve yapı boy oranının, yapının deformasyona bağlı davranışındaki değişimlerle doğru orantılı olarak değiştiği saptanmıştır. Atalete bağlı etkileşimin yapı davranışına olan olumlu katkısı, deformasyonlar çerçevesinde, maksimum 6% olduğu saptanmıştır. Bununla birlikte,

yapı üzerinde artan global süneklik talebinin atalete baėlı yapı zemin etkilişimini azalttığı saptanmıştır. Son olarak, defomasyon talep oranlarında 1'in altındaki azalmayı göstermek üzere, $H/R=0.5$, 1, 2 ve 3 için, dalga parametresinin üst sınırları hesaplanmıştır.

Anahtar Kelimeler: Atalete Dayalı Yapı-zemin Etkileşimi, Kayma Dalgası, Truncated Cone Model, Yüzeysel Temel, doğrusal olmayan dinamik analiz, Serbest Alan Deprem Kayıtı, Deformasyon Talepleri.

To My Parents and My Beloved Wife

ACKNOWLEDGMENTS

The author wishes to express his deepest gratitude to his supervisor Prof. Dr. Polat Gülkan for his guidance, advice, criticism, encouragements and insight throughout the study.

The author is also grateful to Mehmet Şenol (ARTI Architecture, Engineering and Consultancy) for his sincere understanding in the completion of my thesis.

TABLE OF CONTENTS

ABSTRACT.....	iv
ÖZ.....	vi
ACKNOWLEDGMENTS.....	ix
TABLE OF CONTENTS.....	x
LIST OF TABLES.....	xiv
LIST OF FIGURES.....	xx
CHAPTERS	
1. INTRODUCTION.....	1
1.1 Introduction.....	1
1.2 Soil-Structure Interaction.....	2
1.2.1 Kinematic Interaction.....	3
1.2.2 Inertial Interaction.....	3
1.2.3 Parameters of Soil-Structure Interaction.....	4
1.2.4 Possible Approaches to the Solution of Interaction Problem.....	5
1.2.4.1 Finite Element Discretization of Soil-Foundation-Structure System.....	5
1.2.4.2 Equivalent Oscillator.....	6
1.2.4.3 Discrete Element Models for Foundation Vibrations.....	8
1.3 Description of the Problem.....	9
1.4 Aim and Scope.....	11

1.5 Organization of Text.....	13
2. EARTHQUAKE GROUND MOTION RECORDS	14
2.1 Introduction	14
2.2 Classification of Earthquake Events and Associated Acceleration Records	14
2.3 Acceleration Response Spectra	15
2.4 Strong Ground Motion Scaling Schemes	17
3. STRUCTURAL MODELS	23
3.1 Introduction	23
3.2 Frame Properties, Modeling and Analysis Assumptions	24
3.3 Foundation-Soil Interaction Model and Assumptions.....	27
3.4 Frame Models.....	32
3.4.1 Three Story SAC Frame	32
3.4.2 Pairs of Four and Twelve Story Steel Frames	36
3.4.3 Five and Eight Story Steel Frames	40
4. ANALYSIS FRAMEWORK AND RESULTS	46
4.1 Introduction	46
4.2 Analysis Framework.....	47
4.3 The Post-Process	48
4.4 Organization of the Results	49
4.5 Results	53
4.5.1 Deformation State of the Frame Models	53
4.5.2 Variation of the Response Ratio (SSI.TH / FB.TH) in both Global and Local Response Levels	57

5. DISCUSSION OF RESULTS AND CONCLUSION	70
5.1 Summary.....	70
5.2 Discussion of Results	71
5.2.1 Global Deformation State of the Frames	72
5.2.2 Assessment of the Variation in the Demands	73
5.3 Conclusion.....	79
REFERENCES.....	83
APPENDICES	
A. THEORETICAL BACKGROUND OF SOIL-STRUCTURE	
INTERACTION MODEL	91
A.1 Lumped Parameter Model	91
A.2 Truncated Cone Model	96
A.2.1 Construction of Cone Model for Rigid Surface Foundations	96
A.2.2 Low Frequency Limit – Static Stiffness Coefficients and	
Corresponding Apex Height	97
A.2.2.1 Translational Motion in Low Frequency	97
A.2.2.2 Rotational Motion in Low Frequency	101
A.2.2.3 Apex Height for Static Stiffness Coefficients	
(Low Frequency)	103
A.2.3 High Frequency Behavior	104
A.2.3.1 Translational Motion at High Frequency	104
A.2.3.2 Rotational Motion at High Frequency	107
A.2.4 Effect of Nearly Incompressible Soil.....	109
A.2.5. Discrete Element Model	111

A.2.5.1 Translational Motion.....	111
A.2.5.2 Rotational Motion	114
B. EARTHQUAKE GROUND MOTION RECORDS	117
C. TABLES RELATED TO REGRESSION LINES.....	137
D. 2D SCATTER PLOTS RELATED TO STATISTICAL ANALYSIS	147
E. PLOTS OF NONLINEAR STATIC AND NONLINEAR TIME-HISTORY ANALYSES	208
F. INTERSTORY DRIFT PLOTS OBTAINED FROM NTH ANALYSES	220
VITA	263

LIST OF TABLES

TABLES

Table 2.1. Mean and mean plus one standard deviation values of peak ground acceleration, PGA and maximum spectral acceleration, SA(g) values corresponding to SETC and SETD records.....	16
Table 2.2. BSE-1 design spectra coefficients obtained from the mean (μ) and the mean plus one standard deviation ($\mu+\sigma$) response spectra of SET-C1, C2, D1 and D2 records.	16
Table 2.2. Scale factors for SET - SCR2 (Analysis Group III) records in order to produce a spectral acceleration equal to 1g at the effective fundamental period of the frame and associated scale factors to produce the strength reduction factor, R=2 (FEMA356 (2000)).....	18
Table 3.1. Mechanical properties of ASTM type structural steels used in the analysis framework (Gaylord (1992)).	25
Table 3.2. Frequency independent uncoupled stiffness coefficients using FEMA356 (2000) procedure for all degrees of freedom calculated for soil properties given in Table 3.4. Surface foundation is rectangular with L=24m and B=12m.....	30
Table 3.3. Frequency independent coefficients of lumped parameter model using truncated cone model (Wolf (1994)) for both equivalent rigid disk and rigid rectangular foundation. Soil properties are given in Table 3.4.	31
Table 3.4. Basic soil parameters for the evaluation of frequency independent spring-dashpot-mass coefficients	32
Table 3.5. Ratio of frequency independent stiffness coefficients for translation and associated rocking degrees of freedom calculated from FEMA356 (2000) procedure and truncated cone model (Wolf (1994)).....	32

Table 3.6. Geometric, seismic mass and material properties of frame models.....	33
Table 3.7. Structural member sections of frame 3SAC	34
Table 3.8. Modal properties of fixed-base frame models at the fundamental mode	34
Table 3.9. Global yield point of bilinear representation of fixed-base frame models.....	34
Table 3.10. Structural member sections of frame models, 4KatF, 4KatR, 12KatFS, 12KatRS.	36
Table 3.11. . Seismic mass and associated gravity loading of five and eight story steel moment-resisting frame models based on floor design loads.	41
Table 3.12. Variation of fundamental period of vibration according to a selected wave parameter value ($\sigma=9$)	43
Table 3.13. Variation of fundamental period of vibration calculated according to approximate period formulation and associated wave parameter, σ	43
Table 3.14. Wave parameter (σ) values obtained from fundamental periods of vibration of models	43
Table 3.15. Structural member sections of frame models, 5KatS2, 8KatS2.....	44
Table 4.1. Coefficients of the linear regression equations obtained for the roof drift ratio and the first story drift ratio. Equation coefficients are listed for three analysis groups; NS, SC, SCR2, and for four earthquake ground motion sets; SET-C1, C2, D1 and D2.	50
Table 4.2. Coefficients of the linear regression equations obtained for the peak member end rotations at the first story beams and columns. Equation coefficients are listed for Analysis Group I; NS for four earthquake ground motion sets; SET-C1, C2, D1 and D2.	50
Table 4.3. Coefficients of the linear regression equations obtained for the peak member end rotations at the first story beams and columns. Equation coefficients are listed for Analysis Group II; SC for four earthquake ground motion sets; SET-C1, C2, D1 and D2.....	51

Table 4.4. Coefficients of the linear regression equations obtained for the peak member end rotations at the first story beams and columns. Equation coefficients are listed for Analysis Group III; SCR2 for four earthquake ground motion sets; SET-C1, C2, D1 and D2	51
Table 4.5. Number of events among the roof drift ductility demand ranges, which are obtained from nonlinear time-history analyses of flexible-base (interacting) frame models: $\mu=1$, 1-2, 2-4 and >4 . The results are given for analysis group NS.	54
Table 4.6. Number of events among the roof drift ductility demand ranges, which are obtained from nonlinear time-history analyses of flexible-base (interacting) frame models: $\mu=1$, 1-2, 2-4 and >4 . The results are given for analysis group SC	55
Table 4.7. Number of events among the roof drift ductility demand ranges, which are obtained from nonlinear time-history analyses of flexible-base (interacting) frame models: $\mu=1$, 1-2, 2-4 and >4 . The results are given for analysis group SCR2.....	56
Table 4.8. Limiting values of the wave parameter (σ_1) when interaction effects are considered to be beneficial for the structural response, which is expressed in terms of the roof and the first story drift demands. Calculations are performed for H/R=0.5, 1.0, 2.0 and 3.0 and analysis group I: NS	68
Table 4.9. Limiting values of the wave parameter (σ_1) when interaction effects are considered to be beneficial for the structural response, which is expressed in terms of the peak member (Column No.1 and Beam No.1) end rotations at the first story. Calculations are performed for H/R=0.5, 1.0, 2.0 and 3.0 and analysis group I: NS.....	69
Table 5.1. Comparison of the distribution of number of the events with respect to the roof drift ductility ranges among the analysis groups, NS, SC and SCR2, which are obtained from nonlinear time-history analyses of flexible-base (interacting) frame models: $\mu=1$, 1-2, 2-4 and >4	76

Table A.1. Static stiffness and dimensionless coefficients of Monkey-Tail Model for rigid disk on elastic half-space (Wolf (1997)).....	94
Table A.2 Spring, Dashpot and Mass coefficients for disk (or an arbitrary shape) on elastic half-space for Truncated Cone Model (Wolf (1997)).....	99
Table B.1. SET-C1 and SET-D1 Ground motion acceleration records conforming to NEHRP Site Class C and D, respectively: Records containing pulse effects.	118
Table B.2. SET-C2 Ground motion acceleration records conforming to NEHRP Site Class C: Records without pulse effects.....	119
Table B.3. SET-D2 Ground motion acceleration records conforming to NEHRP Site Class D: Records without pulse effects.....	120
Table B.4. Mean (μ), standard deviation (σ), mean plus one standard deviation ($\mu+\sigma$), median, minimum (Min.) and maximum (Max.) values of spectral accelerations for SETC and SETD records calculated at the fundamental period of frame models.....	121
Table B.5. Scale factors for analysis group “SC” for SETC earthquake ground motion acceleration records conforming to NEHRP Site Class C.	122
Table B.6. Scale factors for analysis group “SC” for SETD earthquake ground motion acceleration records conforming to NEHRP Site Class D.....	124
Table B.7. Scale factors for analysis group “SCR2” for SETC earthquake ground motion acceleration records conforming to NEHRP Site Class C.....	126
Table B.8. Scale factors for analysis group “SCR2” for SETD earthquake ground motion acceleration records conforming to NEHRP Site Class D.....	128
Table C.1. Response ratio values (as a percentage of reference base 1.0) for the roof drift ratio evaluated at the minimum and at the maximum values of the wave parameter (9.5 – 65 for SETC and 4.5 – 33 for SETD) and at the respective aspect ratio of the frame models.....	138
Table C.2. Response ratio values (as a percentage of reference base 1.0) for the first story drift ratio evaluated at the minimum and maximum values of	

the wave parameter (9.5 – 65 for SETC and 4.5 – 33 for SETD) and at the respective aspect ratio of the frame models.....	139
Table C.3. Response ratio values (as a percentage of reference base 1.0) for the peak member end rotations at the first story columns and beams evaluated at the minimum and maximum values of the wave parameters (9.5 – 65 for SETC and 4.5 – 33 for SETD) and at the respective aspect ratio of the frame model, 3SAC.....	140
Table C.4. Response ratio values (as a percentage of reference base 1.0) for the peak member end rotations at the first story columns and beams evaluated at the minimum and maximum values of the wave parameters (9.5 – 65 for SETC and 4.5 – 33 for SETD) and at the respective aspect ratio of the frame model, 4KatF.	141
Table C.5. Response ratio values (as a percentage of reference base 1.0) for the peak member end rotations at the first story columns and beams evaluated at the minimum and maximum values of the wave parameters (9.5 – 65 for SETC and 4.5 – 33 for SETD) and at the respective aspect ratio of the frame model, 4KatR.....	142
Table C.6. Response ratio values (as a percentage of reference base 1.0) for the peak member end rotations at the first story columns and beams evaluated at the minimum and maximum values of the wave parameters (9.5 – 65 for SETC and 4.5 – 33 for SETD) and at the respective aspect ratio of the frame model, 5KatS2.	143
Table C.7. Response ratio values (as a percentage of reference base 1.0) for the peak member end rotations at the first story columns and beams evaluated at the minimum and maximum values of the wave parameters (9.5 – 65 for SETC and 4.5 – 33 for SETD) and at the respective aspect ratio of the frame model, 8KatS2.	144
Table C.8. Response ratio values (as a percentage of reference base 1.0) for the peak member end rotations at the first story columns and beams evaluated at the minimum and maximum values of the wave parameters	

(9.5 – 65 for SETC and 4.5 – 33 for SETD) and at the respective aspect ratio of the frame model, 12KatFS.....	145
Table C.9. Response ratio values (as a percentage of reference base 1.0) for the peak member end rotations at the first story columns and beams evaluated at the minimum and maximum values of the wave parameters (9.5 – 65 for SETC and 4.5 – 33 for SETD) and at the respective aspect ratio of the frame model, 12KatRS.....	146

LIST OF FIGURES

FIGURES

Figure 1.1. Finite element discretization of entire soil-foundation-structure system (Mengi, 2002).....	6
Figure 1.2. Equivalent oscillator (FEMA450 (2003); Veletsos and Nair, 1975).....	7
Figure 1.3. Comparison of a typical seismic code design spectrum to actual site-specific spectra from various earthquakes; $\beta=5\%$ (Fig. 3 of Mylonakis and Gazetas (2000)).....	10
Figure 2.1. Response spectra for SETC and SETD records conforming to NEHRP Site Classes C and D, respectively.	19
Figure 2.2. Mean (μ) and mean plus one standard deviation ($\mu+\sigma$) response spectra and equivalent BSE-1 level design spectra for 10% probability of exceedance in 50 years (FEMA356, 2000) for SETC records, conforming to NEHRP Site Class C: Records containing pulse effects and records without pulse effects.....	20
Figure 2.3. Mean (μ) and mean plus one standard deviation ($\mu+\sigma$) response spectra and equivalent BSE-1 level design spectra for 10% probability of exceedance in 50 years (FEMA356, 2000) for SETD records, conforming to NEHRP Site Class D: Records containing pulse effects and records without pulse effects.....	21
Figure 2.4. Mean plus one standard deviation response spectra of SET – NS-C1, SET – NS-C2, SET – NS-D1 and SET – NS-D2 records and the distribution of fundamental periods of frame models: 3SAC ($T_n=1.0s$), 4KatF ($T_n=1.1s$), 4KatR ($T_n=0.72s$), 5KatS2 ($T_n=0.81s$), 8KatS2 ($T_n=1.45s$), 12KatFS ($T_n=2.19s$), 12KatRS ($T_n=1.26s$).....	22

Figure 3.1. Backbone force-deformation relationship for Steel01 material, OpenSees	25
Figure 3.2. Illustration of lumped parameter models for vertical translation and rocking degrees of freedom formulated by truncated cone model (Fig.5; Wolf (1997)).	29
Figure 3.3. Illustration of 3SAC frame model modified with lumped parameter model formulated via truncated cone model (Wolf (1994)). Rigid foundation beams are not included in the figure	29
Figure 3.4. Pushover plots obtained for the frame models: 3SAC, 4KatF, 4KatR, 5KatS2, 8KatS2, 12KatFS and 12KatRS.	35
Figure 3.5. Elevation of four story frame models, 4KatF and 4KatR.....	37
Figure 3.6. Elevation of twelve story frame models, 12KatFS and 12KatRS	38
Figure 3.7. Elevation of five and eight story frame models; 5KatS2, 8KatS2.....	42
Figure 3.8. Capacity ratios obtained for the frame models: 5KatS2, 8KatS2.....	45
Figure 4.1. Comparison of regression lines calculated for the response ratio values associated with the roof drift ratio: SET-NS	59
Figure 4.2. Comparison of regression lines calculated for the response ratio values associated with the roof drift ratio: SET-SC	59
Figure 4.3. Comparison of regression lines calculated for the response ratio values associated with the roof drift ratio: SET-SCR2.....	60
Figure 4.4. Comparison of regression lines calculated for the response ratio values associated with the first story drift ratio: SET-NS	60
Figure 4.5. Comparison of regression lines calculated for the response ratio values associated with the first story drift ratio: SET-SC	61
Figure 4.6. Comparison of regression lines calculated for the response ratio values associated with the first story drift ratio: SET-SCR2.....	61
Figure 4.7. Comparison of regression lines calculated for the response ratio values associated with the peak column (No.1) end rotation at the first story: SET-NS.....	63

Figure 4.8. Comparison of regression lines calculated for the response ratio values associated with the peak beam (No.1) end rotation at the first story: SET-NS.....	63
Figure 4.9. Comparison of regression lines calculated for the response ratio values associated with the peak column (No.1) end rotation at the first story: SET-SC.....	64
Figure 4.10. Comparison of regression lines calculated for the response ratio values associated with the peak beam (No.1) end rotation at the first story: SET-SC.....	64
Figure 4.11. Comparison of regression lines calculated for the response ratio values associated with the peak column (No.1) end rotation at the first story: SET-SCR2	65
Figure 4.12. Comparison of regression lines calculated for the response ratio values associated with the peak beam (No.1) end rotation at the first story: SET-SCR2	65
Figure 4.13. Upper limits of wave parameter for the response ratio equal to 1.0, which are calculated from roof drift and first story drift ratios: Analysis group I, NS	66
Figure 4.14. Upper limits of wave parameter for the response ratio equal to 1.0, which are calculated from peak member end rotations: Analysis group I, NS.....	67
Figure 5.1. 2D scatter plots and associated regression lines for the response ratio values obtained from the roof drift ratio: SET-NS-C1 and D1. In the regression equations ϵ is the mean absolute error (MAE) and s is the standard error (RMSE)	74
Figure 5.2. 2D scatter plots and associated regression lines for the response ratio values obtained from the peak column (no.1) end rotation at the first story: SET-NS-C1 and D1. In the regression equations ϵ is the mean absolute error (MAE) and s is the standard error (RMSE).....	75

Figure 5.3. Comparison of the response ratios of roof and first story drift ratios for SET-NS-C1, C2, D1 and D2 records for H/R=0.5, 1.0, 2.0 and 3.0.....	81
Figure 5.4. Comparison of the response ratios of maximum member end rotations at the first story for SET-NS-C1, C2, D1 and D2 records for H/R=0.5, 1.0, 2.0 and 3.0.....	82
Figure A.1. One dimensional fundamental lumped parameter model (Monkey-Tail Model), Wolf (1997)	92
Figure A.2. Comparison of the dimensionless stiffness and dashpot coefficients between Wolf (1988) and Veletsos and Wei (1971), for the vertical translation and rocking response of disk on elastic half-space (Wolf (1988)). These plots are for Poisson's Ratio, $\nu=0, 1/3$ and $1/2$	95
Figure A.3. Cones for various degrees of freedom with their corresponding apex ratio (Opening Angle), wave propagation velocity and distortion (Fig. 2-1; Wolf (1994))......	98
Figure A.4. Truncated semi-infinite cones (Fig. 2-2; Wolf (1994))	100
Figure A.5. Representation of high frequency limit of dynamic stiffness (Fig. 2-3; Wolf (1994)). In this Figure: (a) Disk foundation, (b) Foundation of arbitrary shape	105
Figure A.6. Analogy of trapped mass to plastic punching (Fig. 2-4; Wolf (1994)). In this Figure: (a) Three-dimensional vertical case (pile), (b) Two-dimensional rocking case (elevation and plan view of roof-shaped volume of soil).....	110
Figure A.7. Discrete element model for translation in the direction normal to foundation (Fig. 2-5; Wolf (1994)).....	112
Figure A.8. Dynamic stiffness coefficients for harmonic loading of disk on homogeneous halfspace in horizontal motion for Poisson's Ratio of $\nu=0, 1/3$ and $1/2$ (Fig. 2-6; Wolf (1994))......	113
Figure A.9. Dynamic-stiffness coefficient for harmonic loading of disk on homogeneous half-space in vertical motion for Poisson's Ratio of $\nu=0, 1/3, 0.45$ and $1/2$ (Fig. 2-7; Wolf (1994))......	113

Figure A.10. Cone Model and Equivalent Discrete-Element Model (Fig.5; Wolf (1997)).	115
Figure A.11. Dynamic stiffness coefficients for harmonic loading of disk on homogeneous halfspace in torsional motion (Fig. 2-20; Wolf (1994)).	115
Figure A.12. Dynamic-stiffness coefficient for harmonic loading of disk on homogeneous halfspace in rocking motion for Poisson's Ratio of $\nu=0, 1/3, 0.45$ and $1/2$ (Fig. 2-7; Wolf (1994)).	116
Figure B.1. Mean plus one standard deviation response spectra of Analysis Group II, SET-SC-C1, SET-SC-C2, SET-SC-D1 and SET-SC-D2 records, obtained for the frame model 3SAC.	130
Figure B.2. Mean plus one standard deviation response spectra of Analysis Group III, SET-SCR2-C1, SET-SCR2-C2, SET-SCR2-D1 and SET-SCR2-D2 records, obtained for the frame model 3SAC.	130
Figure B.3. Mean plus one standard deviation response spectra of Analysis Group II, SET-SC-C1, SET-SC-C2, SET-SC-D1 and SET-SC-D2 records, obtained for the frame model 4KatF.	131
Figure B.4. Mean plus one standard deviation response spectra of Analysis Group III, SET-SCR2-C1, SET-SCR2-C2, SET-SCR2-D1 and SET-SCR2-D2 records, obtained for the frame model 4KatF.	131
Figure B.5. Mean plus one standard deviation response spectra of Analysis Group II, SET-SC-C1, SET-SC-C2, SET-SC-D1 and SET-SC-D2 records, obtained for the frame model 4KatR.	132
Figure B.6. Mean plus one standard deviation response spectra of Analysis Group III, SET-SCR2-C1, SET-SCR2-C2, SET-SCR2-D1 and SET-SCR2-D2 records, obtained for the frame model 4KatR.	132
Figure B.7. Mean plus one standard deviation response spectra of Analysis Group II, SET-SC-C1, SET-SC-C2, SET-SC-D1 and SET-SC-D2 records, obtained for the frame model 5KatS2.	133

Figure B.8. Mean plus one standard deviation response spectra of Analysis Group III, SET-SCR2-C1, SET-SCR2-C2, SET-SCR2-D1 and SET-SCR2-D2 records, obtained for the frame model 5KatS2.....	133
Figure B.9. Mean plus one standard deviation response spectra of Analysis Group II, SET-SC-C1, SET-SC-C2, SET-SC-D1 and SET-SC-D2 records, obtained for the frame model 8KatS2.....	134
Figure B.10. Mean plus one standard deviation response spectra of Analysis Group III, SET-SCR2-C1, SET-SCR2-C2, SET-SCR2-D1 and SET-SCR2-D2 records, obtained for the frame model 8KatS2.....	134
Figure B.11. Mean plus one standard deviation response spectra of Analysis Group II, SET-SC-C1, SET-SC-C2, SET-SC-D1 and SET-SC-D2 records, obtained for the frame model 12KatFS.....	135
Figure B.12. Mean plus one standard deviation response spectra of Analysis Group III, SET-SCR2-C1, SET-SCR2-C2, SET-SCR2-D1 and SET-SCR2-D2 records, obtained for the frame model 12KatFS.....	135
Figure B.13. Mean plus one standard deviation response spectra of Analysis Group II, SET-SC-C1, SET-SC-C2, SET-SC-D1 and SET-SC-D2 records, obtained for the frame model 12KatRS.....	136
Figure B.14. Mean plus one standard deviation response spectra of Analysis Group III, SET-SCR2-C1, SET-SCR2-C2, SET-SCR2-D1 and SET-SCR2-D2 records, obtained for the frame model 12KatRS.....	136
Figure D.1. 2D Scatter plot and associated regression line for the response ratios obtained for Set NS-C1. Response ratios are defined for: Roof drift ratio, first story drift ratio, peak column (foundation end) end and peak beam end rotations at the first story (SSI.TH / FB.TH), while the predictor variables are wave parameter (σ) and aspect ratio (H/R).....	148
Figure D.2. 2D Scatter plot and associated regression line for the response ratios obtained for Set NS-C2. Response ratios are defined for: Roof drift ratio, first story drift ratio, peak column (foundation end) end and peak	

beam end rotations at the first story (SSI.TH / FB.TH), while the predictor variables are wave parameter (σ) and aspect ratio (H/R).....	153
Figure D.3. 2D Scatter plot and associated regression line for the response ratios obtained for Set NS-D1. Response ratios are defined for: Roof drift ratio, first story drift ratio, peak column (foundation end) end and peak beam end rotations at the first story (SSI.TH / FB.TH), while the predictor variables are wave parameter (σ) and aspect ratio (H/R).....	158
Figure D.4. 2D Scatter plot and associated regression line for the response ratios obtained for Set NS-D2. Response ratios are defined for: Roof drift ratio, first story drift ratio, peak column (foundation end) end and peak beam end rotations at the first story (SSI.TH / FB.TH), while the predictor variables are wave parameter (σ) and aspect ratio (H/R).....	163
Figure D.5. 2D Scatter plot and associated regression line for the response ratios obtained for Set SC-C1. Response ratios are defined for: Roof drift ratio, first story drift ratio, peak column (foundation end) end and peak beam end rotations at the first story (SSI.TH / FB.TH), while the predictor variables are wave parameter (σ) and aspect ratio (H/R).....	168
Figure D.6. 2D Scatter plot and associated regression line for the response ratios obtained for Set SC-C2. Response ratios are defined for: Roof drift ratio, first story drift ratio, peak column (foundation end) end and peak beam end rotations at the first story (SSI.TH / FB.TH), while the predictor variables are wave parameter (σ) and aspect ratio (H/R).....	173
Figure D.7. 2D Scatter plot and associated regression line for the response ratios obtained for Set SC-D1. Response ratios are defined for: Roof drift ratio, first story drift ratio, peak column (foundation end) end and peak beam end rotations at the first story (SSI.TH / FB.TH), while the predictor variables are wave parameter (σ) and aspect ratio (H/R).....	178
Figure D.8. 2D Scatter plot and associated regression line for the response ratios obtained for Set SC-D2. Response ratios are defined for: Roof drift ratio, first story drift ratio, peak column (foundation end) end and peak	

beam end rotations at the first story (SSI.TH / FB.TH), while the predictor variables are wave parameter (σ) and aspect ratio (H/R).....	183
Figure D.9. 2D Scatter plot and associated regression line for the response ratios obtained for Set SCR2-C1. Response ratios are defined for: Roof drift ratio, first story drift ratio, peak column (foundation end) end and peak beam end rotations at the first story (SSI.TH / FB.TH), while the predictor variables are wave parameter (σ) and aspect ratio (H/R).....	188
Figure D.10. 2D Scatter plot and associated regression line for the response ratios obtained for Set SCR2-C1. Response ratios are defined for: Roof drift ratio, first story drift ratio, peak column (foundation end) end and peak beam end rotations at the first story (SSI.TH / FB.TH), while the predictor variables are wave parameter (σ) and aspect ratio (H/R).....	193
Figure D.11. 2D Scatter plot and associated regression line for the response ratios obtained for Set SCR2-C1. Response ratios are defined for: Roof drift ratio, first story drift ratio, peak column (foundation end) end and peak beam end rotations at the first story (SSI.TH / FB.TH), while the predictor variables are wave parameter (σ) and aspect ratio (H/R).....	198
Figure D.12. 2D Scatter plot and associated regression line for the response ratios obtained for Set SCR2-C1. Response ratios are defined for: Roof drift ratio, first story drift ratio, peak column (foundation end) end and peak beam end rotations at the first story (SSI.TH / FB.TH), while the predictor variables are wave parameter (σ) and aspect ratio (H/R).....	203
Figure E.1. Pushover curves and performance points obtained from SET-NS-C1, C2, D1 and D2 records for the frame model 3SAC.....	209
Figure E.2. Pushover curves and performance points obtained from SET-SC-C1, C2, D1 and D2 records for the frame model 3SAC.....	209
Figure E.3. Pushover curves and performance points obtained from SET-SCR2-C1, C2, D1 and D2 records for the frame model 3SAC.....	210
Figure E.4. Pushover curves and performance points obtained from SET-NS-C1, C2, D1 and D2 records for the frame model 4KatF.....	210

Figure E.5. Pushover curves and performance points obtained from SET-SC- C1, C2, D1 and D2 records for the frame model 4KatF.....	211
Figure E.6. Pushover curves and performance points obtained from SET- SCR2-C1, C2, D1 and D2 records for the frame model 4KatF.....	211
Figure E.7. Pushover curves and performance points obtained from SET-NS- C1, C2, D1 and D2 records for the frame model 4KatR.	212
Figure E.8. Pushover curves and performance points obtained from SET-SC- C1, C2, D1 and D2 records for the frame model 4KatR.	212
Figure E.9. Pushover curves and performance points obtained from SET- SCR2-C1, C2, D1 and D2 records for the frame model 4KatR.	213
Figure E.10. Pushover curves and performance points obtained from SET-NS- C1, C2, D1 and D2 records for the frame model 5KatS2.....	213
Figure E.11. Pushover curves and performance points obtained from SET-SC- C1, C2, D1 and D2 records for the frame model 5KatS2.....	214
Figure E.12. Pushover curves and performance points obtained from SET- SCR2-C1, C2, D1 and D2 records for the frame model 5KatS2.....	214
Figure E.13. Pushover curves and performance points obtained from SET-NS- C1, C2, D1 and D2 records for the frame model 8KatS2.....	215
Figure E.14. Pushover curves and performance points obtained from SET-SC- C1, C2, D1 and D2 records for the frame model 8KatS2.....	215
Figure E.15. Pushover curves and performance points obtained from SET- SCR2-C1, C2, D1 and D2 records for the frame model 8KatS2.....	216
Figure E.16. Pushover curves and performance points obtained from SET-NS- C1, C2, D1 and D2 records for the frame model 12KatFS.	216
Figure E.17. Pushover curves and performance points obtained from SET-SC- C1, C2, D1 and D2 records for the frame model 12KatFS.	217
Figure E.18. Pushover curves and performance points obtained from SET- SCR2-C1, C2, D1 and D2 records for the frame model 12KatFS.....	217
Figure E.19. Pushover curves and performance points obtained from SET-NS- C1, C2, D1 and D2 records for the frame model 12KatRS.....	218

Figure E.20. Pushover curves and performance points obtained from SET-SC-C1, C2, D1 and D2 records for the frame model 12KatRS.	218
Figure E.21. Pushover curves and performance points obtained from SET-SCR2-C1, C2, D1 and D2 records for the frame model 12KatRS.	219
Figure F.1. Comparison of peak and mean interstory drift demands of Model 3SAC subjected to Set NS-C1, C2, D1, D2 earthquake records.	221
Figure F.2. Comparison of peak and mean interstory drift demands of Model 3SAC subjected to Set SC-C1, C2, D1, D2 earthquake records.	223
Figure F.3. Comparison of peak and mean interstory drift demands of Model 3SAC subjected to Set SCR2-C1, C2, D1, D2 earthquake records.	225
Figure F.4. Comparison of peak and mean interstory drift demands of Model 4KatF subjected to Set NS-C1, C2, D1, D2 earthquake records.	227
Figure F.5. Comparison of peak and mean interstory drift demands of Model 4KatF subjected to Set SC-C1, C2, D1, D2 earthquake records.	229
Figure F.6. Comparison of peak and mean interstory drift demands of Model 4KatF subjected to Set SCR2-C1, C2, D1, D2 earthquake records.	231
Figure F.7. Comparison of peak and mean interstory drift demands of Model 4KatR subjected to Set NS-C1, C2, D1, D2 earthquake records.	233
Figure F.8. Comparison of peak and mean interstory drift demands of Model 4KatR subjected to Set SC-C1, C2, D1, D2 earthquake records.	235
Figure F.9. Comparison of peak and mean interstory drift demands of Model 4KatR subjected to Set SCR2-C1, C2, D1, D2 earthquake records.	237
Figure F.10. Comparison of peak and mean interstory drift demands of Model 5KatS2 subjected to Set NS-C1, C2, D1, D2 earthquake records.	239
Figure F.11. Comparison of peak and mean interstory drift demands of Model 5KatS2 subjected to Set SC-C1, C2, D1, D2 earthquake records.	241
Figure F.12. Comparison of peak and mean interstory drift demands of Model 5KatS2 subjected to Set SCR2-C1, C2, D1, D2 earthquake records.	243
Figure F.13. Comparison of peak and mean interstory drift demands of Model 8KatS2 subjected to Set NS-C1, C2, D1, D2 earthquake records.	245

Figure F.14. Comparison of peak and mean interstory drift demands of Model 8KatS2 subjected to Set SC-C1, C2, D1, D2 earthquake records.	247
Figure F.15. Comparison of peak and mean interstory drift demands of Model 8KatS2 subjected to Set SCR2-C1, C2, D1, D2 earthquake records.....	249
Figure F.16. Comparison of peak and mean interstory drift demands of Model 12KatFS subjected to Set NS-C1, C2, D1, D2 earthquake records.....	251
Figure F.17. Comparison of peak and mean interstory drift demands of Model 12KatFS subjected to Set SC-C1, C2, D1, D2 earthquake records.....	253
Figure F.18. Comparison of peak and mean interstory drift demands of Model 12KatFS subjected to Set SCR2-C1, C2, D1, D2 earthquake records.	255
Figure F.19. Comparison of peak and mean interstory drift demands of Model 12KatRS subjected to Set NS-C1, C2, D1, D2 earthquake records.	257
Figure F.20. Comparison of peak and mean interstory drift demands of Model 12KatRS subjected to Set SC-C1, C2, D1, D2 earthquake records.....	259
Figure F.21. Comparison of peak and mean interstory drift demands of Model 12KatRS subjected to Set SCR2-C1, C2, D1, D2 earthquake records.....	261

CHAPTER 1

INTRODUCTION

1.1 Introduction

Objectives of earthquake resistant building design have been well recognized covering two major goals. The first one is to provide life-safety by forcing structure to have sufficient strength and ductility to resist collapse in severe, yet relatively infrequent earthquakes. The second goal is to control structural and non-structural damage in moderate but likely events. Most of the up to date seismic design codes adopt the approach of proportioning structures under “reduced” design lateral loads from those that would be produced by a design earthquake excitation. These procedures explicitly enforce designer to estimate required strength and deformation capacity by using a direct relation between linearly elastic internal forces and nonlinear deformations. It is a well known fact that the structural response, under strong seismic action, depends primarily on inelastic cyclic behavior of structural members, which are expected to deform considerably beyond their yield limit. In contrast to traditional force based design, which is clearly incapable of monitoring performance of members, performance based procedures are able to address such inelastic behavior by capturing structure’s almost-true strength and deformation distribution. Despite the probabilistic nature of the seismic actions, deterministically allocating ductility in addition to strength would provide an effective tool for ensuring a successful response and prevention of failure at service life. State of the art design and rehabilitation assessment are mostly bound to documents namely ATC-40 (1996); FEMA356 (2000); FEMA440 (2004) and FEMA450 (2003).

Conventional analysis and design in accordance with the seismic response of a structure is customarily based on the assumption that seismic excitation experienced by the foundation of the structure is identical with the free-field motion, which occurs in the absence of structure. This postulation can only be valid if the supporting soil-foundation system is infinitely rigid, which necessitates fixed-base condition of structural system. However, in reality, dynamic response of a structure supported on a compliant soil may vary significantly from the response of same structure when supported on a rigid base. Difference in the motion experienced by foundation with respect to free-field ground motion is based on two factors (Veletsos, 1993):

1. Inability of foundation to conform to the generally non-uniform spatially variable free-field ground motion.
2. The interaction or coupling between the vibrating structure, its foundation, and supporting soils.

Namely; soil-structure-interaction (SSI) has a two fold effect on the dynamic system:

1. Soil-structure interaction increases the fundamental period of the coupled system by introducing the flexibility of supporting soil.
2. Soil-structure interaction usually increases apparent damping of the system by radiation and hysteretic damping.

For the sake of completeness, elementary information will be provided below for the interaction effects.

1.2 Soil-Structure Interaction

Structures supported on a compliant soil experience a different foundation motion relative to the free-field ground motion. A substantial part of their vibrational energy may be dissipated by hysteretic action in the soil and by radiation of waves into the supporting soil medium. Interaction effects are strongly dependent on the dynamic properties of structure, geometrical properties of foundation, properties of supporting medium and the characteristics of the free-field ground motion (Veletsos, Nair (1975)), and are classified into two components: kinematic and inertial interactions.

1.2.1 Kinematic Interaction

During an earthquake excitation, motion in soil at any given instant is generally different from point to point. This spatially variable nature of seismic waves can be expressed by two major phenomena: *First*, incident waves originating from different sources reach the foundation at different instants and strike with different angles; this is called wave passage effect. *Second*, wave characteristics change both in magnitude and phase while waves are propagating through different paths and different soil layers or when they are reflected and scattered around the foundation; this is called ground motion incoherence (Veletsos, 1993). Upon the introduction of relatively stiff surface or embedded foundation elements, spatially variable free-field motions reduce in the form of an averaging and/or scattering effects, which are attributed as base-slab averaging and embedment effects, respectively. Moreover, rotational motions are introduced in addition to reduction in translational motions (FEMA440, 2004).

These effects are referred to as *kinematic interaction* and are very sensitive to wave characteristics. Their significance on the response is maximized for short-period structures subjected to high frequency wave content (Kim and Stewart, 2003). Analytical models for kinematic interaction effects are often expressed as frequency dependent ratios of Fourier amplitudes. Namely, transfer functions relate free-field ground motion to foundation input motion (FIM). Foundation input motion can be expressed as the theoretical motion of the base slab if foundation and structure had no mass.

1.2.2 Inertial Interaction

Inertia developed in an oscillating structure gives rise to base shear and moment, which in turn cause additional translation and rotation of the foundation relative to free-field. This form of difference between foundation and free-field ground motion is called *inertial interaction*, and it leads to dissipation of excitation energy in terms of radiation and hysteretic action in the supporting soil medium (FEMA440, 2004).

Inertial interaction effects are generally pronounced for the fundamental mode's response of flexible-base system, on the other hand, responses associated with higher-modal frequencies are relatively small (Jennings and Bielak (1973); Bielak, 1976 and Veletsos, 1977; Veletsos, 1993). Unlike kinematic interaction, which generally reduces lateral response, inertial interaction may decrease or increase the corresponding response.

1.2.3 Parameters of Soil-Structure Interaction

Over many studies there is a clear agreement on the parameters affecting soil-structure interaction effects. Among these parameters only two of them are selected as key parameters for the purposes of this study:

Wave parameter (Veletsos, Nair (1975)): Wave parameter, σ , expresses the relative stiffness of the foundation medium and the structure. Kim and Stewart (2003) have concluded that the effect of inertial interaction is strongly correlated with wave parameter: “*Inertial interaction on foundation translations increases with decreasing σ* ”. Case studies performed by Stewart et. al. (1999) have shown that inertial interaction is not important for $\sigma > 10$.

$$\sigma = \frac{V_s T_n}{H} \quad (1.1)$$

where,

V_s = Average shear-wave velocity in the soil medium under the foundation

T_n = Fundamental period of the fixed-base structure

H = Structure's effective height ($H \approx 0.7H_{tot}$, if it is a multistory structure)

Aspect Ratio (Veletsos, Nair (1975)): Aspect ratio is a geometric description based on the ratio of the effective height of the structure to the equivalent radius of the foundation. Inertial interaction based on rocking of structure is expected to be more significant with the increasing aspect ratio and decreasing wave parameter.

$$AspectRatio = \frac{H}{R_{eq}} \quad (1.2)$$

where,

R_{eq} = Equivalent radius of the foundation.

1.2.4 Possible Approaches to the Solution of Interaction Problem

Two different modeling approaches can be performed in order to investigate the effects of soil-structure interaction on the response of superstructure: Complete finite element discretization of coupled system and modification of dynamic properties of fixed base structure matching that of interaction case.

1.2.4.1 Finite Element Discretization of Soil-Foundation-Structure System

The first solution involves three dimensional finite element discretization of the entire coupling system including the soil domain, the foundation and the superstructure at the same time (Fig. 1.1). This procedure is often referred to as direct method of analysis. The solution is achieved in two steps. First step is the modification of stipulated free-field ground motion for the driving base-excitation, which is referred to as the site response analysis. The second step is the modification of the model with the transmitting boundaries (also referred to as silent boundaries) which are used to eliminate reflection of outgoing waves travelling from near-field to far-field soil domain. The disadvantage of the direct method is the fact that discretization of the soil domain drastically increases number of degrees of freedom. Large scale and important projects of essential facilities may require application of these rigorous procedures; however, rendering such methods would cost considerable computation effort. Furthermore, modeling complexity makes the analysis more prone to mistakes and this approach becomes unfeasible for practical investigation of structural response to SSI parameters.

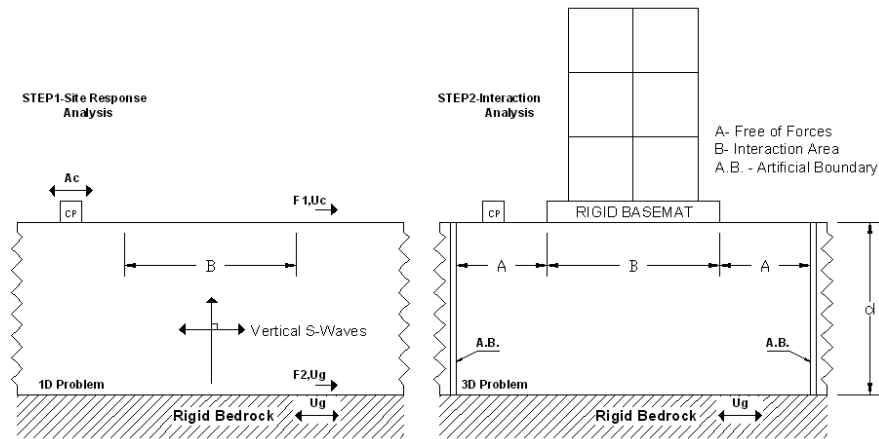


Figure 1.1. Finite element discretization of entire soil-foundation-structure system (Mengi, 2002). In this figure “CP” represents Control Point, at which the ground motion is defined.

An alternative solution for reducing number of degrees of freedom is the utilization of the substructure method. In this method a fictitious boundary is formulated at the soil-structure interface based on wave field properties. This boundary interconnects the soil domain with the superstructure by interaction forces and associated displacements. Formulation of rigorous boundary condition takes forms of frequency dependent dynamic stiffness functions for frequency domain analysis and convolution integrals for time domain analysis.

The major drawback of these analysis schemes is that nonlinearity in both structure and soil domain can not be considered due to the nature of frequency domain analysis.

1.2.4.2 Equivalent Oscillator

In the second approach, an equivalent oscillator; *a linear elastic and damped oscillator supported by a rigid mat foundation, which rests on or is partially embedded in the homogeneous or stratified (visco-) elastic (hysteretic-) half-space*

(FEMA450, 2003); is created by matching the dynamic properties of the actual soil-structure system responding in its fundamental mode of vibration (Fig. 1.2).

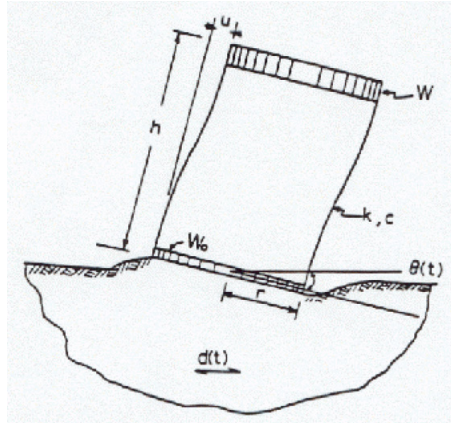


Figure 1.2. Equivalent oscillator (FEMA450 (2003); Veletsos and Nair, 1975). In this figure W , K and C are weight, lateral stiffness and coefficient of viscous damping, respectively.

The response of the pseudo-interacting structure can be solved for the stipulated ground motion. It has been validated that both direct method and equivalent oscillator approaches lead to equivalent results (FEMA450, 2003). Apparently, the second approach is more feasible and practical for the way it handles free-field motion and of modeling the oscillator without dealing with additional degrees of freedom and with introducing complex artificial boundaries; leaving the analysis relatively much simpler to perform and to interpret. This approach has been studied for over three decades regarding the *elastic* response of both supporting medium and structure. Following the studies by Parmalee et al. (1968); Tajimi (1969); Castellani (1970) that provided approximate solutions for dynamic impedances of footings, accurate solutions for rigid mat foundations began to emerge in the beginning of 1970's (Jennings and Bielak (1973); Veletsos and Verbic, 1973; Veletsos and Meek, 1974; Luco, 1974; Veletsos and Nair, 1975; Gazetas, 1975; Veletsos, 1977). They

adequately adopted elastic equivalent oscillator as a replacement of the interacting system by modifying its dynamic properties. Studies have been extended to different types of seismic wave fields, propagation effects, embedment effects, foundation geometry and foundation flexibility effects. However, many of them have remained individual solutions for discrete cases of soil-foundation problems.

1.2.4.3 Discrete Element Models for Foundation Vibrations

Today's practical foundation interaction analyses, including nonlinear response of building structures, can be efficiently solved by the addition of few frequency independent springs, dashpots and masses; namely, lumped parameter models (Dobry and Gazetas (1986); Gazetas, 1991; Wolf, 1994; Wolf, 1997). They can be attached to any multi-degree of freedom system, i.e. at the foundation end of columns, by eliminating over-simplification of the superstructure. Therefore, it allows the analyst to observe individual response of structural elements. ATC-40 (1996) and FEMA356 (2000) documents also point to frequency independent springs which can be evaluated for both surface and embedded foundations of arbitrary shapes. Mathematical formulations of these translational and rotational springs are adopted from Gazetas (1991). However, these documents do not address radiation damping and kinematic interaction. Later, these topics are explicitly included in FEMA440 (2004), Improvement of Nonlinear Static Procedures.

For this study, the truncated cone model (Wolf, 1994) has been preferred among other available models because it provides additional advantages:

- Three dimensional half-space is transformed into a one-dimensional truncated semi-infinite cone by the application of classical strength of materials theory, which provides a better physical insight to foundation behavior.
- Frequency independent dashpots, which simulate radiation damping, can be added in addition to frequency independent springs.
- It is a simple discrete element model and can be directly added to structural model for time-domain analysis.

- Applicability of spring-dashpot and mass models are not limited to special cases and is available for both surface and embedded foundations of arbitrary shapes that rest on/in single or layered halfspace.

Detailed derivations of frequency independent spring, dashpot and mass coefficients for the truncated cone model are given in Appendix A.

1.3 Description of the Problem

It is a common argument that whether soil-structure interaction has beneficial or negative impact on structural response. From the kinematic interaction point of view its beneficial effect in terms of reduction in lateral response of the structure has been briefly discussed in previous sections. From inertial interaction point of view, despite the dominant nature of this effect, its impact on the response is case dependent (Mylonakis and Gazetas (2000)). Assuming an increase in the effective period for the interacting system, when using classical earthquake design spectrum, soil-structure interaction may increase, decrease, or have no effect on the demand forces depending on the location at the spectrum (Bielak (1975); Jennings and Bielak, 1973; Veletsos, 1977; Veletsos and Meek, 1974; Veletsos and Nair, 1975; Veletsos, 1993). Design assessment based on reduced values of base shear and moment due to SSI (FEMA450, (2003)) from the levels applicable to that of fixed-base condition may lead to unsafe design when compared with site-specific procedures (Fig. 1.3). Furthermore, it should be noted that reduction in the base shear due to soil-structure interaction effects at the design stage is only for elastic response of the structure. As will be discussed at the succeeding paragraphs, interaction effects tend to decrease with increasing inelastic action in the structure. In the light of these circumstances, it is a common tendency, even a recommendation by code procedures, to ignore SSI effects at the design phase. From structural deformations point of view, assessment of soil-structure interaction effects may provide clearance limits for controlling pounding of closely spaced buildings due to increased translation and rocking deformations. In addition, second order effects (P-Delta) and yielding of the

structural system may influence exposed deformation and ductility demands at structural members of primary importance.

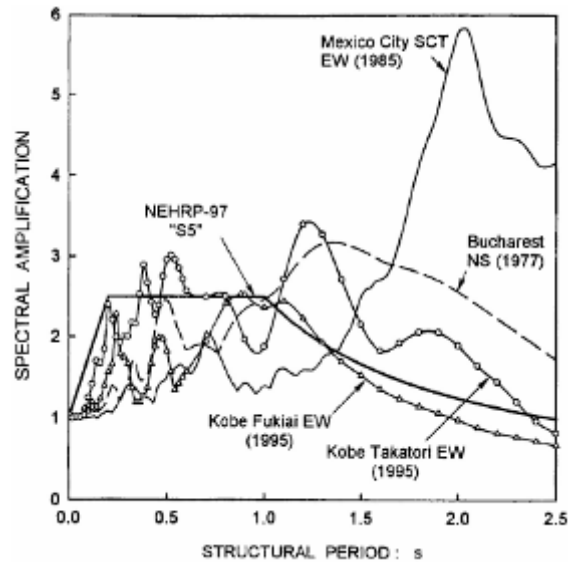


Figure 1.3. Comparison of a typical seismic code design spectrum to actual site-specific spectra from various earthquakes; $\beta=5\%$ (Fig. 3 of Mylonakis and Gazetas (2000)).

Soil-structure interaction effects on yielding structural systems (resting on elastic half-space) have been first studied by Veletsos and Verbic (1973) and later by Priestley and Park (1987); Miranda and Bertero (1994); Ciampoli and Pinto (1995); Elnashai and McClure (1996); Bernal and Youssef (1998); Mylonakis and Gazetas (2000); Aviles and Perez-Rocha (2003). From these studies it has been observed that yielding, which may be globally viewed as a decrease in the stiffness of the structure, leads to a decrease in interaction, hence, variation in response due to SSI effects is less pronounced in inelastic than in elastic systems. In terms of system ductility and member ductility demands there are various studies with conflicting conclusions. It should be noted that conclusions of these studies are specific to analysis assumptions and utilized methods; i.e. idealization of target superstructure, foundation and wave

field characteristics. Based on their comprehensive set of study on simple yielding systems, Ciampoli and Pinto (1995) reported that increased deformations due to SSI effects are mostly based on rigid-body motions, and not because of greater inelastic demands originating from foundation. In addition, they have found that inelastic demands in terms of curvatures remained essentially unaffected by SSI; however, a tendency to decrease which is mostly bound to decreasing trend of base-shear imposed by design response spectra. Studies by Priestley and Park (1987); Bernal and Youssef (1998); Mylonakis and Gazetas (2000); on inelastic bridge piers have showed that an increment in the flexibility of an elastoplastic bridge pier due to the foundation compliance lessens the ductility capacity of the system. Also, they noted that increase in period due to SSI leads to higher relative displacements which, in turn, may cause an increase in seismic demand associated with P-delta effects. This effect, on the contrary, is considered to be of minor importance in FEMA450 (2003).

Under strong earthquake excitation nonlinearity of soil has been identified as an additional issue to be considered. Although lumped parameter models are based on the assumption that soil domain is elastic half-space, validity of this assumption is surely questionable for the affected soil region near the foundation. It is a well known fact that stress-strain relations for soils are nonlinear. Noting that foundation parameters are functions of shear wave velocity; utilization of secant shear modulus, G (based on intensity of seismic action) instead of initial shear modulus, G_0 (corresponds to small amplitude strains) is a common approach (FEMA356 (2000); FEMA440, 2004; FEMA450, 2003; ATC-40, 1996; Veletsos, 1993).

1.4 Aim and Scope

In the light of the facts given in Section 1.3, the dissertation investigates the variation in the response of multistory steel moment-resisting frame structures at both global and local deformation levels as a result of inertial soil-structure interaction effects. Furthermore, this study seeks a tool for the prediction of the change in the response due to the interaction effects by specifying the key parameters of the assessment, which are based on the local soil site condition and the basic geometric and dynamic

properties of the structure. Finally, the limiting values of the key interaction parameters are sought for the case when interaction effects are considered to be beneficial.

The scope of this study is limited to the following structural models, strong ground motion records and foundation and wave field properties and assumptions:

- *Structural models* are; three, four, five, eight and twelve story steel perimeter moment resisting frames (Section 3.4).
- *Two sets of strong ground motion records* compatible with NEHRP Site Classes C and D are compiled in order to perform a comparative structural response with and without the influence of soil-structure interaction effects (Chapter 2).
- *Earthquake acceleration* time-histories are selected as free-field records.
- *The OpenSees* framework is selected as the modeling and analysis software.
- *P-delta effect* is considered in all models.
- *Structural elements* of frames exhibit full material, geometric and element (distributed plasticity) nonlinearities.
- *Wave field* is assumed as vertically propagating horizontally polarized coherent shear waves (SH).
- Structures are supported on *surface foundations*.
- *Foundation* is assumed to be resting on an elastic half-space (surface or shallow foundation, no embedment) and it is assumed that there is full bonding between soil and foundation (Section 3.3).
- *Nonlinearity of soil* is implicitly included in the calculation of frequency independent spring and dashpot coefficients by secant shear modulus.
- *Kinematic interaction* (SSI) is not considered for the type of foundation and assumed wave field.
- *Foundation model* is selected as a lumped parameter model; the truncated cone model (Appendix A). Coefficients are calculated from Wolf (1994).

1.5 Organization of Text

Following the introduction given in this Chapter, details regarding the strong ground motion records are presented in Chapter 2. Details of the structural models (foundation and frames) are given in Chapter 3. Analysis framework and results are given in Chapter 4. Discussion of results and the conclusion are given in Chapter 5. Appendix is provided for further information regarding the derivation of formulations, strong ground motion records and the frame responses.

CHAPTER 2

EARTHQUAKE GROUND MOTION RECORDS

2.1 Introduction

For the purposes of this dissertation two sets of earthquake ground motion records have been compiled from PEER NGA Database¹. These sets represent free-field acceleration records meeting the shear wave velocity requirements of NEHRP Site Classes C ($V_{s30}=360-720$ m/s) and D ($V_{s30}=180-360$ m/s), where V_{s30} is the average shear wave velocity for top 30m soil profile. In this study, these sets are referred to as SETC and SETD records, respectively.

2.2 Classification of Earthquake Events and Associated Acceleration Records

Earthquake events and associated acceleration records bound to SETC and SETD conform to following properties:

- All records are chosen from free-field records.
- Each set (SETC and SETD) contains 50 earthquake events. Their complete listing is given in Appendix B and Tables B.1 - B.3. These tables provide event name, event date, event magnitude, station name, closest distance the rupture surface, shear wave velocity and peak ground acceleration of the recorded event.
- 20 out of 50 events of each set, SETC and SETD, contain pulse effects. These subsets are referred to as SET-C1 and SET-D1. Complementary subsets are referred to as SET-C2 and SET-D2.

¹ <http://peer.berkeley.edu/nga/index.html>, Pacific Earthquake Engineering Research Center.

- Each event record contains two horizontal acceleration components. Both components are included in strong ground motion database. As a sum, there are 80 and 120 acceleration records containing pulse effects and without pulse effects, respectively.
- Earthquake magnitude, M for all records varies from 5.99 to 7.62.
- Shortest distance to the rupture surface, R has a range between:
 - 8km to 77.4km, for SETC records.
 - 7.3km to 77km, for SETD records.
- Peak ground acceleration has a range between:
 - 0.1g - 0.57g, for SET-C1 records.
 - 0.12g - 0.64g, for SET-C2 records.
 - 0.14g - 0.9g, for SET-D1 records.
 - 0.11g - 0.59g, for SET-D2 records.

Mean and mean plus one standard deviation values of peak ground acceleration, PGA and maximum spectral acceleration, $SA(g)$ values corresponding to SETC and SETD records are given in Table 2.1.

- Recording station of earthquake events is selected in order to provide the lowest values of shear wave velocities, V_{s30} to represent the associated NEHRP equivalent site class. Minimum, mean and maximum values of V_{s30} are:
 - 392, 528, 685m/s, for SETC records.
 - 192, 273, 339m/s, for SETD records.

2.3 Acceleration Response Spectra

Acceleration response spectra corresponding to unscaled individual records of sets SETC and SETD, including the mean and the mean plus one standard deviation response spectra, are given in Fig. 2.1. This plot includes response spectra obtained from both records containing pulse effects and records without pulse effects. Therefore, separate plots of the mean and the mean plus one standard deviation response spectra corresponding to SET-C1, C2 and SET-D1, D2 records are given in Fig. 2.2 and Fig. 2.3, respectively.

Table 2.1. Mean and mean plus one standard deviation values of peak ground acceleration, PGA and maximum spectral acceleration, SA(g) values corresponding to SETC and SETD records.

	Peak Ground Acceleration (g)			Maximum Spectral Acceleration (g)		
NEHRP Site Class	All Records			All Records		
	Mean	StDev	Mean+StDev	Mean	StDev	Mean+StDev
C	0.226	0.112	0.339	0.782	0.370	1.151
D	0.251	0.125	0.376	0.851	0.485	1.336
NEHRP Site Class	Records containing Pulse Effects			Records containing Pulse Effects		
	Mean	StDev	Mean+StDev	Mean	StDev	Mean+StDev
C1	0.224	0.102	0.326	0.716	0.327	1.043
D1	0.270	0.136	0.405	0.862	0.447	1.309
NEHRP Site Class	Records without Pulse Effects			Records without Pulse Effects		
	Mean	StDev	Mean+StDev	Mean	StDev	Mean+StDev
C2	0.238	0.116	0.355	0.825	0.392	1.218
D2	0.228	0.120	0.348	0.844	0.512	1.356

Table 2.2. BSE-1 design spectra coefficients obtained from the mean (μ) and the mean plus one standard deviation ($\mu+\sigma$) response spectra of SET-C1, C2, D1 and D2 records.

EQ. RECORD SET	Sxs	Fa	Sxl	Fv	Ss	Sl
SET-C1 μ	0.46	1.2	0.33	1.59	0.38	0.21
SET-C1 $\mu+\sigma$	0.68	1.16	0.57	1.39	0.59	0.41
SET-C2 μ	0.54	1.2	0.18	1.69	0.45	0.11
SET-C2 $\mu+\sigma$	0.80	1.11	0.31	1.61	0.72	0.19
SET-D1 μ	0.56	1.49	0.36	2.10	0.38	0.17
SET-D1 $\mu+\sigma$	0.97	1.17	0.50	1.86	0.83	0.27
SET-D2 μ	0.53	1.51	0.22	2.40	0.35	0.09
SET-D2 $\mu+\sigma$	0.77	1.33	0.42	1.97	0.58	0.22

In order to provide a comparison, equivalent design spectrum of NEHRP, BSE-1 hazard level (10% chance of being exceeded in 50 years; FEMA356 (2000)) representation is superimposed on Fig. 2.2 and Fig. 2.3. Coefficients of BSE-1 design response spectrum are given in Table 2.2. These are: The mapped/design *short* and *long* period spectral response acceleration coefficients (S_s/S_{xs} , S_l/S_{xl}) and the

associated site coefficients (F_a , F_v). The coefficients are calculated from both mean and the mean plus one standard deviation response spectra of SET-C1, C2, D1 and D2 records.

2.4 Strong Ground Motion Scaling Schemes

Three analysis groups are organized according to the applied scaling scheme on the earthquake ground motion acceleration records.

In the *Analysis Group I*, which is also referred to as “SET-NS”, structural responses are evaluated without any scaling of SETC and SETD records. In the related figures, tables and data representation this analysis group is referred to as SET-NS-C1, SET-NS-C2, SET-NS-D1 and SET-NS-D2. Mean plus one standard deviation response spectra of these sets including the distribution of fundamental period of frame models are given in Fig. 2.4.

In the *Analysis Group II*, which is also referred to as “SET-SC”, acceleration records are scaled to mean plus one standard deviation spectral acceleration of each SET-C1, C2, D1 and D2 records, which are calculated at the fundamental period of frame models. In the related figures, tables and data representation this analysis group is referred to as SET-SC-C1, SET-SC-C2, SET-SC-D1 and SET-SC-D2. Mean plus one standard deviation response spectra of these sets scaled at the effective fundamental period of each frame model are given in Appendix B and Figs. B.1 – B.7, respectively. Mean, standard deviation, mean plus one standard deviation, median, minimum and maximum values of spectral accelerations for SETC and SETD records calculated at the fundamental period of frame models are given in Appendix B, Table B.4. Associated scale factors for individual records are given in Appendix B and Tables B.5 and B.6 for SETC and SETD records, respectively.

In the *Analysis Group III*, which is also cited as “SCR2”, each record in each set is individually scaled in order to produce the strength reduction factor, $R=2$ (FEMA356 (2000), Chapter 3, pp. 3-21, eqn. 3-16) at the effective fundamental period of each

frame model. In the related figures, tables and data representation this analysis group is referred to as SET-SCR2-C1, SET-SCR2-C2, SET-SCR2-D1 and SET-SCR2-D2. Mean plus one standard deviation response spectra of these sets scaled at the effective fundamental period of each frame model are given in Appendix B and Figs. B.8 – B.14, respectively. Scale factors in order to produce a spectral acceleration equal to 1.0g at the effective fundamental period of the frame and associated scale factors to produce the strength reduction factor, R=2 are given in Table 2.3. Associated scale factors for individual records are given in Appendix B and Tables B.7 and B.8 for SETC and SETD records, respectively.

Table 2.3. Scale factors for SET-SCR2 (Analysis Group III) records in order to produce a spectral acceleration equal to 1g at the effective fundamental period of the frame and associated scale factors to produce the strength reduction factor, R=2 (FEMA356 (2000)).

Model Name	Te (s)	V_y/Wt (%)	C_m	(SA=1g) R (FEMA356)	SA (g) R=2
3SAC	1.07	24	0.828	3.243	0.617
4KatF	1.21	30	0.874	2.866	0.698
4KatR	0.73	77	0.846	1.085	1.844
5KatS2	0.83	51	0.822	1.612	1.241
8KatS2	1.51	23.5	0.78	3.319	0.603
12KatF	2.24	20	0.786	3.990	0.501
12KatR	1.28	55	0.766	1.393	1.436

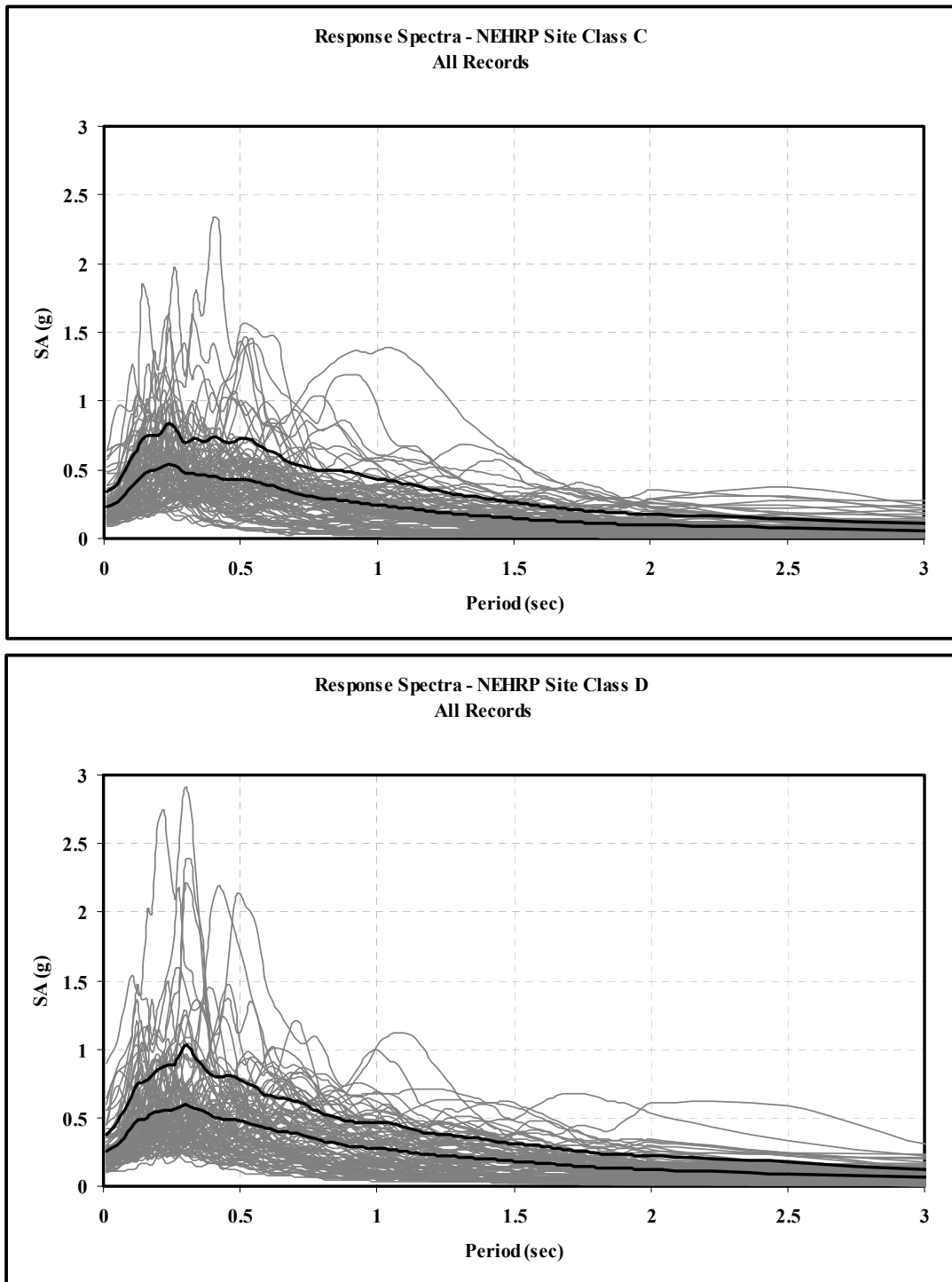


Figure 2.1. Response spectra for SETC and SETD records conforming to NEHRP Site Classes C and D, respectively. In this figure, grey plots represent individual records and dark plot at the bottom and at the top represent mean and mean plus one standard deviation response Spectra, respectively.

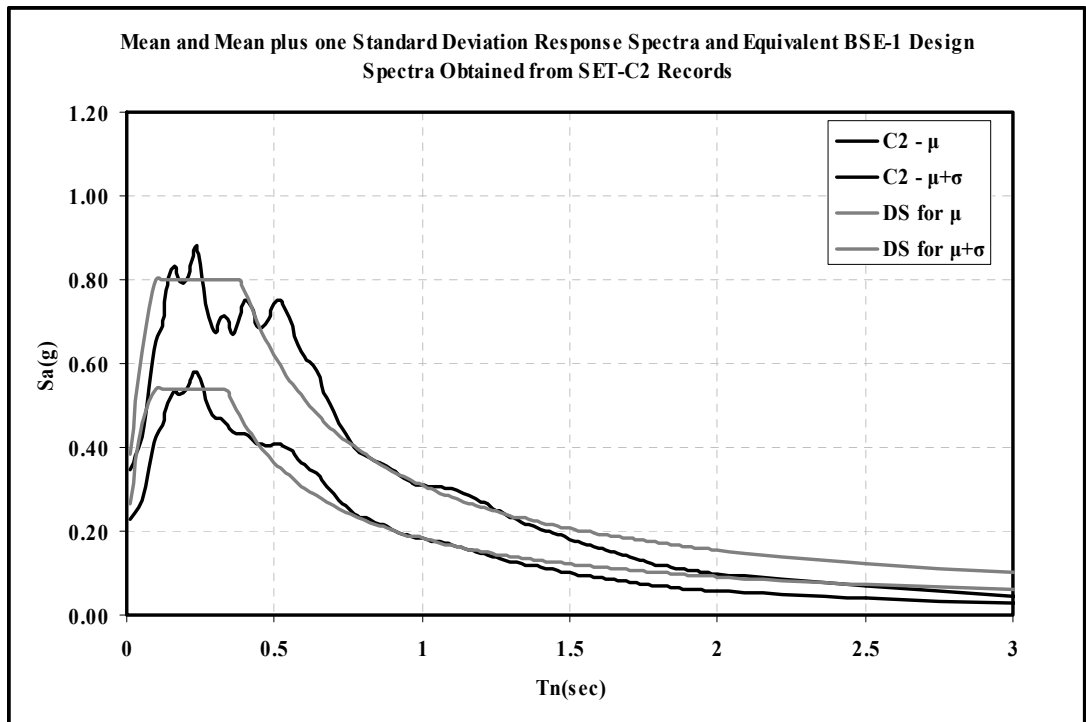
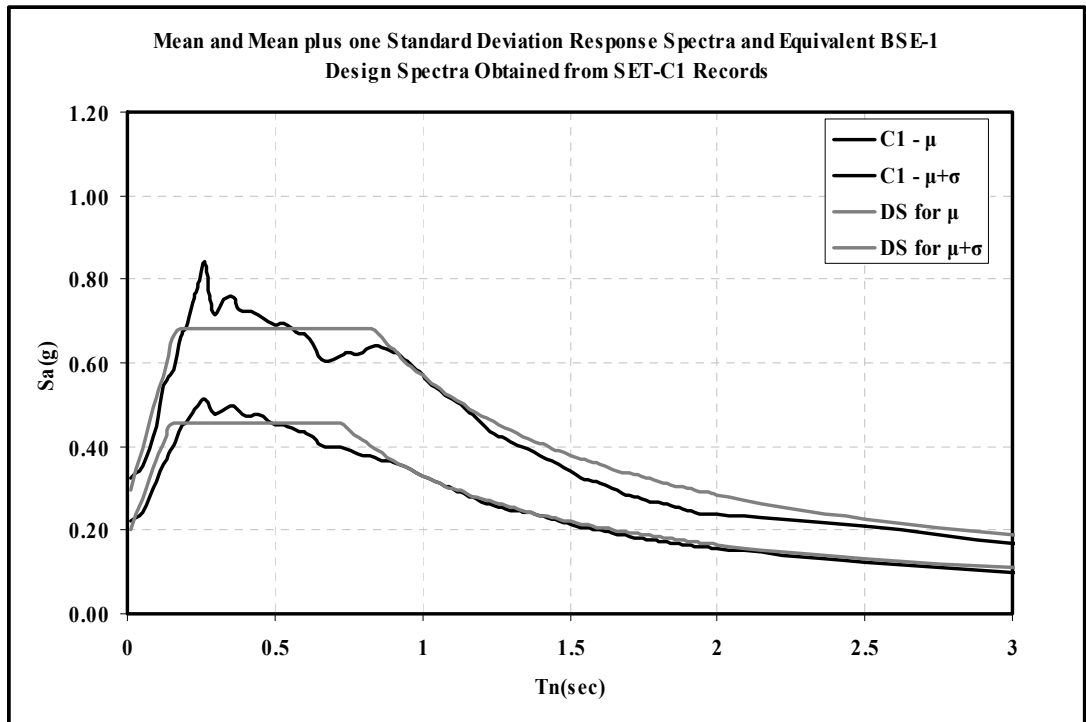


Figure 2.2. Mean (μ) and mean plus one standard deviation ($\mu+\sigma$) response spectra and equivalent BSE-1 level design spectra for 10% probability of exceedance in 50 years (FEMA356, 2000) for SETC records, conforming to NEHRP Site Class C: Records containing pulse effects and records without pulse effects.

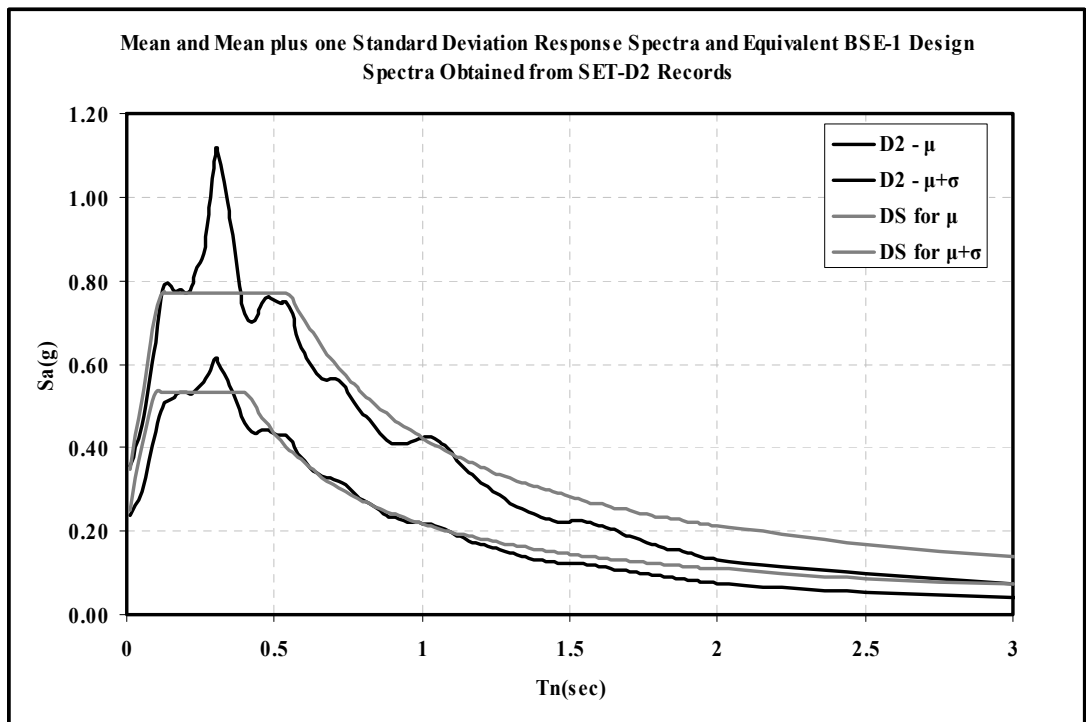
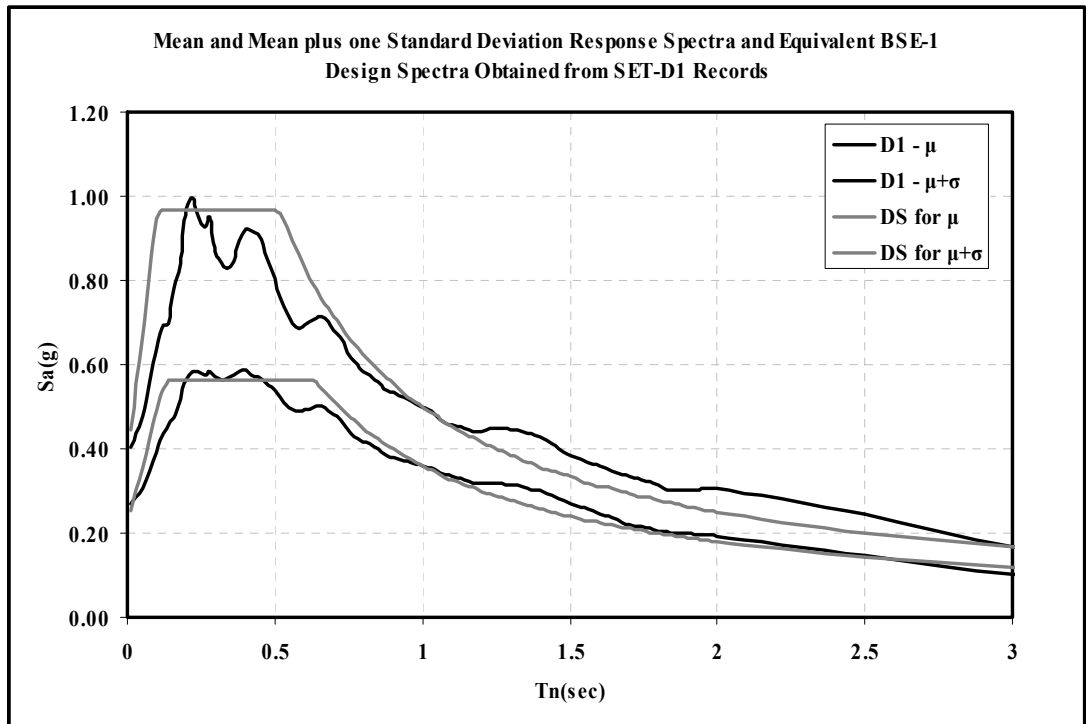


Figure 2.3. Mean (μ) and mean plus one standard deviation ($\mu + \sigma$) response spectra and equivalent BSE-1 level design spectra for 10% probability of exceedance in 50 years (FEMA356, 2000) for SETD records, conforming to NEHRP Site Class D: Records containing pulse effects and records without pulse effects.

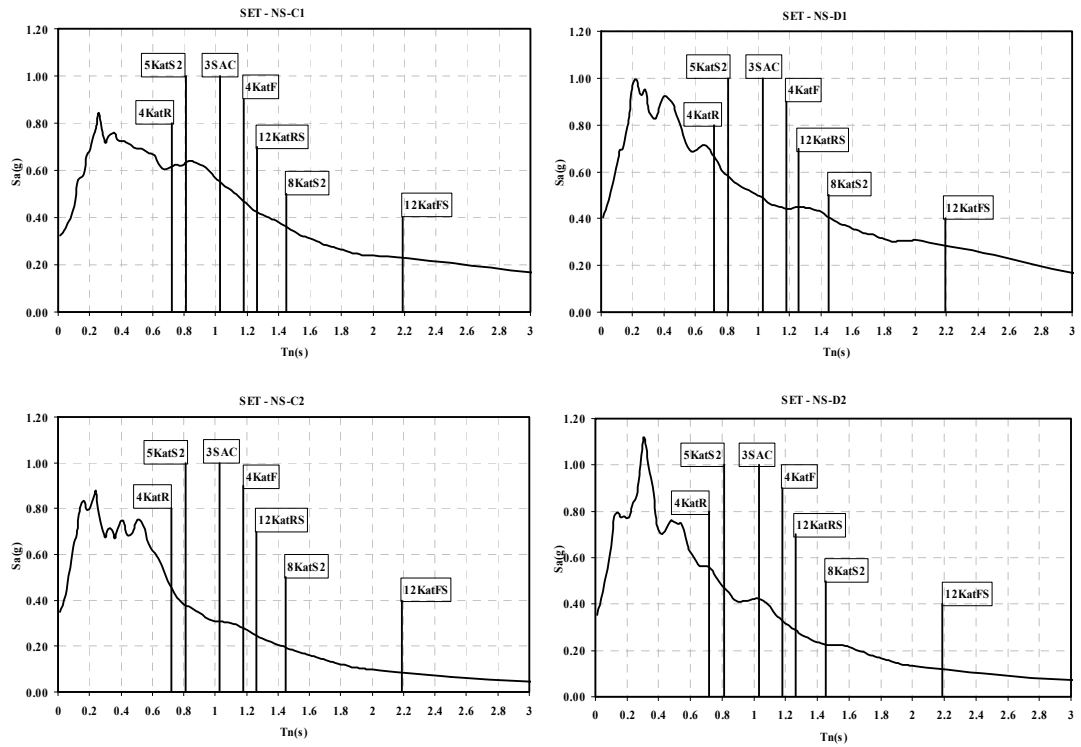


Figure 2.4. Mean plus one standard deviation response spectra of SET-NS-C1, SET-NS-C2, SET-NS-D1 and SET-NS-D2 records and the distribution of fundamental periods of frame models: 3SAC ($T_n=1.0s$), 4KatF ($T_n=1.1s$), 4KatR ($T_n=0.72s$), 5KatS2 ($T_n=0.81s$), 8KatS2 ($T_n=1.45s$), 12KatFS ($T_n=2.19s$), 12KatRS ($T_n=1.26s$).

CHAPTER 3

STRUCTURAL MODELS

3.1 Introduction

7 two-dimensional moment-resisting steel frame models are used in the assessment of nonlinear dynamic analyses. These are:

- N-S Perimeter frame of the three story SAC¹ building. Details are provided in Section 3.4.1.
- Two pairs of four and twelve story frame models (Aschheim (2002)). Details are provided in Section 3.4.2.
 - Four story steel moment-resisting frame – flexible model.
 - Four story steel moment-resisting frame – rigid model.
 - Twelve story steel moment-resisting frame – flexible model.
 - Twelve story steel moment-resisting frame – rigid model.
- Two fictitious frame models prepared particularly for this study by the author. Details are provided in Section 3.4.3.
 - Five story steel moment-resisting frame model.
 - Eight story steel moment-resisting frame model.

Frame models are programmed and analyzed using the finite element analysis framework Opensees. *The Open System for Earthquake Engineering Simulation* is a multiplatform open-source software framework for simulating the seismic response

¹ SAC is a joint venture of three non-profit organizations: The Structural Engineers Association of California (SEAOC), the Applied Technology Council (ATC) and California Universities for Research in Earthquake Engineering (CUREE).

of structural and geotechnical systems. It has been developed as the computational platform for research in performance-based earthquake engineering at the Pacific Earthquake Engineering Research Center. Details about the documentation and examples can be found from official internet address, <http://opensees.berkeley.edu>. Customary properties of the frame models and modeling assumptions are provided in Section 3.2. The foundation is modeled using truncated cone model, (Wolf (1994)) and modeling details are provided in Section 3.3. Their geometric, mass and loading details are provided in Section 3.4.

3.2 Frame Properties, Modeling and Analysis Assumptions

Frame models comprise the following common properties and modeling assumptions:

- Frame models are extracted from the perimeter frame of a steel moment-resisting frame building. The primary lateral load resisting system is the moment-resisting frame around the perimeter of the building. Interior bays of the building structure embrace simple steel framing which resists only gravity loads.
- As a common modeling practice, rigid diaphragm action is assumed at the floor levels. Although masses are assumed to be lumped at joints (at beam-column connections) they are slaved to story master joints.
- Gravity loads are defined by ratios of seismic mass associated to tributary loading area, and they are assumed to be acting uniformly over the span of each steel beam of the perimeter frame.
- It is assumed that each of the opposing perimeter frame share inertia induced story shears equally.
- All beam-column connections are moment-resisting. All column-foundation connections are moment-resisting. Hence, they are modeled as fixed supports.
- All frames are modeled as two dimensional frames with the centerline dimensions of the structural members. In addition, composite action of beam and slab is excluded.

- Analytical model of example frames involve full material and member nonlinearity, including P-Delta effects.
- All structural elements are made of structural steel conforming ASTM A36 and ASTM A572Gr50. Material models are programmed in Opensees via uniaxial bilinear steel material (Fig. 3.1) with the coefficients given by the standards (Table 3.1).

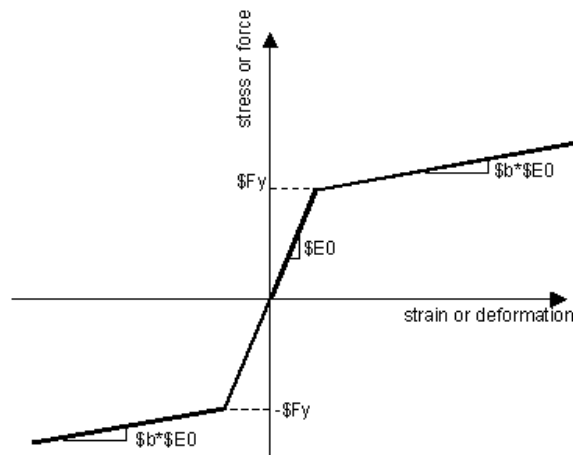


Figure 3.1. Backbone force-deformation relationship for Steel01 material, OpenSees. In this figure F_y is the yield limit; E_0 is the initial tangent, modulus of elasticity; b is the post yield slope.

Table 3.1. Mechanical properties of ASTM type structural steels used in the analysis framework (Gaylord, (1992)). In this table σ_y is the yield stress; σ_u is the ultimate stress; E is the modulus of elasticity; ϵ_y is the yield strain; ϵ_{sh} is the strain at strain hardening; ϵ_u is the ultimate strain; ν is the Poisson's Ratio; G is the shear modulus.

Steel Properties - ASTM						
Steel Class	σ_y (MPa)	σ_u (MPa)	ϵ_y (dL/L)	ϵ_{sh} (dL/L)	ϵ_u (dL/L)	ϵ_r (dL/L)
A36	248.2	399.9	0.00124	0.020	0.140	0.200
A572Gr50	344.7	448.2	0.00172	0.015	0.110	0.170

E (MPa)	ν	G (MPa)	ρ (ton/m ³)	γ (kN/m ³)	α (dL/L/C°)
200000	0.3	76923.1	7.85	77.0	1.17E-05

- All member sections are wide-flange I shapes from AISC (American Institute of Steel Construction) structural steel shape list.
- Element plasticity is associated with the fiber section models that are defined at the integration points along the length of the member. These models are used to obtain sectional response where force-deformation interaction is explicitly defined by a specific material model. Sectional response implicitly includes axial load - moment interaction.
- Beams and columns of the analytical models are programmed with force based nonlinear beam-column elements that are formulated by distributed plasticity integrated along the member length.
- Governing force-deformation mode for structural elements is assumed to be bending in the major axis.
- Beam-column connection and/or panel zone failures are not considered in the analytical models.
- Nonlinear static and dynamic analyses of frame models are performed after the application of associated frame gravity loads. OpenSees has the ability to continue to new loading schemes while preserving former stress-strain levels in sections.
- Nonlinear dynamic analyses are performed by utilizing Rayleigh damping. The damping matrix is calculated from mass and stiffness proportional damping by constraining first and third elastic modes of the analytical model for a fixed damping ratio of $\beta_i=5\%$.
- Structural response is monitored at both global and member levels:
 - Global response: Data is recorded as response-histories of story drifts, story shears and foundation deformation (horizontal translation and rocking degrees of freedom). Maximum deformations and associated forces are also calculated through a post-process scheme over the response histories.
 - Member response: Data is recorded as response-histories of member end moments and end rotations. Maximum values of these responses are also processed in terms of absolute values through a post-process scheme over the response-histories.

- Foundations of structures are assumed to be rigid and rectangular in shape.
- Soil-structure interaction analyses of frames are performed by modifying the original frame with the truncated cone model (Wolf, (1994)). Discrete elements of the model exhibit frequency independent coefficients. Details are provided in Section 3.3.

3.3 Foundation-Soil Interaction Model and Assumptions

Soil-structure interaction analysis is carried out by adding a lumped parameter model to the base of the frame structure. Frequency independent coefficients of spring, dashpot and masses are formulated according to truncated cone model, Wolf (1994). Theoretical background and derivations of the coefficients are provided in Appendix A. Assumptions for the evaluation of foundation parameters and for the preparation of analytical model are as follows:

- Soil domain is assumed as elastic half-space. Parameters are soil mass density, ρ_{soil} ; Poisson's ratio of soil, ν_{soil} ; average shear wave velocity of the top 30m soil profile, V_{s30} .
- Constant values are assumed for soil mass density, $\rho_{\text{soil}}=1.8$ (ton/m³) and Poisson's ratio, $\nu_{\text{soil}}=0.35$. Average shear wave velocity is provided by the station of the recorded strong motion.
- Wave field is assumed as vertically propagating horizontally polarized coherent shear waves (SH).
- The structure is supported by surface foundation (no embedment). The foundation is assumed to be resting on an elastic half-space and there is a full bonding between foundation and soil medium.
- For the selected wave field and taking into account the existence of surface foundation, kinematic interaction effects are not considered.
- The foundation is assumed to be rigid and assumed to be rectangular in shape, covering the whole footprint area of the building structure. Coefficients of the truncated cone model (Wolf (1994)), which is embedded into the two dimensional moment-resisting frame, are calculated for the half of the total

- Nonlinearity of the soil is implicitly included in the calculation of frequency independent spring, dashpot and mass coefficients by strain reduced shear wave velocity, V_{sr} , i.e. secant shear modulus, G ($G=\rho_{soil}(V_{sr})^2$). Strain reduced shear wave velocity can be obtained by multiplying V_{s30} with a coefficient n , which is a function of ground shaking intensity. Values of n as a function of peak ground acceleration are provided in FEMA440 (2004).
- The foundation is modeled with rigid beam-column elements through connecting the bottom ends of ground story columns. Next, lumped parameter model which is illustrated in Fig. 3.2, is inserted in the middle of the foundation while keeping the far end fixed. An illustrative example of a modified frame is provided in Fig. 3.3 for 3SAC (three story SAC frame) model.

In this study, rectangular foundation by equivalent radius analogy is used. A comparative evaluation of frequency independent coefficients formulated according to both FEMA356 (2000) and the truncated cone model, for both rigid disk and rectangular foundation by equivalent radius analogy, is illustrated in Tables 3.2 and 3.3, respectively. A sample local site condition was selected from an earthquake record stored in SETD: Northridge, 1994 ($M=6.69$, $PGA=0.36g$) recorded by “LA-Hollywood Store FF” station. According to station information average shear wave velocity of top 30m soil profile is $V_{s30}=316.46m/s$. Record sequence number and filename are 995 and “NORTHR/PEL360.at2”, respectively. Soil parameters are illustrated in Table 3.4. Calculations are based on a rigid surface rectangular foundation with $L=24m$ and $B=12m$. Translation and rocking spring coefficients calculated for both horizontal components are compared with the FEMA356 (2000) procedure and truncated cone model and illustrated in Table 3.5. Results are presented in terms of ratios of FEMA356 (2000) to truncated cone model outputs and they indicate that equivalent radius analogy for rectangular foundations produce very close results.

Translation

Rocking

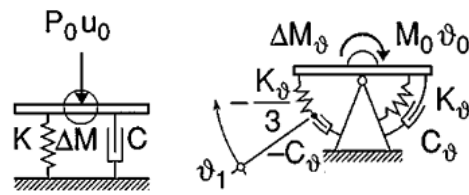


Figure 3.2. Illustration of lumped parameter models for vertical translation and rocking degrees of freedom formulated by truncated cone model (Fig.5; Wolf (1997)).

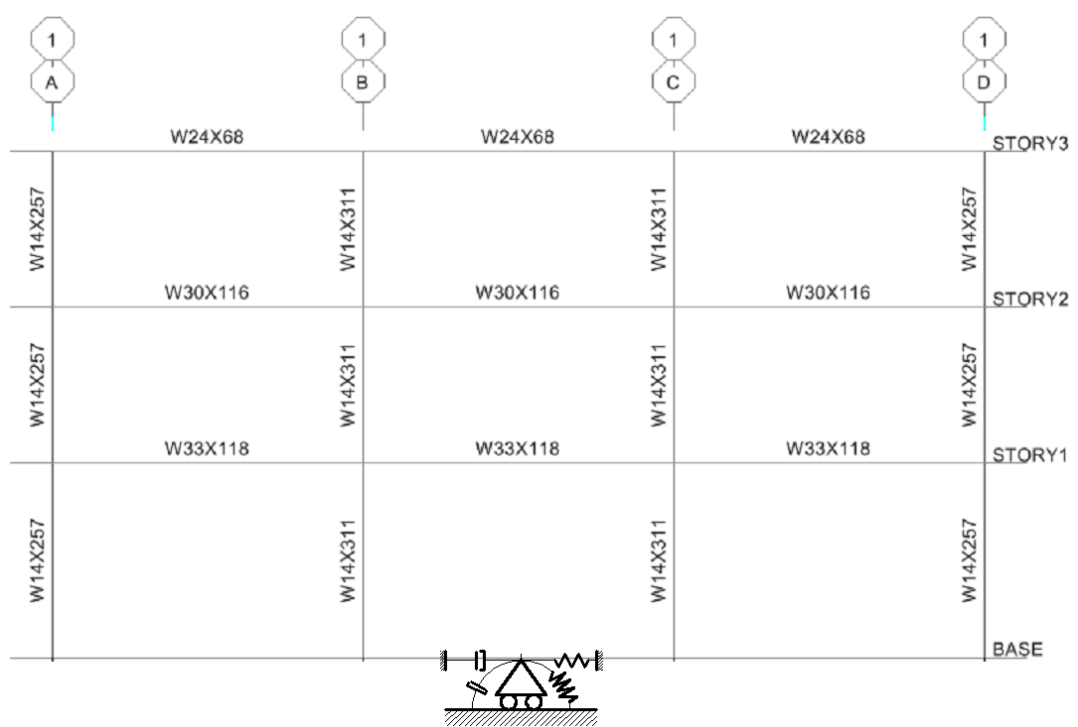


Figure 3.3. Illustration of 3SAC frame model modified with lumped parameter model formulated via truncated cone model (Wolf (1994)). Rigid foundation beams are not included in the figure. Illustration graphics is produced by ETABS (Computers And Structures Inc.).

Table 3.2. Frequency independent uncoupled stiffness coefficients using FEMA356 (2000) procedure for all degrees of freedom calculated for soil properties given in Table 3.4. Surface foundation is rectangular with L=24m and B=12m.

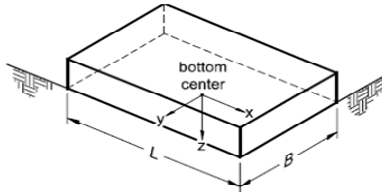
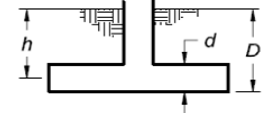
Fema356 Soil Impedance Formulae (L>=B)					
Degree of Freedom	Stiffness of Foundation at Surface			Note	
Translation along x-axis	$K_{x, sur} = \frac{GB}{2-\nu} \left[3.4 \left(\frac{L}{B} \right)^{0.65} + 1.2 \right]$			 <p>Orient axes such that $L \geq B$</p>	
Translation along y-axis	$K_{y, sur} = \frac{GB}{2-\nu} \left[3.4 \left(\frac{L}{B} \right)^{0.65} + 0.4 \frac{L}{B} + 0.8 \right]$				
Translation along z-axis	$K_{z, sur} = \frac{GB}{1-\nu} \left[1.55 \left(\frac{L}{B} \right)^{0.75} + 0.8 \right]$				
Rocking about x-axis	$K_{xx, sur} = \frac{GB^3}{1-\nu} \left[0.4 \left(\frac{L}{B} \right) + 0.1 \right]$				
Rocking about y-axis	$K_{yy, sur} = \frac{GB^3}{1-\nu} \left[0.47 \left(\frac{L}{B} \right)^{2.4} + 0.034 \right]$				
Torsion about z-axis	$K_{zz, sur} = GB^3 \left[0.53 \left(\frac{L}{B} \right)^{2.45} + 0.51 \right]$				
Degree of Freedom	Correction Factor for Embedment			Note	
Translation along x-axis	$\beta_x = \left(1 + 0.21 \sqrt{\frac{D}{B}} \right) \cdot \left[1 + 1.6 \left(\frac{hd(B+L)}{BL^2} \right)^{0.4} \right]$			 <p>d = height of effective sidewall contact (may be less than total foundation height) h = depth to centroid of effective sidewall contact</p> <p>For each degree of freedom, calculate $K_{emb} = \beta K_{sur}$</p>	
Translation along y-axis	$\beta_y = \beta_x$				
Translation along z-axis	$\beta_z = \left[1 + \frac{1}{21} \frac{D}{B} \left(2 + 2.6 \frac{B}{L} \right) \right] \cdot \left[1 + 0.32 \left(\frac{d(B+L)}{BL} \right)^{2/3} \right]$				
Rocking about x-axis	$\beta_{xx} = 1 + 2.5 \frac{d}{B} \left[1 + \frac{2d}{B} \left(\frac{d}{D} \right)^{-0.2} \sqrt{\frac{B}{L}} \right]$				
Rocking about y-axis	$\beta_{yy} = 1 + 1.4 \left(\frac{d}{L} \right)^{0.6} \left[1.5 + 3.7 \left(\frac{d}{L} \right)^{1.9} \left(\frac{d}{D} \right)^{-0.6} \right]$				
Torsion about z-axis	$\beta_{zz} = 1 + 2.6 \left(1 + \frac{B}{L} \right) \left(\frac{d}{B} \right)^{0.9}$				
Figure 4.4. Elastic Solutions for Rigid Footing Spring Constraints, Fema356, Chapter 4					
L(x) (m)	B(y) (m)	Ao (m ²)	I(x) (m ⁴)	I(y) (m ⁴)	I(z)=Ix+Iy (m ⁴)
24	12	288	3456	13824	17280
D (m)	d (m)	h (m)	L/B (-)		
0.00	0.00	0.00	2		
Kx,sur (kN/m)	Ky,sur (kN/m)	Kz,sur (kN/m)	Kxx,sur (kNm/rad)	Kyy,sur (kNm/rad)	Kzz,sur (kNm/rad)
3619855	3841416	4790145	182225754	509153917	448255812
βx	βy	βz	βxx	βyy	βzz
1.0001	1.0001	1.0000	1.0000	1.0001	1.0000
Kx,emb (kN/m)	Ky,emb (kN/m)	Kz,emb (kN/m)	Kxx,emb (kNm/rad)	Kyy,emb (kNm/rad)	Kzz,emb (kNm/rad)
3620083	3841658	4790184	182225792	509193815	448256555

Table 3.3. Frequency independent coefficients of lumped parameter model using truncated cone model (Wolf (1994)) for both equivalent rigid disk and rigid rectangular foundation. Soil properties are given in Table 3.4.

Cone Model Soil Impedance Formulae (Units: kN, tons, m, s, rad)					
Motion	Horizontal	Vertical		Rocking	Torsional
Equivalent radius r_0	$\sqrt{\frac{A_0}{\pi}}$	$\sqrt{\frac{A_0}{\pi}}$		$\sqrt[4]{\frac{4I_0}{\pi}}$	$\sqrt[4]{\frac{2I_0}{\pi}}$
Aspect ratio $\frac{z_0}{r_0}$	$\frac{\pi}{8}(2-v)$	$\frac{\pi}{4}(1-v)\left(\frac{c}{c_s}\right)^2$		$\frac{9\pi}{32}(1-v)\left(\frac{c}{c_s}\right)^2$	$\frac{9\pi}{32}$
Poisson's ratio ν	All ν	$\leq \frac{1}{3}$	$\frac{1}{3} < \nu < \frac{1}{2}$	$\leq \frac{1}{3}$	$\frac{1}{3} < \nu \leq \frac{1}{2}$
Wave velocity c	c_s	c_p	$2c_s$	c_p	$2c_s$
Trapped mass $\Delta M \Delta M_\theta$	0	0	$2.4\left(\nu - \frac{1}{3}\right)\rho A_0 r_0$	0	$1.2\left(\nu - \frac{1}{3}\right)\rho I_0 r_0$
Discrete-element model		$K = \rho c^2 A_0 / z_0$ $C = \rho c A_0$		$K_\theta = 3\rho c^2 I_0 / z_0$ $C_\theta = \rho c I_0$ $M_\theta = \rho I_0 z_0$	
Cone Model Soil Impedance Formulae for Circular Disk					
R (m)	Ao (m²)	Io (m⁴)	Iz (m⁴)		
9.5746	288	6600	13201		
Surface Foundation's Motion (Circular Disk)					
	Horizontal		Vertical	Rocking	
	X	Y	Z	X	Y
Ro(m)	9.575	9.575	9.575	9.575	9.575
c(m/s)	205.699	205.699	411.398	411.398	411.398
Zo/Ro	0.648	0.648	2.042	2.297	2.297
dM	0	0	198.54	2275.09	2275.09
K	3535608.9	3535608.9	4487503.6	274256016.8	274256016.8
C	106634.4	106634.4	213268.7	4887759.1	4887759.1
Mv	0	0	0	261327.2	261327.2
Cone Model Soil Impedance Formulae for Rectangular Foundation, L>=B					
L(x) (m)	B(y) (m)	Ao (m²)	I(x) (m⁴)	I(y) (m⁴)	I(z) (m⁴)
24	12	288	3456	13824	17280
Surface Foundation's Motion (Rectangular)					
	Horizontal		Vertical	Rocking	
	X	Y	Z	X	Y
Ro(m)	9.57	9.57	9.57	8.14	11.52
c(m/s)	205.699	205.699	411.398	411.398	411.398
Zo/Ro	0.648	0.648	2.042	2.297	2.297
dM	0	0	198.54	1013.32	5732.21
K	3535608.9	3535608.9	4487503.6	168812705.7	477474435.9
C	106634.4	106634.4	213268.7	2559224.7	10236898.7
Mv	0	0	0	116394.6	658427.5
M+dM	0	0	199	117408	664160

Table 3.4. Basic soil parameters for the evaluation of frequency independent spring-dashpot-mass coefficients.

Soil Parameters					
ρ (ton/m ³)	ν	V_s (m/s)	n_1	γ (kN/m ³)	V_p (m/s)
1.8	0.35	316.46	0.65	17.7	658.8
V_s' (m/s)	V_p' (m/s)	G_o (N/m ²)	E_o (N/m ²)	G (N/m ²)	E (N/m ²)
205.699	428.2	180264476.9 <i>180.27 MPa</i>	781146066.5 <i>781.15 MPa</i>	76161741.48 <i>76.17 MPa</i>	330034213.1 <i>330.04 MPa</i>

Table 3.5. Ratio of frequency independent stiffness coefficients for translation and associated rocking degrees of freedom calculated from FEMA356 (2000) procedure and truncated cone model (Wolf (1994)).

	Impedance Ratios of Fema to Cone Model			
	K_x/K_x'	K_{yy}/K_{yy}'	K_y/K_y'	K_{xx}/K_{xx}'
FEMA/TCM-C	1.024	1.856	1.086	0.664
FEMA/TCM-R	1.024	1.066	1.086	1.079
<i>TCM-C and TCM-R are Truncated Cone Model - Circular and Rectangular, respectively.</i>				

3.4 Frame Models

3.4.1. Three Story SAC Frame

The frame is adopted from the three story SAC building. Although not actually constructed, it was designed as a part of SAC Phase II Steel Project for Los Angeles, California region. Building's lateral load resisting system is composed of perimeter steel moment-resisting frames having a constant bay width and a story height of 30ft (9.15m) and 13ft (3.96m), respectively. Structure's footprint dimensions are 120ft (36.58m) and 180ft (54.87m) along its North-South (five frames in total) and East-West (7 frames in total) directions, respectively. In this study only one of the N-S perimeter moment-resisting frames is modeled by considering the first three bays

(Fig. 3.3). The fourth bay is omitted because it is not a part of perimeter frame. All beam-column and column-foundation connections are moment-resisting. ASTM A36 and A572Gr50 type structural steel are used for beams and columns, respectively. Typical story and roof seismic weights assigned for the frame model are 4694kN and 5101kN, respectively. For the sake of brevity, this model is referred to as 3SAC throughout the study. Frame's geometric, seismic mass and material properties, member sections, modal properties and global yield level properties are given in Tables 3.6, 3.7, 3.8 and 3.9, respectively. 3SAC frame model including lumped parameter foundation model is also presented in Fig. 3.3. At the base of the frame, rigid beams are defined connecting the end (bottom) nodes of 1st story columns, and lumped parameter model is inserted at the middle of rigid foundation beams. Rigid foundation beams are not included in Fig. 3.3 in order to emphasize the foundation model. Pushover curve of the 3SAC frame model is given in Fig. 3.4.

Table 3.6. Geometric, seismic mass and material properties of frame models.

Frame Model	Number of Stories/Bays	Story Height		Total Height (m)	Bay Width (m)	Total Width (m)
		1st Story (m)	Typical (m)			
3SAC	3/3	3.96	3.96	11.88	9.15	27.5
4KatF, 4KatR	4/3	5	4	17	8	24
5KatS2	5/3	5	4	21	8	24
8KatS2	8/3	5	4	33	8	24
12KatFS, 12KatRS	12/3	5	4	49	8	24

Frame Model	Total Plan Area (m ²)	Story Seismic Mass		Total* Mass (Tons)	Structural Steel Type	
		Typical* (Tons)	Roof* (Tons)		Beam	Columns
3SAC	36.58x54.87	478.5	520	1477	A36	A572Gr50
4KatF, 4KatR	24x24	56.2	56.2	224.8	A36	A36
5KatS2	24x24	212.26	202.86	1051.9	A36	A36
8KatS2	24x24	212.26	202.86	1688.68	A36	A36
12KatFS, 12KatRS	24x24	56.2	56.2	674.4	A36	A36

(*) Seismic mass assigned per frame

Table 3.7. Structural member sections of frame 3SAC.

3SAC			
Story	Beam Section	Int. Col. Section	Ext. Col. Section
1	W33x118	W14x311	W14x257
2	W30x116	W14x311	W14x257
3	W24x68	W14x311	W14x257

Table 3.8. Modal properties of fixed-base frame models at the fundamental mode.

Model Name	nStory	Ht (m)	Wt (kN)	Tn (sec)	α_m	Γ	He (m)	Ke (kN/m)	Me (tons)
3Sac	3	11.88	14489	1.03	0.83	1.27	9.5	41954.5	1223
4KatF	4	17	2204	1.18	0.87	1.27	12.7	5607.3	196
4KatR	4	17	2204	0.72	0.85	1.31	12.9	14548.9	190
5KatS2	5	21	10411	0.81	0.82	1.38	15.6	53120.7	872
8KatS2	8	33	16566	1.45	0.78	1.39	23.8	24870.3	1317
12KatFS	12	49	6612	2.19	0.79	1.37	34.2	4345.5	530
12KatRS	12	49	6612	1.26	0.77	1.41	34.6	12836.4	516

Table 3.9. Global yield point of bilinear representation of fixed-base frame models. Data are obtained from pushover curves (Fig. 3.4). In this table, T_n , T_e , V_y/W_t , DR_y are the fundamental period, effective fundamental period, normalized base shear with respect to seismic weight of the structure and normalized roof drift with respect to the total height of the structure at the global yield level, respectively.

Model Name	T_n (s)	T_e (s)	V_y/W_t (%)	DR_y (%)
3Sac	1.03	1.07	24	0.87
4KatF	1.18	1.21	30	0.93
4KatR	0.72	0.73	77	0.93
5KatS2	0.81	0.83	51	0.72
8KatS2	1.45	1.51	23.5	0.72
12KatFS	2.19	2.24	20	0.89
12KatRS	1.26	1.28	55	0.84

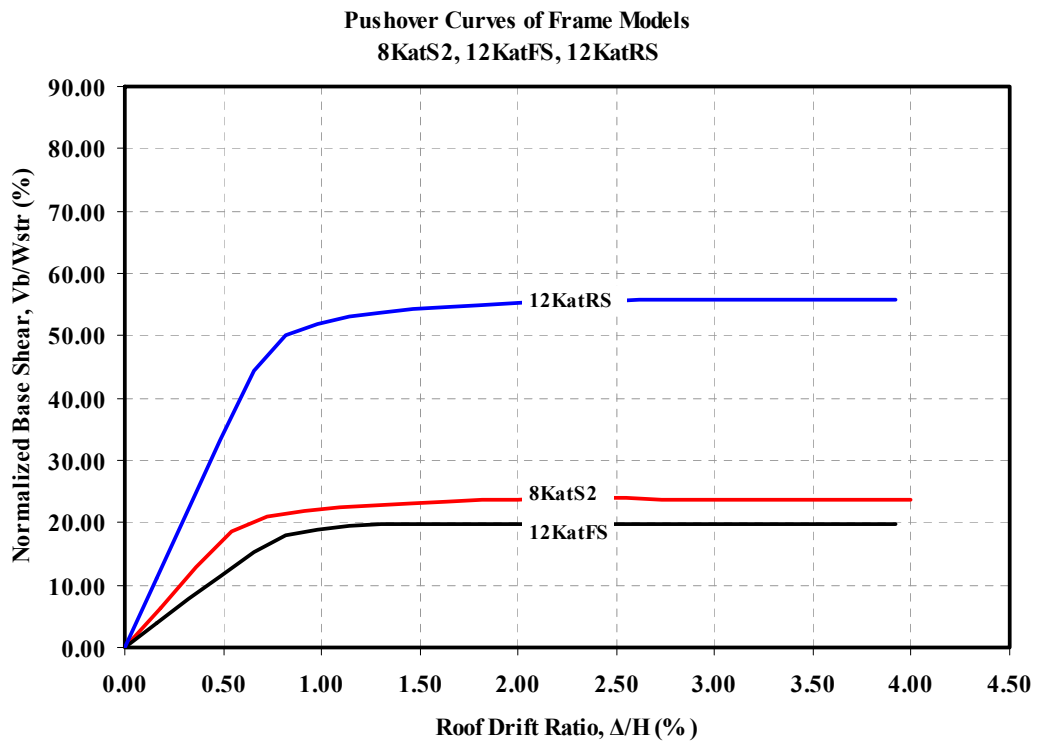
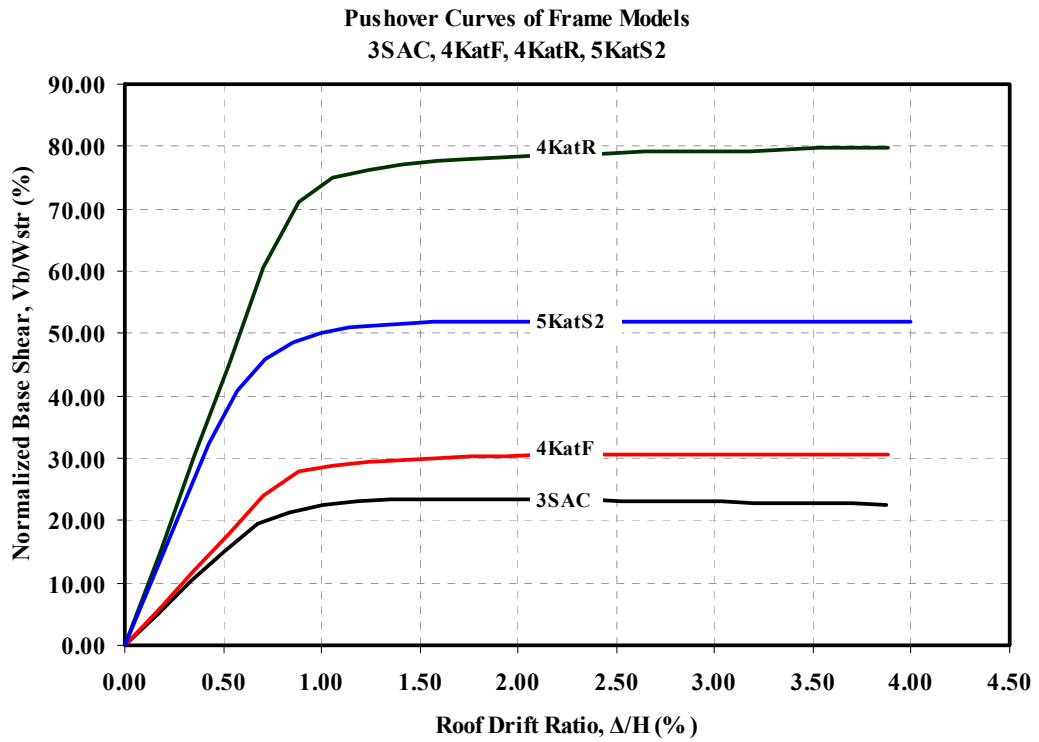


Figure 3.4. Pushover plots obtained for the frame models: 3SAC, 4KatF, 4KatR, 5KatS2, 8KatS2, 12KatFS and 12KatRS. Global yield points are given in Table 3.9.

3.4.2. Pairs of Four and Twelve Story Steel Frames

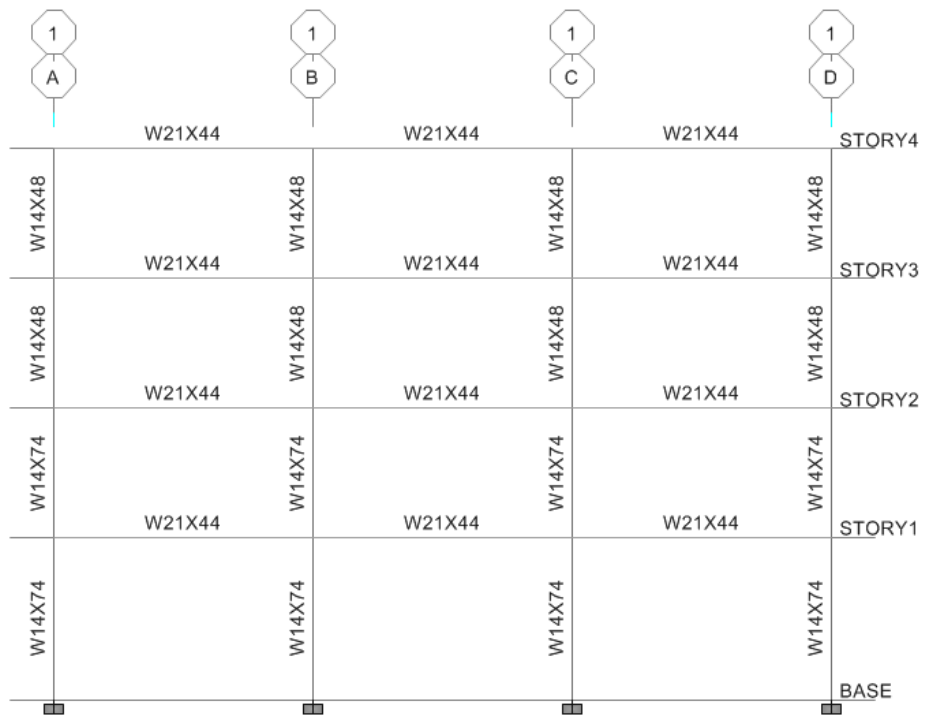
These are pairs of four and twelve story frame (Aschheim (2002)). Each frame of a pair was designed for a limiting roof drift ratio of 1.5% when subjected to specific ground motion with relatively weak or strong intensities (Aschheim (2002)). Resultant design with respect to a relatively strong or weak ground motion was labeled as Rigid or Flexible, respectively. Detailed design specifications can be found from Aschheim (2002). These models are referred to as 4KatF, 4KatR, 12KatF and 12KatR throughout the text in preference to Flexible-4, Rigid-4, Flexible-12 and Rigid-12, respectively. Four and twelve story frame models are illustrated in Figs. 3.5 and 3.6, respectively. Frames have three bays with a constant width of 8m; story heights are constant and equal to 5m and 4m for first and typical stories, respectively. Total heights of the four and twelve story frames are 17m and 49m, respectively. In this study it is assumed that frames are from one side of the perimeter frame of a building structure having a footprint area of 24m x 24m. Seismic weight of each story assigned to the frame model is constant and equal to 551 kN. Frame members comprise ASTM A36 wide flange I sections. Frames' geometric, seismic mass and material properties, modal properties, global yield level properties and member sections are given in Tables 3.6, 3.7, 3.8, 3.9 and 3.10, respectively. Pushover curves of the frame models are given in Fig. 3.4.

Table 3.10. Structural sections of frame models, 4KatF, 4KatR, 12KatFS, 12KatRS.

4KatF			4KatR		
Story	Beam Section	Column Section	Story	Beam Section	Column Section
1, 2	W21x44	W14x74	1, 2	W24x94	W14x176
3, 4	W21x44	W14x48	3, 4	W24x55	W14x99

12KatFS			12KatRS		
Story	Beam Section	Column Section	Story	Beam Section	Column Section
1, 2	W24x76	W14x193	1, 2	W27x194	W14x455
3, 4	W24x76	W14x159	3, 4	W27x161	W14x370
5, 6	W24x68	W14x145	5, 6	W27x146	W14x342
7, 8	W21x68	W14x120	7, 8	W27x129	W14x283
9, 10	W21x57	W14x99	9, 10	W24x104	W14x211
11, 12	W18x46	W14x68	11, 12	W24x68	W14x132

(a) 4KatF



(b) 4KatR

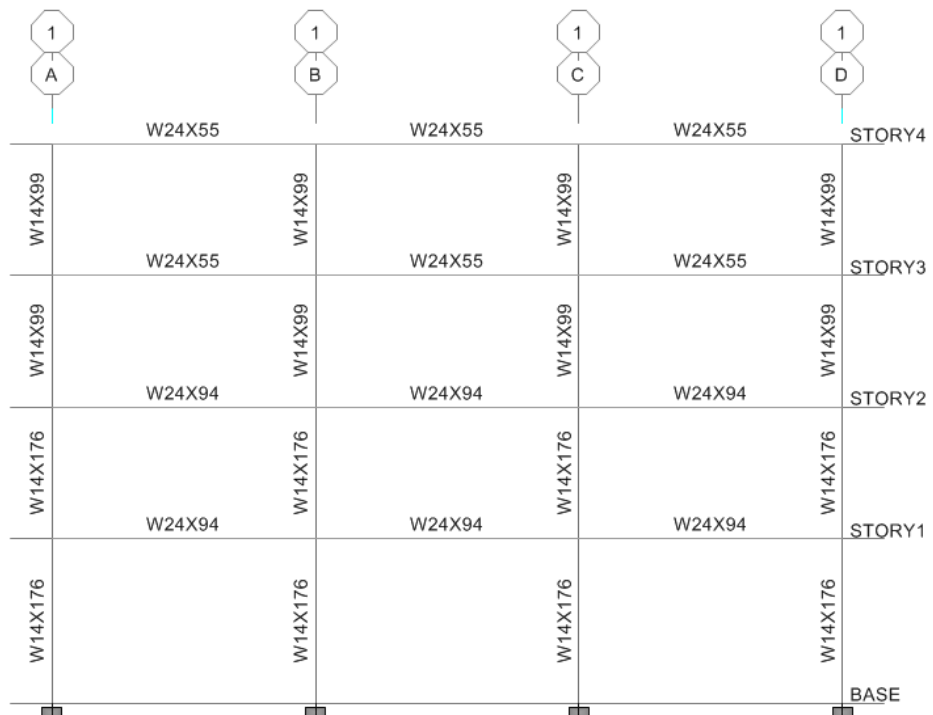


Figure 3.5. Elevation of four story frame models, 4KatF and 4KatR.

(b) 12KatRS

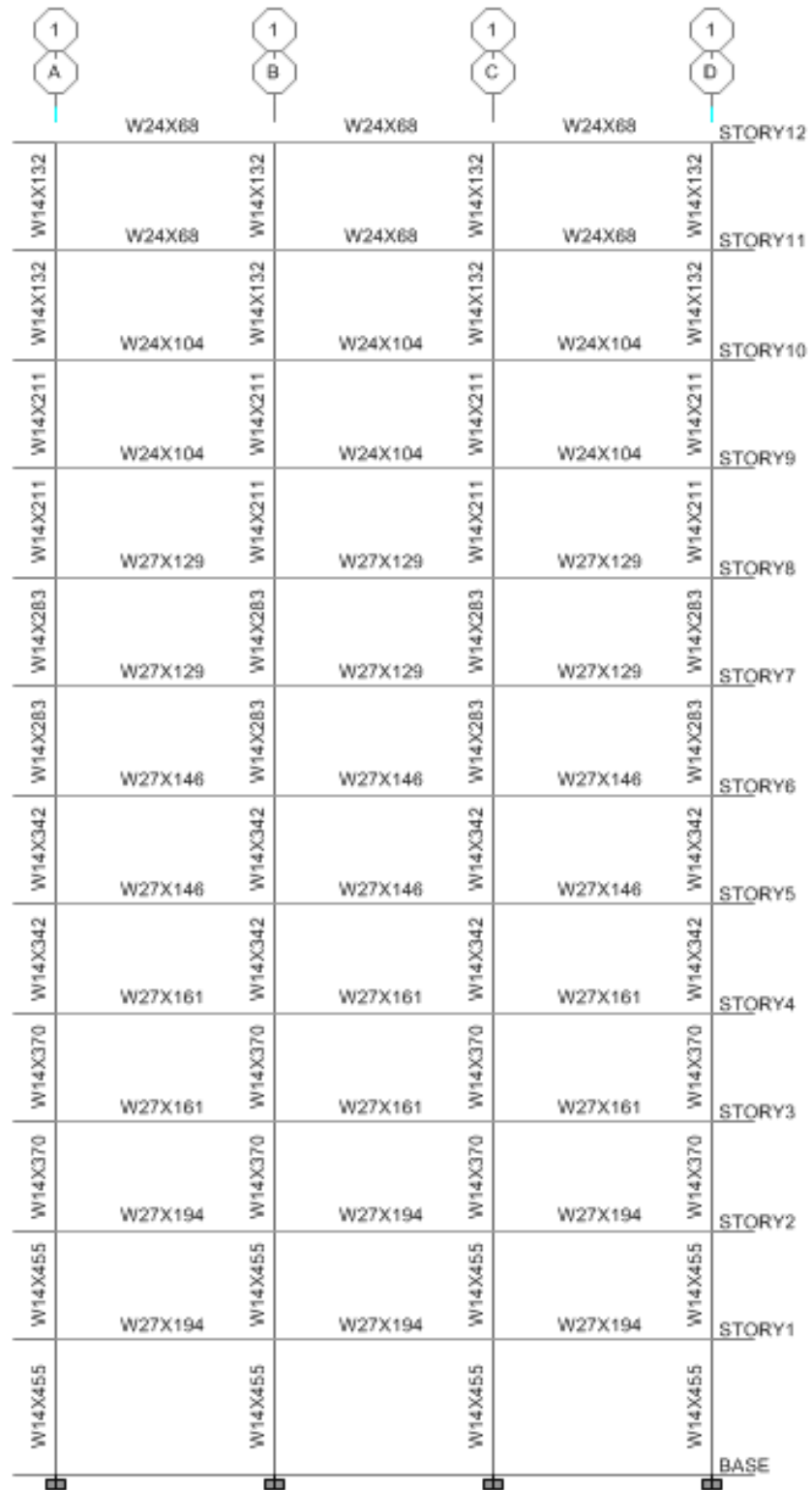


Figure 3.6. (Cont'd)

3.4.3. Five and Eight Story Steel Frames

Design of five (5KatS2) and eight story (8KatS2) steel moment frames involve four stages:

In the First Stage main geometric properties and story design loads are established. In order to create similar frame models, it is assumed that the models have three bays having a constant width of 8m. Story heights are assumed to be constant and equal to 5m and 4m for the first and typical stories, respectively. Total heights of five and eight story frames are 21m and 33m, respectively. It is assumed that building floor plans are square in shape i.e. formed by three bays of constant length at each side having a footprint area of 24m x 24m. Story design gravity loads, associated story seismic weights (typical 2082 kN; roof 1990 kN) and beam loads are given in Table 3.11. It is assumed that gravity loading of structural members is included in story loads. Frame members comprise ASTM A36 wide flange I section. Frame models are illustrated in Fig. 3.7.

Second stage involves determination of fundamental period of vibration of models. This task is accomplished by iterating on the fundamental period of frame model for a target wave parameter (Eq. 1.1):

- *1st Iteration:* Fundamental periods are calculated from a fixed wave parameter value, $\sigma = (V_{sr}T_n)/H = 9$ (Section 1.2.3, Eq. (1.1)) corresponding to four different strain-reduced shear wave velocities, V_{sr} representing mean and mean plus one standard deviation values corresponding to SETC and SETD records. This parameter is selected to observe contribution of soil structure interaction (Stewart et. al. (1999)). Effective height of frame models are based on a fixed ratio of 0.7 for the frame models having more than two stories. Details are provided in Table 3.12.
- *2nd Iteration:* Fundamental periods are calculated from the approximate period formula given by FEMA450 (2003), Equation 5.2-6: $T_a = C_r H^x$, where $C_r=0.0724$ and $x=0.8$. Details are provided in Table 3.13.

Table 3.11. Seismic mass and associated gravity loading of five and eight story steel moment-resisting frame models based on floor design loads.

FLOOR DESIGN LOADS	
Typical Story	
	Load (kN/m²)
13cm Normal Weight Concrete	= 3.12
Steel work + Metal Decking	= 0.46
Finishes	= 2.10
Mechanical Installations	= 0.50
Total Dead Load	= 6.18
Live Load	= 3.50
Additional Live Load	= 0.00
Total Live Load	= 3.50
Roof	
	Load (kN/m²)
13cm Normal Weight Concrete	= 3.12
Steel work + Metal Decking	= 0.46
Cladding + Insulation	= 1.72
Mechanical Installations	= 0.50
Snow Load (as DL)	= 0.30
Total Dead Load	= 6.10
Live Load	= 2.00
Additional Live Load (Snow Load)	= 0.70
Total Live Load	= 2.70

FRAME SEISMIC MASS AND GRAVITY LOADING					
Number of Bays		Bay Width (m)		Slab Area	Total Floor Area
X-Dir	Y-Dir	X-Dir	Y-Dir	(m ²)	(m ²)
3	3	8	8	64	576
Seismic Weight Design Load Contribution Coefficients		Unit Story Weight	Unit Story Mass	Unit Roof Weight	Unit Roof Mass
Dead Load	Live Load	(kN/m ²)	(tons/m ²)	(kN/m ²)	(tons/m ²)
1.0	0.3	7.23	0.74	6.91	0.70
Story Weight	Story Mass	Roof Weight	Roof Mass	Uniform Grider Load, Q (kN/m)	
(kN)	(tons)	(kN)	(tons)	Story	Roof
4164.5	424.5	3980.2	405.7	28.9	27.6

(a) 5KatS2



(b) 8KatS2

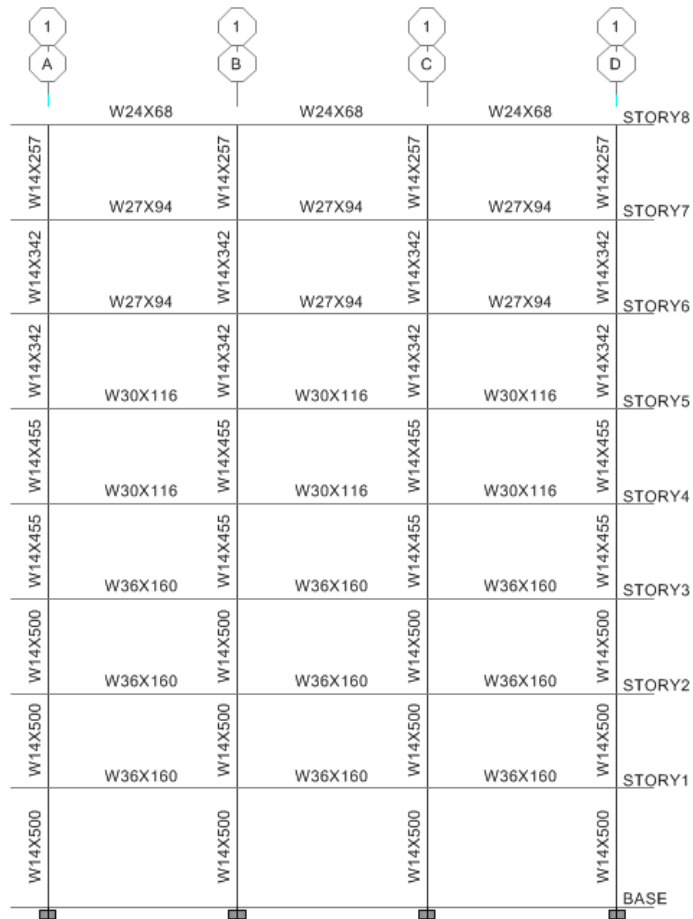


Figure 3.7. Elevation of five and eight story frame models; 5KatS2, 8KatS2.

Table 3.12. Variation of fundamental period of vibration according to a selected wave parameter value ($\sigma=9$).

Vs30 (m/s)	Vsr (m/s)	Target σ	NEHRP Site Class C (Mean)		
528	389	9			
nStory	Htot (m)	H/Htot	H (m)	Target Tn (s)	
5	21	0.7	14.7	0.34	
8	33	0.7	23.1	0.53	

Vs30 (m/s)	Vsr (m/s)	Target σ	NEHRP Site Class C (Mean)		
621	472	9			
nStory	Htot (m)	H/Htot	H (m)	Target Tn (s)	
5	21	0.7	14.7	0.28	
8	33	0.7	23.1	0.44	

Vs30 (m/s)	Vsr (m/s)	Target σ	NEHRP Site Class D (Mean)		
275	197	9			
nStory	Htot (m)	H/Htot	H (m)	Target Tn (s)	
5	21	0.7	14.7	0.67	
8	33	0.7	23.1	1.06	

Vs30 (m/s)	Vsr (m/s)	Target σ	NEHRP Site Class D (Mean)		
321	237	9			
nStory	Htot (m)	H/Htot	H (m)	Target Tn (s)	
5	21	0.7	14.7	0.56	
8	33	0.7	23.1	0.88	

Table 3.13. Variation of fundamental period of vibration calculated according to approximate period formulation and associated wave parameter, σ .

Approximate Fundamental Period Formulation, FEMA450 (Eqn 5.2-6): $T_a=Cr(H)^x$. $Cr=0.0724$, $x=0.8$					σ Corresponding to NEHRP Site Class $WP=Vsr.Ta/H$			
nStory	Htot (m)	H/Htot	H (m)	Ta (s)	Mean		Mean+StDev	
					SETC	SETD	SETC	SETD
5	21	0.7	14.7	0.83	22	11	27	13
8	33	0.7	23.1	1.19	20	10	24	12

Table 3.14. Wave parameter (σ) values obtained from fundamental periods of vibration of models.

Calculated Periods from Designed Frames					σ Corresponding to NEHRP Site Class $\sigma=Vsr.Ta/H$			
nStory	Htot (m)	H/Htot	H (m)	Tn (s)	Mean		Mean+StDev	
					SETC	SETD	SETC	SETD
5	21	0.7	14.7	0.80	21	11	26	13
8	33	0.7	23.1	1.44	24	12	29	15

Target structural periods were selected as 0.83s and 1.19s for five and eight story moment-resisting frame models, respectively. Following the design of these models, final fundamental periods are obtained as 0.81s and 1.45s, respectively. Wave parameter values associated with the designed models are illustrated in Table 3.14. These values are slightly larger than the limiting value of 10.

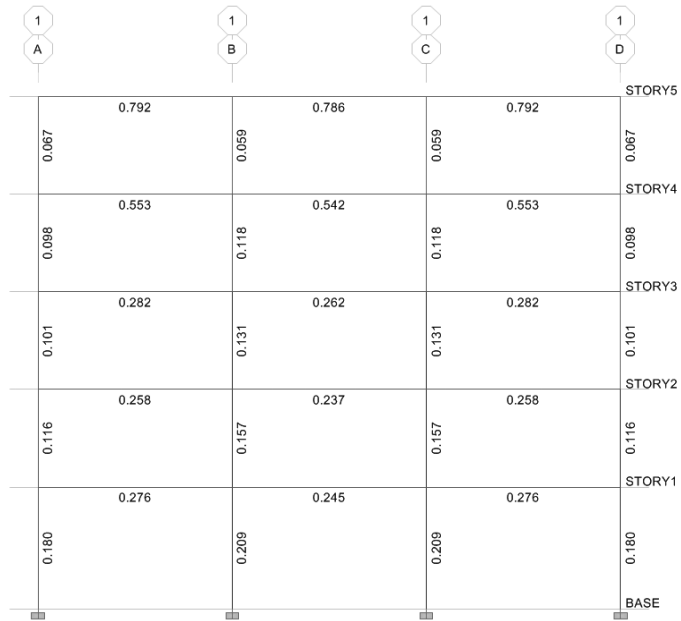
Third stage involves selection and optimization of structural members (selected from AISC wide-flange I profiles). This iterative task is done in such a way that the frame would display progressive yielding by developing plastic hinges at both ends of beams and at ground level ends of columns at the roof drift ratio of 4% from the pushover analysis.

Fourth and final stage is the control of frame models based on design procedure of AISC ASD (2001) and FEMA450 (2003) by assuming the following: Seismic Use Group 2, Design Group E, special steel moment-resisting frame; $R=8$, $\Omega_0=3$, $C_d=5.5$ (Table 3.3-1: FEMA450 (2003)). Designed frames are controlled by response spectrum analysis, where design spectrum is selected as mean plus one standard deviation of SETC and SETD ground motion records. Calculated capacity ratios are illustrated in Fig. 3.8. Frames' geometric, seismic mass and material properties, modal properties, global yield level properties and member sections are given in Tables 3.6, 3.7, 3.8, 3.9 and 3.15, respectively. Pushover curves of the frame models are given in Fig. 3.4.

Table 3.15. Structural member sections of frame models, 5KatS2, 8KatS2.

5KatS2			8KatS2		
Story	Beam Section	Column Section	Story	Beam Section	Column Section
1	W40x183	W14x500	1, 2, 3	W36x160	W14x500
2	W40x183	W14x500	4, 5	W30x116	W14x455
3	W36x160	W14x500	6, 7	W27x94	W14x342
4	W27x94	W14x455	8	W24x68	W14x257
5	W24x68	W14x455			

(a) 5KatS2



(b) 8KatS2

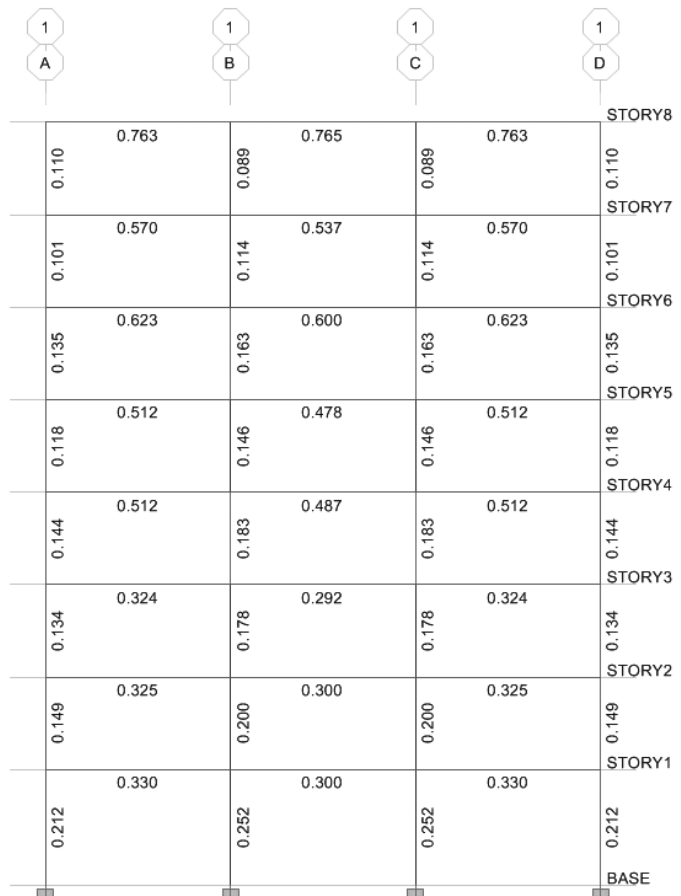


Figure 3.8. Capacity ratios obtained for the frame models: 5KatS2, 8KatS2.

CHAPTER 4

ANALYSIS FRAMEWORK AND RESULTS

4.1 Introduction

The analysis framework is established on a parametric study where the global and the local deformation responses of the steel moment-resisting frame models (Section 3.4) are monitored for variance with respect to inertial soil-structure interaction effects. Main analysis parameters are selected as the wave parameter (Section 1.2.3, Eq. 1.1) and the aspect ratio (Section 1.2.3, Eq. 1.2) of the frame model. Both the wave parameter and the aspect ratio can be calculated easily from local site class properties (shear wave velocity, density and Poisson's ratio of soil) and basic dynamic (modal) properties of the frame structure.

The core analysis is carried out for a single earthquake acceleration record in two steps: Nonlinear time-history analysis of fixed-base frame model and flexible-base (Section 3.3) frame model. In the scope of the framework, the variation in both global and local deformation responses is collected from three analysis groups, which are based on ground motion scaling schemes (Section 2.4). Ultimately, statistical assessment (multiple linear regression procedure) is performed in order to generalize the response trends attributed to inertial soil-structure interaction.

In the following section of this chapter the main components of the analysis framework are given in detail. Next, post-process phase is explained. Finally, analysis results are summarized. In the interest of keeping the text to a minimum

many of its associated figures and tables have been relegated to Appendices C, D, E and F, which contain tables and 2D scatter plots related to statistical analysis of the results, combined plots pushover curves and roof drift demands obtained from nonlinear time-history analyses and peak interstory drift demands, respectively.

4.2 Analysis Framework

Analytical models of the frames and nonlinear static and nonlinear dynamic analyses are programmed in OpenSees. Main modules of the program are listed in the following order:

- *Program parameters*: This section is the user interface of the program at which the header parameters for the requested type of analysis are defined: Modal analysis; nonlinear static analysis, NST; nonlinear dynamic analysis, NTH; solver and postprocessor settings; foundation parameters.
- *Structural model*: This section assembles the analytical model of the frame structure (fixed-base or flexible-base) and the gravity loading. Subsections are: Definition of the geometry, nodes and the constraints; member materials; member sections via fiber models; connectivity of members (including P- Δ) and gravity loading associated with the seismic weight.
- *Recorders*: This section assembles recorders for monitoring required structural response (total deformation) at both global and local levels:
 - Roof drift ratio (roof drift normalized with respect to total height of the frame) vs. normalized base shear (base shear normalized with respect to the seismic weight of the structure).
 - Interstory drift ratio (story drift normalized with respect to story height of the frame) vs. normalized story shear (story shear normalized with respect to the seismic weight of the structure).
 - Maximum column end rotations (foundation end) and maximum beam end rotations at the first story.
- *Analysis module*: First, nonlinear static analysis for the gravity loading is performed. Next, nonlinear time-history analysis, NTH, which is based on the

- *Post-process module*: This is the final section which provides a filtering and assembling process on the raw response data in order to produce statistical analyses and tabular form of tables and figures. Detailed information is given in the following text.

4.3 The Post-Process

Once the nonlinear dynamic analysis is completed the following steps are executed in the following order:

1. Nodal response histories are corrected for rigid-body translation and rotation as a result of elastic base compliance. The correction at each time step is as follows:
 - a) Get the total horizontal translation and the elevation of i^{th} structural node, $U_i(t)$ and h_i , respectively.
 - b) Get the horizontal translation and the rotation of the foundation node, $U_f(t)$ and $R_f(t)$, respectively.
 - c) Calculate the correction for the rigid body translation:

$$U_o(t) = U_f(t) - h_i R_f(t) \quad (4.1)$$
 - d) Correct the total horizontal translation of the i^{th} structural node as:

$$U_i^c(t) = U_i(t) - U_o(t) \quad (4.2)$$
2. Corrected response data are combined in series in order to construct force-deformation tables. In this process response-histories from NTH are scanned for the absolute maximum deformations (and concurrent force).
3. Tabular force-deformation data is transferred to series of predesigned Excel and Matlab workbooks.
4. Through an automation over response data corresponding to each earthquake record:
 - a) Global and member level responses, obtained from both fixed-base and flexible-base (corrected) NTH solution, are extracted and transferred to

- b) Ratio, SSI.TH / FB.TH is calculated for each response variable in order to evaluate the variation in demand due to inertial soil-structure interaction effects. In this context these ratios are referred to as response ratios.
- c) Soil-structure interaction parameters are calculated for the target earthquake record; wave parameter (σ) and aspect ratio (H/R).
- d) Statistical analysis of response ratio (SSI.TH / FB. TH) is the final step of the post-process stage. Multiple linear regression procedure is performed in order to correlate the predictor variables; σ and H/R, to the observed response variable; (SSI.TH / FB. TH).

4.4 Organization of the Results

Results of the dissertation are organized in two sections:

Regression statistics: Statistical assessment is performed by collecting the response ratio values from the pairs of time-history analysis results of SET-C1, C2, D1 and D2 records corresponding to three analysis groups; Group I (NS), Group II (SC) and Group III (SCR2). The regression equation is expressed as:

$$\sigma = c_1 + c_2\sigma + c_3(H/R) \quad (4.3)$$

Where,

σ and (H/R) are the independent predictor variables, wave parameter and aspect ratio, respectively; c_i are the coefficient estimates for the multilinear regression of the response ratio values in y .

The mean absolute error (MAE) and the standard error (RMSE) for the regression equations are given in Tables 4.1 – 4.4, in addition to the regression coefficients c_i .

Table 4.1. Coefficients of the linear regression equations obtained for the roof drift ratio and the first story drift ratio. Equation coefficients are listed for three analysis groups; NS, SC, SCR2, and for four earthquake ground motion sets; SET-C1, C2, D1 and D2. In this table ϵ is the mean absolute error and s is the standard error.

Coefficients of Linear Regression Equation: $y=c1+c2x1+c3x2$: $x1=\sigma$, $x2=H/R$ (SSL.TH / FB.TH)													
Roof Drift Ratio						First Story Drift Ratio							
Set	c1	c2	c3	ϵ	s	Set	c1	c2	c3	ϵ	s		
NS	C1	0.9956	0.0001	-0.0002	0.0069	0.0116	NS	C1	0.9919	0.0002	0.0004	0.0065	0.0096
	C2	0.9840	0.0003	0.0013	0.0065	0.0101		C2	0.9809	0.0004	0.0022	0.0068	0.0105
	D1	0.9390	0.0025	0.0062	0.0248	0.0392		D1	0.9266	0.0031	0.0068	0.0257	0.0407
	D2	0.9234	0.0029	0.0067	0.0235	0.0360		D2	0.9298	0.0026	0.0065	0.0215	0.0330
SC	C1	0.9972	0.0001	-0.0002	0.0063	0.0100	SC	C1	0.9950	0.0001	-0.0001	0.0055	0.0085
	C2	0.9855	0.0003	0.0009	0.0061	0.0097		C2	0.9834	0.0003	0.0017	0.0063	0.0098
	D1	0.9423	0.0027	0.0060	0.0234	0.0370		D1	0.9467	0.0026	0.0038	0.0230	0.0359
	D2	0.9475	0.0023	0.0019	0.0220	0.0347		D2	0.9571	0.0019	0.0011	0.0203	0.0323
SCR2	C1	1.0023	0.0000	-0.0003	0.0039	0.0071	SCR2	C1	0.9975	0.0000	0.0002	0.0056	0.0104
	C2	0.9937	0.0001	0.0028	0.0061	0.0319		C2	0.9946	0.0000	0.0032	0.0095	0.0456
	D1	1.0040	-0.0002	-0.0010	0.0143	0.0309		D1	0.9983	0.0003	-0.0032	0.0197	0.0376
	D2	0.9864	0.0005	0.0019	0.0085	0.0154		D2	0.9815	0.0007	0.0006	0.0122	0.0198

Table 4.2. Coefficients of the linear regression equations obtained for the peak member end rotations at the first story beams and columns. Equation coefficients are listed for Analysis Group I; NS for four earthquake ground motion sets; SET-C1, C2, D1 and D2. In this table ϵ is the mean absolute error and s is the standard error.

Analysis Group I, NS: (SSL.TH / FB.TH) Coefficients of Linear Regression Equation: $y=c1+c2x1+c3x2$: $x1=\sigma$, $x2=H/R$ Peak Member End Rotations at the First Story													
Set	c1	c2	c3	ϵ	s	Set	c1	c2	c3	ϵ	s		
C1	Col.1	0.9919	0.0002	0.0002	0.0072	0.0114	D1	Col.1	0.9263	0.0030	0.0078	0.0259	0.0398
	Col.2	0.9923	0.0002	0.0003	0.0072	0.0114		Col.2	0.9172	0.0034	0.0088	0.0280	0.0424
	Col.3	0.9922	0.0002	0.0003	0.0073	0.0114		Col.3	0.9175	0.0034	0.0088	0.0280	0.0423
	Col.4	0.9931	0.0001	0.0002	0.0073	0.0117		Col.4	0.9293	0.0030	0.0062	0.0265	0.0415
	Bm.1	0.9911	0.0002	0.0003	0.0070	0.0104		Bm.1	0.9034	0.0042	0.0119	0.0304	0.0476
	Bm.2	0.9917	0.0002	0.0002	0.0070	0.0104		Bm.2	0.9209	0.0034	0.0078	0.0276	0.0435
	Bm.3	0.9918	0.0002	0.0001	0.0072	0.0106		Bm.3	0.9075	0.0040	0.0108	0.0301	0.0465
	Bm.4	0.9918	0.0002	0.0001	0.0072	0.0106		Bm.4	0.9075	0.0040	0.0108	0.0301	0.0465
C2	Col.1	0.9801	0.0004	0.0024	0.0072	0.0110	D2	Col.1	0.9258	0.0027	0.0071	0.0213	0.0330
	Col.2	0.9808	0.0004	0.0022	0.0070	0.0107		Col.2	0.9255	0.0026	0.0075	0.0223	0.0359
	Col.3	0.9803	0.0004	0.0023	0.0071	0.0107		Col.3	0.9244	0.0027	0.0078	0.0224	0.0360
	Col.4	0.9815	0.0003	0.0021	0.0068	0.0103		Col.4	0.9307	0.0025	0.0063	0.0212	0.0331
	Bm.1	0.9825	0.0003	0.0012	0.0067	0.0105		Bm.1	0.9455	0.0017	-0.0017	0.0223	0.0352
	Bm.2	0.9835	0.0003	0.0007	0.0067	0.0106		Bm.2	0.9444	0.0016	-0.0014	0.0224	0.0355
	Bm.3	0.9820	0.0004	0.0012	0.0068	0.0108		Bm.3	0.9462	0.0017	-0.0021	0.0220	0.0346
	Bm.4	0.9820	0.0004	0.0012	0.0068	0.0108		Bm.4	0.9462	0.0017	-0.0021	0.0220	0.0346

Table 4.3. Coefficients of the linear regression equations obtained for the peak member end rotations at the first story beams and columns. Equation coefficients are listed for Analysis Group II; SC for four earthquake ground motion sets; SET-C1, C2, D1 and D2. In this table ϵ is the mean absolute error and s is the standard error.

Analysis Group II, SC: (SSI.TH / FB.TH)													
Coefficients of Linear Regression Equation: $y=c1+c2x1+c3x2$: $x1=\sigma$, $x2=H/R$													
Peak Member End Rotations at the First Story													
Set		c1	c2	c3	ϵ	s	Set		c1	c2	c3	ϵ	s
C1	Col.1	0.9943	0.0001	0.0001	0.0071	0.0118	D1	Col.1	0.9545	0.0021	0.0035	0.0249	0.0387
	Col.2	0.9919	0.0002	0.0004	0.0084	0.0158		Col.2	0.9401	0.0026	0.0059	0.0294	0.0468
	Col.3	0.9925	0.0001	0.0003	0.0083	0.0157		Col.3	0.9411	0.0026	0.0057	0.0293	0.0468
	Col.4	0.9927	0.0001	0.0004	0.0069	0.0108		Col.4	0.9535	0.0020	0.0034	0.0268	0.0422
	Bm.1	0.9904	0.0002	0.0012	0.0071	0.0114		Bm.1	0.9291	0.0033	0.0054	0.0312	0.0491
	Bm.2	0.9936	0.0002	0.0005	0.0059	0.0091		Bm.2	0.9491	0.0024	0.0014	0.0261	0.0410
	Bm.4	0.9906	0.0002	0.0012	0.0070	0.0112		Bm.4	0.9281	0.0034	0.0059	0.0303	0.0467
C2	Col.1	0.9812	0.0004	0.0022	0.0068	0.0112	D2	Col.1	0.9496	0.0019	0.0030	0.0228	0.0345
	Col.2	0.9796	0.0004	0.0026	0.0073	0.0116		Col.2	0.9431	0.0021	0.0044	0.0241	0.0363
	Col.3	0.9798	0.0004	0.0026	0.0072	0.0116		Col.3	0.9431	0.0021	0.0044	0.0241	0.0362
	Col.4	0.9804	0.0004	0.0025	0.0069	0.0113		Col.4	0.9464	0.0020	0.0039	0.0232	0.0349
	Bm.1	0.9847	0.0003	0.0005	0.0066	0.0102		Bm.1	0.9689	0.0010	-0.0082	0.0229	0.0381
	Bm.2	0.9859	0.0003	0.0003	0.0064	0.0097		Bm.2	0.9699	0.0010	-0.0086	0.0212	0.0338
	Bm.4	0.9839	0.0003	0.0007	0.0066	0.0102		Bm.4	0.9677	0.0011	-0.0076	0.0226	0.0374

Table 4.4. Coefficients of the linear regression equations obtained for the peak member end rotations at the first story beams and columns. Equation coefficients are listed for Analysis Group III; SCR2 for four earthquake ground motion sets; SET-C1, C2, D1 and D2. In this table ϵ is the mean absolute error and s is the standard error.

Analysis Group III, SCR2: (SSI.TH / FB.TH)													
Coefficients of Linear Regression Equation: $y=c1+c2x1+c3x2$: $x1=\sigma$, $x2=H/R$													
Peak Member End Rotations at the First Story													
Set		c1	c2	c3	ϵ	s	Set		c1	c2	c3	ϵ	s
C1	Col.1	0.9919	0.0001	0.0008	0.0110	0.0196	D1	Col.1	0.9841	0.0010	-0.0041	0.0376	0.0681
	Col.2	0.9929	0.0002	0.0002	0.0104	0.0189		Col.2	0.9953	0.0007	-0.0073	0.0357	0.0689
	Col.3	0.9867	0.0003	0.0013	0.0115	0.0239		Col.3	0.9933	0.0007	-0.0069	0.0357	0.0659
	Col.4	0.9928	0.0001	0.0006	0.0115	0.0211		Col.4	0.9871	0.0010	-0.0054	0.0390	0.0744
	Bm.1	0.9972	0.0001	-0.0009	0.0060	0.0115		Bm.1	1.0052	-0.0001	-0.0066	0.0222	0.0441
	Bm.2	0.9977	0.0001	-0.0012	0.0072	0.0146		Bm.2	1.0110	-0.0004	-0.0086	0.0260	0.0514
	Bm.4	0.9970	0.0001	-0.0008	0.0060	0.0116		Bm.4	1.0067	-0.0003	-0.0072	0.0220	0.0438
C2	Col.1	0.9889	0.0000	0.0066	0.0189	0.0859	D2	Col.1	0.9658	0.0012	0.0016	0.0269	0.0474
	Col.2	0.9884	0.0000	0.0062	0.0172	0.0758		Col.2	0.9723	0.0011	0.0001	0.0245	0.0430
	Col.3	0.9916	0.0000	0.0054	0.0168	0.0761		Col.3	0.9731	0.0010	-0.0001	0.0246	0.0430
	Col.4	0.9874	0.0000	0.0071	0.0204	0.0925		Col.4	0.9690	0.0011	0.0007	0.0270	0.0487
	Bm.1	0.9891	0.0003	0.0066	0.0090	0.0441		Bm.1	0.9860	0.0004	-0.0026	0.0124	0.0208
	Bm.2	0.9842	0.0003	0.0086	0.0107	0.0491		Bm.2	0.9830	0.0006	-0.0021	0.0141	0.0235
	Bm.4	0.9872	0.0003	0.0075	0.0089	0.0432		Bm.4	0.9866	0.0004	-0.0029	0.0126	0.0213

The variation in the demands is examined by utilizing the regression lines which are defined between the minimum and maximum values of the wave parameter associated with the ground motion sets (9.5 – 65 for SETC and 4.5 – 33 for SETD) and at the respective aspect ratio of the frame models. The limiting value of the response ratio is assumed to be 1.0 in which the structural deformation obtained from the flexible-base frame model approaches to that obtained from fixed-base model. Hence, the response ratio values, which are presented in the related tables, are expressed as percentages in reference to base 1.0, i.e. a value of -4.4% means 0.956. Complete set of the results are given in Appendix C; Tables C.1 – C.9, for the roof and the first story drift ratios and peak end rotations of columns and beams at the first story, which are obtained from each frame model, respectively.

In order to visualize the data distribution, which are obtained from both the global and the local deformation response ratios, and the associated linear regression lines, series of 2D scatter plots are prepared. In these plots, x axis corresponds to the predictor variable, σ and y axis corresponds to the observed response variable; the response ratio (SSI.TH / FB.TH). Each plot contains scatter plots of 7 data series associated with the aspect ratio (H/R) of frame models. Complete set of plots obtained from the three analysis groups are given in Appendix D and Figs. D.1 – D.12.

Pushover curves and peak interstory drift demands: Pushover curves are plotted for the roof drift ratio vs. normalized base shear for the fixed-base frame models. These plots are given in Chapter 3; Fig. 3.4. Combined plots of the pushover curves with the peak roof drift demands obtained from nonlinear analyses of both fixed-base and flexible-base frame models are given in Appendix E; Figs. E.1 – E.21. Peak interstory drift demands, which are obtained from the responses of both fixed-base and flexible-base models, are given in Appendix F; Figs. F.1 – F.21, These plots are provided for each of the analysis group; NS, SC and SCR2; and the ground motion set; SET-C1, C2, D1 and D2. In these figures, comparison is illustrated in terms of individual demand traces in addition to the mean of the set.

4.5 Results

The statistical assessment of the results is established on three parameters of interest: Deformation state of the frame models, the wave parameter and the aspect ratio.

4.5.1 Deformation State of the Frame Models

Global deformation state provides information regarding the contribution of inertial soil-structure interaction effects in the response of the flexible-base (interacting) frames deforming in the nonlinear range (Section 1.3). For this purpose, the pushover curve of each frame model is combined with the peak roof drift demands obtained from the nonlinear time-history analyses of each earthquake ground motion set corresponding to each analysis group (Appendix E, Figs. E.1 – E.21). These plots are summarized in Tables 4.5 – 4.7. In these tables the roof drift ductility demands are sorted with respect to ductility ranges. From these tables following trends are observed for each analysis group:

Analysis Group I (NS): Table 4.5 illustrates that responses obtained from 87.9%, 82.9%, 97.4% and 94.5% of the events corresponding to SET-NS-C1, D1, C2 and D2 remain in the elastic range ($\mu=1$). In this analysis group, only 4KatR and 12KatRS remain essentially in the elastic range (minimum 95%). Rest of the frame models are observed in the inelastic range $\mu < 2$. Among the frames, only 3SAC frame model is deformed further in the range of $\mu=2.0 - 4.0$ (7.5% of SET-C1). It is also observed that the responses obtained from SET-C1 and D1 (records including pulse effects) are deformed significantly more in the inelastic range than in SET-C2 and D2 (14.1% and 4%, respectively).

Analysis Group II (SC): Table 4.6 illustrates that most of the events still remain in the elastic range, however, more frames deform in the nonlinear range. 61.8%, 50%, 95.5% and 84.8% of the events corresponding to SET-NS-C1, D1, C2 and D2 remain in the elastic range ($\mu=1$).

Table 4.5. Number of events among the roof drift ductility demand ranges, which are obtained from nonlinear time-history analyses of flexible-base (interacting) frame models: $\mu=1$, 1-2, 2-4 and >4 . The results are given for analysis group NS.

Analysis Group I: NS										
Frame Model	Eq. Set	Number of Events Among the Roof Drift Ductility Demand Ranges								
		$\mu=1$		$\mu=(1 - 2)$		$\mu=(2 - 4)$		$\mu>4$		Total
3SAC	C1	27	67.5%	10	25%	3	7.5%	0	0%	40
	C2	54	90%	6	10%	0	0%	0	0%	60
	D1	17	42.5%	23	57.5%	0	0%	0	0%	40
	D2	50	83.3%	10	16.7%	0	0%	0	0%	60
4KatF	C1	33	82.5%	7	17.5%	0	0%	0	0%	40
	C2	56	93.3%	4	6.7%	0	0%	0	0%	60
	D1	31	77.5%	9	22.5%	0	0%	0	0%	40
	D2	55	91.7%	5	8.3%	0	0%	0	0%	60
4KatR	C1	38	95%	2	5%	0	0%	0	0%	40
	C2	60	100%	0	0%	0	0%	0	0%	60
	D1	38	95%	2	5%	0	0%	0	0%	40
	D2	60	100%	0	0%	0	0%	0	0%	60
5KatS2	C1	35	87.5%	5	12.5%	0	0%	0	0%	40
	C2	60	100%	0	0%	0	0%	0	0%	60
	D1	40	100%	0	0%	0	0%	0	0%	40
	D2	56	93.3%	4	6.7%	0	0%	0	0%	60
8KatS2	C1	36	90%	4	10%	0	0%	0	0%	40
	C2	59	98.3%	1	1.7%	0	0%	0	0%	60
	D1	32	80%	8	20%	0	0%	0	0%	40
	D2	56	93.3%	4	6.7%	0	0%	0	0%	60
12KatFS	C1	38	95%	2	5%	0	0%	0	0%	40
	C2	60	100%	0	0%	0	0%	0	0%	60
	D1	34	85%	6	15%	0	0%	0	0%	40
	D2	60	100%	0	0%	0	0%	0	0%	60
12KatRS	C1	39	97.5%	1	2.5%	0	0%	0	0%	40
	C2	60	100%	0	0%	0	0%	0	0%	60
	D1	40	100%	0	0%	0	0%	0	0%	40
	D2	60	100%	0	0%	0	0%	0	0%	60
TOTAL	C1	246	87.9%	31	11.1%	3	1.1%	0	0%	280
	D1	232	82.9%	48	17.1%	0	0%	0	0%	280
	SUM	478	85.4%	79	14.1%	3	0.5%	0	0%	560
	C2	409	97.4%	11	2.6%	0	0%	0	0%	420
	D2	397	94.5%	23	5.5%	0	0%	0	0%	420
	SUM	806	96%	34	4%	0	0%	0	0%	840

Table 4.6. Number of events among the roof drift ductility demand ranges, which are obtained from nonlinear time-history analyses of flexible-base (interacting) frame models: $\mu=1$, 1-2, 2-4 and >4 . The results are given for analysis group SC.

Analysis Group II: SC										
Frame Model	Eq. Set	Number of Events Among the Roof Drift Ductility Demand Ranges								
		$\mu=1$		$\mu=(1 - 2)$		$\mu=(2 - 4)$		$\mu>4$		Total
3SAC	C1	0	0%	30	75%	9	22.5%	1	2.5%	40
	C2	41	68.3%	19	31.7%	0	0%	0	0%	60
	D1	0	0%	37	92.5%	3	7.5%	0	0%	40
	D2	1	1.7%	58	96.7%	1	1.7%	0	0%	60
4KatF	C1	2	5%	38	95%	0	0%	0	0%	40
	C2	60	100%	0	0%	0	0%	0	0%	60
	D1	3	7.5%	37	92.5%	0	0%	0	0%	40
	D2	56	93.3%	4	6.7%	0	0%	0	0%	60
4KatR	C1	40	100%	0	0%	0	0%	0	0%	40
	C2	60	100%	0	0%	0	0%	0	0%	60
	D1	40	100%	0	0%	0	0%	0	0%	40
	D2	60	100%	0	0%	0	0%	0	0%	60
5KatS2	C1	37	92.5%	3	7.5%	0	0%	0	0%	40
	C2	60	100%	0	0%	0	0%	0	0%	60
	D1	39	97.5%	1	2.5%	0	0%	0	0%	40
	D2	60	100%	0	0%	0	0%	0	0%	60
8KatS2	C1	14	35%	26	65%	0	0%	0	0%	40
	C2	60	100%	0	0%	0	0%	0	0%	60
	D1	7	17.5%	33	82.5%	0	0%	0	0%	40
	D2	59	98.3%	1	1.7%	0	0%	0	0%	60
12KatFS	C1	40	100%	0	0%	0	0%	0	0%	40
	C2	60	100%	0	0%	0	0%	0	0%	60
	D1	11	27.5%	29	72.5%	0	0%	0	0%	40
	D2	60	100%	0	0%	0	0%	0	0%	60
12KatRS	C1	40	100%	0	0%	0	0%	0	0%	40
	C2	60	100%	0	0%	0	0%	0	0%	60
	D1	40	100%	0	0%	0	0%	0	0%	40
	D2	60	100%	0	0%	0	0%	0	0%	60
TOTAL	C1	173	61.8%	97	34.6%	9	3.2%	1	0.4%	280
	D1	140	50%	137	48.9%	3	1.1%	0	0%	280
	SUM	313	55.9%	234	41.8%	12	2.1%	1	0.2%	560
	C2	401	95.5%	19	4.5%	0	0%	0	0%	420
	D2	356	84.8%	63	15%	1	0.2%	0	0%	420
	SUM	757	90.1%	82	9.8%	1	0.1%	0	0%	840

Table 4.7. Number of events among the roof drift ductility demand ranges, which are obtained from nonlinear time-history analyses of flexible-base (interacting) frame models: $\mu=1$, 1-2, 2-4 and >4 . The results are given for analysis group SCR2.

Analysis Group III: SCR2										
Frame Model	Eq. Set	Number of Events Among the Roof Drift Ductility Demand Ranges								
		$\mu=1$		$\mu=(1 - 2)$		$\mu=(2 - 4)$		$\mu>4$		Total
3SAC	C1	0	0%	17	42.5%	23	57.5%	0	0%	40
	C2	0	0%	40	66.7%	18	30%	2	3.3%	60
	D1	0	0%	17	42.5%	23	57.5%	0	0%	40
	D2	0	0%	41	68.3%	19	31.7%	0	0%	60
4KatF	C1	0	0%	27	67.5%	10	25%	3	7.5%	40
	C2	0	0%	49	81.7%	10	16.7%	1	1.7%	60
	D1	0	0%	28	70%	11	27.5%	1	2.5%	40
	D2	0	0%	49	81.7%	11	18.3%	0	0%	60
4KatR	C1	0	0%	19	47.5%	19	47.5%	2	5%	40
	C2	0	0%	42	70%	18	30%	0	0%	60
	D1	0	0%	25	62.5%	13	32.5%	2	5%	40
	D2	0	0%	45	75%	15	25%	0	0%	60
5KatS2	C1	0	0%	26	65%	13	32.5%	1	2.5%	40
	C2	0	0%	42	70%	18	30%	0	0%	60
	D1	0	0%	22	55%	16	40%	2	5%	40
	D2	1	1.7%	46	76.7%	13	21.7%	0	0%	60
8KatS2	C1	0	0%	26	65%	13	32.5%	1	2.5%	40
	C2	0	0%	50	83.3%	10	16.7%	0	0%	60
	D1	0	0%	32	80%	8	20%	0	0%	40
	D2	0	0%	48	80%	12	20%	0	0%	60
12KatFS	C1	0	0%	32	80%	7	17.5%	1	2.5%	40
	C2	0	0%	50	83.3%	10	16.7%	0	0%	60
	D1	0	0%	35	87.5%	5	12.5%	0	0%	40
	D2	0	0%	56	93.3%	4	6.7%	0	0%	60
12KatRS	C1	0	0%	24	60%	14	35%	2	5%	40
	C2	0	0%	50	83.3%	9	15%	1	1.7%	60
	D1	0	0%	30	75%	9	22.5%	1	2.5%	40
	D2	0	0%	46	76.7%	14	23.3%	0	0%	60
TOTAL	C1	0	0%	171	61.1%	99	35.4%	10	3.6%	280
	D1	0	0%	189	67.5%	85	30.4%	6	2.1%	280
	SUM	0	0%	360	64.3%	184	32.9%	16	2.9%	560
	C2	0	0%	323	76.9%	93	22.1%	4	1%	420
	D2	1	0.2%	331	78.8%	88	21%	0	0%	420
	SUM	1	0.1%	654	77.9%	181	21.5%	4	0.5%	840

In analysis group II, 4katR and 12KatRS frame models' responses are observed to be completely in the elastic range. Conversely, 3SAC frame model is observed to be deforming in the inelastic range ($\mu > 1$) with the highest event participation percentages among the other frames. Similar to the results obtained from analysis group I, it is observed that the responses obtained from SET-C1 and D1 (records including pulse effects) are deformed significantly more in the inelastic range than in SET-C2 and D2 (41.8% and 9.8%, respectively).

Analysis Group III (SCR2): Table 4.7 illustrates that all of the events (except 1 event at $\mu=1$; 5KatS2) result in the responses varying in the nonlinear range, with a greater percentage of the events concentrated in the $\mu=1.0 - 2.0$ range. These are 61.1%, 67.5%, 76.9% and 78.8% for SET-NS-C1, D1, C2 and D2, respectively. Among the frame models 3SAC frame model is observed to be deformed relatively more in the inelastic range, $\mu=2.0 - 4.0$.

As a summary, it is observed that, most of the events corresponding to analysis groups NS and SC are within the elastic range, while SC events produce relatively increased deformation demands. However, in SCR2 all of the events are observed in the nonlinear range.

4.5.2 Variation of the Response Ratio (SSI.TH / FB.TH) in both Global and Local Response Levels

In the following text the results are summarized with respect to roof drift demands, first story drift demands and peak member end rotation demands at the first story of each frame model. In this context, for the sake of brevity, the response ratio values are referred to as RR.

Roof drift ratio: RR values for the roof drift ratio are illustrated at Appendix C and Table C.1. Comparison of the associated regression lines are given in Figs. 4.1 – 4.3, for the analysis groups NS, SC and SCR2, respectively. As a summary:

- RR is observed to be directly proportional to σ . The opposite trend is only observed at SET-SCR2-C1 and SET-SCR2-D1 (Fig. 4.3).
- RR is observed to be directly proportional to H/R, except SET-C1 (Table C.1). However, the difference varies in 1%, which is significantly small.
- The maximum reduction in the RR is attained in NS at the bottom limit of σ and is equal to -1.22% and -6% for SETC and SETD, respectively.
- The reductions are observed to be in a decreasing trend among the analysis groups, in the order of NS, SC, and SCR2. The difference between NS and SC varies between 0.01–0.15% and 0.3–1.9% and the difference between NS and SCR2 varies between 0.5–1.3% and 3–5% for SETC and SETD, respectively.
- Reduction in RR is relatively more in SET-C2 and SET-D2 with respect to SET-C1 and SET-D1 (ground motion sets which contain records without and with pulse effects, respectively). However, the difference is generally less than 1%.
- Slopes of the fit lines associated with SETD records are observed to be higher than the ones observed from SETC records (Figs 4.1 – 4.3).

First story drift ratio: RR values for the first story drift ratio are illustrated at Appendix C and Table C.2. Comparison of the associated regression lines are given in Figs. 4.4 – 4.6, for the analysis groups NS, SC and SCR2, respectively. As a summary:

- RR is observed to be directly proportional to σ .
- RR is observed to be directly proportional to H/R, except SET-SC-C1 and SET-SCR2-D1. However, the differences are small (0.02% and 0.99%, respectively).
- The maximum reduction in the RR is attained in NS at the bottom limit of σ and is equal to -1.45% and -5.53%, respectively (Fig. 4.4).
- The reductions are observed to be in a decreasing trend among the analysis groups, in the order of NS, SC, and SCR2. The difference between NS and SC varies between 0.04–0.21% and 0.5–2.15% and the difference between NS and SCR2 varies between 0.3–1.4% and 2.2–4.4% for SETC and SETD, respectively.
- Slopes of the fit lines associated with SETD records are observed to be higher than the ones observed from SETC records (Figs 4.4 – 4.6).

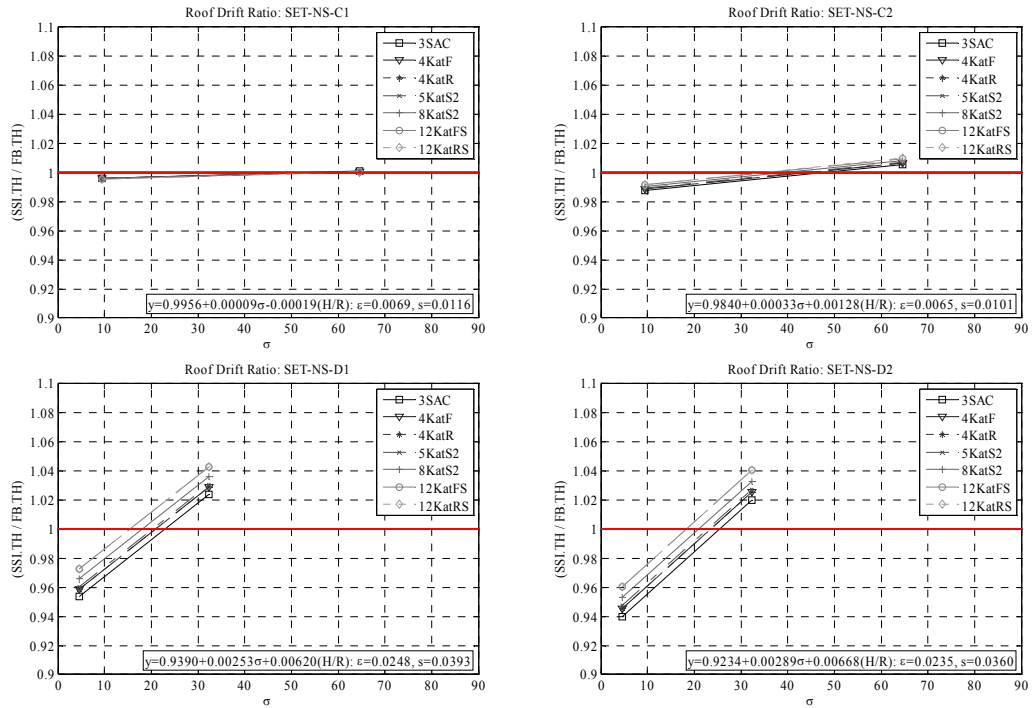


Figure 4.1. Comparison of regression lines calculated for the response ratio values associated with the roof drift ratio: SET-NS.

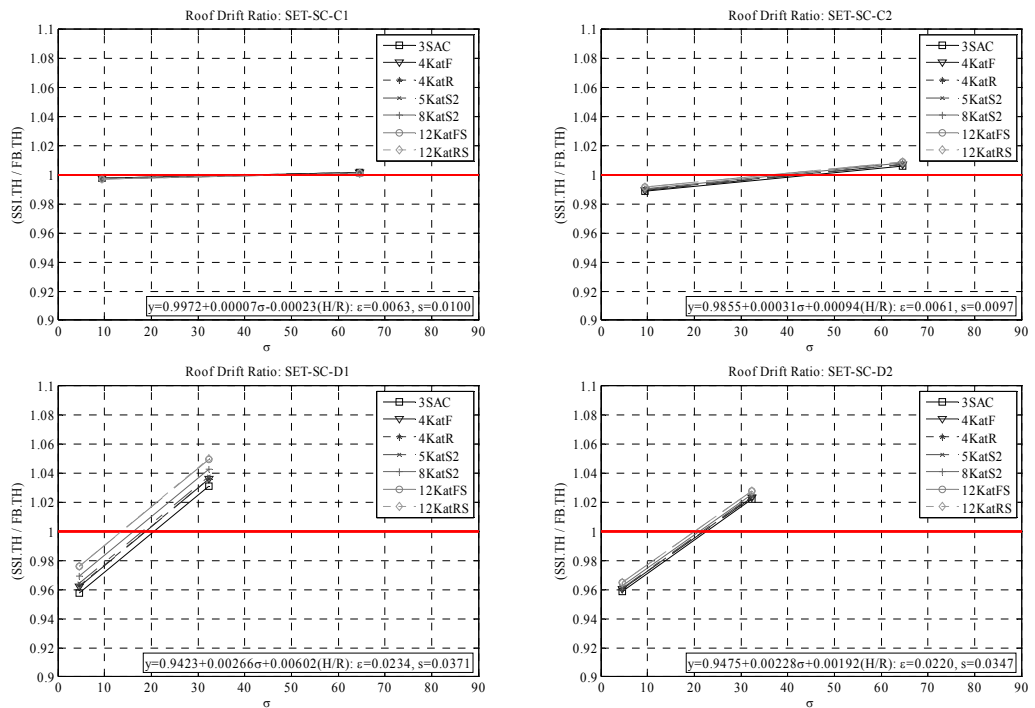


Figure 4.2. Comparison of regression lines calculated for the response ratio values associated with the roof drift ratio: SET-SC.

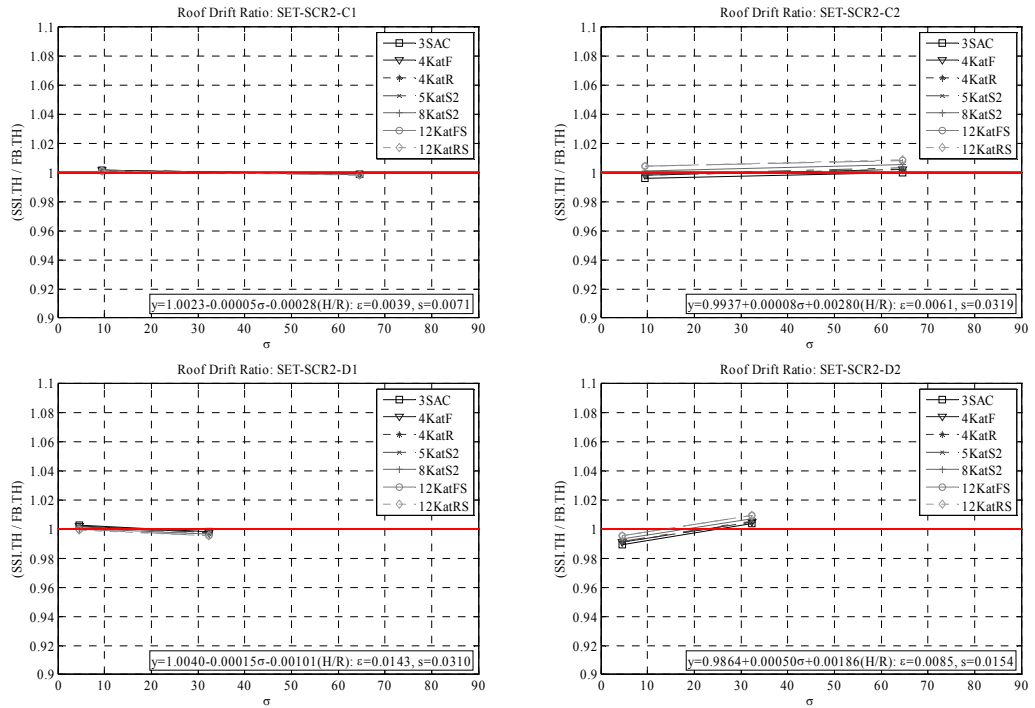


Figure 4.3. Comparison of regression lines calculated for the response ratio values associated with the roof drift ratio: SET-SCR2.

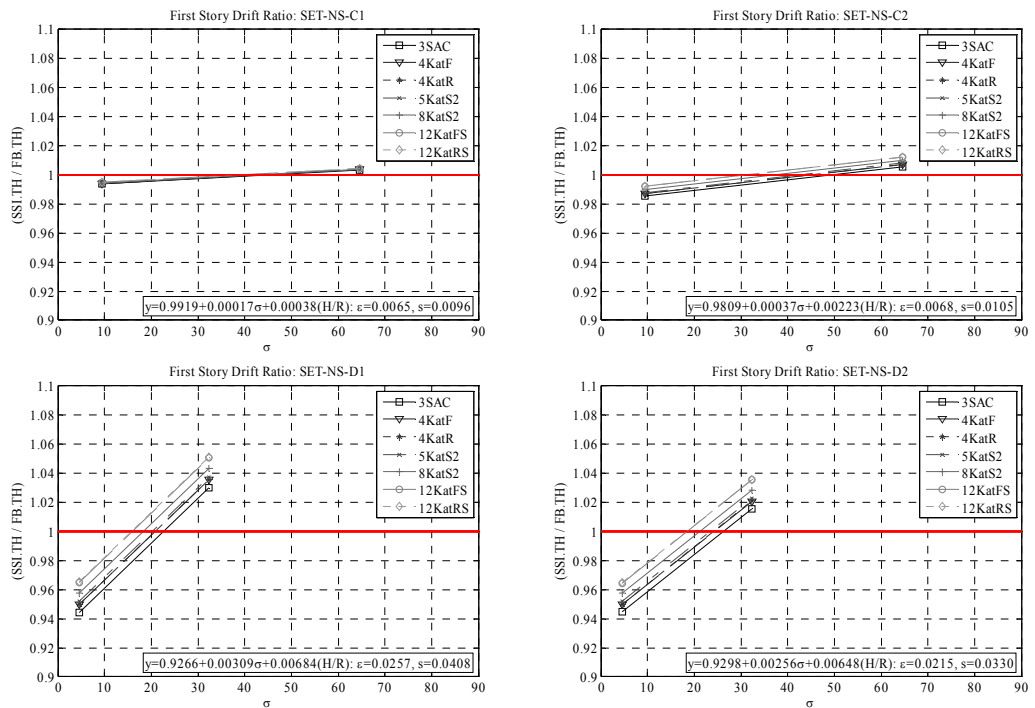


Figure 4.4. Comparison of regression lines calculated for the response ratio values associated with the first story drift ratio: SET-NS.

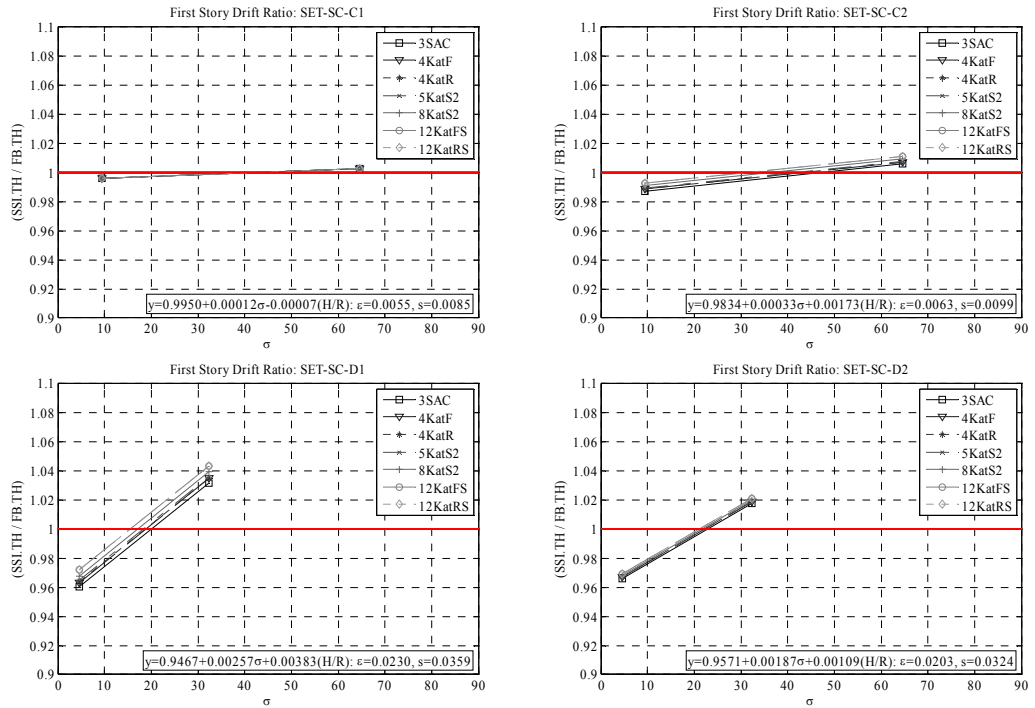


Figure 4.5. Comparison of regression lines calculated for the response ratio values associated with the first story drift ratio: SET-SC.

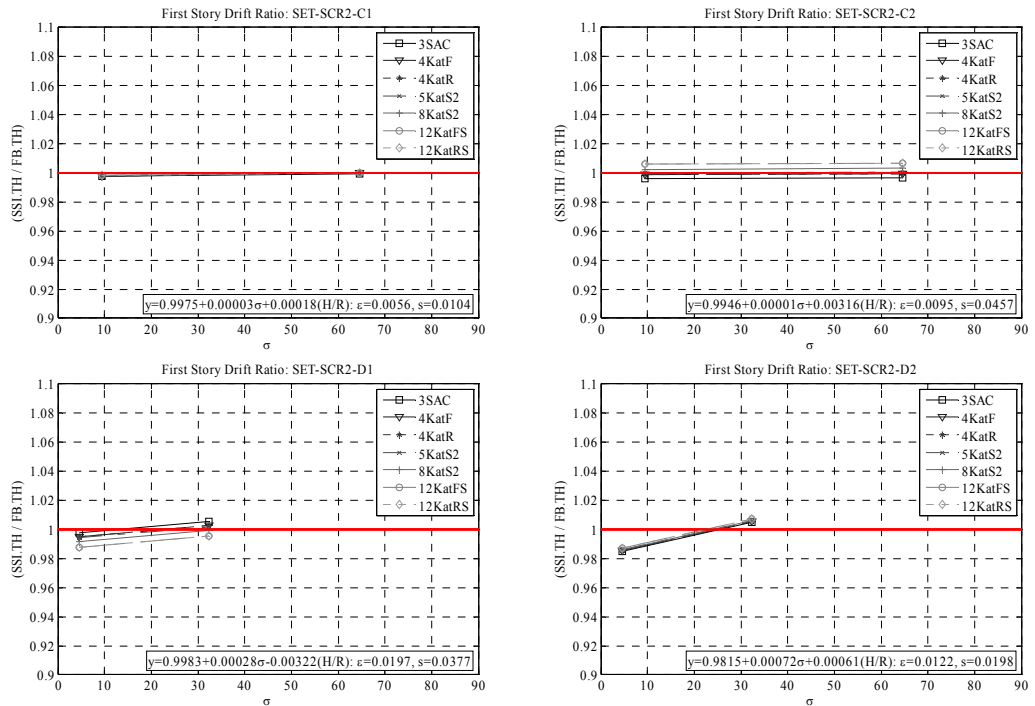


Figure 4.6. Comparison of regression lines calculated for the response ratio values associated with the first story drift ratio: SET-SCR2.

Peak member end rotations at the first story: RR values for the peak column and beam end rotations at the first story are illustrated at Appendix C and Tables C.3 – C.9. Comparison of the associated regression lines for Column1 and Beam1 (elements located at the farthest left of the frame) are given in Figs. 4.7 – 4.8, Figs. 4.9 – 4.10 and Figs. 4.11 – 4.12 for analysis groups NS, SC and SCR2, respectively. As a summary:

- RR is observed to be directly proportional to σ , except SET-SCR2-C2.
- RR is observed to be directly proportional to H/R.
- The reductions are observed to be in a decreasing trend among the analysis groups, in the order of NS, SC, and SCR2.
- Maximum reductions in RR which are observed in the elements at the bottom limit of σ are summarized as ranges between the maximum H/R (12KatRS)=3.62 and the minimum H/R(3SAC)=0.53:
 - NS: -0.78% – -1.52% and -3.64% – -6.3%, for the columns in SETC and SETD, respectively. -1.09% – -1.41% and -5.33% – -7.13%, for the beams in SETC and SETD, respectively.
 - SC: -0.75% – -1.55% and -3.17% – -4.5%, for the columns at SETC and SETD, respectively. -1.06% – -1.22% and -5.73% – -5.31%, for the beams at SETC and SETD, respectively.
 - SCR2: -0.61% – -1% and -2.83% – -2.8%, for the columns at SETC and SETD, respectively. -0.57% – -0.88% and -2.21% – -1.54%, for the beams at SETC and SETD, respectively.

From the observations it has been found that the variation in response, in terms of a beneficial effect of inertial soil-structure interaction, is more pronounced SETD and for the records without pulse effects. However, the difference in RR is 6-7% in the most extreme cases. The upper limits of the wave parameter (σ) representing the beneficial reduction in the response due to inertial interaction effects are illustrated in Figs.4.13 – 4.14 and Tables 4.8 – 4.9. These plots are prepared for both the roof and the first story drift ratios and the peak member (elements located at the farthest left: Column1 and Beam1) end rotations obtained from analysis group I, NS, respectively.

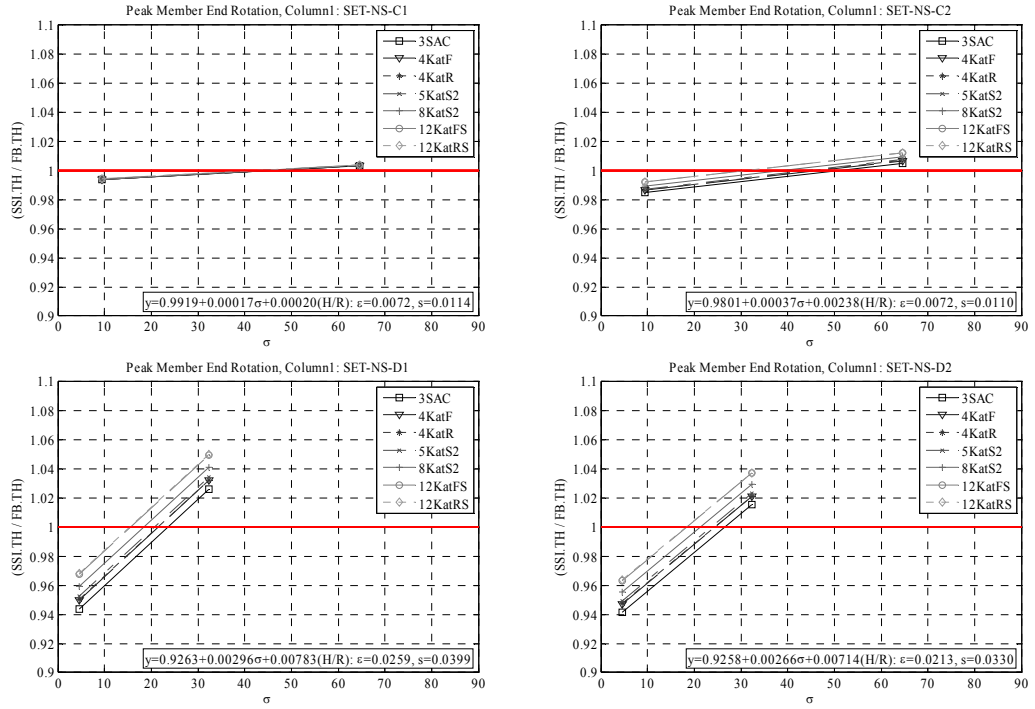


Figure 4.7. Comparison of regression lines calculated for the response ratio values associated with the peak column (No.1) end rotation at the first story: SET-NS.

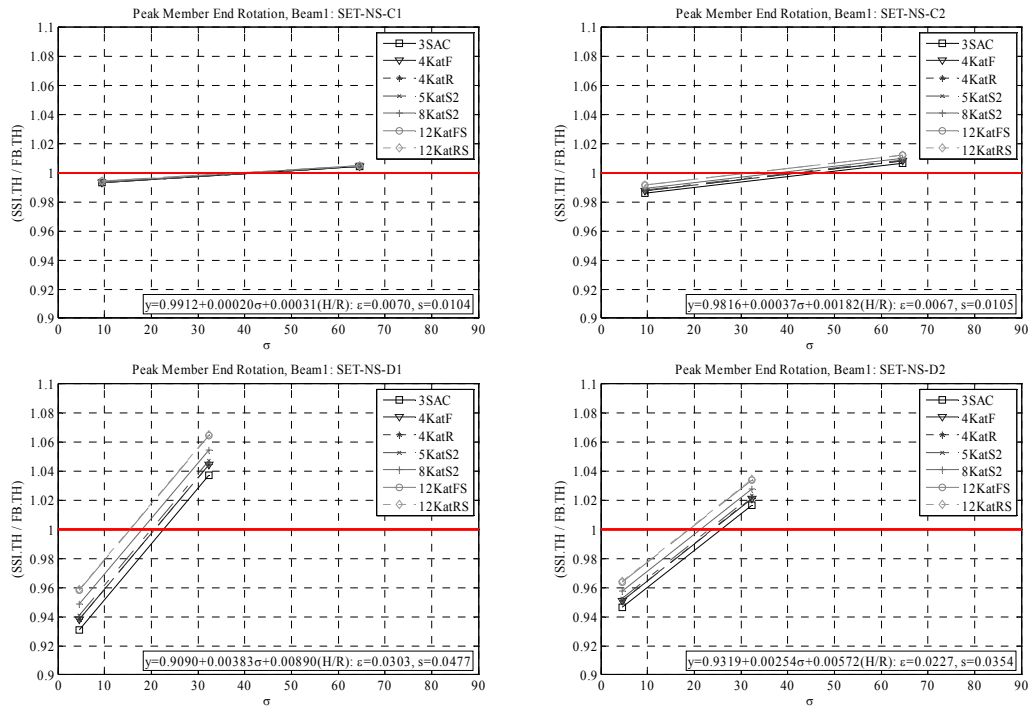


Figure 4.8. Comparison of regression lines calculated for the response ratio values associated with the peak beam (No.1) end rotation at the first story: SET-NS.

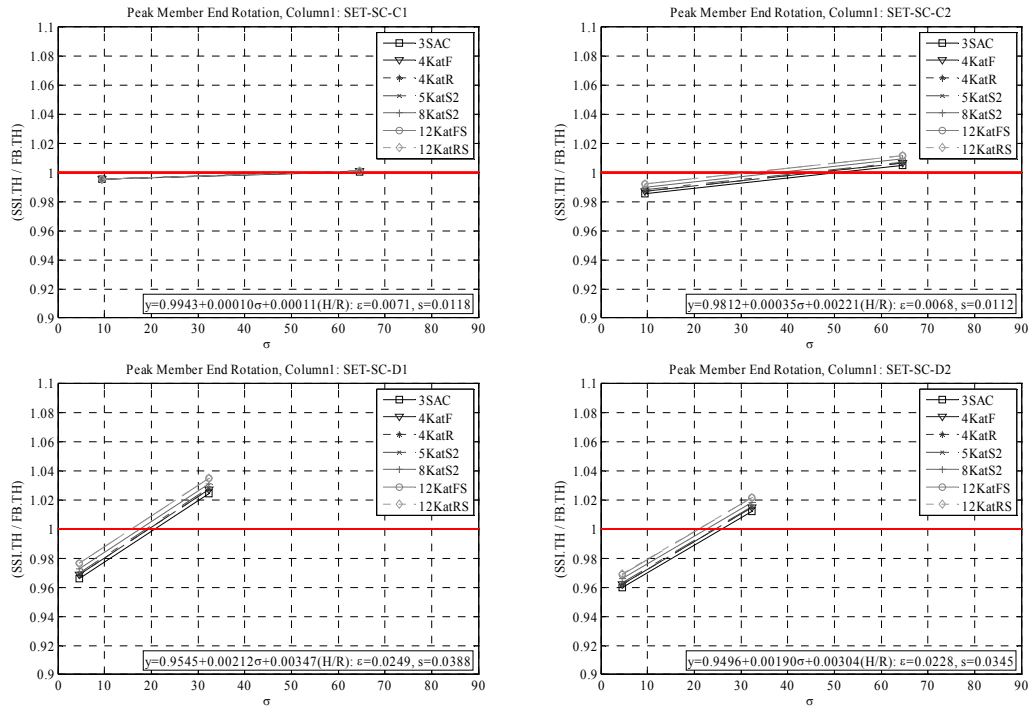


Figure 4.9. Comparison of regression lines calculated for the response ratio values associated with the peak column (No.1) end rotation at the first story: SET-SC.

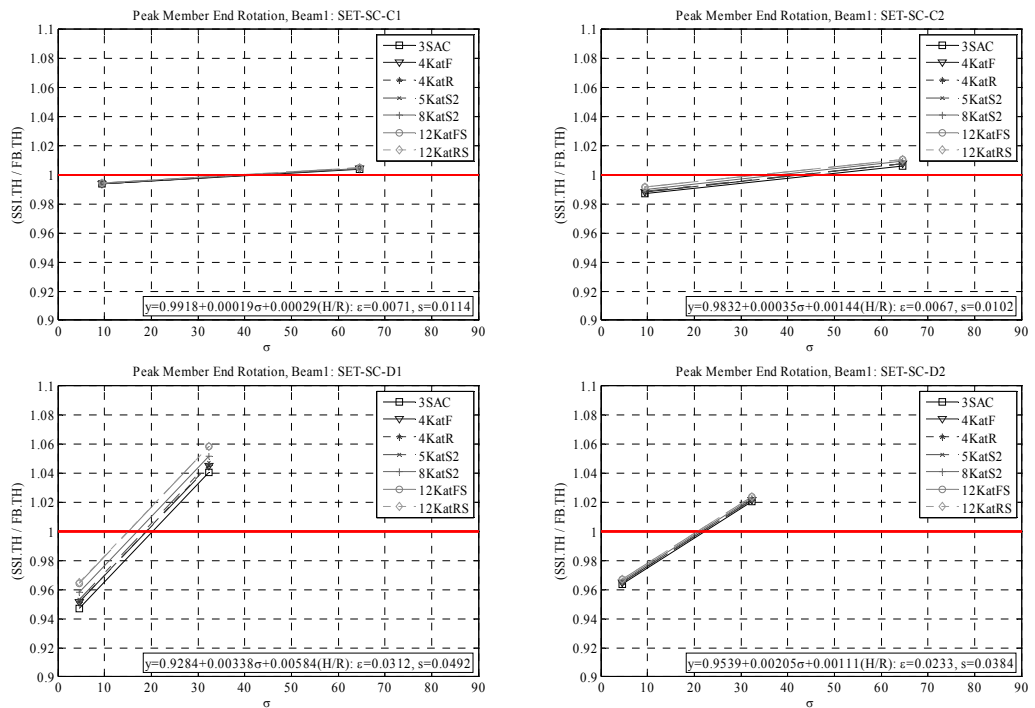


Figure 4.10. Comparison of regression lines calculated for the response ratio values associated with the peak beam (No.1) end rotation at the first story: SET-SC.

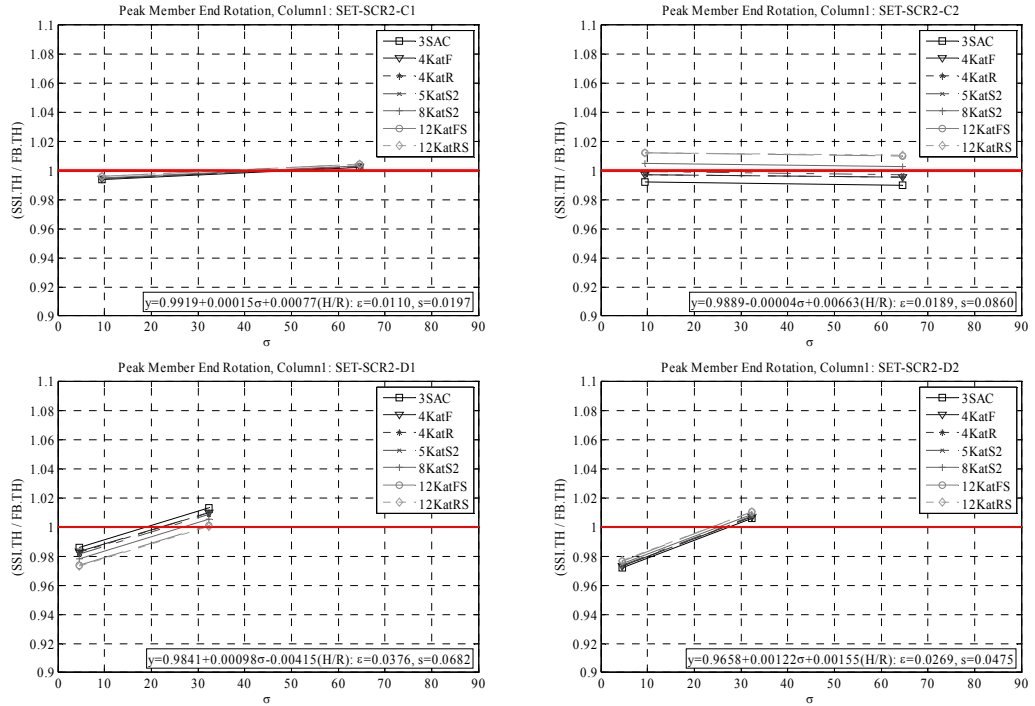


Figure 4.11. Comparison of regression lines calculated for the response ratio values associated with the peak column (No.1) end rotation at the first story: SET-SCR2.

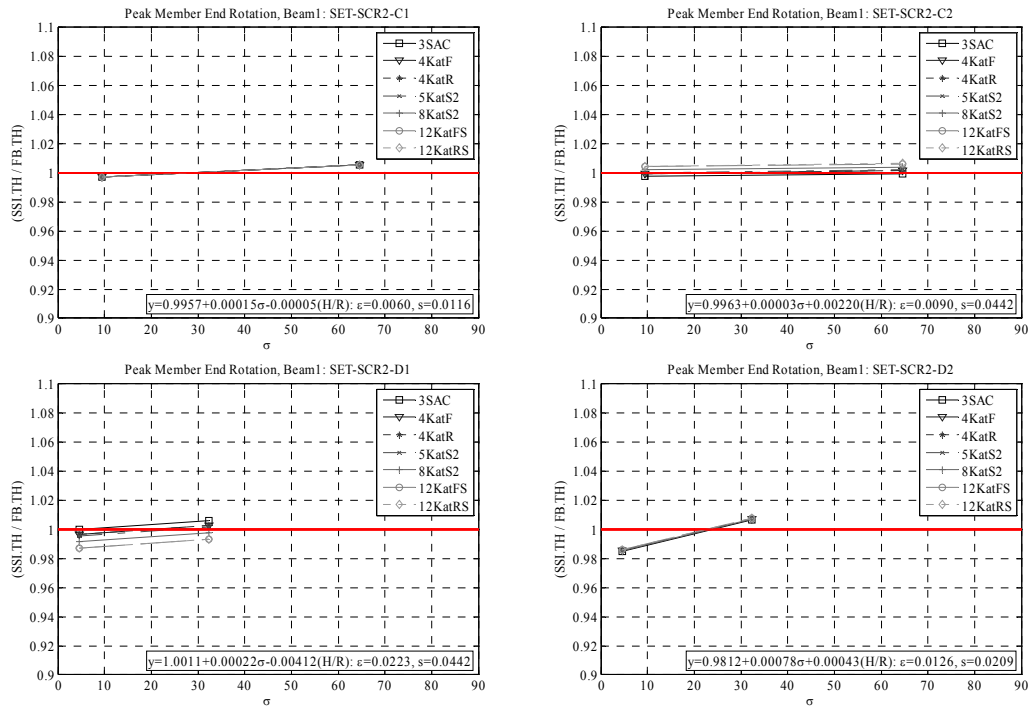


Figure 4.12. Comparison of regression lines calculated for the response ratio values associated with the peak beam (No.1) end rotation at the first story: SET-SCR2.

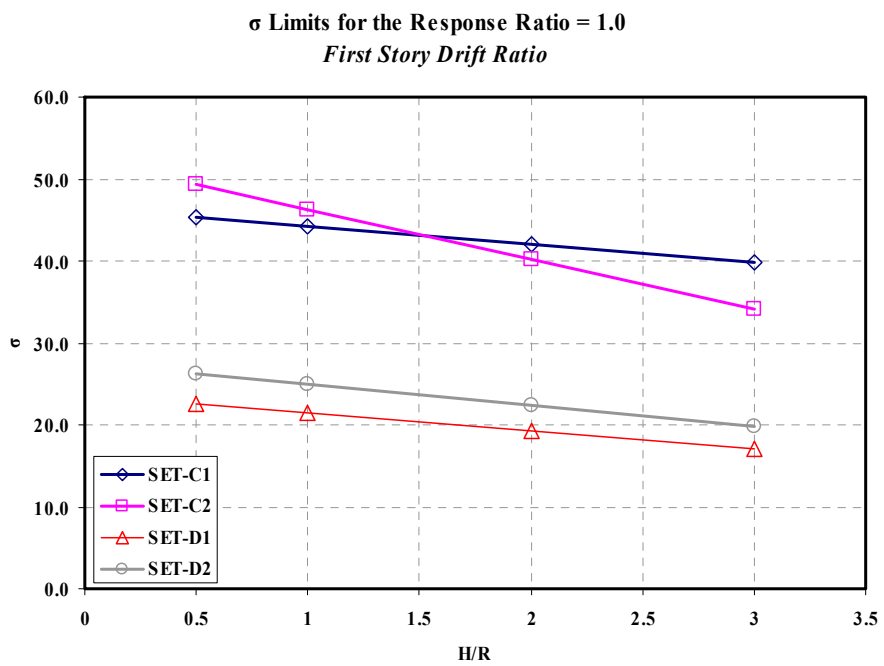
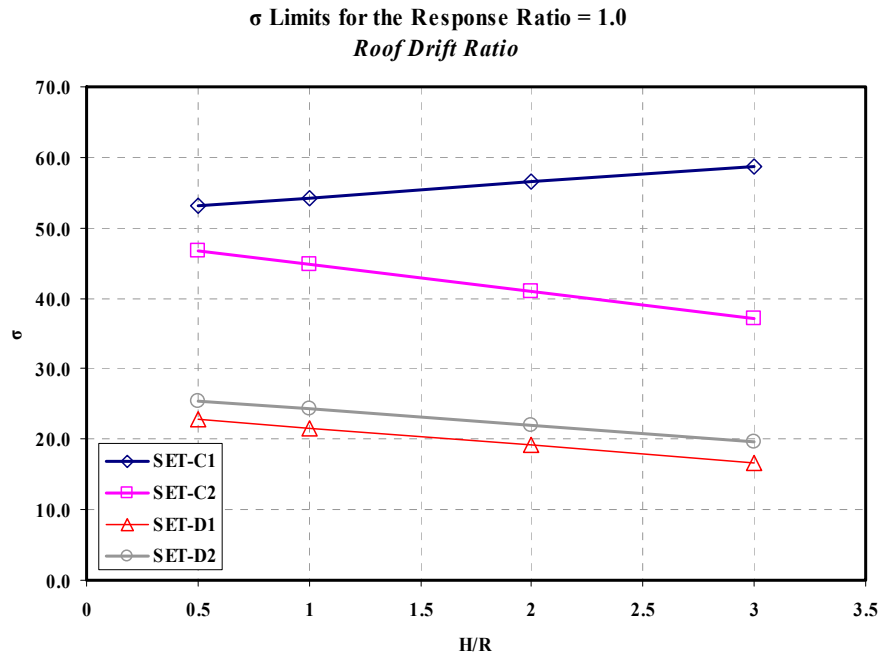


Figure 4.13. Upper limits of wave parameter for the response ratio equal to 1.0, which are calculated from roof drift and first story drift ratios: Analysis group I, NS.

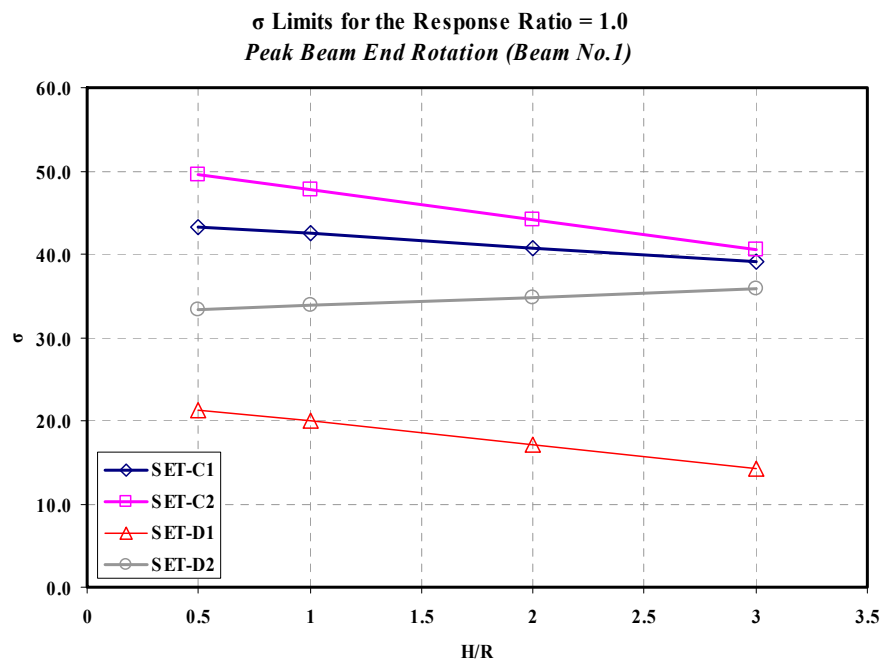
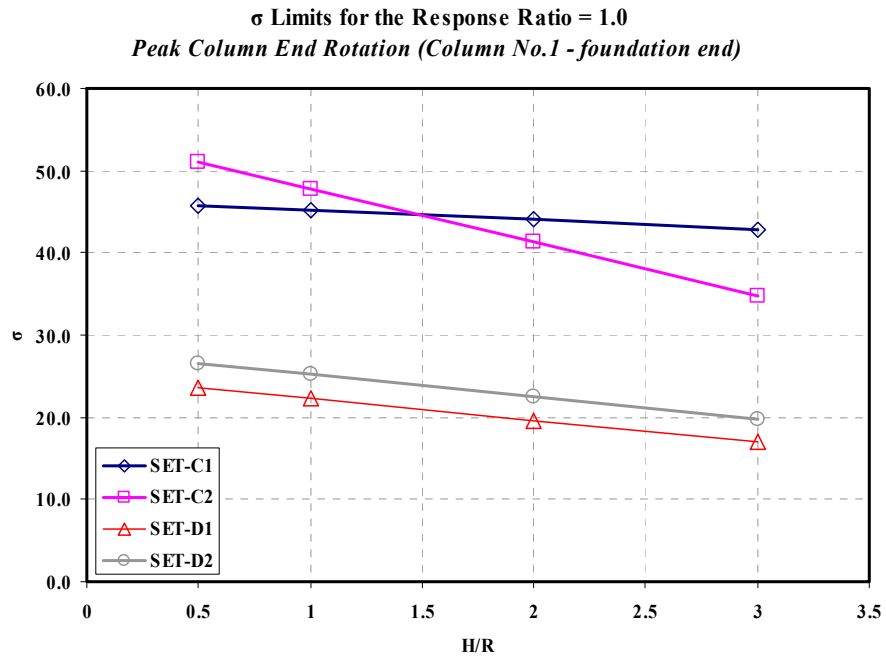


Figure 4.14. Upper limits of wave parameter for the response ratio equal to 1.0, which are calculated from peak member end rotations: Analysis group I, NS.

Table 4.8. Limiting values of the wave parameter (σ_1) when interaction effects are considered to be beneficial for the structural response, which is expressed in terms of the roof and the first story drift demands. Calculations are performed for H/R=0.5, 1.0, 2.0 and 3.0 and analysis group I: NS.

Roof Drift Ratio							
H/R=0.5				H/R=1			
Set	σ	RR1(%)	σ_1	Set	σ	RR1(%)	σ_1
C1	10	-0.4	53.0	C1	10	-0.4	54.2
	60	0.1			60	0.0	
C2	10	-1.2	46.8	C2	10	-1.1	44.9
	60	0.4			60	0.5	
D1	5	-4.5	22.9	D1	5	-4.2	21.6
	30	1.8			30	2.1	
D2	5	-5.9	25.4	D2	5	-5.5	24.2
	30	1.3			30	1.7	
H/R=2				H/R=3			
Set	σ	RR1(%)	σ_1	Set	σ	RR1(%)	σ_1
C1	10	-0.4	56.5	C1	10	-0.4	58.8
	60	0.0			60	0.0	
C2	10	-1.0	41.0	C2	10	-0.9	37.1
	60	0.6			60	0.8	
D1	5	-3.6	19.2	D1	5	-3.0	16.7
	30	2.7			30	3.4	
D2	5	-4.9	21.9	D2	5	-4.2	19.6
	30	2.3			30	3.0	

First Story Drift Ratio							
H/R=0.5				H/R=1			
Set	σ	RR1(%)	σ_1	Set	σ	RR1(%)	σ_1
C1	10	-0.6	45.3	C1	10	-0.6	44.2
	60	0.3			60	0.3	
C2	10	-1.4	49.3	C2	10	-1.3	46.3
	60	0.4			60	0.5	
D1	5	-5.4	22.6	D1	5	-5.1	21.5
	30	2.3			30	2.6	
D2	5	-5.4	26.2	D2	5	-5.1	24.9
	30	1.0			30	1.3	
H/R=2				H/R=3			
Set	σ	RR1(%)	σ_1	Set	σ	RR1(%)	σ_1
C1	10	-0.6	42.0	C1	10	-0.5	39.8
	60	0.3			60	0.4	
C2	10	-1.1	40.2	C2	10	-0.9	34.1
	60	0.7			60	0.9	
D1	5	-4.4	19.3	D1	5	-3.7	17.1
	30	3.3			30	4.0	
D2	5	-4.4	22.4	D2	5	-3.8	19.9
	30	1.9			30	2.6	

Table 4.9. Limiting values of the wave parameter (σ_1) when interaction effects are considered to be beneficial for the structural response, which is expressed in terms of the peak member (Column No.1 and Beam No.1) end rotations at the first story. Calculations are performed for H/R=0.5, 1.0, 2.0 and 3.0 and analysis group I: NS.

H/R=0.5					H/R=1				
Set	Member	σ	RR1(%)	σ_1	Set	Member	σ	RR1(%)	σ_1
C1	Col.1	10	-0.6	45.7	C1	Col.1	10	-0.6	45.2
		60	0.2				60	0.3	
	Bm.1	10	-0.7	43.3		Bm.1	10	-0.7	42.4
		60	0.3				60	0.4	
C2	Col.1	10	-1.5	51.0	C2	Col.1	10	-1.4	47.8
		60	0.3				60	0.4	
	Bm.1	10	-1.3	49.5		Bm.1	10	-1.3	47.7
		60	0.4				60	0.4	
D1	Col.1	5	-5.5	23.6	D1	Col.1	5	-5.1	22.3
		30	1.9				30	2.3	
	Bm.1	5	-7.0	21.3		Bm.1	5	-6.4	19.9
		30	3.7				30	4.3	
D2	Col.1	5	-5.7	26.5	D2	Col.1	5	-5.4	25.2
		30	0.9				30	1.3	
	Bm.1	5	-4.7	33.3		Bm.1	5	-4.8	33.8
		30	-0.6				30	-0.6	

H/R=2					H/R=3				
Set	Member	σ	RR1(%)	σ_1	Set	Member	σ	RR1(%)	σ_1
C1	Col.1	10	-0.6	44.0	C1	Col.1	10	-0.6	42.9
		60	0.3				60	0.3	
	Bm.1	10	-0.6	40.8		Bm.1	10	-0.6	39.1
		60	0.4				60	0.4	
C2	Col.1	10	-1.1	41.3	C2	Col.1	10	-0.9	34.8
		60	0.7				60	0.9	
	Bm.1	10	-1.2	44.1		Bm.1	10	-1.0	40.5
		60	0.5				60	0.7	
D1	Col.1	5	-4.3	19.6	D1	Col.1	5	-3.5	17.0
		30	3.1				30	3.9	
	Bm.1	5	-5.2	17.1		Bm.1	5	-4.0	14.3
		30	5.5				30	6.7	
D2	Col.1	5	-4.7	22.5	D2	Col.1	5	-3.9	19.8
		30	2.0				30	2.7	
	Bm.1	5	-4.9	34.8		Bm.1	5	-5.1	35.8
		30	-0.8				30	-1.0	

CHAPTER 5

DISCUSSION OF RESULTS AND CONCLUSION

5.1 Summary

A parametric study is conducted for the investigation of the variation in the global and the local deformation demands caused by the inertial soil-structure interaction effects. For this purpose nonlinear time-history analyses are performed on both fixed-base and flexible-base (interacting) frame structures. Consequently, this study has sought to develop a tool for the prediction of the variation in the demands, which is based on the statistical assessment of the results of the parametric study. In addition, the limiting values of the key interaction parameter (the wave parameter) are sought for the case when interaction effects are considered to be beneficial for the structural response.

The results presented in the dissertation are limited to the following principal cases:

- *Frame models (Section 3.4)*: There are 7 steel moment-resisting frame models: 3 story SAC frame, 3SAC; 2 pairs of 4 story frames, 4KatF, 4KatR; 5 story frame, 5KatS2; 8 Story frame, 8KatS2; 2 pairs of 12 story frames, 12KatFS, 12KatRS.
- *Foundation type and foundation model (Section 3.3)*: The foundation is assumed to be resting on an elastic half-space and there is a full bonding between the foundation and the soil medium. Rigid surface foundation is represented by truncated cone model (Wolf, 1994) with frequency independent coefficients.
- *Wave field (Section 3.3)*: The wave field is assumed as vertically propagating horizontally polarized coherent shear waves (SH).

- *Local site properties and strong ground motion records (Section 2.2):* There are 2 x 50 free-field earthquake event records conforming to NEHRP equivalent site classes C and D, respectively. 20 out of 50 events of each set contain pulse effects. These subsets are referred to as SET-C1 and SET-D1. Complementary sets are referred to as SET-C2 and SET-D2.
- *Analysis groups (Section 2.4):* Parametric study is established on three analysis groups, Group I (NS); II (SC) and III (SCR2), based on the scaling of SET-C1, C2, D1 and D2 records. In NS, records are not scaled; in SC, records are scaled to the mean plus one standard deviation spectral acceleration of each subset at the fundamental period of each frame model; in SCR2, each record is scaled in order to produce the strength reduction factor, $R=2$ (FEMA356, 2000) at the effective fundamental period of each frame model.
- *Structural response:* The scope of the study is limited to the following structural responses: Roof drift ratio (roof drift normalized with respect to total height of the frame), first story drift ratio (story drift normalized with respect to story height of the frame), maximum column end rotations (at the foundation end) and maximum beam end rotations at the first story.
- *Parameters of the soil-structure interaction assessment (Section 1.2.3):* Soil-structure interaction parameters which are used in the parametric study are the wave parameter, $\sigma = V_s T_n / H$ (Eq. 1.1), which expresses the relative stiffness of the foundation medium and the structure, and the aspect ratio, H/R (Eq. 1.2), which is a geometrical description of the frame height with respect to the equivalent radius of the foundation. These variables, which are based on the local site condition of each earthquake event record and modal and geometric properties of the frame and the foundation, respectively, are used as the predictor variables of the statistical evaluation (multiple linear regression) of the variation in the structural response.

5.2 Discussion of Results

The difference in the deformation demands is investigated in terms of response ratio.

This is defined as the ratio of flexible-base (interacting) frame model's response to that of obtained from the fixed-base frame model. The limiting value of the response ratio is assumed to be 1.0 in which the structural deformation obtained from the flexible-base frame model approaches to that of obtained from fixed-base model. Hence, the response ratio values, which are presented in the related tables, are expressed as percentages in reference to base 1.0, i.e. a value of -4.4% means 0.956.

Deformation responses, in the form of response ratios, are collected from the analysis groups NS, SC and SCR2 with respect to the SSI parameters (σ and H/R). For the statistical assessment, multiple linear regression procedure is performed for the derivation of the regression equations which are expressed in the following form: $y=c_1+c_2\sigma+c_3(H/R)$ (Eq. 4.3). The regression equations and the associated 2D scatter data are given in Chapter 4 and Tables 4.1 – 4.4; Appendix D and Figs. D.1 – D.12, respectively. In the figures, linear regression lines are also superimposed on the associated response ratio values (for each of the 7 frame model's aspect ratios). When these plots are examined it is observed that the dispersion in the scatter groups from the SETD records is more dominant with respect to SETD records (Figs.5.1 – 5.2). This observation is also supported from the difference between the mean absolute error (MAE) and standard error (RMSE) calculated for the associated regression equations. However, both MAE (up to 0.039) and RMSE (up to 0.093) are observed to be small. Hence, the regression equations are utilized in order to investigate the general tendency of the contribution of inertial interaction effects within the scope of the study. In the following text, the results are summarized in terms of the σ and H/R based on the global deformation level of the frame models.

5.2.1 Global Deformation State of the Frames

As the structure begins to yield and deform inelastically, the effective fundamental period of the structure tends to lengthen and the structure becomes more flexible. The influence of the increased deformation demands on the inertial interaction effects are examined by comparing the response ratio values among the analysis groups. For this purpose, roof drift ductility demands, which are obtained from the

nonlinear time-history analyses of the flexible-base frame models, are summarized in Table 5.1 with respect to the following ranges: $\mu=1$, $\mu=1.0 - 2.0$, $\mu=2.0 - 4.0$ and $\mu>4.0$. From this table it is concluded that the deformation demands in the frame models (with respect to the roof drift ductility demands) increase by following the order of the analysis groups: NS, SC and SCR2:

- In analysis group I, NS: At least 82.9% (D1) and 94.5% (D2) of the events associated with the records containing pulse effects and without pulse effects produced responses in the elastic range ($\mu=1.0$), respectively.
- In analysis group II, SC: At least 50.0% (D1) and 84.8% (C2) of the events associated with the records containing pulse effects and without pulse effects produced responses in the elastic range, respectively. The percentages related to the responses in the nonlinear range, $\mu=1.0 - 2.0$, are 34.6% (C1) and 4.5% (C2), respectively.
- In analysis group III, SCR2: At least 61.1% (C1) and 76.9% (C2) of the events associated with the records containing pulse effects and without pulse effects produced responses in the nonlinear range, $\mu=1.0 - 2.0$, respectively. The percentages related to the responses in the nonlinear range, $\mu=2.0 - 4.0$, are 30.4% (D1) and 21% (D2), respectively.
- From all analysis groups it is observed that sets containing records with pulse effects (SET-C1 and SET-D1) lead to increased deformations in the nonlinear range.

Detailed information regarding the distribution of events for each frame model is given in Section 4.5.1 and Tables 4.5 – 4.7.

5.2.2. Assessment of the Variation in the Demands

The mean variation in the demands is assessed by utilizing the regression equations for the range of σ and H/R given in Table 5.2. Detailed tabular results are presented in Appendix C and Tables C.1 – C.9 and associated plots are given in Chapter 4 and Figs. 4.1 – 4.12. The summary of these tables are given in the following text.

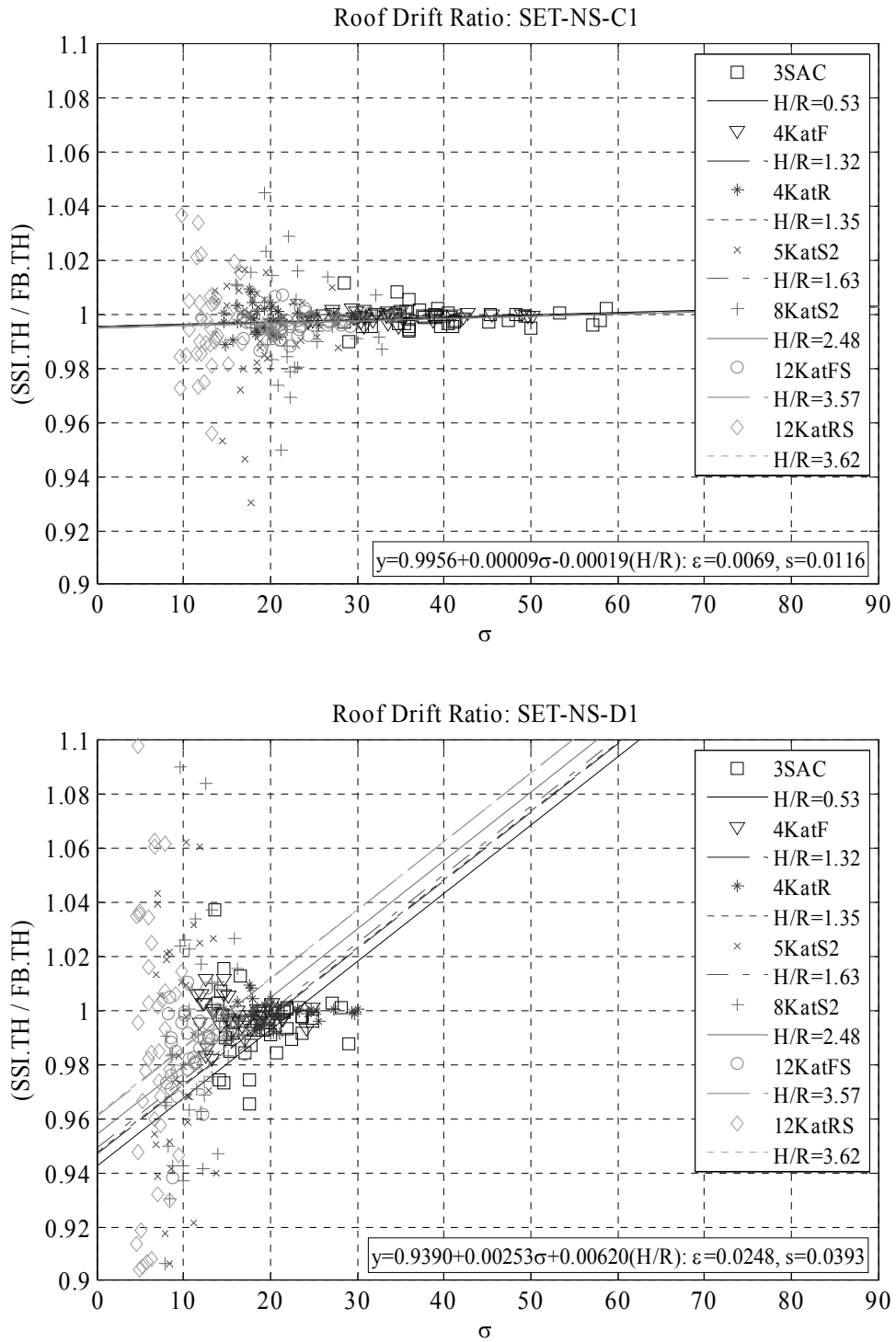


Figure 5.1. 2D scatter plots and associated regression lines for the response ratio values obtained from the roof drift ratio: SET-NS-C1 and D1. In the regression equations ε is the mean absolute error (MAE) and s is the standard error (RMSE).

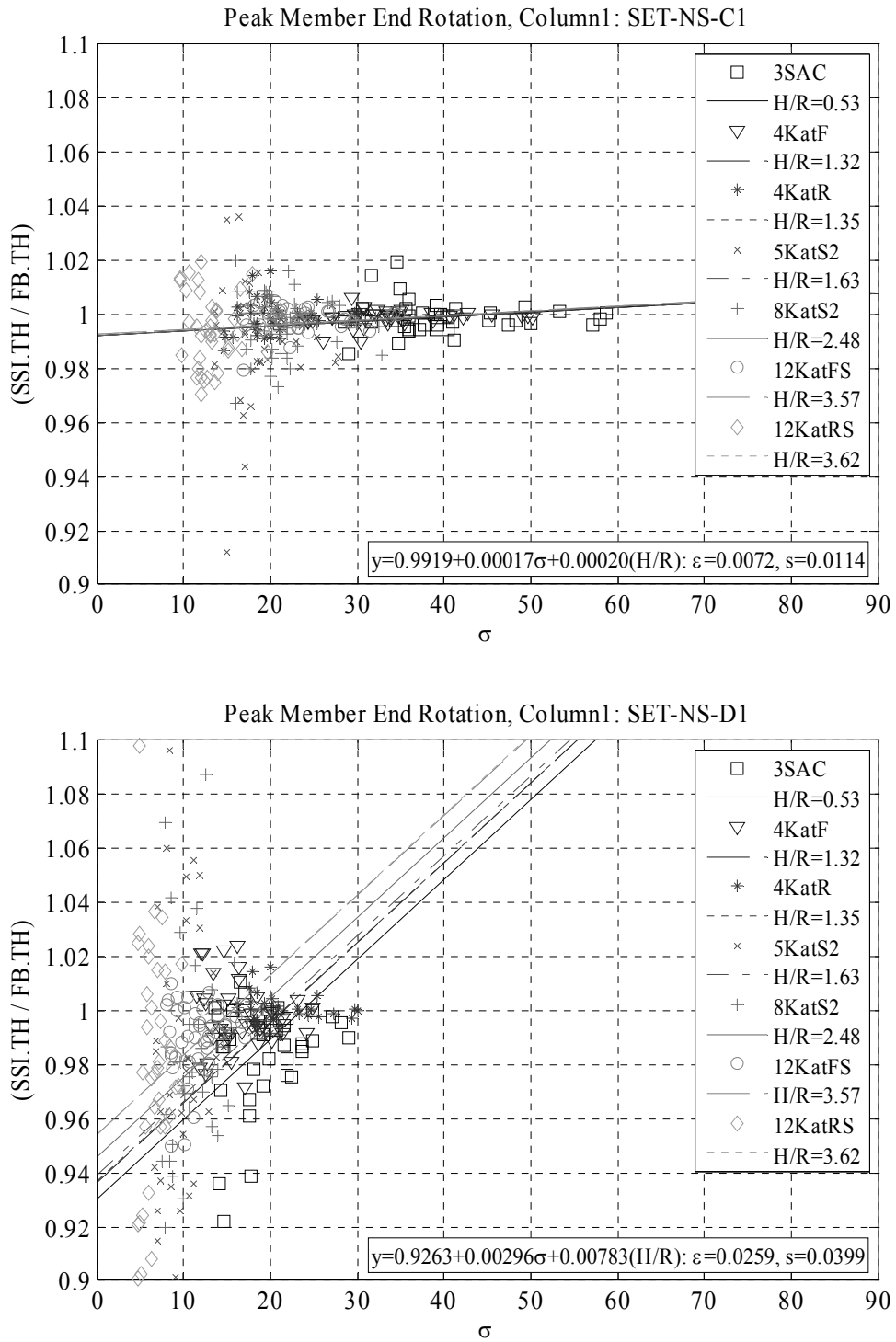


Figure 5.2. 2D scatter plots and associated regression lines for the response ratio values obtained from the peak column (no.1) end rotation at the first story: SET-NS-C1 and D1. In the regression equations ε is the mean absolute error (MAE) and s is the standard error (RMSE).

Table 5.1. Comparison of the distribution of number of the events with respect to the roof drift ductility ranges among the analysis groups, NS, SC and SCR2, which are obtained from nonlinear time-history analyses of flexible-base (interacting) frame models: $\mu=1$, 1-2, 2-4 and >4 .

Analysis Group	Eq. Set	Number of Events Among the Roof Drift Ductility Demand Ranges								
		$\mu=1$		$\mu=(1 - 2)$		$\mu=(2 - 4)$		$\mu>4$		Total
NS	C1	246	87.9%	31	11.1%	3	1.1%	0	0%	280
	D1	232	82.9%	48	17.1%	0	0%	0	0%	280
	C1+D1	478	85.4%	79	14.1%	3	0.5%	0	0%	560
	C2	409	97.4%	11	2.6%	0	0%	0	0%	420
	D2	397	94.5%	23	5.5%	0	0%	0	0%	420
	C2+D2	806	96%	34	4%	0	0%	0	0%	840
SC	C1	173	61.8%	97	34.6%	9	3.2%	1	0.4%	280
	D1	140	50%	137	48.9%	3	1.1%	0	0%	280
	C1+D1	313	55.9%	234	41.8%	12	2.1%	1	0.2%	560
	C2	401	95.5%	19	4.5%	0	0%	0	0%	420
	D2	356	84.8%	63	15%	1	0.2%	0	0%	420
	C2+D2	757	90.1%	82	9.8%	1	0.1%	0	0%	840
SCR2	C1	0	0%	171	61.1%	99	35.4%	10	3.6%	280
	D1	0	0%	189	67.5%	85	30.4%	6	2.1%	280
	C1+D1	0	0%	360	64.3%	184	32.9%	16	2.9%	560
	C2	0	0%	323	76.9%	93	22.1%	4	1%	420
	D2	1	0.2%	331	78.8%	88	21%	0	0%	420
	C2+D2	1	0.1%	654	77.9%	181	21.5%	4	0.5%	840

Roof drift ratio:

The maximum reduction in the demands, which is calculated from the regression lines with respect to analysis groups and soil site classification, is as follows:

- Analysis group NS: Between -0.37% and -1.22%; -2.71% and -6% for SETC and SETD records, respectively. Maximum standard errors for SETC and SETD are observed to be equal to 1.2% and 3.9%, respectively.
- Analysis group SC: Between -0.22% and -1.1%; -2.4% and 4.25% for SETC and SETD records, respectively. Maximum standard errors for SETC and SETD are observed to be equal to 1% and 3.7%, respectively.
- Analysis group SCR2: Between -0.09% and -0.41%; -0.03% and -1.03% for SETC and SETD records, respectively. Maximum standard errors for SETC and SETD are observed to be equal to 3.2% and 3%, respectively.

Standard errors for SETC are observed to be low (~1.2%) in the analysis groups NS and SC in contrast to SCR2 (3.2%); for SETD, the standard error varies between 3–4%. When the mean absolute error (MAE) and the standard error (RMSE) are compared to diagnose the variation in the response ratio values RMSE is observed to be larger than MAE. The difference between the two parameters is observed to be larger for SETD. The trend is also visible in Figs. 5.1 – 5.2.

As a general trend, σ and H/R are observed to be directly proportional to the response ratios. For the exceptions the variation in the demands are observed to be within 1%, which is significantly small. The maximum reduction in the demands, which can be considered as the beneficial aspect of the inertial interaction, is attained at the bottom limit of σ (Table 5.2) and is equal to -1.38% and -6% for SETC and SETD, respectively. The intermediate values of the response ratio can be observed in Chapter 4 and Figs. 4.1 – 4.3. Furthermore, the response ratio values obtained from the ground motion sets which include pulse effects, SET-C1 and D1, are relatively smaller than the ones obtained from the complementary sets, SET-C2 and SET-D2. The differences are observed to be within 1% and 1.4% for SETC and SETD, respectively. When the results are compared among the analysis groups NS, SC and SCR2, reduction due to interaction effects are more pronounced in NS and less pronounced in SCR2. The differences vary between 2%–3% and 0.1%–0.8% for SETD and SETC records between analysis groups NS-SC and SC-SCR2, respectively. These trends are recognized as the effect of the relatively increased flexibility of the inelastically deformed structure with respect to the foundation medium, which leads to a decrease in the contribution of the interaction effects. The upper limits of σ representing the beneficial reduction in the response due to inertial interaction effects are illustrated in Fig. 5.3; Chapter 4 and Table 4.8 and Fig. 4.13, for the analysis group NS. In the figure, the response ratio values are plotted at the discrete values of H/R=0.5, 1, 2 and 3 and are capped at 1.0.

First story drift ratio:

The maximum reduction in the demands, which is calculated from the regression lines, with respect to analysis groups and soil site classification is as follows:

- Analysis group NS: Between -0.5% and -1.45%; -3.47% and -5.58% for SETC and SETD records, respectively. Maximum standard errors for SETC and SETD are observed to be equal to 1% and 4%, respectively.
- Analysis group SC: Between -0.39% and -1.25%; -2.78% and 3.96% for SETC and SETD records, respectively. Maximum standard errors for SETC and SETD are observed to be equal to 1% and 3.6%, respectively.
- Analysis group SCR2: Between -0.02% and -0.37%; -0.06% and -1.5% for SETC and SETD records, respectively. Maximum standard errors for SETC and SETD are observed to be equal to 4.6% and 3.8%, respectively.

The general trend of the response ratio values obtained for the first story drift ratio are observed to be similar to the conclusions derived from the roof drift ratio. In this case the maximum reduction in the demands, which can be considered as the beneficial aspect of the inertial interaction, is limited to -5.6% for SETD records. The intermediate values of the response ratio can be observed in Chapter 4 and Figs. 4.4 – 4.6. The upper limits of σ representing the beneficial reduction in the response due to inertial interaction effects are illustrated in Fig. 5.3; Chapter 4 and Table 4.8 and Fig. 4.13, for the analysis group NS.

Maximum member end rotations at the first story:

In order to keep the text to a minimum the response ratio values are compared among the results associated with the minimum, intermediate and maximum H/R of interest. These are H/R=0.53 (3SAC frame), H/R=1.63 (5KatS2 frame) and H/R=3.62 (12KatRS), given in Appendix C; Tables C.3, C.6 and C.9, respectively. In these tables it is observed that the response ratio values for SETC records associated with analysis groups NS, SC and SCR2 are less than -1.55%, therefore, further details are not addressed in the text. The maximum reduction in the demands with respect to minimum, intermediate and maximum H/R (SETD) is as follows:

- NS-SETD: Response ratio values vary between -6.3%, -5.33%, -3.64% and -7.13%, -5.81%, -5.33% for columns and beams, respectively.

- SC-SETD: Response ratio values vary between -4.52%, -4.04%, -3.17% and -5.31%, -4.71%, -5.73% for columns and beams, respectively.
- SCR2-SETD: Response ratio values vary between -2.79%, -2.62%, -2.83% and -1.54%, -1.77%, -2.21% for columns and beams, respectively.

Similar to the previous findings, response ratio values obtained from the analysis group NS-SETD are relatively more affected from the interaction effects. The intermediate values of the response ratio can be observed in Chapter 4 and Figs. 4.7 – 4.12. The upper limits of σ representing the beneficial reduction in the response due to inertial interaction effects are illustrated in Fig. 5.4; Chapter 4 and Table 4.9 and Fig. 4.14, for the analysis group NS. In the table and figures, response ratio values are illustrated for the exterior (left) members: Column No.1 and Beam No.1.

5.3 Conclusion

Based on these range of SSI parameters, σ and H/R; ground motion sets, SET-C1, SET-C2, SET-D1 and SET-D2; following conclusions are drawn from the assessment of the contribution of inertial soil-structure interaction effects:

- The flexibility introduced by the supporting foundation medium leads to a decrease in the demands, which is more pronounced at soft soil sites and for the decreasing values of the wave parameter.
- As a general trend, the wave parameter and the aspect ratio are observed to be directly proportional to the response ratios: Decreasing trends in the wave parameter value and aspect ratio lead to a higher reduction in the demands. The reduction is relatively more pronounced in SETD (up to -7.13%) than in SETC (up to -1.5%) records.
- Maximum reduction among the roof and first story drift demands and peak member end rotation demands at the first story of the frame models are observed to be close to each other: -1.22% – -1.52% and -5.58% – -7.13% for SETC and SETD, respectively.

- Increasing inelastic deformation of the frames (among the analysis groups NS, SC and SCR2), which can be regarded as an increase in the flexibility of structure, leads to a decrease in the contribution of inertial interaction effects (~5% difference in maximum).
- Linear regression equations are derived for the prediction of the response ratio (Chapter 4; Tables 4.1 – 4.4), which is defined as the ratio of the demands obtained from the flexible-base frame structure to the fixed-base frame structure. These equations can be used to predict the variation in both the roof and the first story drift ratios and the peak member end rotations at the first story. Both mean absolute error (MAE) and standard error (RMSE) of the regression equations are observed to be low.
- The limiting values of the wave parameter (σ_l) are calculated for the variation in the deformation demands when the inertial interaction effects are beneficial (Chapter 4; Tables 4.8 – 4.9).

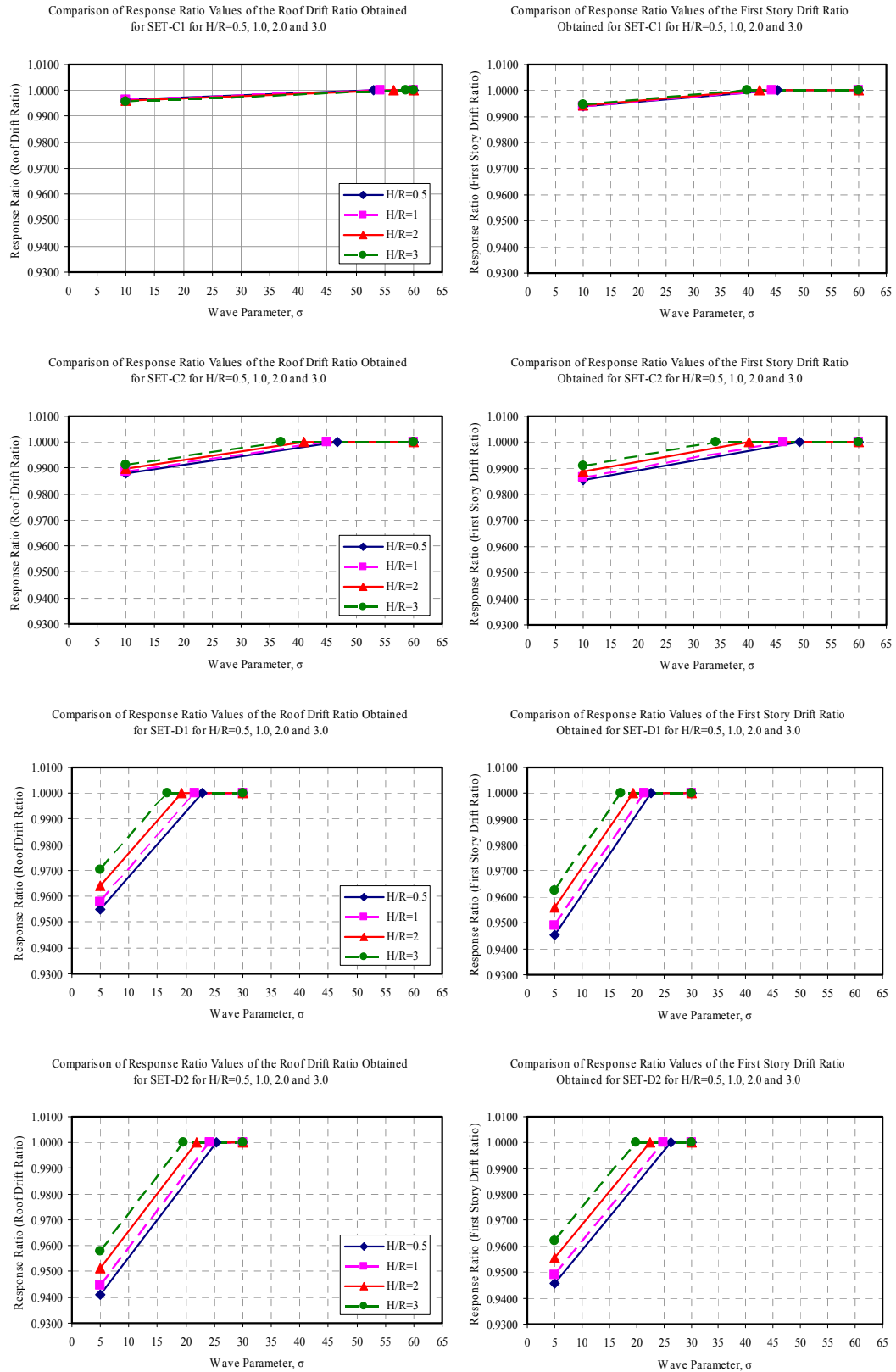


Figure 5.2. Comparison of the response ratios of roof and first story drift ratios for SET-NS-C1, C2, D1 and D2 records for $H/R=0.5, 1.0, 2.0$ and 3.0 .

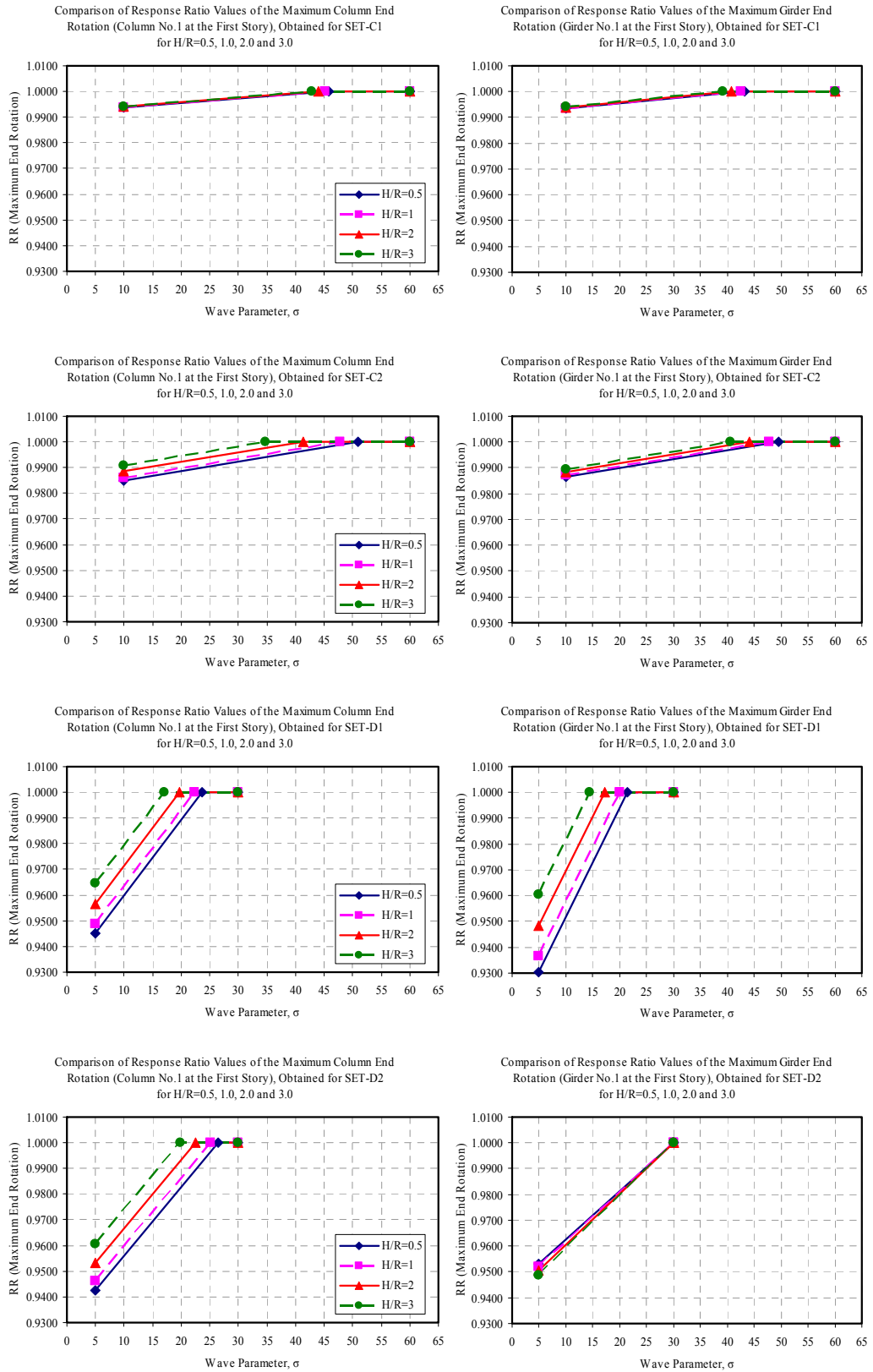


Figure 5.3. Comparison of the response ratios of maximum member end rotations at the first story for SET-NS-C1, C2, D1 and D2 records for H/R=0.5, 1.0, 2.0 and 3.0.

REFERENCES

ActiveState, Sophos, TCL, “Active TCL, Tool Command Language”.

Akkar, S., Gülkan, P., 2000, “Comparative performance evaluation of displacement based design procedures for near field earthquakes,” Proceedings of the 12th World Conference on Earthquake Engineering, New Zealand Society for Earthquake Engineering, Upper Hutt, New Zealand.

Akkar, S., Miranda, E., 2003, “Critical Review Of Equivalent Linear Methods In ATC-40”, Paper No: Ae-019, Fifth National Conference On Earthquake Engineering, 26-30 May 2003, Istanbul, Turkey.

Akkar, S., Miranda, E., Ruiz-García, J., 2003, “Critical Review Of Displacement Modification Factors In Fema-273/356”, Paper No: Ae-018, Fifth National Conference On Earthquake Engineering, 26-30 May 2003, Istanbul, Turkey.

Albanesi, T., Nuti, C., Vanzi, I., 2000, “A simplified procedure to assess the seismic response of nonlinear structures,” Earthquake Spectra, Vol. 16, No. 4, Earthquake Engineering Research Institute, Oakland, California, pp. 715-734.

Aschheim, M., 2002, “Seismic Design Based on the Yield Displacement”, Earthquake Spectra, Vol. 18, No. 4, pp. 581–600.

ATC-40, 1996, “Seismic Evaluation and Retrofit of Concrete Buildings, Volume 1”, Applied Technology Council, CA, USA.

Aviles, J., Perez-Rocha, L., E., 2003, “Soil-Structure Interaction in Yielding Systems”, Earthquake Engineering and Structural Dynamics, Vol. 32, pp.1749-1771.

Bernal, D., Youssef, A., “Hybrid-methods for nonlinear soil-structure interaction”, 12th Engineering Mechanics Conference, La Jolla, CA, 1998.

Bielak, J., 1975. "Dynamic Behavior of Structures with Embedded Foundations", *Earthquake Engineering and Structural Dynamics*, Vol. 3, pp. 259-274.

Bielak, J., 1976, "Modal analysis for building-soil interaction", *Journal of Engineering Mechanics Division, ASCE*, Vol. 102, pp. 771-786.

Castellani, A., 1970. "Foundation compliance effects on earthquake response spectra", *Journal of Soil Mechanics and Foundations Division of ASCE*, Vol. 96, No. 4, pp. 1335-1355.

Chang, C., Y., Mok, C. M., Power, M., S., Tang, Y., K., Tang A. T., Stepp, J. C., 1990, "Equivalent linear and nonlinear ground response analyses at Lotung seismic experiment site.", *Proc., 4th U.S. National Conf. on Earthquake Engineering*, 1, Earthquake Engineering Research Institute, Oakland, Calif., pp. 327-336.

Chopra, A., K., Goel, R.K. 2000. "Evaluation of NSP to estimate seismic deformation: SDOF systems", *Journal of Structural Engineering*, Vol. 126, No. 4, April 2000, pp. 482-490.

Chopra, A., K., 2001, "Dynamics of Structures, Theory and Applications to Earthquake Engineering, Second Ed.", Prentice-Hall, Upper Saddle River, NJ.

Ciampoli, M., Pinto, P., E., 1995, "Effects of soil-structure interaction on inelastic seismic response of bridge piers", *Journal of Structural Engineering, ASCE*, Vol. 121, No. 5, pp. 806-814.

Computers and Structures Inc., ETABS, "Integrated Analysis, Design And Drafting of Building Systems", 1995 University Ave., Berkeley, CA, 94704.

Day S.M., 1978, "Seismic response of embedded foundations", *Proc. ASCE Convention, Chicago, Illinois, October*, Preprint No. 3450.

Dobry, R., Gazetas, G., 1986. "Dynamic Response of Arbitrarily Shaped Foundations", *Journal of Geotechnical Engineering, ASCE*, Vol. 112, No.2, pp. 109-135.

Elgamal, A. W., Zeghal, M., Tang, H. T., Stepp, J. C., 1995. "Lotung downhole array. I: Evaluation of site dynamic properties", *Journal of Geotechnical Engineering*, Vol. 121, No.4, pp.350-362.

Elnashai, A. S., McClure, D. C., 1996. "Effect of modeling assumptions and input motion characteristics on seismic design parameters of RC bridge piers foundations", *Earthquake Engineering and Structural Dynamics*, Vol. 25, pp. 435-463.

Elsabee, F., Morray, J. P., 1977. "Dynamic behavior of embedded foundations", Rep. No. R77-33, Department of Civil Engineering, MIT, Cambridge, Mass., USA.

FEMA273, 1997, "NEHRP Guidelines for the Seismic Rehabilitation of Buildings, FEMA 273 Report (Guidelines) and FEMA 274 Report (Commentary) prepared by the Applied Technology Council for the Building Seismic Safety Council", Federal Emergency Management Agency, Washington, D.C.

FEMA356, 2000, "Prestandard and Commentary for the Seismic Rehabilitation of Buildings", Building Seismic Safety Council, Washington DC, USA.

FEMA440, 2004, "Improvement of Nonlinear Static Seismic Analysis Procedures, Applied Technology Council (ATC-55 Project)", Federal Emergency Management Agency, Washington DC, USA.

FEMA450, 2003, "NEHRP Recommended Provisions for Seismic Regulations for New Buildings and Other Structures, Parts 1 and 2", Building Seismic Safety Council, Washington DC, USA.

Gaylord, E. H., Jr., Gaylord, C. N., Stallmeyer J. E., 1992, "Design of Steel Structures, Third Edition", McGraw-Hill International..

Gazetas G., 1975. "Dynamic stiffness functions of strip and rectangular footings on layered soil", SM thesis, Massachusetts Institute of Technology, (MIT), Boston, Massachusetts, USA.

Gazetas G., 1991. "Formulas and Charts for Impedances of Surface and Embedded Foundations", *Journal of Geotechnical Engineering*, Vol. 117, No.9, pp. 1363-1381.

Jennings and Bielak, 1973. "Dynamics of building-soil interaction", Bull. Seism., Am., Vol. 63, pp. 9-48.

Kim S., Stewart J. P., 2003. "Kinematic Soil-Structure Interaction from Strong Motion Recordings", Journal of Geotechnical and Geoenvironmental Engineering, Vol. 129, No.4, ASCE, pp. 323-335.

Kuhlemeyer R. L., Lysmer J., 1973. "Finite element Method Accuracy for Wave Propagation Problems", Journal of Soil Mechanics & Foundations, Div. ASCE, 99(SM5), pp. 421-427.

Luco J. E., Hadjian A. H., 1974, "Two Dimensional Approximation to the Three-Dimensional Soil-Structure Interaction Problem", Nuclear Engineering and Design, Vol. 31, pp. 195-203.

Luco J. E., 1974. "Impedance Functions for a Rigid Foundation on a Layered Medium", Nuclear Engineering and Design, Vol. 31, pp. 204-217.

Luco J. E., Wong H. L., 1986, "Response of a rigid foundation to a spatially random ground motion", Earthquake Engineering and Structural Dynamics, Vol. 14 No.6, pp. 891-908.

Luco J. E., Mita A., 1987a, "Response of circular foundation to spatially random ground motion", Journal of Engineering Mechanics Division ASCE, Vol. 113, No.1, pp. 1-15.

Luco J. E., Mita A., 1987b, "Response of a Circular Foundation on a Uniform Halfspace to Elastic Waves", Earthquake Engineering and Structural Dynamics, Vol. 15, pp. 105-118.

MacRae, G., Tagawa, H., 2001, "Methods to Estimate Displacements of PG&E Structures", draft report on research conducted under PGE/PEER Task No. 505, University of Washington.

McKenna, Frank, Fenves, Gregory L., "OpenSees, Open System for Earthquake Engineering Simulation Software", Pacific Earthquake Engineering Research Center, University of California, Berkeley.

Mengi Y., 2002, "Lecture notes on Soil-Structure Interaction", Middle East Technical University, Ankara, Turkey.

Miranda E., 1991, "Seismic Evaluation and Upgrading of Existing Buildings," Ph.D. Dissertation, University of California, Berkeley.

Miranda E., Bertero V.V., 1994. "Evaluation of Strength Reduction Factors for Earthquake Resistant Design", *Earthquake Spectra*, Vol. 10, No. 2, pp. 357-380.

Mylonakis G., Gazetas G., 2000, "Seismic SSI Beneficial or Detrimental", *Journal of Earthquake Engineering*, Vol. 4, No. 3, pp. 277-301.

Naimi M., Galal K., 2007, "Nonlinear dynamic behavior of R/C tall structures subjected to near-fault earthquakes including soil structure interaction", Ninth Canadian Conference On Earthquake Engineering Ottawa, Ontario, Canada June 2007, pp.26-29.

Newmark N. M., Hall W. J., 1973, "Seismic design criteria for nuclear reactor facilities", Report No. 46, Building Practices for Disaster Mitigation National Bureau of Standards, US Department of Commerce, pp. 209-236.

Newmark N. M., Hall W. J., Morgan J. R., 1977, "Comparison of building response and free field motion in earthquake." Proc., 6th World Conf. Earthquake Engineering, New Delhi, India, Vol. II, 972-978.

Parmalee R. A., Perelman D. S., Lee S. L., Keer I., M., 1968. "Seismic response of structure foundation systems", *Journal of Engineering Mechanics*, ASCE, Vol. 94, No. 6, pp. 1245-1315.

Priestley M. J. N., Park R., 1987. "Strength and ductility of concrete bridge columns under seismic loading", *ACI Structural Journal* Vol. 84, No.1, pp. 61- 76.

Scanlan, R. H., 1976, "Seismic wave effects on soil-structure interaction", *Earthquake Engineering and Structural Dynamics*, Vol. 4, pp. 379-388.

Shome N., Cornell C. A., Bazzurro P., Carballo J. E., 1998, "Earthquakes, records, and nonlinear responses", *Earthquake Spectra*, Vol. 14, No.3, pp. 469-500.

Silva W., 1986, "Soil response to earthquake ground motion", Report No. RP2556-07, Electric Power Research Institute, Palo Alto, California, USA.

Stewart J. P., Fenves G. L., Seed R. B., 1999, "Seismic Soil-Structure Interaction In Buildings, I: Analytical Methods", *Journal of Geotechnical and Geoenvironmental Engineering*, Vol. 125, No.1, pp. 26-37.

Tajimi H., 1969. "Dynamic analysis of a structure embedded in an elastic stratum", Proc., 4th World Conference on Earthquake Engineering, Editorial Universitaria, Santiago, Chile., Vol. 3, pp. 53-70.

Tsopelas, P., Constantinou, M.C., Kircher, C.A., Whittaker, A.S., 1997, "Evaluation of Simplified Methods of Analysis of Yielding Structures", Technical Report NCEER-97-0012, National Center for Earthquake Engineering Research, State University of New York, Buffalo, New York.

Veletsos A. S., Wei Y. T., 1971, "Lateral and Rocking Vibration of Footings", *Journal of the Soil Mechanics and Foundation Division, ASCE*, Vol. 97, pp. 1227-1248.

Veletsos A. S., Verbic B., 1973, "Vibration of viscoelastic foundations", *Earthquake Engineering and Structural Dynamics*, Vol. 2, No.1 , pp. 87–102.

Veletsos A. S., Verbic B., 1974, "Basic Response Functions for Elastic Foundations", *Journal of the Engineering Mechanics Division, ASCE*, Vol. 100, pp. 189-202.

Veletsos A. S., Meek J. W, 1974. "Dynamic Behavior of Building Foundation Systems", *Earthquake Engineering and Structural Dynamics* Vol. 3, No. 2, pp.121-138.

Veletsos A. S., Nair V. D., 1974, "Response of Torsionally Excited Foundations", *Journal of the Geotechnical Engineering Division, ASCE*, Vol. 100, pp. 476-482.

Veletsos A. S., Nair V. D., 1975, “Seismic Interaction of Structures on Hysteretic Foundations”, *Journal of the Structural Division, ASCE*, Vol. 101, pp. 109-129.

Veletsos, A. S. 1977. “Dynamics of structure-foundation systems”, In *Structural and Geotechnical Mechanics, A Volume Honoring N. M. Newmark*, edited by W. J. Hall, pp. 333-361. Englewood Cliffs, New Jersey: Prentice-Hall.

Veletsos A. S., Prasad A. M., 1989, “Seismic interaction of structures and soils: Stochastic approach.”, *Journal of Structural Engineering*, Vol. 115, No.4, ASCE, pp. 935–956.

Veletsos A. S., 1993, “Design Concepts for Dynamics of Soil-Structure Interaction”, P. Gülkan and R. W. Clough (eds.), *Developments in Dynamic Soil-Structure Interaction*, pp. 307-325.

Veletsos A. S., Prasad A. M., Wu W. H., 1997, “Transfer functions for rigid rectangular foundations.”, *Earthquake Engineering and Structural Dynamics*, Vol. 26, No.1, pp. 5–17.

Wilson E. L., 2002, “Three-Dimensional Static and Dynamic Analysis of Structures, A Physical Approach with Emphasis on Earthquake Engineering, Third Ed.”, Computers and Structures, Inc., 1995 University Avenue, Berkeley, California 94704 USA.

Wolf J. P., 1985, “Dynamic Soil-Structure Interaction”, Prentice-Hall, Englewood Cliffs, New Jersey.

Wolf J. P., 1988, “Soil Structure-Interaction Analysis in Time Domain”, Prentice-Hall, Englewood Cliffs, New Jersey.

Wolf J. P., 1994, “Foundation Vibration Analysis Using Simple Physical Models”, Prentice-Hill, Englewood Cliffs, New Jersey.

Wolf J. P., 1997, “Spring-Dashpot-Mass Models for Foundation Vibrations”, *Earthquake Engineering and Structural Dynamics*, Vol. 26, pp. 931-949.

Yamahara H., 1970, “Ground motions during earthquakes and the input loss of earthquake power to an excitation of buildings”, *Soils Found.*, Vol. 10, No. 2, pp. 145–161.

APPENDIX A

THEORETICAL BACKGROUND OF SSI MODEL

A.1 Lumped Parameter Model

As discussed in the preceding section, analysis using discretization of soil layer or shifting to rigorous solution leads to increased computational effort. Instead, there are approximate models to simulate the dynamic behavior of rigid disc on surface of elastic half-space. These discrete element models are easy to interpret and they can be added to the structural model without any difficulty. One of the most common discrete element forms is the fundamental lumped parameter model by Wolf (1994). It is also referred as monkey-tail model and is illustrated in Fig. A.1.

Monkey-tail model is composed of four lumped parameters, C_1 , M_1 , C_0 and M_0 defined independently for each deformation mode (translational and rotational), in addition to static stiffness coefficient for the direction under consideration. Static stiffness coefficient of the spring is equal to static coefficient obtained from the exact solution of disk on elastic half-space. Lumped parameters are utilized to attain an optimum fit between dynamic stiffness coefficients of lumped parameter model and exact solution of disk. In this model there exist two dynamic degrees of freedom for each deformation mode (Wolf (1994)):

- The first one is represented by mass or mass moment of inertia M_0 , which is located at the basemat. It is connected to the far end rigid support by a translational or rotational spring and a dashpot with coefficients K and C_0 , respectively.

- The second one (referred as the monkey tail) is represented by or mass moment of inertia M_1 , which is connected to basemat by a translational or rotational dashpot with coefficient C_1 .

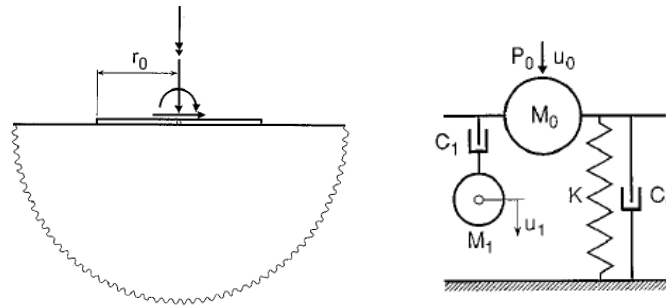


Figure A.1. One dimensional fundamental lumped parameter model (Monkey-Tail Model), Wolf (1997).

For the sake of illustration, dynamic equilibrium is derived for the translational deformation in the vertical direction (Fig. A.1):

$$\begin{aligned}
 M_0 \ddot{u}_0 + (C_0 + C_1) \dot{u}_0 - C_1 \dot{u}_1 + K u_0 &= P \\
 M_1 \ddot{u}_1 - C_1 \dot{u}_0 + C_1 \dot{u}_1 &= 0
 \end{aligned}
 \tag{A.1}$$

where,

u_0 and u_1 are translational degree of freedoms associated with mass or mass moment of inertia M_0 and M_1 , respectively.

These equilibrium equations can be expressed for harmonic excitation; where w is frequency parameter:

$$\begin{aligned}
-w^2 M_0 u_0(w) + iw(C_0 + C_1)u_0(w) - iwC_1 u_1(w) + K u_0(w) &= P(w) \\
-w^2 M_1 u_1(w) - iwC_1 u_0(w) + C_1 u_1(w) &= 0
\end{aligned} \tag{A.2}$$

Solving Eq. A.2 for $P(w)$ by eliminating $u_1(w)$ and by regrouping for $u_0(w)$ leads to classical impedance function for interaction force-displacement relation:

$$P(w) = S(w)u_0(w) \tag{A.3.a}$$

$$S(w) = K [\hat{k} + iw\hat{c}] \tag{A.3.b}$$

$$\hat{k} = \left(1 - \frac{\frac{w^2 M_1}{K}}{1 + \frac{w^2 M_1^2}{C_1^2}} - \frac{w^2 M_0}{K} \right) \tag{A.3.c}$$

$$\hat{c} = \left(\frac{M_1}{C_1} \frac{\frac{w^2 M_1}{K}}{1 + \frac{w^2 M_1^2}{C_1^2}} + \frac{C_0}{K} \right) \tag{A.3.d}$$

Upon substituting dimensionless frequency parameter $a_o = wR/C_s$ Eq. A.3 can be rearranged and expressed as (refer to Table A.1 for other dimensionless parameters):

$$P(a_o) = K [k + ia_o c] u_0(a_o) \tag{A.4.a}$$

$$k = \left(1 - \frac{\mu_1 a_o^2}{1 + \frac{\mu_1^2}{\gamma_1^2} a_o^2} - \mu_0 a_o^2 \right) \tag{A.4.b}$$

$$c = \left(\frac{\mu_1}{\gamma_1} \frac{\mu_1 a_o^2}{1 + \frac{\mu_1^2}{\gamma_1^2} a_o^2} + \gamma_0 \right) \tag{A.4.c}$$

Table A.1. Static stiffness and dimensionless coefficients of Monkey-Tail Model for rigid disk on elastic half-space (Wolf (1997)).

	Static stiffness K	Dimensionless coefficients of			
		Dashpots		Masses	
		γ_0	γ_1	μ_0	μ_1
Horizontal	$\frac{8Gr_0}{2-\nu}$	0.78-0.4 ν	—	—	—
Vertical	$\frac{4Gr_0}{1-\nu}$	0.8	0.34-4.3 ν^4	$\nu < \frac{1}{3}$	0
				$\nu > \frac{1}{3}$	$0.9\left(\nu - \frac{1}{3}\right)$
Rocking	$\frac{8Gr_0^3}{3(1-\nu)}$	—	0.42-0.3 ν^2	$\nu < \frac{1}{3}$	0
				$\nu > \frac{1}{3}$	$0.16\left(\nu - \frac{1}{3}\right)$
Torsional	$\frac{16Gr_0^3}{3}$	0.017	0.291	—	0.171

Through further simplification of Eq. A.4 and defining lumped parameters as (refer to Table A.1 for values associated with required degree of freedom):

$$P(a_0) = K [k(a_0) + ia_0c(a_0)]u_0(a_0) \quad (\text{A.5.a})$$

$$C_0 = \frac{r_0}{c_s} \gamma_0 K \quad , \quad C_1 = \frac{r_0}{c_s} \gamma_1 K \quad (\text{A.5.b})$$

$$M_0 = \frac{r_0^2}{c_s^2} \gamma_0 K \quad , \quad M_1 = \frac{r_0^2}{c_s^2} \gamma_1 K \quad (\text{A.5.c})$$

where,

r_0 = Characteristic length or the radius of the basemat.

K = Static stiffness.

μ_0, μ_1 = Dimensionless coefficients of masses.

γ_0, γ_1 = Dimensionless coefficients of dashpots.

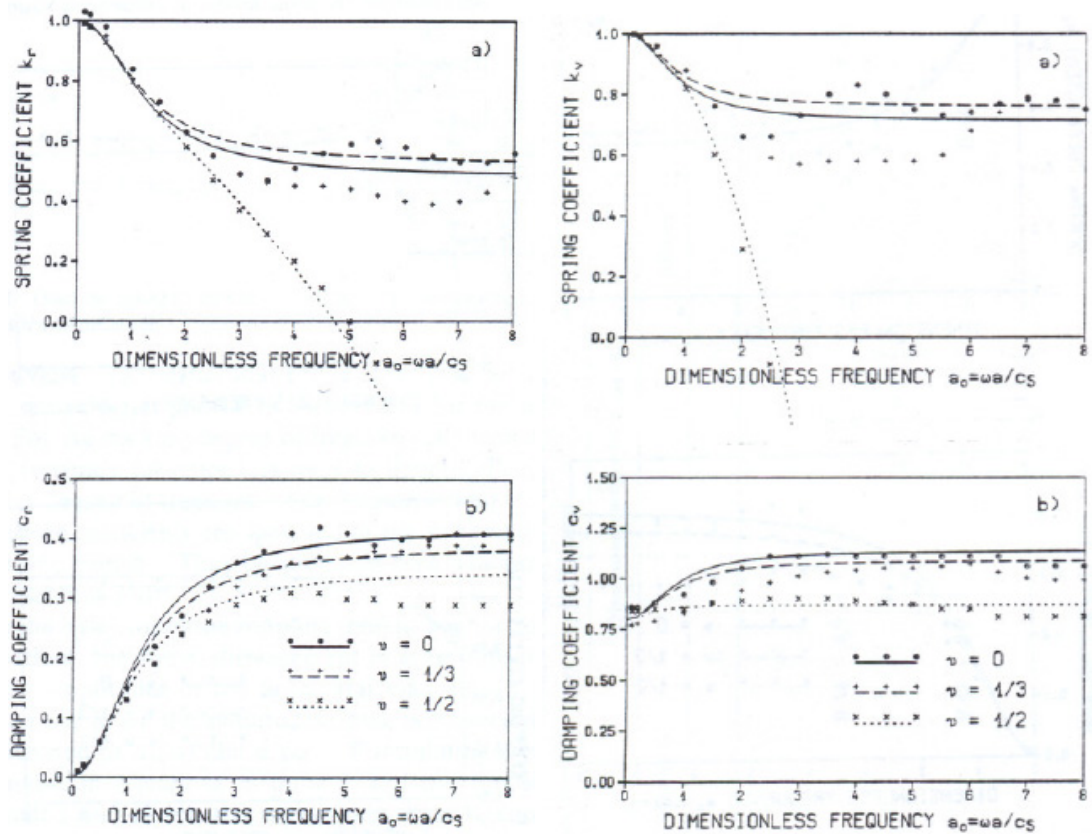


Figure A.2. Comparison of the dimensionless stiffness and dashpot coefficients between Wolf (1988) and Veletsos and Wei (1971), for the vertical translation and rocking response of disk on elastic half-space (Wolf (1988)). These plots are for Poisson's Ratio, $\nu=0, 1/3$ and $1/2$.

Dimensionless stiffness and damping coefficients for rocking and vertical translation ($k(a_0)$ and $c(a_0)$) had been compared for accuracy by Wolf (1988), with the values obtained from Veletsos and Wei (1971) in Fig. A.2. Plots were prepared for three values of Poisson's ratio, $\nu=0, 1/3$ and $1/2$. The sudden drop at $\nu > 1/3$ in both non-dimensional stiffness coefficients is due to the presence of additional mass that vibrates in phase with the basemat. As a general trend, the agreement between plots was found to be satisfactory (Wolf (1988)).

A.2 Truncated Cone Model

Discrete foundation model used through out the study is based on truncated cone model. Derivation of closed form equations is summarized from Wolf (1994). Figures and tables used in this section are directly taken from the same source without any modification unless otherwise stated.

A.2.1 Construction of Cone Model for Rigid Surface Foundations

Cones are doubly asymptotic approximations, which are exact at very low and at very high frequencies, and are based on strength of materials instead of the theory of elastic half-space. Illustration of physical interpretation of cone models for translation and rotation degrees of freedom are given in Fig. A.3. Assumptions associated with the model are as follows:

- Soil is idealized as an unlayered, homogenous, linearly elastic, semi-infinite medium.
- Soil is assumed to be undamped.
- Soil is defined by mass density (ρ), Poisson's ratio (ν) and average wave velocity (c), which are constant in the truncated soil domain (cone).
- Soil is idealized for each degree of freedom (deformation mode as vertical and horizontal translation and rocking and torsional rotation) with an independent semi-infinite elastic cone having a specific apex height, z_0 .
- Radius of a semi-infinite elastic cone increases linearly with the increasing depth of soil (Fig. A.3).
- Soil domain outside the cone is ignored.
- Foundation is a rigid massless surface disk (or an arbitrary shape, which can be expressed with equivalent radius, area, moment of inertia and polar moment of inertia).
- Application of a load on the disk leads to stresses in the soil half space acting on an area that increases with depth.

- The displacement pattern over the area is assumed to be equal to the corresponding value on the axis of cone.

Following sections provide a brief summary for the derivation of static spring and dashpot coefficients at low and high frequency limits, respectively. These coefficients and associated parameters are given in Table A.2. Refer to Wolf (1994) for further details.

A.2.2 Low Frequency Limit – Static Stiffness Coefficients and Corresponding Apex Height

At low frequency limit static spring coefficients are determined by relating the deformation u_0 to loading P_0 and v_0 to M_0 for translational and rotational degrees of freedom, respectively. Cone representing each degree of freedom has a unique apex height. For a specific basemat with an equivalent radius, aspect ratio can be calculated as z_0/r_0 . Aspect ratio is obtained by equating the static stiffness coefficient for a rigid disk calculated from well known closed form solution to that of cone.

A.2.2.1 Translational Motion in Low Frequency

In this section derivation of the static stiffness for vertical motion, which is parallel to axis normal to basemat, is explained. Derivation of horizontal stiffness is analogous to vertical motion. Force equilibrium is obtained by considering an infinitesimal slice at cone's cross section at depth z (Fig. A.4.a). Then static stiffness is obtained by relating displacement u_0 to load P_0 .

$$-N + N + N_{,z}dz = 0 \tag{A.6}$$

where,

N = Axial force acting in the cross section at depth z .

$N_{,z}$ = Single derivative of N with respect to z .

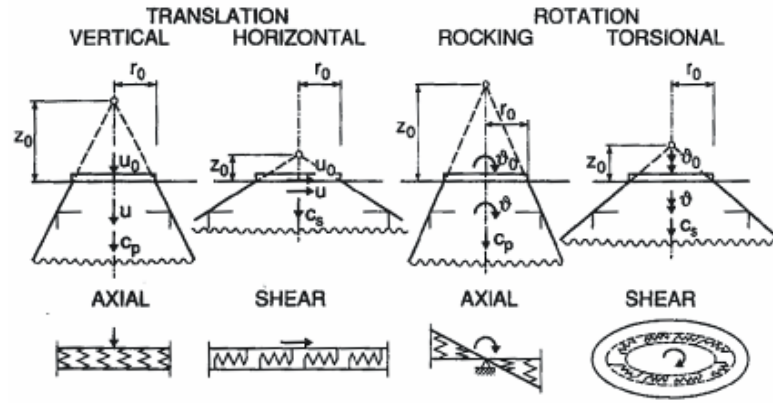


Figure A.3. Cones for various degrees of freedom with their corresponding apex ratio (Opening Angle), wave propagation velocity and distortion (Fig. 2-1; Wolf (1994)).

Corresponding force-displacement relation can be stated as:

$$N = E_c A u_{,z} \quad (\text{A.7})$$

where,

$$E_c = 2G \frac{1-\nu}{1-2\nu} \text{ is the constrained elastic modulus, which is also equal to } \rho c_p^2.$$

$$A = (z/z_0)^2 A_0 \text{ is the effective cross sectional area of the cone at depth } z.$$

$$A_0 = \pi r_0^2 \text{ is the area of the disk with radius (or equivalent radius) } r_0.$$

Substituting Eq. A.7 to Eq. A.6 leads to the following differential equation:

$$z u_{,zz} + 2 u_{,z} = 0 \quad (\text{A.8})$$

Assuming a solution of the form $u = z^\alpha$ and with $\alpha = -1$, leads to:

$$(uz)_{,zz} = 0 \quad (\text{A.9})$$

$$uz = c_1 + c_2 z$$

where,

$c_1, c_2 =$ Integration constants to be determined by imposing boundary conditions.

Table A.2. Spring, Dashpot and Mass coefficients for disk (or an arbitrary shape) on elastic half-space for Truncated Cone Model (Wolf (1997)).

Motion	Horizontal	Vertical	Rocking	Torsional
Equivalent radius r_o	$\sqrt{\frac{A_o}{\pi}}$	$\sqrt{\frac{A_o}{\pi}}$	$\sqrt[4]{\frac{4I_o}{\pi}}$	$\sqrt[4]{\frac{2I_o}{\pi}}$
Aspect ratio $\frac{z_o}{r_o}$	$\frac{\pi}{8}(2-\nu)$	$\frac{\pi}{4}(1-\nu)\left(\frac{c}{c_s}\right)^2$	$\frac{9\pi}{32}(1-\nu)\left(\frac{c}{c_s}\right)^2$	$\frac{9\pi}{32}$
Poisson's ratio ν	All ν	$\leq \frac{1}{3}$ $\frac{1}{3} < \nu < \frac{1}{2}$	$\leq \frac{1}{3}$ $\frac{1}{3} < \nu \leq \frac{1}{2}$	All ν
Wave velocity c	c_s	c_p $2c_s$	c_p $2c_s$	c_s
Trapped mass $\Delta M \Delta M_g$	0	0 $2.4\left(\nu - \frac{1}{3}\right)\rho A_o r_o$	0 $1.2\left(\nu - \frac{1}{3}\right)\rho I_o r_o$	0
Discrete- element model		$K = \rho c^2 A_o / z_o$ $C = \rho c A_o$		$K_g = 3\rho c^2 I_o / z_o$ $C_g = \rho c I_o$ $M_g = \rho I_o z_o$

At $z=z_o$, loading on disk is equal to P_o (Fig. A.4). In addition, deformation will be theoretically zero for infinite depth. Imposing the following boundary conditions with substitution of Eq. A.9 leads to:

$$\left\{ \begin{array}{l} u(z = z_o) = u_o \\ u(z = \infty) = 0 \end{array} \right\} \rightarrow u = \frac{z_o}{z} u_o \quad (\text{A.10})$$

$$P_o = -N(z = z_o, u = u_o) = -E_c A_o u_{o,z} \quad (\text{A.11})$$

where,

P_o is the applied load on the disk and u_o is the corresponding deformation.

Finally, substituting Eq. A.10 into Eq. A.11 leads to force-deformation relation, static stiffness coefficient for vertical motion:

$$P_o = \left(\frac{E_c A_o}{z_o} \right) u_o, \quad K = \frac{E_c A_o}{z_o} \quad (\text{A.12})$$

For the horizontal motion; constrained modulus, E_c , is replaced by shear modulus, G :

$$K = \frac{GA_0}{z_0} \quad (\text{A.13})$$

Expanding shear modulus in Eq. A.13 leads to general representation of static stiffness coefficient for the translational motion:

$$K = \frac{\rho c^2 A_0}{z_0} \quad (\text{A.14})$$

where,

c = Wave propagation velocity.

For horizontal translation wave propagation velocity is $c=c_s$.

For vertical translation wave propagation velocity is a function of Poisson's ratio, ν .

- For Poisson's ratio, $\nu < 1/3$, wave propagation velocity is $c=c_p$.
- For Poisson's ratio, $1/3 < \nu < 1/2$, wave propagation velocity is $c=2c_s$ (Section A.2.4).

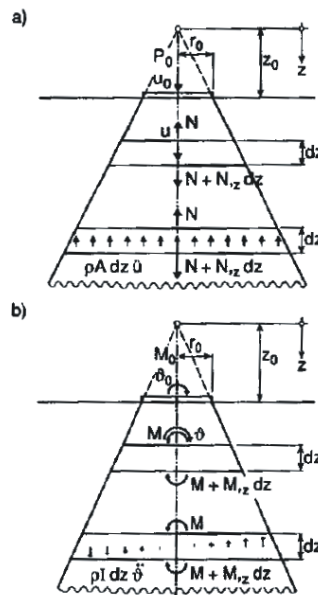


Figure A.4. Truncated semi-infinite cones (Fig. 2-2; Wolf (1994)). In this Figure: (a) Translational cone with nomenclature for vertical motion and static and dynamic equilibrium of infinitesimal element, (b) Rotational cone with nomenclature for rocking motion and static and dynamic equilibrium of infinitesimal element.

A.2.2.2 Rotational Motion in Low Frequency

Force equilibrium is obtained for moment once more by considering an infinitesimal slice at cone's cross section at depth z (Fig. A.4.b). Next, static stiffness for rotation is obtained by relating rotation v_0 to moment M_0 .

$$-M + M + M_{,z} dz = 0 \quad (\text{A.15})$$

where, M is the bending moment acting in the cross section at depth z .

Force-displacement relation for bending moment can be expressed as:

$$M = E_c I v_{,z} \quad (\text{A.16})$$

where,

$I = (z/z_0)^2 I_0 =$ Moment of inertia of the cross section at depth z .

$I_0 = \frac{\pi}{4} r_0^4 =$ Moment of inertia of the disk for rocking with radius (or equivalent radius) r_0 .

$I_0 = \frac{\pi}{2} r_0^4 =$ Polar moment of inertia of the disk for torsion with radius (or equivalent radius) r_0 .

Substituting Eq. A.16 to Eq. A.15 leads to the following differential equation:

$$v_{,zz} + \frac{4}{z} v_{,z} = 0 \quad (\text{A.17})$$

Assuming a solution of the form $u = z^\alpha$ and with $\alpha=0, -3$ ($\alpha^2+3\alpha=0$) leads to:

$$v = c_1 + c_2 z^{-3} \quad (\text{A.18})$$

where,

c_1 and c_2 are integration constants to be determined by imposing boundary conditions.

Imposing following boundary conditions to Eq. A.16 and Eq. A.18 leads to:

$$\left\{ \begin{array}{l} v(z = z_0) = v_0 \\ v(z = \infty) = 0 \end{array} \right\} \rightarrow v = \left(\frac{z_0}{z} \right)^3 v_0 \quad (\text{A.19})$$

$$M_0 = -M(z = z_0, v = v_0) = -E_c I_0 v_{0,z} \quad (\text{A.20})$$

where,

M_0 = Applied bending moment on the disk and v_0 is the corresponding rotational deformation.

Finally, substituting Eq. A.19 into Eq. A.20 leads to force-deformation relation, static stiffness coefficient for rocking motion.

$$M_0 = \left(\frac{3E_c I_0}{z_0} \right) v_0, \quad K = \frac{3E_c I_0}{z_0} \quad (\text{A.21})$$

For torsional motion, constrained modulus, E_c and moment of inertia, I_0 are replaced by shear modulus, G and polar moment of inertia, $I_0 = \frac{\pi}{2} r_0^4$, respectively:

$$K = \frac{3GI_0}{z_0} \quad (\text{A.22})$$

Expanding shear modulus in Eq. A.22 leads to general representation of static stiffness coefficients for the rotational motion:

$$K = \frac{3\rho c^2 I_0}{z_0} \quad (\text{A.23})$$

where,

For torsional motion:

- I_0 = Polar moment of inertia.

- Wave propagation velocity is $c=c_s$.

For rocking motion:

- I_o = Moment of inertia.
- Wave propagation velocity is a function of Poisson's ratio, ν .
 - For Poisson's ratio, $\nu < 1/3$, wave propagation velocity is $c=c_p$.
 - For Poisson's ratio, $1/3 < \nu < 1/2$, wave propagation velocity is $c=2c_s$.

A.2.2.3 Apex Height for Static Stiffness Coefficients (Low Frequency)

In order to evaluate both translational and rotational static stiffness coefficients, apex height z_0 must be evaluated. For a specific disk radius (or equivalent radius) aspect ratio z_0/r_0 turns out to be a more meaningful parameter and is calculated by equating static stiffness terms for cone to static stiffness coefficients of half space. Please refer to Table A.2 for the summary of coefficients associated with degrees of freedom.

For horizontal translation,

$$K_{hor}^{halfspace} = \frac{8Gr_0}{2-\nu} \quad (A.24.a)$$

$$K_{hor}^{halfspace} = K_{hor}^{cone} = \frac{GA_0}{z_0} \quad (A.24.b)$$

$$\rightarrow \left(\frac{z_0}{r_0} \right) = \frac{\pi}{8}(2-\nu) \quad (A.24.c)$$

And for rocking,

$$K_{rocking}^{halfspace} = \frac{8Gr_0^3}{3(1-\nu)} \quad (A.25.a)$$

$$K_{rocking}^{halfspace} = K_{rocking}^{cone} = \frac{3E_c I_0}{z_0} \quad (\text{A.25.b})$$

$$\rightarrow \left(\frac{z_0}{r_0} \right) = \frac{9\pi}{8} (1-\nu) \left(\frac{c_p}{c_s} \right)^2 \quad (\text{A.25.c})$$

A.2.3 High Frequency Behavior

Static stiffness coefficients were determined for zero frequency state as the bottom limit. The upper limit is obtained by considering the dynamic stiffness when frequency is approaching infinity.

Spring stiffness coefficients were determined for bottom limit case (Section A.2.2) where frequency approaches to zero (static stiffness). The upper limit case, where frequency tends to infinity, provides dashpot coefficients (dynamic stiffness).

As will be illustrated in the following two sections (Fig. A.5):

High frequency coefficients, C and C_v are independent of apex height. The same relationships for the high-frequency dashpots may be derived simply by assuming that every surface in contact with the soil possesses an inherent amount of radiation damping equal to density times appropriate wave velocity, ρc , per unit area and multiplying this quantity by the contact area A_0 for the translational motions and by the contact moment of inertia I_0 for the rotational motions (Wolf (1994)).

A.2.3.1 Translational Motion at High Frequency

From Fig. A.4.a, by referencing the differential slice (the one illustrated at the bottom), dynamic equilibrium in the vertical direction (normal to foundation area) can be derived as:

$$-N + N + N_{,z} dz - \rho A dz \ddot{u} = 0 \quad (\text{A.26})$$

where, \ddot{u} is the second time derivative (acceleration) of the displacement in the vertical direction.

Substituting Eq. A.7 ($N = E_c A u_{,z}$) to Eq. A.26, one-dimensional wave equation is obtained for the waves propagating in the positive z direction (outgoing waves simulating radiation) as:

$$(uz)_{,zz} - \frac{(zu)''}{c_p^2} = 0 \quad (\text{A.27.a})$$

$$uz = z_0 f\left(t - \frac{z - z_0}{c_p}\right) \quad (\text{A.27.b})$$

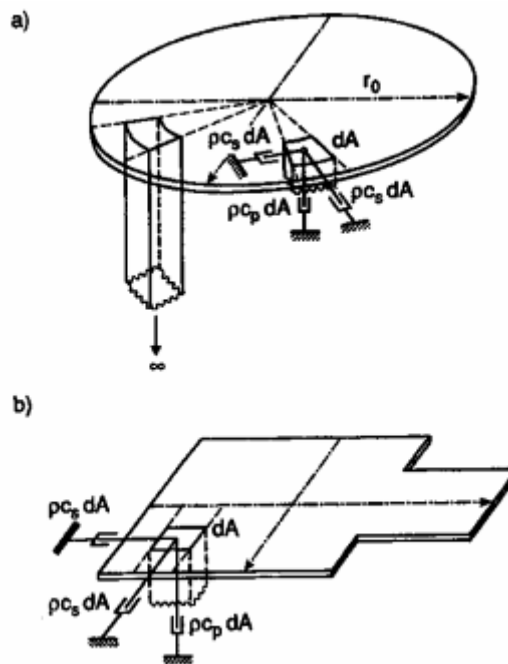


Figure A.5. Representation of high frequency limit of dynamic stiffness (Fig. 2-3; Wolf (1994)). In this Figure: (a) Disk foundation, (b) Foundation of arbitrary shape.

Imposing boundary condition, $u(z=z_0)=u_0$ to Eq. A.27 leads to $f(t)=u_0$. Hence, Eq. A.27 can be rewritten as:

$$u(z,t) = \frac{z_0}{z} u_0 \left(t - \frac{z-z_0}{c_p} \right) \quad (\text{A.28})$$

Solving Eq. A.28 and Eq. A.11 simultaneously will lead to:

$$u_{,z} = -\frac{z_0}{z^2} u_0 \left(t - \frac{z-z_0}{c_p} \right) - \frac{z_0}{zc_p} u_0' \left(t - \frac{z-z_0}{c_p} \right) \quad (\text{A.29})$$

where,

$u_0' \left(t - (z-z_0)/c_p \right)$ = Differentiation of u_0 with respect to the argument $\left(t - (z-z_0)/c_p \right)$. When $z=z_0$ then $u_0' = \dot{u}_0$.

As a result following relation is obtained:

$$P_0 = \frac{E_c A_0}{z_0} u_0 + \rho c_p A_0 \dot{u}_0 \quad (\text{A.30})$$

Expanding constrained elastic modulus in Eq. A.30 leads to general representation for the translational motion:

$$P_0 = \frac{\rho c^2 A_0}{z_0} u_0 + \rho c A_0 \dot{u}_0 = K u_0 + C \dot{u}_0 \quad (\text{A.31})$$

It should be noted that interaction force-displacement relation defined by Eq. A.31 is valid for complete frequency range. For harmonic loading, Eq. A.31 is modified as:

$$P_0(w) = [K + (iw)C] u_0(w) = S(w) u_0(w) \quad (\text{A.32})$$

it is clear from Eq. A.32 that imaginary term, $(iw)C$, dominates the impedance function, $S(w)$, as forcing frequency, w , tends to infinity. Hence, at high frequency limit Eq. A.32 can be expressed as:

$$P_0(w) \approx (iw)Cu_0(w) \rightarrow P_0 \approx Ci\dot{u}_0 \quad (\text{A.33})$$

A.2.3.2 Rotational Motion at High Frequency

Constructing dynamic equilibrium for rotational motion as illustrated at the bottom slice in Fig. A.4.b leads to:

$$-M + M + M_{,z} - \rho I dz \ddot{v} = 0 \quad (\text{A.34})$$

Substituting force displacement relation given at Eq. A.16 to Eq. A.34 leads to:

$$v_{,zz} + \frac{4}{z} v_{,z} - \frac{\ddot{v}}{c_p^2} = 0 \quad (\text{A.35})$$

For high-frequency limit, asymptotic solution of Eq. A.35 in frequency domain for vertically propagating waves in the positive z axis leads to:

$$\ddot{v}(w) = -w^2 v(w) \quad (\text{A.36.a})$$

$$v(w)_{,zz} + \frac{4}{z} v(w)_{,z} + \frac{w^2}{c_p^2} v(w) = 0 \quad (\text{A.36.b})$$

$$v(w) = v_0(w) \left(\frac{z_0}{z} \right)^m e^{-i \frac{w}{c_p} (z-z_0)} \quad (\text{A.36.c})$$

Where,

m is a constant to be determined by substituting Eq. A.36 to Eq. A.35.c in frequency domain.

Coefficient m is determined by multiplying $v(w)$ by e^{+iwt} resulting in a term $e^{+iwt-(Z-z_0)/C_p}$. As a result substituting Eq. A.36.c in Eq. A.36.b, $m^2 - 3m + \frac{iwz}{cp}(2m - 4) = 0$ is obtained. As w approaches infinity, the third term, which can be vanished by $m=2$, governs the equation. Solving derivative of Eq. A.36 for $m=2$ with the following relation:

$$M_0(w) = -E_c I_0 v_0(w),_z \quad (A.37)$$

Finally, substituting the derivative of Eq. A.36.c to Eq. A.37 leads to the interaction moment-rotation relationship in the high-frequency limit as follows:

$$M_0(w) = \left(\frac{2\rho c^2 I_0}{z_0} + iw\rho c I_0 \right) v_0(w)$$

$$\downarrow$$

$$M_0(w) = (K_{v\infty} + iwC_v) v_0(w) \quad (A.38)$$

where,

$K_{v\infty} = 2/3K_v$ (K_v is the static stiffness coefficient for rocking - Eq. A.21).

For torsional degree of freedom propagation wave velocity, $c=c_s$.

For rocking degree of freedom propagation wave propagation velocity is a function of Poisson's ratio, ν .

- For Poisson's ratio, $\nu < 1/3$, wave propagation velocity is $c=c_p$.
- For Poisson's ratio, $1/3 < \nu < 1/2$, wave propagation velocity is $c=2c_s$.

As w approaches infinity, M_0 can be expressed as:

$$M_0 = c_v \dot{v}_0 \quad (A.39)$$

It is clear from Fig. A.5.a and Eq. A.38 that when z_0 tends to infinity cone transforms into a prismatic bar having a static stiffness coefficient $K=0$ and a finite value of

dashpot coefficient per unit area. These coefficients are ρc_s and ρc_p in two horizontal/tangential directions and in the direction of wave propagation (vertical), respectively. Please refer to Table A.2 for the summary of coefficients associated with degrees of freedom.

A.2.4 Effect of Nearly Incompressible Soil

Regarding the static stiffness coefficients obtained from low frequency limit, it was shown that aspect ratio of a cone associated with any degree of freedom is a function of Poisson's ratio (Table A.2). For the case of shearing, where horizontal translation and torsional rotation degrees of freedom are defined by shear wave velocity, c_s , associated aspect ratio is a finite number. However, for vertical translation and rocking motion, where dilatational wave velocity, c_p , dominates the action, aspect ratio is not a finite number and it tends to infinity while Poisson's ratio, ν , approaches $1/2$. This is the case for nearly incompressible soils; i.e. saturated soils. In addition, while c_p tends to infinity associated radiation damping given by dashpot coefficients C and C_v would produce unrealistic (overestimated) results. Same pitfall also exists for rigorous boundary element solution for the dynamic stiffness of the rigid disk. This problem can be solved by introducing two conditions for vertical and rocking degree of freedoms for the range of $1/3 < \nu < 1/2$.

- Radiation damping is capped by twice the shear wave velocity, $2c_s$, instead of dilatational wave velocity, c_p .
- A trapped mass ΔM and a trapped mass moment of inertia ΔM_v at the basemat which increases linearly with Poisson's ratio are introduced.

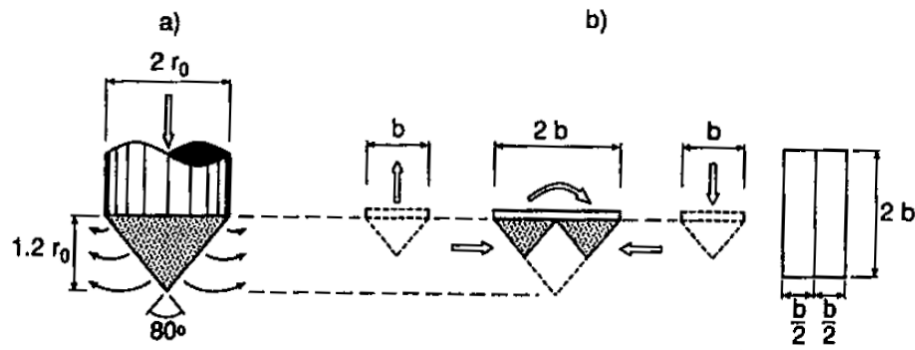


Figure A.6. Analogy of trapped mass to plastic punching (Fig. 2-4; Wolf (1994)). In this Figure: (a) Three-dimensional vertical case (pile), (b) Two-dimensional rocking case (elevation and plan view of roof-shaped volume of soil).

Trapped mass is based on a physical reasoning. In practice it has been observed that blunt end piles were driven in the ground as easy as pointed tip piles. The pile creates its own pointed tip (Fig. A.6.a) and a cone of trapped soil forms and moves as a rigid body with the pile.

By curve fitting, following relations are obtained for vertical (Eq. A.40) and rocking (Eq.A.51) motions, respectively.

$$\Delta M = \mu \rho r_0^2 \quad , \quad \mu = 2.4\pi(\nu - 1/3) \quad (\text{A.40})$$

$$\Delta M_v = \mu_v \rho r_0^5 \quad , \quad \mu_v = 0.3\pi(\nu - 1/3) \quad (\text{A.41})$$

The introduction of trapped mass and limited wave propagation velocity for nearly incompressible soil is questioned by Wolf (1994) for its validity on violating the basic assumption; doubly asymptotic approximation. It has been stated that:

- For low-frequency/static case there is no problem since cone model parameters are based on disk on elastic half-space solution.
- For high-frequency case both models' dynamic stiffness coefficients lead to infinity:
 - For $\nu=1/2$, real valued mass term dominates (no effect of the dashpot).

- For $\nu < 1/2$, trapped mass term is eliminated and damping term starts to dominate in the disk on elastic half-space solution.
- In either way, when dynamic stiffness approaches infinity resulting deformation goes zero for high-frequency excitation.

A.2.5. Discrete Element Model

The application of the cone model as a simple mathematical model is summarized in the proceeding two sections for both translational and rotational degrees of freedom of rigid disk.

A.2.5.1 Translational Motion

General formulation for interaction-displacement relation in time domain for translational motion of massless surface basemat is as follows (Fig. A.7):

$$P_0(t) = Ku_0(t) + C\dot{u}_0(t) + \Delta M\ddot{u}_0(t) \quad (\text{A.42})$$

where,

$K = \frac{\rho c^2 A_0}{z_0}$ is the frequency independent stiffness coefficient (Eq. A.14).

$C = \rho c A_0$ is the frequency independent dashpot coefficient (Eq. A.31).

$\Delta M = \mu \rho r_0^2$ is the trapped mass *only* for vertical motion for $1/3 < \nu < 1/2$ (Eq. A.40).

The dynamic stiffness is expressed with non-dimensional coefficients as:

$$S(a_0) = K [k(a_0) + ia_0 c(a_0)] \quad (\text{A.43})$$

where,

$a_0 = \frac{\omega r_0}{c_s} = \frac{r_0}{z_0} \frac{c}{c_s} b_0$ is the dimensionless frequency parameter.

$k(a_0) = 1 - \frac{\mu}{\pi} \frac{z_0}{r_0} \frac{c_s^2}{c^2} a_0^2$ is the real part – stiffness term of the dynamic stiffness relation.

$c(a_0) = \frac{z_0}{r_0} \frac{c_s}{c}$ is the imaginary part – damping term of the dynamic stiffness relation.

Accuracy of the cone model in horizontal translational motion is evaluated by comparing with the values calculated by Veletsos and Wei (1971) as a function of dimensionless frequency parameter, a_0 , for $\nu=0, 1/3$ and $1/2$ (Fig. A.8) and a good agreement are found.

Next, vertical translational motion as a function of dimensionless frequency parameter, a_0 , of the cone model is compared with the values obtained from Veletsos and Verbic (1974) and Luco and Mita (1987b) for Poisson's ratio of $\nu=0, 1/3, 1/2$ and 0.45 (Fig. A.9). For values $\nu=1/2$ and 0.45 , k_v , which is described as a second degree parabola, demonstrate a decreasing trend as a result of the effect of the inertial load for intermediate and high-frequency ranges. In other words dynamic stiffness is governed by damping coefficient, which is accurate for intermediate and high-frequency ranges. However, for low frequency range ($a_0 < 2$) for $\nu < 1/3$ cone model overestimates the damping.

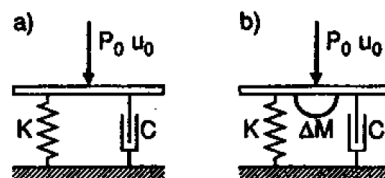


Figure A.7. Discrete element model for translation in the direction normal to foundation (Fig. 2-5; Wolf (1994)). In this Figure: (a) Horizontal motion and vertical motion for compressible soil, (b) Vertical motion for nearly incompressible soil.

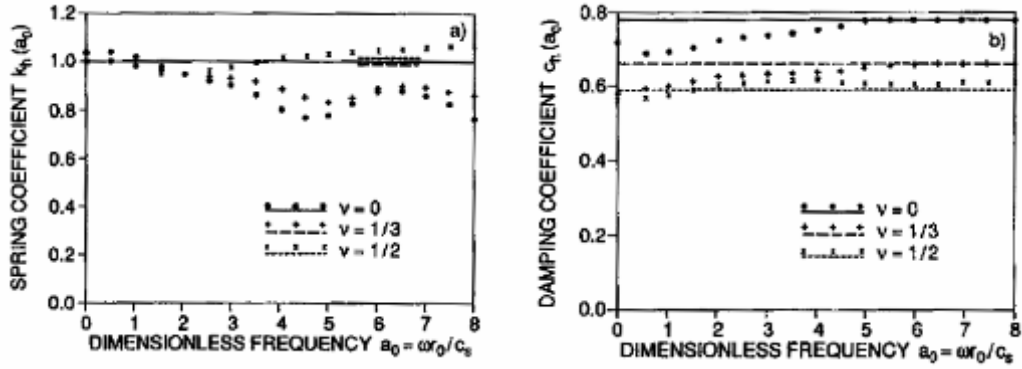


Figure A.8. Dynamic stiffness coefficients for harmonic loading of disk on homogeneous halfspace in horizontal motion for Poisson's Ratio of $\nu=0$, $1/3$ and $1/2$ (Fig. 2-6; Wolf (1994)). In this Figure, accuracy of cone model is compared to that of Veletsos and Wei (1971).

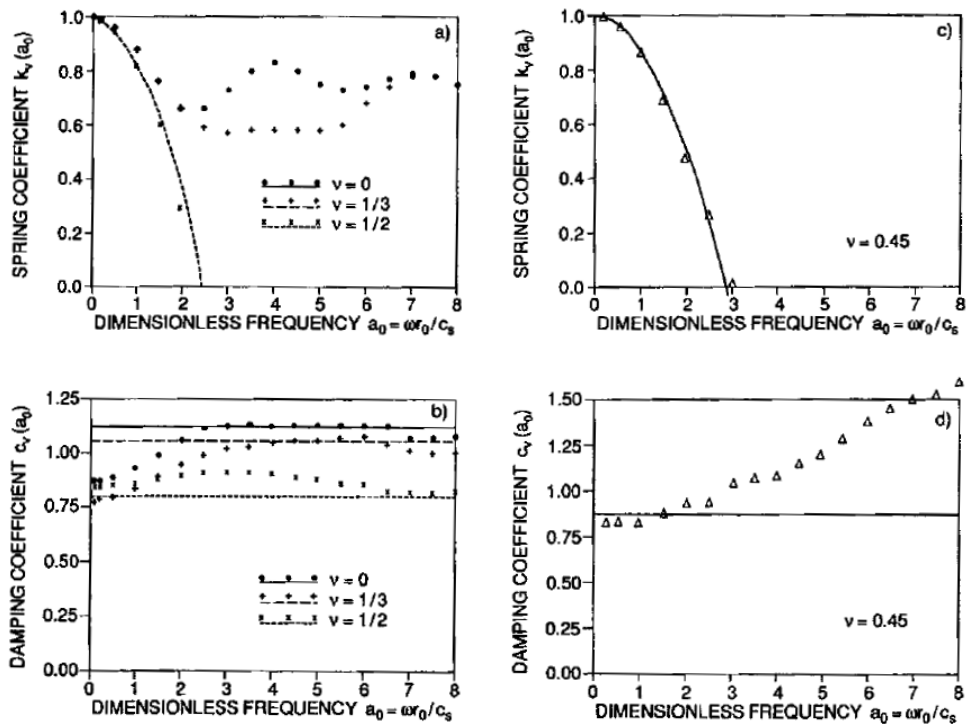


Figure A.9. Dynamic-stiffness coefficient for harmonic loading of disk on homogeneous half-space in vertical motion for Poisson's Ratio of $\nu=0$, $1/3$, 0.45 and $1/2$ (Fig. 2-7; Wolf (1994)). In this Figure, accuracy of cone model is compared to that of Veletsos and Verbic (1974) and Luco and Mita (1987b).

A.2.5.2 Rotational Motion

The illustration given in Fig. A.10.c is the discrete element model of truncated cone model in rotation. Unlike translational model there is an additional rotational degree of freedom defined between rigid support and the basemat. The massless model has a rotational spring with stiffness coefficient, $-K_v/3$, connecting basemat and internal degree of freedom, and a dashpot with coefficient, $-C_v$, connecting internal degree of freedom and the rigid support. Negative coefficients are not real and are used for best fit. The negative coefficients are avoided in the next model with internal mass, namely monkey-tail model. It is claimed by the author that in practical applications either of the *discrete-element models with one internal degree of freedom* shown in Fig. A.10.c may be attached to the underside of the structural system as an *exact equivalent representation of the rotational cone*. The dynamic-stiffness relation for rocking and torsion for harmonic loading is given as:

$$S_v(a_0) = K_v [k_v(a_0) + ia_0 c_v(a_0)] \quad (\text{A.44})$$

where,

K_v is zero-frequency stiffness given by Eq. A.23.

$$k_v(a_0) = 1 - \frac{4}{3} \frac{\mu_v}{\pi} \frac{z_0}{r_0} \frac{c_s^2}{c^2} a_0^2 - \frac{1}{3} \frac{a_0^2}{\left(\frac{r_0 c}{z_0 c_s}\right)^2 + a_0^2} \text{ is the real part / stiffness term.}$$

$$c_v(a_0) = \frac{z_0}{3r_0} \frac{c_s}{c} \frac{a_0^2}{\left(\frac{r_0 c}{z_0 c_s}\right)^2 + a_0^2} \text{ is the imaginary part / damping term.}$$

For the torsional motion wave propagation velocity, $c=c_s$ and $\mu_v=0$ for all Poisson's ratio, ν , and corresponding opening angle for apex is $z_0/r_0=0.884$. For rocking motion $c=c_p$ and $\mu_v=0$ for $\nu \leq 1/3$, $c=2c_s$ and μ_v is defined in Equation A.51 for $1/3 < \nu < 1/2$. The opening angle, z_0/r_0 , for rocking motion for all ν is given in Eq. A.25.

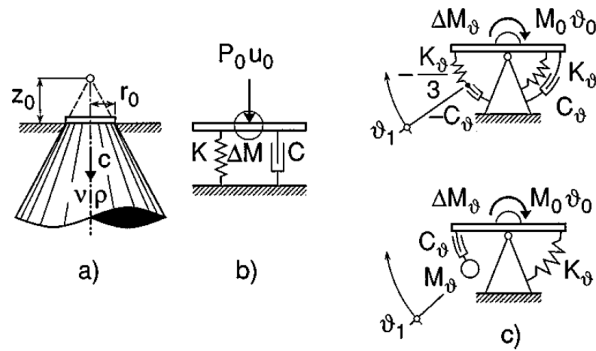


Figure A.10. Cone model and equivalent discrete-element model (Fig.5; Wolf (1997)). In this Figure: (a) Cone, (b) Discrete-element model for translation, (c) Discrete-element model for rotation.

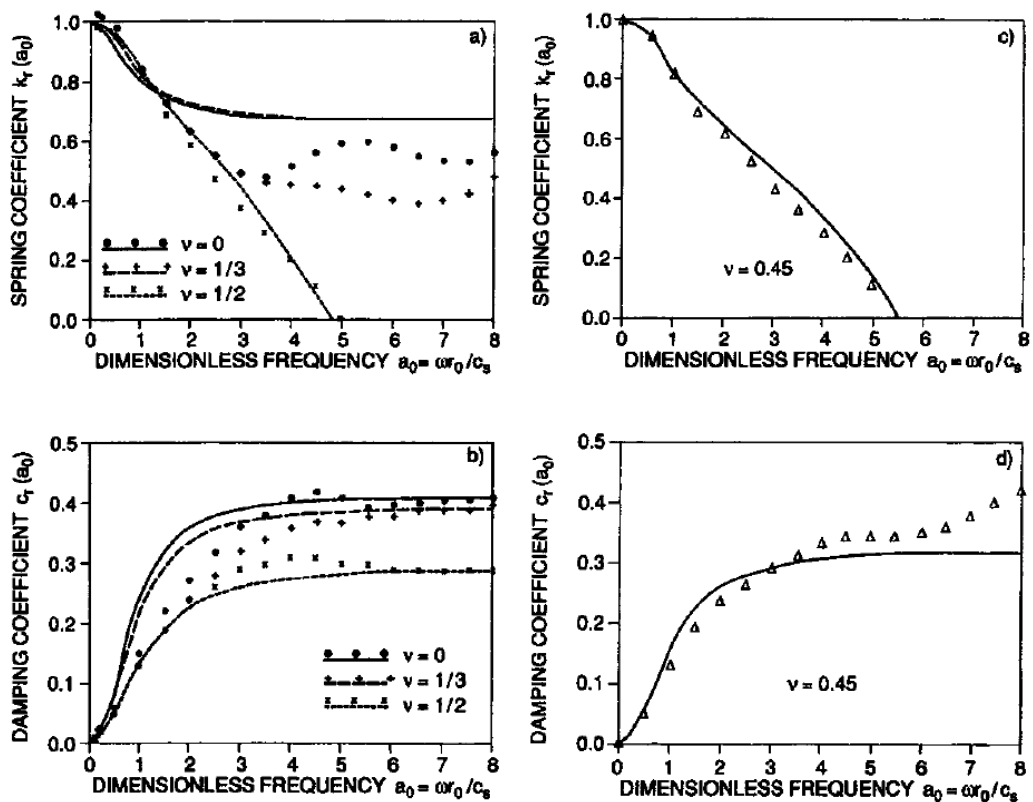


Figure A.11. Dynamic-stiffness coefficient for harmonic loading of disk on homogeneous halfspace in rocking motion for Poisson's Ratio of $\nu=0$, $1/3$, 0.45 and $1/2$ (Fig. 2-7; Wolf (1994)). In this Figure, accuracy of cone model is compared to that of Veletsos and Wei, 1971 and Luco and Mita (1987b).

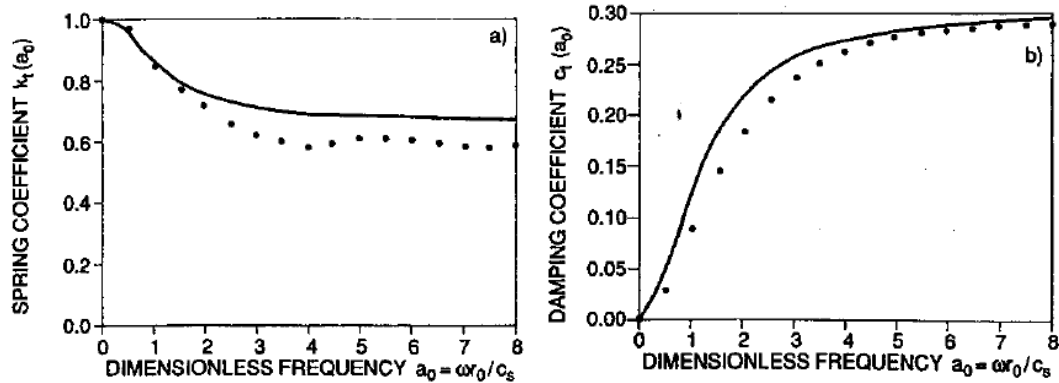


Figure A.12. Dynamic stiffness coefficients for harmonic loading of disk on homogeneous halfspace in torsional motion (Fig. 2-20; Wolf (1994)). In this Figure, accuracy of cone model is compared to that of Veletsos and Nair (1974).

The torsional motion is analyzed by comparing cone's results with values of Veletsos and Nair (1974) in Fig. A.11 for all ν . The rocking motion is illustrated in Fig. A.12 for which the cones results are compared with values of Veletsos and Wei (1971) and Luco and Mita (1987b) for $\nu=0, 1/3, 1/2$ and 0.45 .

From Fig. A.12 it is clear that in general the agreement is satisfactory for all ν . It must be noted that for $\nu \leq 1/3$ and lower-frequency, which has a practical importance, the damping is overestimated slightly. The same behavior is also observed for translational cones. For other ranges cone models are accurate.

The power of the simple models lies in their applicability directly in the time domain by the virtue of regular finite element programs. However, there is a pitfall when using with seismic excitation. The effective seismic input motion can not be applied at the far end of the simple model (rigid support) of the soil that contains masses. Instead, in the case of total displacement formulation, the foundation input motion should be applied to the foundation system at the connection interface of the superstructure without the presence of superstructure. Then, the obtained driving forces are applied at the interface node of the complete dynamic system.

APPENDIX B

EARTHQUAKE GROUND MOTION RECORDS

Complete listing of SETC and SETD earthquake ground motion acceleration records, which conform to NEHRP Site Classes C and D, respectively; are given in Tables B.1 - B.3. Mean, standard deviation, mean plus one standard deviation, median, minimum and maximum values of spectral accelerations for SETC and SETD records calculated at the fundamental period of frame models are given in Table B.4. Scale factors for the earthquake acceleration records which are used in analysis groups SC and SCR2 are given in Tables B.5 – B.8. Mean plus one standard deviation response spectra of Analysis Group II (SC) and Analysis Group III (SCR2) records computed at the initial and effective fundamental periods of frame models, respectively, are given in Figs. B.1 – B.14.

Table B.1. SET-C1 and SET-D1 Ground motion acceleration records conforming to NEHRP Site Class C and D, respectively: Records containing pulse effects.

SET-C1 - Ground Motion Acceleration Records Conforming to NEHRP Site Class C: Records Containing Pulse Effects								
Ref. No.	Rec. No.	Eq. Name	Eq. Mag.	Year	Station Name	ClstD (km)	Vs30 (m/s)	PGA (g)
3	1548	Chi-Chi, Taiwan	7.62	1999	TCU128	13.15	599.64	0.17
4	1208	Chi-Chi, Taiwan	7.62	1999	CHY046	24.11	442.15	0.18
5	1535	Chi-Chi, Taiwan	7.62	1999	TCU109	13.08	473.9	0.16
6	1476	Chi-Chi, Taiwan	7.62	1999	TCU029	28.05	473.9	0.20
7	1482	Chi-Chi, Taiwan	7.62	1999	TCU039	19.9	540.66	0.21
9	1479	Chi-Chi, Taiwan	7.62	1999	TCU034	35.69	393.77	0.25
11	1193	Chi-Chi, Taiwan	7.62	1999	CHY024	9.64	427.73	0.28
12	1546	Chi-Chi, Taiwan	7.62	1999	TCU122	9.35	475.46	0.26
14	1202	Chi-Chi, Taiwan	7.62	1999	CHY035	12.65	473.9	0.25
16	2461	Chi-Chi, Taiwan-03	6.2	1999	CHY028	24.38	542.61	0.17
18	2655	Chi-Chi, Taiwan-03	6.2	1999	TCU122	19.3	475.46	0.20
20	2495	Chi-Chi, Taiwan-03	6.2	1999	CHY080	22.37	553.4	0.48
21	2703	Chi-Chi, Taiwan-04	6.2	1999	CHY028	17.7	542.61	0.20
25	3274	Chi-Chi, Taiwan-06	6.3	1999	CHY035	41.58	473.9	0.17
29	369	Coalinga-01	6.36	1983	Slack Canyon	27.46	684.935	0.17
33	796	Loma Prieta	6.93	1989	SF - Presidio	77.43	594.47	0.20
35	739	Loma Prieta	6.93	1989	Anderson Dam (Downstream)	20.26	488.77	0.24
42	1009	Northridge-01	6.69	1994	LA - Wadsworth VA Hospital North	23.6	392.24	0.25
45	963	Northridge-01	6.69	1994	Castaic - Old Ridge Route	20.72	450.28	0.57
46	33	Parkfield	6.19	1966	Temblor pre-1969	15.96	527.92	0.36

SET-D1 - Ground Motion Acceleration Records Conforming to NEHRP Site Class D: Records Containing Pulse Effects								
Ref. No.	Rec. No.	Eq. Name	Eq. Mag.	Year	Station Name	ClstD (km)	Vs30 (m/s)	PGA (g)
1	829	Cape Mendocino	7.01	1992	Rio Dell Overpass - FF	14.33	311.8	0.55
2	826	Cape Mendocino	7.01	1992	Eureka - Myrtle & West	41.97	338.5	0.18
3	1536	Chi-Chi, Taiwan	7.62	1999	TCU110	11.60	212.7	0.18
5	1246	Chi-Chi, Taiwan	7.62	1999	CHY104	18.04	223.2	0.19
6	1209	Chi-Chi, Taiwan	7.62	1999	CHY047	24.14	272.6	0.19
7	1484	Chi-Chi, Taiwan	7.62	1999	TCU042	26.32	272.6	0.25
9	2618	Chi-Chi, Taiwan-03	6.2	1999	TCU065	26.05	305.9	0.35
12	3275	Chi-Chi, Taiwan-06	6.3	1999	CHY036	46.19	233.1	0.20
16	359	Coalinga-01	6.36	1983	Parkfield - Vineyard Cany 1E	26.38	338.539	0.23
21	165	Imperial Valley-06	6.53	1979	Chihuahua	7.29	274.5	0.27
22	170	Imperial Valley-06	6.53	1979	EC County Center FF	7.31	192.05	0.24
26	766	Loma Prieta	6.93	1989	Gilroy Array #2	11.07	270.84	0.37
27	754	Loma Prieta	6.93	1989	Coyote Lake Dam (Downst)	20.8	295.01	0.18
29	778	Loma Prieta	6.93	1989	Hollister Diff. Array	24.82	215.54	0.28
30	783	Loma Prieta	6.93	1989	Oakland - Outer Harbor Wharf	74.26	248.62	0.29
31	758	Loma Prieta	6.93	1989	Emeryville - 6363 Christie	76.97	198.74	0.27
37	1077	Northridge-01	6.69	1994	Santa Monica City Hall	26.45	336.2	0.90
43	725	Superstition Hills-02	6.54	1987	Poe Road (temp)	11.16	207.469	0.45
44	721	Superstition Hills-02	6.54	1987	El Centro Imp. Co. Cent	18.2	192.05	0.36
45	729	Superstition Hills-02	6.54	1987	Wildlife Liquef. Array	23.85	207.469	0.21

Table B.2. SET-C2 Ground motion acceleration records conforming to NEHRP Site Class C: Records without pulse effects.

SET-C2 - Ground Motion Acceleration Records Conforming to NEHRP Site Class C: Records Without Pulse Effects								
Ref. No.	Rec. No.	Eq. Name	Eq. Mag.	Year	Station Name	ClstD (km)	Vs30 (m/s)	PGA (g)
1	830	Cape Mendocino	7.01	1992	Shelter Cove Airport	28.78	513.703	0.23
2	1234	Chi-Chi, Taiwan	7.62	1999	CHY086	28.42	553.4	0.20
8	1350	Chi-Chi, Taiwan	7.62	1999	ILA067	38.82	553.4	0.20
10	1184	Chi-Chi, Taiwan	7.62	1999	CHY010	19.96	473.9	0.23
13	1186	Chi-Chi, Taiwan	7.62	1999	CHY014	34.18	473.9	0.26
15	1205	Chi-Chi, Taiwan	7.62	1999	CHY041	19.83	492.26	0.64
17	2623	Chi-Chi, Taiwan-03	6.2	1999	TCU072	22.53	468.14	0.17
19	2622	Chi-Chi, Taiwan-03	6.2	1999	TCU071	16.46	624.85	0.38
22	3208	Chi-Chi, Taiwan-05	6.2	1999	TCU109	54.11	473.9	0.19
23	2942	Chi-Chi, Taiwan-05	6.2	1999	CHY024	48.65	427.73	0.26
24	3268	Chi-Chi, Taiwan-06	6.3	1999	CHY028	33.61	542.61	0.15
26	3278	Chi-Chi, Taiwan-06	6.3	1999	CHY041	46.76	492.26	0.18
27	352	Coalinga-01	6.36	1983	Parkfield - Gold Hill 3W	39.12	438.339	0.14
28	330	Coalinga-01	6.36	1983	Parkfield - Cholame 4W	46.35	438.339	0.14
30	1618	Duzce, Turkey	7.14	1999	Lamont 531	8.03	659.6	0.16
31	1787	Hector Mine	7.13	1999	Hector	11.66	684.935	0.34
32	164	Imperial Valley-06	6.53	1979	Cerro Prieto	15.19	659.6	0.17
34	769	Loma Prieta	6.93	1989	Gilroy Array #6	18.33	663.31	0.17
36	801	Loma Prieta	6.93	1989	San Jose - Santa Teresa Hills	14.69	671.77	0.28
37	459	Morgan Hill	6.19	1984	Gilroy Array #6	9.86	663.31	0.29
38	537	N. Palm Springs	6.06	1986	Silent Valley - Poppet Flat	17.03	684.935	0.14
39	1031	Northridge-01	6.69	1994	Leona Valley #5 - Ritter	37.8	445.983	0.15
40	1023	Northridge-01	6.69	1994	Lake Hughes #9	25.36	670.84	0.22
41	1020	Northridge-01	6.69	1994	Lake Hughes #12A	21.36	602.1	0.26
43	1010	Northridge-01	6.69	1994	LA - Wadsworth VA Hospital South	23.6	413.81	0.38
44	1006	Northridge-01	6.69	1994	LA - UCLA Grounds	22.49	398.42	0.49
47	73	San Fernando	6.61	1971	Lake Hughes #9	22.57	670.84	0.16
48	57	San Fernando	6.61	1971	Castaic - Old Ridge Route	22.63	450.28	0.33
49	265	Victoria, Mexico	6.33	1980	Cerro Prieto	14.37	659.6	0.64
50	646	Whittier Narrows-01	5.99	1987	LB - Rancho Los Cerritos	28.56	405.189	0.19

Table B.3. SET-D2 Ground motion acceleration records conforming to NEHRP Site Class D: Records without pulse effects.

SET-D2 - Ground Motion Acceleration Records Conforming to NEHRP Site Class D: Records Without Pulse Effects								
Ref. No.	Rec. No.	Eq. Name	Eq. Mag.	Year	Station Name	ClstD (km)	Vs30 (m/s)	PGA (g)
4	1203	Chi-Chi, Taiwan	7.62	1999	CHY036	16.06	233.1	0.29
8	1236	Chi-Chi, Taiwan	7.62	1999	CHY088	37.48	272.6	0.22
10	3222	Chi-Chi, Taiwan-05	6.2	1999	TCU141	60.33	215.0	0.20
11	2955	Chi-Chi, Taiwan-05	6.2	1999	CHY047	71.26	272.6	0.25
13	3282	Chi-Chi, Taiwan-06	6.3	1999	CHY047	54.47	272.6	0.24
14	3306	Chi-Chi, Taiwan-06	6.3	1999	CHY082	61.76	193.69	0.20
15	368	Coalinga-01	6.36	1983	Pleasant Valley P.P. - yard	8.41	257.38	0.59
17	340	Coalinga-01	6.36	1983	Parkfield - Fault Zone 16	27.67	338.539	0.20
18	338	Coalinga-01	6.36	1983	Parkfield - Fault Zone 14	29.48	338.539	0.29
19	334	Coalinga-01	6.36	1983	Parkfield - Fault Zone 1	41.99	338.539	0.20
20	1615	Duzce, Turkey	7.14	1999	Lamont 1062	9.15	338	0.26
23	167	Imperial Valley-06	6.53	1979	Compuertas	15.3	274.5	0.19
24	169	Imperial Valley-06	6.53	1979	Delta	22.03	274.5	0.36
25	848	Landers	7.28	1992	Coolwater	19.74	271.441	0.42
28	770	Loma Prieta	6.93	1989	Gilroy Array #7	22.68	333.85	0.32
32	460	Morgan Hill	6.19	1984	Gilroy Array #7	12.07	333.85	0.19
33	456	Morgan Hill	6.19	1984	Gilroy Array #2	13.69	270.84	0.21
34	530	N. Palm Springs	6.06	1986	Palm Springs Airport	10.84	207.469	0.19
35	988	Northridge-01	6.69	1994	LA - Century City CC North	23.41	277.98	0.26
36	995	Northridge-01	6.69	1994	LA - Hollywood Stor FF	24.03	316.46	0.36
38	985	Northridge-01	6.69	1994	LA - Baldwin Hills	29.88	297.07	0.24
39	1000	Northridge-01	6.69	1994	LA - Pico & Sentous	31.33	270.19	0.19
40	1032	Northridge-01	6.69	1994	Leona Valley #6	38.03	327.44	0.18
41	30	Parkfield	6.19	1966	Cholame - Shandon Array #5	9.58	289.56	0.45
42	68	San Fernando	6.61	1971	LA - Hollywood Stor FF	22.77	316.46	0.22
46	668	Whittier Narrows-01	5.99	1987	Norwalk - Imp Hwy, S Grnd	20.42	270.19	0.25
47	635	Whittier Narrows-01	5.99	1987	LA - Hollywood Stor FF	24.08	316.46	0.22
48	625	Whittier Narrows-01	5.99	1987	Inglewood - Union Oil	25.86	316.02	0.30
49	627	Whittier Narrows-01	5.99	1987	LA - Baldwin Hills	25.94	297.07	0.16
50	700	Whittier Narrows-01	5.99	1987	Tarzana - Cedar Hill	41.22	257.21	0.65

Table B.4. Mean (μ), standard deviation (σ), mean plus one standard deviation ($\mu+\sigma$), median, minimum (Min.) and maximum (Max.) values of spectral accelerations for SETC and SETD records calculated at the fundamental period of frame models.

Model	3SAC	4KatF	4KatR	5KatS2	8KatS2	12KatF	12KatR
Tn (sec)	<i>1.03</i>	<i>1.18</i>	<i>0.72</i>	<i>0.81</i>	<i>1.45</i>	<i>2.19</i>	<i>1.26</i>
Records Containing Pulse Effects (SET-C1)							
μ	0.32	0.28	0.40	0.38	0.22	0.14	0.25
σ	0.23	0.20	0.22	0.25	0.14	0.08	0.17
$\mu+\sigma$	0.55	0.47	0.61	0.63	0.36	0.22	0.43
Median	0.26	0.23	0.33	0.31	0.21	0.13	0.23
Min.	0.08	0.06	0.10	0.08	0.04	0.04	0.05
Max.	1.39	1.22	1.02	1.22	0.68	0.33	1.03
Records Containing Pulse Effects (SET-D1)							
μ	0.35	0.32	0.47	0.42	0.29	0.18	0.32
σ	0.13	0.12	0.20	0.17	0.12	0.11	0.13
$\mu+\sigma$	0.48	0.44	0.67	0.58	0.41	0.28	0.45
Median	0.34	0.31	0.45	0.41	0.26	0.16	0.31
Min.	0.14	0.13	0.16	0.13	0.12	0.05	0.11
Max.	0.68	0.71	0.92	0.82	0.61	0.60	0.70
Records Without Pulse Effects (SET-C2)							
μ	0.18	0.15	0.28	0.23	0.11	0.05	0.14
σ	0.13	0.13	0.19	0.15	0.09	0.04	0.11
$\mu+\sigma$	0.31	0.28	0.46	0.38	0.20	0.09	0.25
Median	0.17	0.14	0.25	0.23	0.09	0.04	0.12
Min.	0.02	0.01	0.03	0.03	0.01	0.00	0.01
Max.	0.61	0.62	0.91	0.65	0.46	0.18	0.51
Records Without Pulse Effects (SET-D2)							
μ	0.21	0.17	0.32	0.27	0.13	0.07	0.15
σ	0.21	0.16	0.24	0.20	0.10	0.05	0.13
$\mu+\sigma$	0.42	0.33	0.56	0.48	0.23	0.12	0.29
Median	0.15	0.13	0.22	0.20	0.08	0.05	0.12
Min.	0.03	0.03	0.07	0.05	0.02	0.01	0.03
Max.	1.09	1.00	1.19	1.01	0.42	0.22	0.77
All Records(SETC)							
μ	0.23	0.20	0.33	0.29	0.15	0.09	0.18
σ	0.19	0.17	0.21	0.21	0.12	0.07	0.15
$\mu+\sigma$	0.42	0.37	0.53	0.50	0.28	0.16	0.33
Median	0.21	0.17	0.31	0.28	0.13	0.06	0.15
Min.	0.02	0.01	0.03	0.03	0.01	0.00	0.01
Max.	1.39	1.22	1.02	1.22	0.68	0.33	1.03
All Records (SETD)							
μ	0.27	0.23	0.38	0.33	0.19	0.11	0.22
σ	0.19	0.16	0.23	0.20	0.14	0.09	0.15
$\mu+\sigma$	0.46	0.39	0.62	0.53	0.33	0.21	0.37
Median	0.22	0.20	0.32	0.29	0.18	0.10	0.18
Min.	0.03	0.03	0.07	0.05	0.02	0.01	0.03
Max.	1.09	1.00	1.19	1.01	0.61	0.60	0.77

Table B.5. Scale factors for analysis group “SC” for SETC earthquake ground motion acceleration records conforming to NEHRP Site Class C.

SETC - NEHRP Site Class C							
Model <i>T_i</i> (sec)	3SAC <i>1.03</i>	4KatF <i>1.18</i>	4KatR <i>0.72</i>	5KatS2 <i>0.81</i>	8KatS2 <i>1.45</i>	12KatFS <i>2.19</i>	12KatRS <i>1.26</i>
<i>EQ No.1</i>	1.951	2.173	2.985	2.769	1.292	1.404	1.723
<i>2</i>	2.159	2.215	2.170	1.550	1.587	0.938	2.587
<i>3</i>	3.559	3.278	2.534	2.767	3.319	1.146	3.446
<i>4</i>	1.890	2.084	1.311	1.758	1.679	1.956	1.869
<i>5</i>	2.209	1.615	1.502	1.313	1.181	0.703	1.464
<i>6</i>	1.259	1.983	1.674	1.685	1.609	0.678	1.805
<i>7</i>	3.012	2.981	1.901	2.280	3.111	1.951	2.730
<i>8</i>	1.938	2.452	1.841	1.782	2.445	1.451	3.035
<i>9</i>	1.616	1.742	1.765	2.287	1.399	0.767	1.396
<i>10</i>	2.387	2.333	1.789	1.997	1.572	0.962	2.117
<i>11</i>	2.427	2.979	1.993	2.281	2.105	1.446	3.171
<i>12</i>	2.367	1.678	2.068	2.807	1.320	1.426	1.509
<i>13</i>	1.158	1.343	1.175	2.049	1.332	0.982	1.630
<i>14</i>	1.491	1.749	2.210	2.079	1.569	0.957	1.728
<i>15</i>	2.402	1.577	1.407	1.854	1.775	1.650	1.645
<i>16</i>	1.410	1.246	2.275	1.977	1.466	1.031	1.168
<i>17</i>	0.924	0.875	1.005	0.789	0.588	1.192	0.667
<i>18</i>	1.097	1.532	0.763	0.797	1.097	1.773	1.279
<i>19</i>	1.449	1.705	1.298	1.305	2.768	1.988	2.411
<i>20</i>	2.411	2.098	1.883	2.099	1.832	1.791	1.911
<i>21</i>	2.212	1.712	1.834	1.982	1.968	1.590	1.777
<i>22</i>	6.206	4.523	3.202	4.409	5.229	3.979	4.179
<i>23</i>	0.404	0.386	0.604	0.516	0.540	1.117	0.414
<i>24</i>	0.959	1.033	0.927	1.178	1.615	5.188	1.160
<i>25</i>	7.021	7.900	6.131	5.673	7.706	4.753	8.975
<i>26</i>	6.768	7.843	6.417	7.764	8.136	3.774	7.746
<i>27</i>	1.485	1.128	1.346	1.644	1.120	2.629	0.944
<i>28</i>	3.104	2.775	2.304	2.892	2.057	2.555	2.444
<i>29</i>	2.492	2.468	2.063	1.644	2.507	2.753	2.464
<i>30</i>	1.920	1.236	2.006	2.280	2.400	5.131	1.369
<i>31</i>	2.813	3.643	1.777	2.554	3.783	4.412	3.550
<i>32</i>	2.015	1.725	1.537	1.673	1.645	2.138	1.524
<i>33</i>	2.727	3.170	1.665	2.151	2.548	2.612	2.538
<i>34</i>	3.554	3.743	1.039	2.108	2.320	3.060	2.679
<i>35</i>	1.932	1.520	1.835	2.171	1.753	1.257	1.674
<i>36</i>	2.673	2.717	1.921	1.655	2.230	3.056	2.673
<i>37</i>	1.095	1.233	0.679	0.613	0.943	1.170	1.146
<i>38</i>	0.645	0.758	0.648	0.652	0.638	0.920	0.956
<i>39</i>	2.661	2.922	3.590	4.234	4.538	6.391	3.169
<i>40</i>	4.897	3.420	4.804	6.999	4.575	4.521	2.964
<i>41</i>	12.375	18.470	12.272	13.571	17.281	9.708	16.197
<i>42</i>	12.356	11.244	9.052	10.850	8.237	9.977	8.759
<i>43</i>	1.725	1.199	1.453	1.299	1.164	1.199	1.086
<i>44</i>	1.105	1.437	0.804	0.584	2.011	1.964	1.733
<i>45</i>	1.854	1.802	1.533	1.514	2.428	1.872	1.795
<i>46</i>	1.247	1.631	1.346	1.136	1.866	2.716	1.669
<i>47</i>	1.733	1.958	1.456	1.268	1.300	0.965	1.708
<i>48</i>	1.720	1.586	1.533	1.466	1.329	0.911	1.566
<i>49</i>	1.583	2.366	0.727	1.015	2.361	2.048	2.596
<i>50</i>	1.353	1.798	0.512	0.765	2.310	1.527	1.801

Table B.5. (Continued)

SETC - NEHRP Site Class C							
Model <i>T_i</i> (sec)	3SAC <i>1.03</i>	4KatF <i>1.18</i>	4KatR <i>0.72</i>	5KatS2 <i>0.81</i>	8KatS2 <i>1.45</i>	12KatFS <i>2.19</i>	12KatRS <i>1.26</i>
EQ. No. 51	0.872	1.399	1.154	1.260	1.774	1.722	1.723
52	1.059	2.062	0.611	0.937	1.850	1.429	1.958
53	7.391	5.055	4.099	4.935	4.282	3.954	4.675
54	5.100	6.800	3.421	4.227	7.594	4.981	8.009
55	3.647	3.158	2.060	1.906	2.598	3.249	2.872
56	3.981	4.148	6.385	5.279	3.028	2.184	3.702
57	3.479	5.367	2.914	3.483	6.994	3.879	6.660
58	3.430	5.015	4.344	4.719	5.890	3.999	5.714
59	6.037	7.689	2.825	3.809	6.812	4.270	7.245
60	6.449	7.432	4.325	4.214	7.180	6.608	7.363
61	0.955	1.365	1.863	1.555	1.308	0.897	1.311
62	1.683	1.483	1.802	1.584	1.061	1.157	1.254
63	2.694	2.013	2.510	2.184	2.213	2.227	1.799
64	1.467	1.280	1.384	1.401	1.645	1.796	1.265
65	1.643	1.468	3.873	3.231	1.494	1.509	1.361
66	2.224	2.046	2.774	2.920	1.618	2.658	1.856
67	2.775	3.777	1.200	2.144	4.410	2.181	3.838
68	3.916	4.524	2.593	2.519	3.687	3.110	4.288
69	1.931	2.446	2.554	2.271	1.656	2.680	2.738
70	4.300	6.889	3.191	2.885	3.480	3.853	5.682
71	0.822	0.618	1.532	1.116	0.689	0.940	0.628
72	0.785	0.554	1.249	1.274	0.426	0.464	0.487
73	3.125	1.843	2.217	2.321	1.994	1.607	1.828
74	0.998	0.893	1.177	0.916	1.403	1.113	1.030
75	1.554	2.543	2.288	2.525	1.835	1.405	2.337
76	1.467	1.319	2.461	2.376	1.356	1.569	1.337
77	1.666	2.111	1.144	1.251	1.304	1.795	1.535
78	1.226	1.469	1.671	1.292	1.042	1.198	1.232
79	2.520	2.140	1.393	1.394	2.757	4.388	2.502
80	0.546	0.505	0.726	0.582	0.601	1.019	0.517
81	18.453	22.511	13.279	11.418	22.570	17.845	23.960
82	8.521	11.017	13.964	8.699	19.422	14.625	12.683
83	0.866	1.176	1.352	1.067	2.360	2.233	1.467
84	2.032	2.517	2.659	1.744	2.195	0.918	2.571
85	9.934	7.627	6.382	7.171	5.429	3.914	6.169
86	8.799	9.599	6.879	7.181	7.992	3.374	9.027
87	7.449	9.142	5.376	4.680	5.970	2.351	8.137
88	4.165	6.023	4.821	5.041	5.513	2.475	5.772
89	0.878	0.868	1.029	1.237	0.724	0.711	0.802
90	1.193	1.467	0.994	0.844	1.203	0.942	1.410
91	1.476	2.544	0.980	1.190	1.531	1.539	2.513
92	1.251	1.210	1.404	1.444	0.792	0.547	1.098
93	7.225	6.809	7.751	7.583	5.951	6.426	7.640
94	9.689	10.744	7.507	6.659	7.494	4.795	11.039
95	1.840	2.088	2.088	1.721	2.376	2.736	2.284
96	0.996	1.306	1.090	0.901	1.379	1.571	1.286
97	0.514	0.457	0.889	0.782	0.613	0.962	0.509
98	1.206	2.002	1.246	1.236	2.014	1.134	2.492
99	1.294	1.738	1.144	1.060	2.606	2.918	1.997
100	1.605	1.801	1.264	1.247	2.756	3.310	2.285

Table B.6. Scale factors for analysis group “SC” for SETD earthquake ground motion acceleration records conforming to NEHRP Site Class D.

SETD - NEHRP Site Class D							
Model <i>T_i</i> (sec)	3SAC <i>1.03</i>	4KatF <i>1.18</i>	4KatR <i>0.72</i>	5KatS2 <i>0.81</i>	8KatS2 <i>1.45</i>	12KatFS <i>2.19</i>	12KatRS <i>1.26</i>
<i>EQ No.1</i>	0.915	0.945	0.947	1.106	1.203	2.267	0.989
<i>2</i>	1.248	1.232	1.281	1.491	1.593	4.533	1.406
<i>3</i>	3.432	2.682	3.249	3.790	2.095	2.863	2.552
<i>4</i>	2.053	1.509	4.059	4.111	1.454	1.833	1.441
<i>5</i>	1.054	1.534	1.546	1.298	1.152	0.473	1.362
<i>6</i>	0.833	1.012	1.229	1.228	0.741	0.612	0.796
<i>7</i>	1.660	2.012	1.043	0.948	1.655	1.041	2.310
<i>8</i>	1.531	1.343	0.964	1.083	1.603	0.957	1.236
<i>9</i>	2.503	2.336	1.992	1.750	1.932	1.527	2.205
<i>10</i>	3.451	2.470	2.825	3.366	3.181	2.335	2.770
<i>11</i>	1.726	1.942	1.635	1.556	1.995	1.827	2.062
<i>12</i>	1.816	1.536	1.869	1.690	1.792	1.784	1.763
<i>13</i>	1.227	1.148	2.478	2.029	1.303	2.297	1.234
<i>14</i>	1.166	0.989	1.526	1.182	1.852	3.812	1.256
<i>15</i>	2.141	2.337	1.806	2.245	2.761	1.805	2.470
<i>16</i>	2.920	3.137	4.038	4.414	2.883	3.257	3.572
<i>17</i>	1.000	1.640	1.764	1.742	2.837	2.566	2.602
<i>18</i>	0.899	0.996	2.639	1.721	2.148	2.821	1.337
<i>19</i>	1.861	1.921	1.072	1.162	2.124	2.810	2.100
<i>20</i>	1.211	1.388	0.808	0.929	1.837	2.495	1.764
<i>21</i>	1.179	1.086	1.472	1.413	0.991	1.724	0.916
<i>22</i>	1.415	1.338	1.249	1.242	0.906	1.198	1.142
<i>23</i>	1.651	1.689	0.944	1.073	1.380	2.556	1.488
<i>24</i>	1.185	0.741	1.307	1.435	0.681	1.393	0.710
<i>25</i>	3.310	3.333	3.774	3.009	3.374	6.124	3.947
<i>26</i>	2.969	3.355	2.758	2.002	2.036	2.766	2.882
<i>27</i>	1.450	1.217	0.801	0.887	1.309	1.209	1.254
<i>28</i>	0.969	1.539	1.096	0.860	2.343	2.128	1.871
<i>29</i>	1.032	1.228	0.726	0.714	0.851	1.747	1.303
<i>30</i>	0.742	1.097	1.027	0.898	1.139	1.746	1.142
<i>31</i>	0.728	0.622	0.995	0.976	0.668	1.460	0.642
<i>32</i>	1.352	1.445	1.289	1.350	1.134	4.323	1.266
<i>33</i>	1.519	1.579	1.314	1.215	1.274	1.146	1.503
<i>34</i>	1.370	1.338	1.565	1.874	1.409	1.680	1.474
<i>35</i>	1.480	1.427	1.602	1.464	1.789	1.927	1.411
<i>36</i>	1.518	1.466	1.662	1.708	1.890	1.676	1.737
<i>37</i>	1.536	0.973	1.089	1.047	1.222	1.705	0.975
<i>38</i>	1.966	1.371	2.679	3.291	1.336	0.944	1.465
<i>39</i>	2.174	1.962	2.495	2.251	1.831	1.360	2.255
<i>40</i>	1.153	1.032	1.169	1.121	1.191	0.928	0.961
<i>41</i>	0.710	1.061	0.652	0.612	0.625	0.533	0.868
<i>42</i>	1.445	1.453	0.703	0.839	1.062	0.738	1.591
<i>43</i>	1.561	1.891	1.404	1.349	1.889	1.053	1.987
<i>44</i>	2.224	2.359	1.406	1.563	1.643	0.893	2.317
<i>45</i>	7.073	5.003	8.303	6.809	7.275	4.231	6.477
<i>46</i>	6.569	6.171	5.234	4.035	5.015	4.423	5.368
<i>47</i>	9.288	8.204	4.757	6.273	6.722	6.037	9.973
<i>48</i>	7.858	7.726	3.322	3.205	5.699	3.861	5.481
<i>49</i>	4.304	2.872	5.457	5.154	1.899	1.512	2.479
<i>50</i>	2.798	2.044	2.513	3.120	1.942	0.695	2.006

Table B.6. (Continued)

SETD - NEHRP Site Class D							
Model <i>T_i</i> (sec)	3SAC <i>1.03</i>	4KatF <i>1.18</i>	4KatR <i>0.72</i>	5KatS2 <i>0.81</i>	8KatS2 <i>1.45</i>	12KatFS <i>2.19</i>	12KatRS <i>1.26</i>
EQ. No. 51	4.606	3.971	5.035	4.651	3.307	1.649	4.156
52	4.617	4.546	1.972	2.479	4.526	2.927	4.133
53	0.437	0.566	0.535	0.470	0.604	0.912	0.550
54	0.782	1.090	0.647	0.707	1.108	2.093	1.140
55	1.369	1.486	2.551	2.276	2.418	2.253	1.808
56	3.294	2.468	2.923	3.550	2.620	2.682	2.356
57	0.398	0.333	1.317	0.821	0.536	0.838	0.374
58	0.628	0.655	1.115	0.664	0.739	1.341	0.678
59	0.848	0.894	1.277	1.342	0.866	1.006	0.835
60	2.085	1.631	2.756	2.546	1.215	1.239	1.344
61	2.275	2.037	1.468	1.882	1.232	2.576	2.031
62	4.352	5.099	3.998	5.487	2.915	3.841	3.329
63	4.411	3.646	2.584	3.028	3.286	3.032	2.648
64	7.770	8.122	5.667	5.944	4.361	3.962	6.477
65	1.939	1.781	1.025	0.984	1.189	0.796	1.578
66	0.920	1.121	0.887	1.156	0.664	0.582	0.898
67	2.262	1.636	1.268	1.079	1.690	2.023	1.842
68	1.208	0.781	0.473	0.725	0.656	1.150	0.657
69	4.047	4.129	1.494	1.977	4.613	3.149	4.224
70	5.107	4.213	1.999	3.251	4.625	4.959	3.915
71	8.082	5.654	6.507	8.210	9.346	11.044	5.383
72	13.374	11.436	6.022	8.995	6.283	9.418	8.980
73	4.866	3.849	6.329	7.120	3.075	5.579	3.880
74	4.173	4.075	2.658	2.971	3.008	2.623	3.469
75	2.331	2.597	2.080	1.796	2.683	1.941	2.395
76	2.580	2.292	3.412	2.845	2.746	2.526	2.440
77	1.623	1.284	1.863	1.393	1.137	0.804	1.265
78	1.013	1.064	1.290	1.242	0.925	1.171	1.080
79	1.701	1.355	1.062	1.617	1.147	1.346	1.609
80	0.932	1.053	0.976	0.773	1.321	2.310	1.247
81	2.660	2.432	2.104	1.998	1.632	1.073	1.770
82	2.582	2.363	2.549	1.769	1.145	1.330	1.841
83	3.904	2.548	3.338	3.760	2.532	1.735	2.864
84	2.840	1.997	1.786	1.862	2.577	3.218	1.715
85	5.672	5.225	2.504	2.722	4.412	2.179	5.357
86	2.678	3.017	2.918	2.552	4.536	5.654	3.539
87	2.316	1.719	2.081	2.488	2.642	1.054	1.506
88	2.872	3.763	2.111	2.083	3.736	2.956	3.766
89	1.752	1.360	2.874	1.558	0.918	1.522	1.123
90	3.063	3.477	3.231	3.471	3.525	1.297	3.330
91	3.915	4.315	4.038	3.412	4.207	7.354	4.503
92	1.813	2.073	1.183	1.241	2.422	2.043	2.170
93	3.727	3.133	2.894	2.453	4.969	4.192	3.491
94	4.303	2.565	3.023	2.355	4.380	6.722	3.288
95	7.427	7.283	3.881	4.705	7.166	12.552	6.714
96	1.930	2.338	1.214	1.143	3.471	6.315	2.661
97	4.137	3.750	3.342	3.985	3.960	6.071	3.611
98	4.448	4.666	3.082	3.656	6.201	10.318	5.197
99	5.463	6.753	2.882	3.213	6.267	9.419	6.278
100	5.176	4.686	1.942	2.302	4.029	7.190	4.876

Table B.7. Scale factors for analysis group “SCR2” for SETC earthquake ground motion acceleration records conforming to NEHRP Site Class C.

SETC - NEHRP Site Class C							
Model <i>Te</i> (sec)	3SAC <i>1.07</i>	4KatF <i>1.21</i>	4KatR <i>0.73</i>	5KatS2 <i>0.83</i>	8KatS2 <i>1.51</i>	12KatFS <i>2.24</i>	12KatRS <i>1.28</i>
<i>EQ No.1</i>	2.217	3.092	8.831	5.814	2.701	3.168	5.493
<i>2</i>	2.454	3.687	6.066	3.390	2.780	2.125	8.027
<i>3</i>	3.639	4.967	7.226	5.382	4.996	2.695	13.071
<i>4</i>	2.611	3.103	4.009	3.457	2.887	4.463	6.202
<i>5</i>	1.850	2.443	4.359	2.753	1.950	1.522	4.912
<i>6</i>	1.560	2.820	4.967	3.225	2.484	1.541	6.424
<i>7</i>	4.225	4.359	5.966	4.693	5.595	4.295	9.792
<i>8</i>	2.362	4.428	5.975	3.403	4.190	3.150	10.689
<i>9</i>	2.141	2.338	5.853	4.731	2.133	1.698	4.596
<i>10</i>	2.886	3.640	5.523	3.881	2.244	2.218	6.574
<i>11</i>	3.385	4.823	6.307	4.506	3.547	3.303	10.817
<i>12</i>	2.484	2.401	6.024	6.139	2.308	3.433	5.158
<i>13</i>	1.713	2.165	3.813	4.015	2.301	2.116	5.308
<i>14</i>	1.934	2.653	6.557	4.437	2.442	2.122	6.076
<i>15</i>	2.329	2.646	4.466	3.979	3.050	3.616	5.579
<i>16</i>	1.355	1.876	6.502	3.617	1.983	2.454	4.124
<i>17</i>	1.053	1.207	2.760	1.520	1.068	2.847	2.130
<i>18</i>	1.727	2.199	2.197	1.524	1.788	4.207	3.999
<i>19</i>	1.620	3.082	3.901	2.606	4.893	4.574	8.571
<i>20</i>	2.711	3.079	5.610	4.428	3.179	4.177	6.445
<i>21</i>	2.183	2.654	5.381	3.930	3.344	3.390	6.070
<i>22</i>	6.451	6.609	10.478	8.959	8.868	9.195	14.220
<i>23</i>	0.451	0.610	1.730	0.988	1.045	2.611	1.473
<i>24</i>	1.128	1.662	2.833	2.449	3.313	12.217	4.218
<i>25</i>	8.444	13.204	19.438	10.620	12.459	11.025	30.922
<i>26</i>	9.455	11.438	20.686	15.567	12.790	8.521	27.646
<i>27</i>	1.688	1.556	4.134	3.456	2.197	6.153	3.208
<i>28</i>	3.611	3.993	7.094	6.016	3.672	5.928	8.168
<i>29</i>	3.272	3.761	6.348	3.031	4.029	6.515	8.580
<i>30</i>	1.722	1.932	5.908	5.121	5.030	11.986	5.043
<i>31</i>	3.812	5.546	5.455	5.263	7.336	10.106	12.352
<i>32</i>	2.416	2.473	4.590	3.374	3.029	4.998	5.181
<i>33</i>	3.424	4.282	5.294	4.257	3.786	6.193	8.568
<i>34</i>	4.531	5.267	3.342	4.949	4.445	7.308	8.309
<i>35</i>	1.795	2.446	5.591	4.383	2.858	2.876	5.936
<i>36</i>	3.031	4.203	5.719	3.327	3.850	7.261	9.099
<i>37</i>	1.395	1.877	1.936	1.282	1.612	2.776	3.702
<i>38</i>	0.914	1.312	2.002	1.124	1.229	2.148	3.236
<i>39</i>	2.951	4.924	11.141	8.490	9.271	14.593	11.218
<i>40</i>	5.140	4.810	15.200	13.286	8.511	10.498	10.124
<i>41</i>	36.573	43.672	51.023	45.368	47.881	61.572	94.900
<i>42</i>	30.670	23.639	36.969	37.195	25.822	60.991	52.585
<i>43</i>	2.759	3.043	5.930	4.179	4.809	7.264	6.065
<i>44</i>	2.366	4.255	2.962	2.003	5.817	11.528	10.432
<i>45</i>	3.986	4.600	5.964	5.294	8.123	11.111	10.938
<i>46</i>	2.953	4.350	5.593	3.816	7.068	16.487	9.593
<i>47</i>	3.468	4.800	5.888	4.283	4.500	6.051	9.911
<i>48</i>	3.452	4.061	6.204	5.740	3.858	5.549	9.496
<i>49</i>	3.755	6.468	3.116	3.795	7.723	12.628	16.050
<i>50</i>	3.851	4.463	2.191	2.818	7.092	9.525	11.321

Table B.7. (Continued)

SETC - NEHRP Site Class C							
Model	3SAC	4KatF	4KatR	5KatS2	8KatS2	12KatFS	12KatRS
<i>Te (sec)</i>	<i>1.07</i>	<i>1.21</i>	<i>0.73</i>	<i>0.83</i>	<i>1.51</i>	<i>2.24</i>	<i>1.28</i>
EQ. No. 51	2.080	4.273	4.843	4.547	5.278	10.194	10.301
52	2.848	5.613	2.754	3.326	6.246	8.720	10.994
53	13.633	11.973	17.501	17.455	14.016	23.482	28.037
54	11.231	19.215	14.333	13.813	22.732	31.456	46.165
55	8.135	7.911	8.605	6.924	9.914	19.249	17.002
56	8.790	10.322	24.448	17.110	9.247	13.357	21.273
57	8.682	15.516	11.564	13.422	23.651	21.970	40.720
58	7.234	15.012	17.137	17.549	20.437	23.172	33.896
59	14.043	19.546	11.883	14.892	21.177	25.979	42.112
60	14.309	19.444	17.532	14.841	25.351	40.160	43.184
61	2.028	3.500	8.093	4.873	4.666	5.442	7.501
62	3.194	3.625	7.386	5.548	3.588	6.955	7.082
63	5.294	4.670	10.924	6.753	7.829	13.442	11.268
64	2.793	3.265	5.674	4.782	5.340	10.987	7.819
65	3.262	3.658	15.589	9.970	5.616	8.912	8.032
66	4.114	5.057	11.583	9.831	6.854	16.163	10.829
67	6.572	9.969	5.129	8.692	13.732	12.702	22.620
68	8.620	11.696	10.252	8.690	11.607	19.134	23.984
69	4.279	6.903	10.926	7.241	5.182	16.315	16.012
70	11.490	16.930	13.502	9.047	11.981	23.175	29.761
71	1.433	1.616	6.222	3.767	2.512	5.668	3.798
72	1.364	1.338	5.183	3.802	1.403	2.895	2.825
73	5.036	4.645	9.760	7.219	6.741	9.805	11.293
74	1.613	2.315	4.474	3.029	4.832	6.955	7.386
75	3.549	6.465	10.072	8.408	5.106	8.705	13.359
76	2.801	3.424	10.249	7.720	4.732	9.621	8.092
77	3.943	4.752	4.969	3.978	4.332	11.195	8.478
78	3.268	3.461	6.979	3.701	3.475	7.284	7.175
79	4.403	5.954	5.436	5.102	9.250	26.704	15.010
80	1.086	1.317	2.840	1.878	2.142	6.380	3.140
81	41.594	60.475	50.806	38.266	61.305	102.593	139.677
82	19.021	30.516	53.405	27.638	72.879	87.178	79.575
83	1.899	3.466	5.498	3.468	8.361	13.954	9.188
84	4.630	6.619	9.928	6.064	5.953	5.803	15.272
85	17.331	16.850	28.077	26.112	17.084	23.450	36.224
86	23.333	23.857	29.342	24.398	23.896	19.513	53.267
87	17.504	22.856	20.792	16.446	18.716	13.500	45.898
88	11.009	15.610	19.180	17.756	17.413	15.329	31.932
89	1.944	2.165	4.648	3.988	2.195	4.272	4.711
90	2.707	3.843	4.106	2.817	3.404	5.513	8.011
91	3.479	7.121	4.206	4.002	4.497	9.198	13.658
92	2.408	3.053	5.918	4.814	2.459	3.204	6.245
93	15.766	18.217	31.932	25.581	19.799	40.388	43.342
94	22.794	28.552	30.413	22.990	23.673	29.669	60.550
95	3.710	5.652	8.481	5.422	8.033	16.918	14.111
96	2.323	3.374	4.367	2.987	4.873	9.724	7.624
97	0.951	1.241	3.760	2.360	2.307	5.924	3.085
98	2.881	6.146	5.077	3.849	6.515	7.106	14.260
99	2.914	4.860	4.613	3.568	9.459	17.041	12.323
100	3.959	5.014	5.184	4.269	9.807	20.594	14.081

Table B.8. Scale factors for analysis group “SCR2” for SETD earthquake ground motion acceleration records conforming to NEHRP Site Class D.

SETD - NEHRP Site Class D							
Model <i>Te</i> (sec)	3SAC <i>1.07</i>	4KatF <i>1.21</i>	4KatR <i>0.73</i>	5KatS2 <i>0.83</i>	8KatS2 <i>1.51</i>	12KatFS <i>2.24</i>	12KatRS <i>1.28</i>
<i>EQ No.1</i>	1.205	1.506	2.734	2.449	2.102	4.169	3.188
<i>2</i>	1.552	2.042	3.784	3.341	2.706	8.291	4.506
<i>3</i>	4.236	4.041	9.231	8.877	3.001	5.314	7.977
<i>4</i>	2.449	2.262	11.505	9.190	2.313	3.292	4.551
<i>5</i>	1.614	2.219	4.277	2.555	1.567	0.843	4.000
<i>6</i>	1.130	1.412	3.520	2.467	1.214	1.140	2.558
<i>7</i>	2.583	3.301	3.024	2.070	2.491	1.904	7.439
<i>8</i>	1.843	1.978	2.640	2.724	2.285	1.749	4.104
<i>9</i>	3.073	3.457	5.563	3.549	2.707	2.792	6.923
<i>10</i>	4.596	4.122	8.030	7.752	3.691	4.028	8.323
<i>11</i>	2.465	3.158	4.545	3.430	2.797	3.314	6.633
<i>12</i>	2.448	2.479	5.007	3.489	2.694	3.334	5.952
<i>13</i>	1.538	1.839	6.888	3.989	2.131	4.285	3.986
<i>14</i>	1.371	1.680	4.062	2.515	3.182	6.907	4.407
<i>15</i>	3.451	3.506	5.073	5.294	4.447	3.278	7.596
<i>16</i>	3.282	5.370	11.799	9.998	4.253	5.915	11.190
<i>17</i>	1.519	3.211	4.855	3.487	3.919	4.778	8.609
<i>18</i>	1.163	1.776	7.180	3.319	3.682	5.215	4.583
<i>19</i>	2.365	3.241	3.307	2.692	3.092	5.269	6.271
<i>20</i>	1.908	2.588	2.227	1.996	3.172	4.488	5.683
<i>21</i>	1.546	1.529	4.382	2.913	1.832	3.159	2.835
<i>22</i>	1.938	1.974	3.454	2.925	1.481	2.112	3.314
<i>23</i>	2.122	2.482	2.658	2.610	2.136	4.818	4.595
<i>24</i>	1.231	1.111	3.626	3.126	1.055	2.634	2.248
<i>25</i>	4.229	5.561	10.535	6.050	5.419	11.245	12.914
<i>26</i>	3.996	4.830	7.844	3.944	3.211	5.022	8.440
<i>27</i>	1.919	1.895	2.242	2.061	1.968	2.248	4.022
<i>28</i>	1.564	2.630	3.087	1.786	3.411	3.844	6.258
<i>29</i>	1.386	2.113	2.091	1.561	1.278	3.273	3.988
<i>30</i>	1.148	1.768	2.965	1.853	1.847	3.141	3.583
<i>31</i>	0.911	0.972	2.835	2.089	1.002	2.762	2.062
<i>32</i>	1.797	2.185	3.673	2.972	2.002	8.254	3.783
<i>33</i>	2.026	2.344	3.685	2.670	1.777	2.065	4.782
<i>34</i>	1.669	2.243	4.608	4.386	2.494	2.936	4.516
<i>35</i>	1.597	2.265	4.479	3.137	3.252	3.395	4.478
<i>36</i>	2.274	2.534	4.941	3.449	3.363	3.010	5.701
<i>37</i>	1.684	1.467	3.014	2.404	2.106	3.095	3.187
<i>38</i>	2.247	2.181	7.950	7.369	1.950	1.733	4.618
<i>39</i>	2.258	3.242	6.518	5.017	3.003	2.505	7.251
<i>40</i>	1.700	1.542	3.204	2.550	1.997	1.717	3.109
<i>41</i>	1.219	2.187	2.130	1.631	1.559	2.452	4.258
<i>42</i>	1.941	3.344	2.333	2.555	2.536	3.146	7.935
<i>43</i>	2.829	4.321	4.599	3.595	5.341	4.725	10.443
<i>44</i>	3.531	5.494	4.811	3.910	3.931	4.010	11.020
<i>45</i>	10.850	11.617	27.448	17.740	25.185	18.596	36.998
<i>46</i>	9.652	13.257	17.065	10.758	16.058	19.673	26.482
<i>47</i>	12.327	20.734	16.517	17.662	16.592	26.257	49.304
<i>48</i>	12.257	13.761	11.285	8.934	15.046	17.352	28.608
<i>49</i>	5.881	6.036	17.566	12.829	5.303	6.707	12.078
<i>50</i>	3.795	4.513	8.819	8.811	4.482	2.925	10.271

Table B.8. (Continued)

SETD - NEHRP Site Class D							
Model	3SAC	4KatF	4KatR	5KatS2	8KatS2	12KatFS	12KatRS
<i>Te (sec)</i>	<i>1.07</i>	<i>1.21</i>	<i>0.73</i>	<i>0.83</i>	<i>1.51</i>	<i>2.24</i>	<i>1.28</i>
EQ. No. 51	7.452	9.721	17.392	12.945	7.546	7.112	18.908
52	7.575	10.006	6.956	7.251	10.648	12.145	20.420
53	0.700	1.232	1.770	1.378	1.561	3.981	2.868
54	1.169	2.499	2.184	1.876	3.513	9.169	5.965
55	2.179	3.585	8.483	5.657	7.280	9.790	10.214
56	5.472	5.227	10.894	8.918	7.769	12.154	12.456
57	0.549	0.787	4.213	2.029	1.573	3.679	2.019
58	0.957	1.503	3.503	1.703	2.255	5.865	3.521
59	1.325	1.897	4.290	3.657	2.623	4.335	4.321
60	3.016	3.372	9.005	6.690	2.767	5.248	6.552
61	3.665	4.834	4.946	5.750	2.959	11.349	9.920
62	7.186	10.557	13.756	13.116	9.440	16.851	14.472
63	6.778	6.656	8.643	7.697	10.418	13.241	13.313
64	12.753	17.475	19.263	16.516	13.630	16.806	29.504
65	3.088	3.757	3.380	2.742	2.816	3.410	7.897
66	1.688	2.034	2.951	2.742	1.524	2.520	4.569
67	3.425	3.724	4.384	2.692	5.383	9.069	10.115
68	1.985	1.538	1.644	2.099	2.107	5.039	3.244
69	6.515	9.266	5.285	5.741	12.699	13.773	22.064
70	7.043	8.992	7.346	9.350	11.997	21.296	20.068
71	9.614	12.197	22.168	24.544	26.362	47.988	28.421
72	21.015	22.869	21.050	25.524	16.182	41.908	43.250
73	5.970	8.282	22.945	18.329	9.214	25.744	21.252
74	5.695	8.606	8.722	9.001	9.673	11.678	16.656
75	3.192	5.513	6.772	4.931	8.437	8.658	12.563
76	3.832	5.029	11.338	7.293	6.927	11.104	13.984
77	2.701	2.741	5.961	3.711	2.778	3.398	6.592
78	1.558	2.437	4.534	3.186	2.778	4.971	5.381
79	2.003	3.554	3.534	4.976	2.845	5.910	7.711
80	1.427	2.602	3.145	1.919	3.830	9.969	6.634
81	3.618	5.011	6.508	5.977	4.194	4.796	8.329
82	4.079	4.699	7.972	4.765	3.176	5.642	8.695
83	5.152	5.923	11.831	9.736	6.094	7.816	14.407
84	4.241	4.000	6.163	4.886	6.874	13.824	8.879
85	8.624	11.546	8.671	7.460	10.514	9.683	27.972
86	4.252	7.215	9.860	6.677	14.363	24.671	19.359
87	3.236	3.364	6.832	6.954	6.493	4.626	8.272
88	4.853	8.528	6.989	5.414	12.102	12.240	17.439
89	2.824	2.710	9.211	3.653	2.898	6.360	5.299
90	5.114	7.708	11.174	8.933	9.786	5.712	17.059
91	6.465	9.978	13.236	8.947	12.871	33.046	23.180
92	3.084	4.716	4.060	3.381	7.021	8.902	11.362
93	5.813	7.132	8.877	7.105	18.087	18.705	19.170
94	5.563	5.962	9.663	6.027	12.133	29.731	20.021
95	12.240	16.659	13.102	13.534	20.658	56.400	33.075
96	3.308	5.528	4.007	3.165	10.757	28.032	14.320
97	6.440	7.897	11.481	11.809	11.680	27.096	19.520
98	6.825	10.825	10.523	10.824	20.352	45.497	27.914
99	9.741	14.543	9.938	9.083	18.885	41.762	31.677
100	7.452	11.043	6.578	6.892	12.130	32.087	23.786

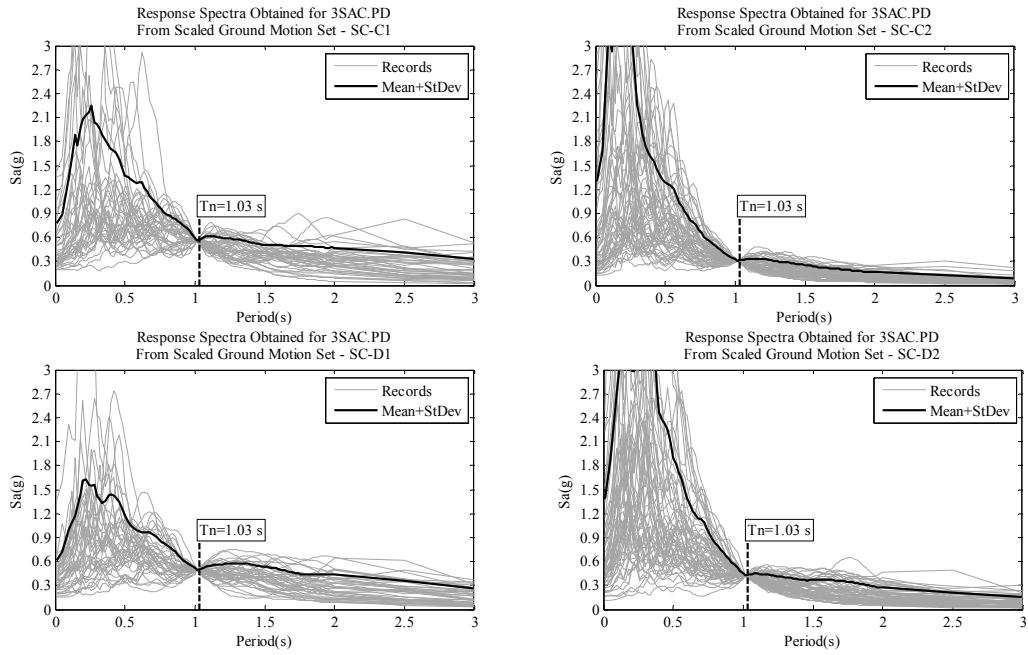


Figure B.1. Mean plus one standard deviation response spectra of Analysis Group II, SET-SC-C1, SET-SC-C2, SET-SC-D1 and SET-SC-D2 records, obtained for the frame model 3SAC.

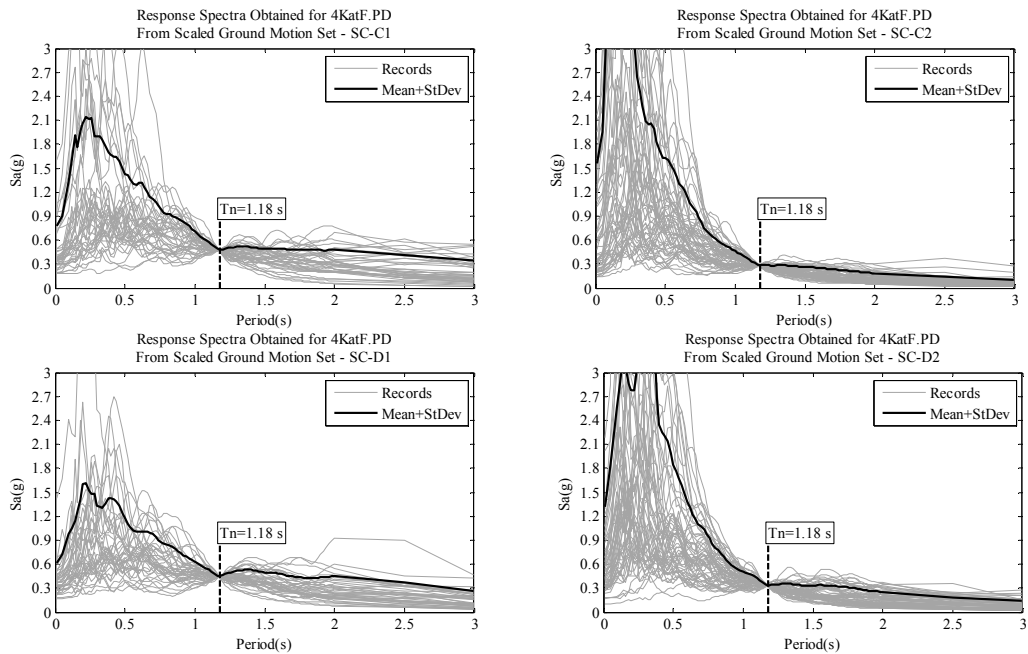


Figure B.2. Mean plus one standard deviation response spectra of Analysis Group II, SET-SC-C1, SET-SC-C2, SET-SC-D1 and SET-SC-D2 records, obtained for the frame model 4KatF.

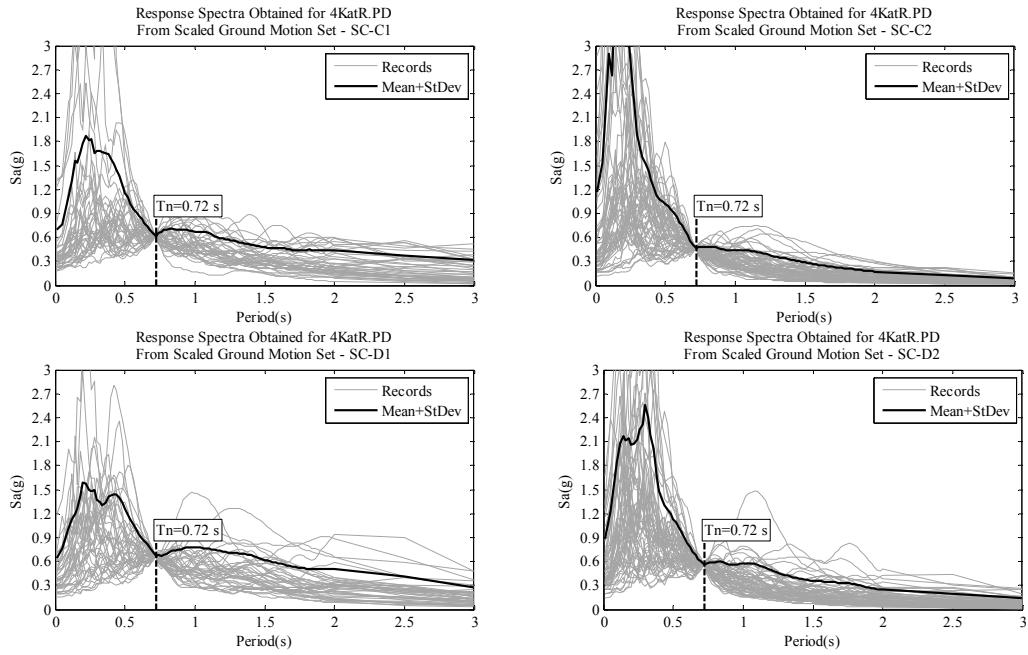


Figure B.3. Mean plus one standard deviation response spectra of Analysis Group II, SET-SC-C1, SET-SC-C2, SET-SC-D1 and SET-SC-D2 records, obtained for the frame model 4KatR.

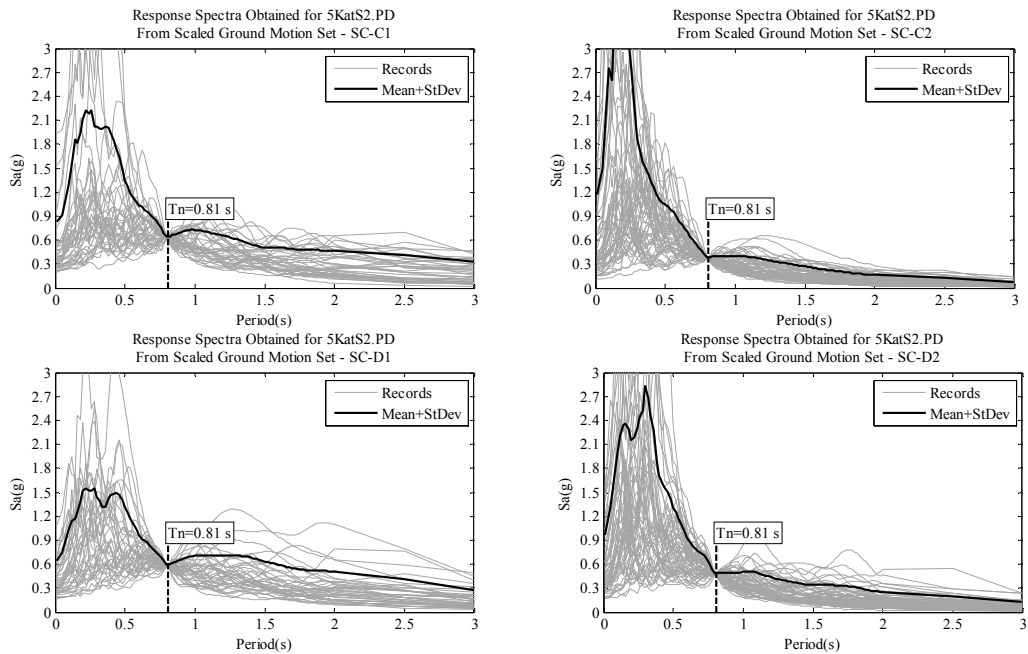


Figure B.4. Mean plus one standard deviation response spectra of Analysis Group II, SET-SC-C1, SET-SC-C2, SET-SC-D1 and SET-SC-D2 records, obtained for the frame model 5KatS2.

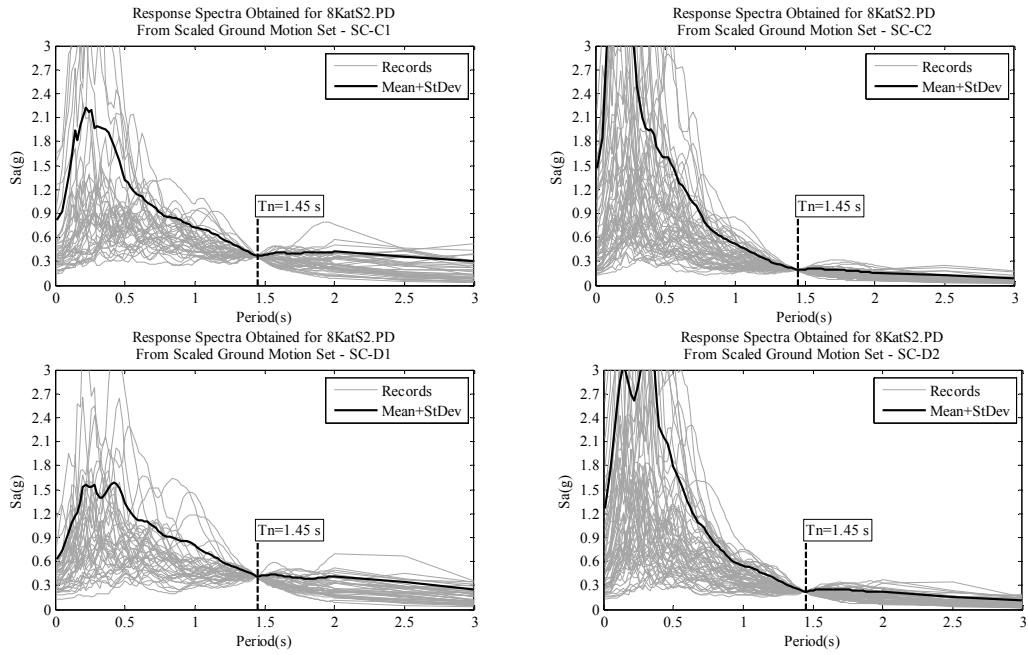


Figure B.5. Mean plus one standard deviation response spectra of Analysis Group II, SET-SC-C1, SET-SC-C2, SET-SC-D1 and SET-SC-D2 records, obtained for the frame model 8KatS2.

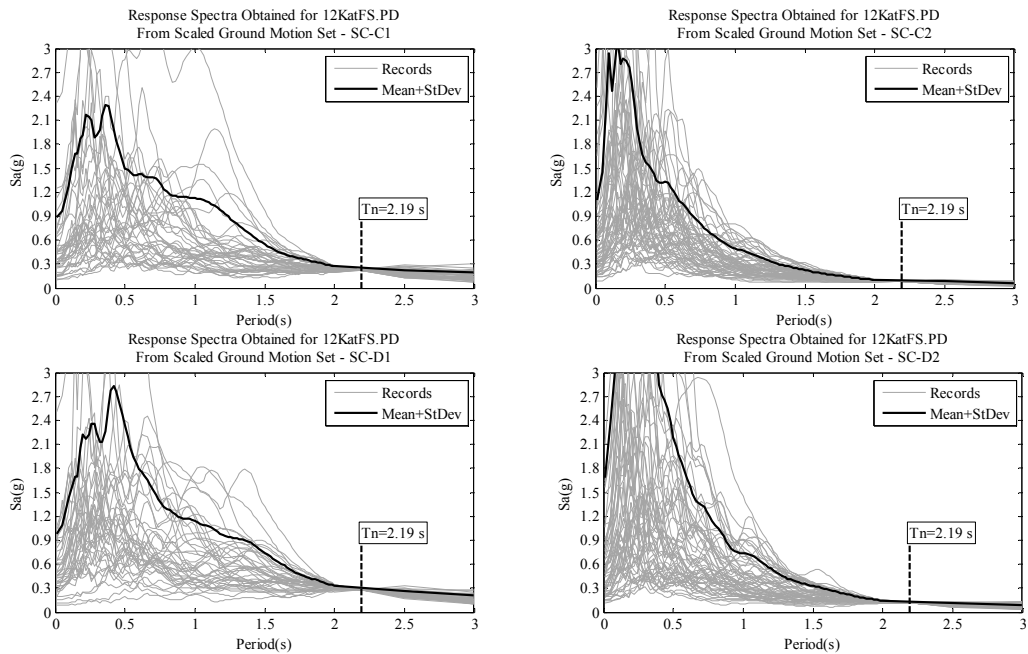


Figure B.6. Mean plus one standard deviation response spectra of Analysis Group II, SET-SC-C1, SET-SC-C2, SET-SC-D1 and SET-SC-D2 records, obtained for the frame model 12KatFS.

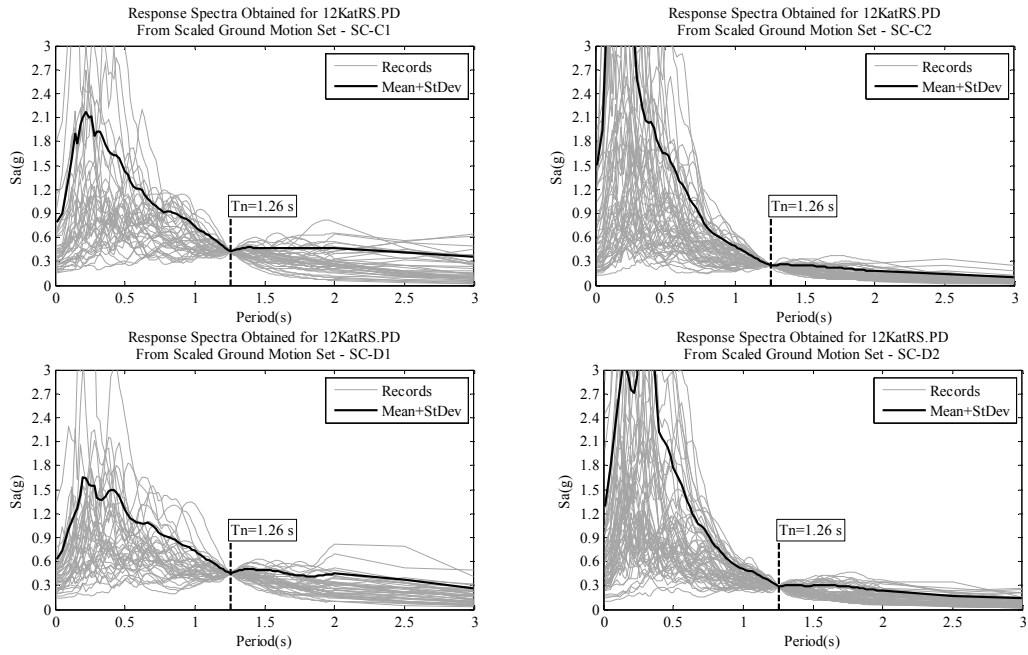


Figure B.7. Mean plus one standard deviation response spectra of Analysis Group II, SET-SC-C1, SET-SC-C2, SET-SC-D1 and SET-SC-D2 records, obtained for the frame model 12KatRS.

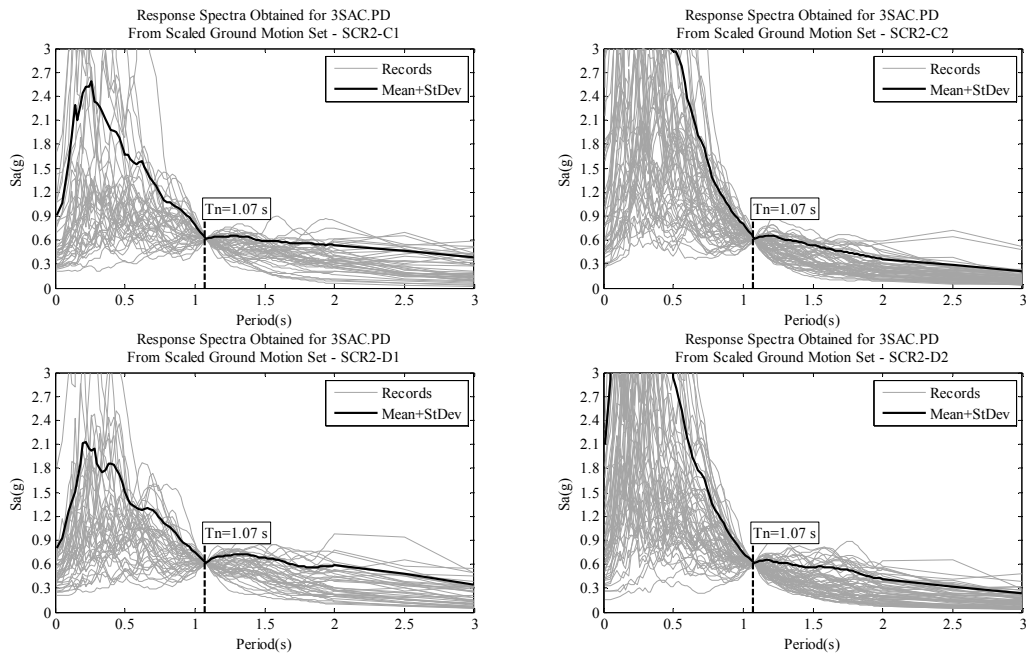


Figure B.8. Mean plus one standard deviation response spectra of Analysis Group III, SET-SCR2-C1, SET-SCR2-C2, SET-SCR2-D1 and SET-SCR2-D2 records, obtained for the frame model 3SAC.

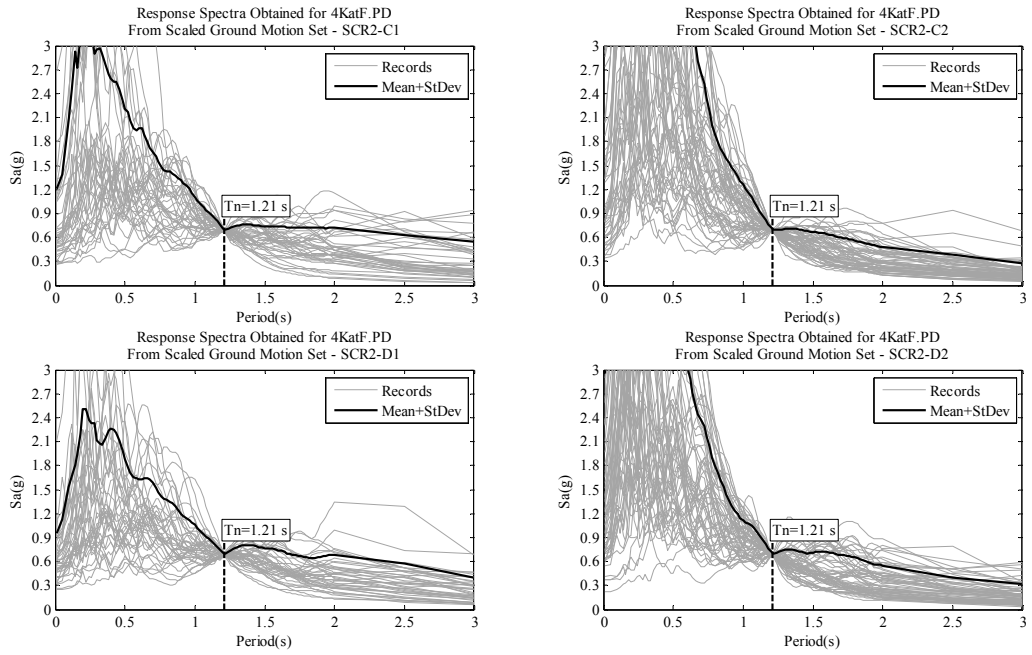


Figure B.9. Mean plus one standard deviation response spectra of Analysis Group III, SET-SCR2-C1, SET-SCR2-C2, SET-SCR2-D1 and SET-SCR2-D2 records, obtained for the frame model 4KatF.

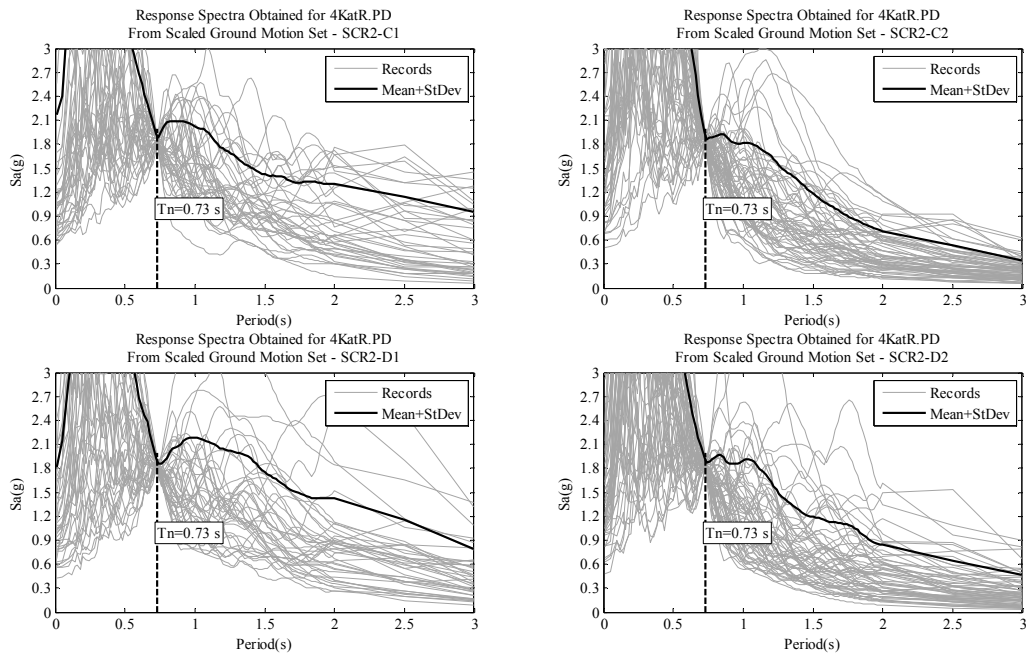


Figure B.10. Mean plus one standard deviation response spectra of Analysis Group III, SET-SCR2-C1, SET-SCR2-C2, SET-SCR2-D1 and SET-SCR2-D2 records, obtained for the frame model 4KatR.

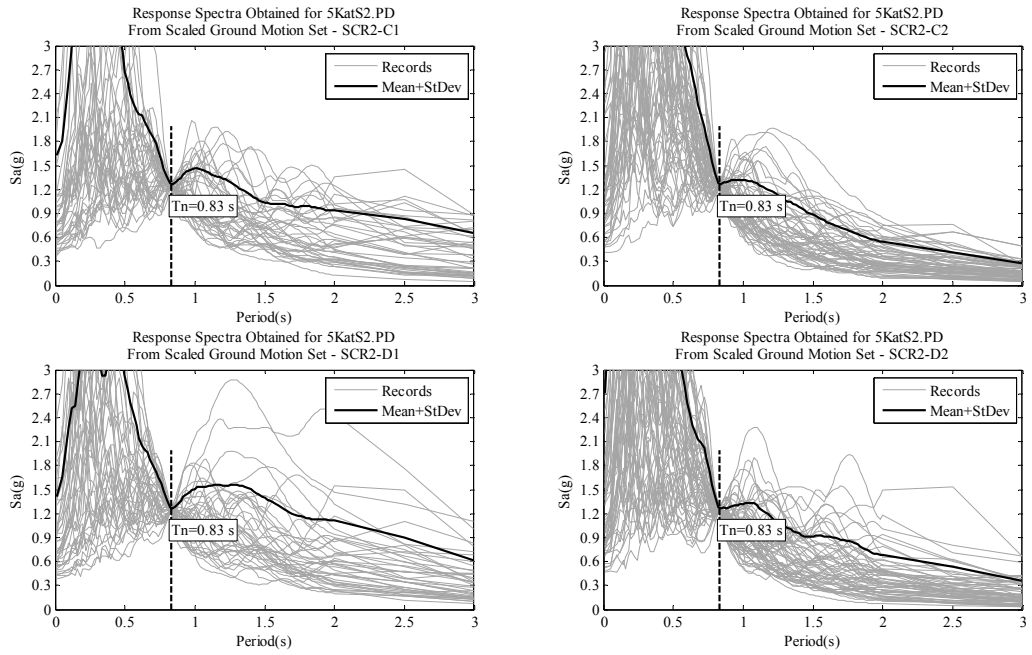


Figure B.11. Mean plus one standard deviation response spectra of Analysis Group III, SET-SCR2-C1, SET-SCR2-C2, SET-SCR2-D1 and SET-SCR2-D2 records, obtained for the frame model 5KatS2.

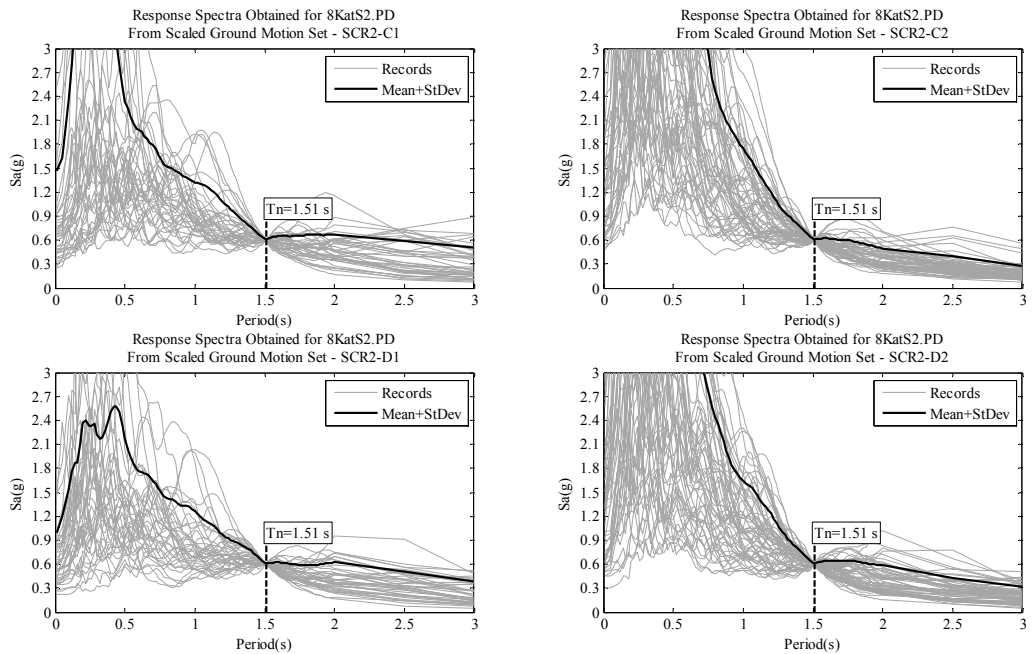


Figure B.12. Mean plus one standard deviation response spectra of Analysis Group III, SET-SCR2-C1, SET-SCR2-C2, SET-SCR2-D1 and SET-SCR2-D2 records, obtained for the frame model 8KatS2.

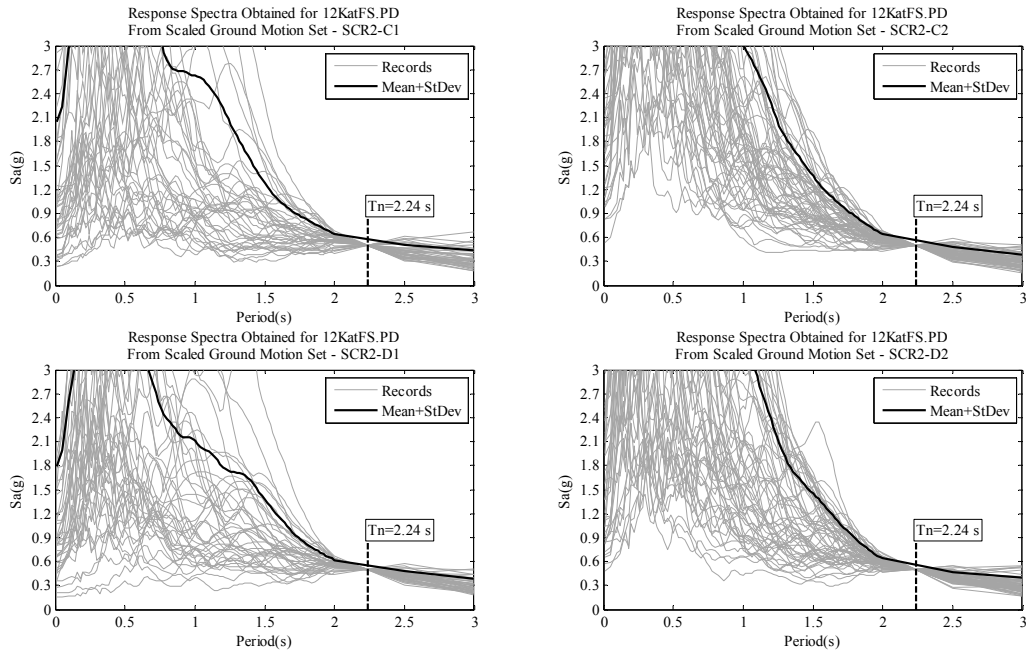


Figure B.13. Mean plus one standard deviation response spectra of Analysis Group III, SET-SCR2-C1, SET-SCR2-C2, SET-SCR2-D1 and SET-SCR2-D2 records, obtained for the frame model 12KatFS.

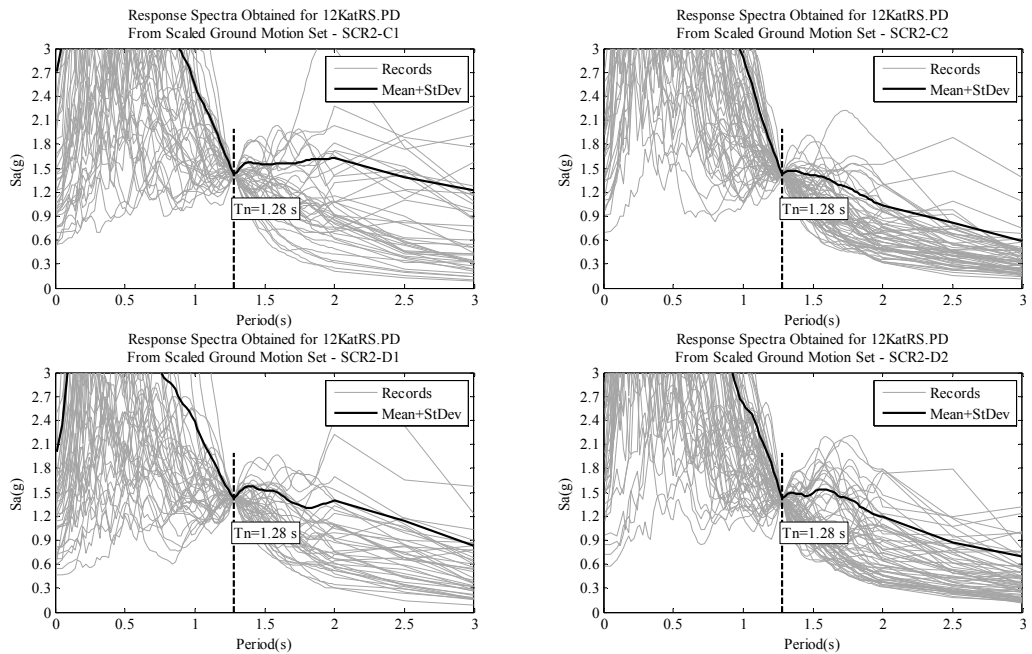


Figure B.14. Mean plus one standard deviation response spectra of Analysis Group III, SET-SCR2-C1, SET-SCR2-C2, SET-SCR2-D1 and SET-SCR2-D2 records, obtained for the frame model 12KatRS.

APPENDIX C

TABLES RELATED TO REGRESSION LINES

Response ratio (SSI.TH / FB.TH) values corresponding to both global and local level deformations are recalculated by employing the linear regression equations derived in Chapter 4 and Tables 4.1 – 4.4. Response ratio values are evaluated at the minimum and at the maximum limits of the wave parameter which are associated with the ground motion sets (9.5 – 65 for SETC and 4.5 – 33 for SETD) and at the respective aspect ratio of the frame models. The results, which are expressed as a percentage of reference base 1.0 (i.e. a value of -4.4% means 0.956), are organized as follows:

- Response ratio values calculated for the roof drift ratio (Table C.1),
- Response ratio values calculated for the first story drift ratio (Table C.2),
- Response ratio values calculated for the peak member end rotations at the first story (Table C.3 – C.9):
 - Response ratio values associated with the column end rotation are obtained at the foundation end.
 - Response ratio values associated with the peak beam end rotation are obtained from the maximum of the either ends of the element.
 - Aspect ratio of the frame models 3SAC, 4KatF, 4KatR, 5KatS2, 8KatS2, 12KatFS and 12KatRS are equal to 0.53, 1.32, 1.35, 1.63, 2.48, 3.57 and 3.62, respectively.

Table C.1. Response ratio values (as a percentage of reference base 1.0) for the roof drift ratio evaluated at the minimum and at the maximum values of the wave parameter (9.5 – 65 for SETC and 4.5 – 33 for SETD) and at the respective aspect ratio of the frame models.

Response Ratio Values Predicted for the Roof Drift Ratio (as a percentage of reference base 1.0)								
H/R	Analysis Group I, NS							
	SET-C1		SET-C2		SET-D1		SET-D2	
	$\sigma=9.5$	$\sigma=65$	$\sigma=9.5$	$\sigma=65$	$\sigma=4.5$	$\sigma=33$	$\sigma=4.5$	$\sigma=33$
0.53	<i>-0.37</i>	0.10	<i>-1.22</i>	0.60	<i>-4.63</i>	2.59	<i>-6.00</i>	2.22
1.32	<i>-0.39</i>	0.09	<i>-1.12</i>	0.70	<i>-4.14</i>	3.08	<i>-5.47</i>	2.75
1.35	<i>-0.39</i>	0.09	<i>-1.11</i>	0.70	<i>-4.12</i>	3.09	<i>-5.46</i>	2.76
1.63	<i>-0.39</i>	0.08	<i>-1.08</i>	0.74	<i>-3.94</i>	3.27	<i>-5.27</i>	2.95
2.48	<i>-0.41</i>	0.06	<i>-0.97</i>	0.85	<i>-3.42</i>	3.80	<i>-4.70</i>	3.52
3.57	<i>-0.43</i>	0.04	<i>-0.83</i>	0.99	<i>-2.74</i>	4.47	<i>-3.97</i>	4.25
3.62	<i>-0.43</i>	0.04	<i>-0.82</i>	0.99	<i>-2.71</i>	4.50	<i>-3.94</i>	4.28
H/R	Analysis Group II, SC							
	SET-C1		SET-C2		SET-D1		SET-D2	
	$\sigma=9.5$	$\sigma=65$	$\sigma=9.5$	$\sigma=65$	$\sigma=4.5$	$\sigma=33$	$\sigma=4.5$	$\sigma=33$
0.53	<i>-0.22</i>	0.17	<i>-1.10</i>	0.64	<i>-4.25</i>	3.33	<i>-4.12</i>	2.38
1.32	<i>-0.24</i>	0.15	<i>-1.03</i>	0.72	<i>-3.78</i>	3.81	<i>-3.97</i>	2.53
1.35	<i>-0.24</i>	0.15	<i>-1.03</i>	0.72	<i>-3.76</i>	3.82	<i>-3.96</i>	2.53
1.63	<i>-0.25</i>	0.14	<i>-1.00</i>	0.74	<i>-3.59</i>	4.00	<i>-3.91</i>	2.59
2.48	<i>-0.27</i>	0.12	<i>-0.92</i>	0.82	<i>-3.08</i>	4.51	<i>-3.75</i>	2.75
3.57	<i>-0.29</i>	0.10	<i>-0.82</i>	0.93	<i>-2.42</i>	5.16	<i>-3.54</i>	2.96
3.62	<i>-0.29</i>	0.10	<i>-0.81</i>	0.93	<i>-2.40</i>	5.19	<i>-3.53</i>	2.97
H/R	Analysis Group III, SCR2							
	SET-C1		SET-C2		SET-D1		SET-D2	
	$\sigma=9.5$	$\sigma=65$	$\sigma=9.5$	$\sigma=65$	$\sigma=4.5$	$\sigma=33$	$\sigma=4.5$	$\sigma=33$
0.53	0.17	<i>-0.09</i>	<i>-0.41</i>	0.01	0.28	<i>-0.16</i>	<i>-1.03</i>	0.40
1.32	0.15	<i>-0.11</i>	<i>-0.19</i>	0.23	0.20	<i>-0.23</i>	<i>-0.89</i>	0.55
1.35	0.15	<i>-0.11</i>	<i>-0.18</i>	0.24	0.20	<i>-0.24</i>	<i>-0.88</i>	0.56
1.63	0.14	<i>-0.12</i>	<i>-0.10</i>	0.32	0.17	<i>-0.27</i>	<i>-0.83</i>	0.61
2.48	0.12	<i>-0.14</i>	0.14	0.55	0.08	<i>-0.35</i>	<i>-0.67</i>	0.77
3.57	0.09	<i>-0.17</i>	0.44	0.86	<i>-0.03</i>	<i>-0.46</i>	<i>-0.47</i>	0.97
3.62	0.08	<i>-0.17</i>	0.45	0.87	<i>-0.03</i>	<i>-0.47</i>	<i>-0.46</i>	0.98

Table C.2. Response ratio values (as a percentage of reference base 1.0) for the first story drift ratio evaluated at the minimum and at the maximum values of the wave parameter (9.5 – 65 for SETC and 4.5 – 33 for SETD) and at the respective aspect ratio of the frame models.

Response Ratio Values Predicted for the First Story Drift Ratio (as a percentage of reference base 1.0)								
H/R	Analysis Group I, NS							
	SET-C1		SET-C2		SET-D1		SET-D2	
	$\sigma=9.5$	$\sigma=65$	$\sigma=9.5$	$\sigma=65$	$\sigma=4.5$	$\sigma=33$	$\sigma=4.5$	$\sigma=33$
0.53	-0.62	0.34	-1.45	0.58	-5.58	3.23	-5.53	1.76
1.32	-0.59	0.37	-1.27	0.76	-5.04	3.77	-5.01	2.27
1.35	-0.59	0.38	-1.27	0.76	-5.02	3.79	-5.00	2.29
1.63	-0.58	0.39	-1.20	0.83	-4.83	3.98	-4.81	2.47
2.48	-0.55	0.42	-1.01	1.01	-4.25	4.56	-4.26	3.02
3.57	-0.51	0.46	-0.77	1.26	-3.50	5.31	-3.56	3.73
3.62	-0.50	0.46	-0.76	1.27	-3.47	5.34	-3.53	3.76
H/R	Analysis Group II, SC							
	SET-C1		SET-C2		SET-D1		SET-D2	
	$\sigma=9.5$	$\sigma=65$	$\sigma=9.5$	$\sigma=65$	$\sigma=4.5$	$\sigma=33$	$\sigma=4.5$	$\sigma=33$
0.53	-0.39	0.28	-1.25	0.60	-3.96	3.37	-3.39	1.93
1.32	-0.40	0.28	-1.12	0.74	-3.66	3.67	-3.31	2.02
1.35	-0.40	0.28	-1.11	0.74	-3.65	3.68	-3.30	2.02
1.63	-0.40	0.28	-1.06	0.79	-3.54	3.79	-3.27	2.05
2.48	-0.40	0.27	-0.92	0.94	-3.22	4.11	-3.18	2.14
3.57	-0.41	0.26	-0.73	1.13	-2.80	4.53	-3.06	2.26
3.62	-0.41	0.26	-0.72	1.14	-2.78	4.55	-3.06	2.27
H/R	Analysis Group III, SCR2							
	SET-C1		SET-C2		SET-D1		SET-D2	
	$\sigma=9.5$	$\sigma=65$	$\sigma=9.5$	$\sigma=65$	$\sigma=4.5$	$\sigma=33$	$\sigma=4.5$	$\sigma=33$
0.53	-0.21	-0.03	-0.37	-0.31	-0.22	0.57	-1.49	0.57
1.32	-0.20	-0.02	-0.12	-0.06	-0.47	0.31	-1.44	0.62
1.35	-0.20	-0.01	-0.11	-0.05	-0.48	0.31	-1.44	0.62
1.63	-0.19	-0.01	-0.02	0.04	-0.57	0.21	-1.42	0.64
2.48	-0.18	0.01	0.25	0.31	-0.85	-0.06	-1.37	0.69
3.57	-0.16	0.03	0.59	0.65	-1.20	-0.41	-1.30	0.76
3.62	-0.16	0.03	0.61	0.67	-1.21	-0.43	-1.30	0.76

Table C.3. Response ratio values (as a percentage of reference base 1.0) for the peak member end rotations at the first story columns and beams evaluated at the minimum and at the maximum values of the wave parameter (9.5 – 65 for SETC and 4.5 – 33 for SETD) and at the respective aspect ratio of the frame model, 3SAC.

H/R=0.53								
(Response ratio values as a percentage of reference base 1.0)								
Member	Analysis Group I: NS							
	SET-C1		SET-C2		SET-D1		SET-D2	
	$\sigma=9.5$	$\sigma=65$	$\sigma=9.5$	$\sigma=65$	$\sigma=4.5$	$\sigma=33$	$\sigma=4.5$	$\sigma=33$
Col.1	-0.63	0.34	-1.52	0.52	-5.63	2.81	-5.85	1.74
Col.2	-0.60	0.25	-1.45	0.57	-6.30	3.31	-5.86	1.67
Col.3	-0.61	0.28	-1.49	0.58	-6.27	3.29	-5.94	1.66
Col.4	-0.54	0.26	-1.41	0.48	-5.40	3.10	-5.46	1.73
Bm.1	-0.68	0.44	-1.36	0.53	-7.13	4.99	-4.79	-0.06
Bm.2	-0.67	0.28	-1.35	0.34	-5.98	3.70	-4.92	-0.23
Bm.3	-0.68	0.33	-1.41	0.59	-5.26	2.75	-4.65	0.07
Member	Analysis Group II: SC							
	SET-C1		SET-C2		SET-D1		SET-D2	
	$\sigma=9.5$	$\sigma=65$	$\sigma=9.5$	$\sigma=65$	$\sigma=4.5$	$\sigma=33$	$\sigma=4.5$	$\sigma=33$
Col.1	-0.47	0.08	-1.43	0.51	-3.42	2.61	-4.02	1.38
Col.2	-0.63	0.25	-1.55	0.48	-4.51	2.95	-4.52	1.44
Col.3	-0.60	0.22	-1.54	0.50	-4.43	2.88	-4.52	1.42
Col.4	-0.58	0.12	-1.49	0.47	-3.56	2.23	-4.28	1.29
Bm.1	-0.67	0.69	-1.22	0.40	-5.31	4.18	-3.12	-0.25
Bm.2	-0.46	0.43	-1.14	0.34	-3.94	2.90	-3.04	-0.31
Bm.3	-0.36	0.23	-1.15	0.36	-3.07	1.77	-2.95	-0.32
Member	Analysis Group III: SCR2							
	SET-C1		SET-C2		SET-D1		SET-D2	
	$\sigma=9.5$	$\sigma=65$	$\sigma=9.5$	$\sigma=65$	$\sigma=4.5$	$\sigma=33$	$\sigma=4.5$	$\sigma=33$
Col.1	-0.63	0.20	-0.79	-0.99	-1.37	1.42	-2.79	0.68
Col.2	-0.55	0.30	-0.83	-0.80	-0.56	1.34	-2.29	0.74
Col.3	-1.00	0.59	-0.58	-0.69	-0.71	1.36	-2.23	0.72
Col.4	-0.57	0.12	-0.90	-1.00	-1.12	1.78	-2.56	0.64
Bm.1	-0.24	0.31	-0.47	1.18	0.12	-0.19	-1.34	-0.06
Bm.2	-0.23	0.35	-0.83	1.20	0.41	-0.73	-1.54	0.22
Bm.3	-0.19	0.26	-0.88	0.63	0.23	-0.52	-1.50	0.26

Table C.4. Response ratio values (as a percentage of reference base 1.0) for the peak member end rotations at the first story columns and beams evaluated at the minimum and at the maximum values of the wave parameter (9.5 – 65 for SETC and 4.5 – 33 for SETD) and at the respective aspect ratio of the frame model, 4KatF.

H/R=1.32 (Response ratio values as a percentage of reference base 1.0)								
Member	Analysis Group I: NS							
	SET-C1		SET-C2		SET-D1		SET-D2	
	$\sigma=9.5$	$\sigma=65$	$\sigma=9.5$	$\sigma=65$	$\sigma=4.5$	$\sigma=33$	$\sigma=4.5$	$\sigma=33$
Col.1	-0.61	0.35	-1.33	0.71	-5.01	3.42	-5.28	2.30
Col.2	-0.58	0.27	-1.28	0.75	-5.60	4.01	-5.26	2.27
Col.3	-0.59	0.31	-1.30	0.77	-5.58	3.98	-5.33	2.28
Col.4	-0.53	0.27	-1.25	0.64	-4.91	3.59	-4.96	2.23
Bm.1	-0.65	0.46	-1.26	0.63	-6.18	5.93	-4.92	-0.19
Bm.2	-0.66	0.30	-1.28	0.41	-5.36	4.31	-5.03	-0.34
Bm.3	-0.66	0.34	-1.31	0.69	-4.88	3.12	-4.79	-0.07
Member	Analysis Group II: SC							
	SET-C1		SET-C2		SET-D1		SET-D2	
	$\sigma=9.5$	$\sigma=65$	$\sigma=9.5$	$\sigma=65$	$\sigma=4.5$	$\sigma=33$	$\sigma=4.5$	$\sigma=33$
Col.1	-0.46	0.09	-1.26	0.68	-3.14	2.88	-3.78	1.62
Col.2	-0.60	0.28	-1.35	0.69	-4.04	3.41	-4.17	1.79
Col.3	-0.57	0.25	-1.33	0.70	-3.98	3.33	-4.17	1.76
Col.4	-0.55	0.16	-1.29	0.67	-3.29	2.50	-3.97	1.60
Bm.1	-0.57	0.79	-1.18	0.44	-4.88	4.61	-3.76	-0.89
Bm.2	-0.42	0.47	-1.12	0.36	-3.82	3.01	-3.72	-0.99
Bm.3	-0.38	0.21	-1.11	0.39	-3.24	1.60	-3.66	-1.03
Member	Analysis Group III: SCR2							
	SET-C1		SET-C2		SET-D1		SET-D2	
	$\sigma=9.5$	$\sigma=65$	$\sigma=9.5$	$\sigma=65$	$\sigma=4.5$	$\sigma=33$	$\sigma=4.5$	$\sigma=33$
Col.1	-0.57	0.26	-0.27	-0.47	-1.70	1.09	-2.67	0.80
Col.2	-0.54	0.31	-0.34	-0.31	-1.14	0.76	-2.28	0.74
Col.3	-0.90	0.69	-0.15	-0.26	-1.25	0.81	-2.24	0.71
Col.4	-0.51	0.18	-0.33	-0.44	-1.55	1.35	-2.51	0.69
Bm.1	-0.31	0.23	0.06	1.71	-0.40	-0.72	-1.54	-0.27
Bm.2	-0.32	0.26	-0.15	1.88	-0.26	-1.40	-1.70	0.05
Bm.3	-0.28	0.17	-0.19	1.31	-0.37	-1.12	-1.65	0.11

Table C.5. Response ratio values (as a percentage of reference base 1.0) for the peak member end rotations at the first story columns and beams evaluated at the minimum and at the maximum values of the wave parameter (9.5 – 65 for SETC and 4.5 – 33 for SETD) and at the respective aspect ratio of the frame model, 4KatR.

H/R=1.35								
(Response ratio values as a percentage of reference base 1.0)								
Member	Analysis Group I: NS							
	SET-C1		SET-C2		SET-D1		SET-D2	
	$\sigma=9.5$	$\sigma=65$	$\sigma=9.5$	$\sigma=65$	$\sigma=4.5$	$\sigma=33$	$\sigma=4.5$	$\sigma=33$
Col.1	-0.61	0.35	-1.32	0.72	-4.99	3.45	-5.26	2.32
Col.2	-0.58	0.27	-1.27	0.76	-5.57	4.03	-5.24	2.29
Col.3	-0.59	0.31	-1.30	0.77	-5.55	4.01	-5.31	2.30
Col.4	-0.53	0.27	-1.24	0.65	-4.89	3.61	-4.94	2.25
Bm.1	-0.65	0.46	-1.26	0.63	-6.15	5.97	-4.92	-0.19
Bm.2	-0.66	0.30	-1.28	0.41	-5.34	4.34	-5.03	-0.34
Bm.3	-0.66	0.34	-1.31	0.69	-4.87	3.14	-4.79	-0.07
Member	Analysis Group II: SC							
	SET-C1		SET-C2		SET-D1		SET-D2	
	$\sigma=9.5$	$\sigma=65$	$\sigma=9.5$	$\sigma=65$	$\sigma=4.5$	$\sigma=33$	$\sigma=4.5$	$\sigma=33$
Col.1	-0.46	0.09	-1.25	0.69	-3.13	2.90	-3.78	1.63
Col.2	-0.60	0.29	-1.34	0.70	-4.02	3.43	-4.16	1.80
Col.3	-0.57	0.25	-1.33	0.71	-3.96	3.35	-4.16	1.77
Col.4	-0.55	0.16	-1.28	0.68	-3.28	2.51	-3.96	1.61
Bm.1	-0.57	0.79	-1.18	0.44	-4.87	4.62	-3.79	-0.92
Bm.2	-0.42	0.47	-1.12	0.36	-3.82	3.02	-3.74	-1.02
Bm.3	-0.38	0.21	-1.11	0.39	-3.24	1.60	-3.69	-1.05
Member	Analysis Group III: SCR2							
	SET-C1		SET-C2		SET-D1		SET-D2	
	$\sigma=9.5$	$\sigma=65$	$\sigma=9.5$	$\sigma=65$	$\sigma=4.5$	$\sigma=33$	$\sigma=4.5$	$\sigma=33$
Col.1	-0.56	0.27	-0.25	-0.45	-1.71	1.08	-2.67	0.80
Col.2	-0.54	0.31	-0.32	-0.29	-1.16	0.74	-2.28	0.74
Col.3	-0.89	0.69	-0.13	-0.24	-1.27	0.79	-2.24	0.71
Col.4	-0.51	0.18	-0.31	-0.41	-1.57	1.33	-2.50	0.69
Bm.1	-0.32	0.23	0.08	1.73	-0.42	-0.74	-1.55	-0.27
Bm.2	-0.32	0.26	-0.12	1.91	-0.28	-1.43	-1.71	0.05
Bm.3	-0.29	0.16	-0.17	1.34	-0.39	-1.14	-1.65	0.10

Table C.6. Response ratio values (as a percentage of reference base 1.0) for the peak member end rotations at the first story columns and beams evaluated at the minimum and at the maximum values of the wave parameter (9.5 – 65 for SETC and 4.5 – 33 for SETD) and at the respective aspect ratio of the frame model, 5KatS2.

H/R=1.63								
(Response ratio values as a percentage of reference base 1.0)								
Member	Analysis Group I: NS							
	SET-C1		SET-C2		SET-D1		SET-D2	
	$\sigma=9.5$	$\sigma=65$	$\sigma=9.5$	$\sigma=65$	$\sigma=4.5$	$\sigma=33$	$\sigma=4.5$	$\sigma=33$
Col.1	-0.61	0.36	-1.26	0.78	-4.77	3.67	-5.06	2.52
Col.2	-0.57	0.28	-1.21	0.82	-5.33	4.28	-5.03	2.50
Col.3	-0.58	0.32	-1.23	0.84	-5.31	4.26	-5.09	2.52
Col.4	-0.53	0.28	-1.18	0.71	-4.71	3.78	-4.77	2.43
Bm.1	-0.64	0.47	-1.22	0.67	-5.81	6.31	-4.97	-0.24
Bm.2	-0.65	0.30	-1.26	0.44	-5.12	4.56	-5.07	-0.38
Bm.3	-0.66	0.35	-1.27	0.73	-4.73	3.27	-4.84	-0.12
Member	Analysis Group II: SC							
	SET-C1		SET-C2		SET-D1		SET-D2	
	$\sigma=9.5$	$\sigma=65$	$\sigma=9.5$	$\sigma=65$	$\sigma=4.5$	$\sigma=33$	$\sigma=4.5$	$\sigma=33$
Col.1	-0.46	0.09	-1.19	0.75	-3.04	2.99	-3.69	1.71
Col.2	-0.59	0.30	-1.26	0.77	-3.86	3.60	-4.04	1.92
Col.3	-0.56	0.26	-1.25	0.78	-3.80	3.51	-4.04	1.90
Col.4	-0.53	0.17	-1.21	0.75	-3.18	2.61	-3.85	1.72
Bm.1	-0.54	0.82	-1.17	0.45	-4.71	4.77	-4.01	-1.15
Bm.2	-0.41	0.49	-1.11	0.37	-3.78	3.06	-3.99	-1.26
Bm.3	-0.38	0.21	-1.10	0.41	-3.30	1.54	-3.94	-1.30
Member	Analysis Group III: SCR2							
	SET-C1		SET-C2		SET-D1		SET-D2	
	$\sigma=9.5$	$\sigma=65$	$\sigma=9.5$	$\sigma=65$	$\sigma=4.5$	$\sigma=33$	$\sigma=4.5$	$\sigma=33$
Col.1	-0.54	0.29	-0.07	-0.26	-1.83	0.96	-2.62	0.85
Col.2	-0.53	0.32	-0.15	-0.12	-1.37	0.53	-2.28	0.75
Col.3	-0.86	0.73	0.02	-0.09	-1.46	0.60	-2.24	0.71
Col.4	-0.49	0.20	-0.11	-0.21	-1.72	1.18	-2.48	0.71
Bm.1	-0.34	0.20	0.27	1.91	-0.61	-0.92	-1.62	-0.34
Bm.2	-0.35	0.23	0.12	2.15	-0.52	-1.66	-1.77	-0.01
Bm.3	-0.32	0.13	0.07	1.58	-0.61	-1.36	-1.71	0.05

Table C.7. Response ratio values (as a percentage of reference base 1.0) for the peak member end rotations at the first story columns and beams evaluated at the minimum and at the maximum values of the wave parameter (9.5 – 65 for SETC and 4.5 – 33 for SETD) and at the respective aspect ratio of the frame model, 8KatS2.

H/R=2.48								
(Response ratio values as a percentage of reference base 1.0)								
Member	Analysis Group I: NS							
	SET-C1		SET-C2		SET-D1		SET-D2	
	$\sigma=9.5$	$\sigma=65$	$\sigma=9.5$	$\sigma=65$	$\sigma=4.5$	$\sigma=33$	$\sigma=4.5$	$\sigma=33$
Col.1	-0.59	0.37	-1.05	0.99	-4.10	4.33	-4.45	3.13
Col.2	-0.54	0.31	-1.02	1.01	-4.58	5.03	-4.39	3.14
Col.3	-0.55	0.34	-1.03	1.04	-4.56	5.00	-4.42	3.18
Col.4	-0.51	0.29	-1.00	0.89	-4.19	4.31	-4.23	2.96
Bm.1	-0.61	0.50	-1.12	0.77	-4.80	7.32	-5.11	-0.38
Bm.2	-0.63	0.32	-1.19	0.51	-4.46	5.22	-5.18	-0.49
Bm.3	-0.64	0.36	-1.17	0.83	-4.33	3.68	-4.98	-0.26
Member	Analysis Group II: SC							
	SET-C1		SET-C2		SET-D1		SET-D2	
	$\sigma=9.5$	$\sigma=65$	$\sigma=9.5$	$\sigma=65$	$\sigma=4.5$	$\sigma=33$	$\sigma=4.5$	$\sigma=33$
Col.1	-0.45	0.10	-1.00	0.94	-2.74	3.29	-3.43	1.97
Col.2	-0.55	0.33	-1.04	1.00	-3.36	4.10	-3.67	2.29
Col.3	-0.53	0.29	-1.04	1.00	-3.31	4.00	-3.67	2.27
Col.4	-0.50	0.21	-1.00	0.96	-2.90	2.89	-3.52	2.04
Bm.1	-0.43	0.93	-1.12	0.50	-4.25	5.23	-4.71	-1.84
Bm.2	-0.37	0.53	-1.09	0.39	-3.65	3.18	-4.72	-1.99
Bm.3	-0.40	0.19	-1.06	0.45	-3.48	1.36	-4.71	-2.07
Member	Analysis Group III: SCR2							
	SET-C1		SET-C2		SET-D1		SET-D2	
	$\sigma=9.5$	$\sigma=65$	$\sigma=9.5$	$\sigma=65$	$\sigma=4.5$	$\sigma=33$	$\sigma=4.5$	$\sigma=33$
Col.1	-0.48	0.35	0.50	0.30	-2.18	0.61	-2.49	0.98
Col.2	-0.52	0.33	0.37	0.40	-1.99	-0.09	-2.27	0.75
Col.3	-0.75	0.83	0.47	0.36	-2.05	0.02	-2.25	0.70
Col.4	-0.44	0.25	0.49	0.39	-2.18	0.72	-2.43	0.77
Bm.1	-0.42	0.13	0.83	2.48	-1.17	-1.48	-1.84	-0.56
Bm.2	-0.44	0.14	0.85	2.88	-1.24	-2.38	-1.95	-0.19
Bm.3	-0.41	0.04	0.80	2.31	-1.25	-2.00	-1.87	-0.11

Table C.8. Response ratio values (as a percentage of reference base 1.0) for the peak member end rotations at the first story columns and beams evaluated at the minimum and at the maximum values of the wave parameter (9.5 – 65 for SETC and 4.5 – 33 for SETD) and at the respective aspect ratio of the frame model, 12KatFS.

H/R=3.57								
(Response ratio values as a percentage of reference base 1.0)								
Member	Analysis Group I: NS							
	SET-C1		SET-C2		SET-D1		SET-D2	
	$\sigma=9.5$	$\sigma=65$	$\sigma=9.5$	$\sigma=65$	$\sigma=4.5$	$\sigma=33$	$\sigma=4.5$	$\sigma=33$
Col.1	-0.57	0.40	-0.79	1.25	-3.25	5.19	-3.67	3.91
Col.2	-0.51	0.35	-0.77	1.25	-3.62	5.99	-3.57	3.96
Col.3	-0.51	0.38	-0.78	1.30	-3.60	5.96	-3.57	4.03
Col.4	-0.49	0.31	-0.77	1.12	-3.51	4.99	-3.54	3.65
Bm.1	-0.58	0.54	-0.99	0.90	-3.50	8.62	-5.29	-0.56
Bm.2	-0.61	0.35	-1.09	0.60	-3.60	6.07	-5.32	-0.64
Bm.3	-0.62	0.38	-1.04	0.97	-3.81	4.20	-5.17	-0.45
Member	Analysis Group II: SC							
	SET-C1		SET-C2		SET-D1		SET-D2	
	$\sigma=9.5$	$\sigma=65$	$\sigma=9.5$	$\sigma=65$	$\sigma=4.5$	$\sigma=33$	$\sigma=4.5$	$\sigma=33$
Col.1	-0.43	0.12	-0.76	1.18	-2.36	3.67	-3.10	2.30
Col.2	-0.51	0.38	-0.75	1.28	-2.71	4.74	-3.19	2.77
Col.3	-0.49	0.32	-0.76	1.27	-2.69	4.62	-3.19	2.74
Col.4	-0.45	0.26	-0.73	1.23	-2.53	3.26	-3.10	2.47
Bm.1	-0.30	1.06	-1.07	0.55	-3.66	5.83	-5.60	-2.73
Bm.2	-0.31	0.58	-1.05	0.42	-3.49	3.34	-5.66	-2.93
Bm.3	-0.43	0.16	-1.01	0.49	-3.72	1.12	-5.69	-3.05
Member	Analysis Group III: SCR2							
	SET-C1		SET-C2		SET-D1		SET-D2	
	$\sigma=9.5$	$\sigma=65$	$\sigma=9.5$	$\sigma=65$	$\sigma=4.5$	$\sigma=33$	$\sigma=4.5$	$\sigma=33$
Col.1	-0.39	0.44	1.22	1.02	-2.63	0.15	-2.32	1.15
Col.2	-0.50	0.35	1.04	1.07	-2.78	-0.89	-2.26	0.76
Col.3	-0.61	0.97	1.06	0.95	-2.80	-0.74	-2.26	0.69
Col.4	-0.37	0.32	1.27	1.17	-2.78	0.12	-2.35	0.84
Bm.1	-0.52	0.03	1.56	3.21	-1.89	-2.20	-2.12	-0.84
Bm.2	-0.56	0.02	1.79	3.82	-2.16	-3.31	-2.18	-0.43
Bm.3	-0.53	-0.08	1.74	3.25	-2.08	-2.83	-2.08	-0.32

Table C.9. Response ratio values (as a percentage of reference base 1.0) for the peak member end rotations at the first story columns and beams evaluated at the minimum and at the maximum values of the wave parameter (9.5 – 65 for SETC and 4.5 – 33 for SETD) and at the respective aspect ratio of the frame model, 12KatRS.

H/R=3.62								
(Response ratio values as a percentage of reference base 1.0)								
Member	Analysis Group I: NS							
	SET-C1		SET-C2		SET-D1		SET-D2	
	$\sigma=9.5$	$\sigma=65$	$\sigma=9.5$	$\sigma=65$	$\sigma=4.5$	$\sigma=33$	$\sigma=4.5$	$\sigma=33$
Col.1	-0.57	0.40	-0.78	1.26	-3.21	5.22	-3.64	3.95
Col.2	-0.50	0.35	-0.76	1.26	-3.57	6.04	-3.53	4.00
Col.3	-0.51	0.38	-0.77	1.31	-3.56	6.01	-3.54	4.07
Col.4	-0.49	0.31	-0.76	1.13	-3.48	5.02	-3.51	3.68
Bm.1	-0.57	0.54	-0.98	0.91	-3.44	8.68	-5.30	-0.57
Bm.2	-0.61	0.35	-1.09	0.60	-3.57	6.11	-5.33	-0.64
Bm.3	-0.62	0.38	-1.03	0.97	-3.78	4.22	-5.18	-0.46
Member	Analysis Group II: SC							
	SET-C1		SET-C2		SET-D1		SET-D2	
	$\sigma=9.5$	$\sigma=65$	$\sigma=9.5$	$\sigma=65$	$\sigma=4.5$	$\sigma=33$	$\sigma=4.5$	$\sigma=33$
Col.1	-0.43	0.12	-0.75	1.19	-2.35	3.68	-3.09	2.32
Col.2	-0.51	0.38	-0.74	1.30	-2.69	4.77	-3.17	2.79
Col.3	-0.49	0.32	-0.74	1.29	-2.66	4.65	-3.17	2.77
Col.4	-0.45	0.26	-0.72	1.24	-2.51	3.28	-3.08	2.49
Bm.1	-0.29	1.07	-1.06	0.56	-3.63	5.85	-5.64	-2.77
Bm.2	-0.31	0.58	-1.05	0.43	-3.48	3.35	-5.70	-2.98
Bm.3	-0.43	0.16	-1.01	0.50	-3.73	1.11	-5.73	-3.09
Member	Analysis Group III: SCR2							
	SET-C1		SET-C2		SET-D1		SET-D2	
	$\sigma=9.5$	$\sigma=65$	$\sigma=9.5$	$\sigma=65$	$\sigma=4.5$	$\sigma=33$	$\sigma=4.5$	$\sigma=33$
Col.1	-0.39	0.44	1.25	1.06	-2.65	0.13	-2.31	1.16
Col.2	-0.50	0.36	1.08	1.10	-2.82	-0.92	-2.26	0.76
Col.3	-0.61	0.98	1.09	0.98	-2.83	-0.77	-2.26	0.68
Col.4	-0.37	0.32	1.30	1.20	-2.80	0.10	-2.35	0.85
Bm.1	-0.52	0.02	1.59	3.24	-1.93	-2.24	-2.13	-0.85
Bm.2	-0.57	0.02	1.84	3.87	-2.21	-3.35	-2.19	-0.44
Bm.3	-0.54	-0.09	1.79	3.29	-2.12	-2.87	-2.09	-0.33

APPENDIX D

2D SCATTER PLOTS RELATED TO STATISTICAL ANALYSIS

In this appendix, 2D scatter plots of the response ratio values and the associated linear regression lines related to statistical analysis of Analysis Groups I, II and III are given. Plots contain (SSI.TH / FB.TH) values for the roof and the first story drift ratios and the peak member end rotations of the first story columns and beams with respect to the wave parameter (σ) and aspect ratio (H/R) of the frame models. Response ratio values associated with the peak column end rotation are obtained at the foundation end. Response ratio values associated with the peak beam end rotation are obtained from the maximum of the either ends of the element.

Figs. D.1 – D.4 are obtained for Analysis Group I; SET-NS-C1, C2, D1 and D2, respectively. Figs. D.5 – D.8 are obtained for Analysis Group II; SET-SC-C1, C2, D1 and D2, respectively. Figs. D.9 – D.12 are obtained for Analysis Group III; SET-SCR2-C1, C2, D1 and D2, respectively.

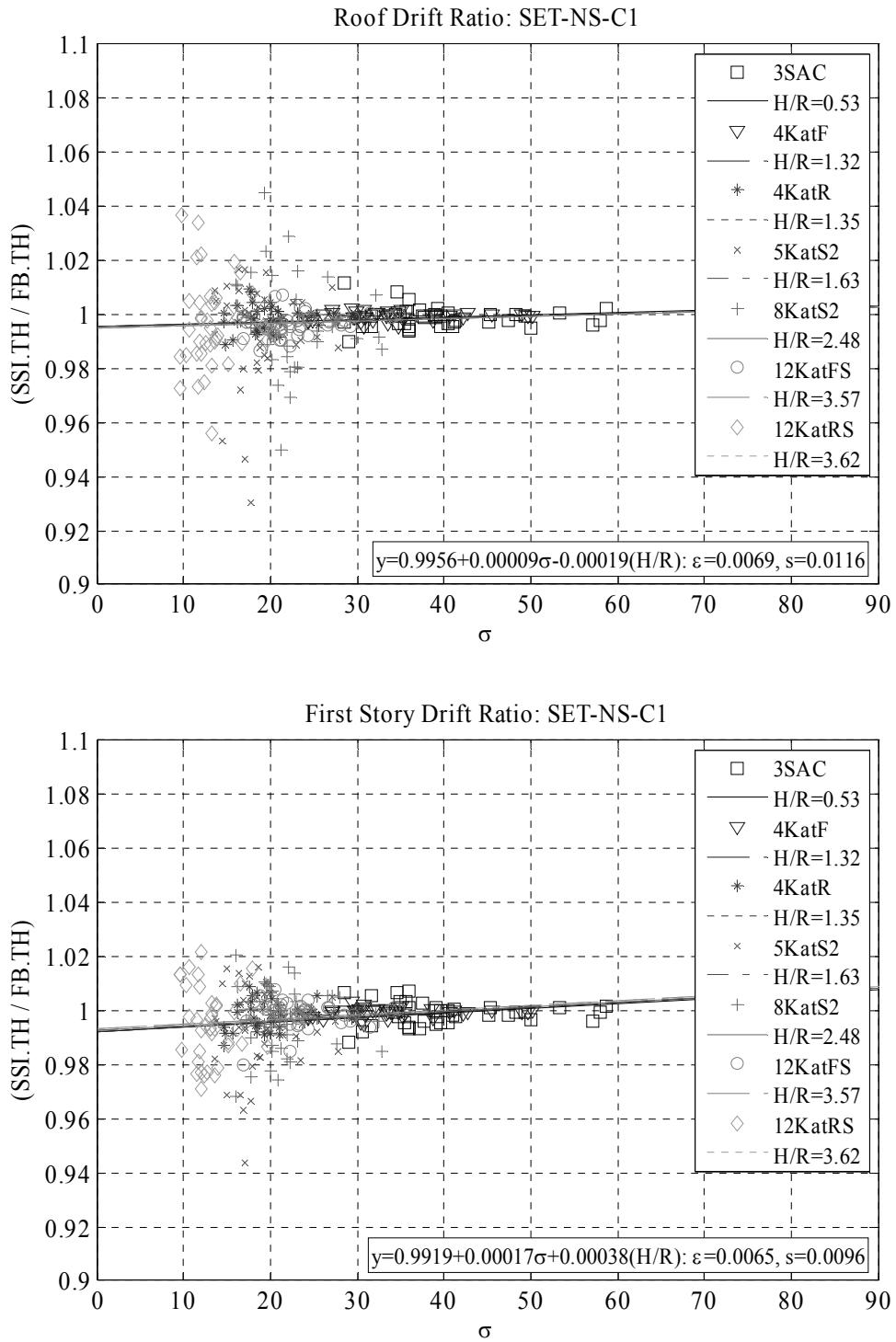


Figure D.1. 2D Scatter plot and associated regression line for the response ratios obtained for SET-NS-C1. Response ratios are calculated for: Roof drift ratio, first story drift ratio, peak column (foundation end) end and peak beam end rotations at the first story (SSI.TH / FB.TH), while the predictor variables are wave parameter (σ) and aspect ratio (H/R), ε is the mean absolute error and s is the standard error.

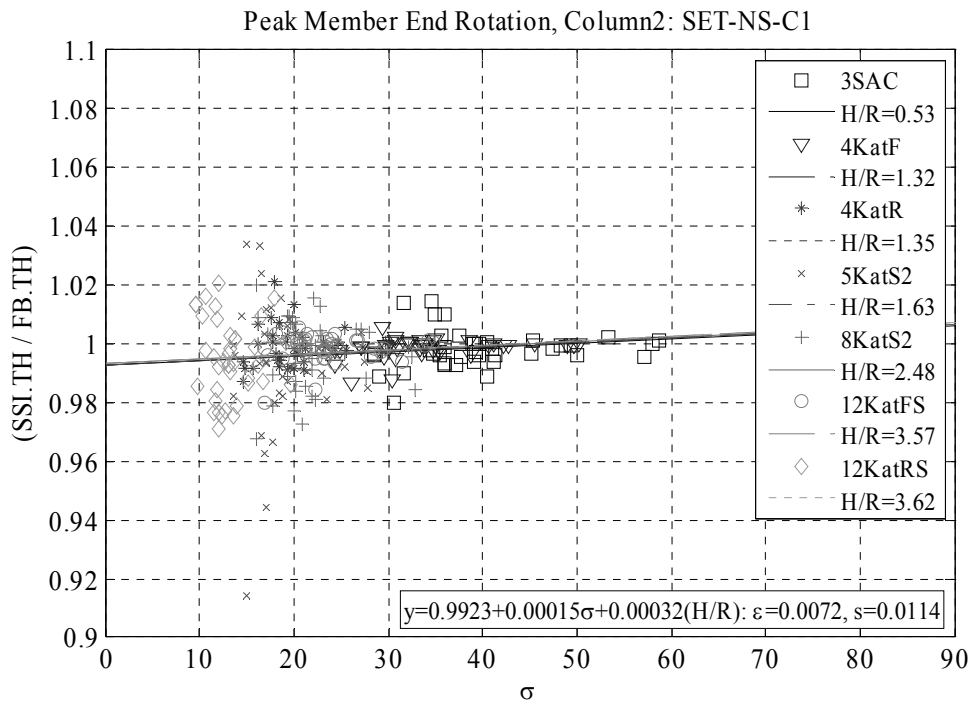
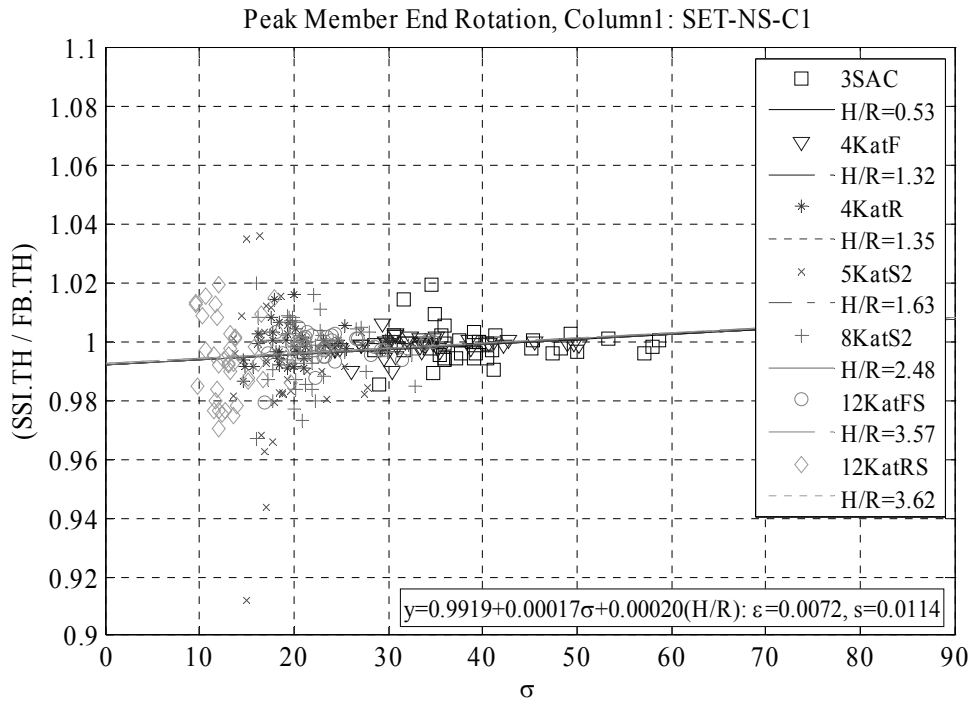


Figure D.1. (Cont'd)

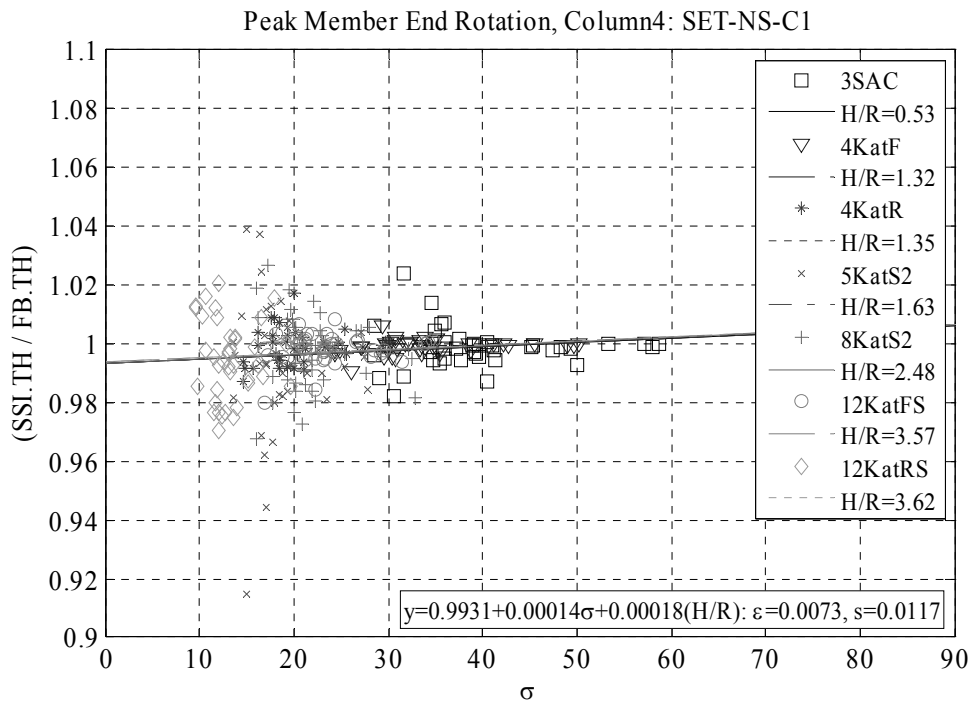
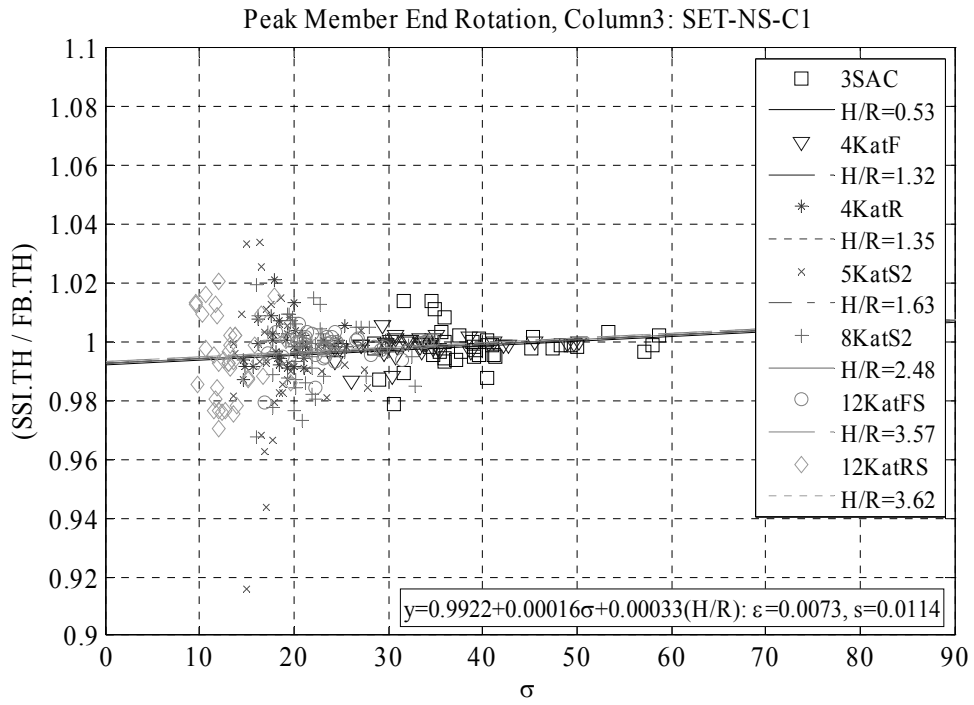


Figure D.1. (Cont'd)

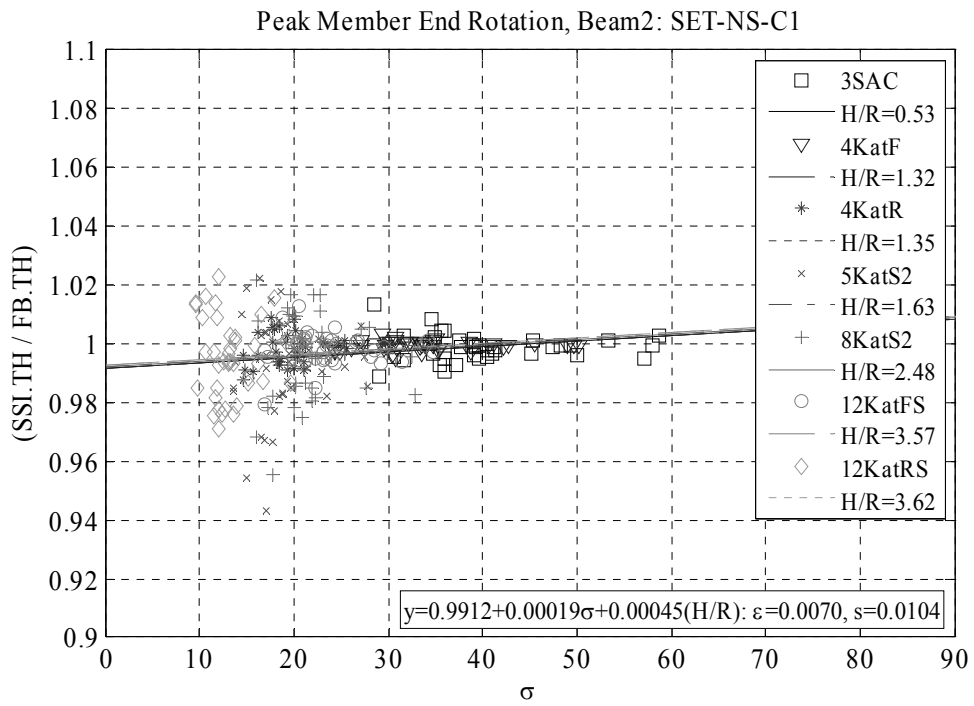
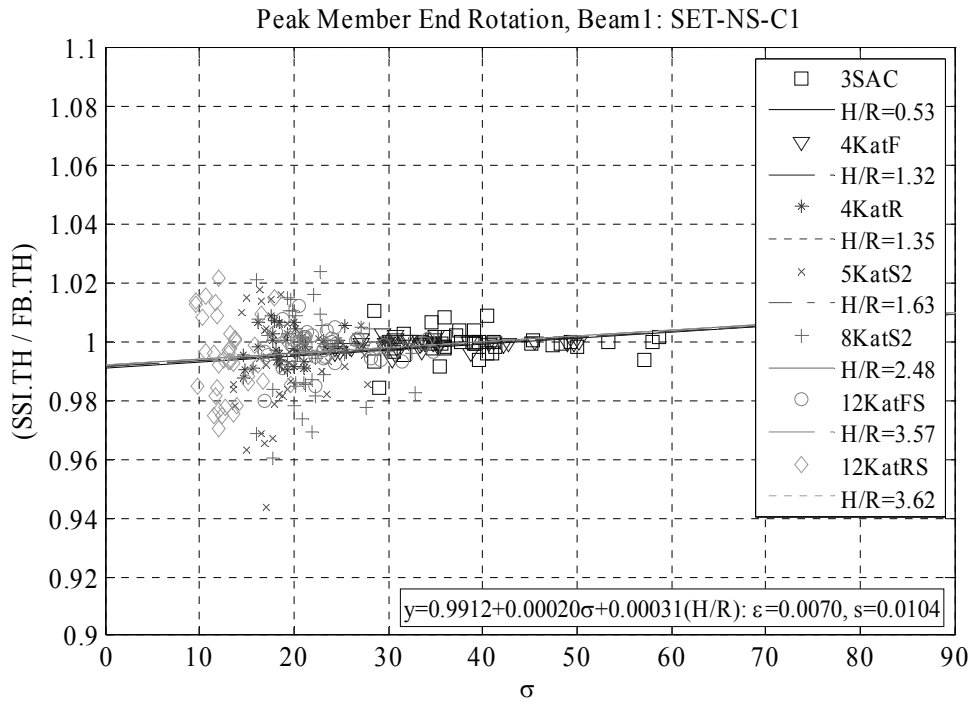


Figure D.1. (Cont'd)

Peak Member End Rotation, Beam3: SET-NS-C1

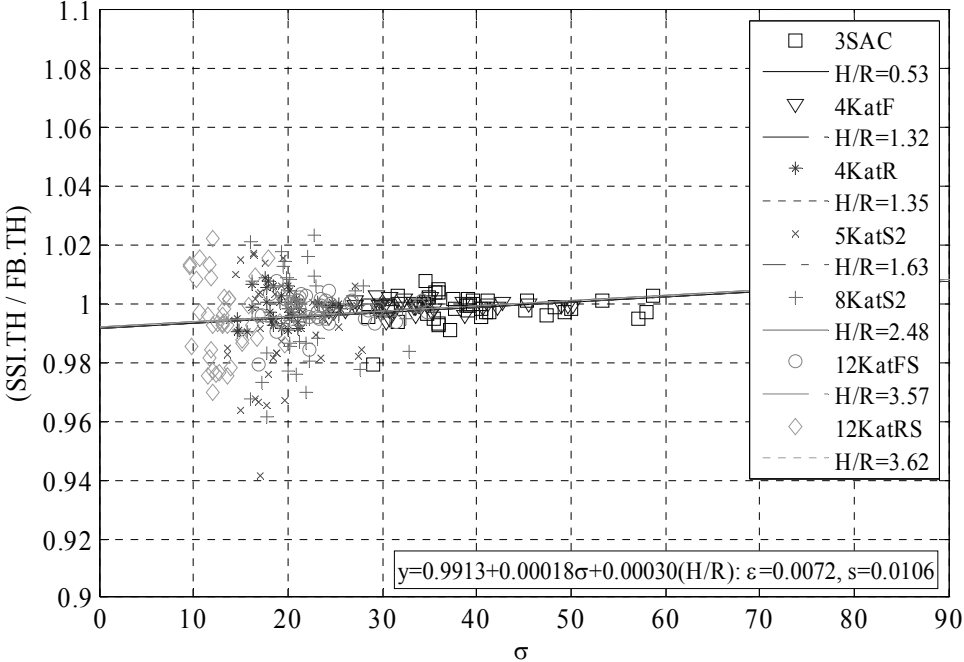


Figure D.1. (Cont'd)

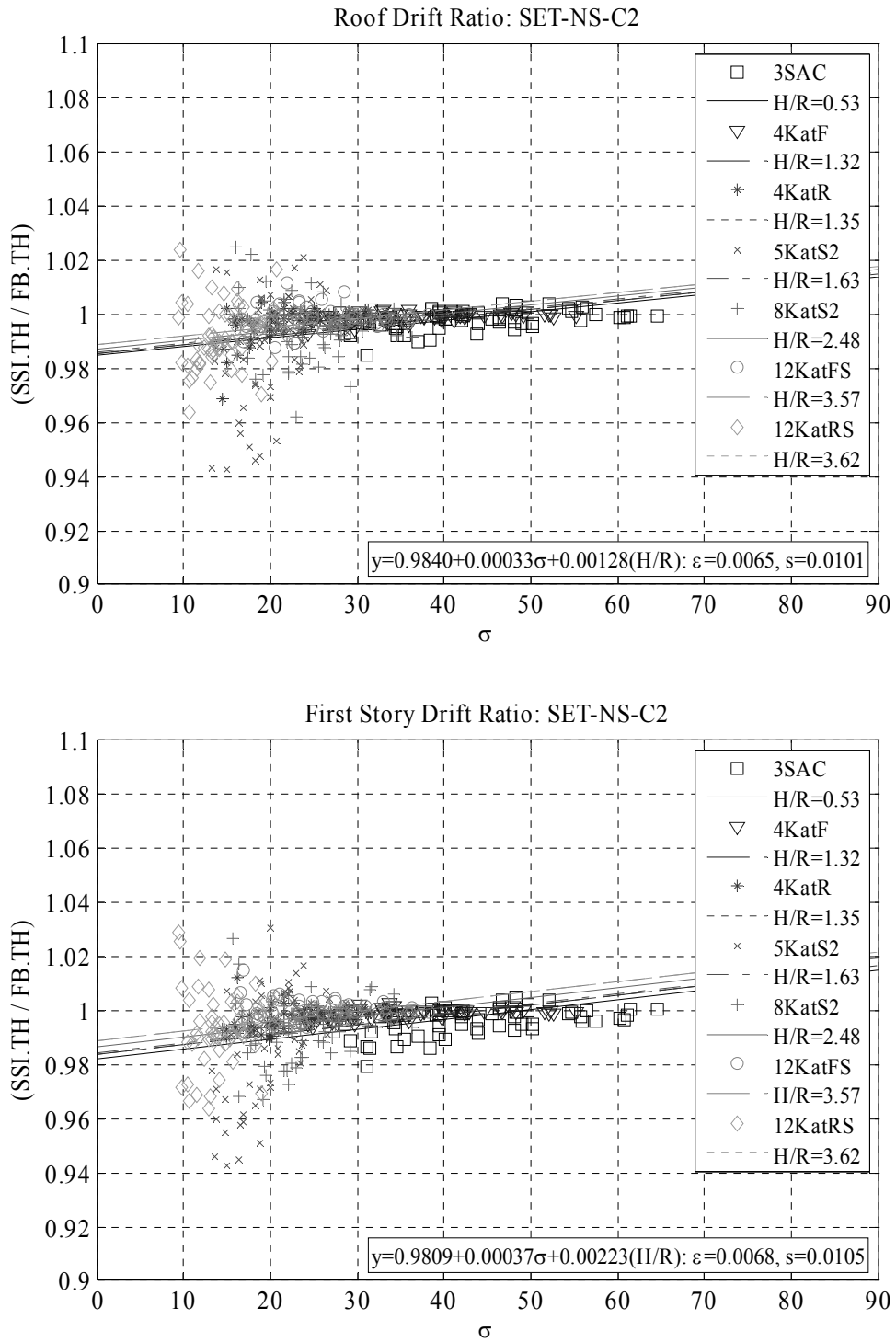


Figure D.2. 2D Scatter plot and associated regression line for the response ratios obtained for SET-NS-C2. Response ratios are calculated for: Roof drift ratio, first story drift ratio, peak column (foundation end) end and peak beam end rotations at the first story (SSI.TH / FB.TH), while the predictor variables are wave parameter (σ) and aspect ratio (H/R), ε is the mean absolute error and s is the standard error.

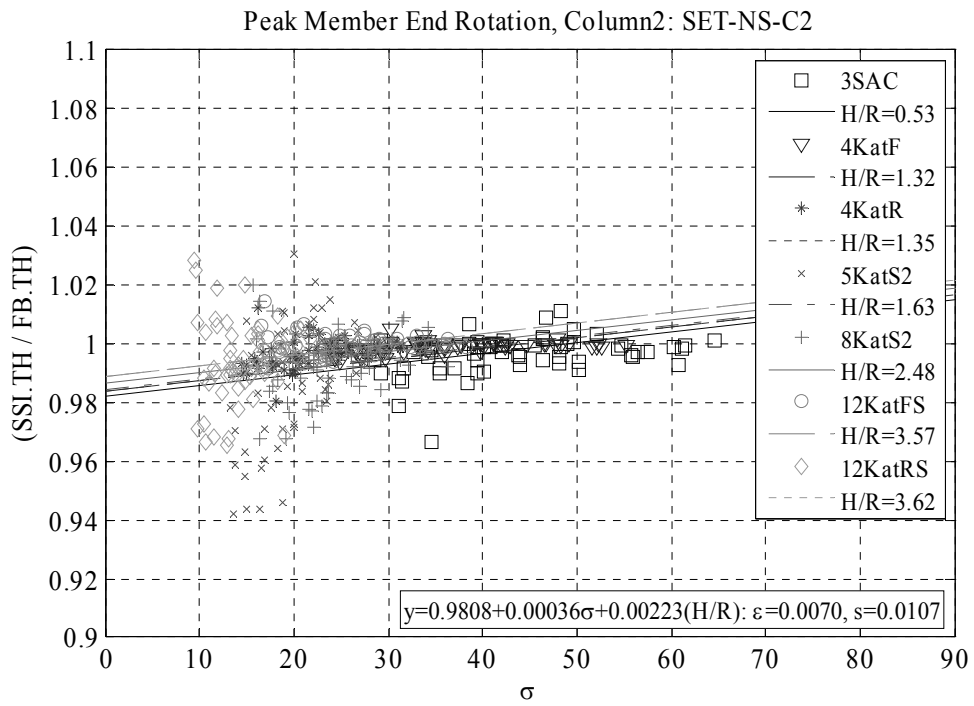
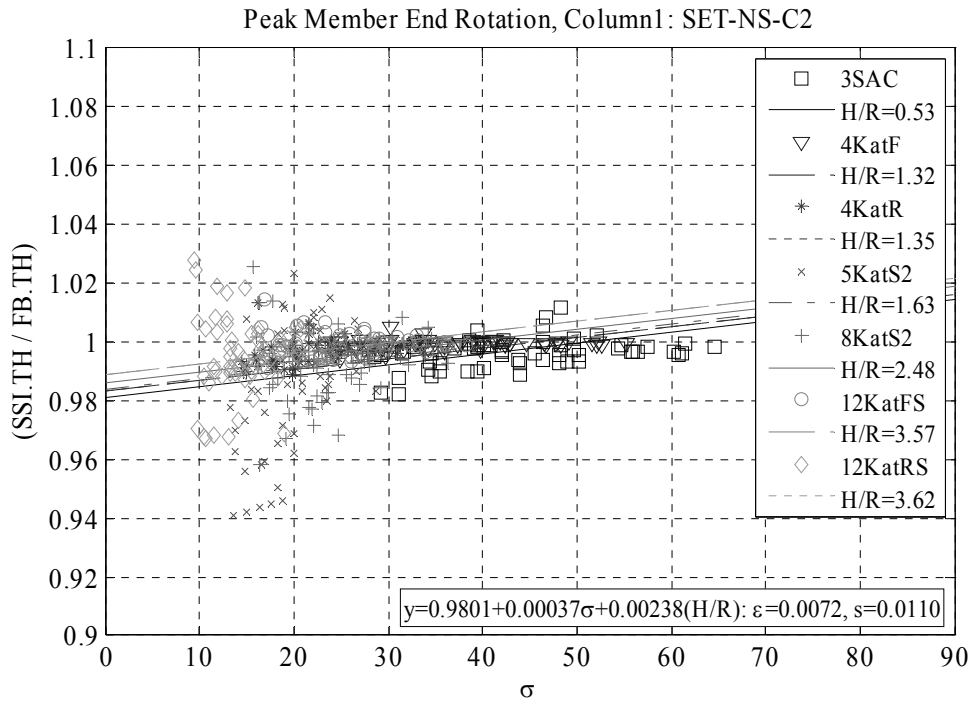


Figure D.2. (Cont'd)

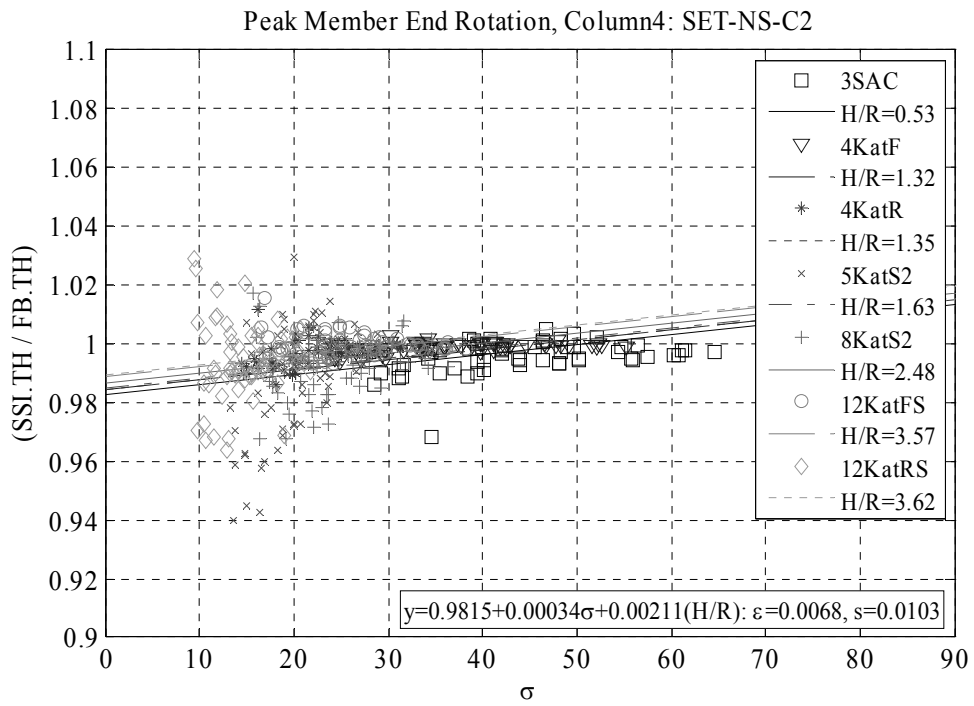
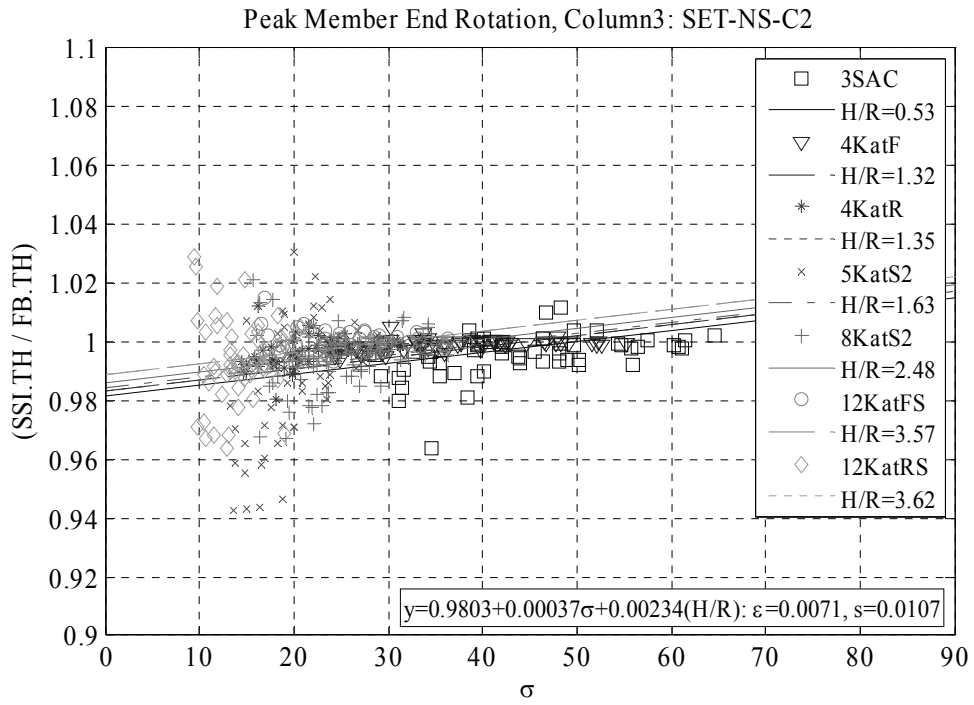


Figure D.2. (Cont'd)

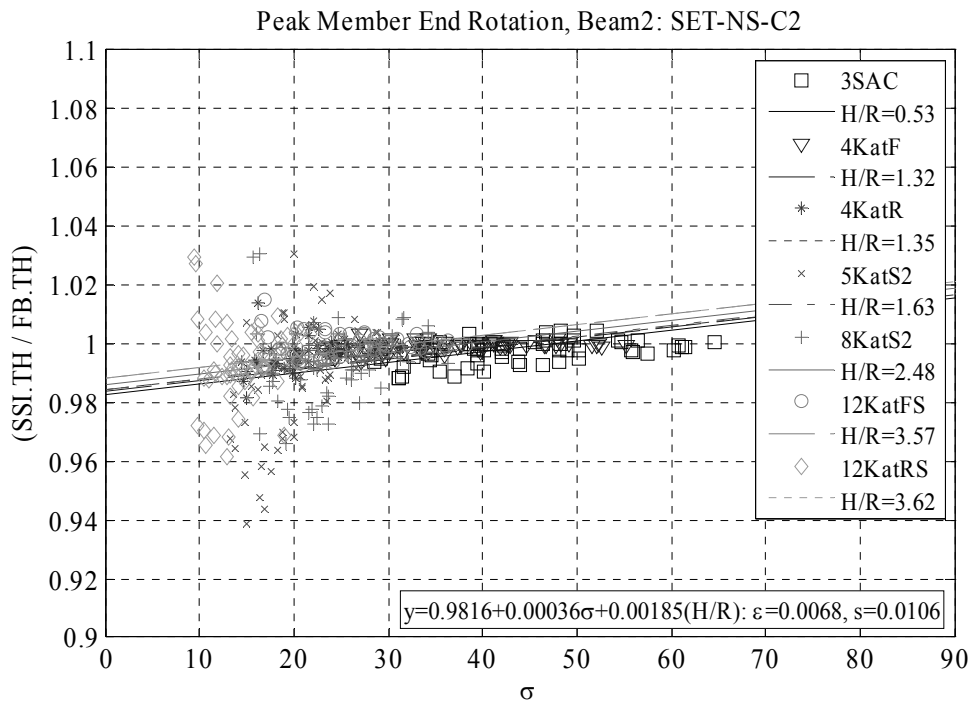
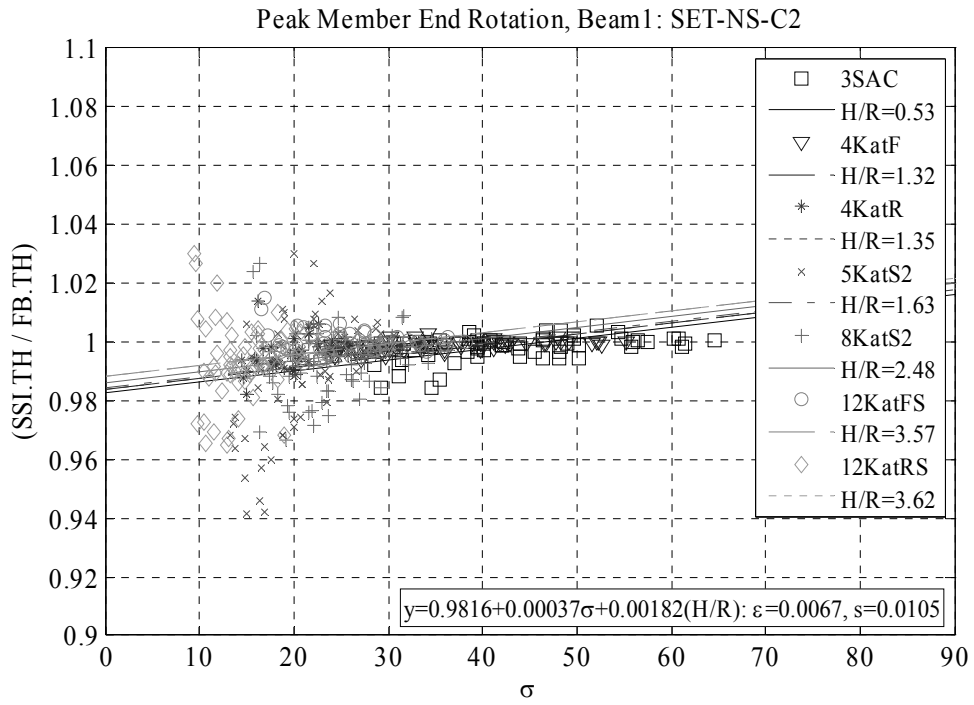


Figure D.2. (Cont'd)

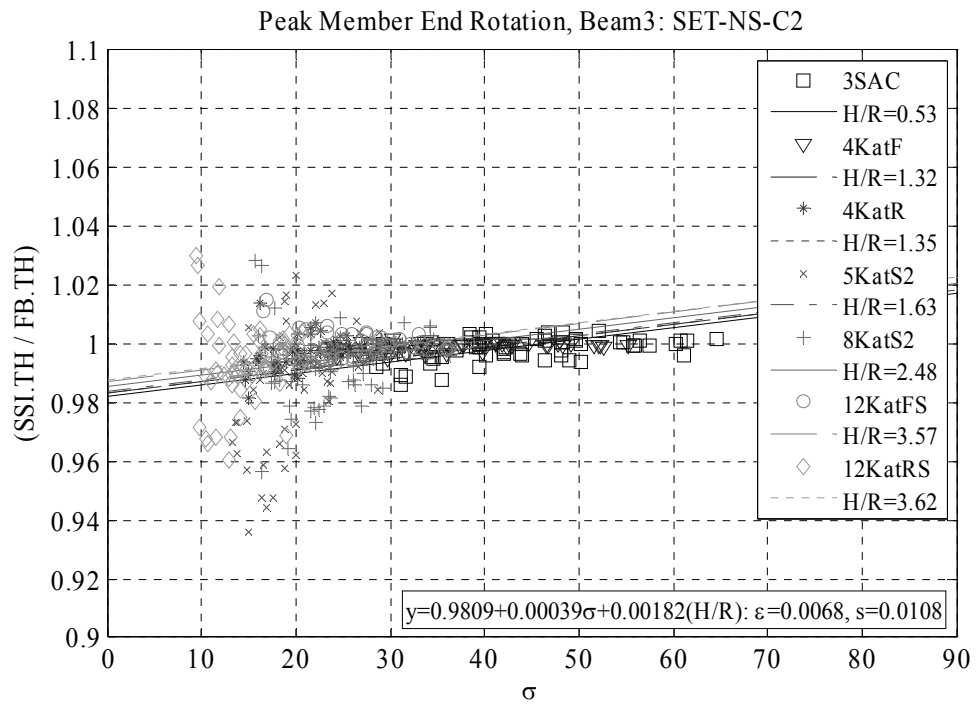


Figure D.2. (Cont'd)

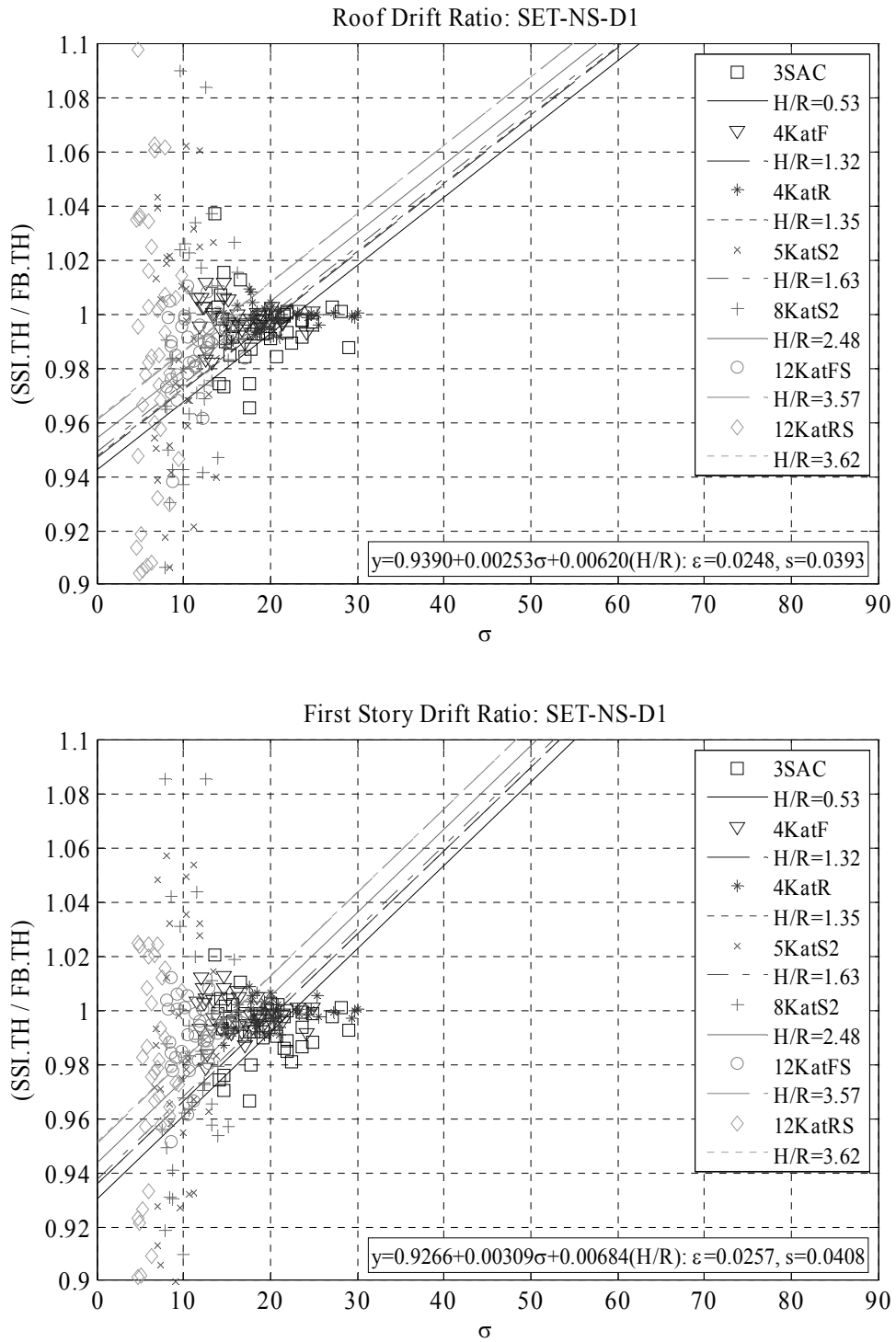


Figure D.3. 2D Scatter plot and associated regression line for the response ratios obtained for SET-NS-D1. Response ratios are calculated for: Roof drift ratio, first story drift ratio, peak column (foundation end) end and peak beam end rotations at the first story (SSI.TH / FB.TH), while the predictor variables are wave parameter (σ) and aspect ratio (H/R), ε is the mean absolute error and s is the standard error.

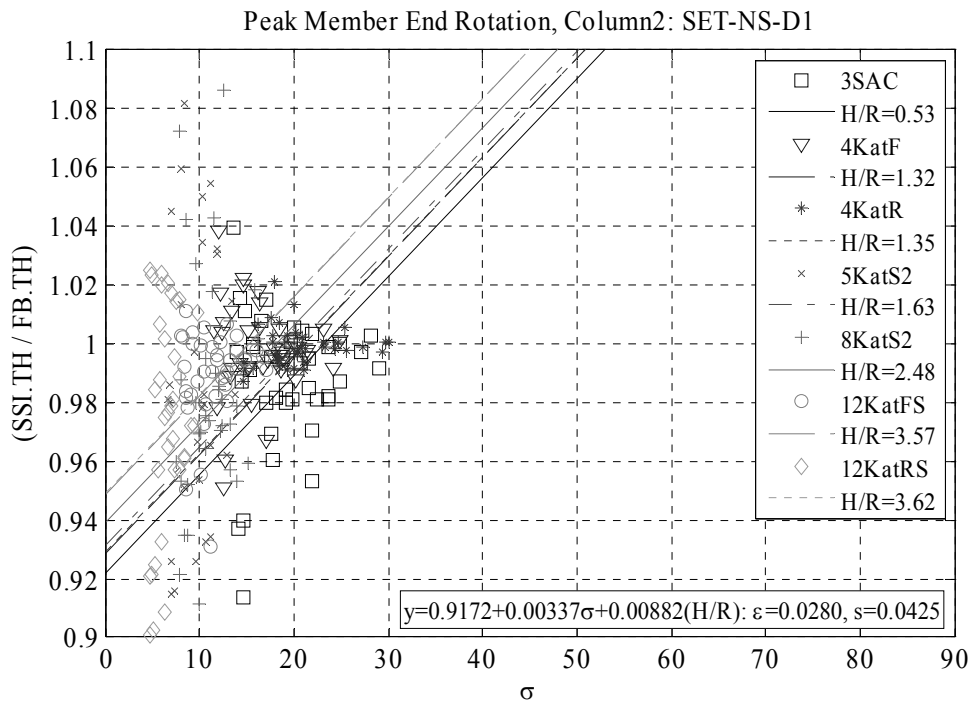
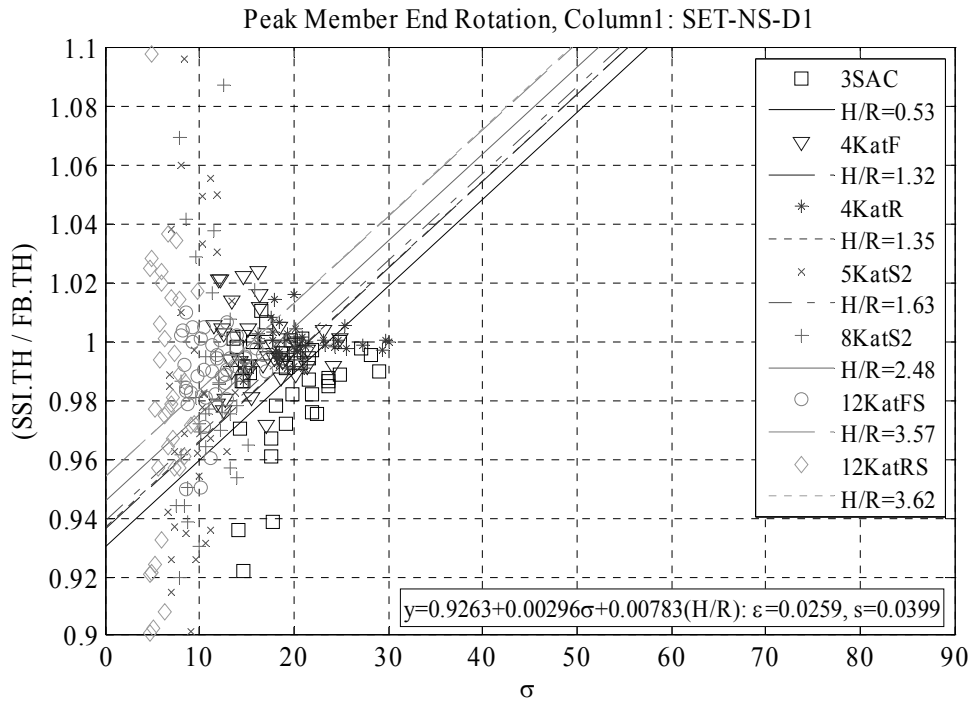


Figure D.3. (Cont'd)

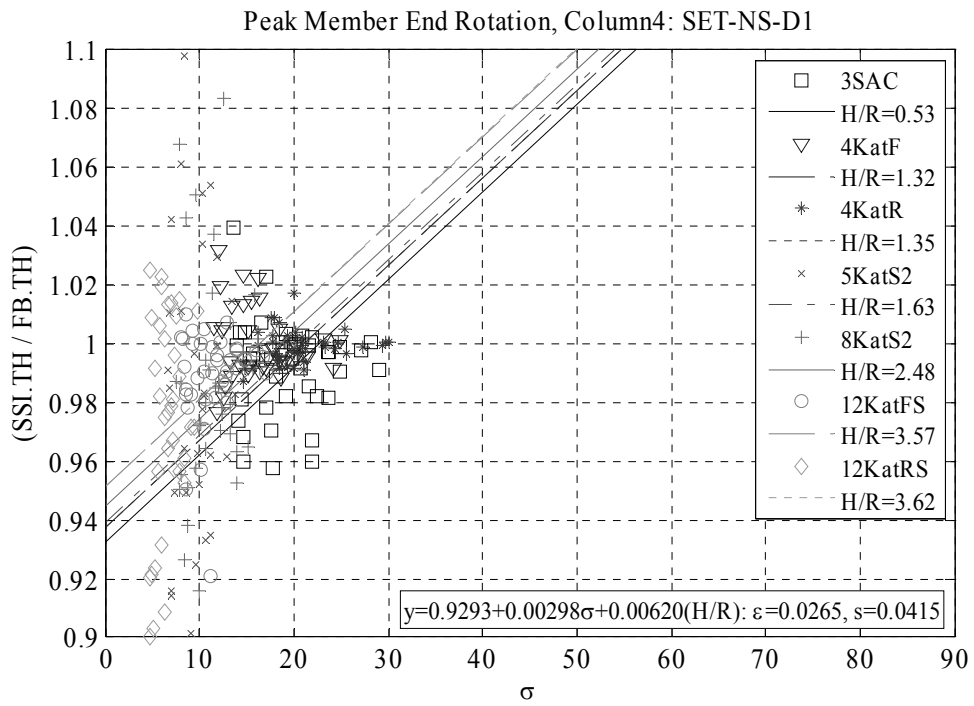
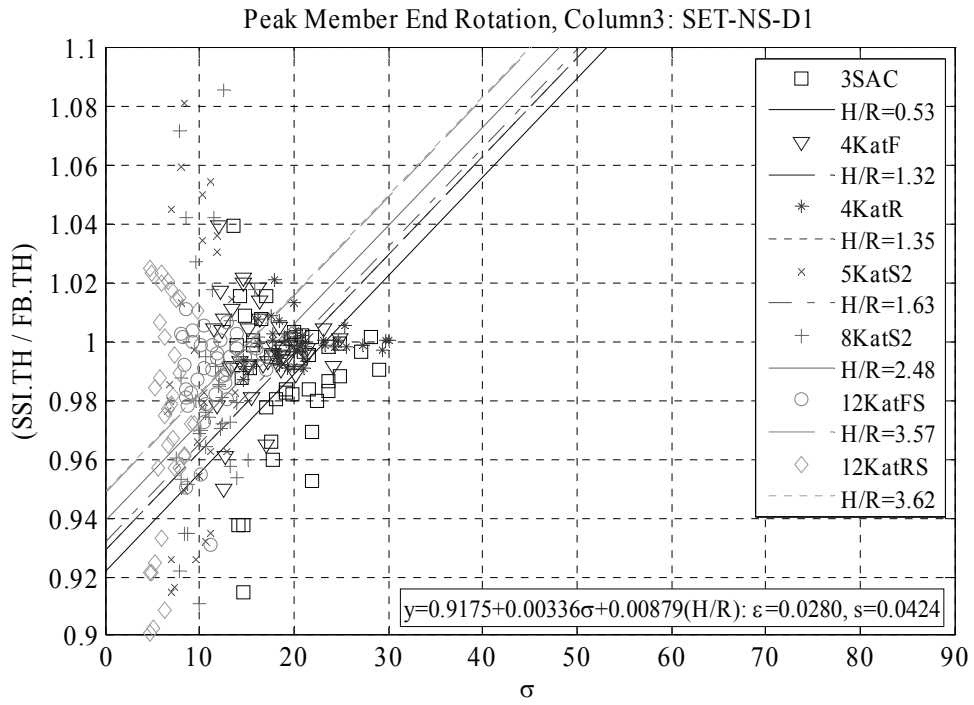


Figure D.3. (Cont'd)

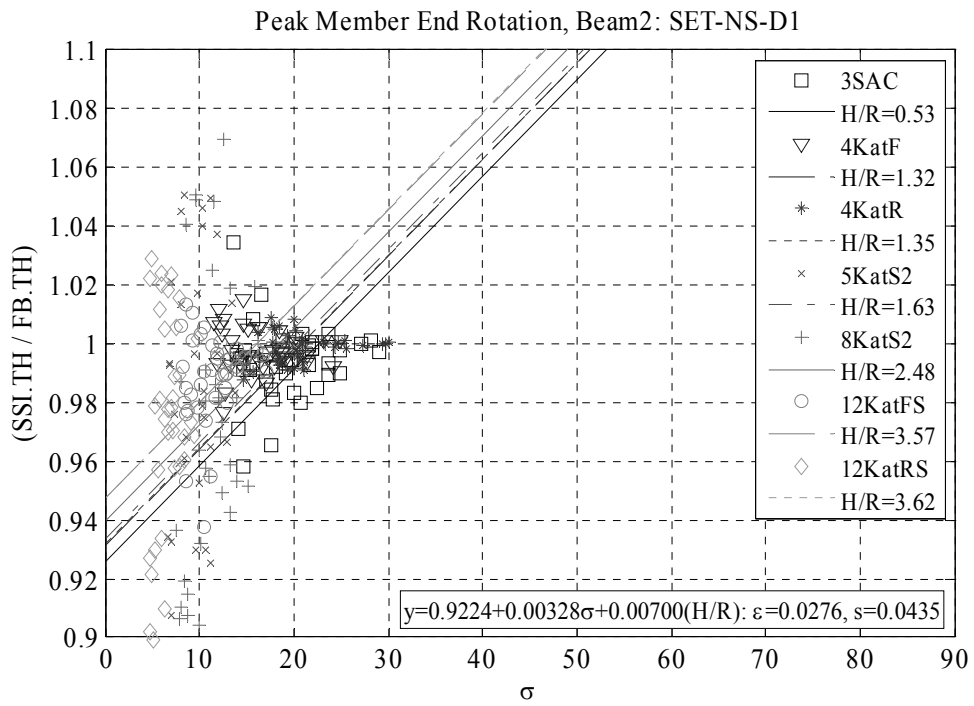
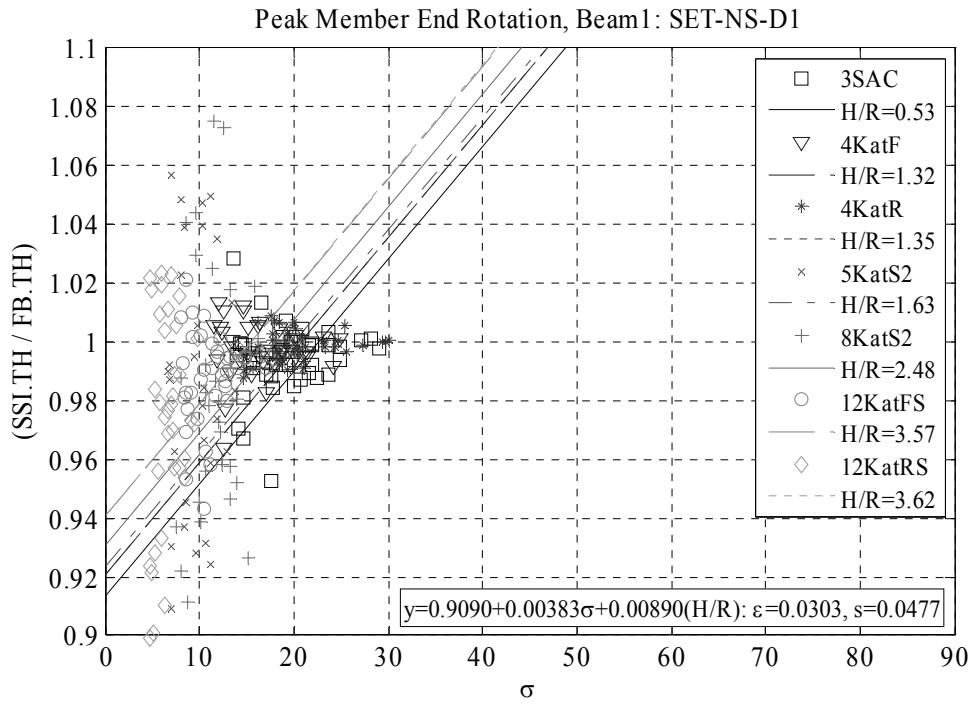


Figure D.3. (Cont'd)

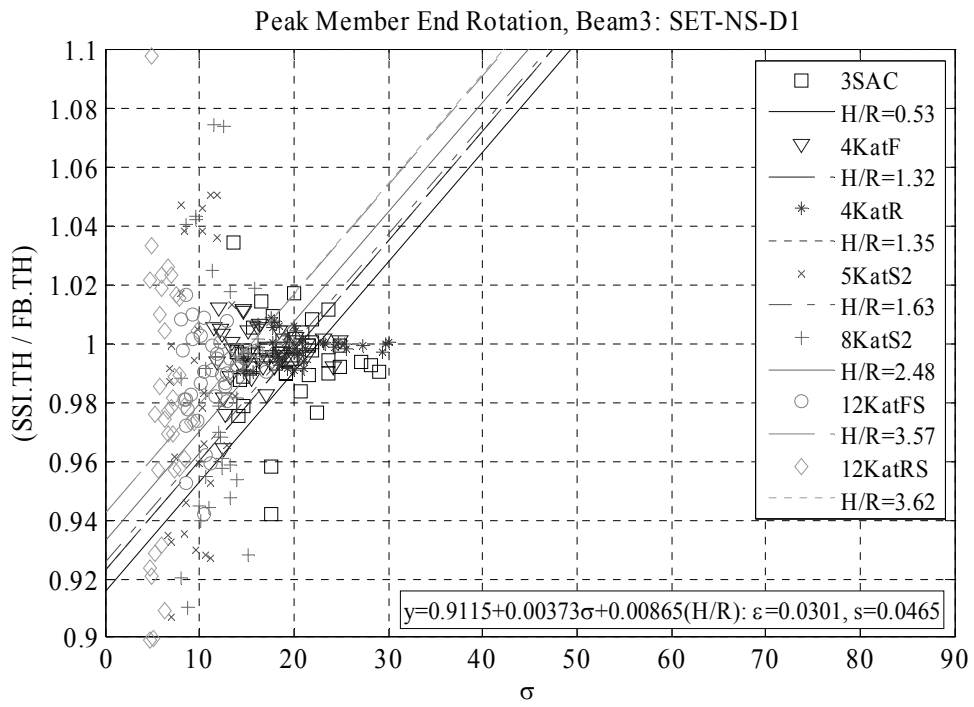


Figure D.3. (Cont'd)

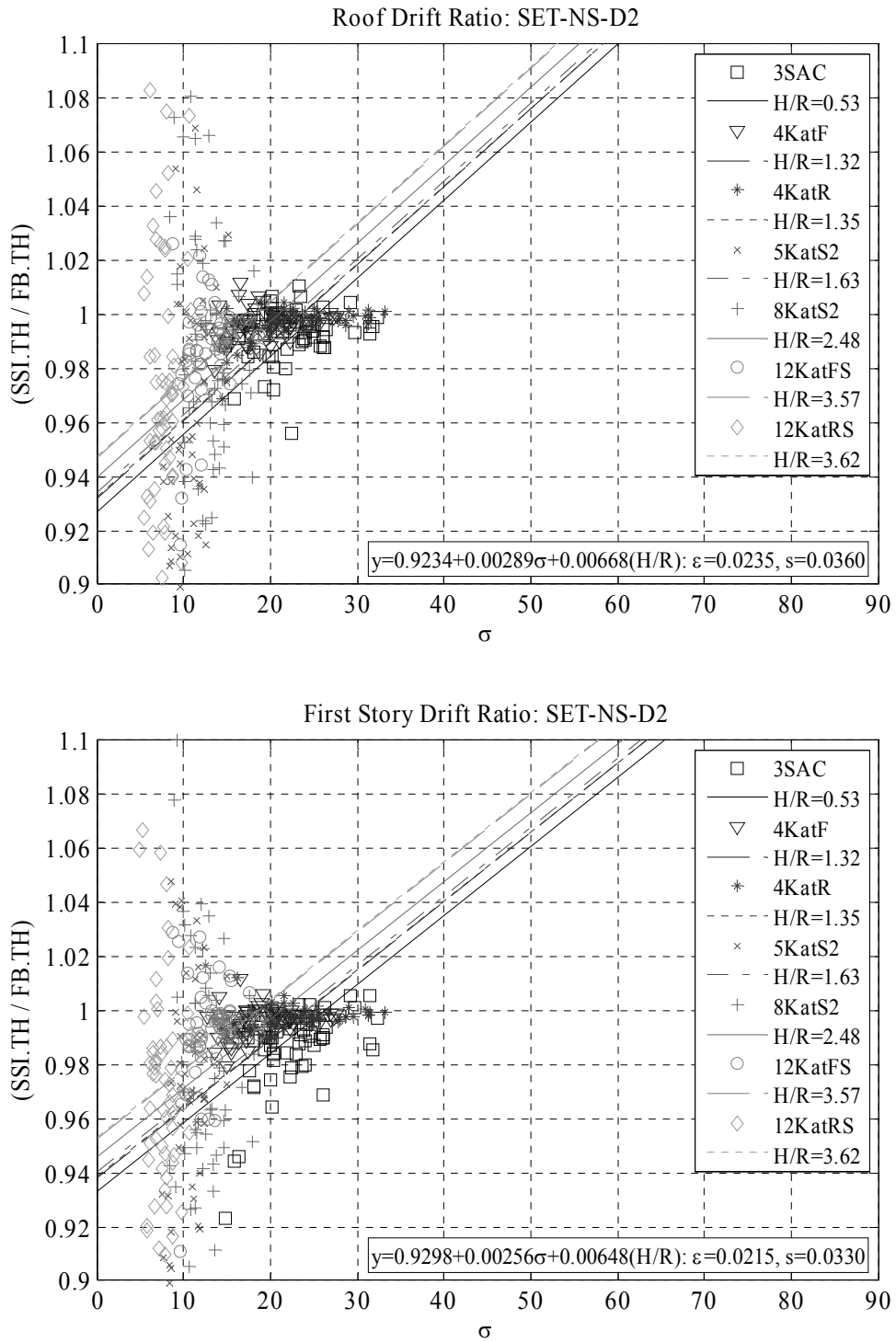


Figure D.4. 2D Scatter plot and associated regression line for the response ratios obtained for SET-NS-D2. Response ratios are calculated for: Roof drift ratio, first story drift ratio, peak column (foundation end) end and peak beam end rotations at the first story (SSI.TH / FB.TH), while the predictor variables are wave parameter (σ) and aspect ratio (H/R), ε is the mean absolute error and s is the standard error.

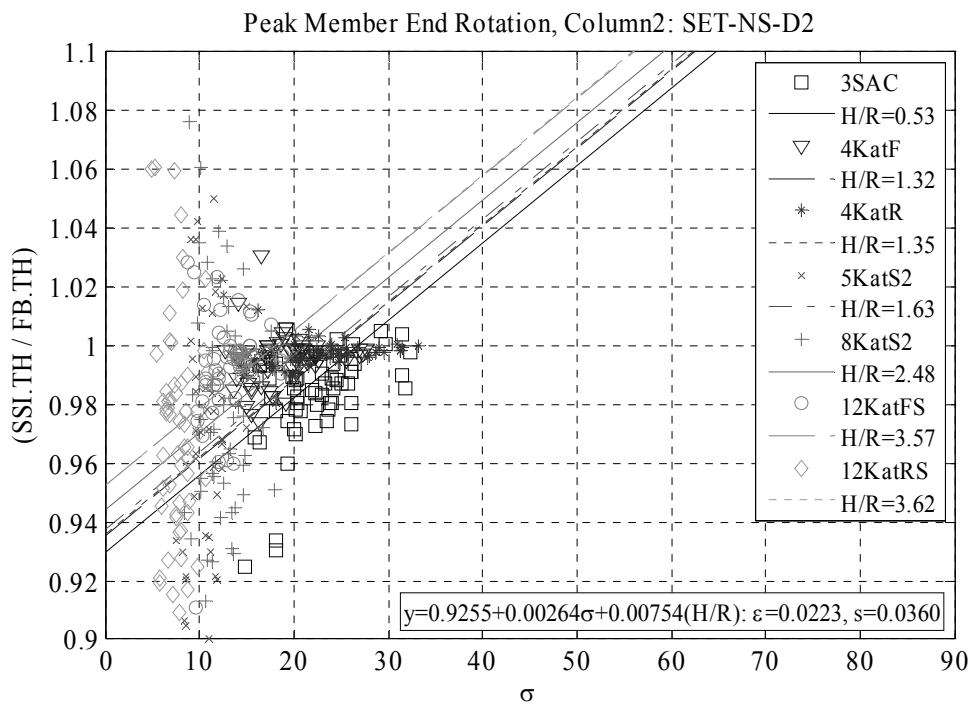
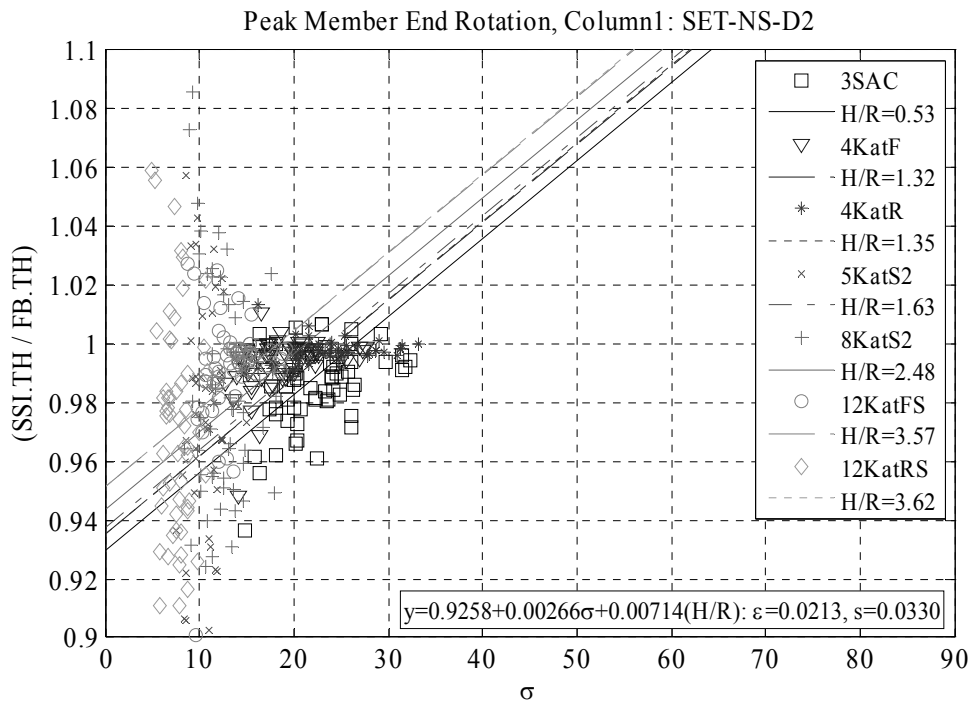


Figure D.4. (Cont'd)

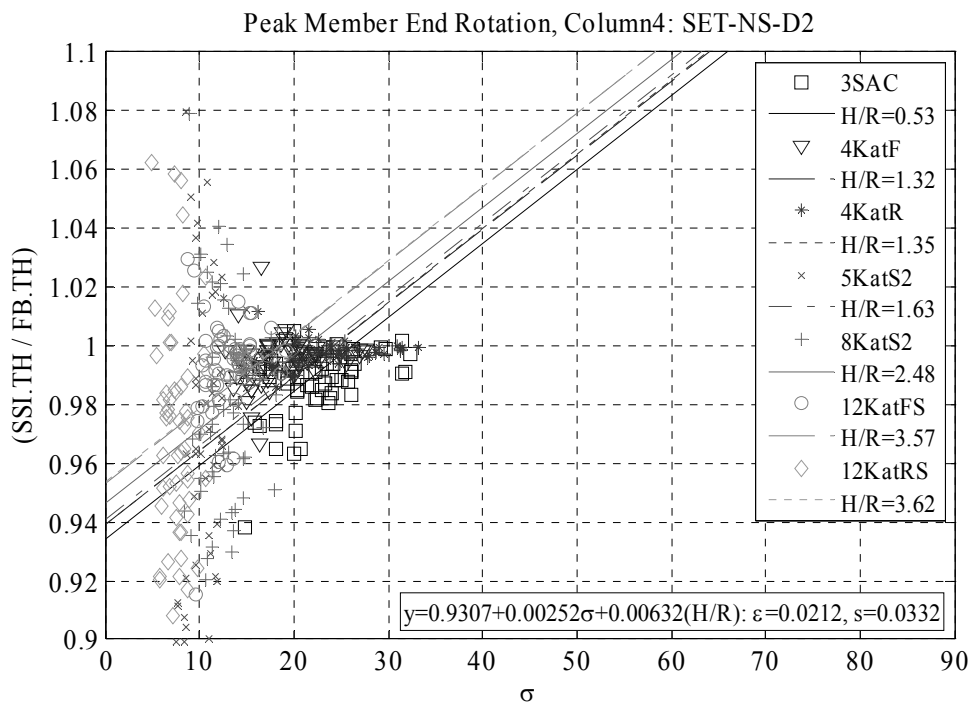
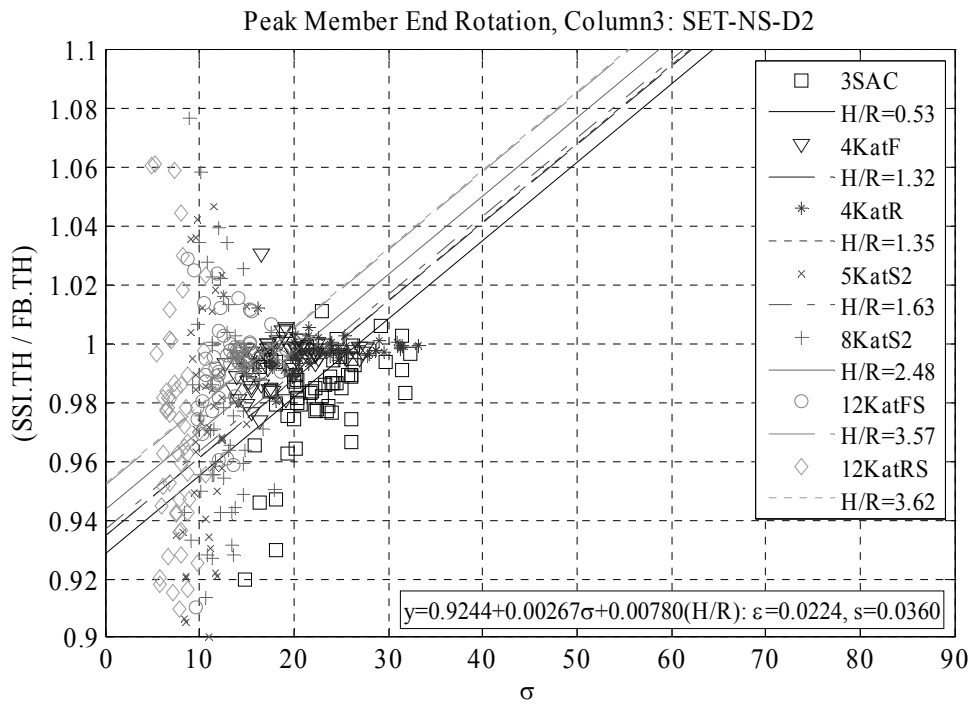


Figure D.4. (Cont'd)

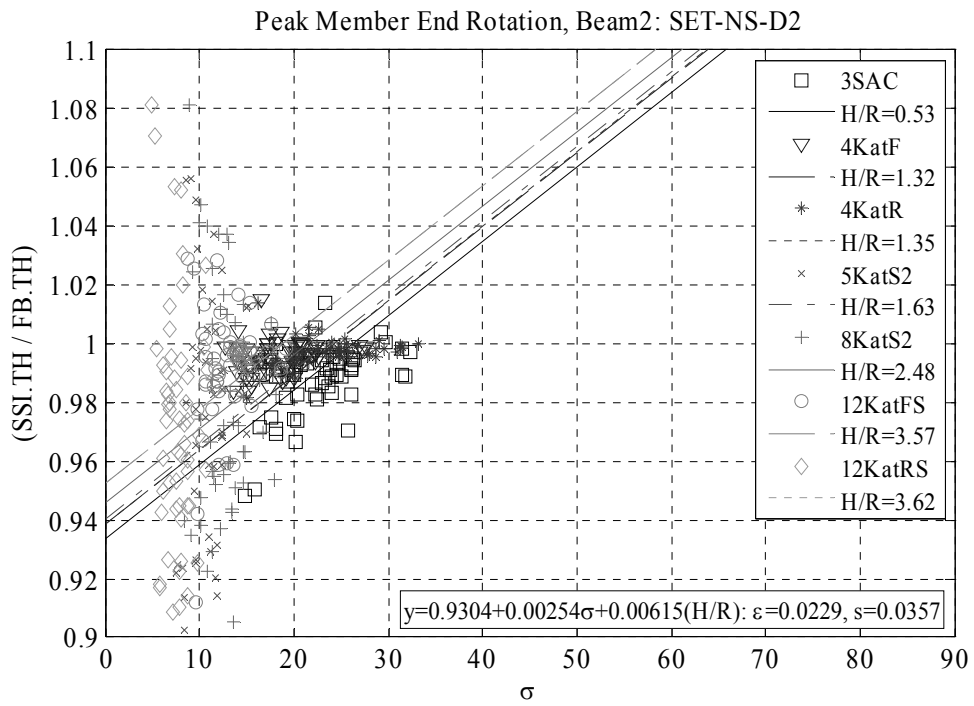
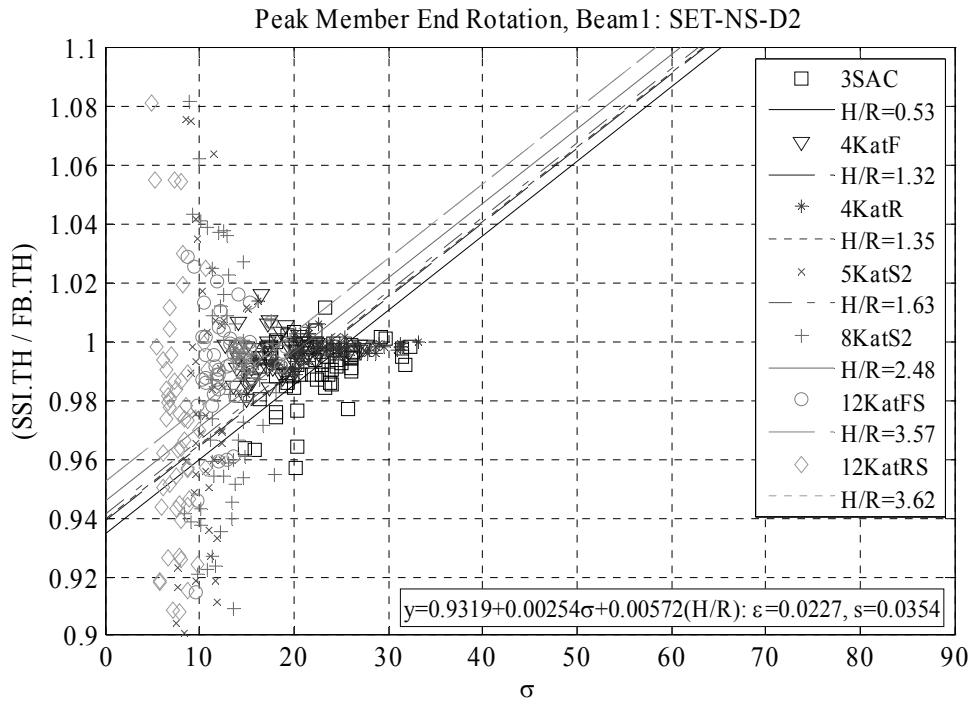


Figure D.4. (Cont'd)

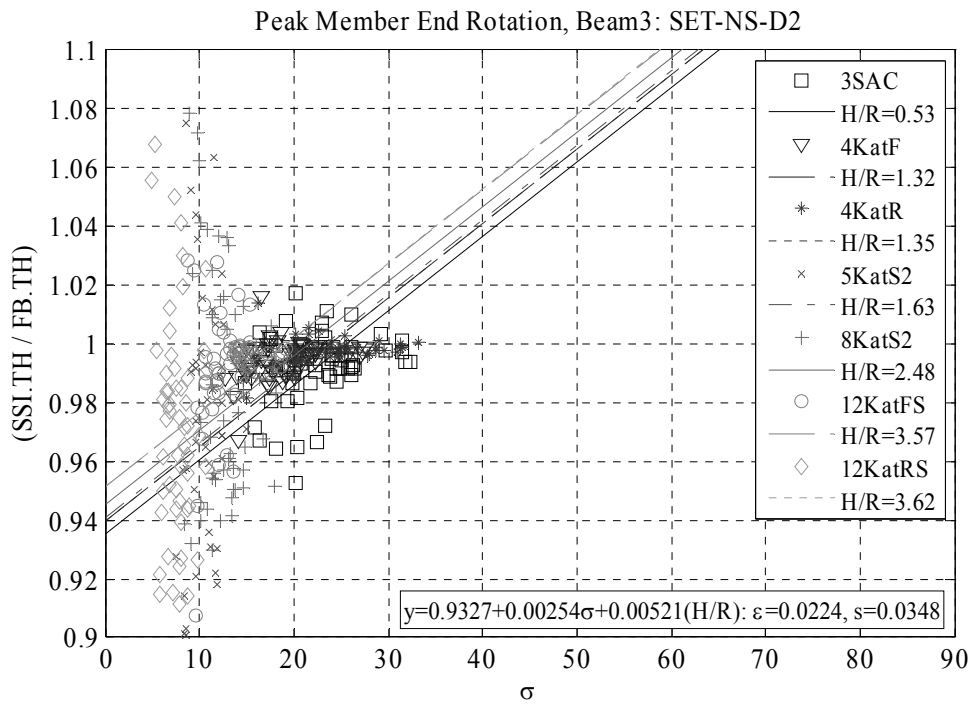


Figure D.4. (Cont'd)

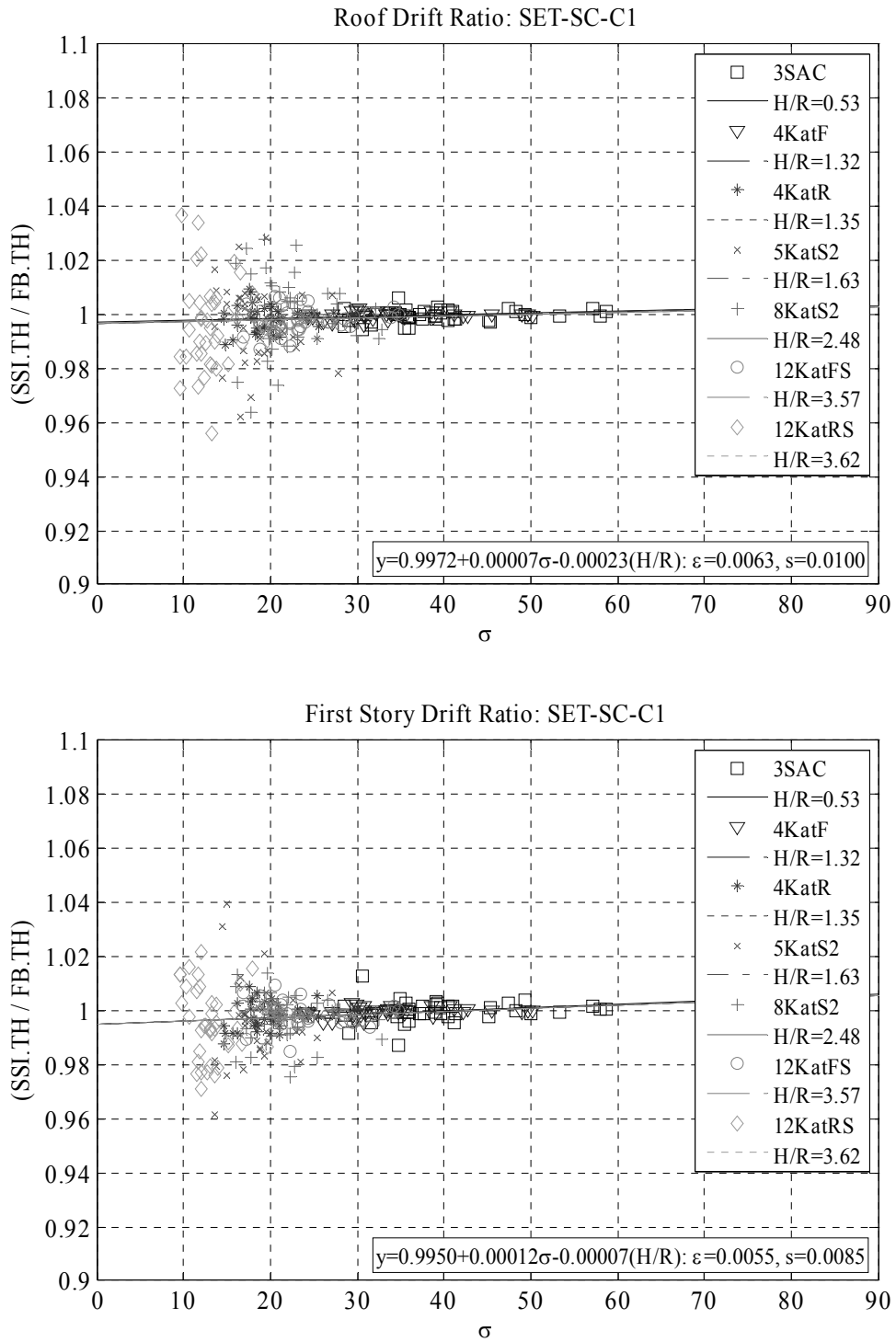


Figure D.5. 2D Scatter plot and associated regression line for the response ratios obtained for SET-SC-C1. Response ratios are calculated for: Roof drift ratio, first story drift ratio, peak column (foundation end) end and peak beam end rotations at the first story (SSI.TH / FB.TH), while the predictor variables are wave parameter (σ) and aspect ratio (H/R), ε is the mean absolute error and s is the standard error.

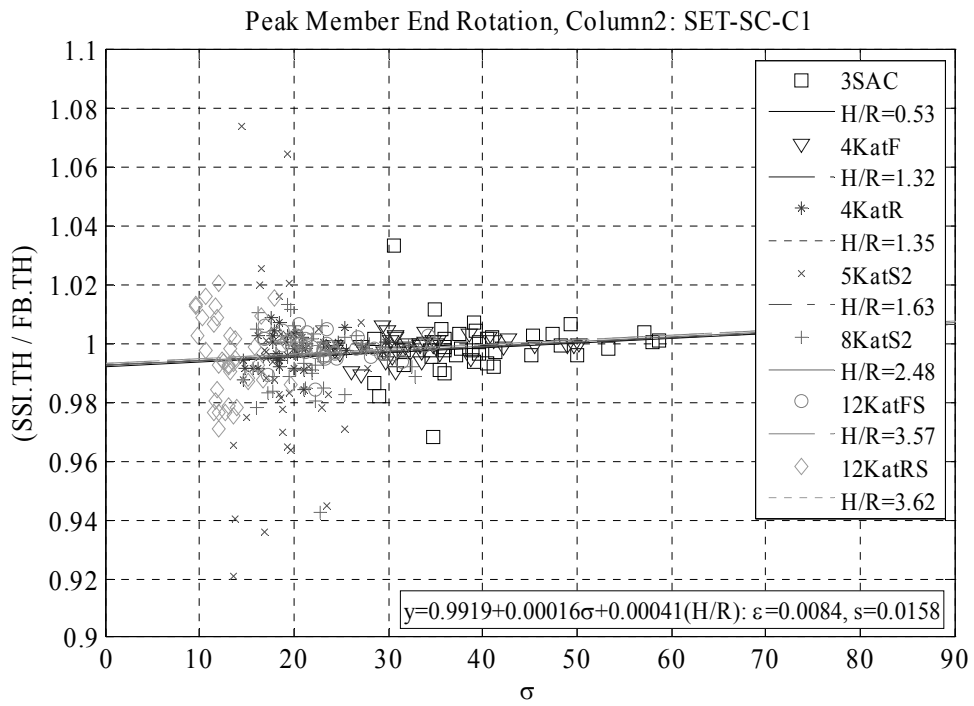
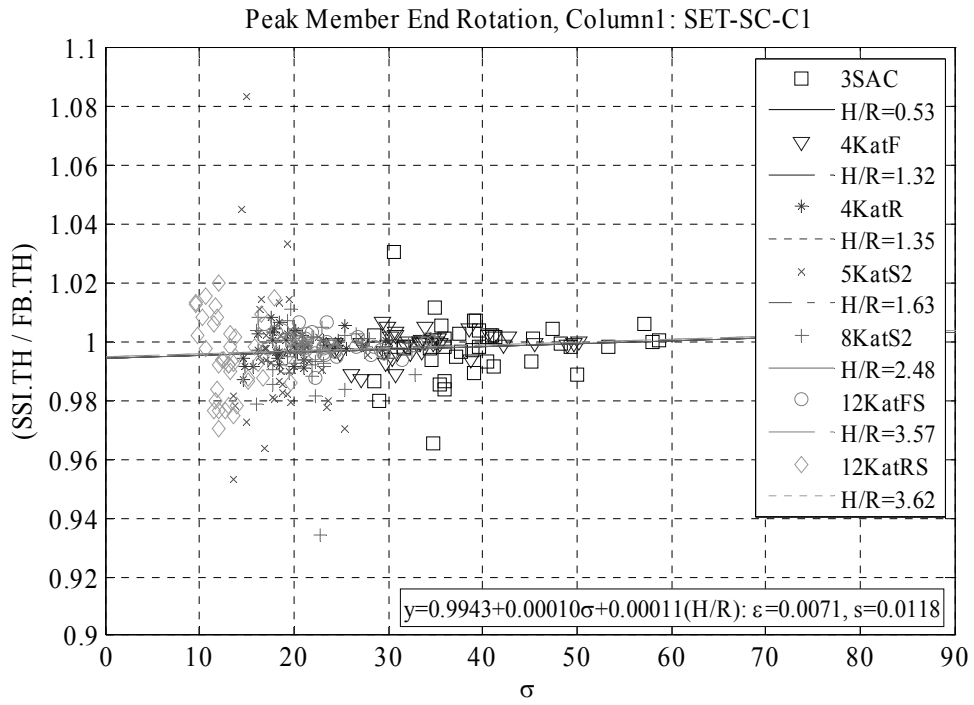


Figure D.5. (Cont'd)

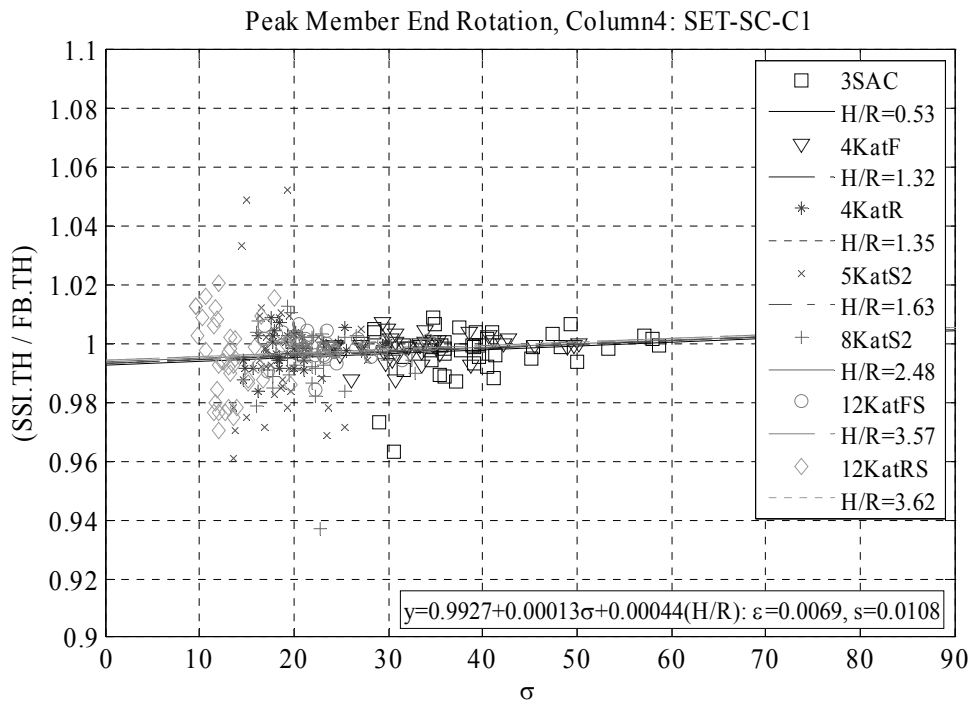
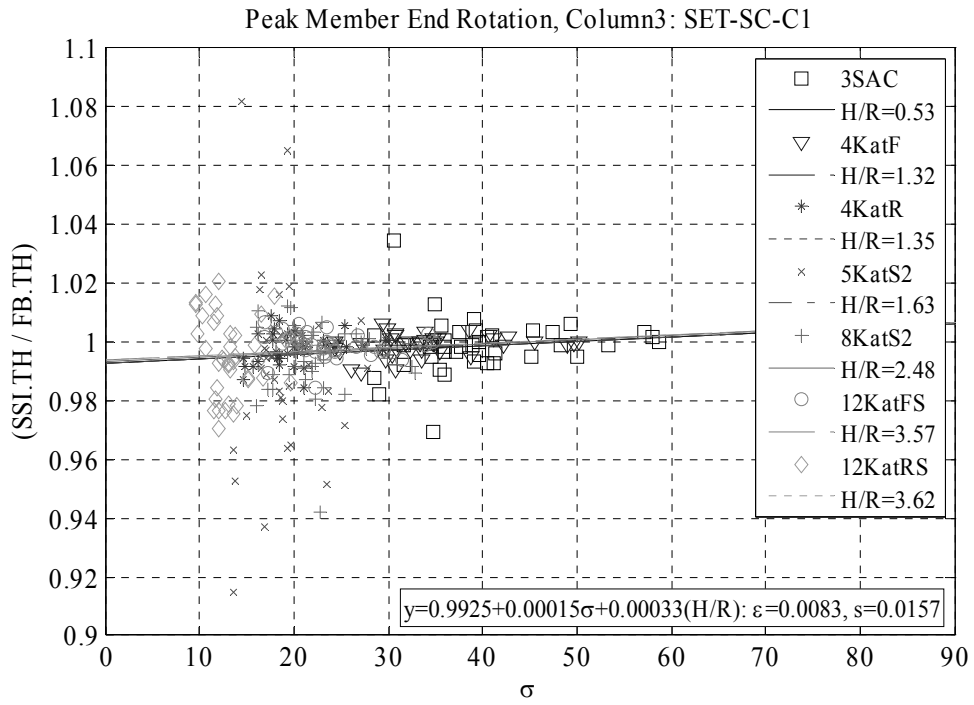


Figure D.5. (Cont'd)

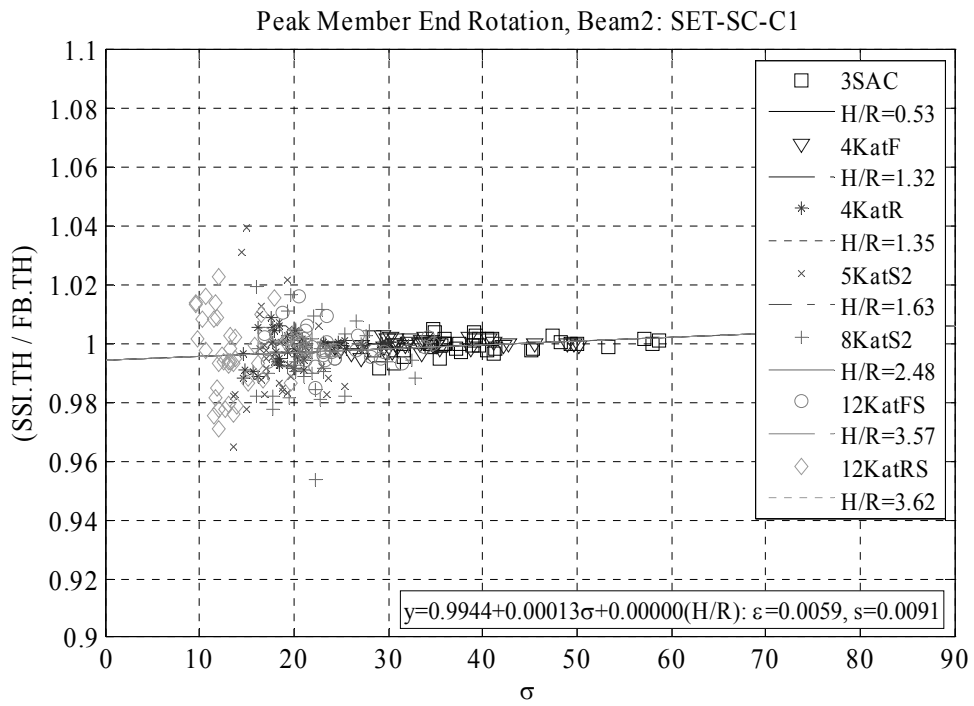
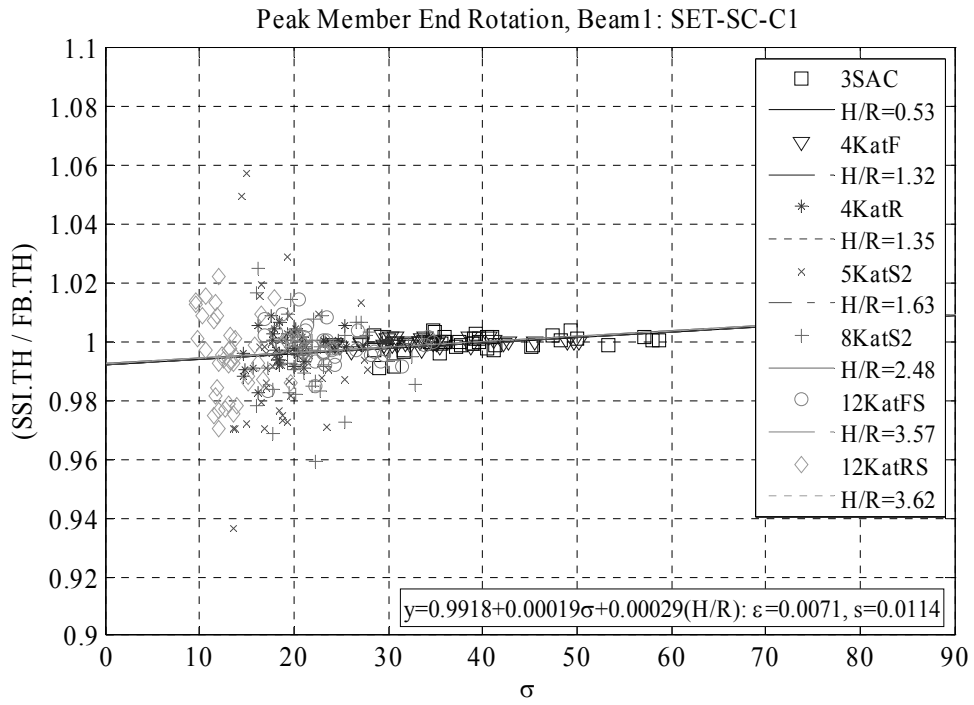


Figure D.5. (Cont'd)

Peak Member End Rotation, Beam3: SET-SC-C1

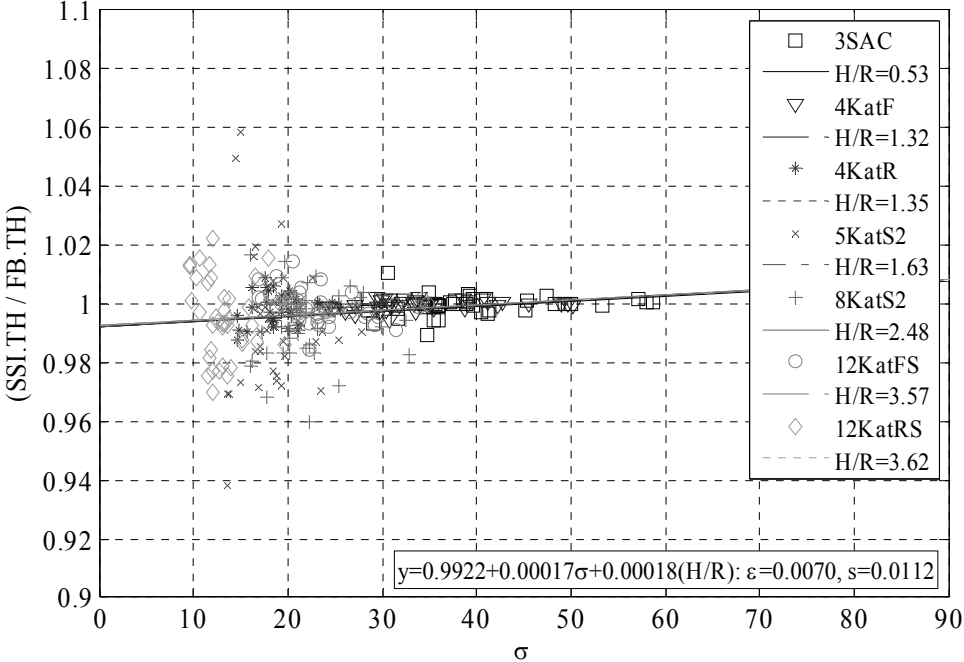


Figure D.5. (Cont'd)

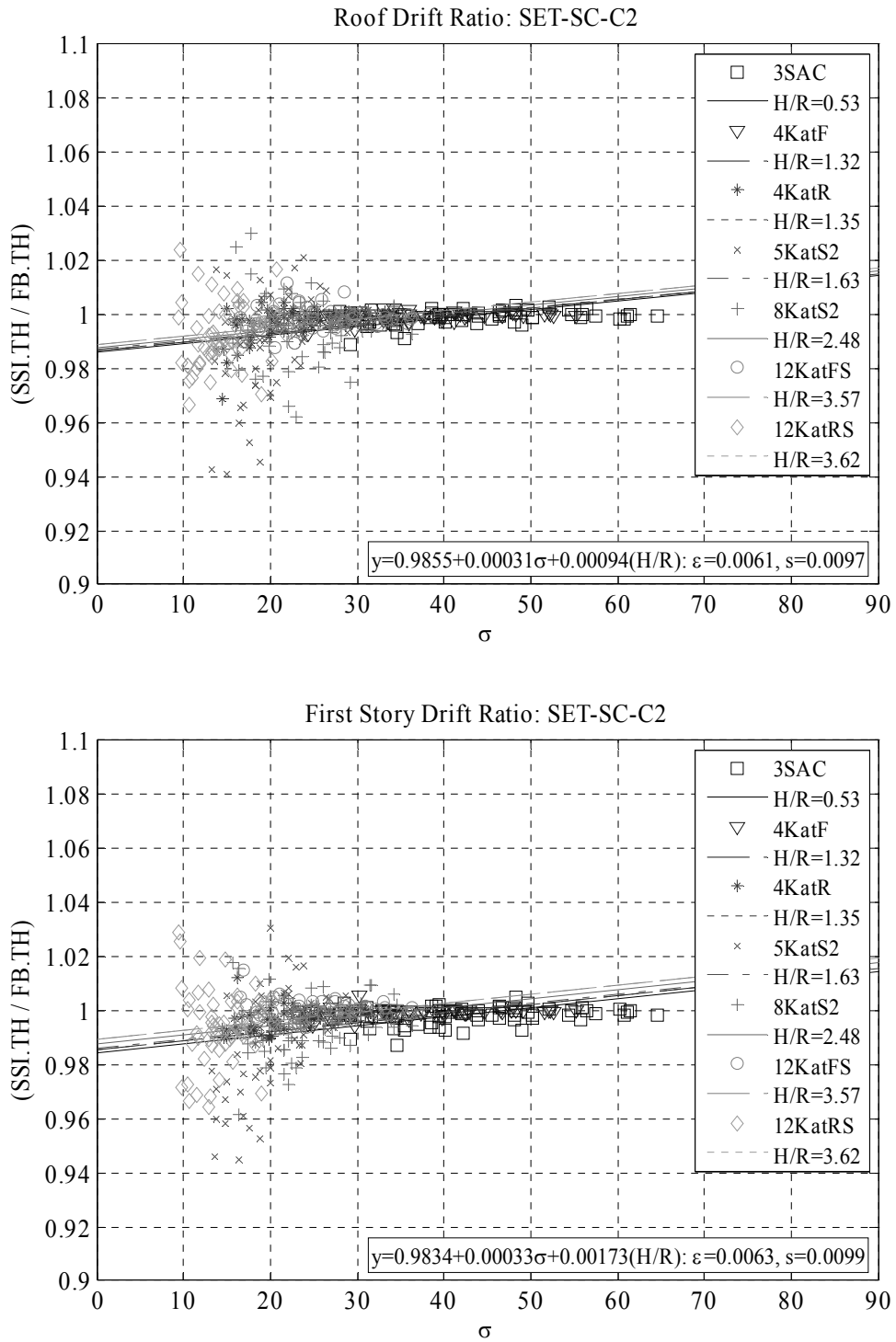


Figure D.6. 2D Scatter plot and associated regression line for the response ratios obtained for SET-SC-C2. Response ratios are calculated for: Roof drift ratio, first story drift ratio, peak column (foundation end) end and peak beam end rotations at the first story (SSI.TH / FB.TH), while the predictor variables are wave parameter (σ) and aspect ratio (H/R), ε is the mean absolute error and s is the standard error.

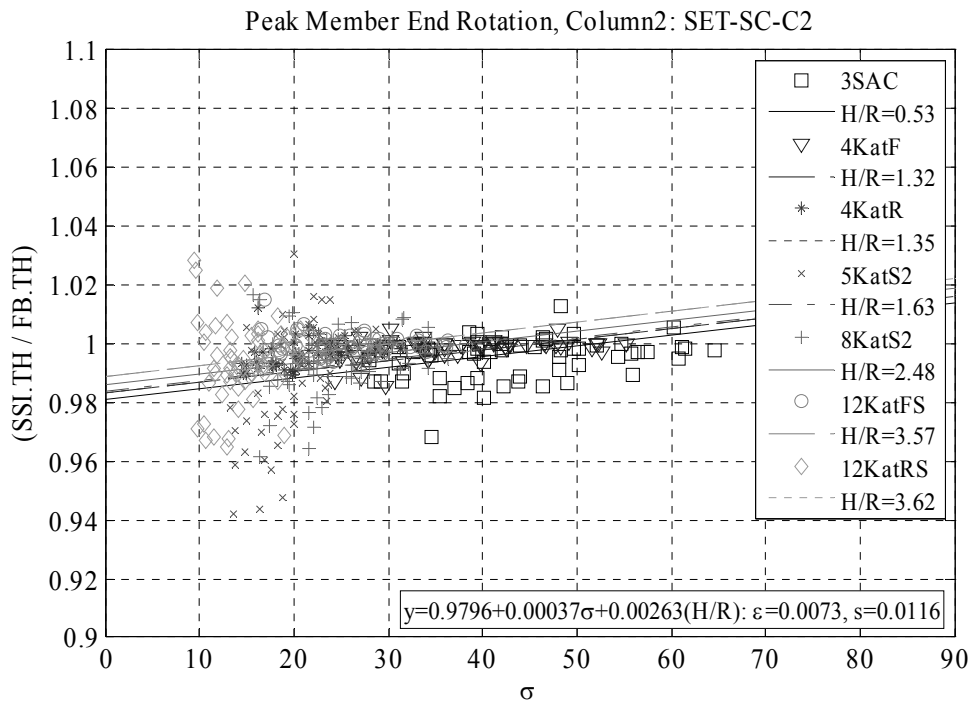
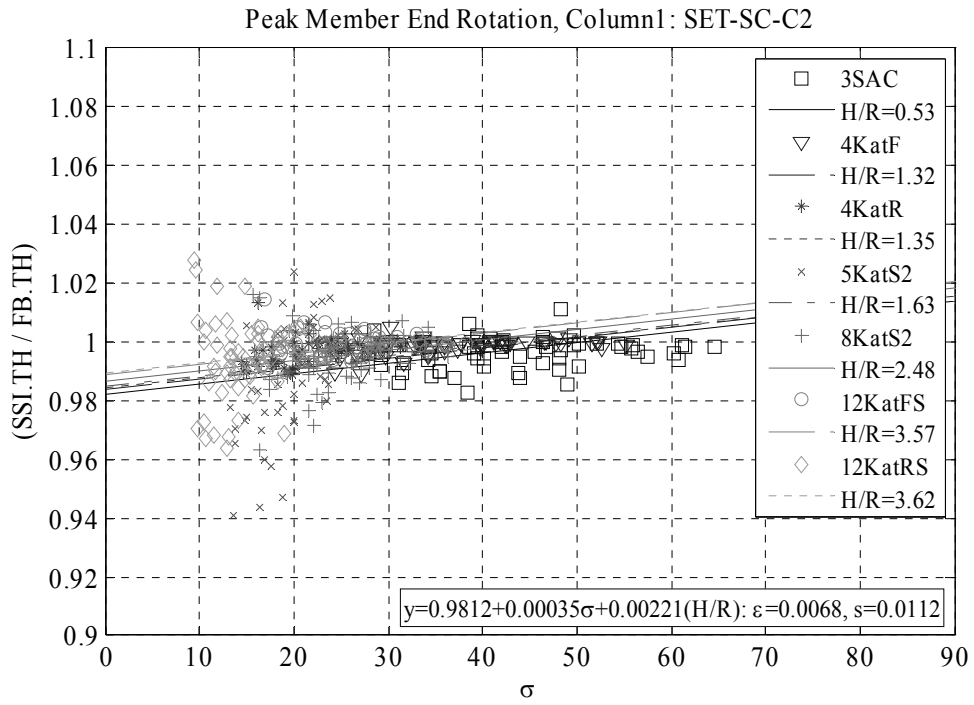


Figure D.6. (Cont'd)

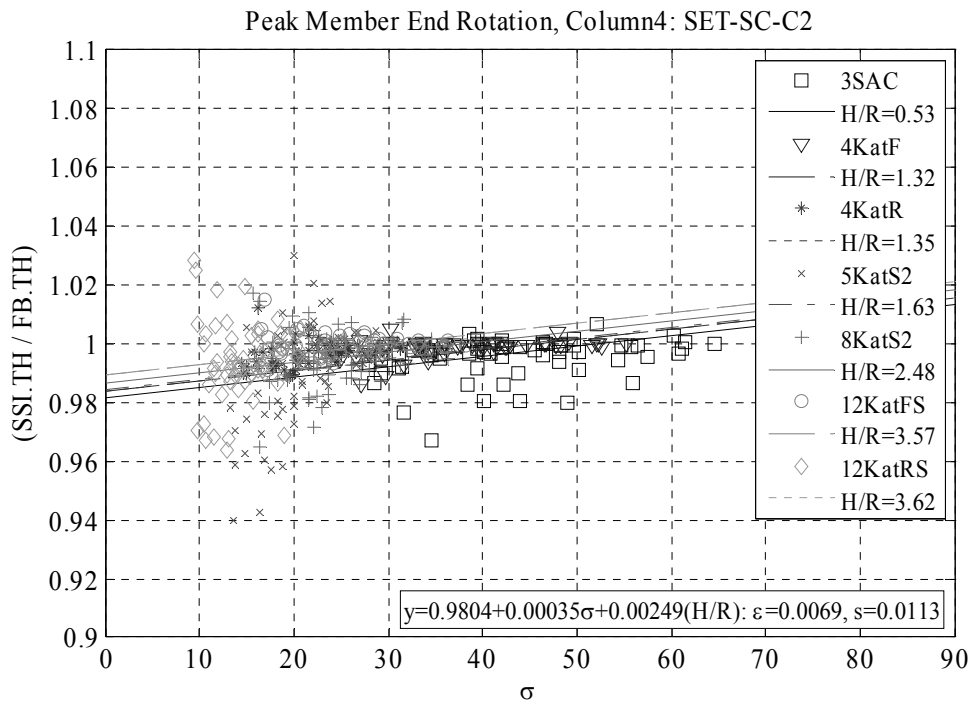
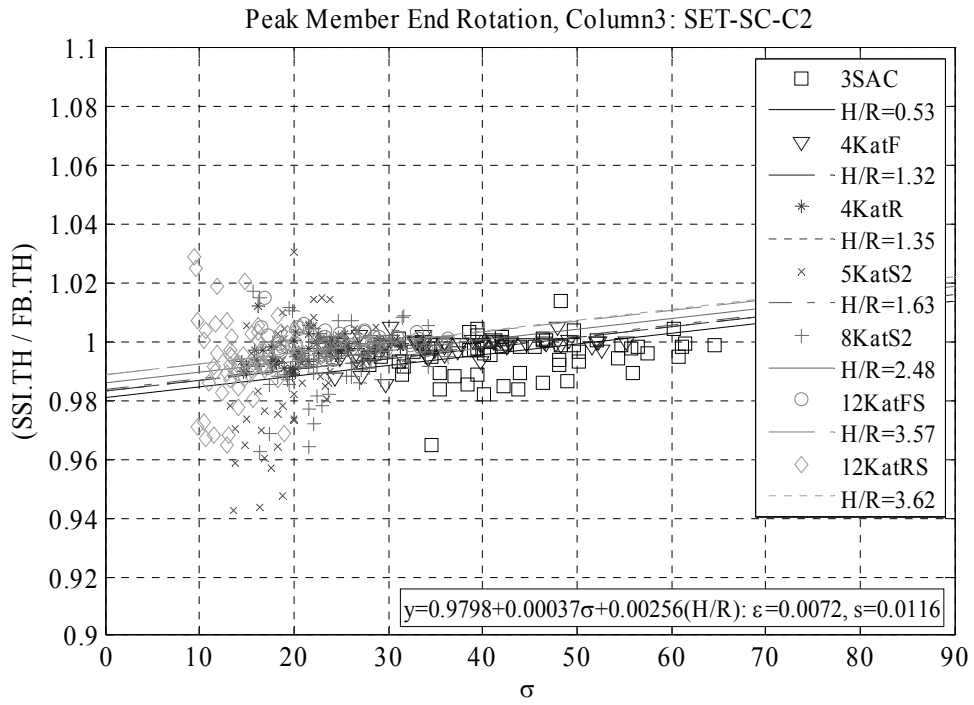


Figure D.6. (Cont'd)

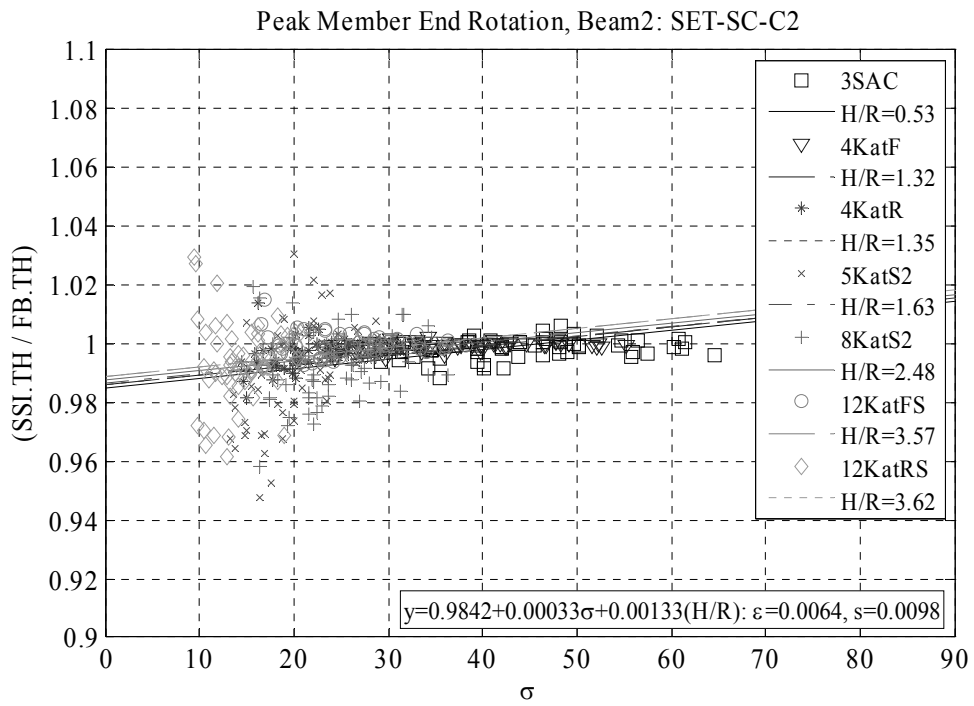
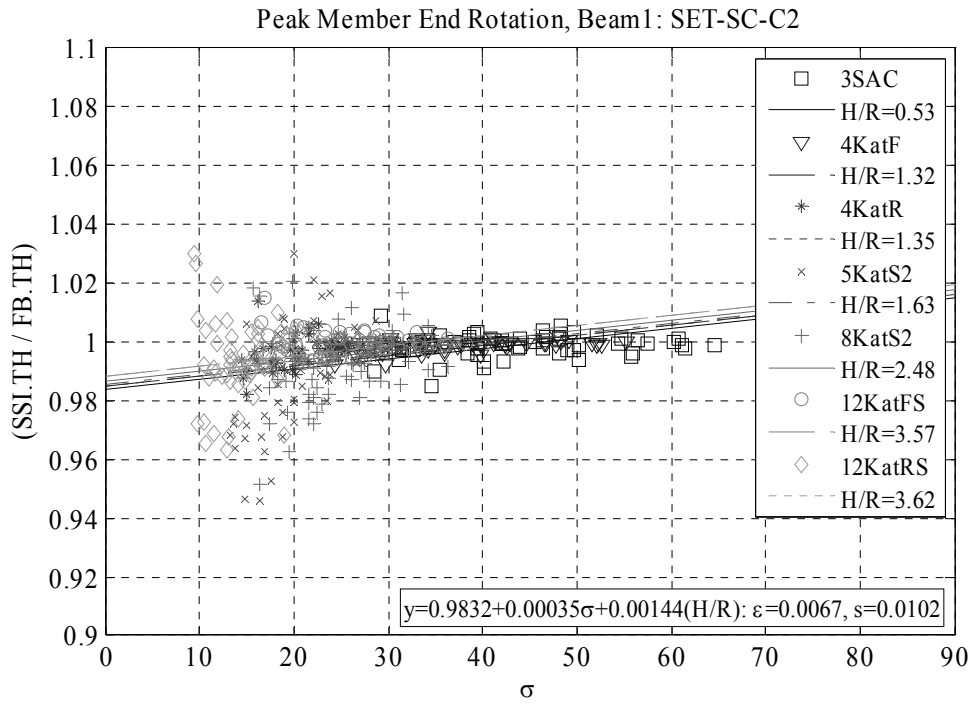


Figure D.6. (Cont'd)

Peak Member End Rotation, Beam3: SET-SC-C2

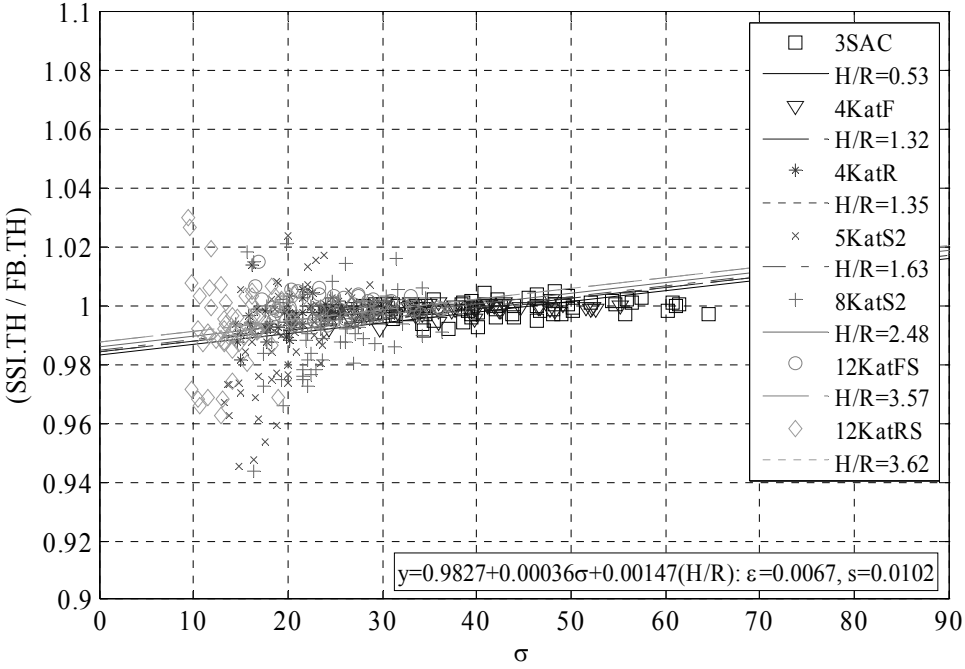


Figure D.6. (Cont'd)

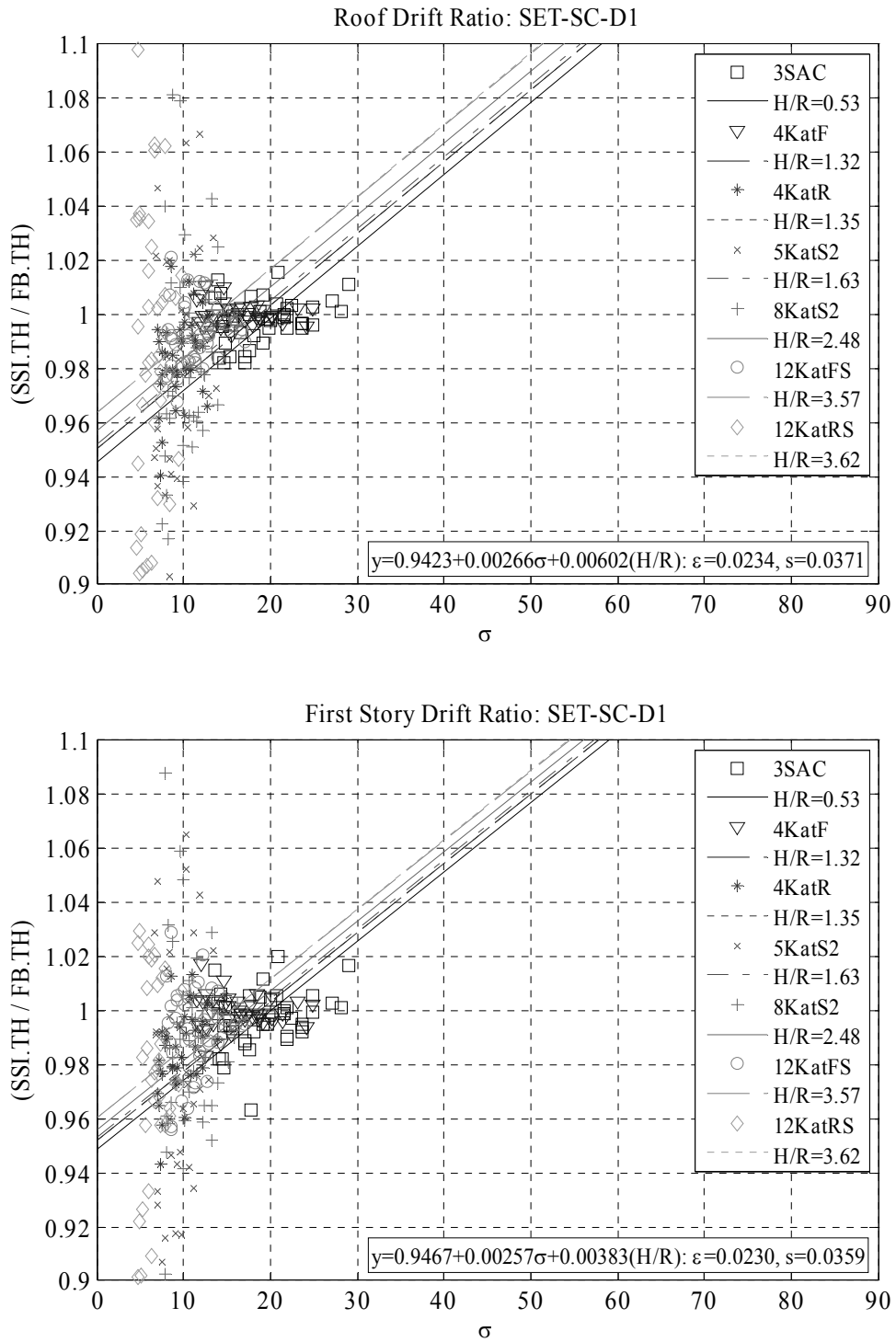


Figure D.7. 2D Scatter plot and associated regression line for the response ratios obtained for SET-SC-D1. Response ratios are calculated for: Roof drift ratio, first story drift ratio, peak column (foundation end) end and peak beam end rotations at the first story (SSI.TH / FB.TH), while the predictor variables are wave parameter (σ) and aspect ratio (H/R), ε is the mean absolute error and s is the standard error.

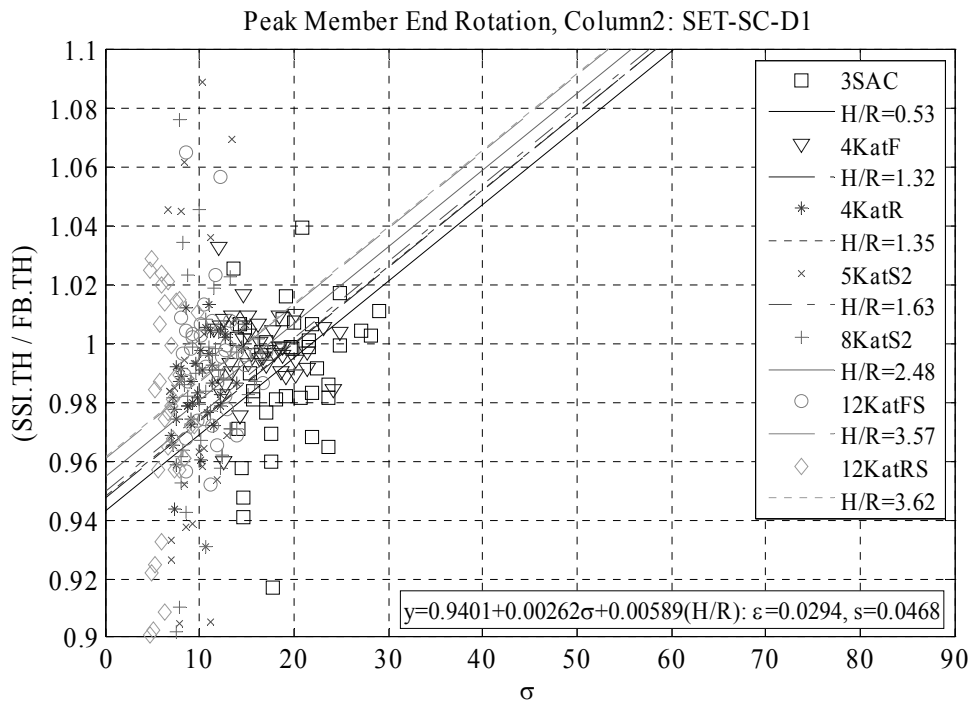
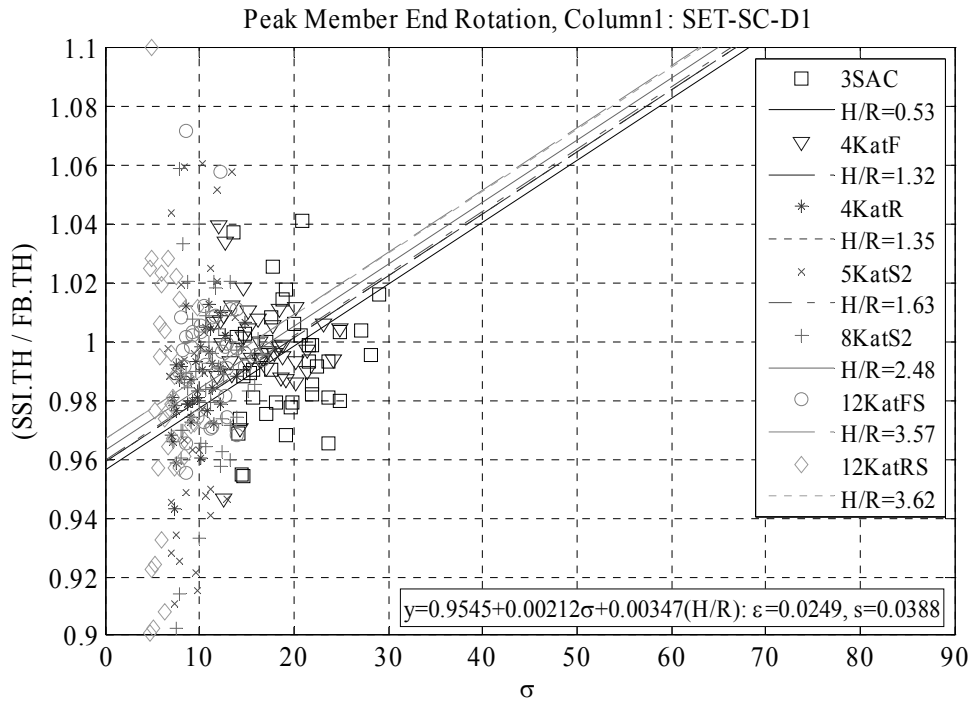


Figure D.7. (Cont'd)

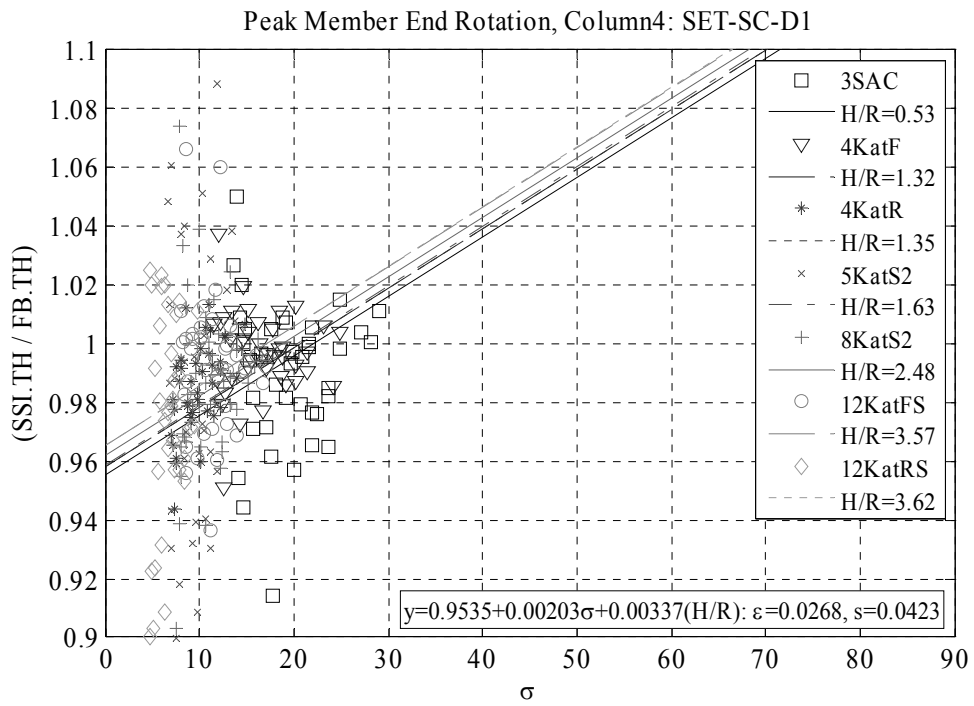
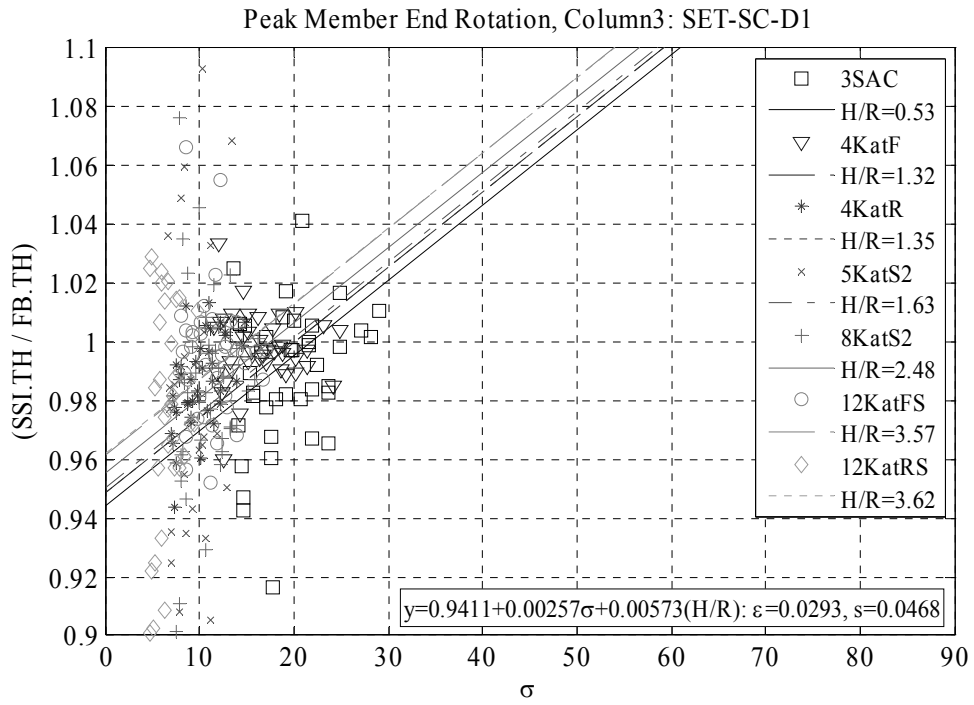


Figure D.7. (Cont'd)

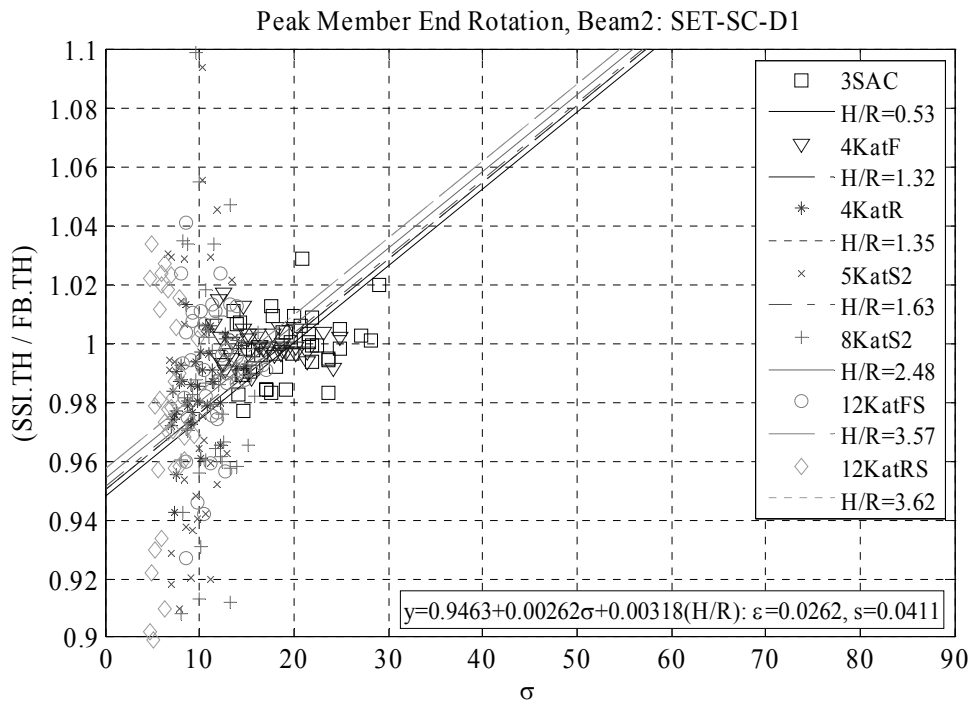
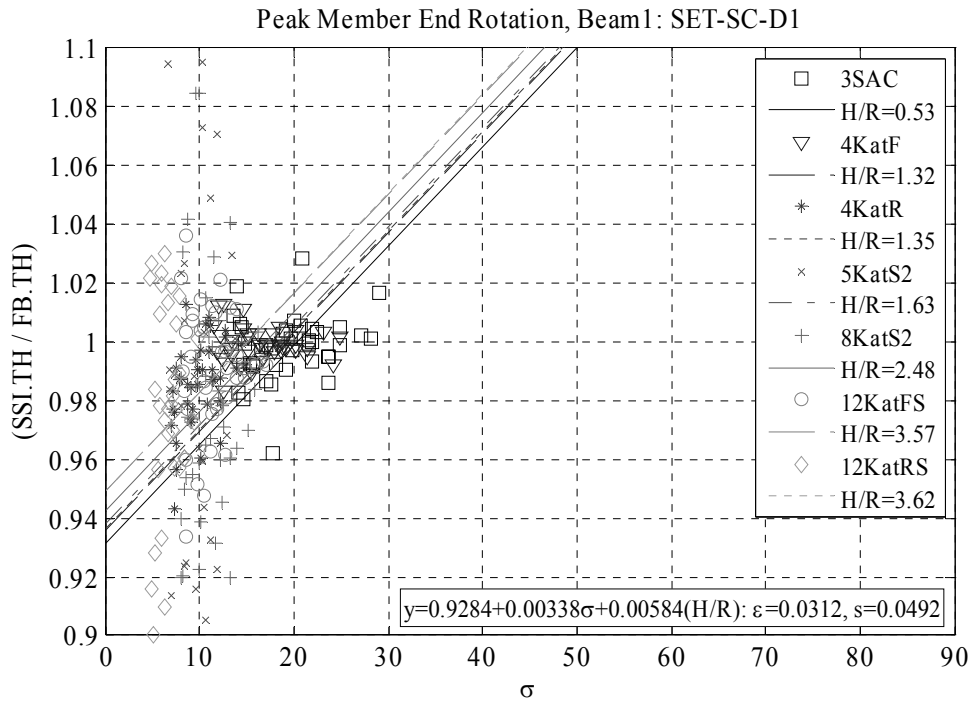


Figure D.7. (Cont'd)

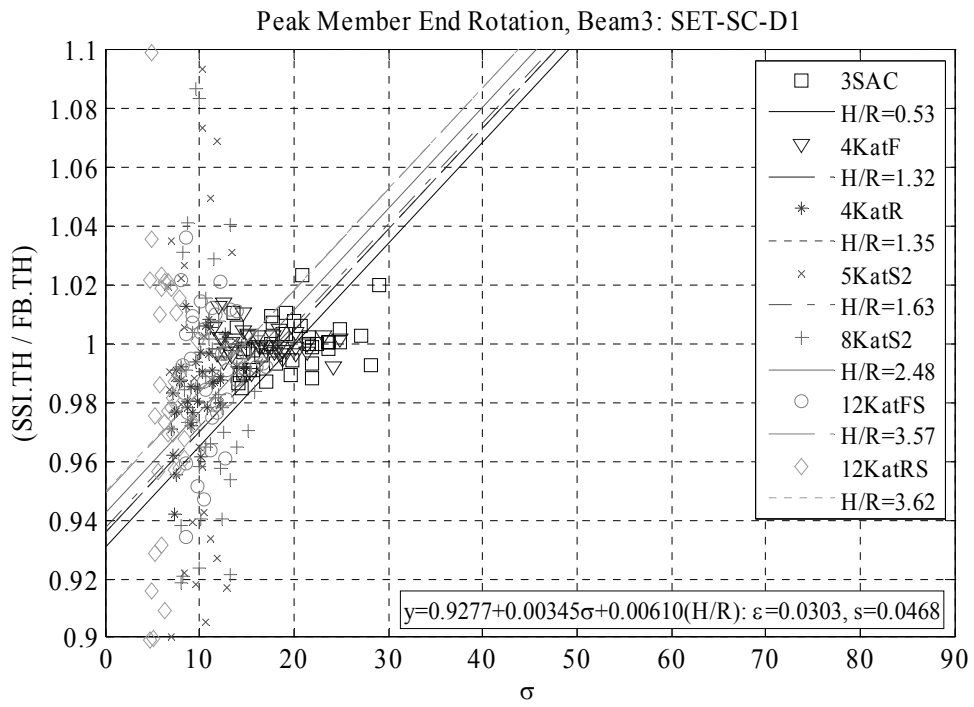


Figure D.7. (Cont'd)

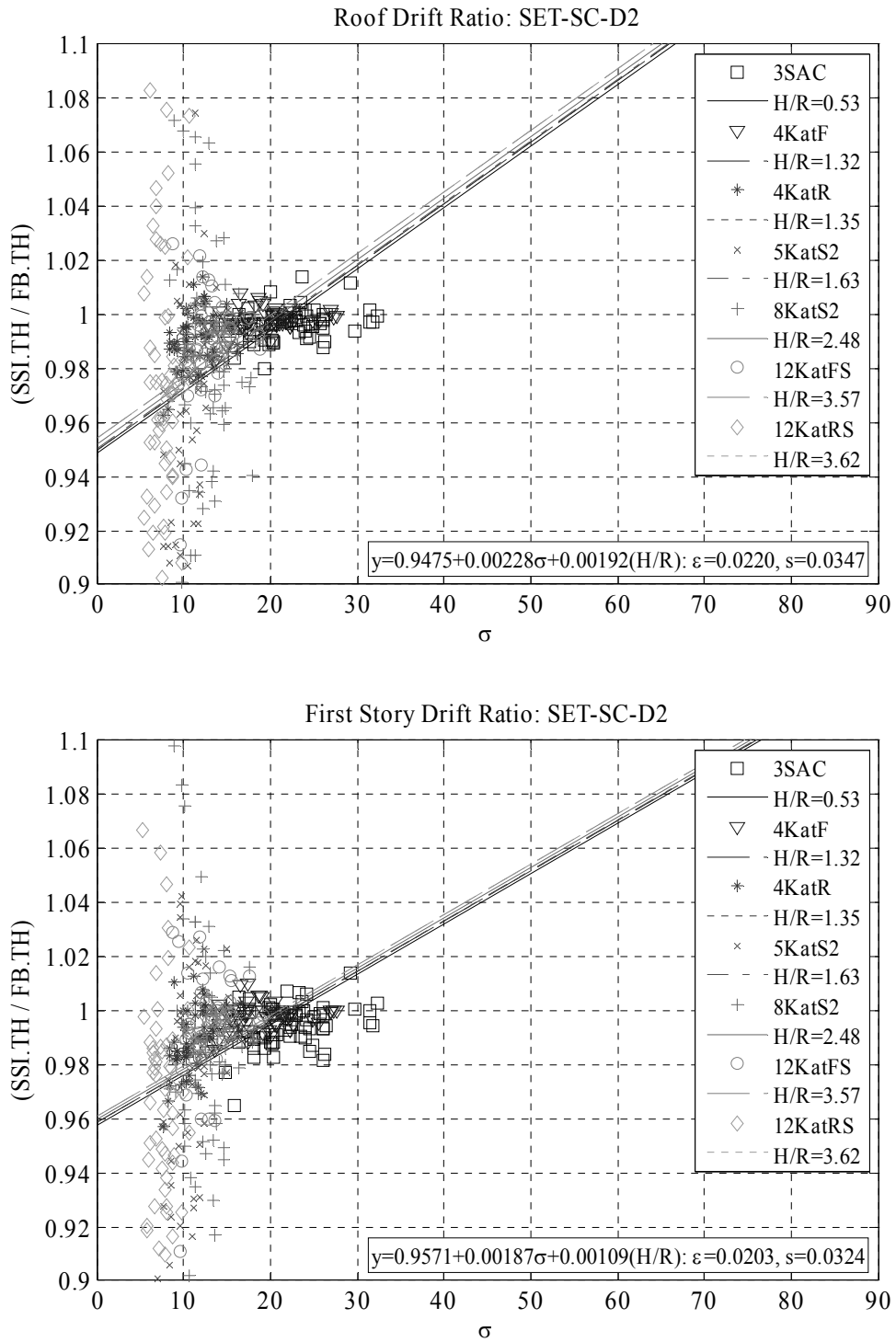


Figure D.8. 2D Scatter plot and associated regression line for the response ratios obtained for SET-SC-D2. Response ratios are calculated for: Roof drift ratio, first story drift ratio, peak column (foundation end) end and peak beam end rotations at the first story (SSI.TH / FB.TH), while the predictor variables are wave parameter (σ) and aspect ratio (H/R), ε is the mean absolute error and s is the standard error.

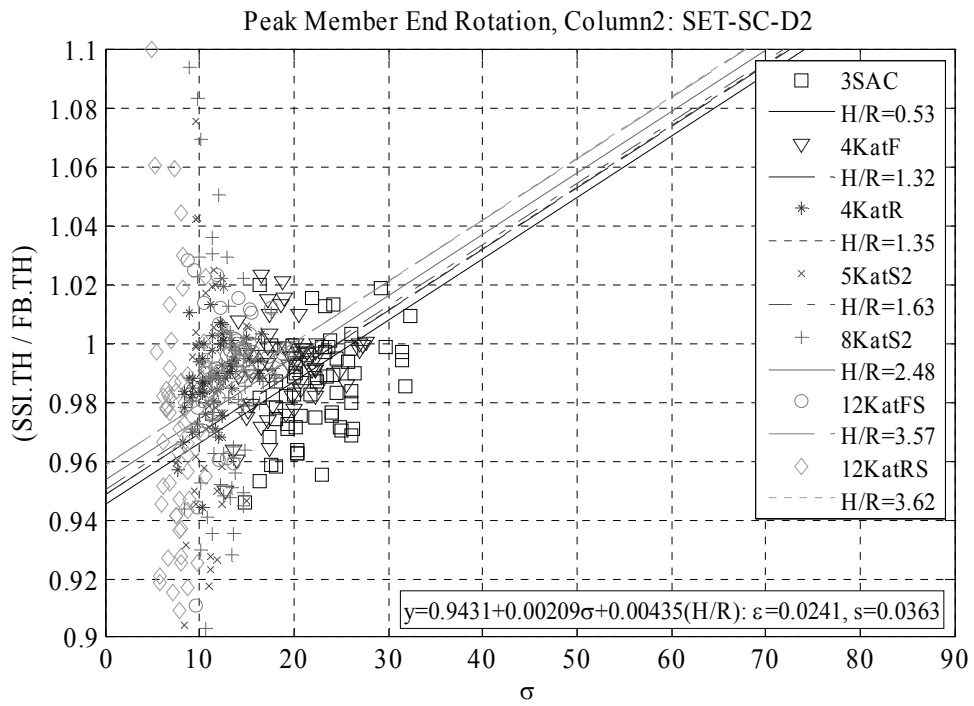
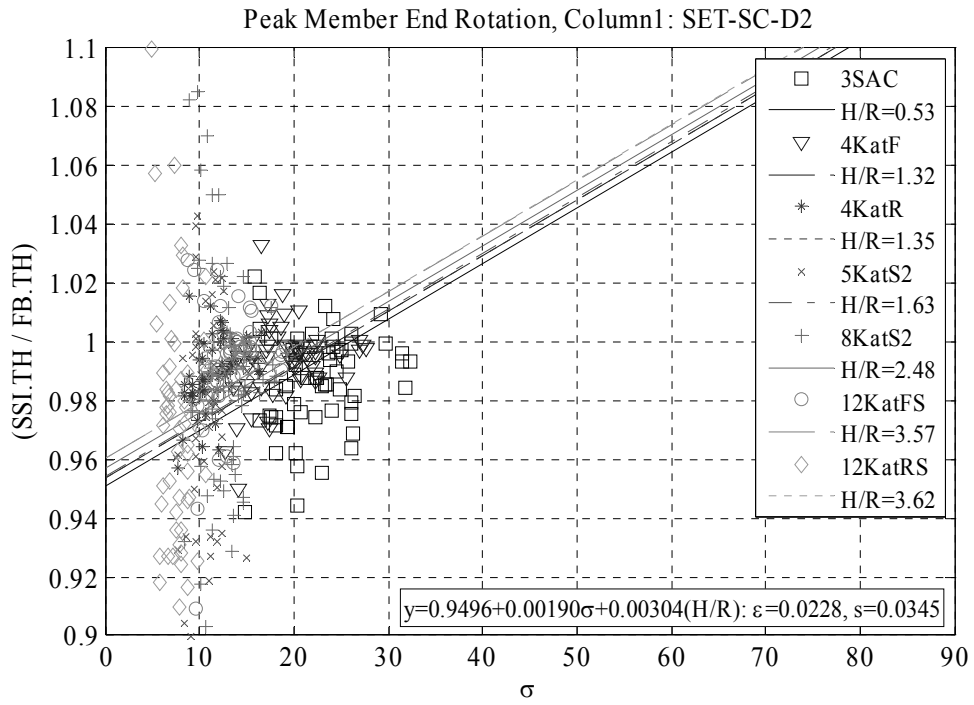


Figure D.8. (Cont'd)

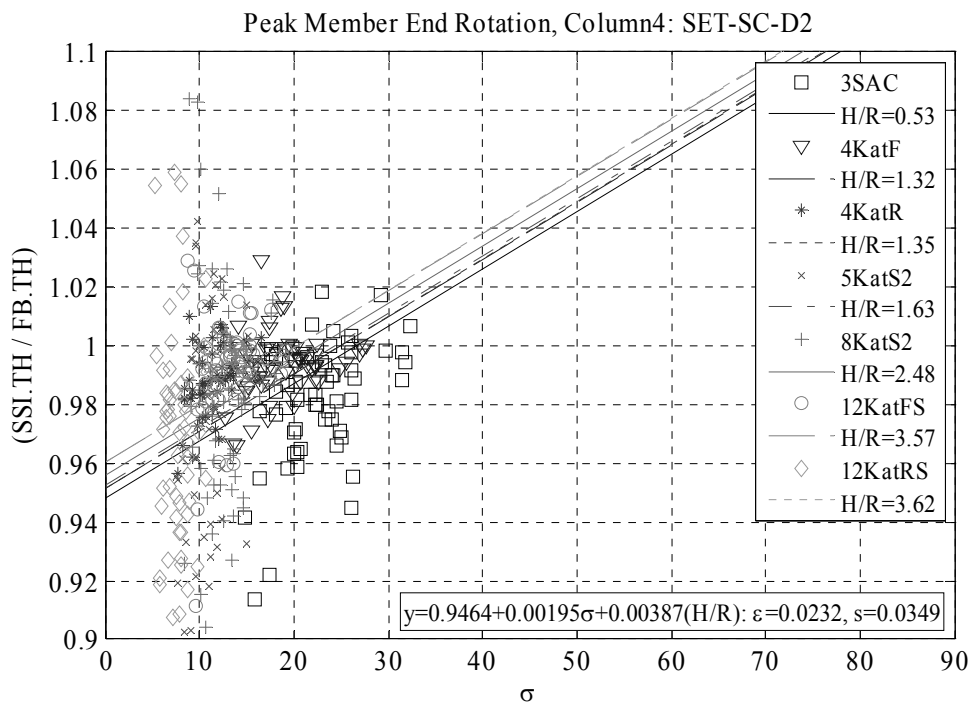
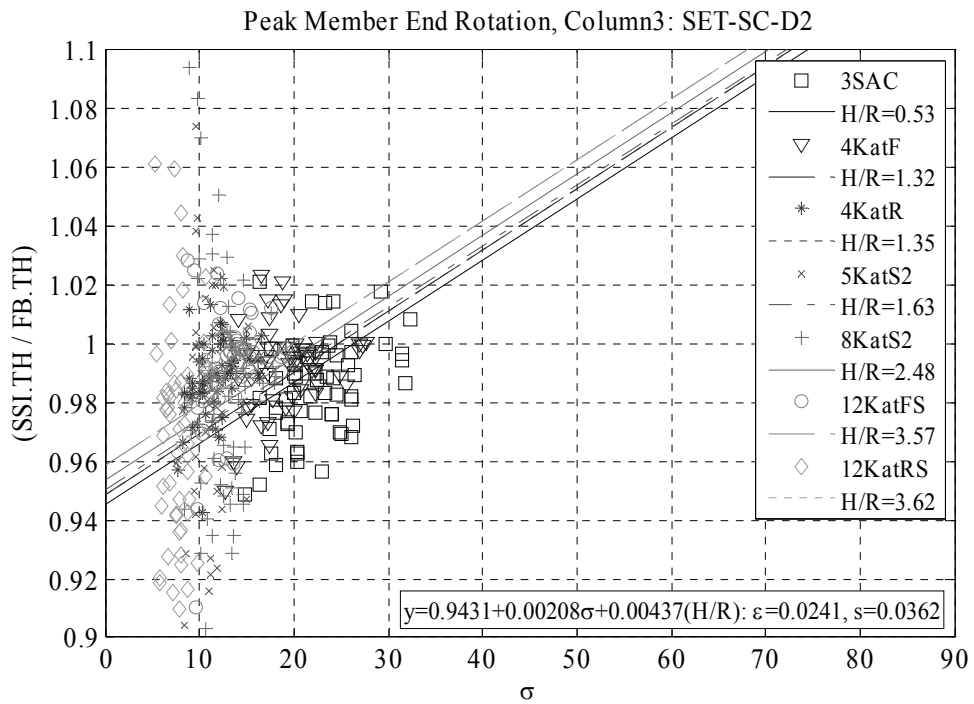


Figure D.8. (Cont'd)

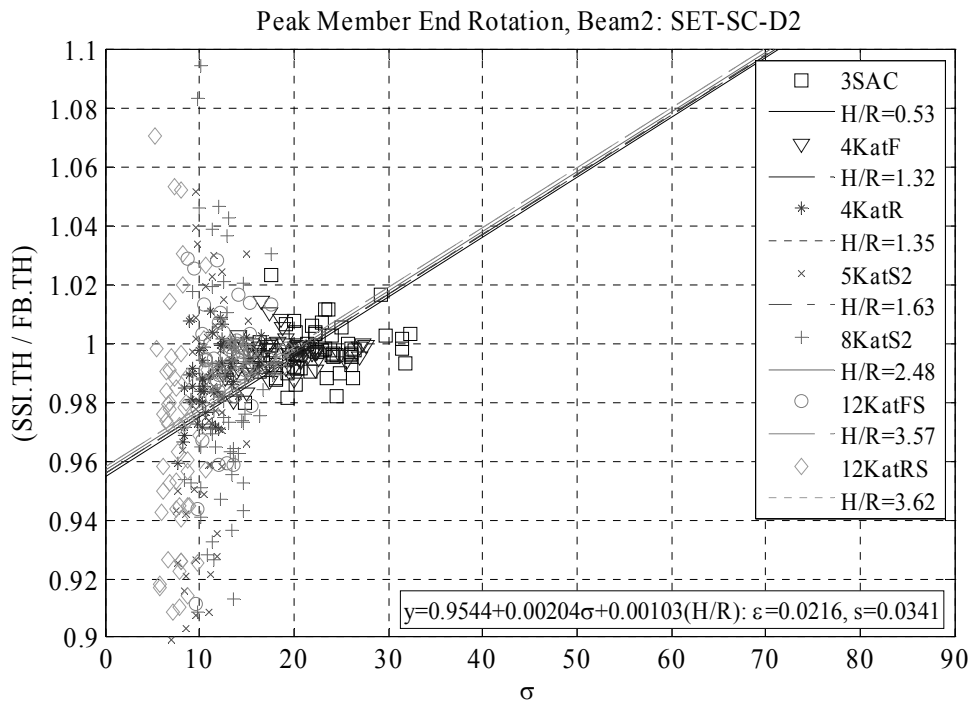
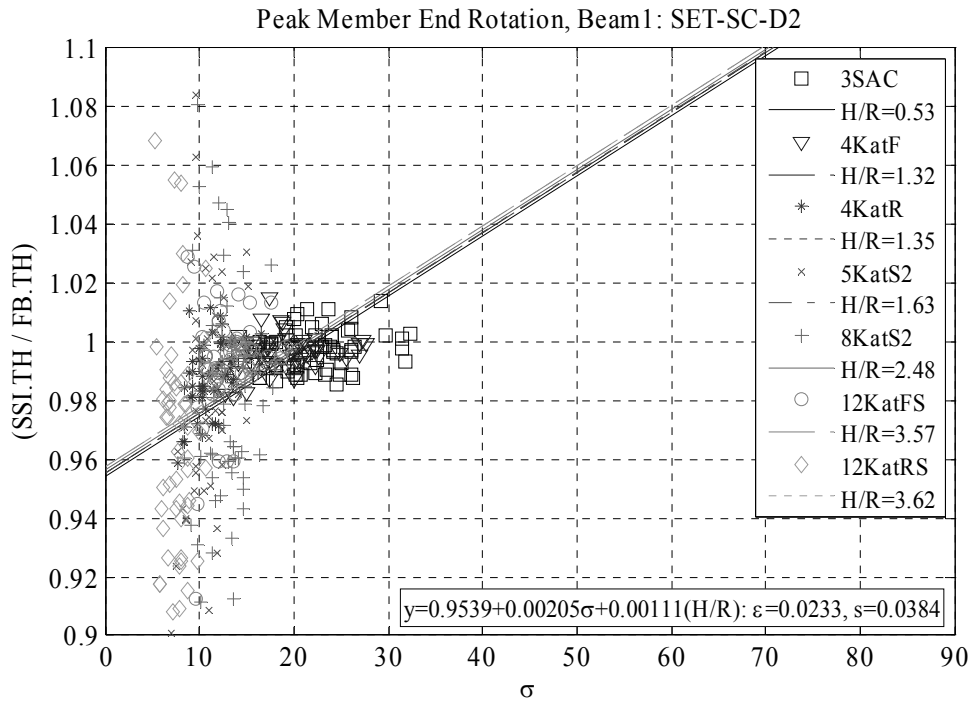


Figure D.8. (Cont'd)

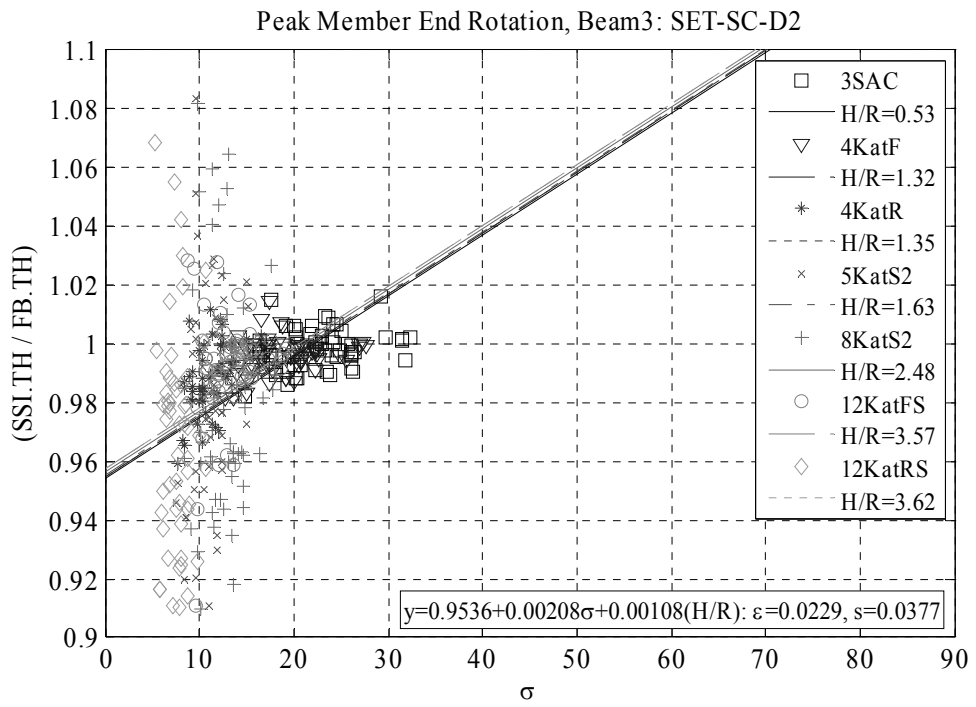


Figure D.8. (Cont'd)

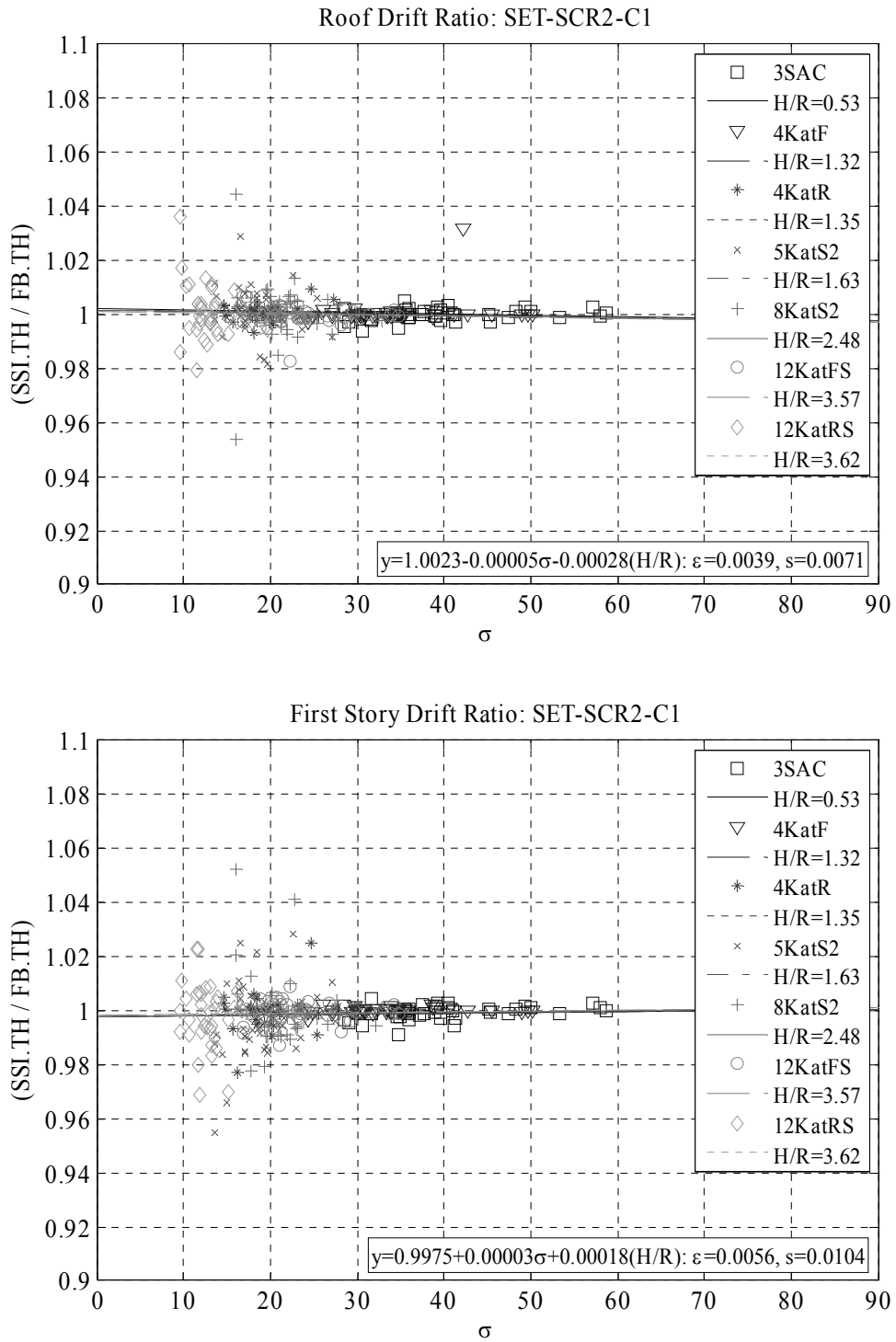


Figure D.9. 2D Scatter plot and associated regression line for the response ratios obtained for SET-SCR2-C1. Response ratios are calculated for: Roof drift ratio, first story drift ratio, peak column (foundation end) end and peak beam end rotations at the first story (SSI.TH / FB.TH), while the predictor variables are wave parameter (σ) and aspect ratio (H/R), ϵ is the mean absolute error and s is the standard error.

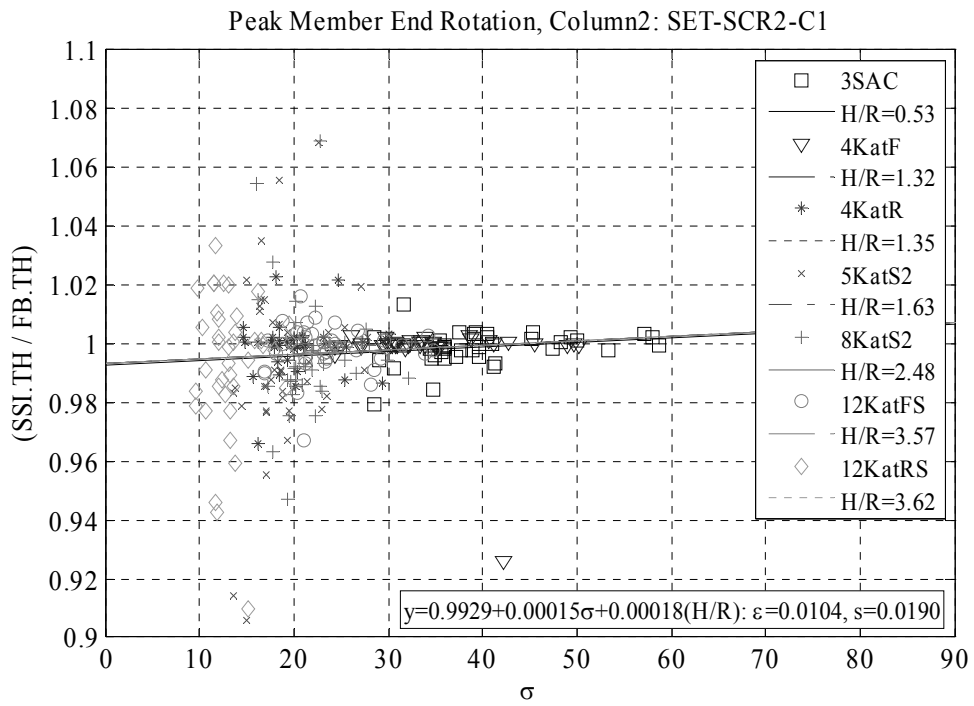
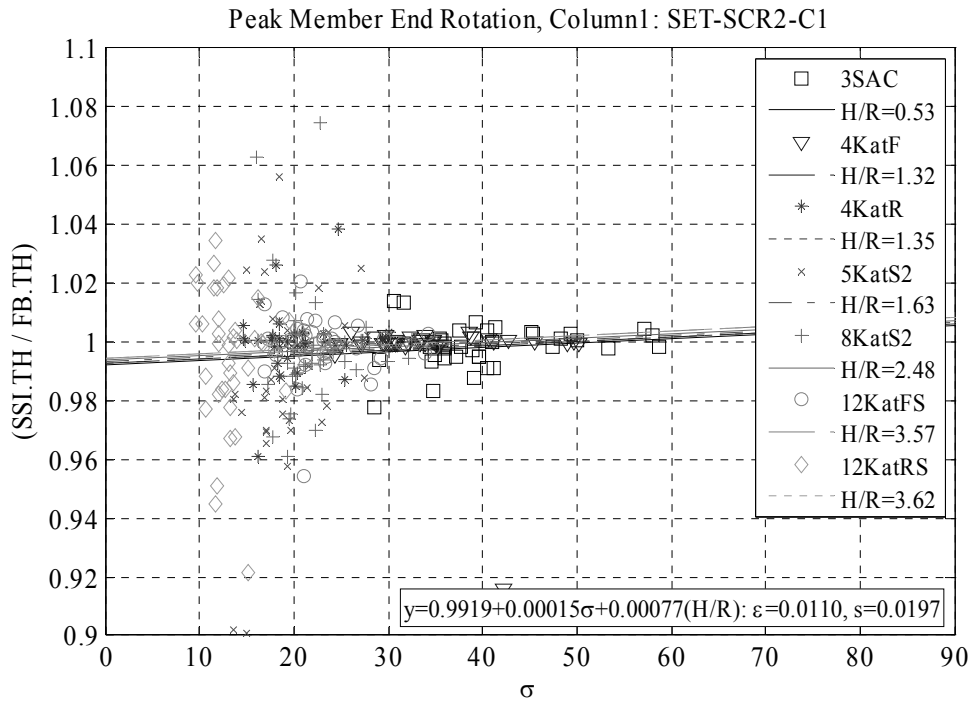


Figure D.9. (Cont'd)

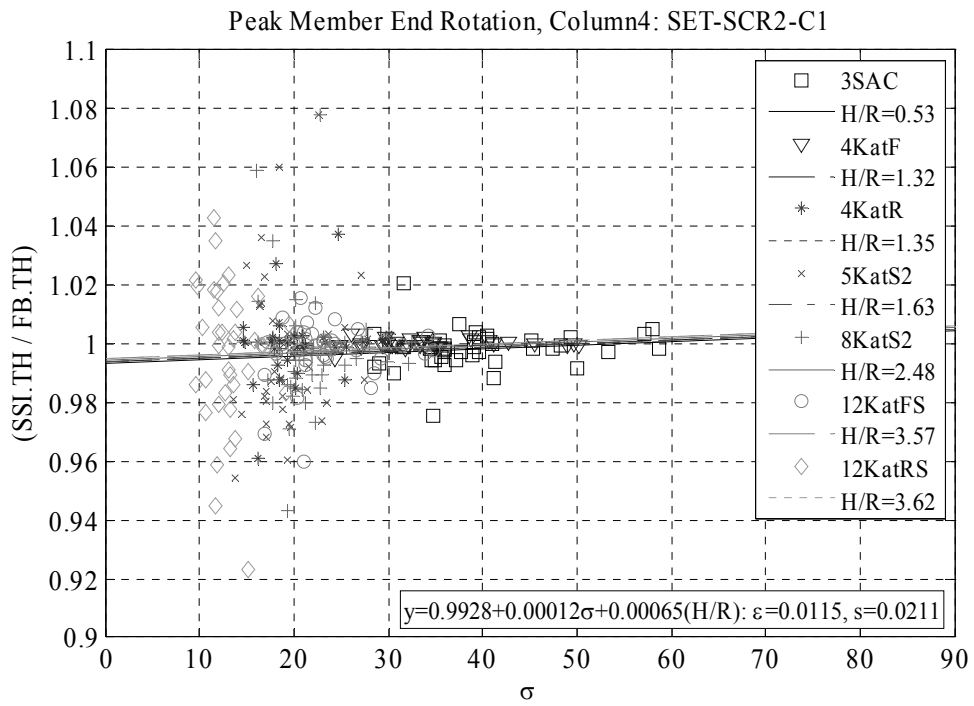
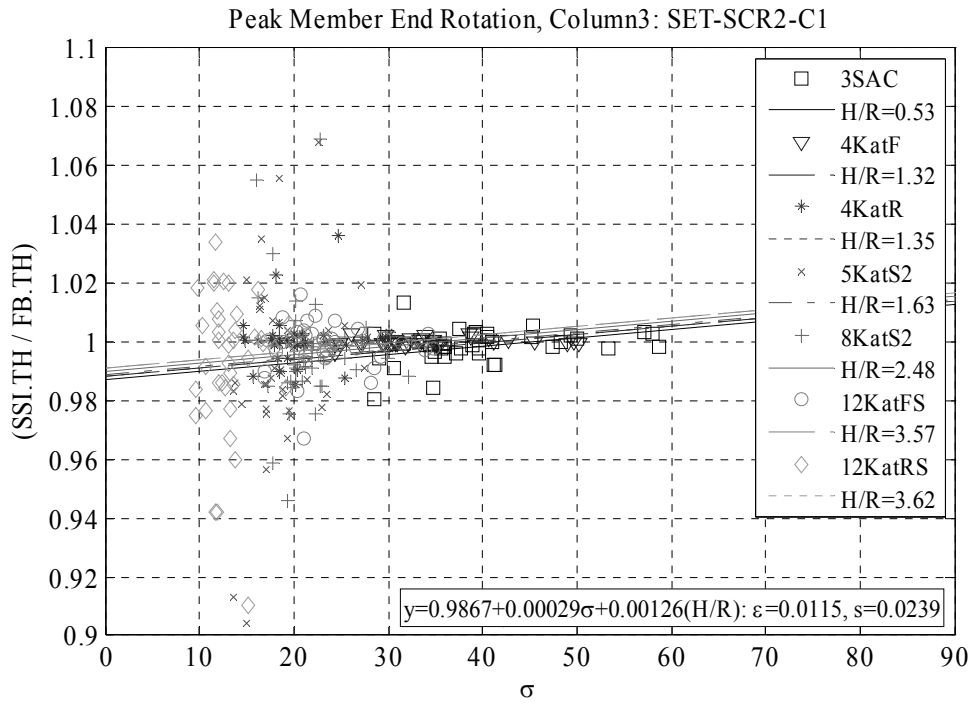


Figure D.9. (Cont'd)

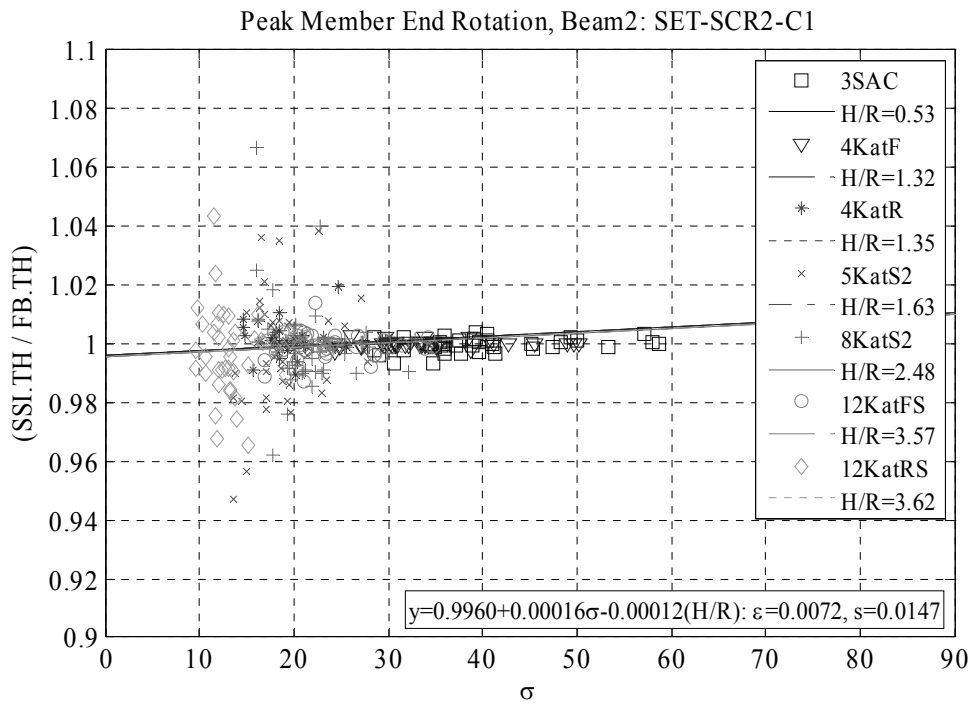
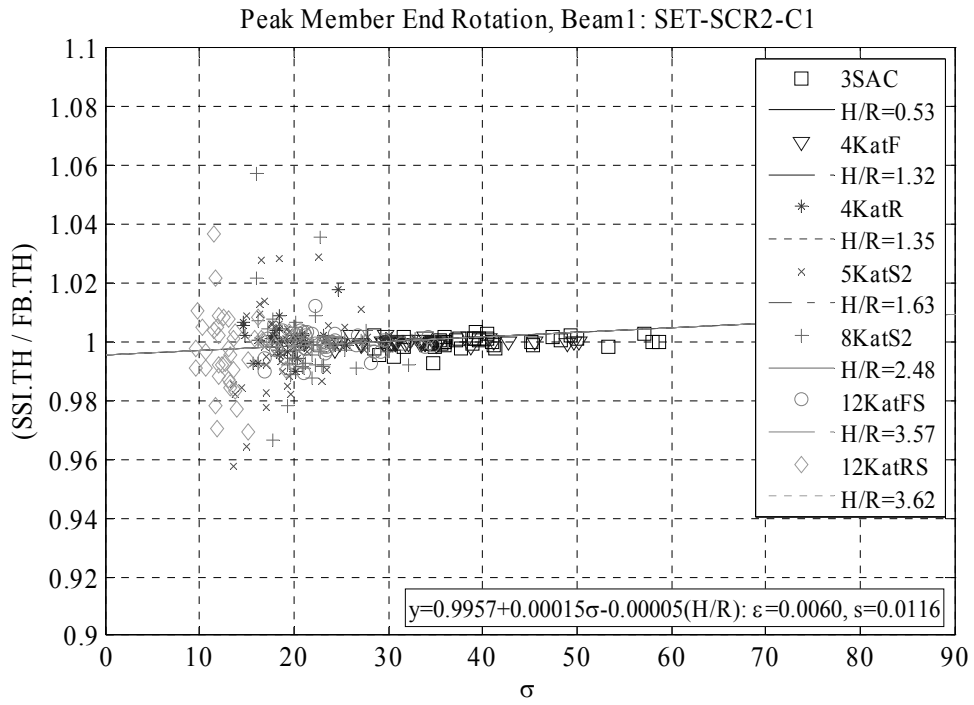


Figure D.9. (Cont'd)

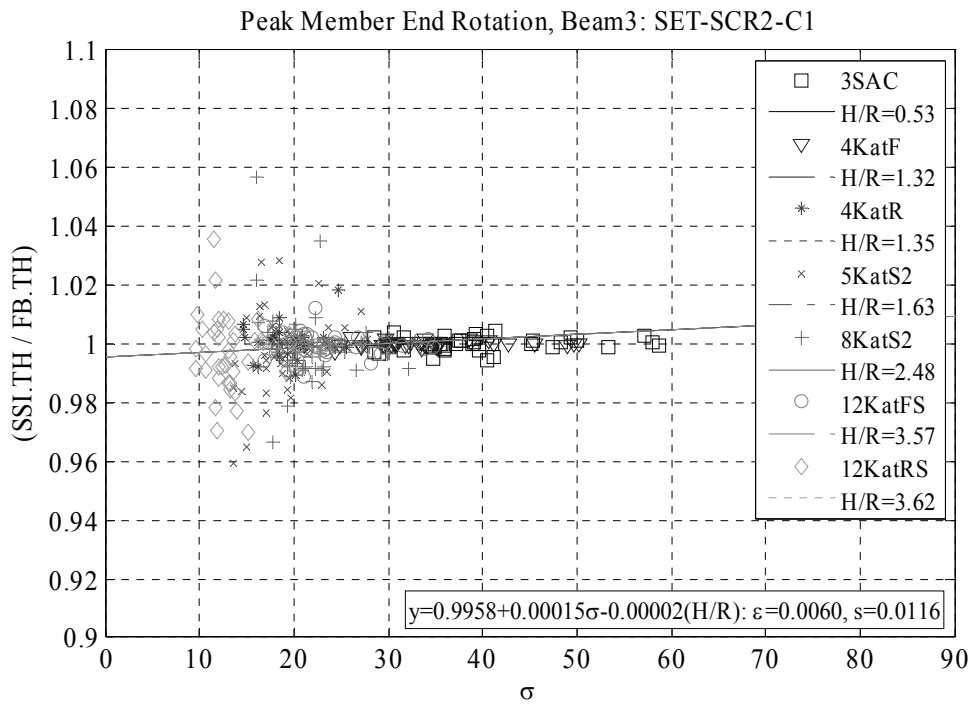


Figure D.9. (Cont'd)

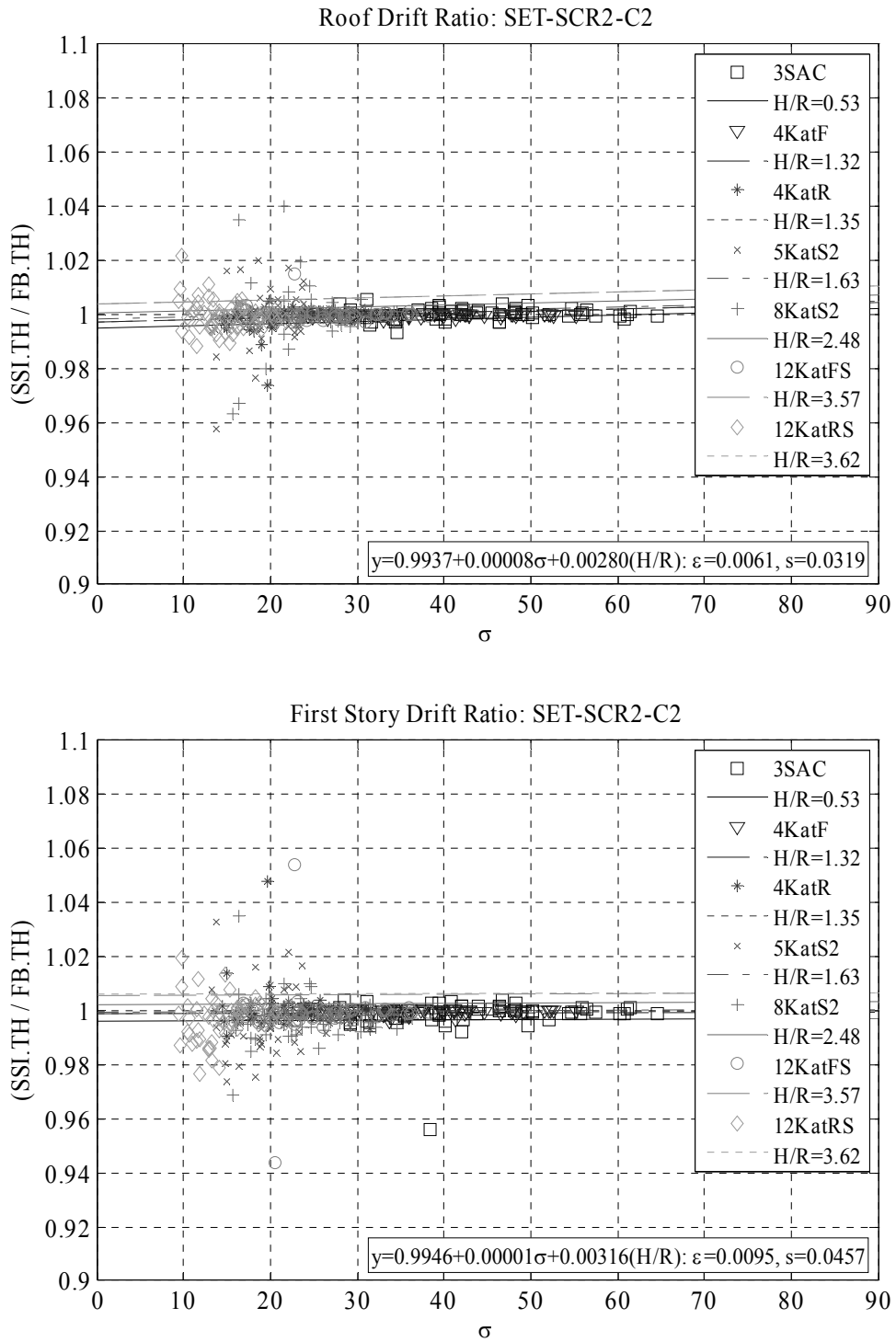


Figure D.10. 2D Scatter plot and associated regression line for the response ratios obtained for SET-SCR2-C2. Response ratios are calculated for: Roof drift ratio, first story drift ratio, peak column (foundation end) end and peak beam end rotations at the first story (SSI.TH / FB.TH), while the predictor variables are wave parameter (σ) and aspect ratio (H/R), ε is the mean absolute error and s is the standard error.

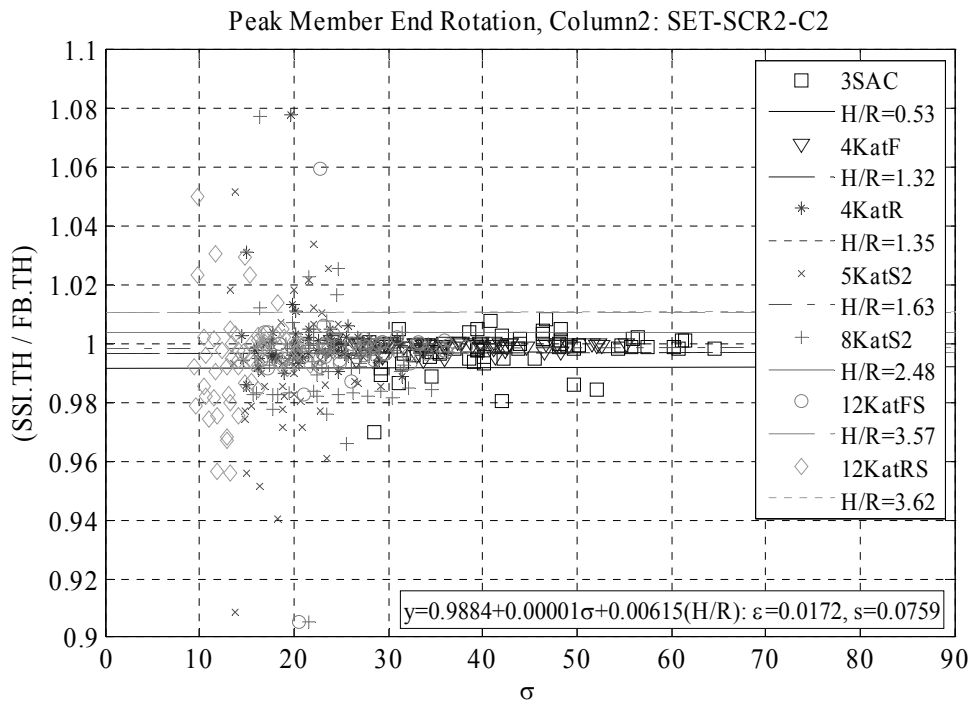
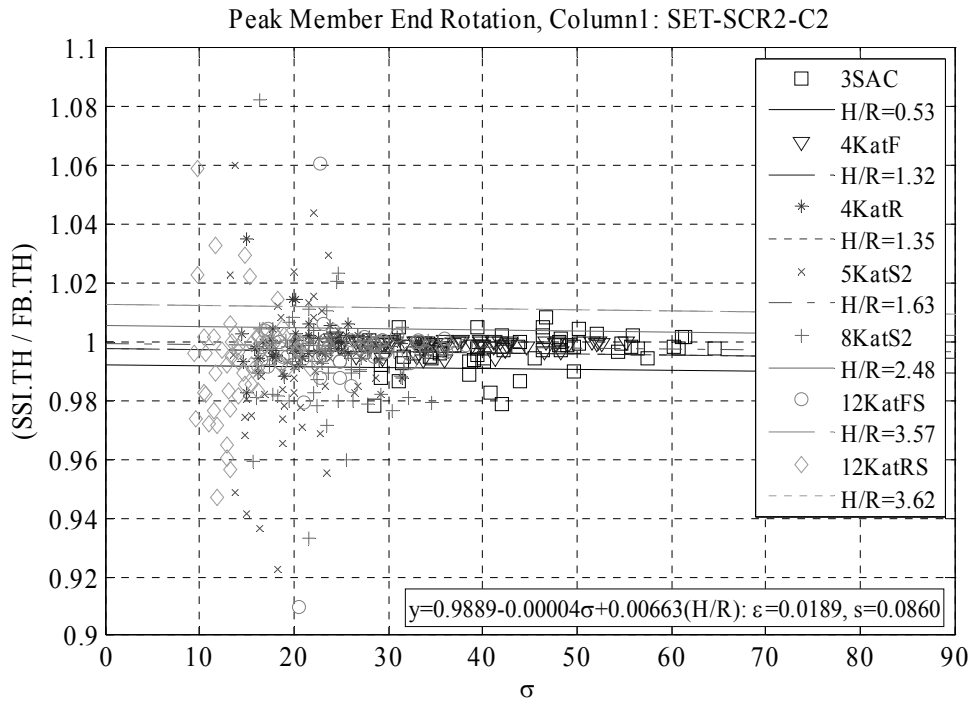


Figure D.10. (Cont'd)

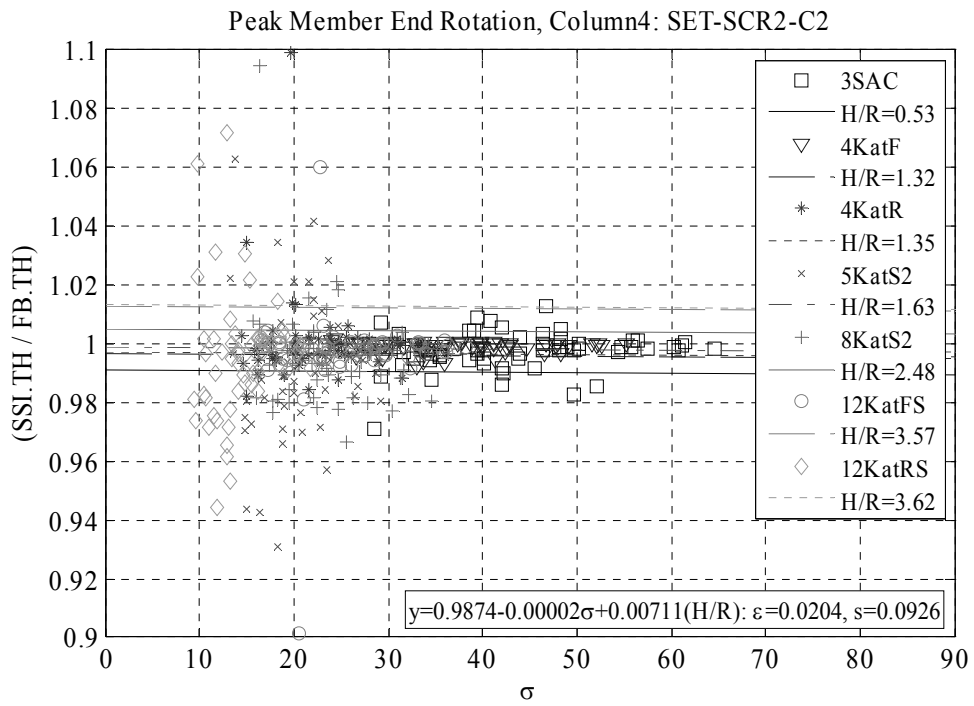
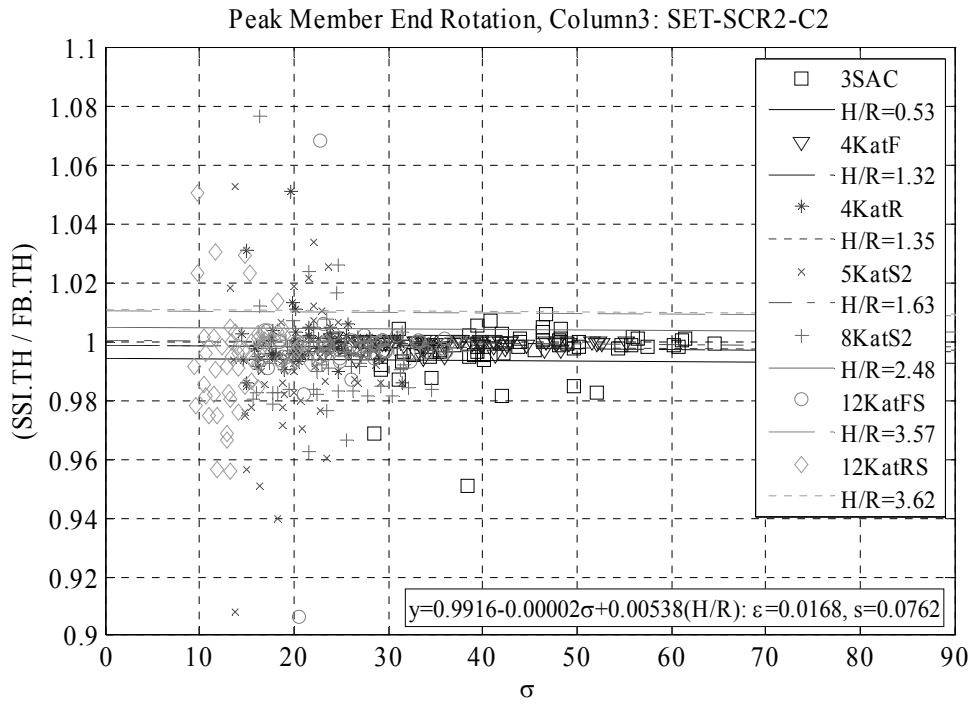


Figure D.10. (Cont'd)

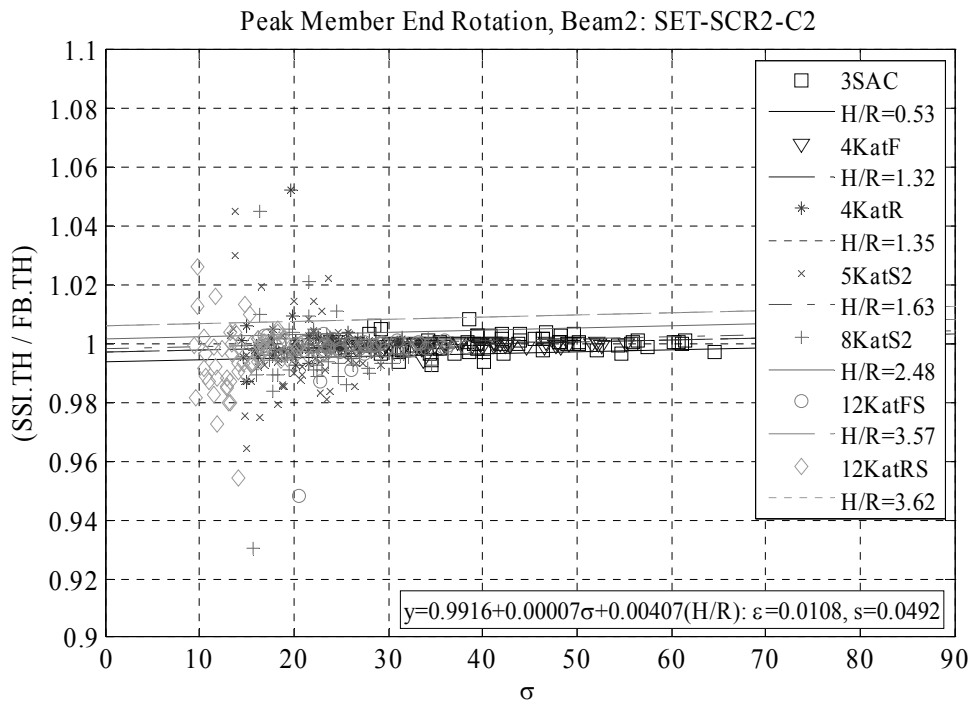
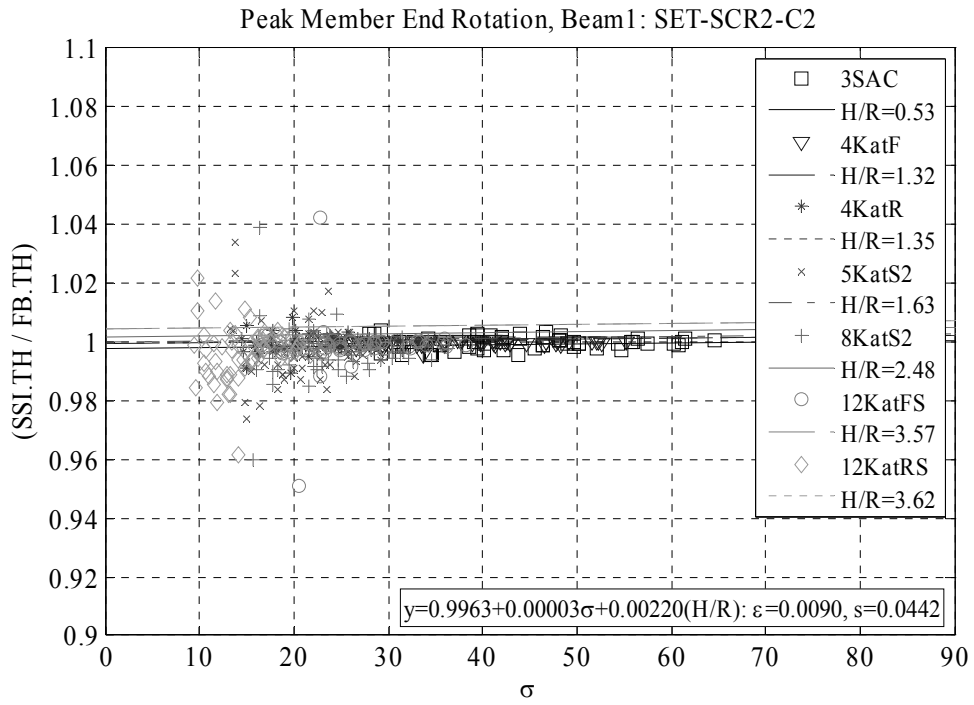


Figure D.10. (Cont'd)

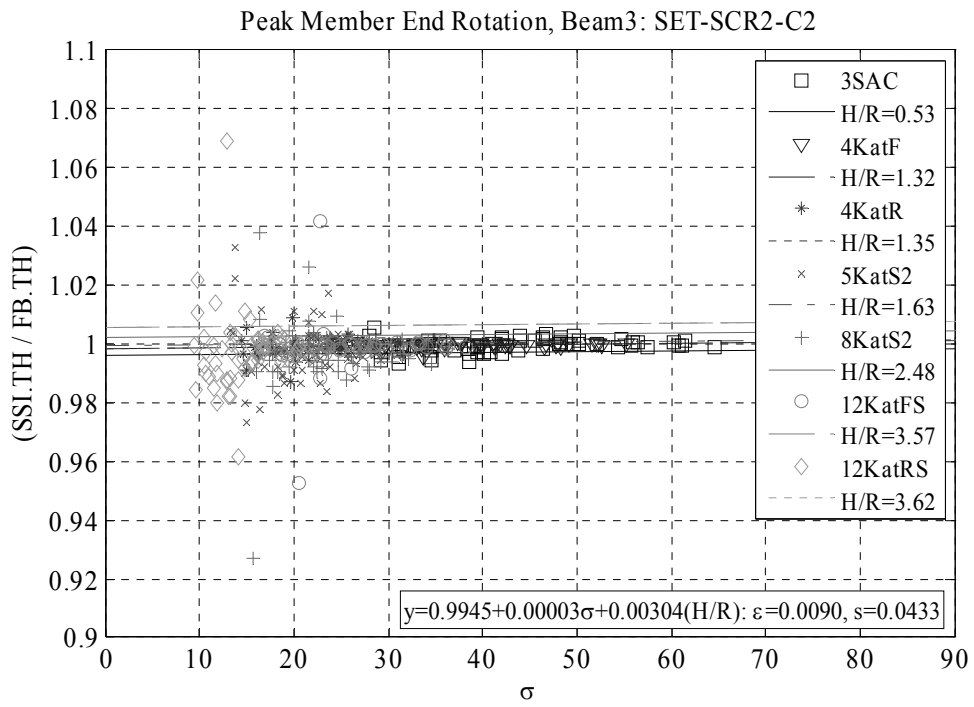


Figure D.10. (Cont'd)

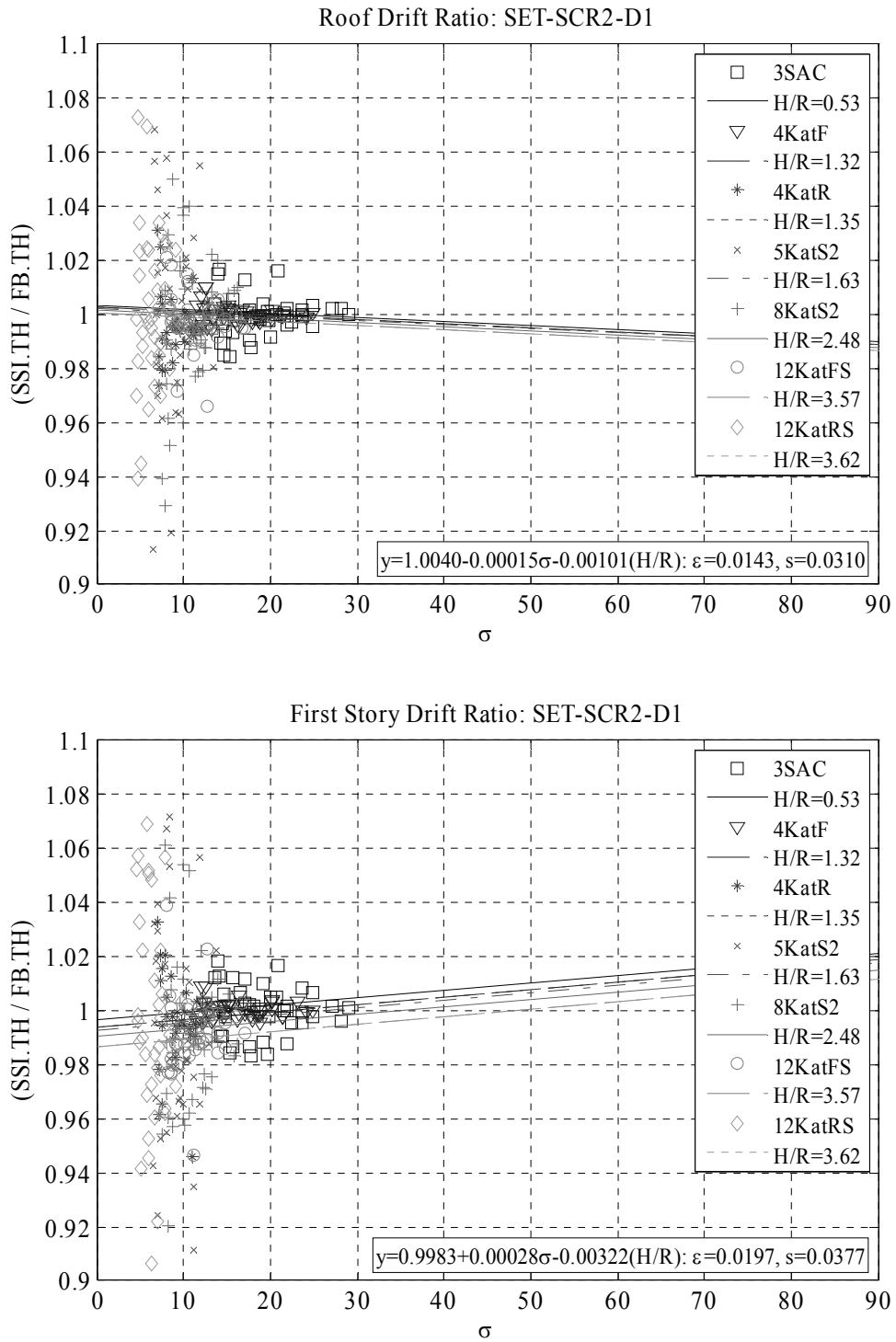


Figure D.11. 2D Scatter plot and associated regression line for the response ratios obtained for SET-SCR2-D1. Response ratios are calculated for: Roof drift ratio, first story drift ratio, peak column (foundation end) end and peak beam end rotations at the first story (SSI.TH / FB.TH), while the predictor variables are wave parameter (σ) and aspect ratio (H/R), ε is the mean absolute error and s is the standard error.

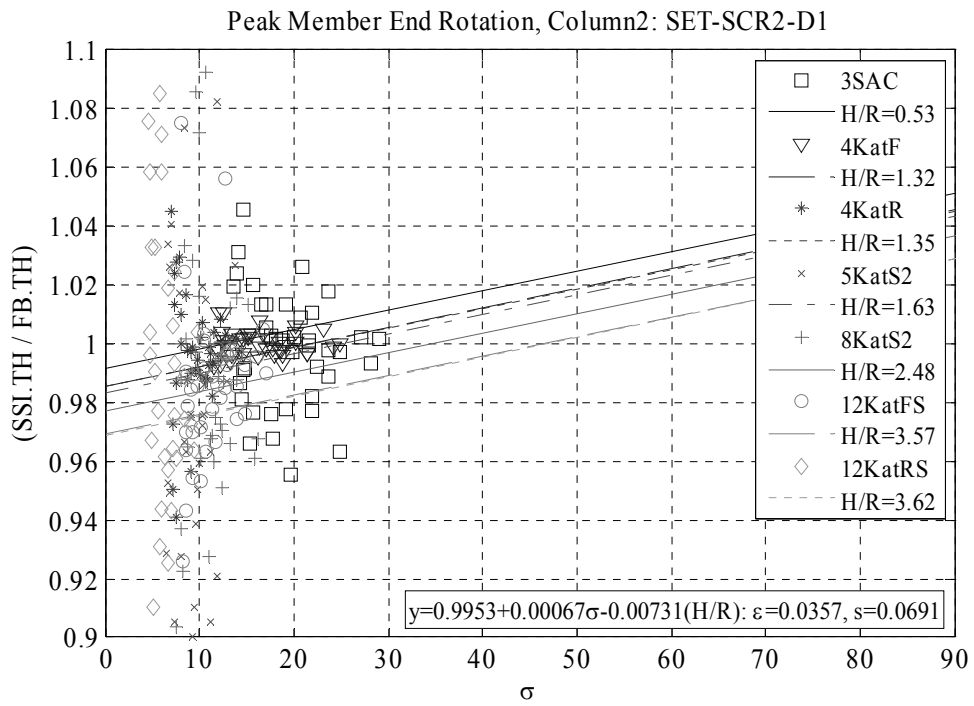
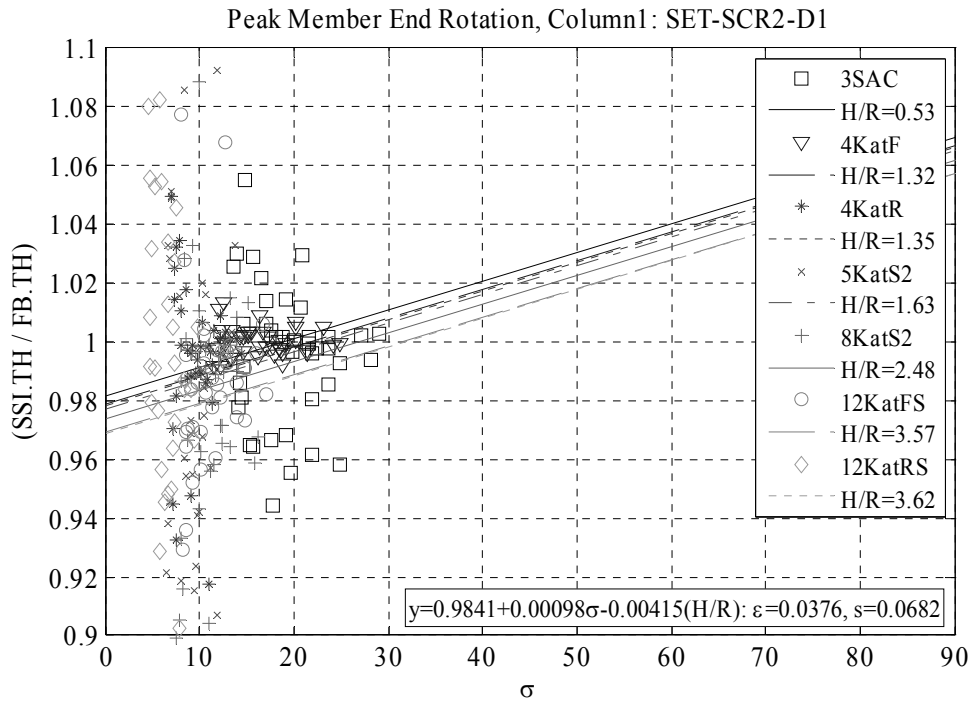


Figure D.11. (Cont'd)

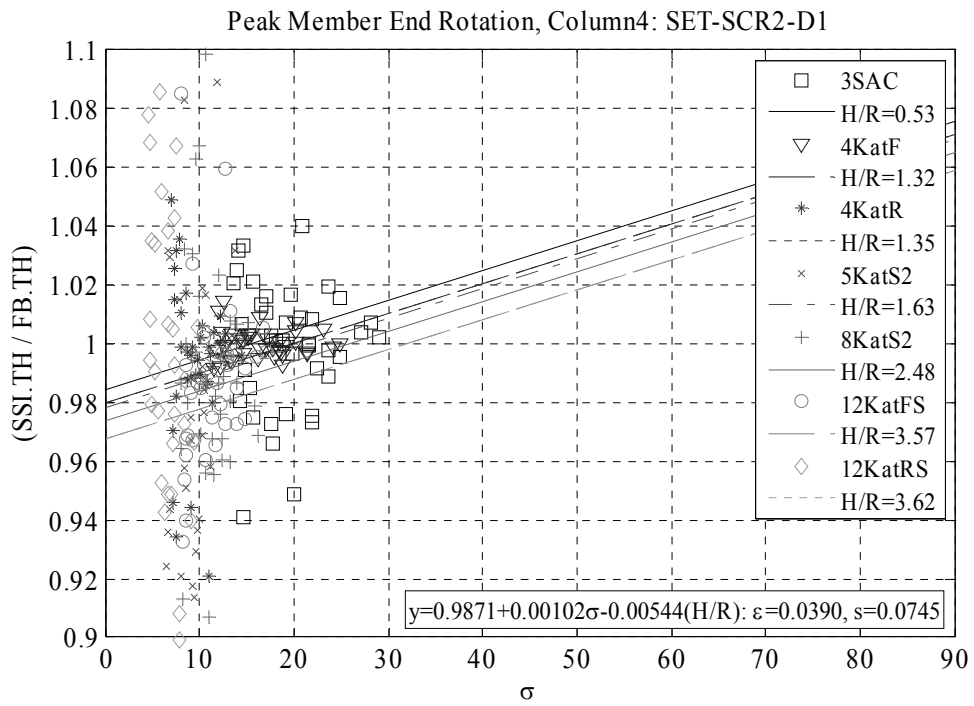
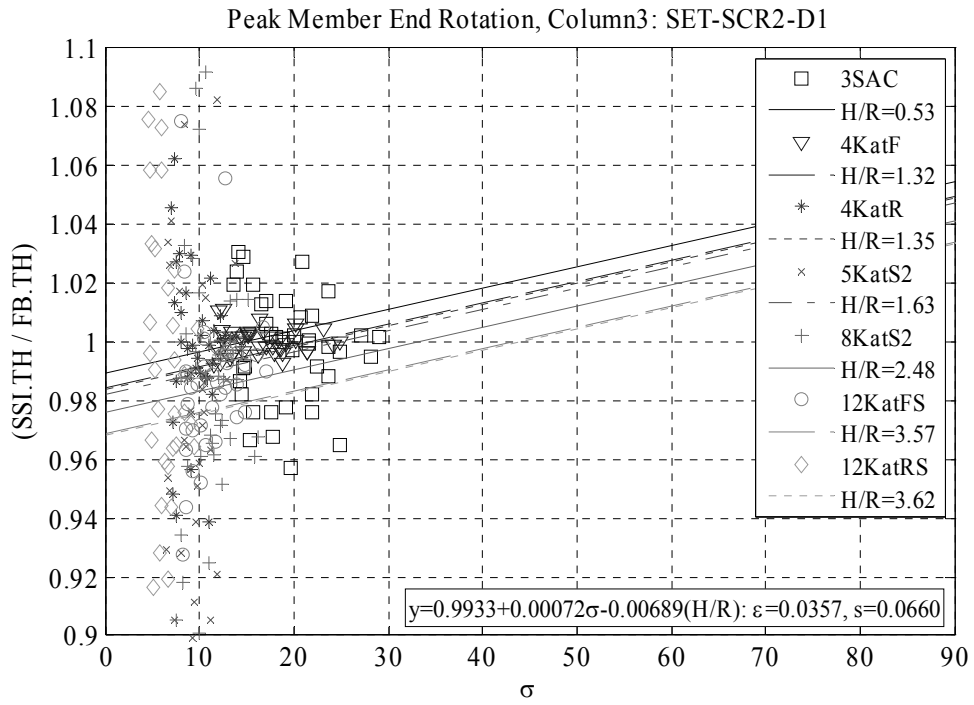


Figure D.11. (Cont'd)

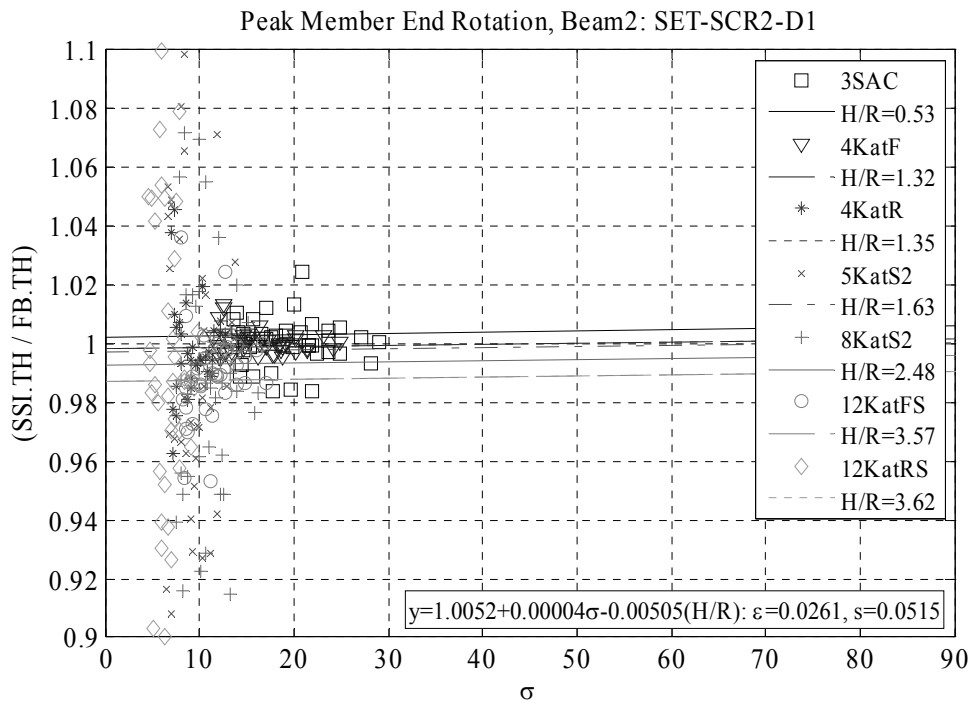
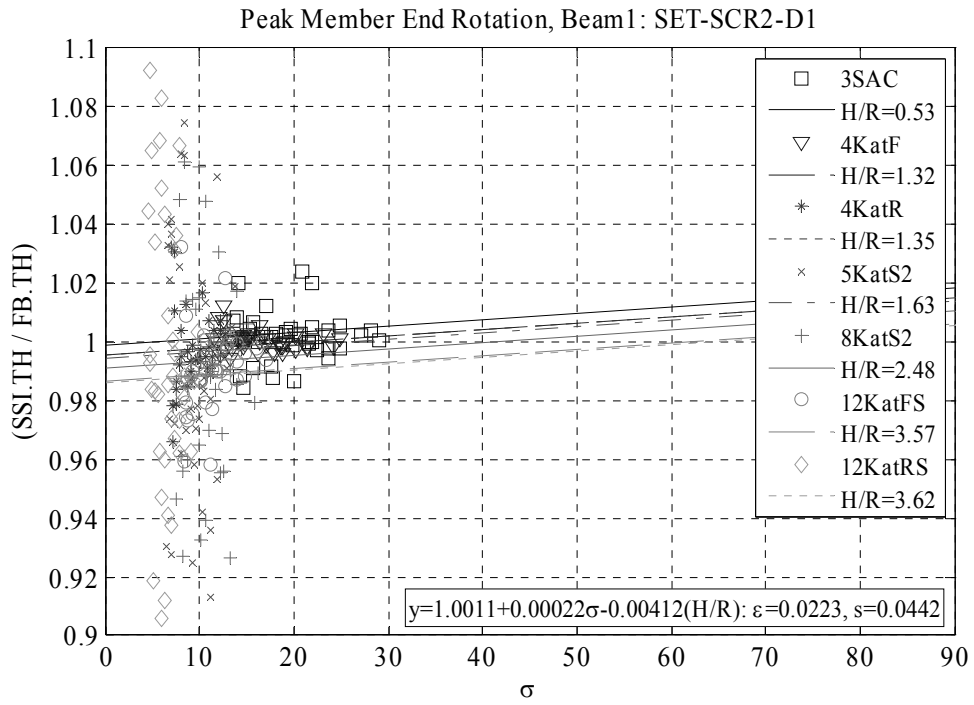


Figure D.11. (Cont'd)

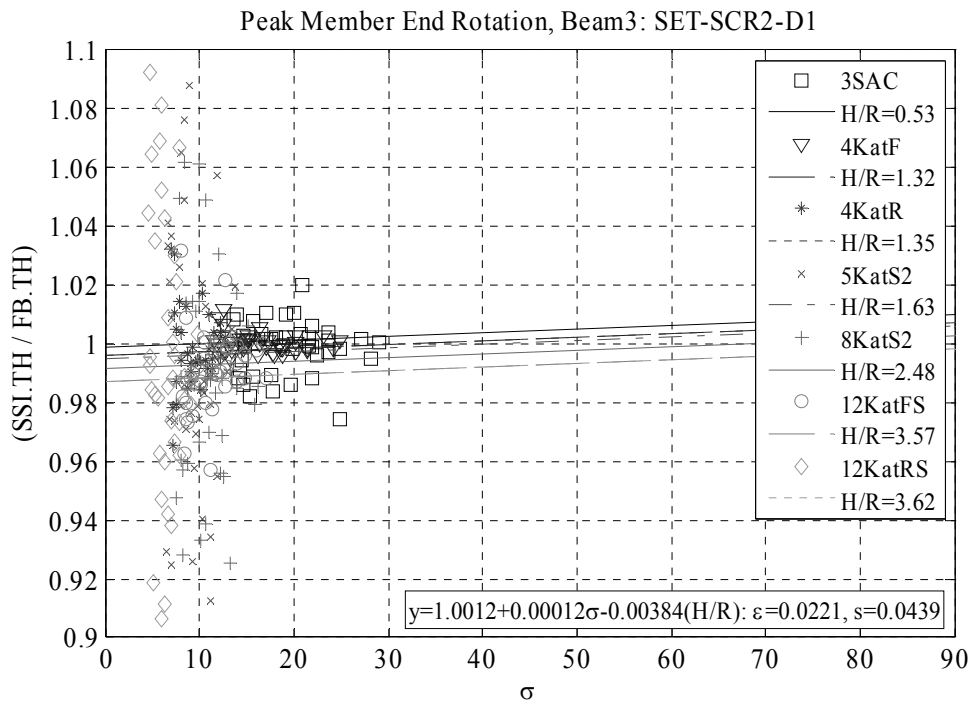


Figure D.11. (Cont'd)

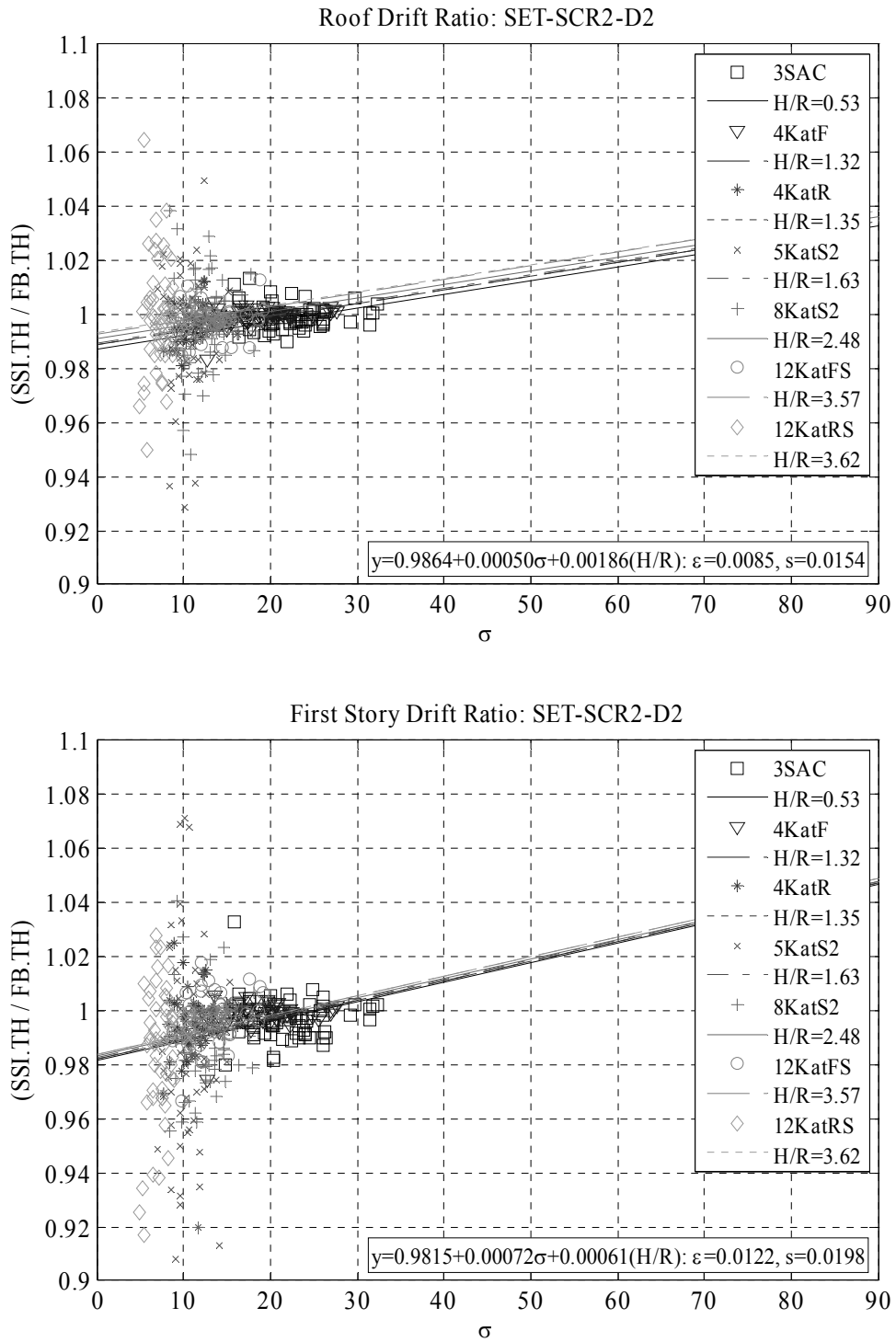


Figure D.12. 2D Scatter plot and associated regression line for the response ratios obtained for SET-SCR2-D2. Response ratios are calculated for: Roof drift ratio, first story drift ratio, peak column (foundation end) end and peak beam end rotations at the first story (SSI.TH / FB.TH), while the predictor variables are wave parameter (σ) and aspect ratio (H/R), ε is the mean absolute error and s is the standard error.

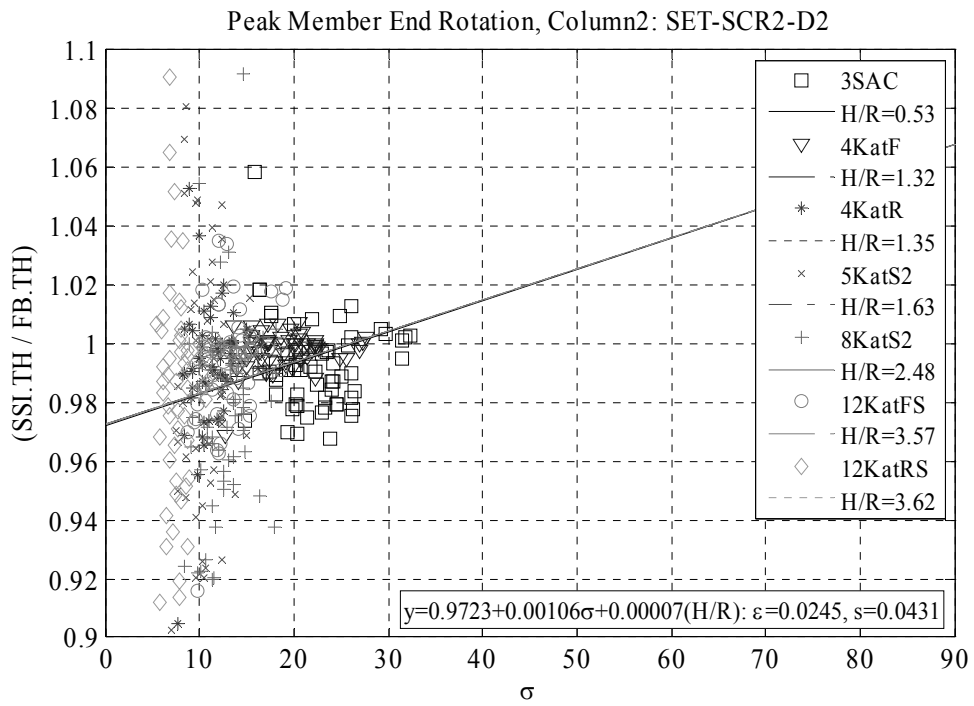
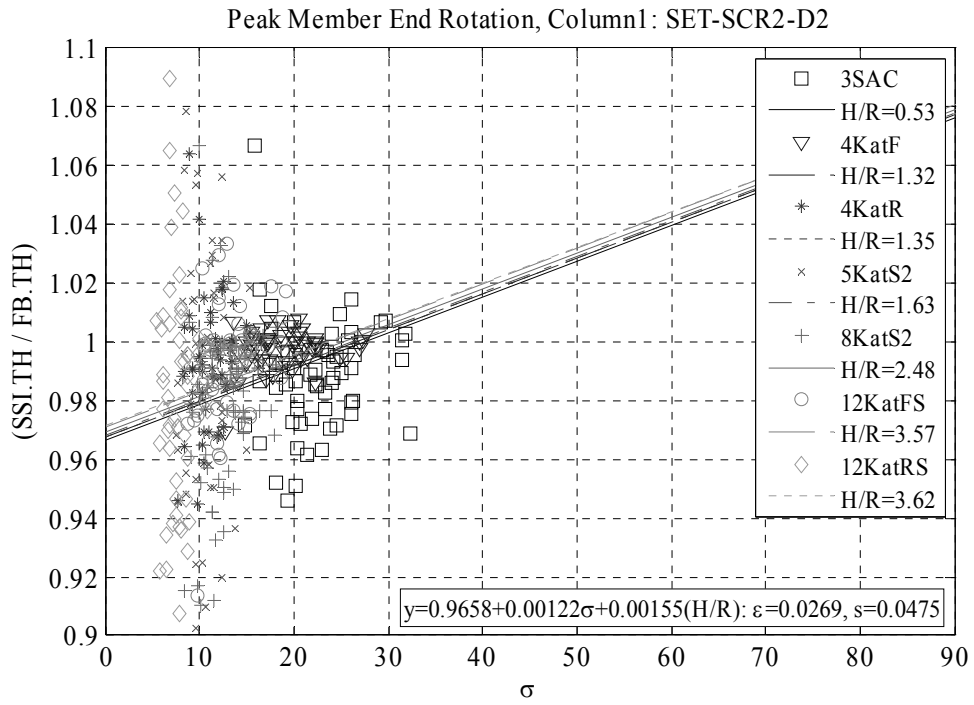


Figure D.12. (Cont'd)

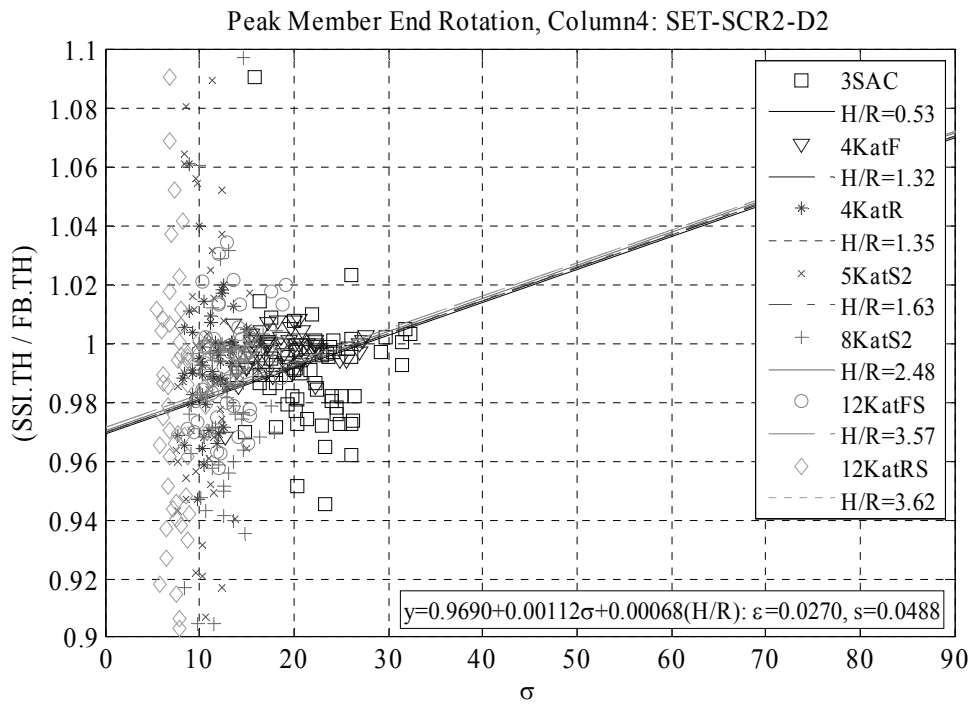
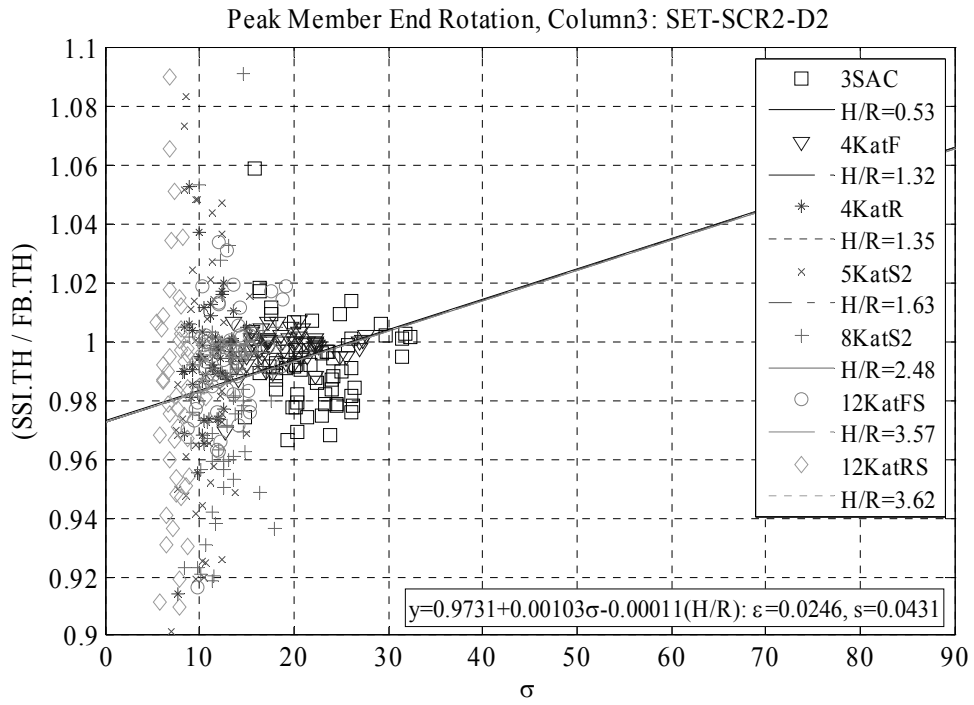


Figure D.12. (Cont'd)

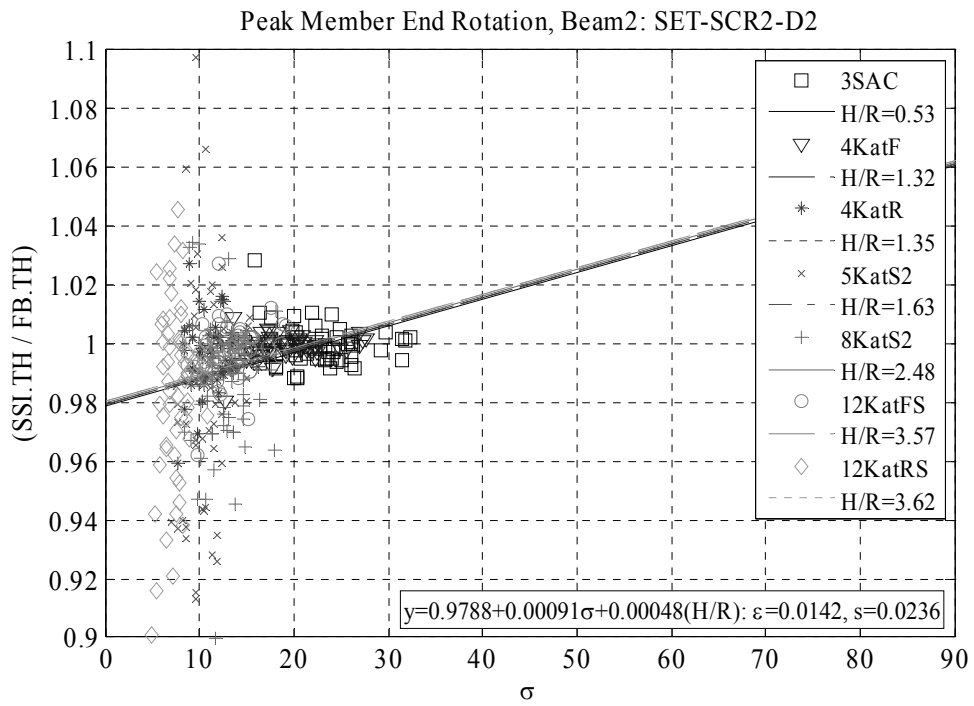
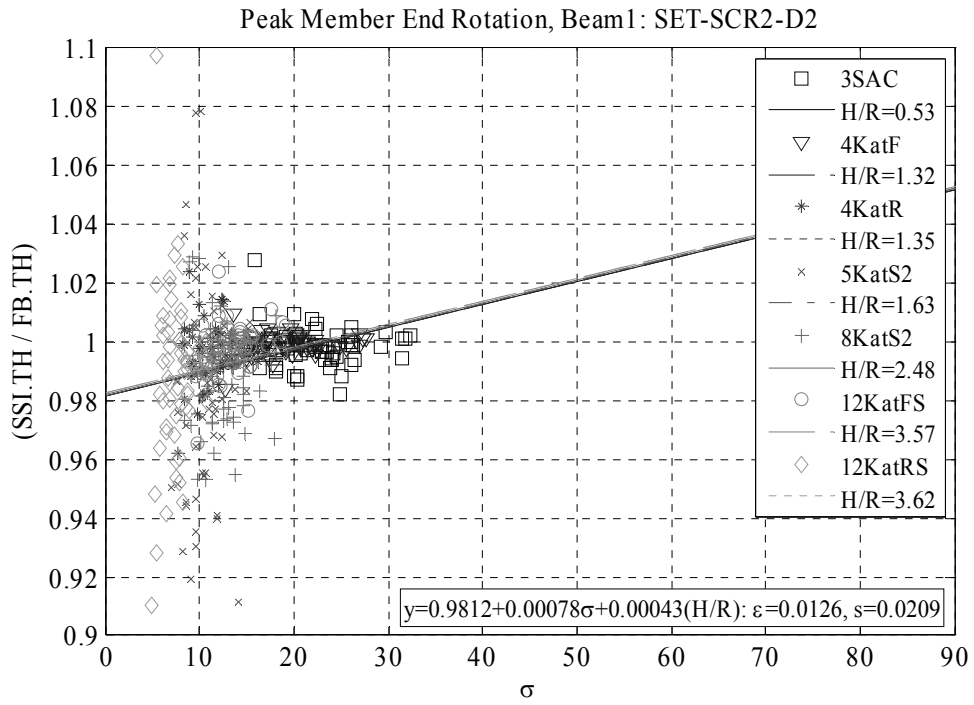


Figure D.12. (Cont'd)

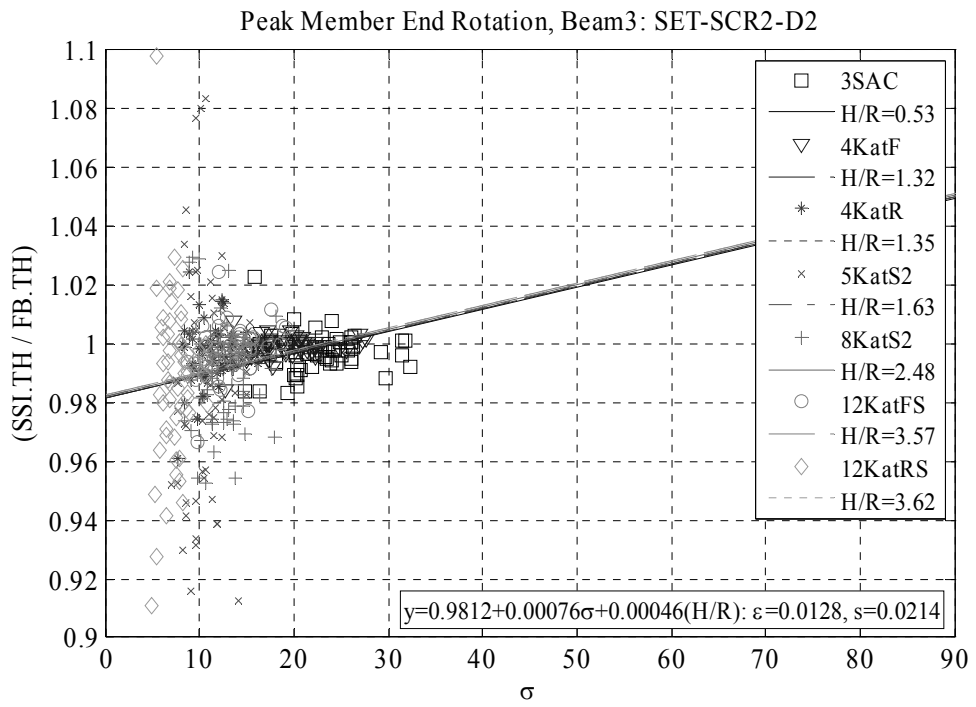


Figure D.12. (Cont'd)

APPENDIX E

PLOTS OF NONLINEAR STATIC AND NONLINEAR TIME-HISTORY ANALYSES

In this appendix, combined plots of the pushover curves with the peak roof drift demands obtained from NTH analyses are given. NTH events include both fixed-base (FB.TH) and flexible-base (SSI.TH) frame models' responses.

- Figs. E.1 – F.3 are obtained for 3SAC frame model for SET-C1, C2, D1 and D2 ground motion sets corresponding to Groups I, II and III, respectively.
- Figs. E.4 – F.6 are obtained for 4KatF frame model for SET-C1, C2, D1 and D2 ground motion sets corresponding to Groups I, II and III, respectively.
- Figs. E.7 – F.9 are obtained for 4KatR frame model for SET-C1, C2, D1 and D2 ground motion sets corresponding to Groups I, II and III, respectively.
- Figs. E.10 – F.12 are obtained for 5KatS2 frame model for SET-C1, C2, D1 and D2 ground motion sets corresponding to Groups I, II and III, respectively.
- Figs. E.13 – F.15 are obtained for 8KatS2 frame model for SET-C1, C2, D1 and D2 ground motion sets corresponding to Groups I, II and III, respectively.
- Figs. E.16 – F.18 are obtained for 12KatFS frame model for SET-C1, C2, D1 and D2 ground motion sets corresponding to Groups I, II and III, respectively.
- Figs. E.19 – F.21 are obtained for 12KatRS frame model for SET-C1, C2, D1 and D2 ground motion sets corresponding to Groups I, II and III, respectively.

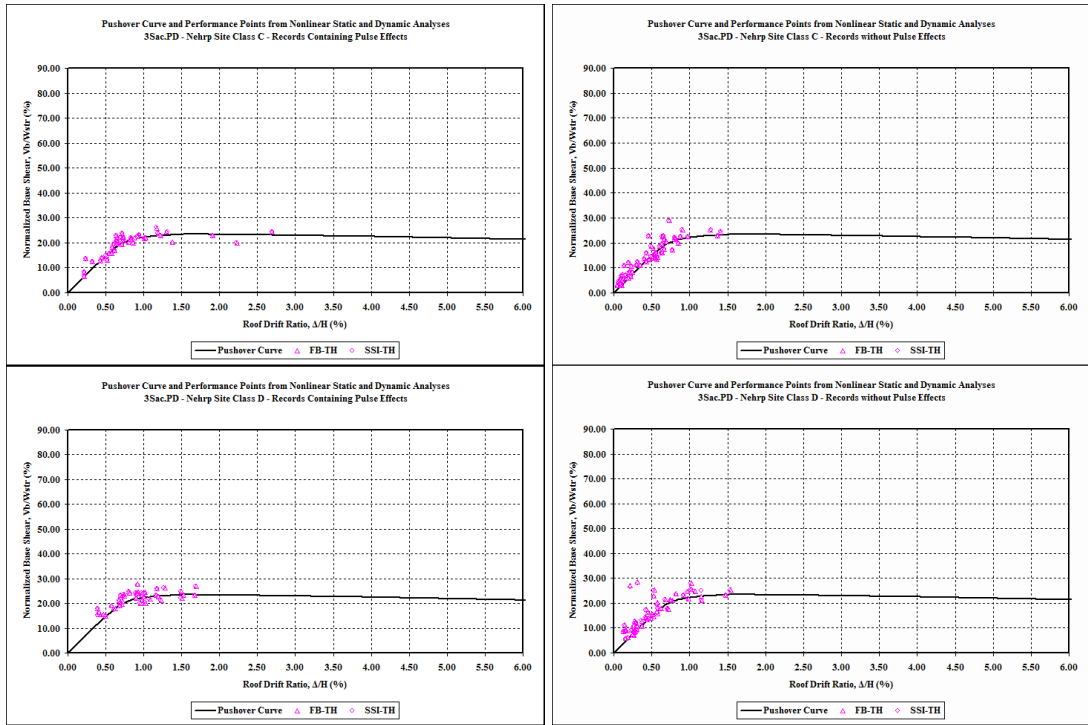


Figure E.1. Pushover curves and peak roof drift demands obtained from SET-NS-C1, C2, D1 and D2 records for the frame model 3SAC.

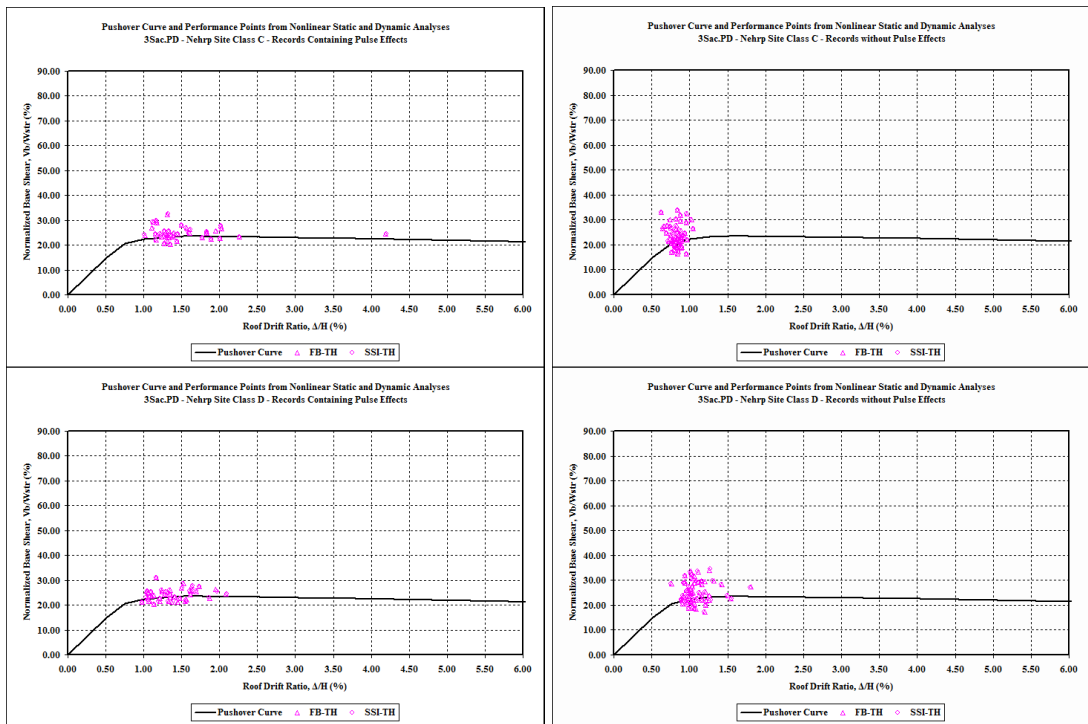


Figure E.2. Pushover curves and peak roof drift demands obtained from SET-SC-C1, C2, D1 and D2 records for the frame model 3SAC.

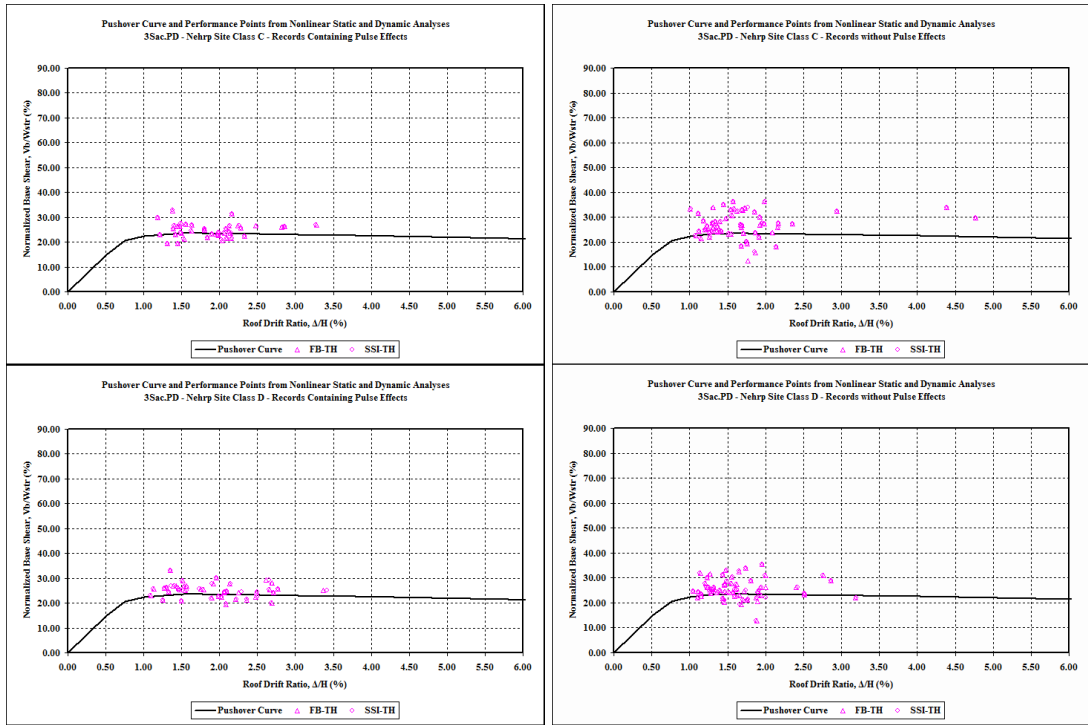


Figure E.3. Pushover curves and peak roof drift demands obtained from SET-SCR2-C1, C2, D1 and D2 records for the frame model 3SAC.

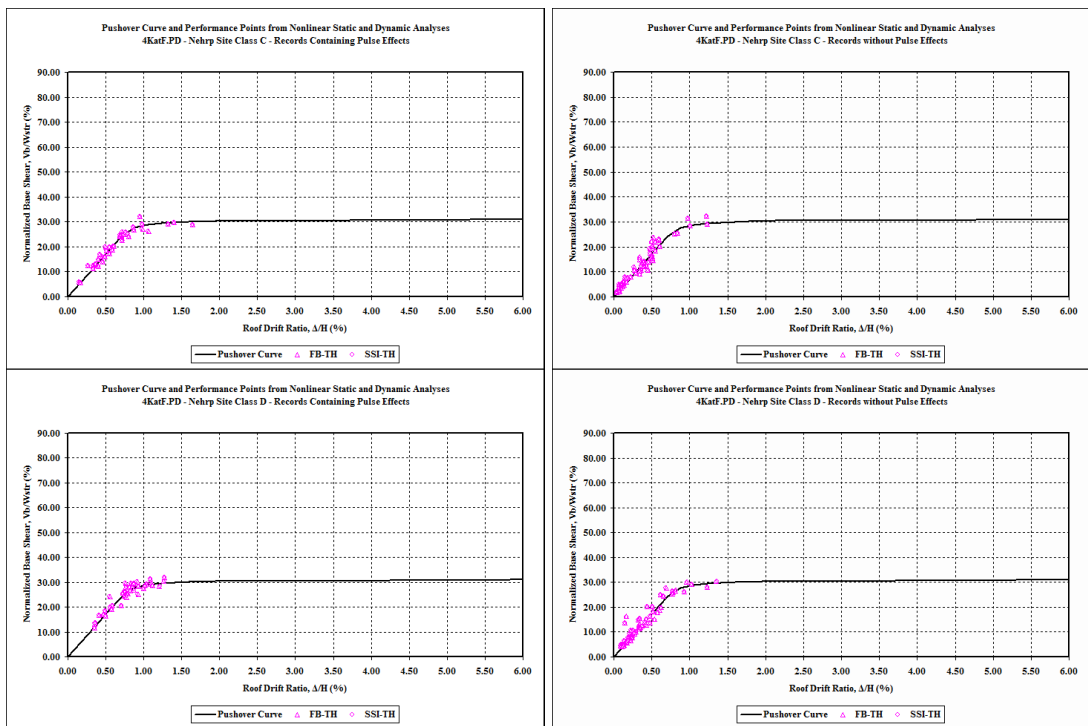


Figure E.4. Pushover curves and peak roof drift demands obtained from SET-NS-C1, C2, D1 and D2 records for the frame model 4KatF.

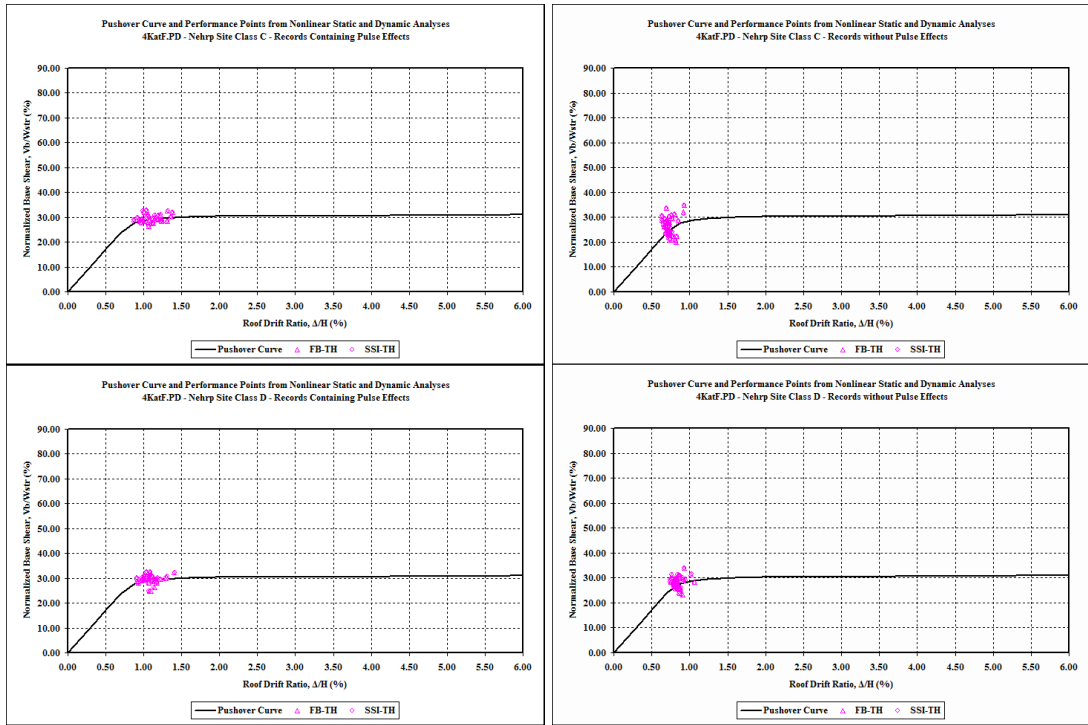


Figure E.5. Pushover curves and peak roof drift demands obtained from SET-SC-C1, C2, D1 and D2 records for the frame model 4KatF.

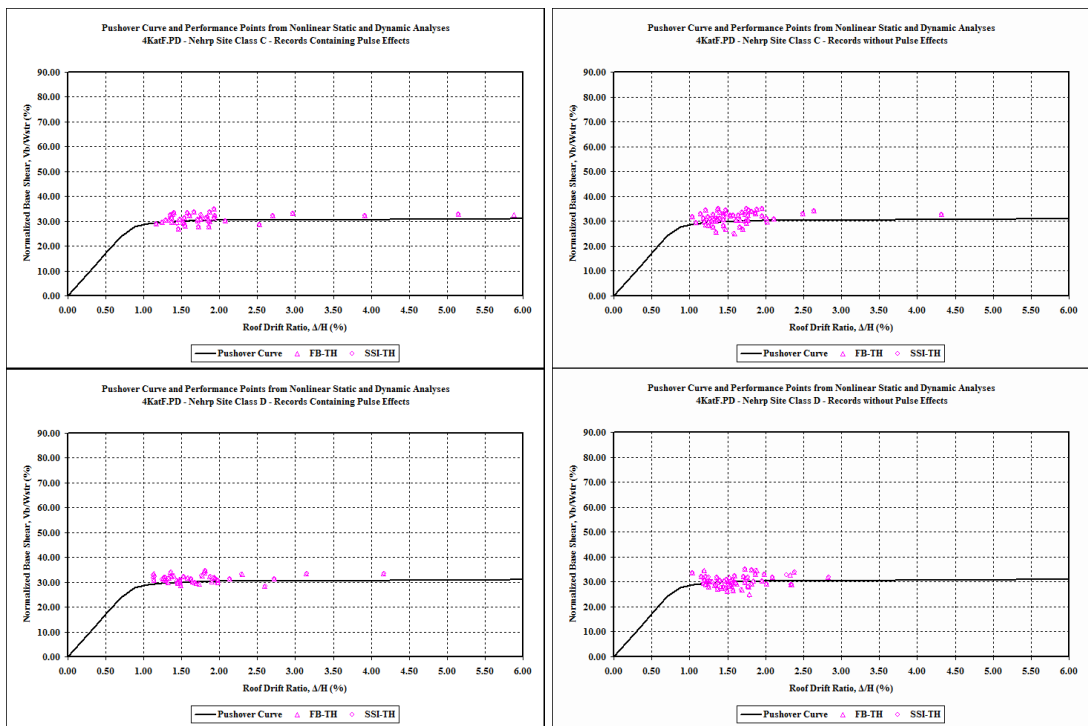


Figure E.6. Pushover curves and peak roof drift demands obtained from SET-SCR2-C1, C2, D1 and D2 records for the frame model 4KatF.

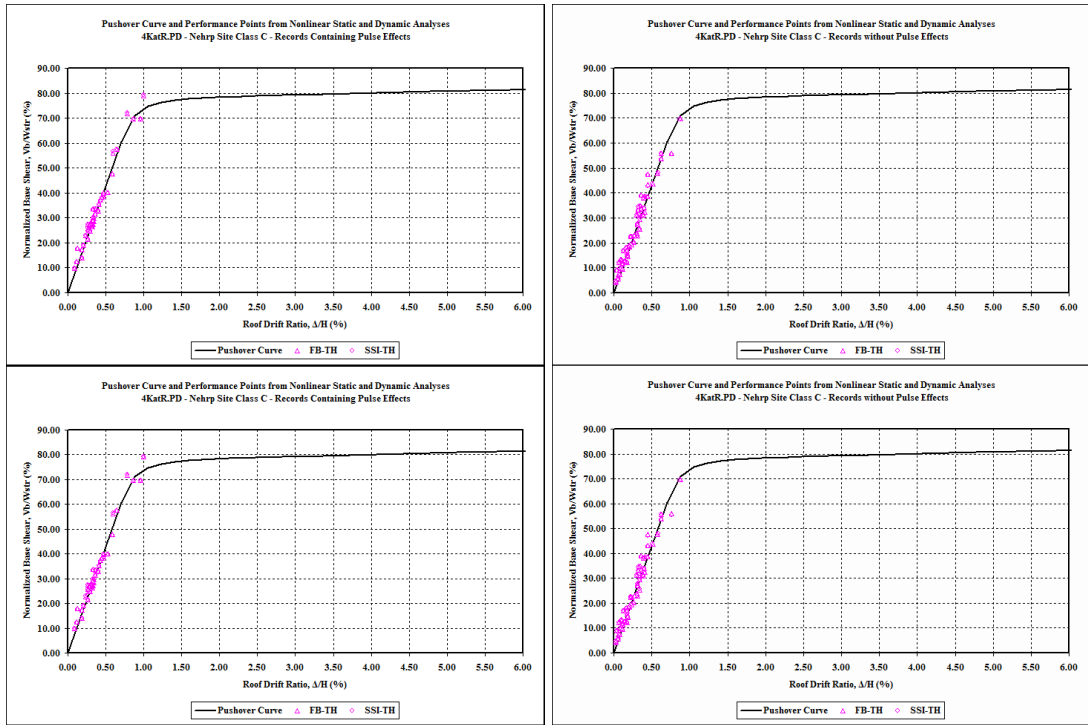


Figure E.7. Pushover curves and peak roof drift demands obtained from SET-NS-C1, C2, D1 and D2 records for the frame model 4KatR.

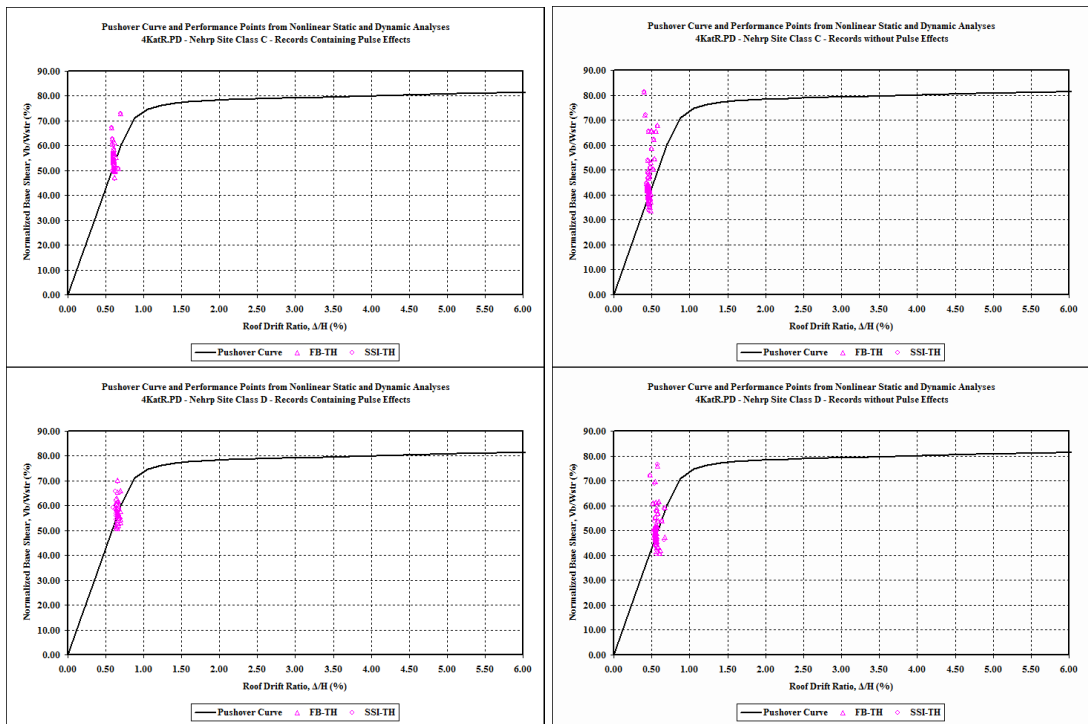


Figure E.8. Pushover curves and peak roof drift demands obtained from SET-SC-C1, C2, D1 and D2 records for the frame model 4KatR.

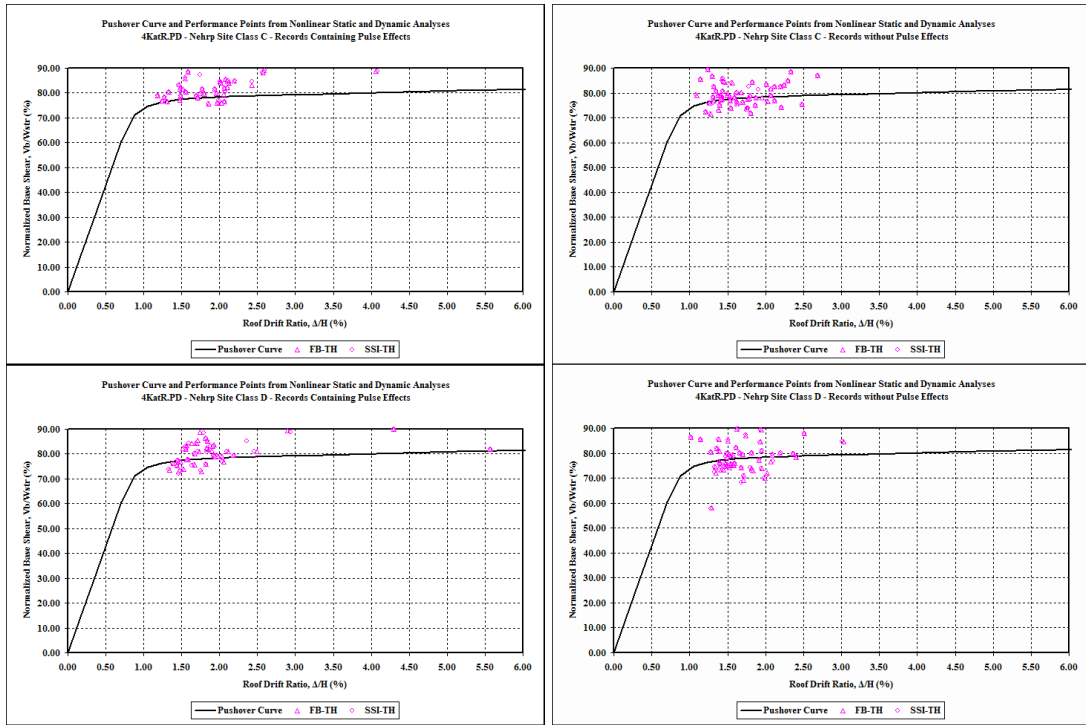


Figure E.9. Pushover curves and peak roof drift demands obtained from SET-SCR2-C1, C2, D1 and D2 records for the frame model 4KatR.

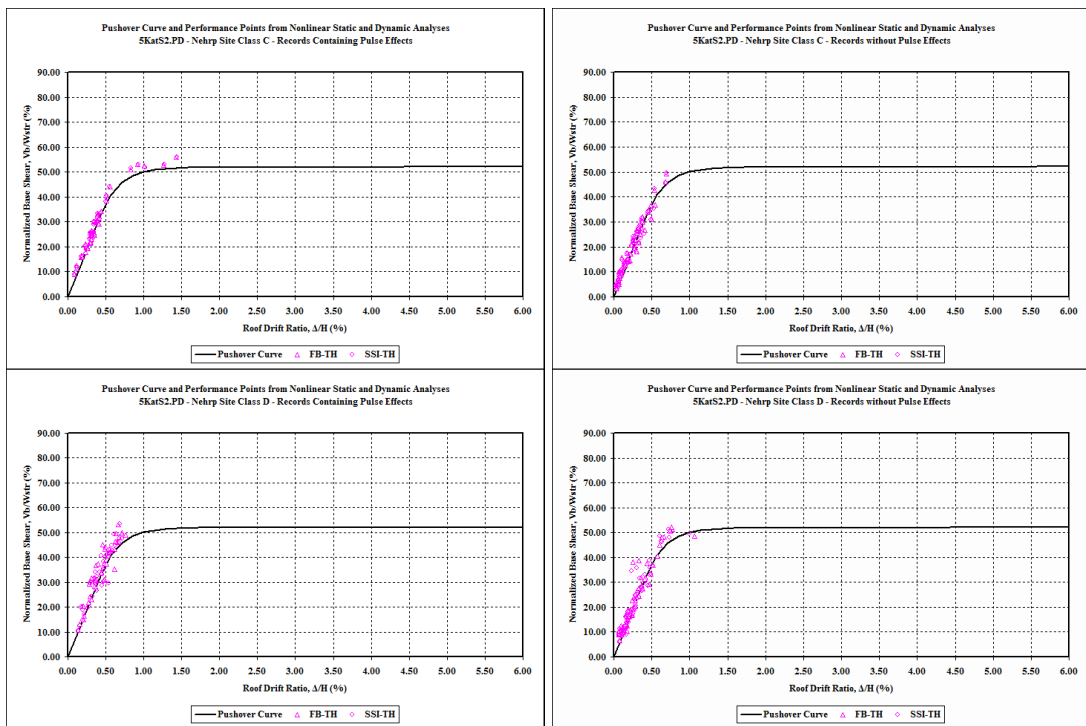


Figure E.10. Pushover curves and peak roof drift demands obtained from SET-NS-C1, C2, D1 and D2 records for the frame model 5KatS2.

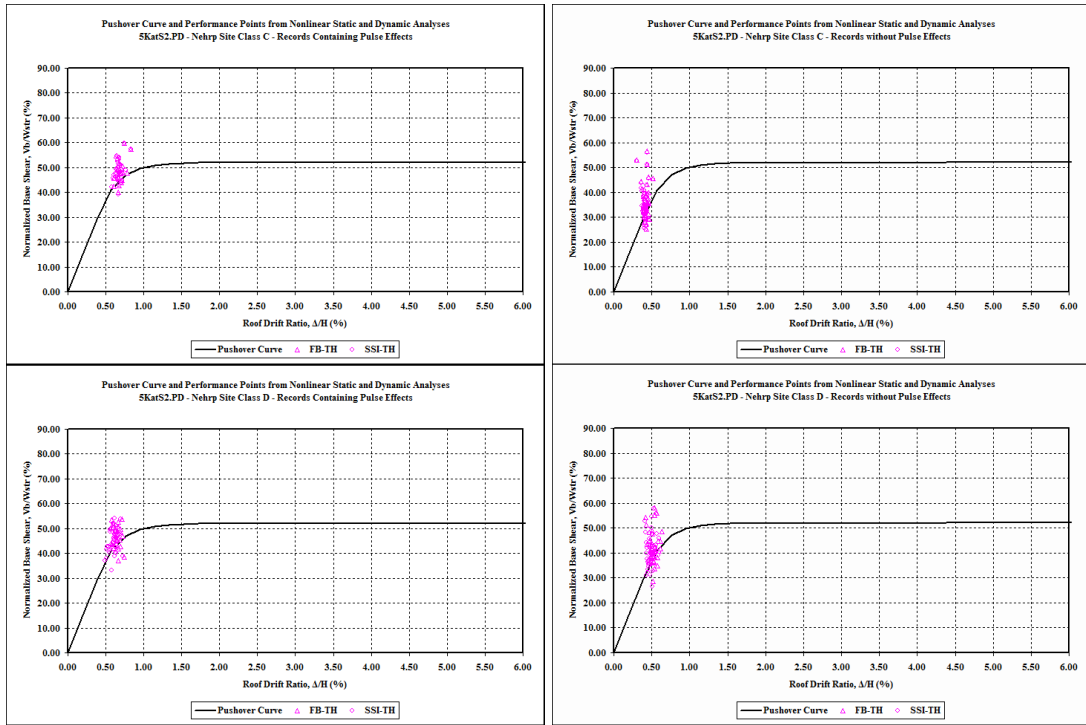


Figure E.11. Pushover curves and peak roof drift demands obtained from SET-SC-C1, C2, D1 and D2 records for the frame model 5KatS2.

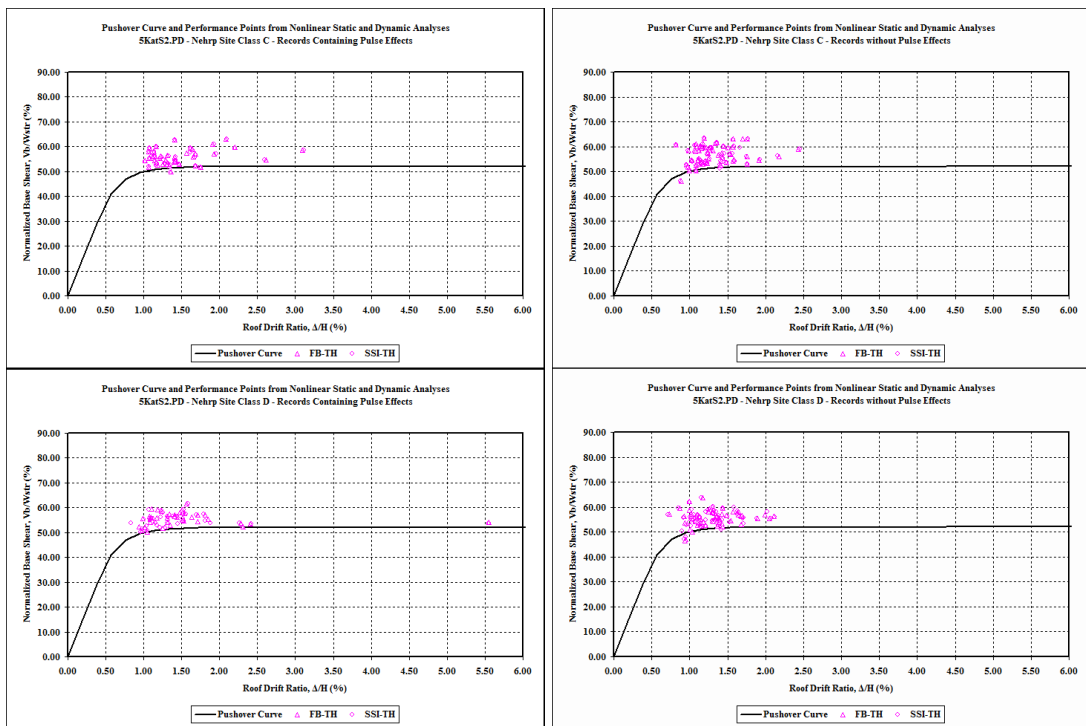


Figure E.12. Pushover curves and peak roof drift demands obtained from SET-SCR2-C1, C2, D1 and D2 records for the frame model 5KatS2.

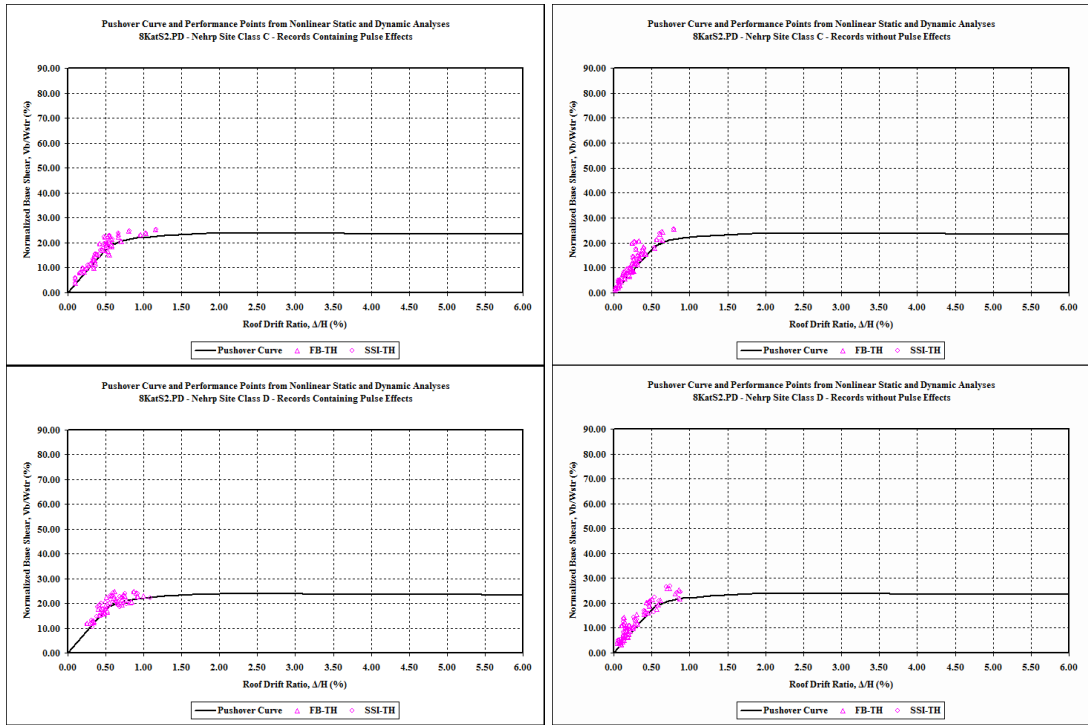


Figure E.13. Pushover curves and peak roof drift demands obtained from SET-NS-C1, C2, D1 and D2 records for the frame model 8KatS2.

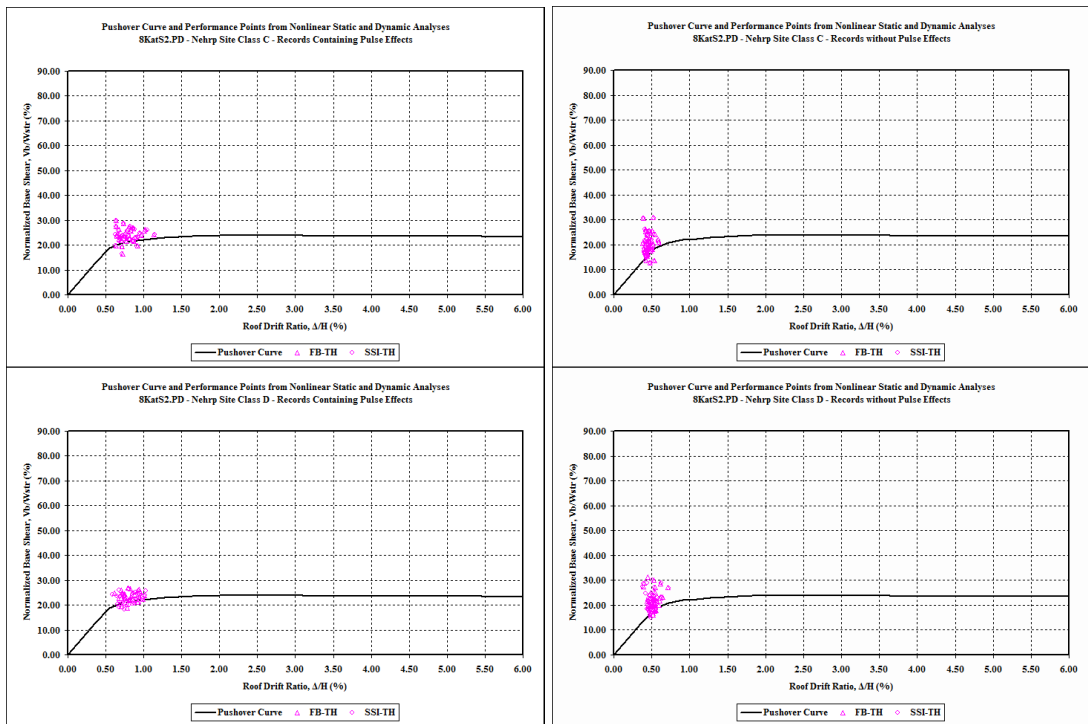


Figure E.14. Pushover curves and peak roof drift demands obtained from SET-SC-C1, C2, D1 and D2 records for the frame model 8KatS2.

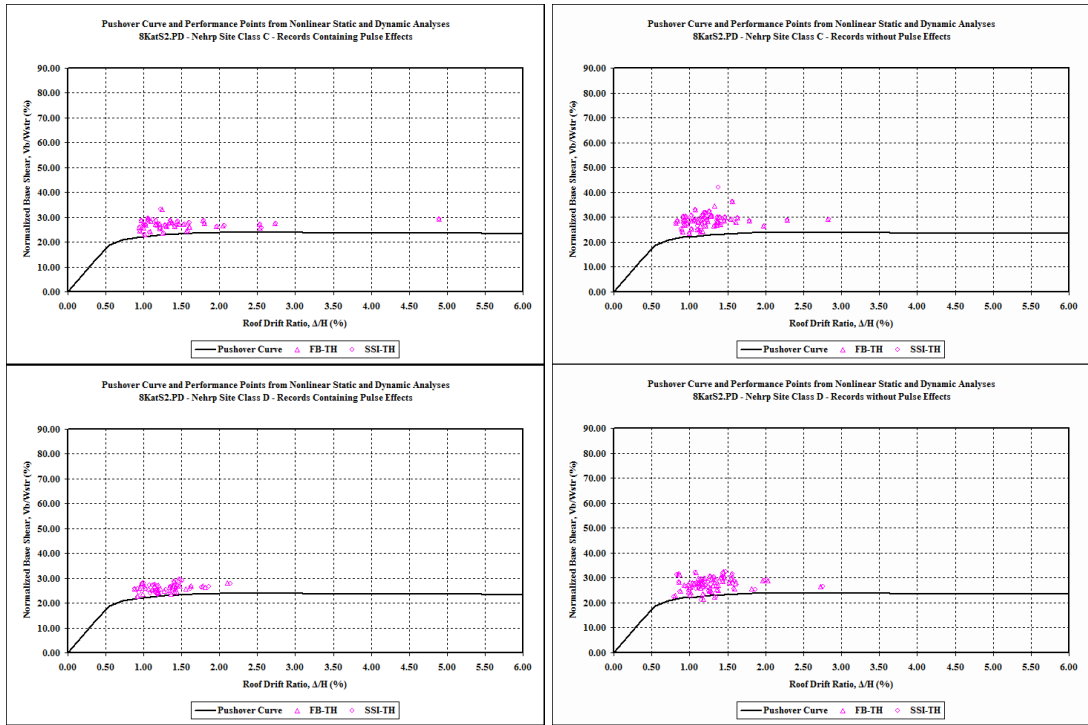


Figure E.15. Pushover curves and peak roof drift demands obtained from SET-SCR2-C1, C2, D1 and D2 records for the frame model 8KatS2.

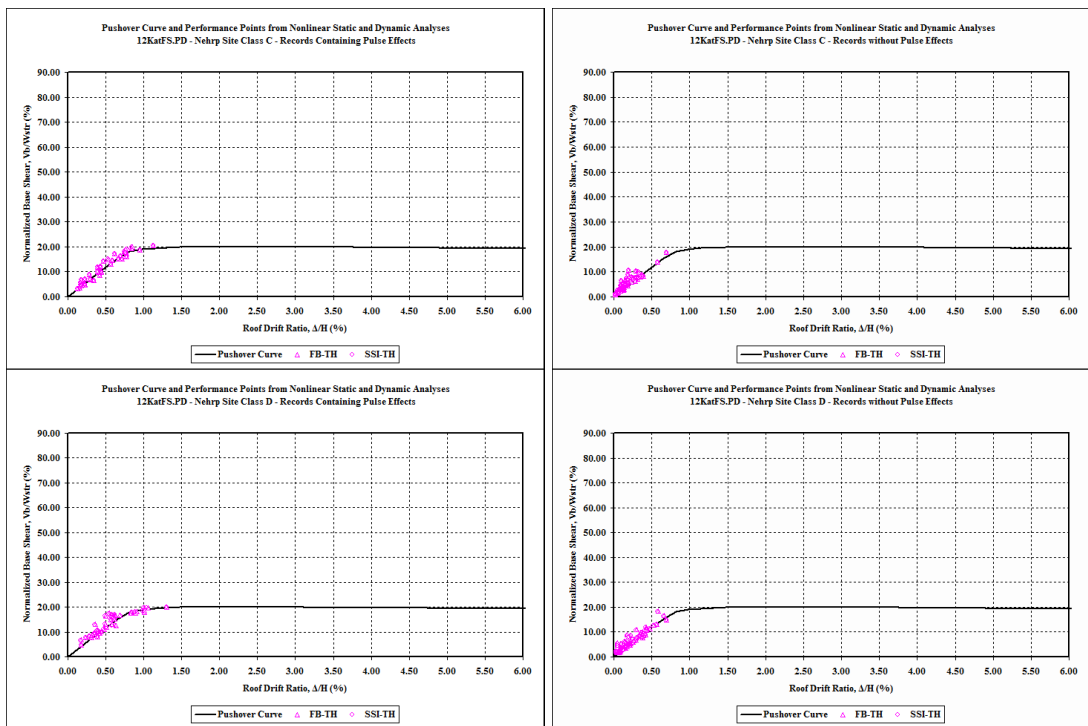


Figure E.16. Pushover curves and peak roof drift demands obtained from SET-NS-C1, C2, D1 and D2 records for the frame model 12KatFS.

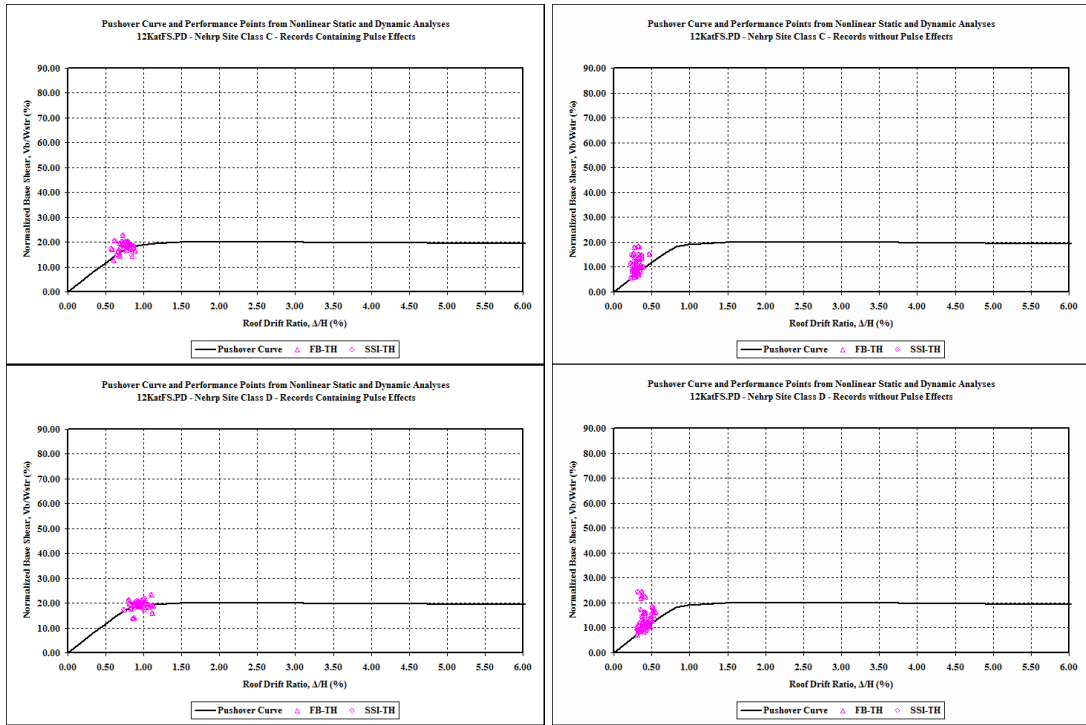


Figure E.17. Pushover curves and peak roof drift demands obtained from SET-SC-C1, C2, D1 and D2 records for the frame model 12KatFS.

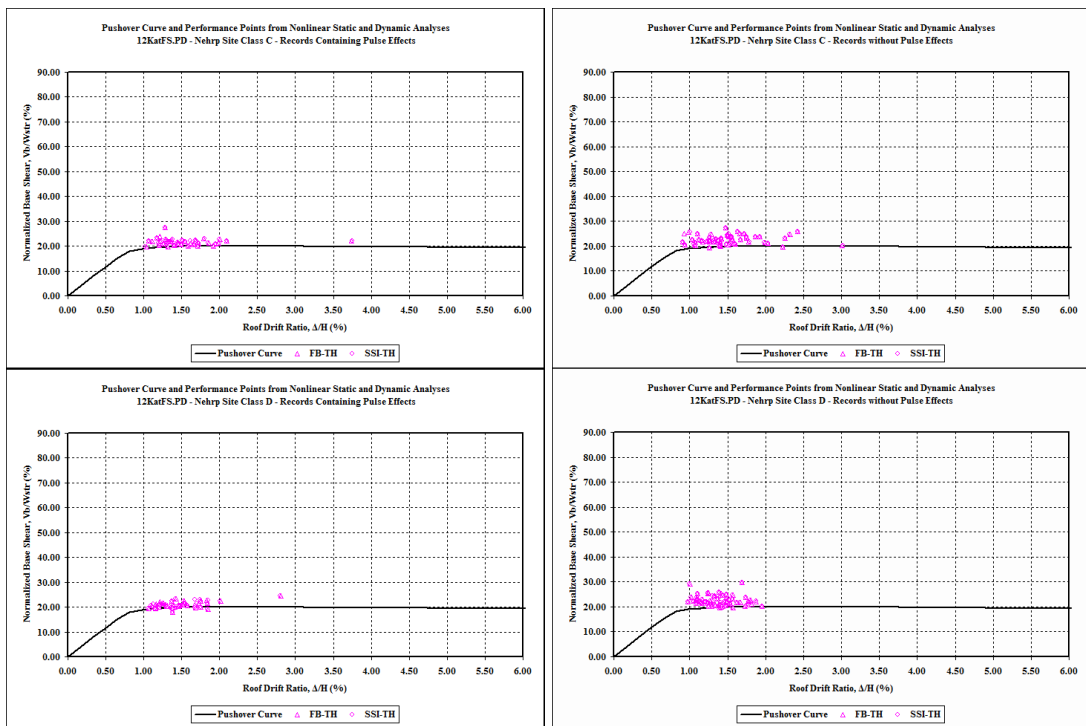


Figure E.18. Pushover curves and peak roof drift demands obtained from SET-SCR2-C1, C2, D1 and D2 records for the frame model 12KatFS.

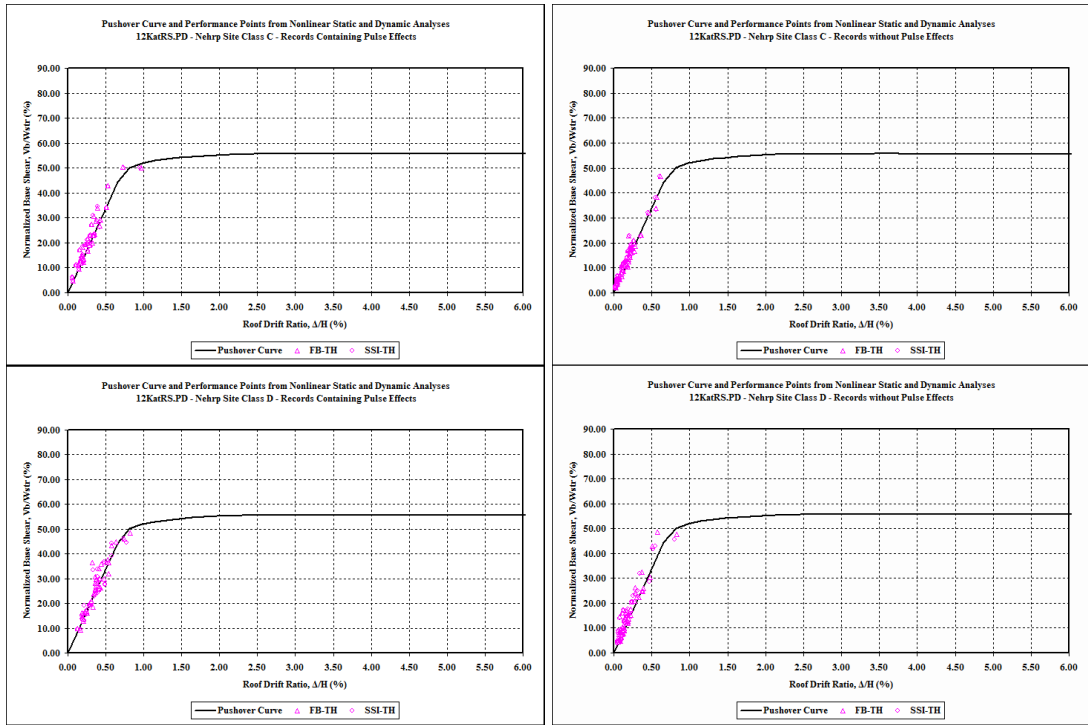


Figure E.19. Pushover curves and peak roof drift demands obtained from SET-NS-C1, C2, D1 and D2 records for the frame model 12KatRS.

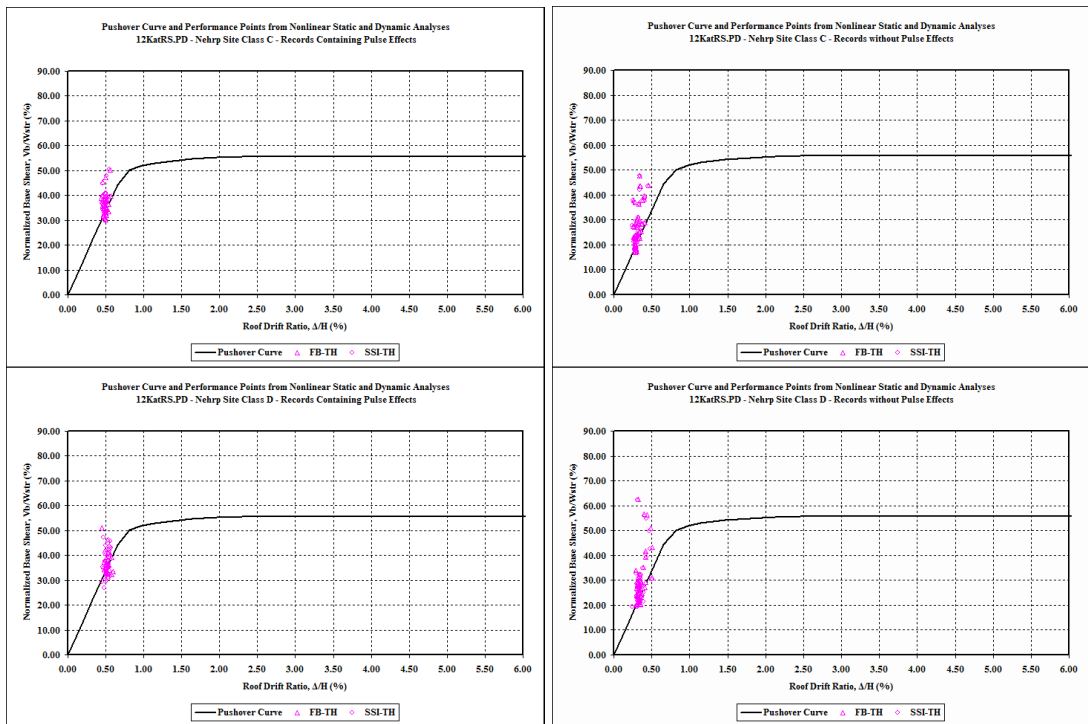


Figure E.20. Pushover curves and peak roof drift demands obtained from SET-SC-C1, C2, D1 and D2 records for the frame model 12KatRS.

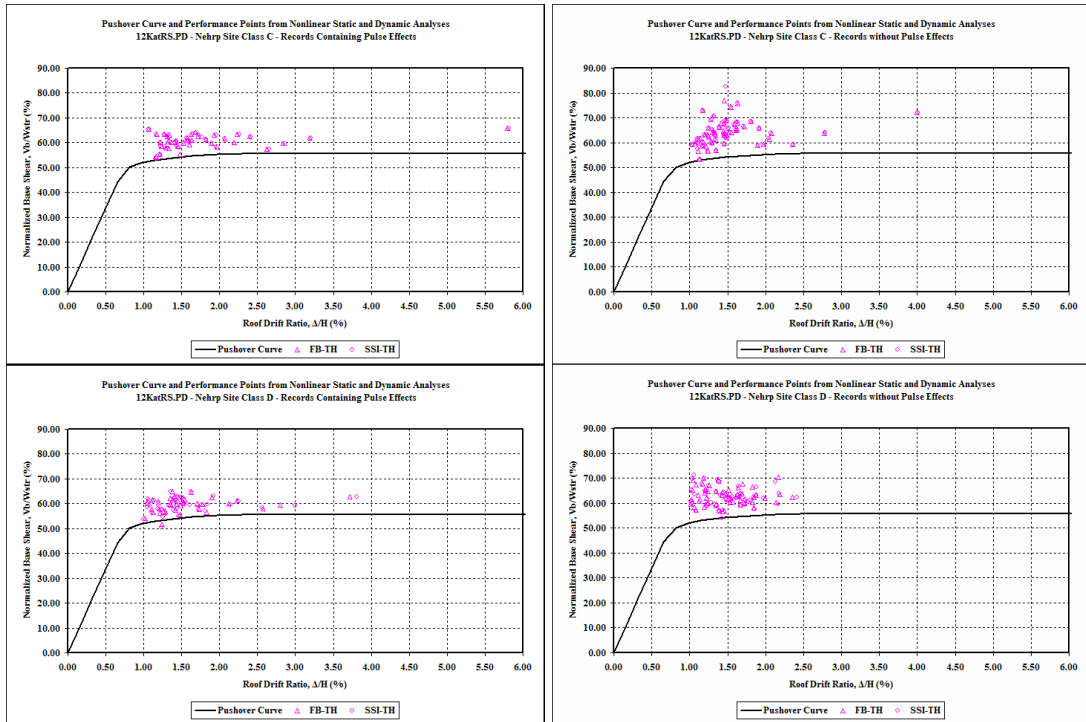


Figure E.21. Pushover curves and peak roof drift demands obtained from SET-SCR2-C1, C2, D1 and D2 records for the frame model 12KatRS.

APPENDIX F

INTERSTORY DRIFT PLOTS OBTAINED FROM NTH ANALYSES

In this appendix, predicted peak and mean interstory drift demands from nonlinear time-history analyses of both fixed-base (FB.TH) and flexible-base (SSI.TH) frame models corresponding to Analysis Groups I, II and III are given. These figures are organized in the following order:

- Figs. F.1 – F.3 are obtained for 3SAC frame model for SET-C1, C2, D1 and D2 ground motion sets corresponding to Groups I, II and III, respectively.
- Figs. F.4 – F.6 are obtained for 4KatF frame model for SET-C1, C2, D1 and D2 ground motion sets corresponding to Groups I, II and III, respectively.
- Figs. F.7 – F.9 are obtained for 4KatR frame model for SET-C1, C2, D1 and D2 ground motion sets corresponding to Groups I, II and III, respectively.
- Figs. F.10 – F.12 are obtained for 5KatS2 frame model for SET-C1, C2, D1 and D2 ground motion sets corresponding to Groups I, II and III, respectively.
- Figs. F.13 – F.15 are obtained for 8KatS2 frame model for SET-C1, C2, D1 and D2 ground motion sets corresponding to Groups I, II and III, respectively.
- Figs. F.16 – F.18 are obtained for 12KatFS frame model for SET-C1, C2, D1 and D2 ground motion sets corresponding to Groups I, II and III, respectively.
- Figs. F.19 – F.21 are obtained for 12KatRS frame model for SET-C1, C2, D1 and D2 ground motion sets corresponding to Groups I, II and III, respectively.

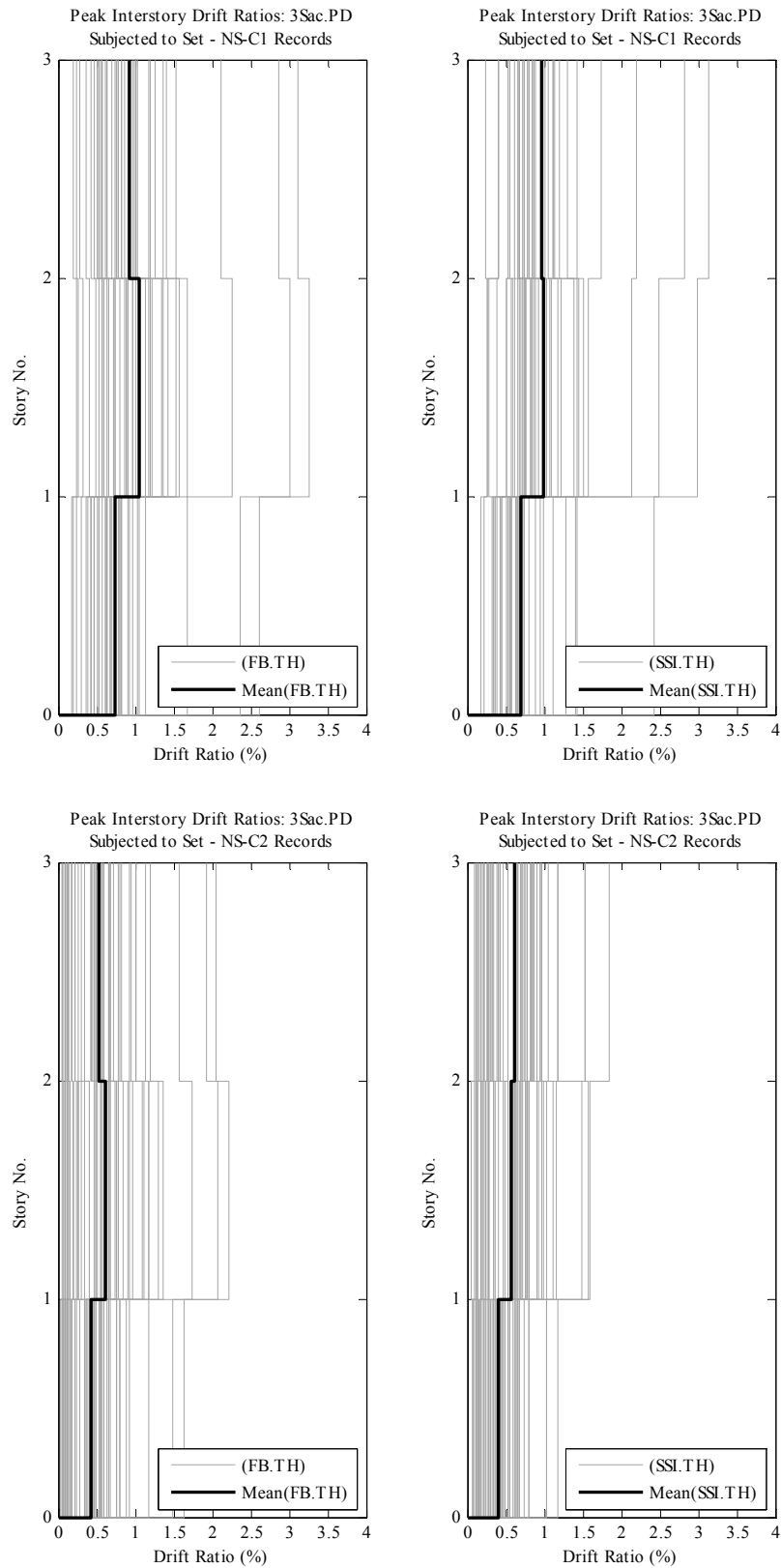


Figure F.1. Comparison of peak and mean interstory drift demands of Model 3SAC subjected to Set NS-C1, C2, D1, D2 earthquake records.

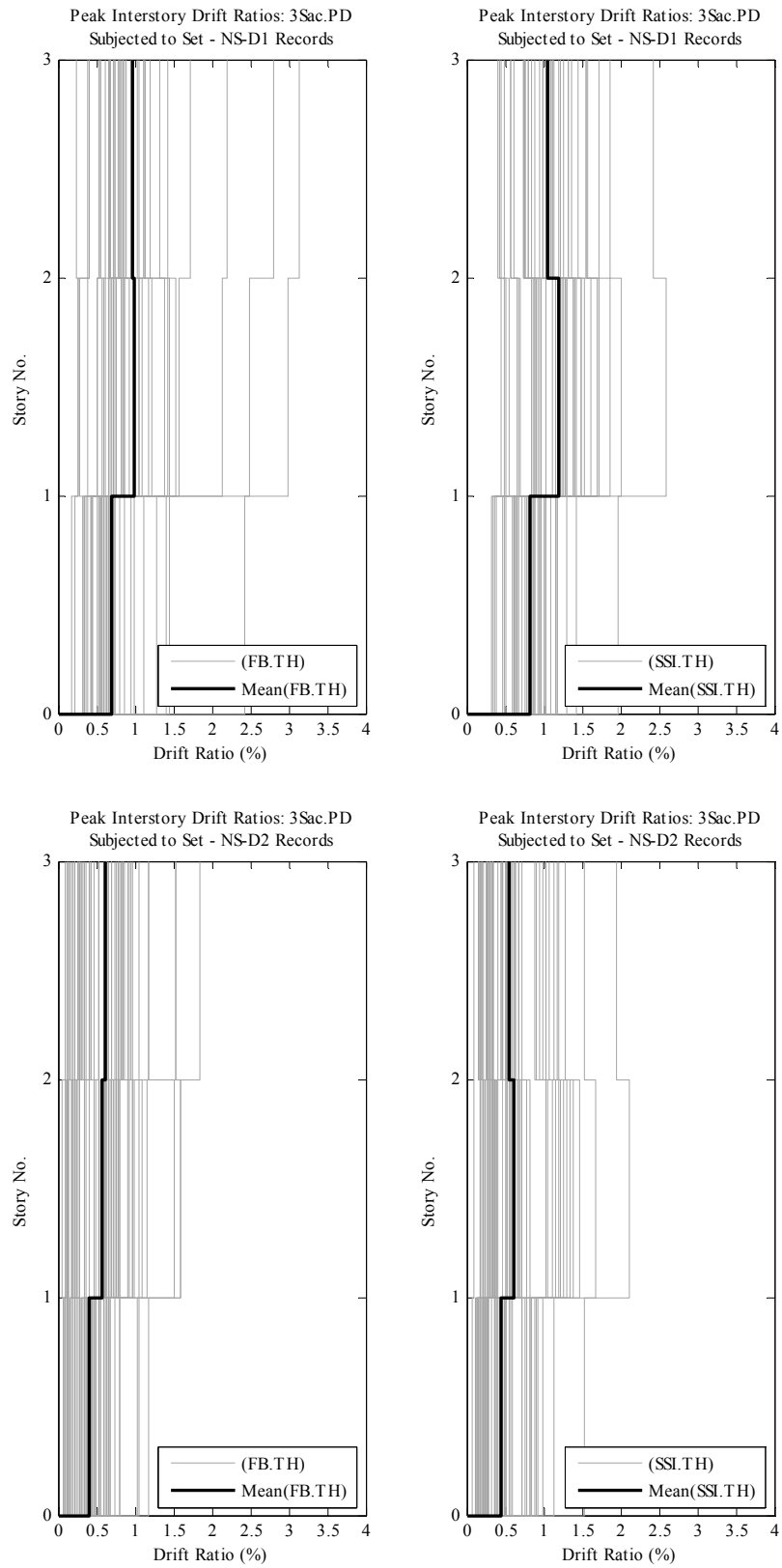


Figure F.1. (Cont'd)

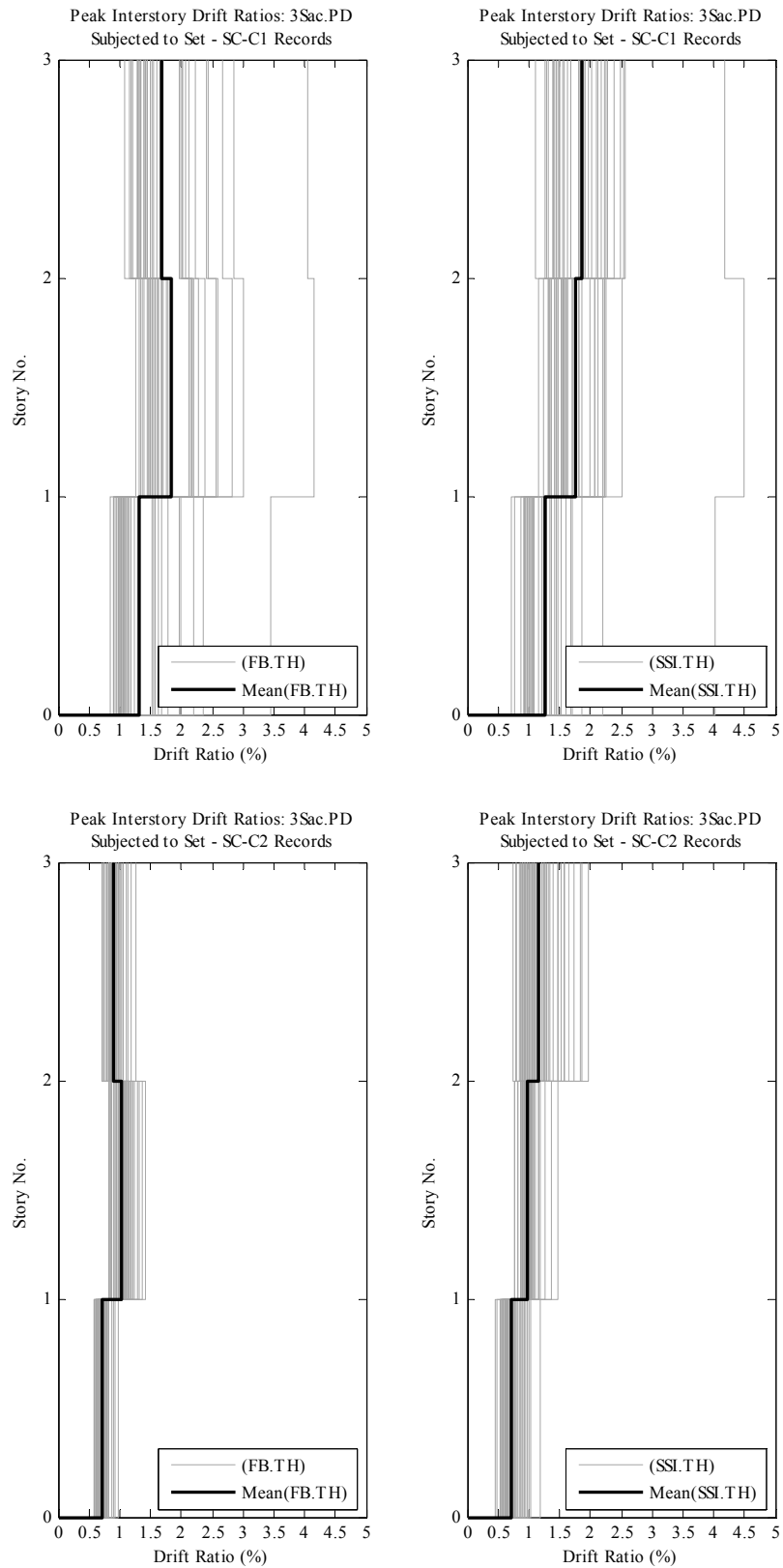


Figure F.2. Comparison of peak and mean interstory drift demands of Model 3SAC subjected to Set SC-C1, C2, D1, D2 earthquake records.

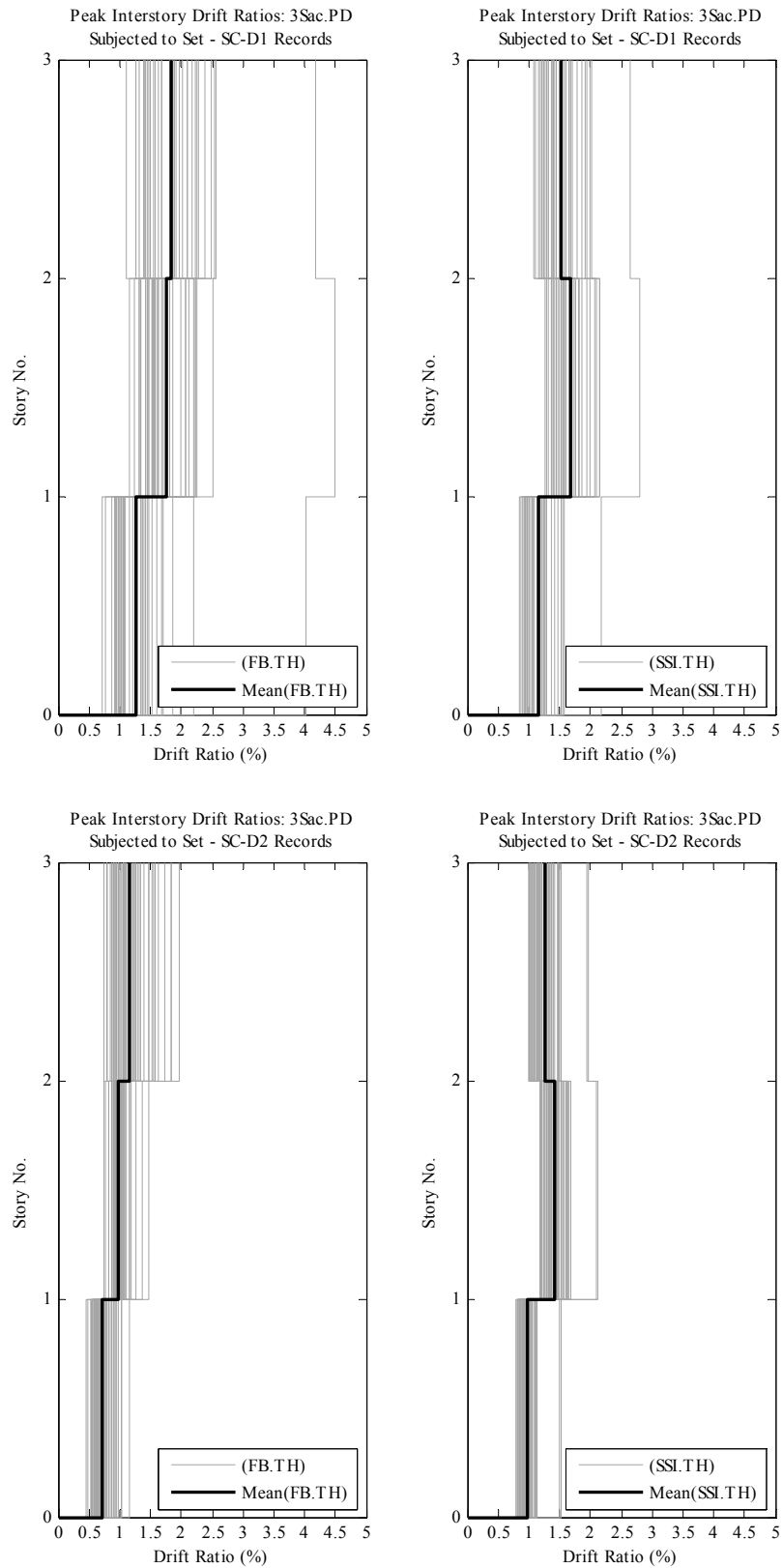


Figure F.2. (Cont'd)

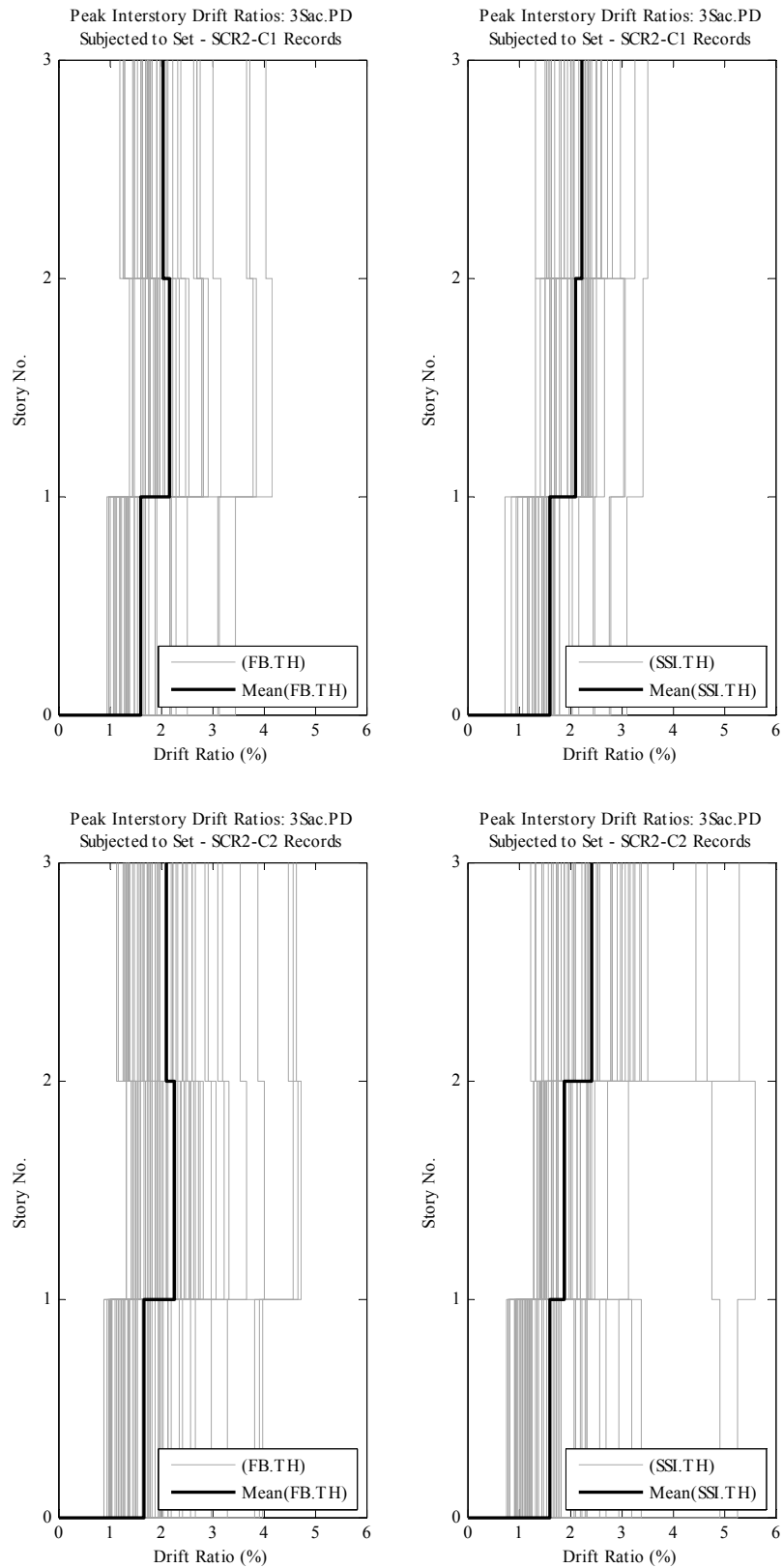


Figure F.3. Comparison of peak and mean interstory drift demands of Model 3SAC subjected to Set SCR2-C1, C2, D1, D2 earthquake records.

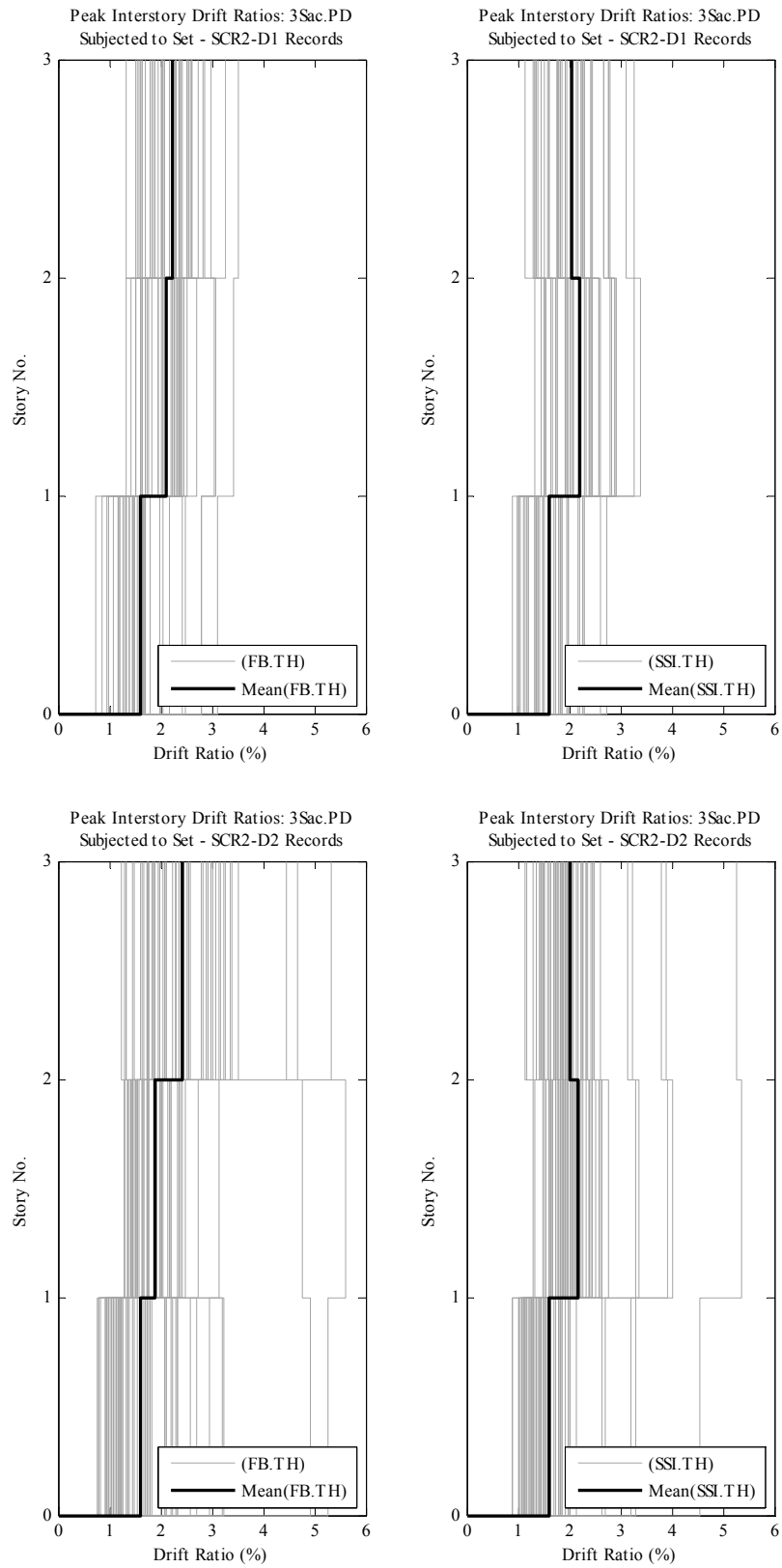


Figure F.3. (Cont'd)

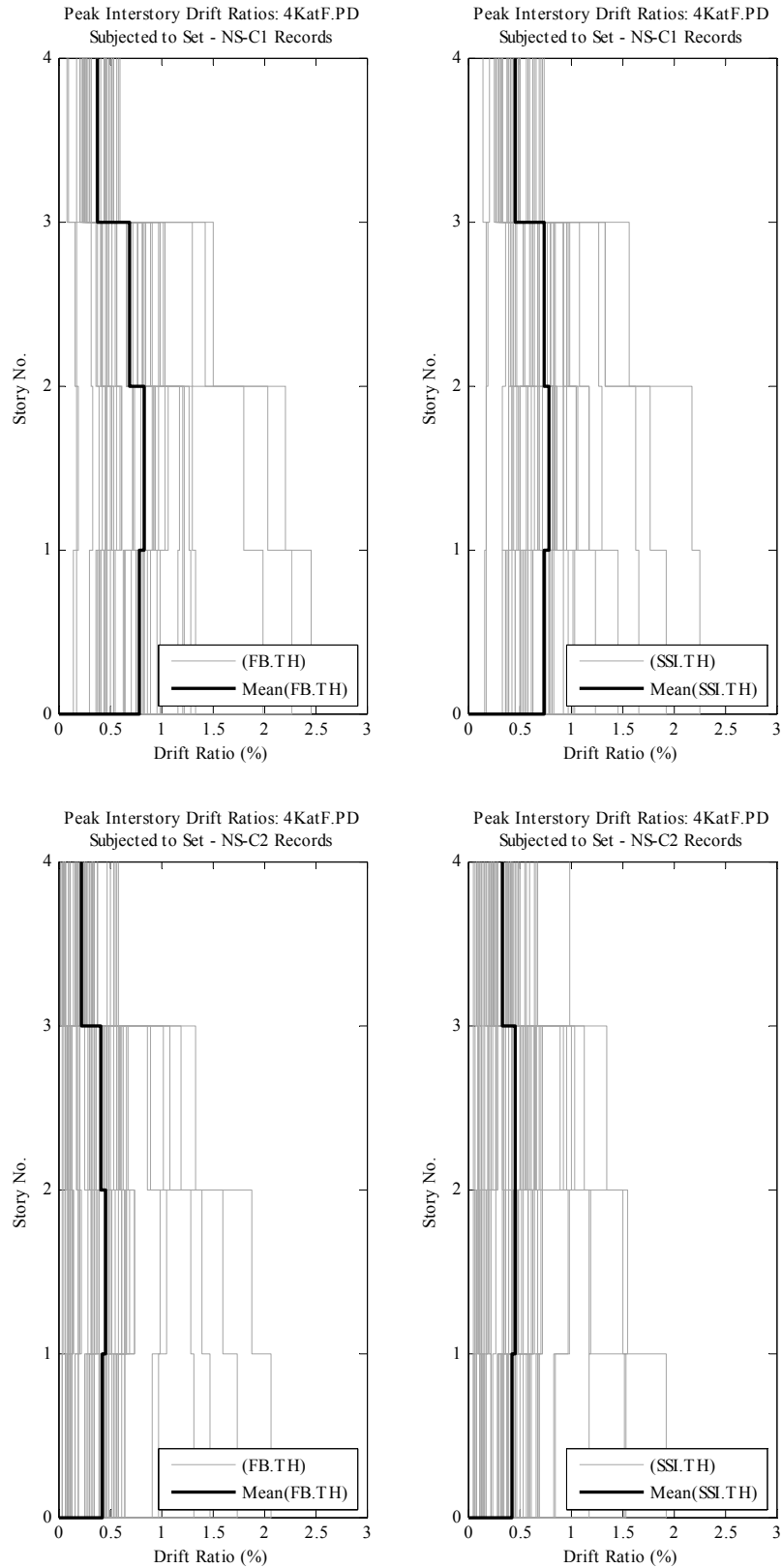


Figure F.4. Comparison of peak and mean interstory drift demands of Model 4KatF subjected to Set NS-C1, C2, D1, D2 earthquake records.

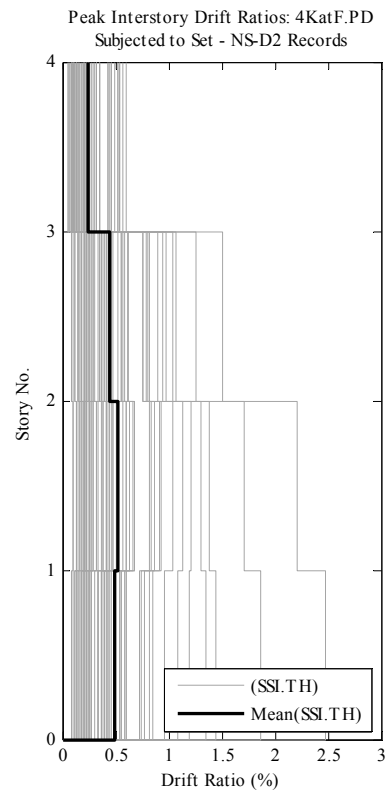
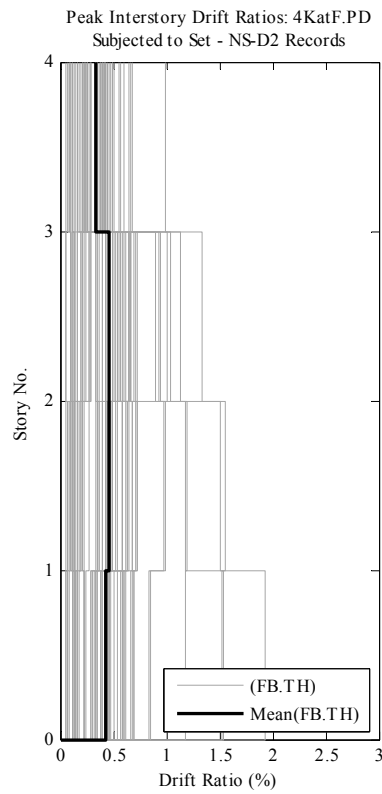
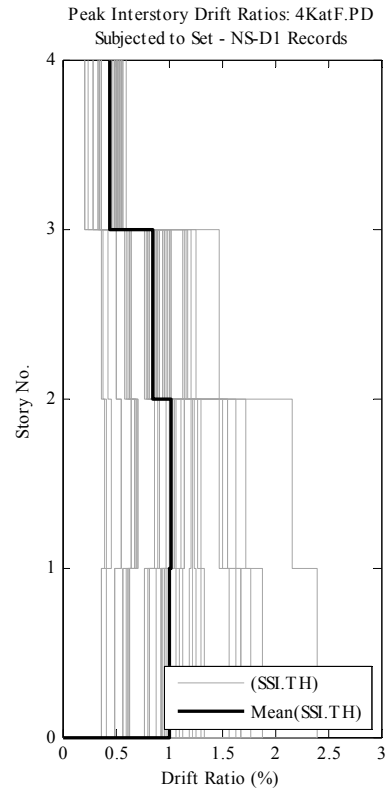
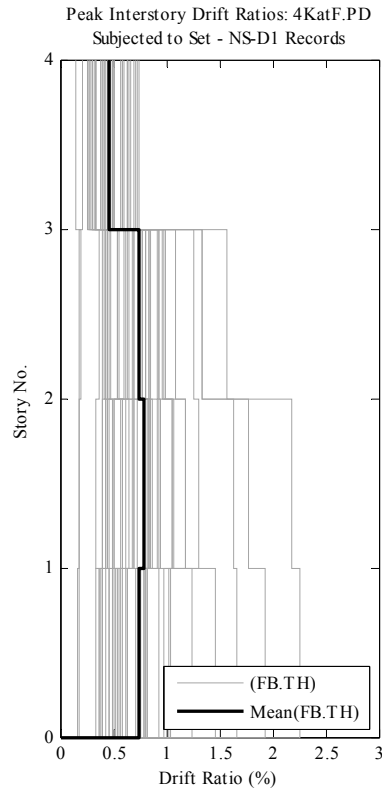


Figure F.4. (Cont'd)

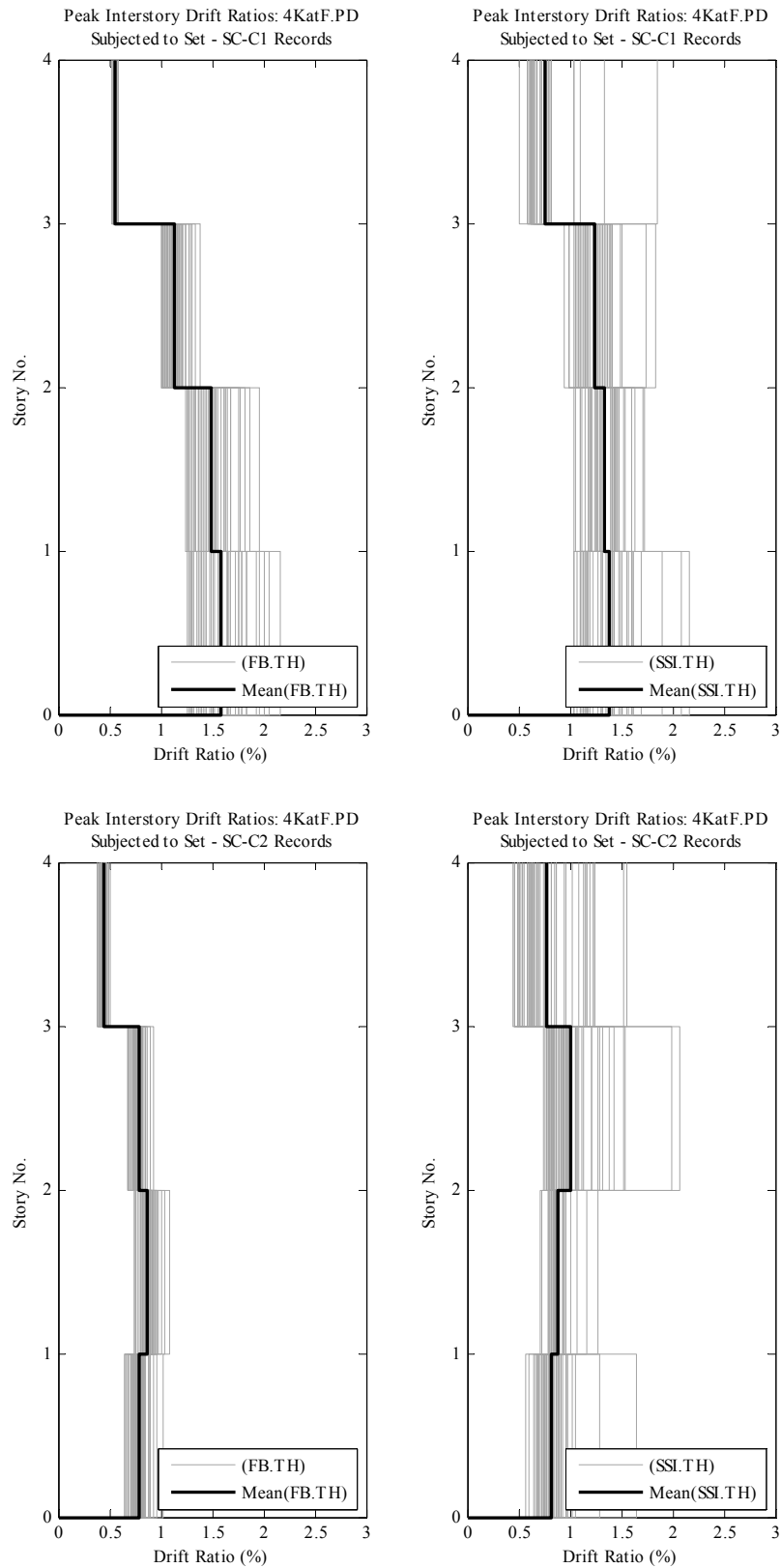


Figure F.5. Comparison of peak and mean interstory drift demands of Model 4KatF subjected to Set SC-C1, C2, D1, D2 earthquake records.

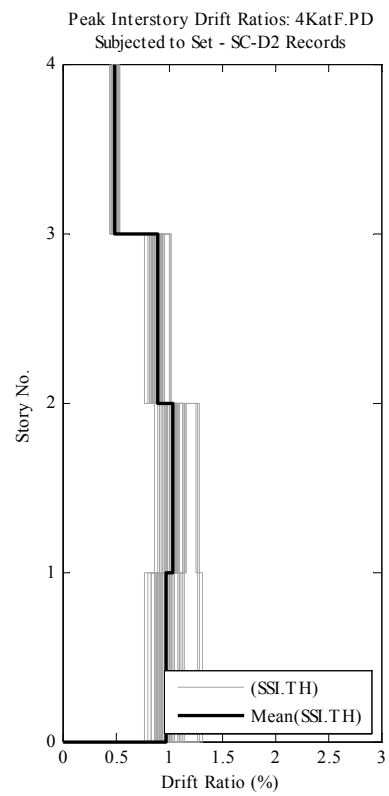
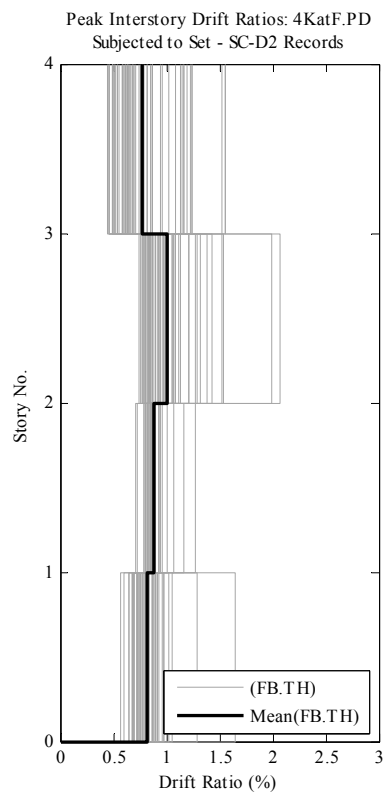
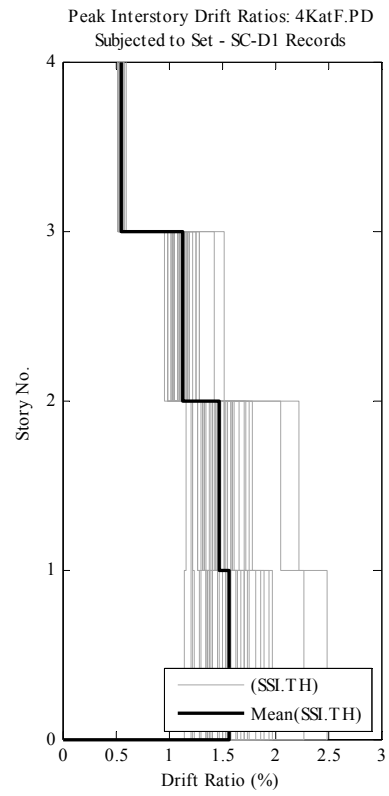
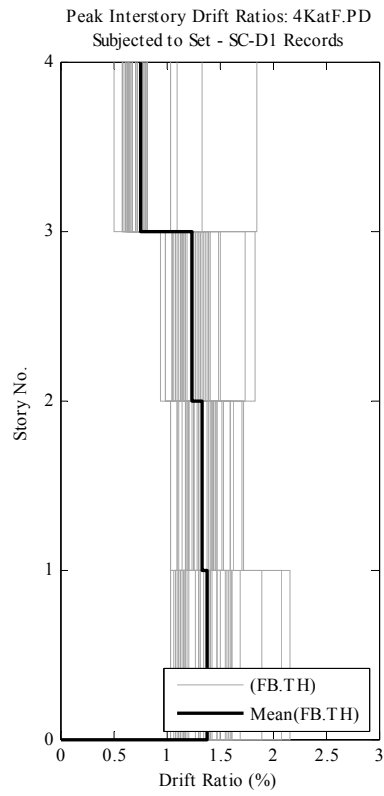


Figure F.5. (Cont'd)

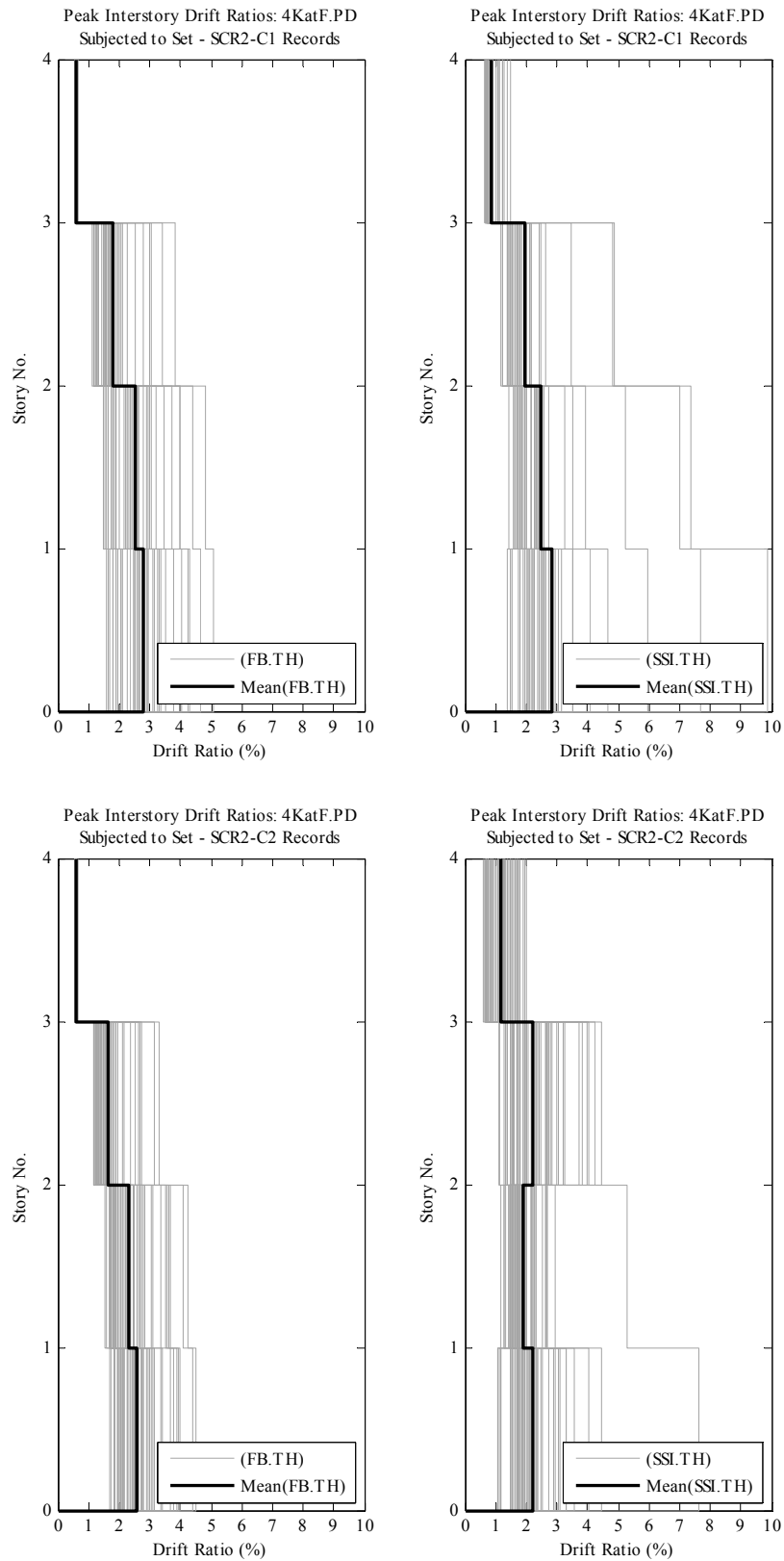


Figure F.6. Comparison of peak and mean interstory drift demands of Model 4KatF subjected to Set SCR2-C1, C2, D1, D2 earthquake records.

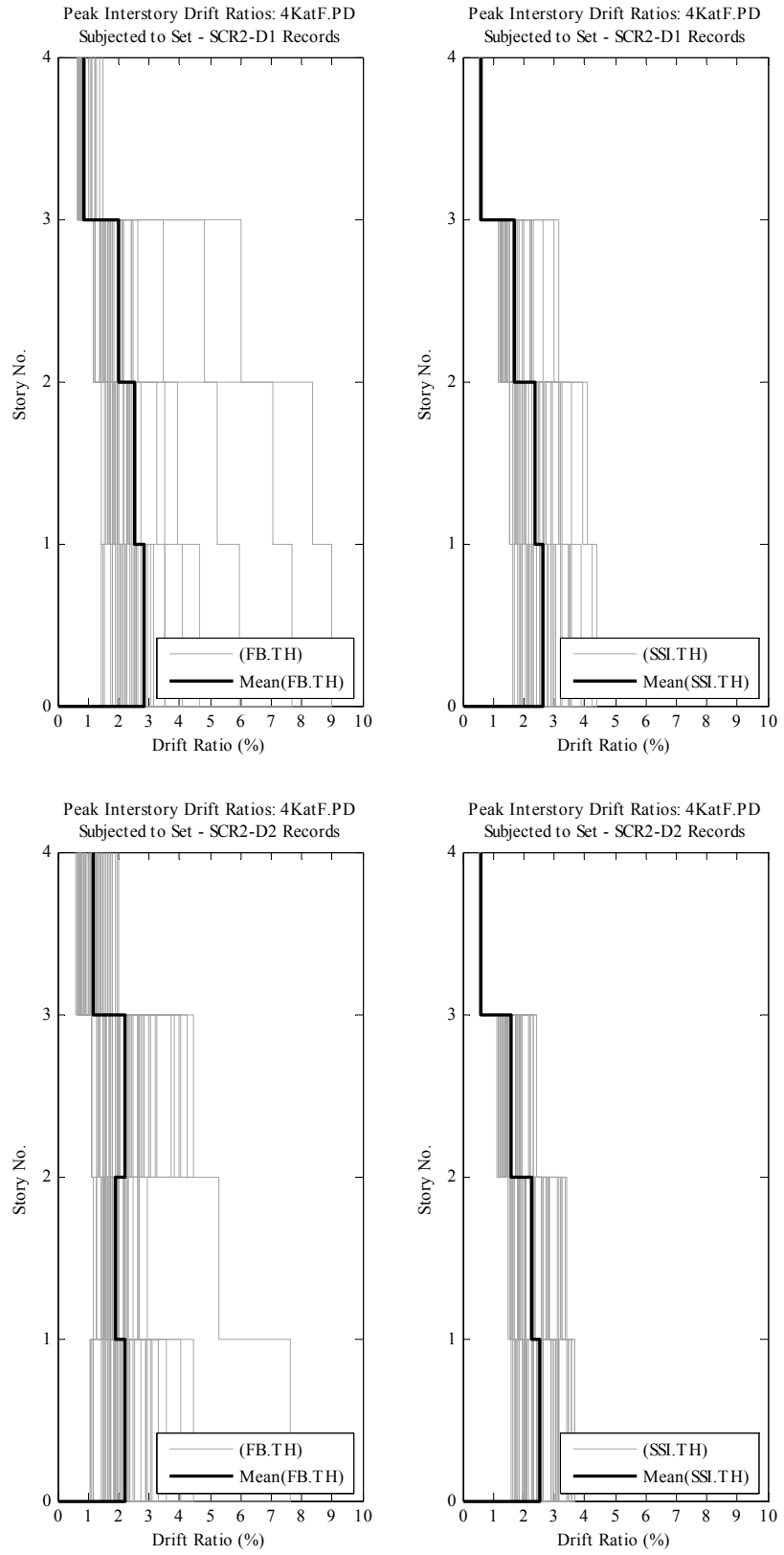


Figure F.6. (Cont'd)

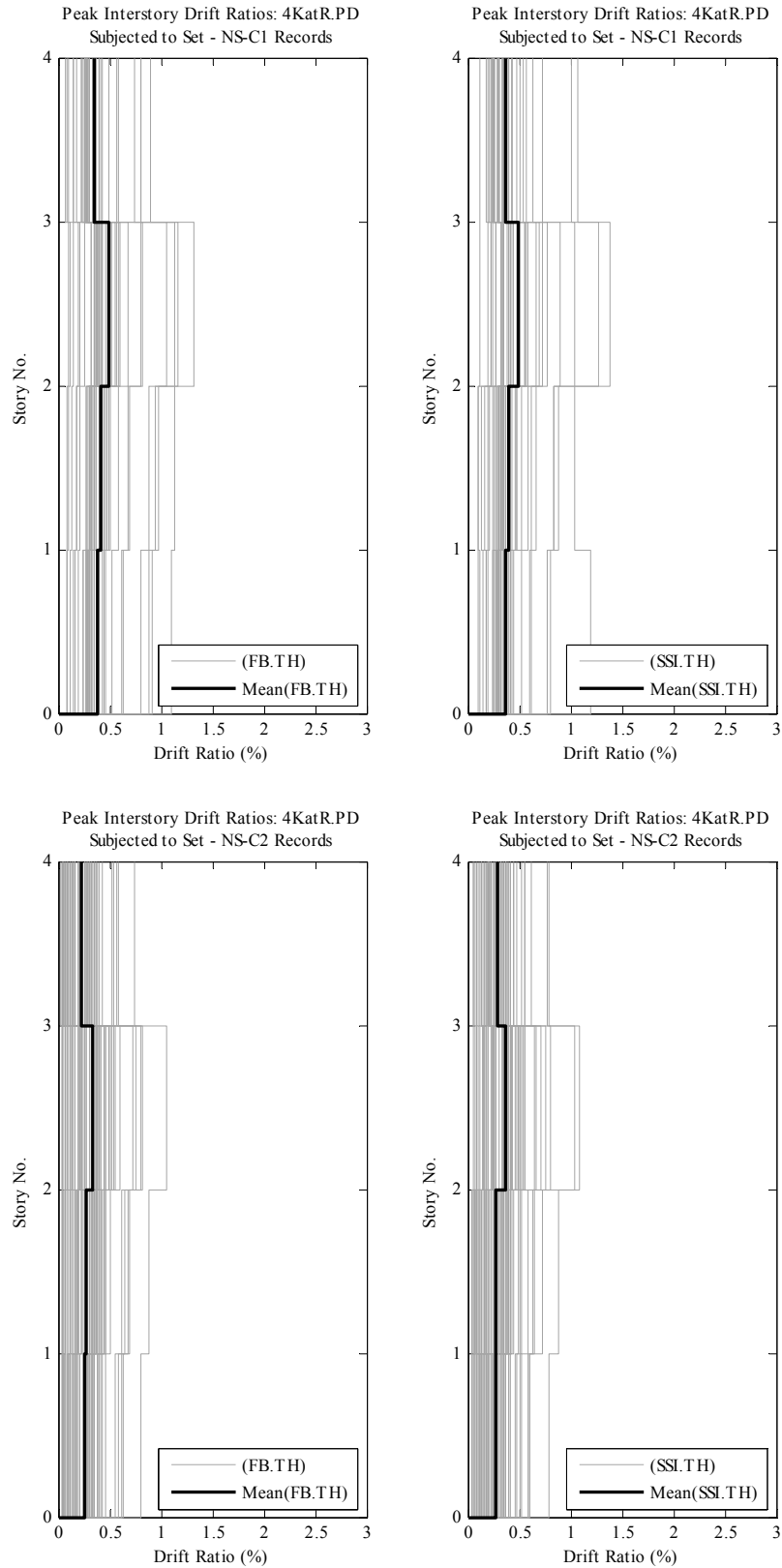


Figure F.7. Comparison of peak and mean interstory drift demands of Model 4KatR subjected to Set NS-C1, C2, D1, D2 earthquake records.

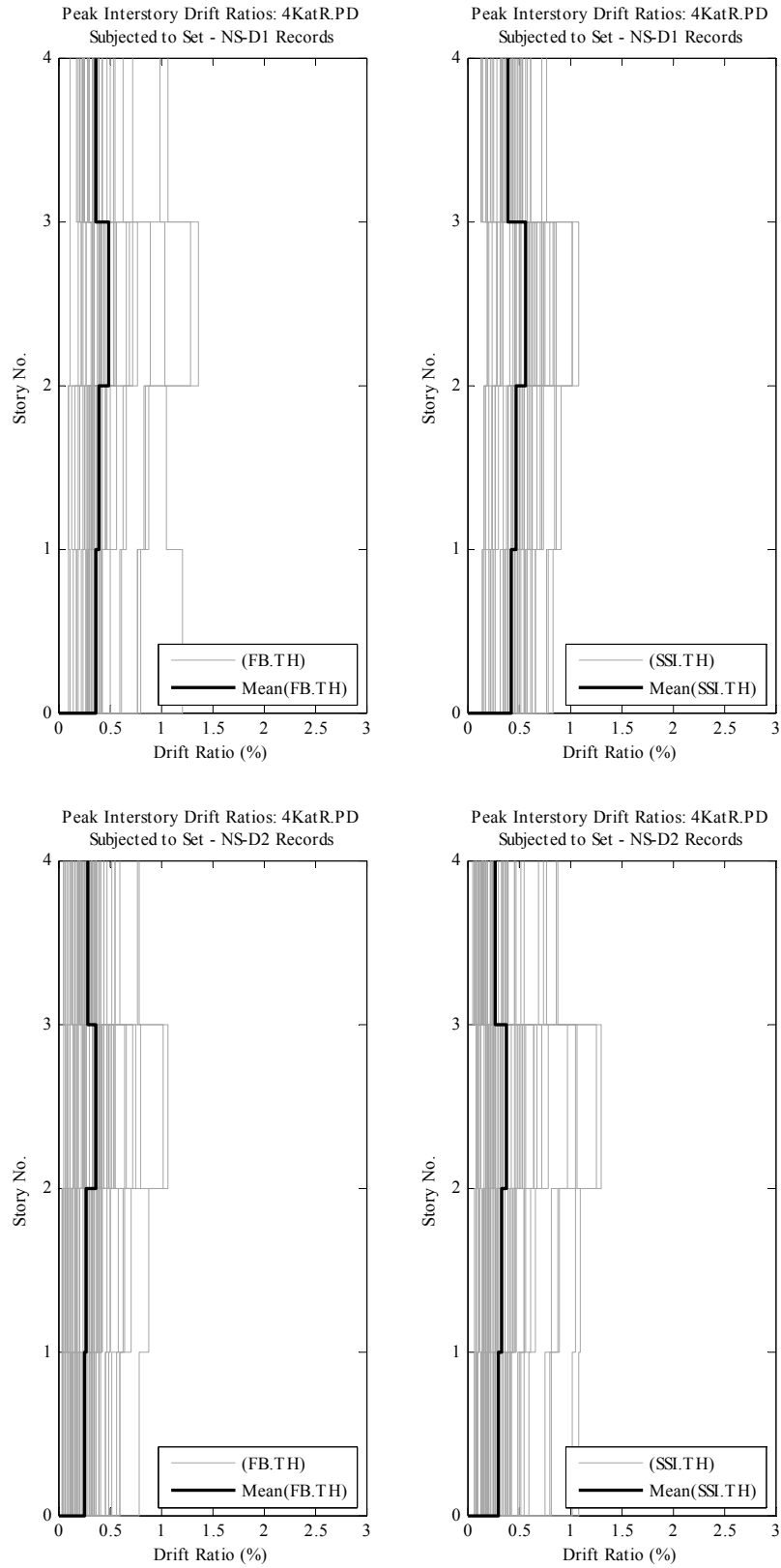


Figure F.7. (Cont'd)

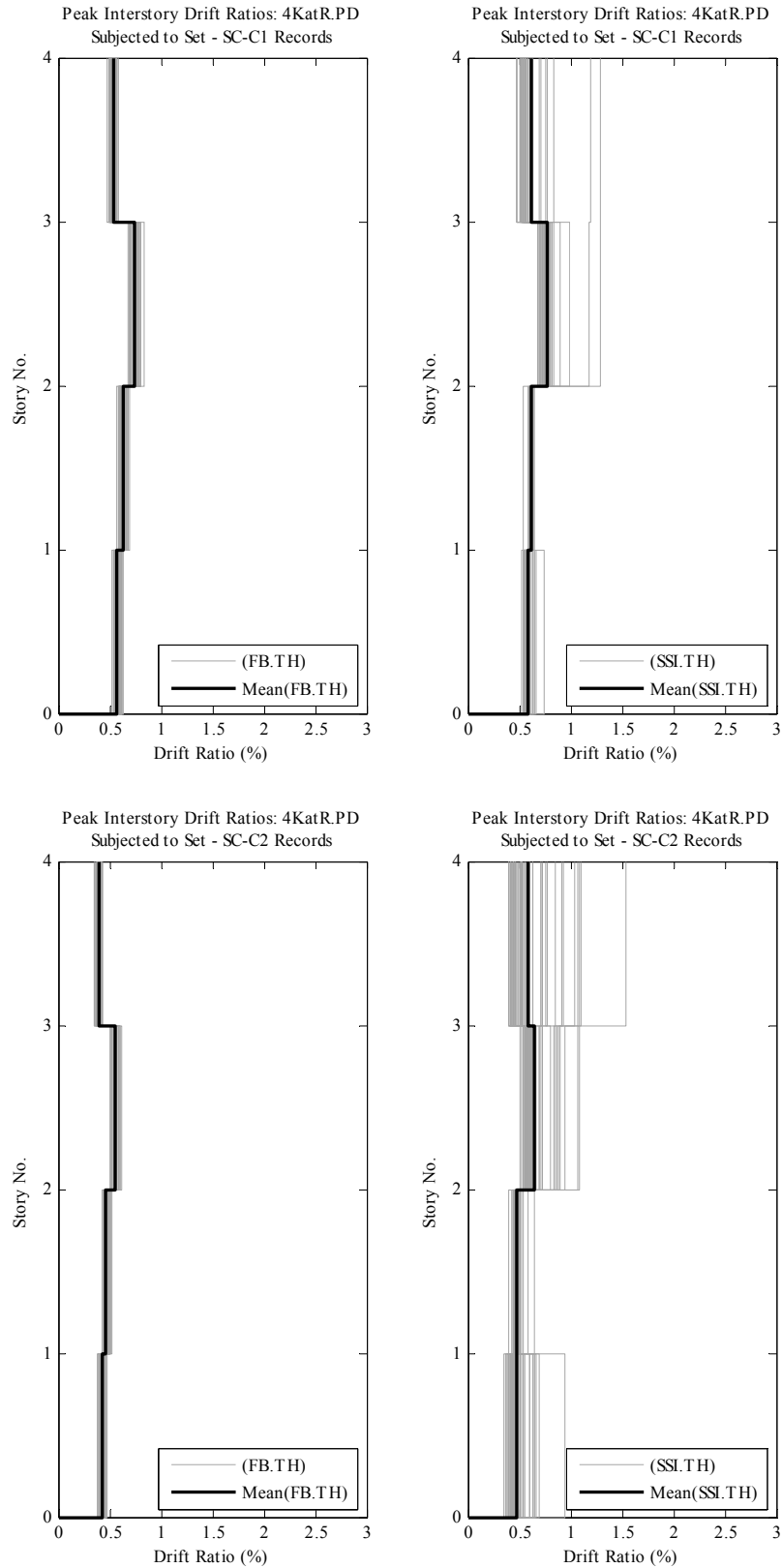


Figure F.8. Comparison of peak and mean interstory drift demands of Model 4KatR subjected to Set SC-C1, C2, D1, D2 earthquake records.

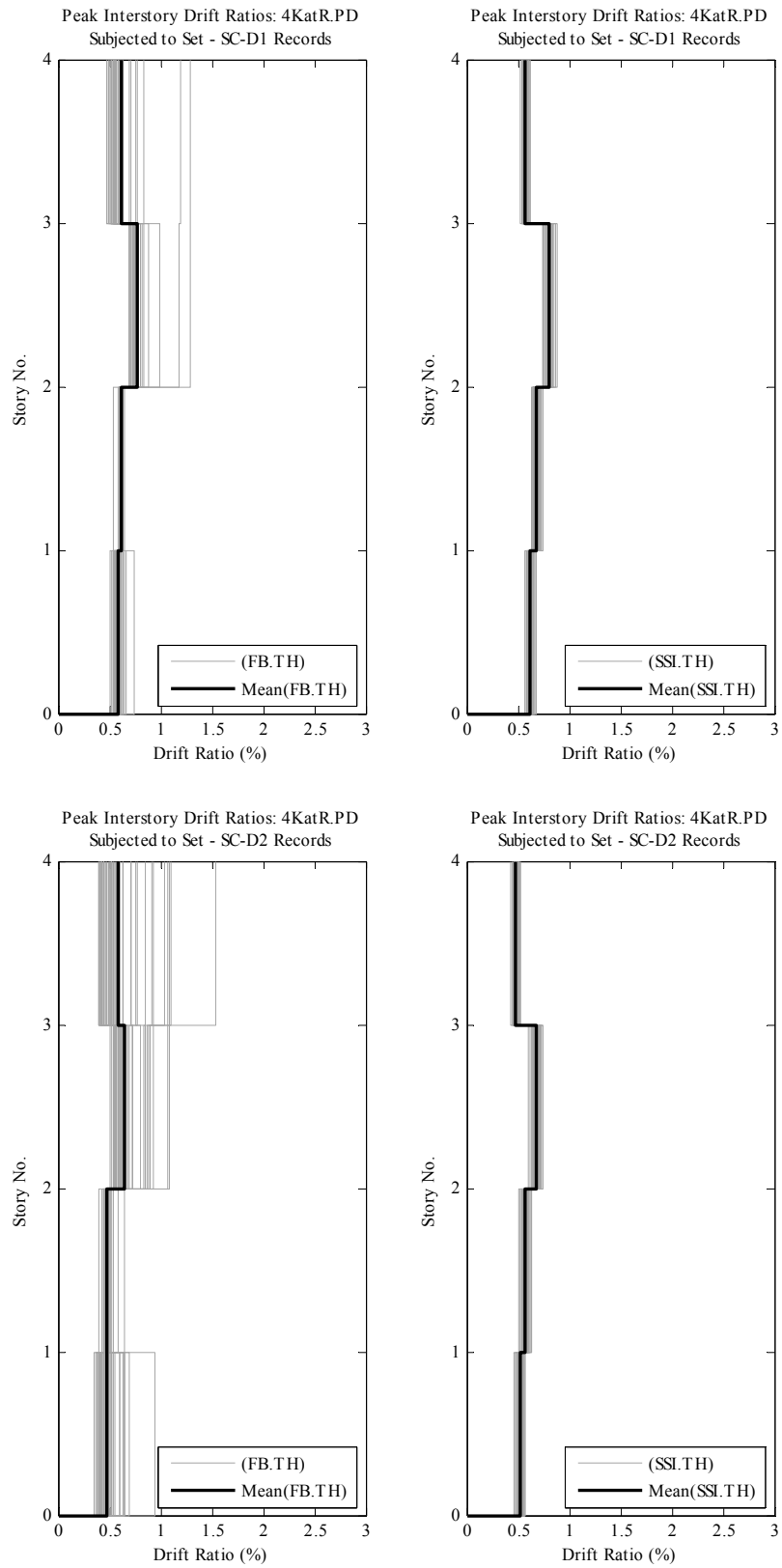


Figure F.8. (Cont'd)

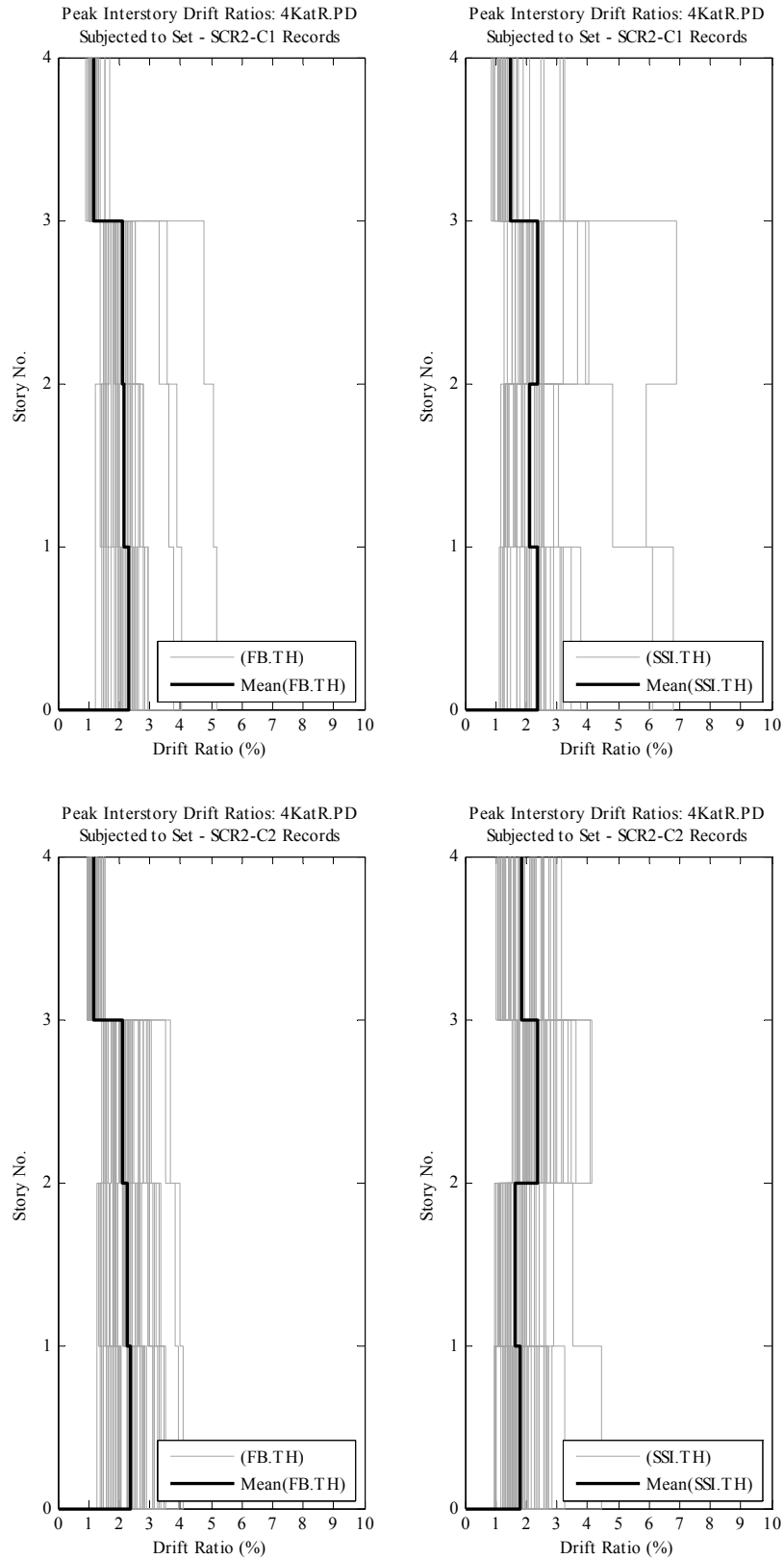


Figure F.9. Comparison of peak and mean interstory drift demands of Model 4KatR subjected to Set SCR2-C1, C2, D1, D2 earthquake records.

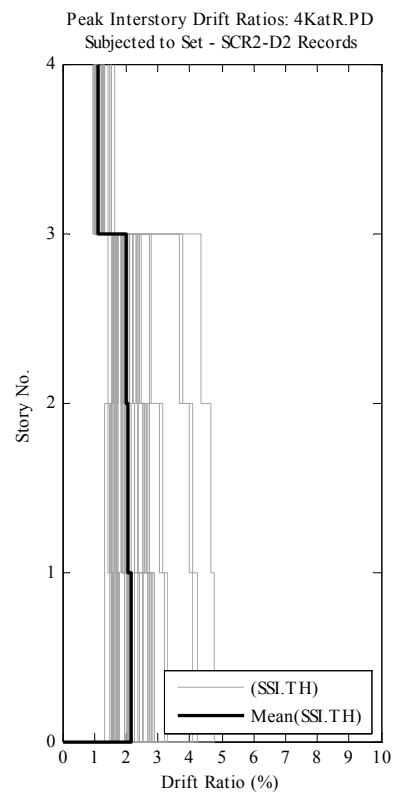
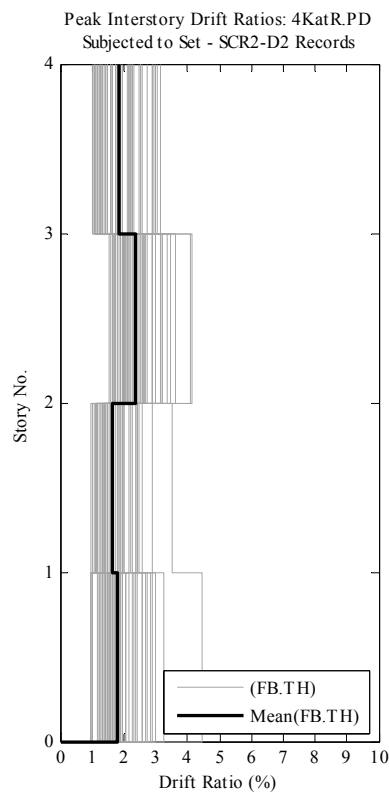
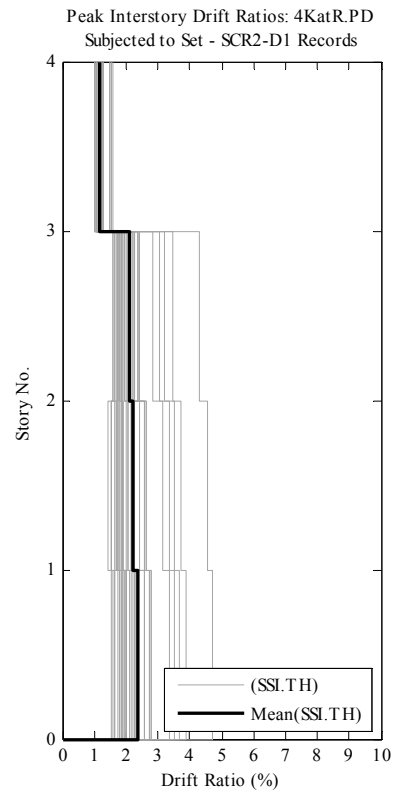
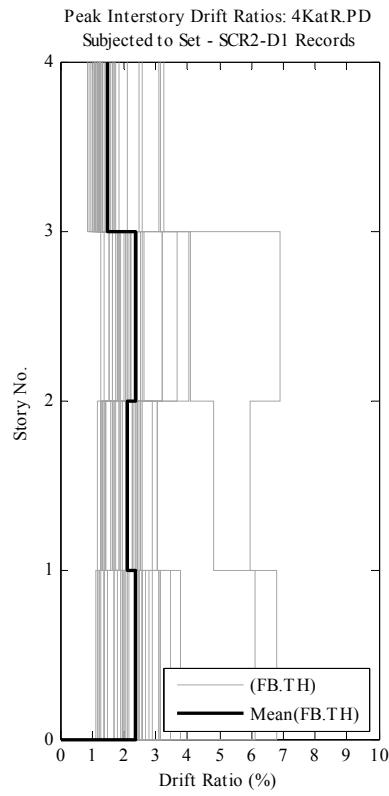


Figure F.9. (Cont'd)

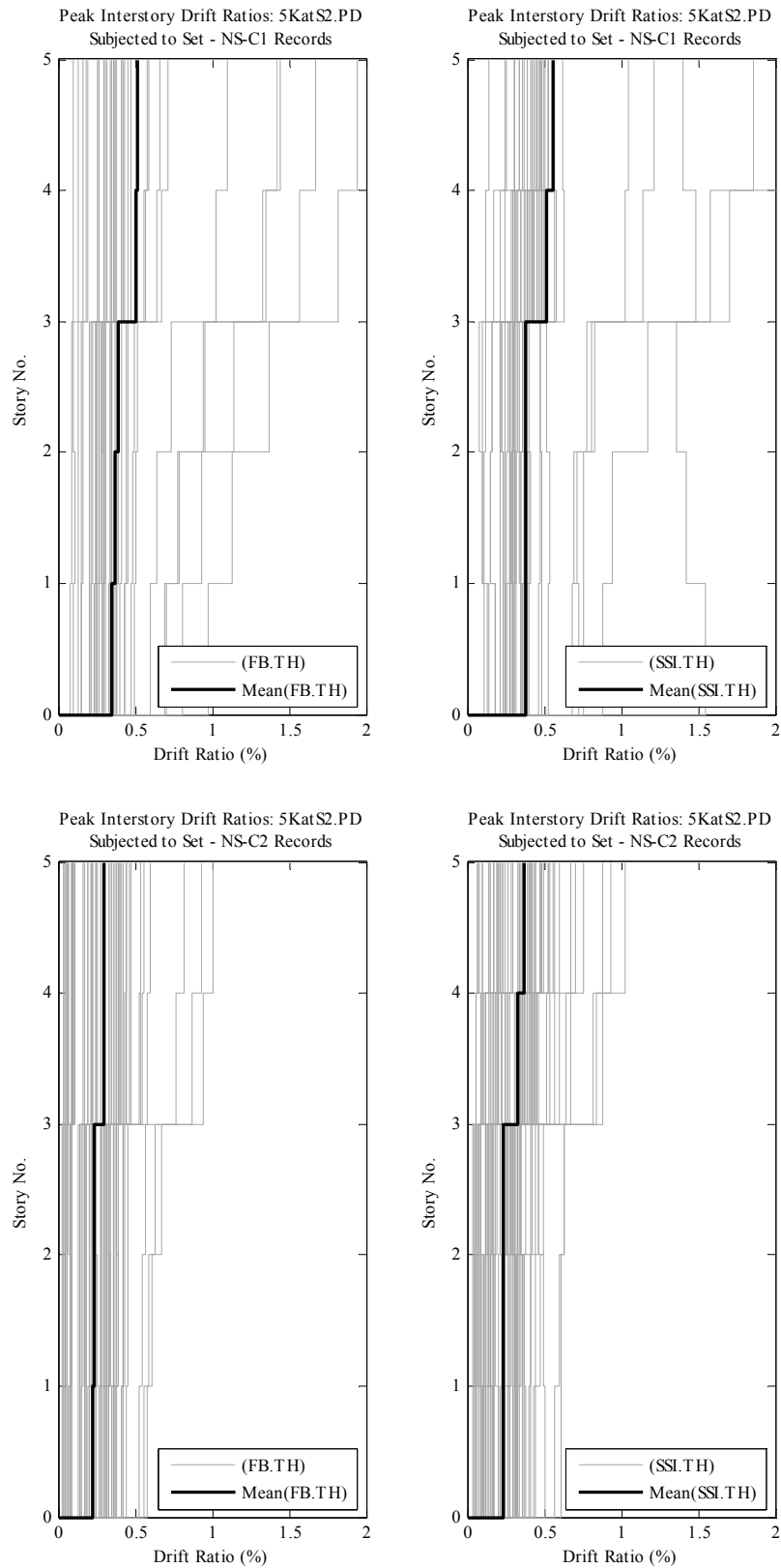


Figure F.10. Comparison of peak and mean interstory drift demands of Model 5KatS2 subjected to Set NS-C1, C2, D1, D2 earthquake records.

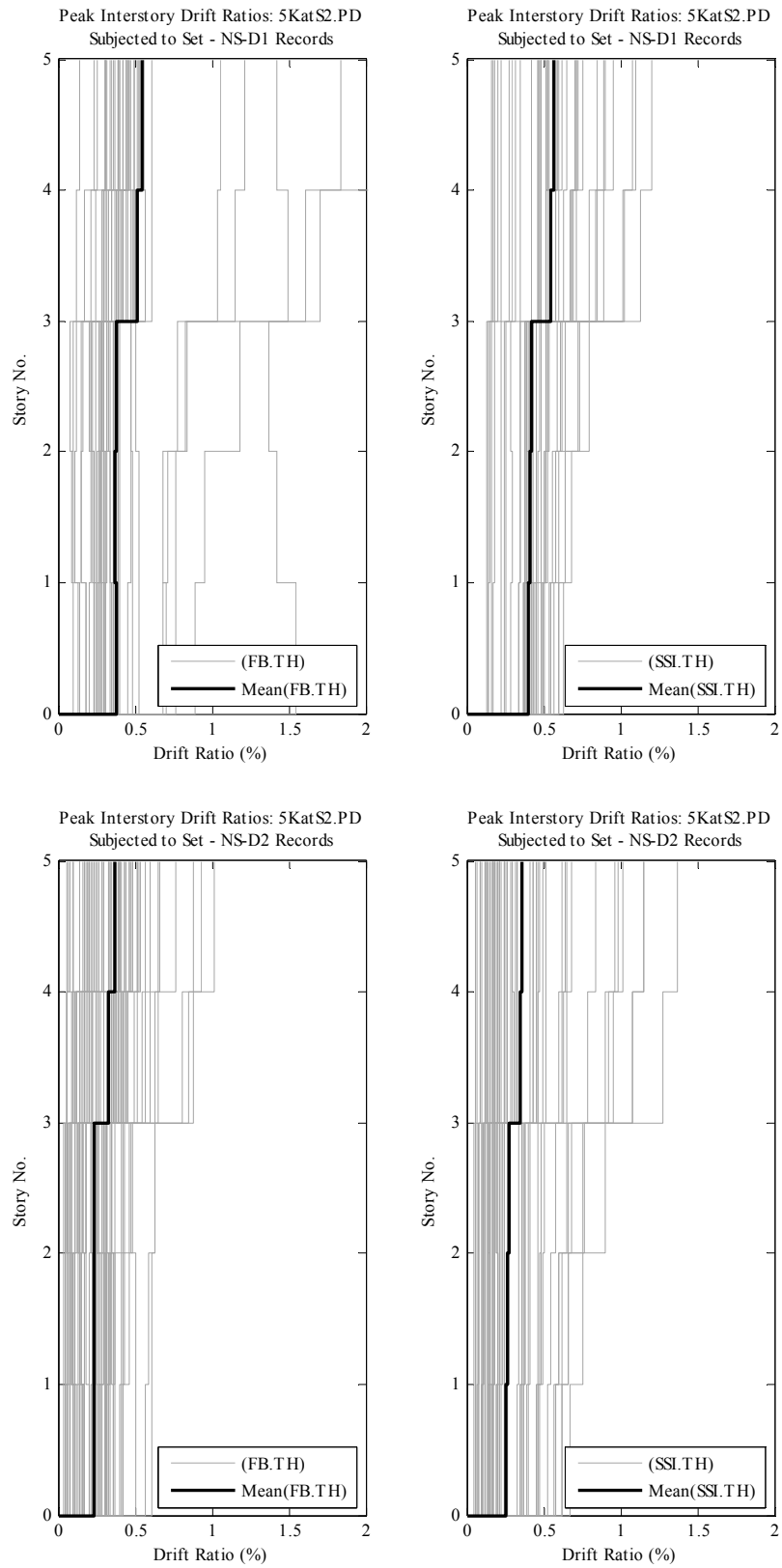


Figure F.10. (Cont'd)

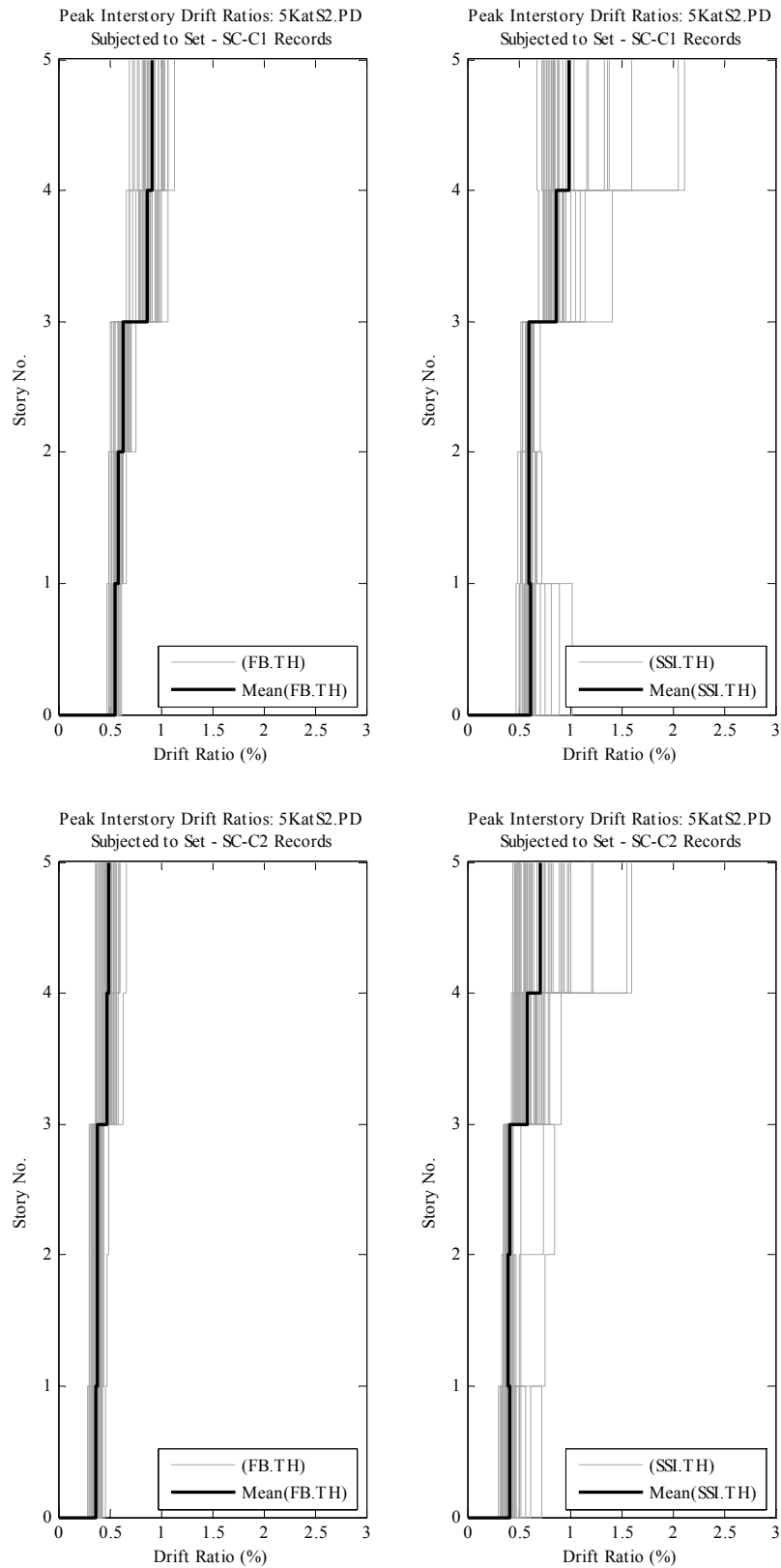


Figure F.11. Comparison of peak and mean interstory drift demands of Model 5KatS2 subjected to Set SC-C1, C2, D1, D2 earthquake records.

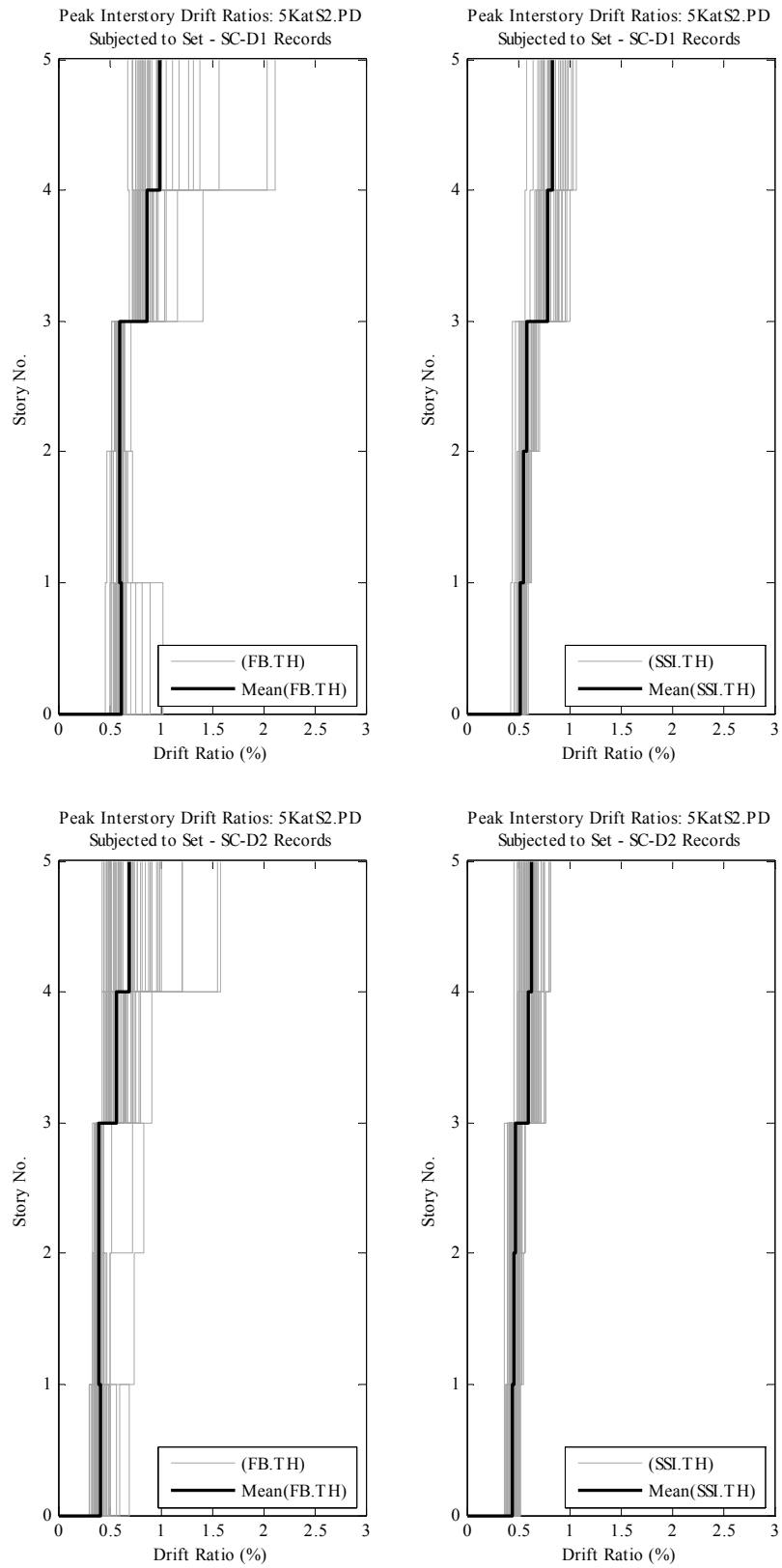


Figure F.11. (Cont'd)

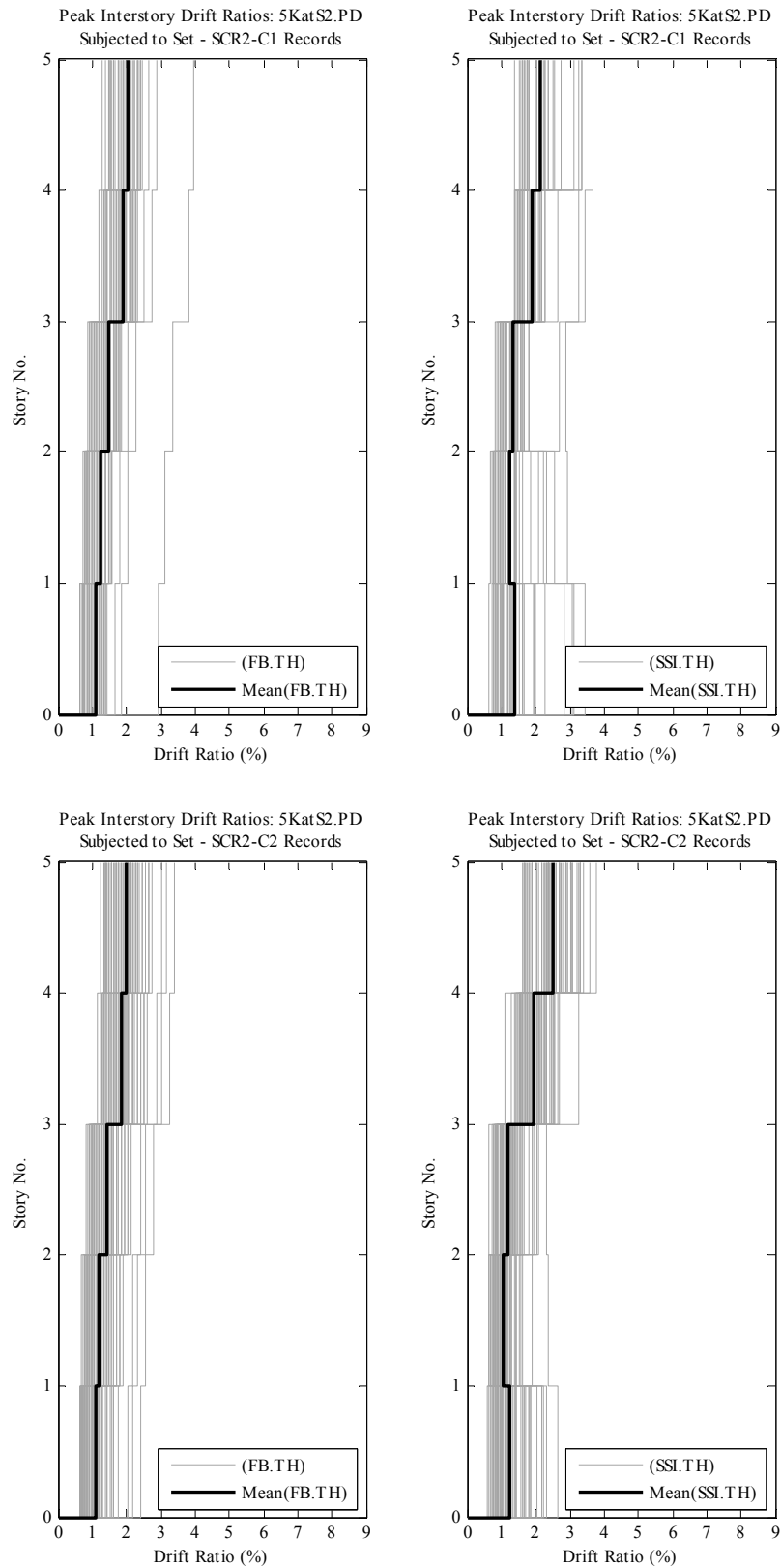


Figure F.12. Comparison of peak and mean interstory drift demands of Model 5KatS2 subjected to Set SCR2-C1, C2, D1, D2 earthquake records.

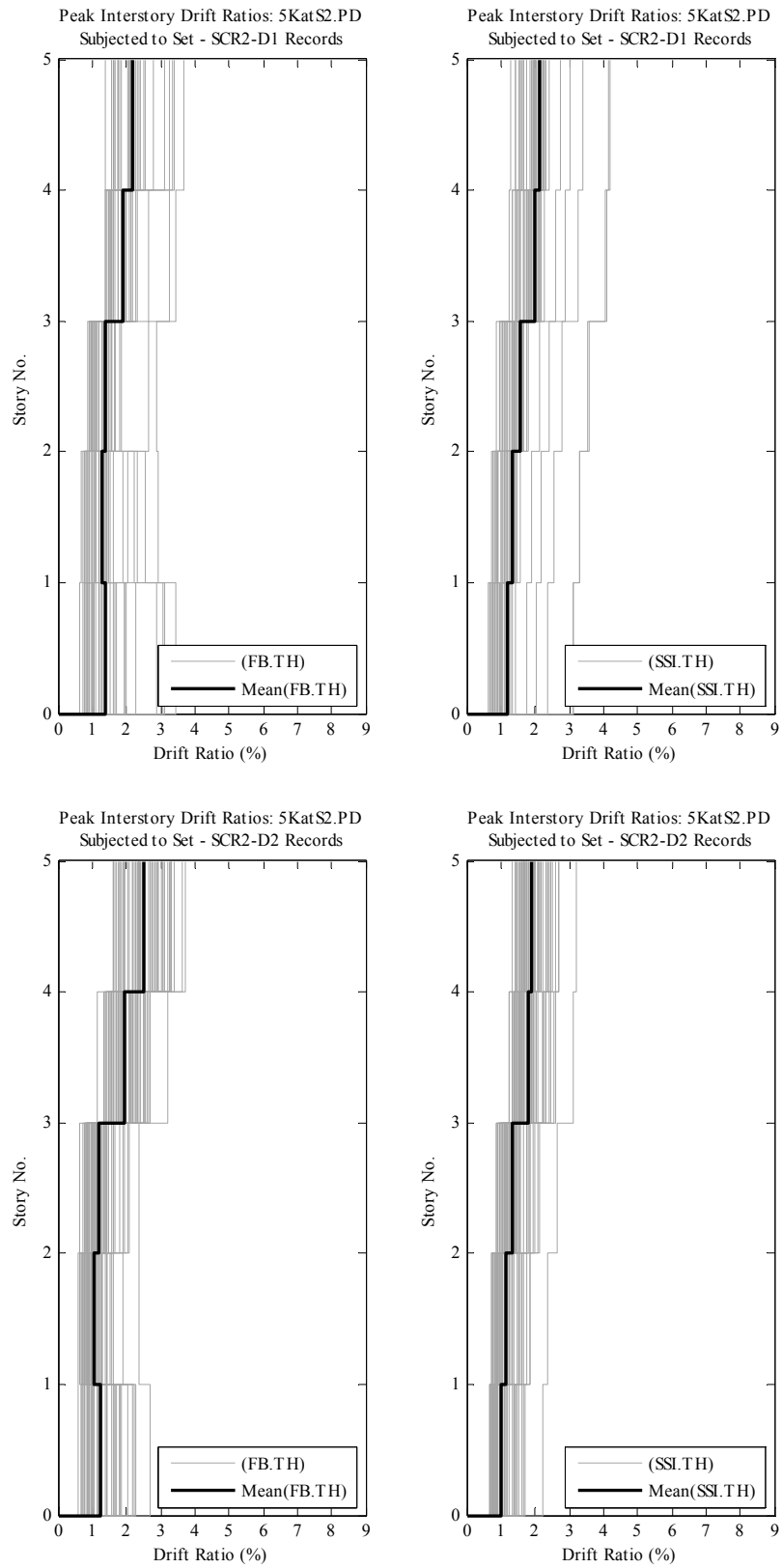


Figure F.12. (Cont'd)

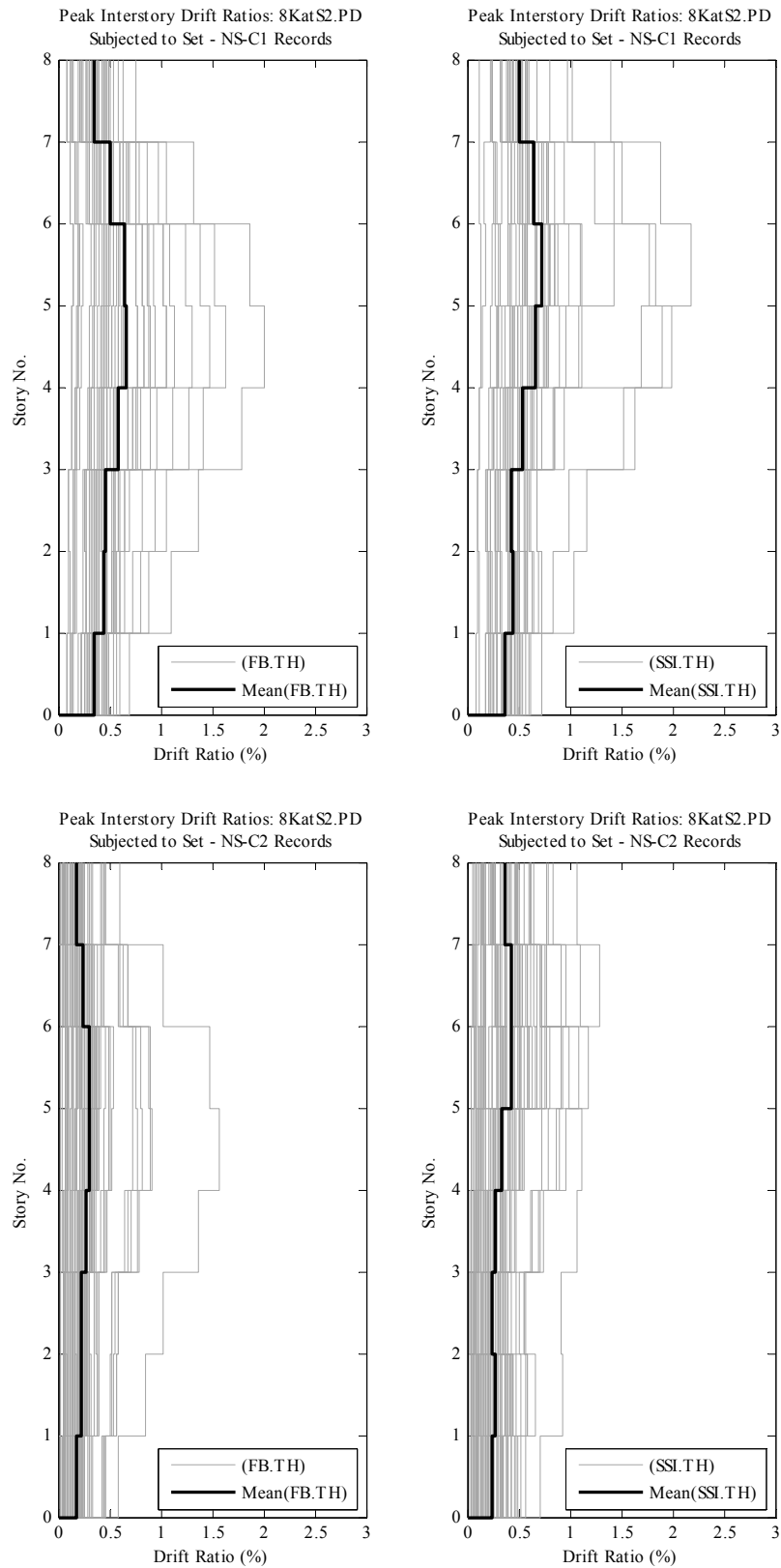


Figure F.13. Comparison of peak and mean interstory drift demands of Model 8KatS2 subjected to Set NS-C1, C2, D1, D2 earthquake records.

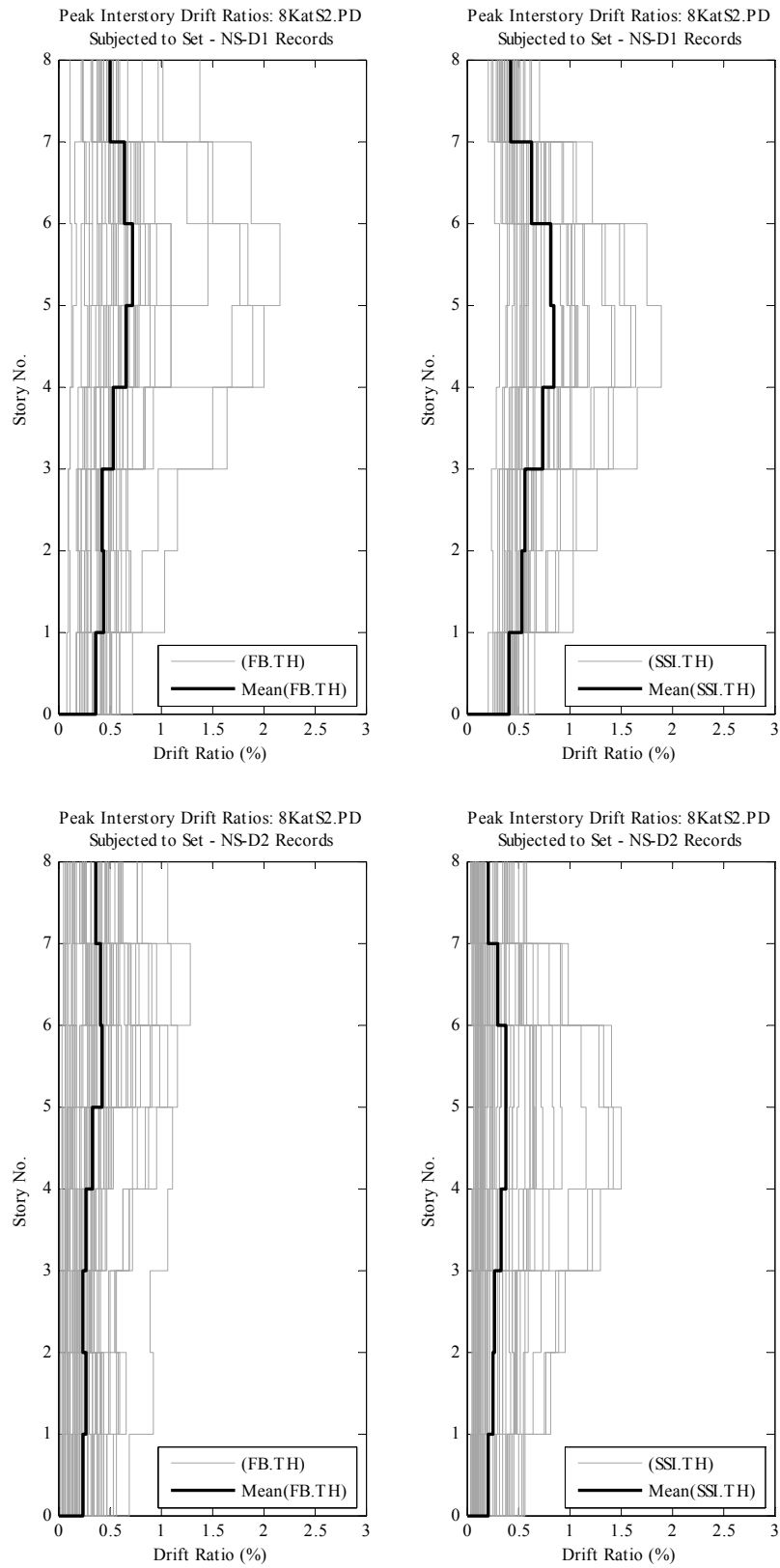


Figure F.13. (Cont'd)

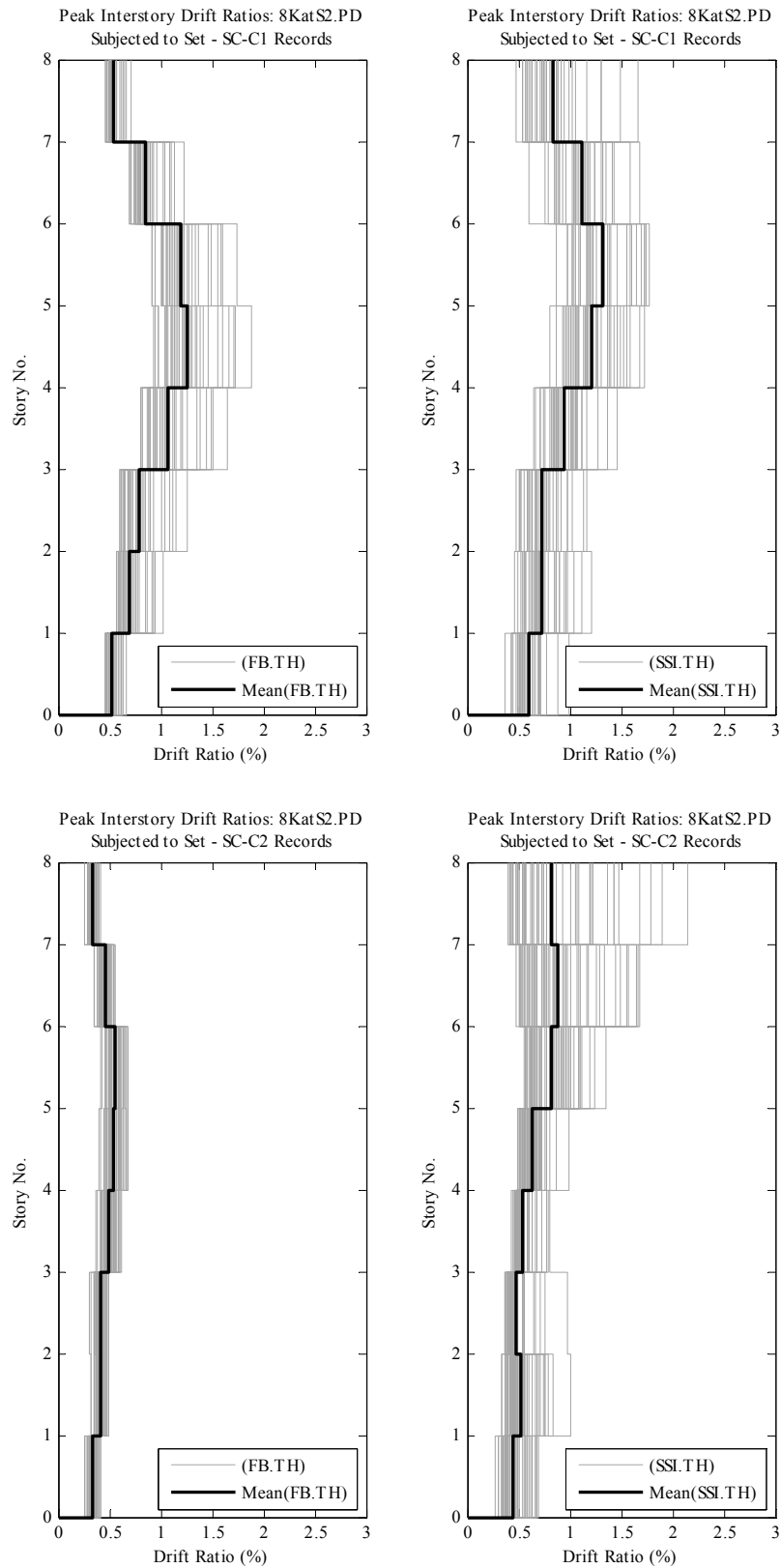


Figure F.14. Comparison of peak and mean interstory drift demands of Model 8KatS2 subjected to Set SC-C1, C2, D1, D2 earthquake records.

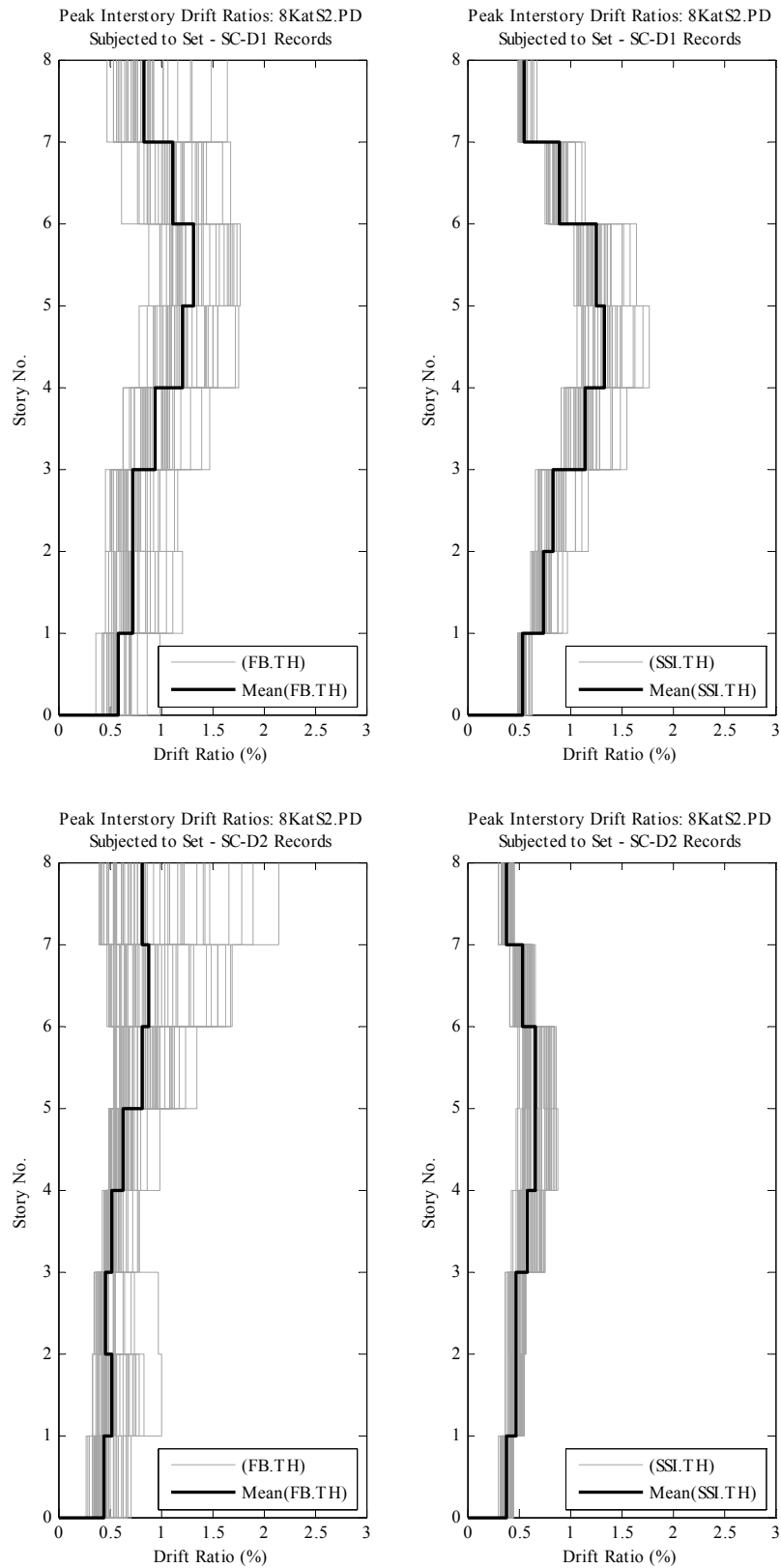


Figure F.14. (Cont'd)

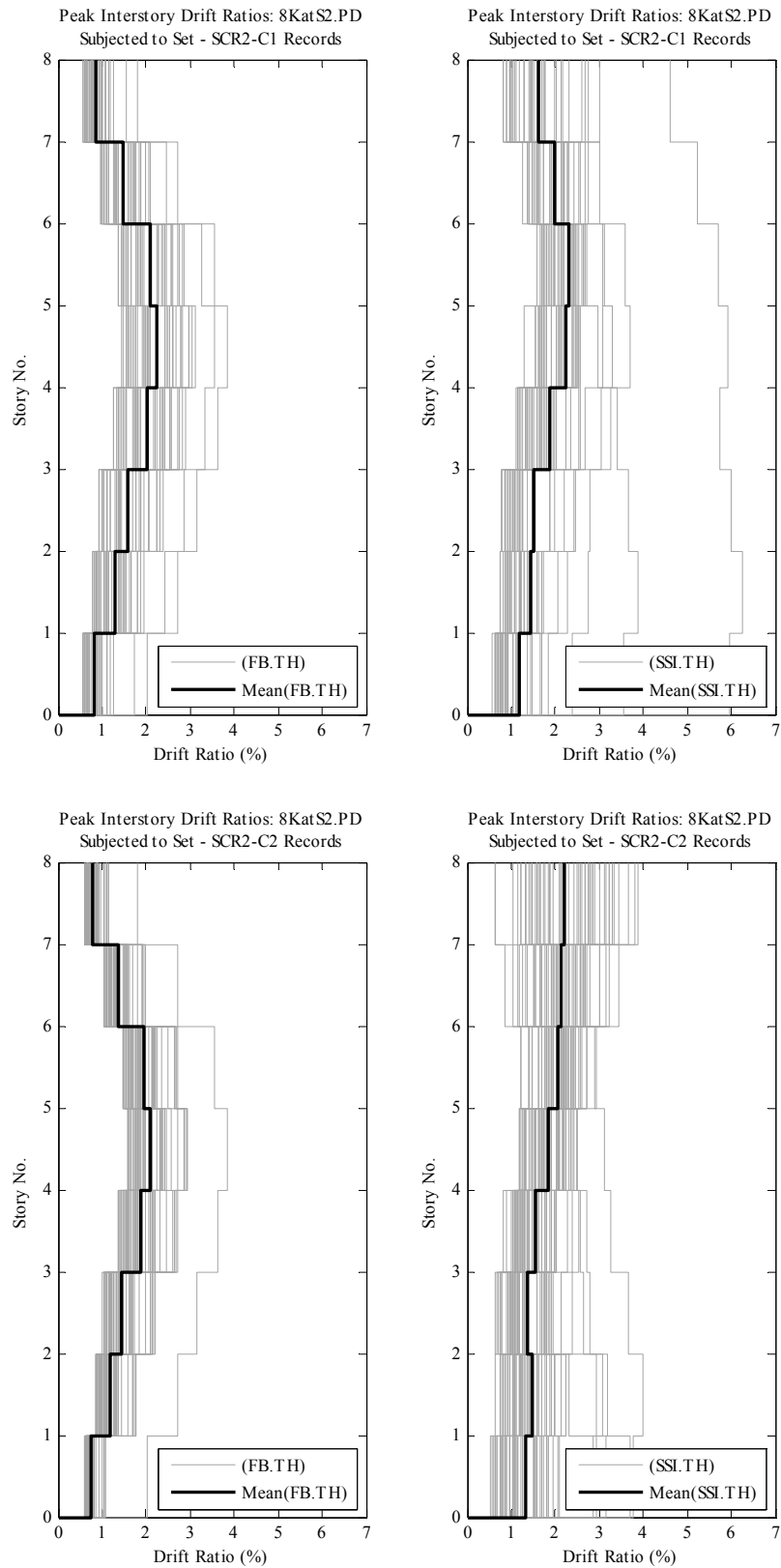


Figure F.15. Comparison of peak and mean interstory drift demands of Model 8KatS2 subjected to Set SCR2-C1, C2, D1, D2 earthquake records.

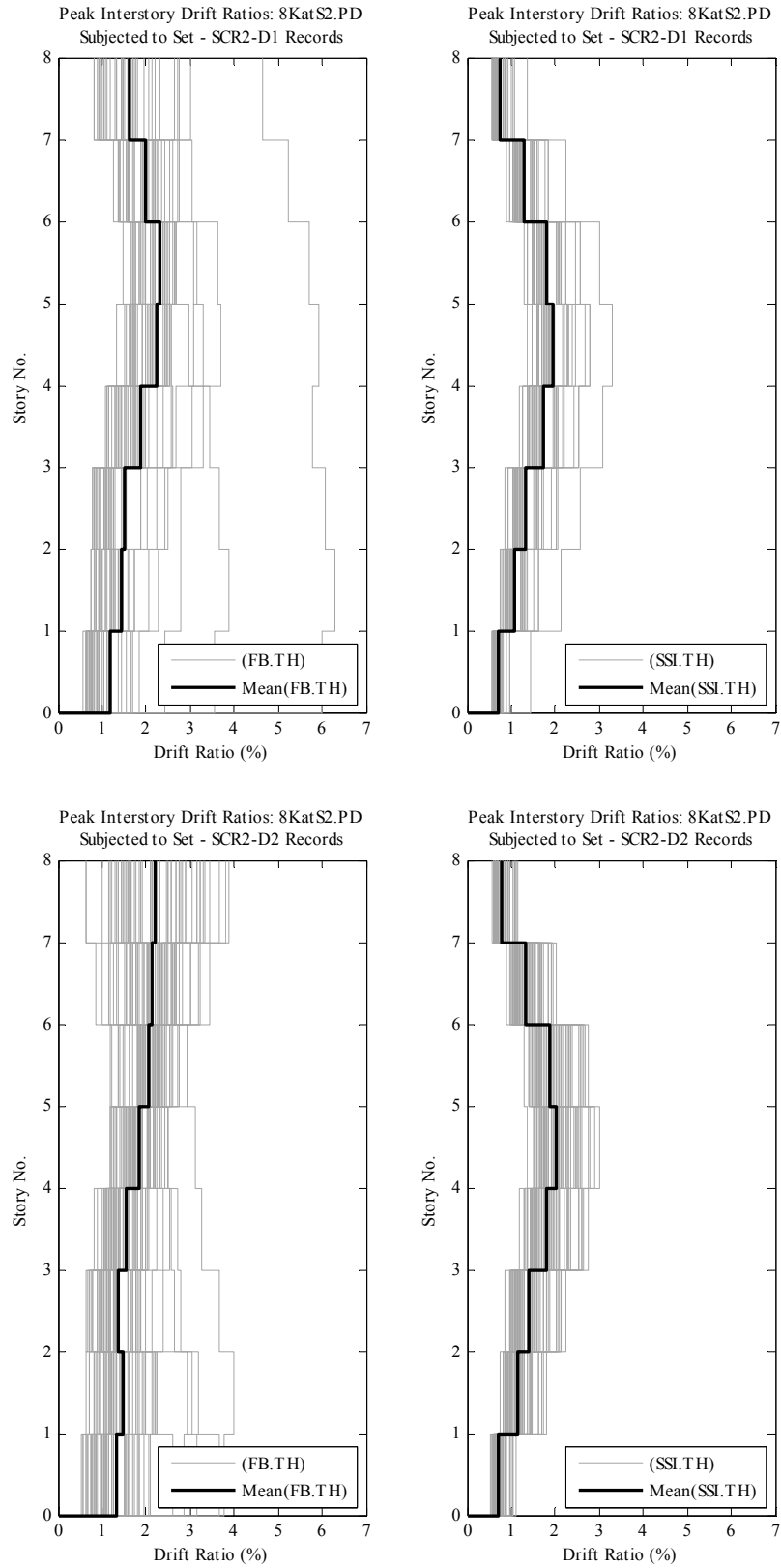


Figure F.15. (Cont'd)

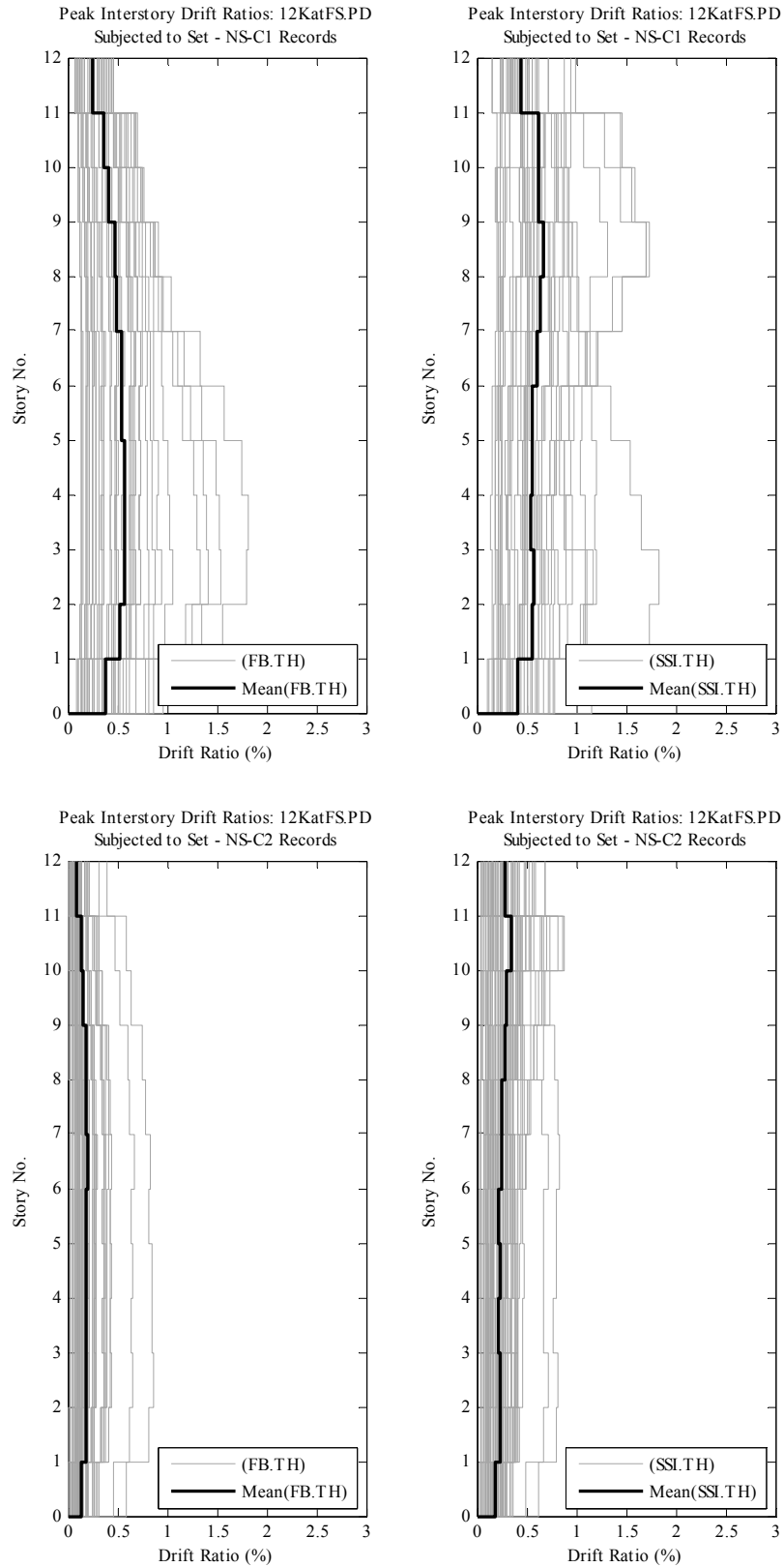


Figure F.16. Comparison of peak and mean interstory drift demands of Model 12KatFS subjected to Set NS-C1, C2, D1, D2 earthquake records.

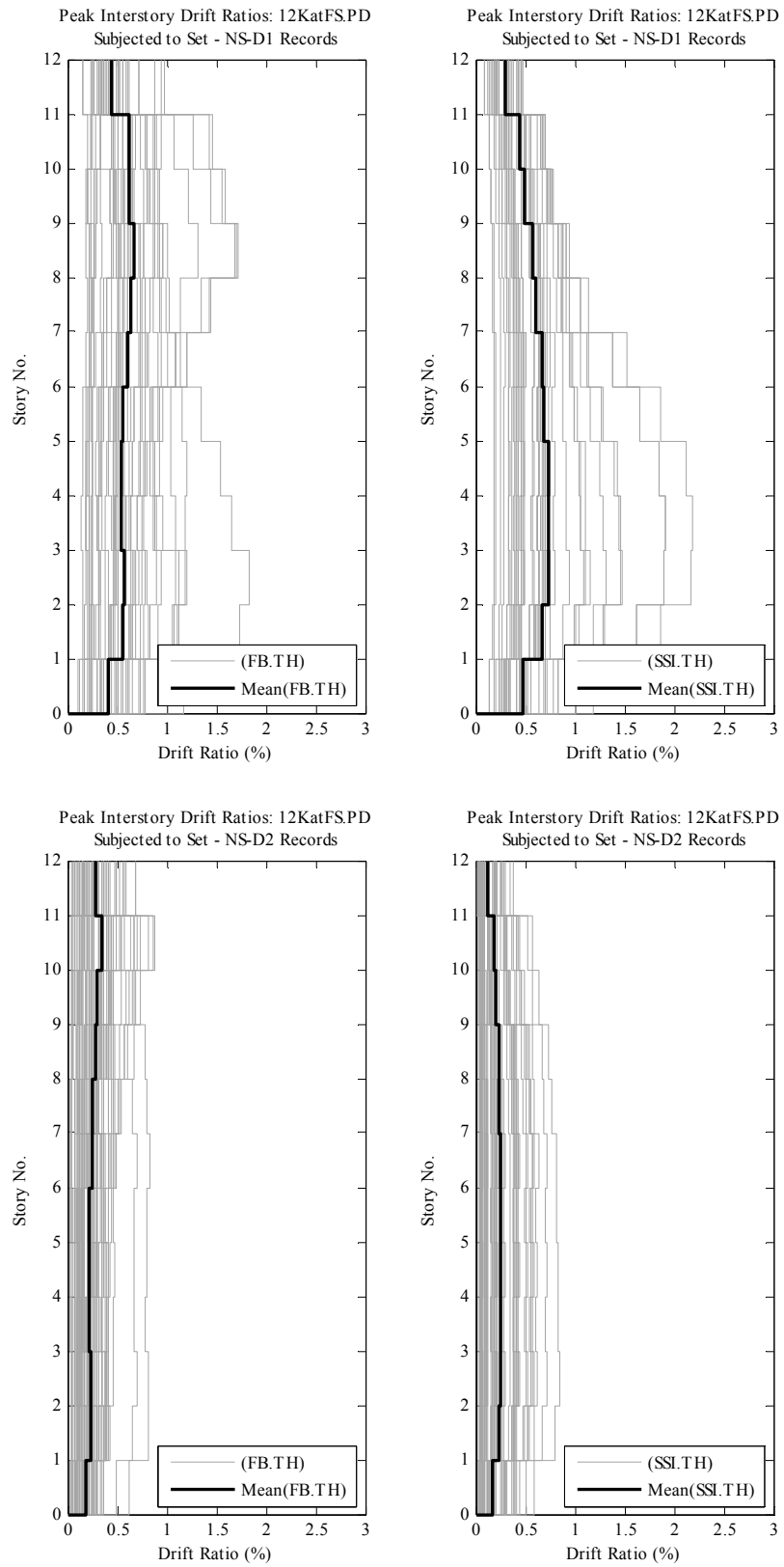


Figure F.16. (Cont'd)

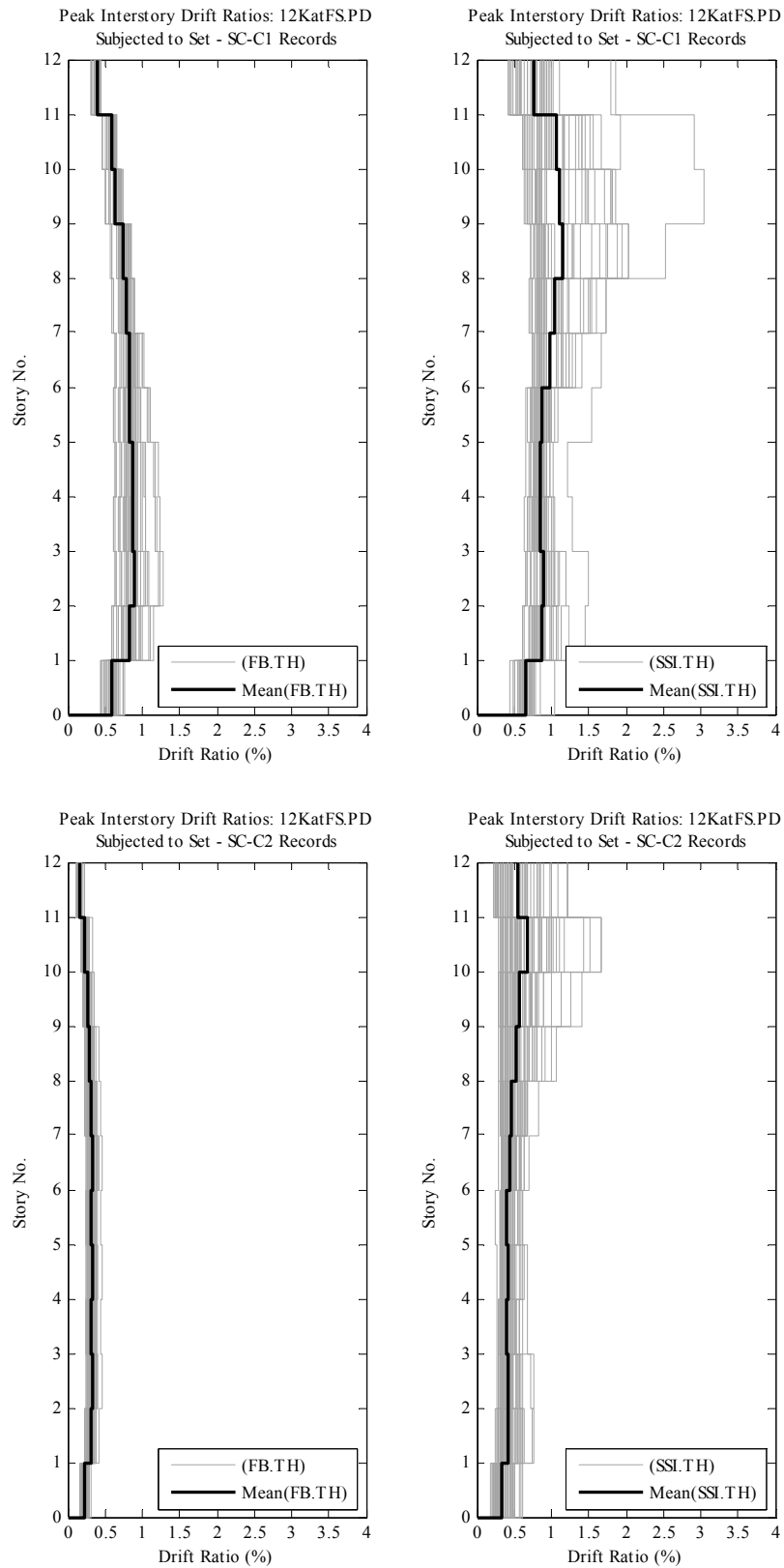


Figure F.17. Comparison of peak and mean interstory drift demands of Model 12KatFS subjected to Set SC-C1, C2, D1, D2 earthquake records.

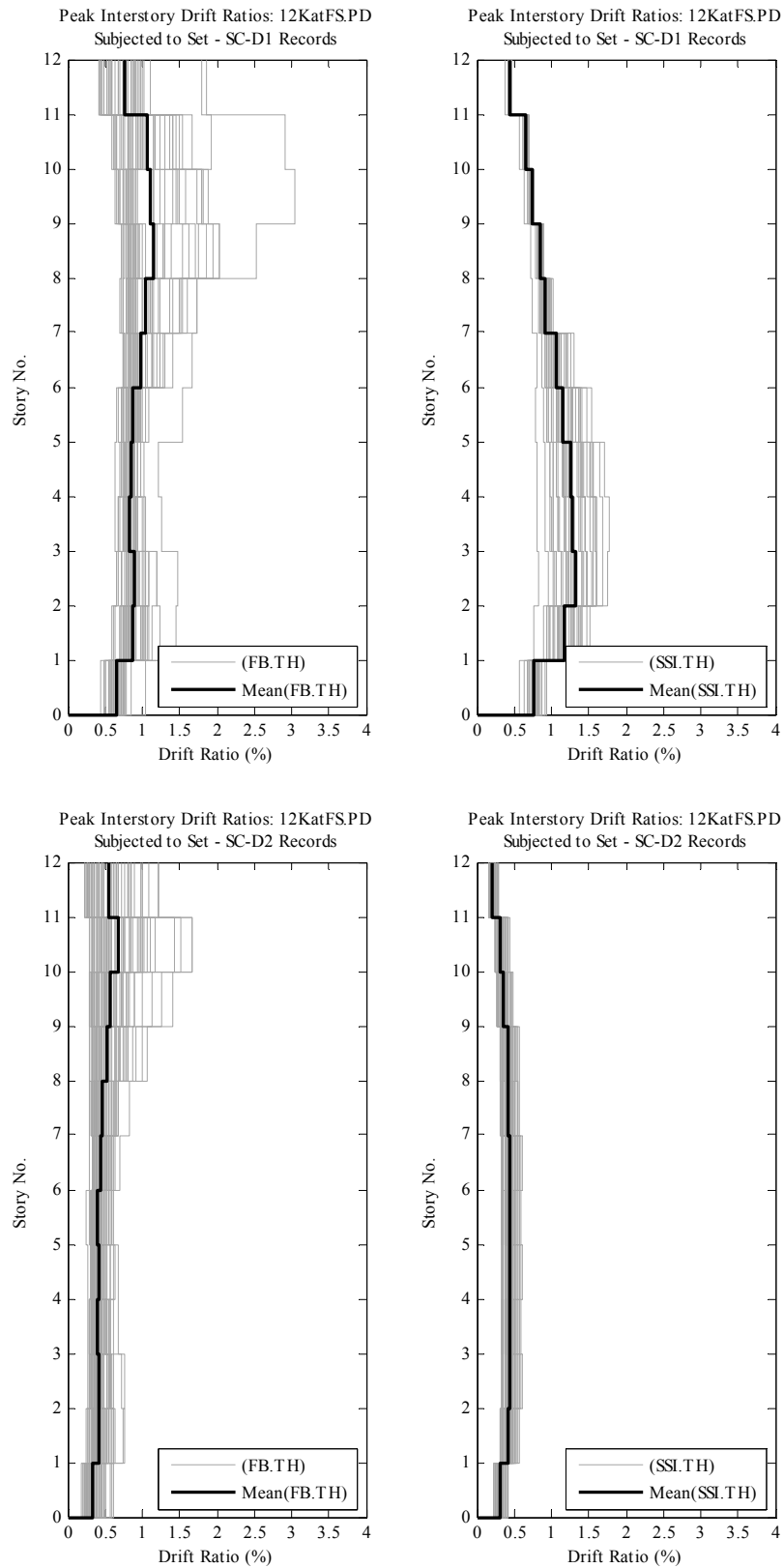


Figure F.17. (Cont'd)

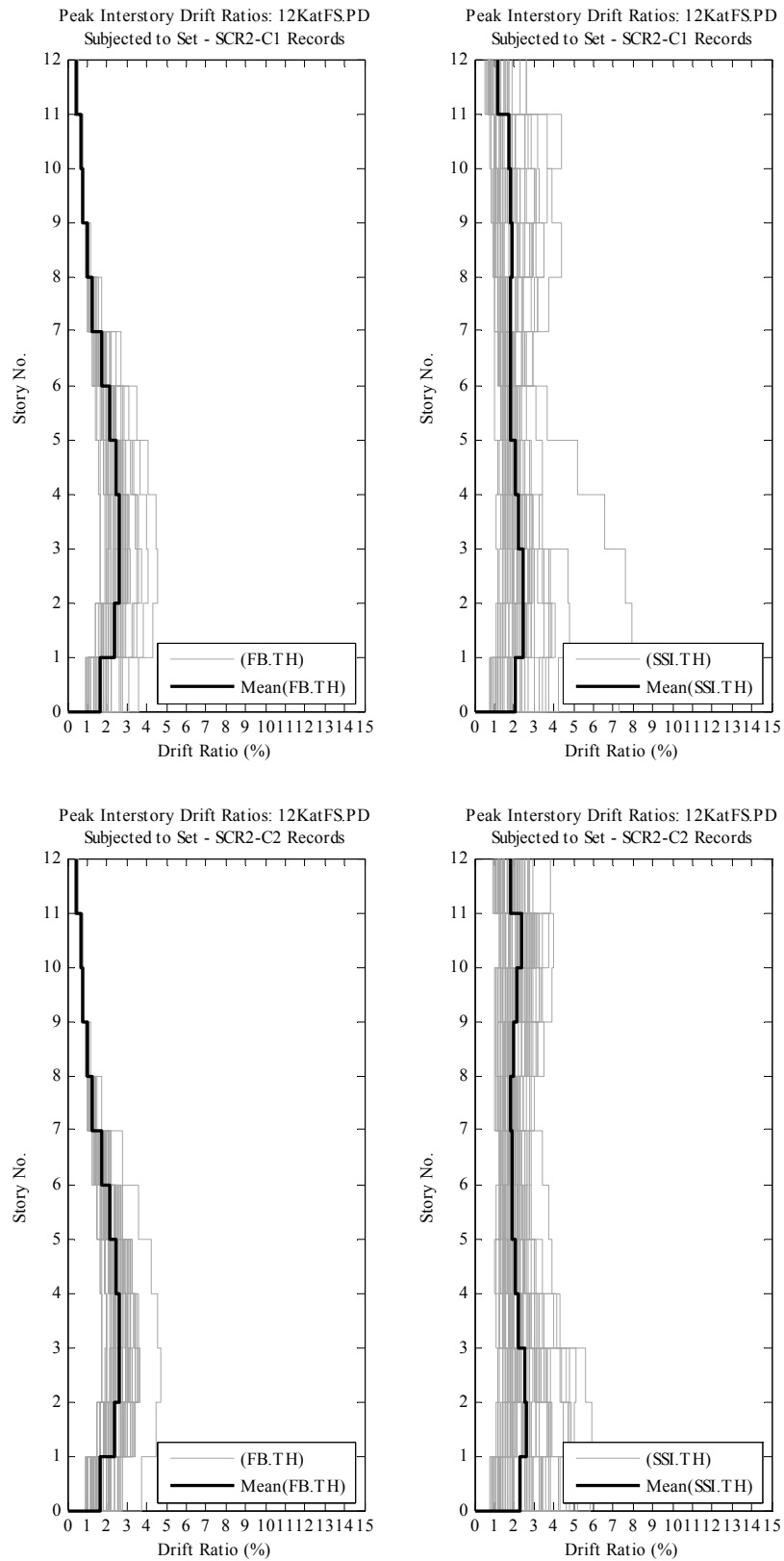


Figure F.18. Comparison of peak and mean interstory drift demands of Model 12KatFS subjected to Set SCR2-C1, C2, D1, D2 earthquake records.

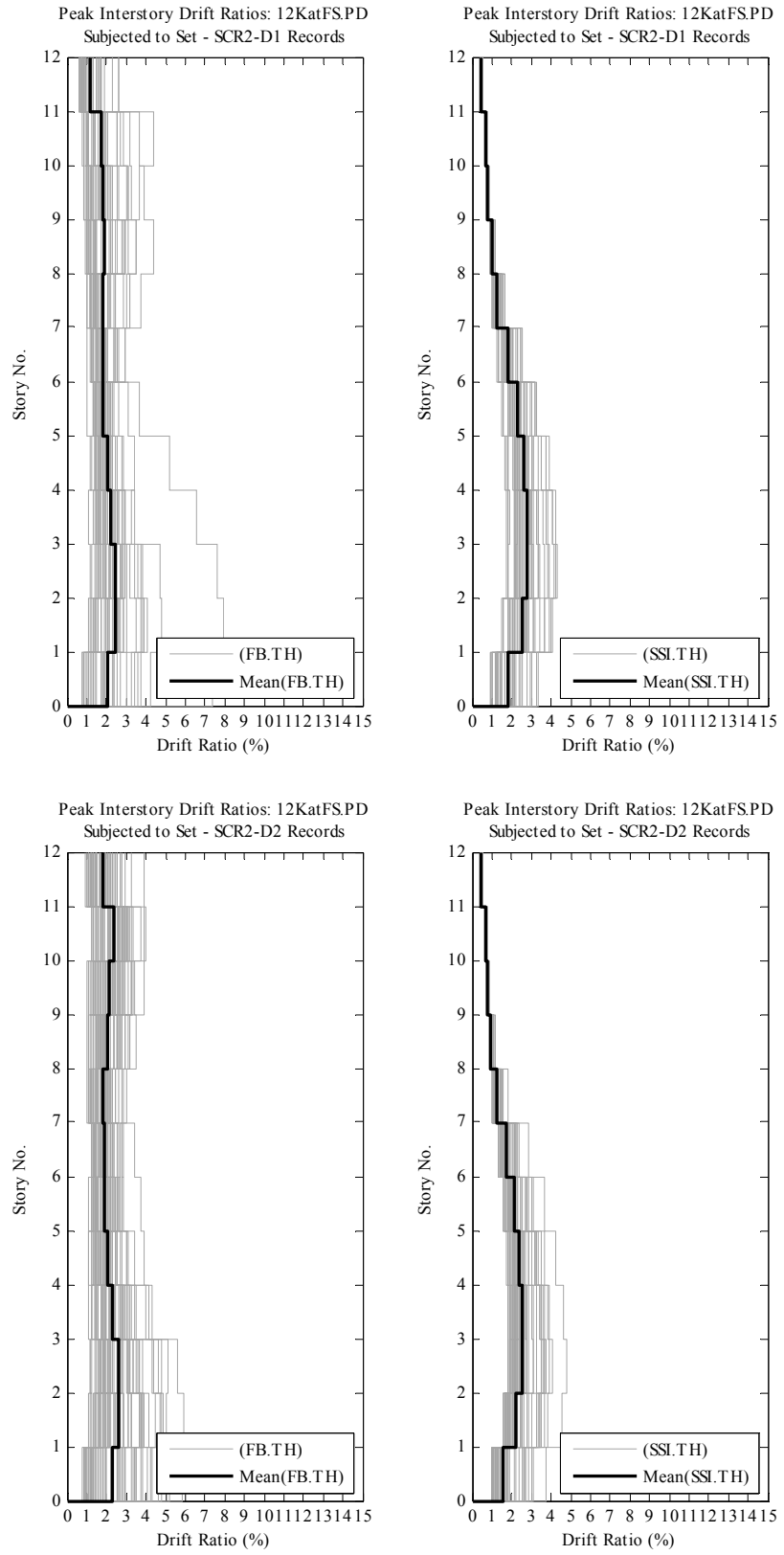


Figure F.18. (Cont'd)

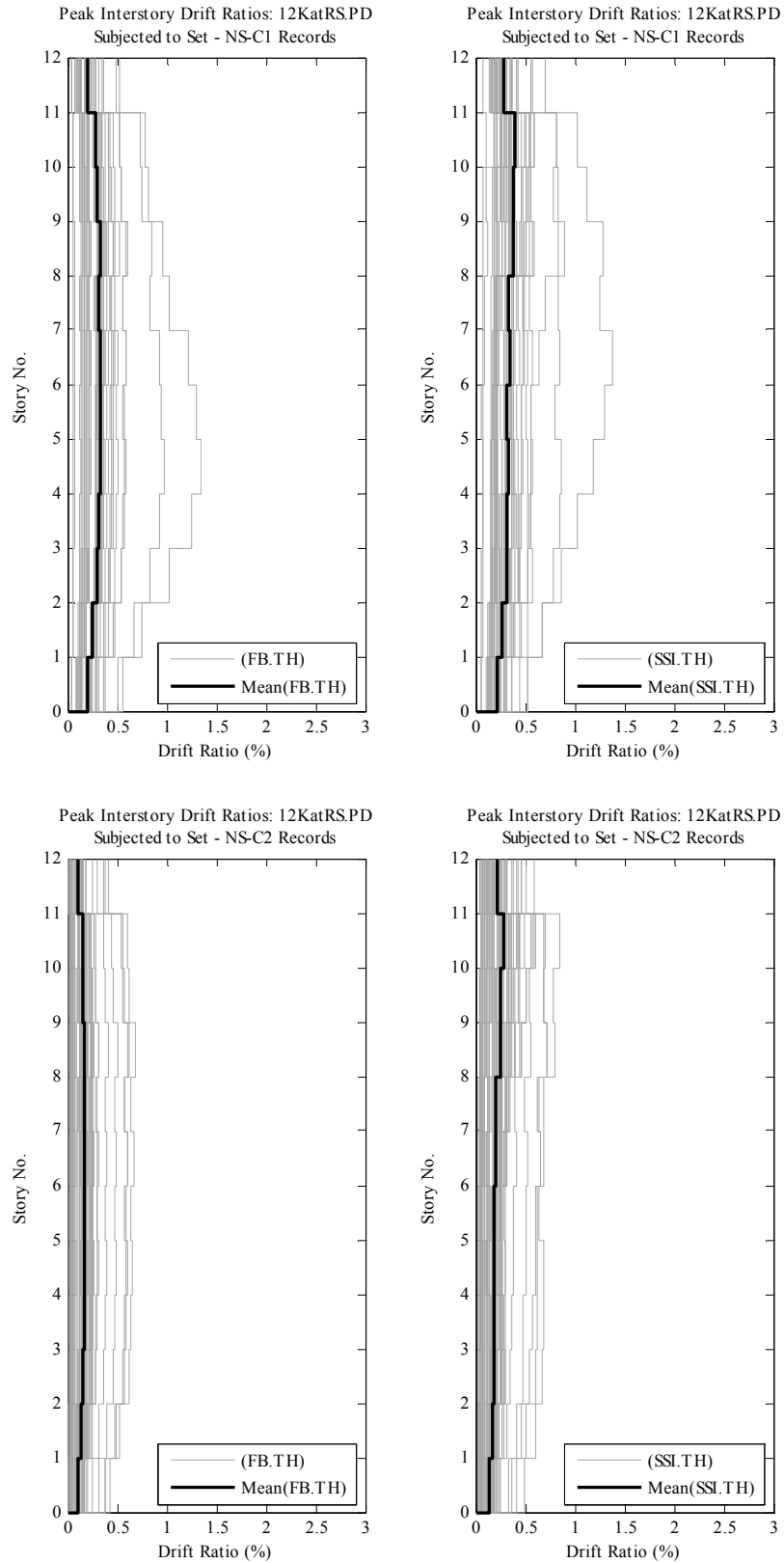


Figure F.19. Comparison of peak and mean interstory drift demands of Model 12KatRS subjected to Set NS-C1, C2, D1, D2 earthquake records.

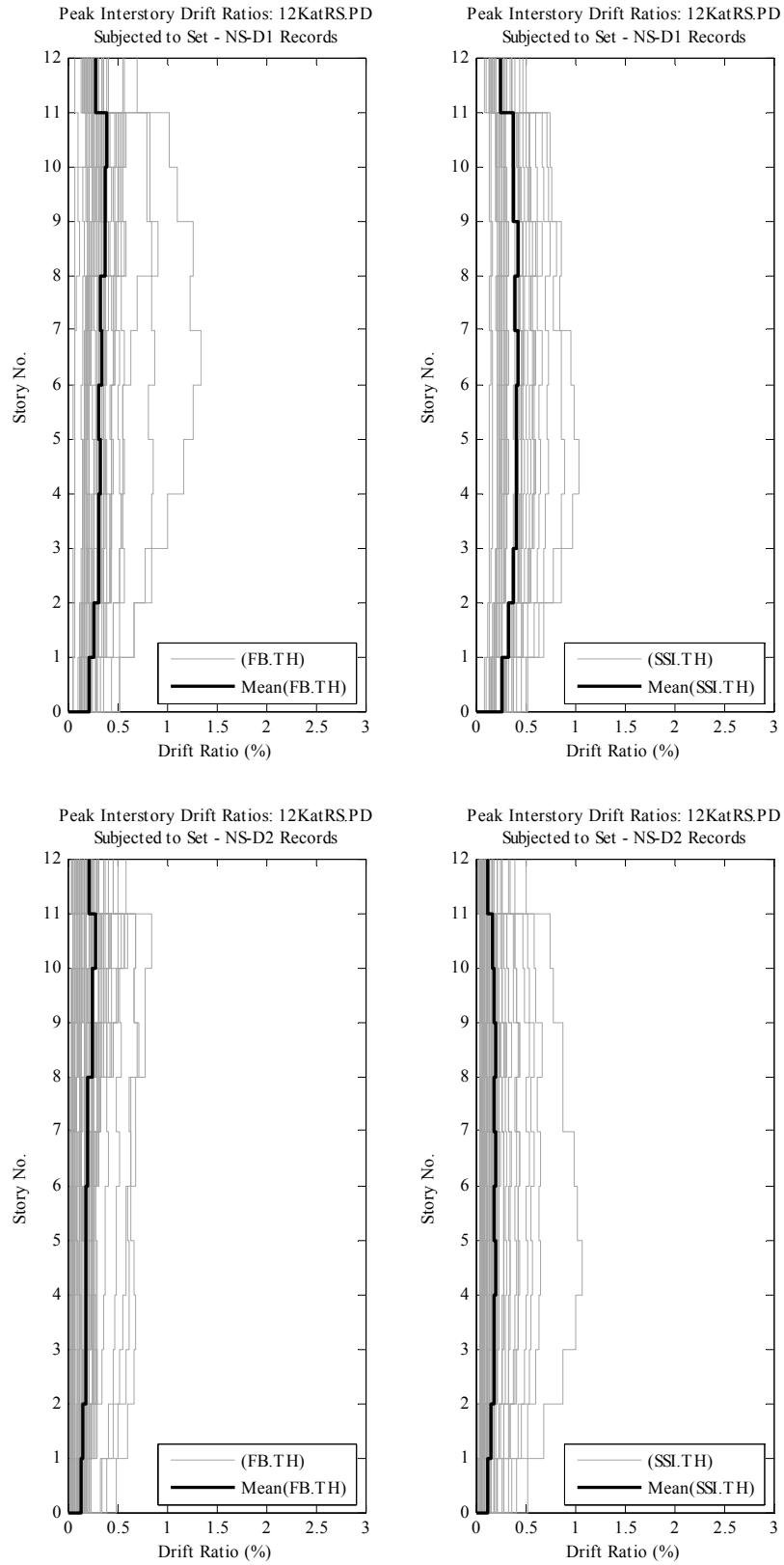


Figure F.19. (Cont'd)

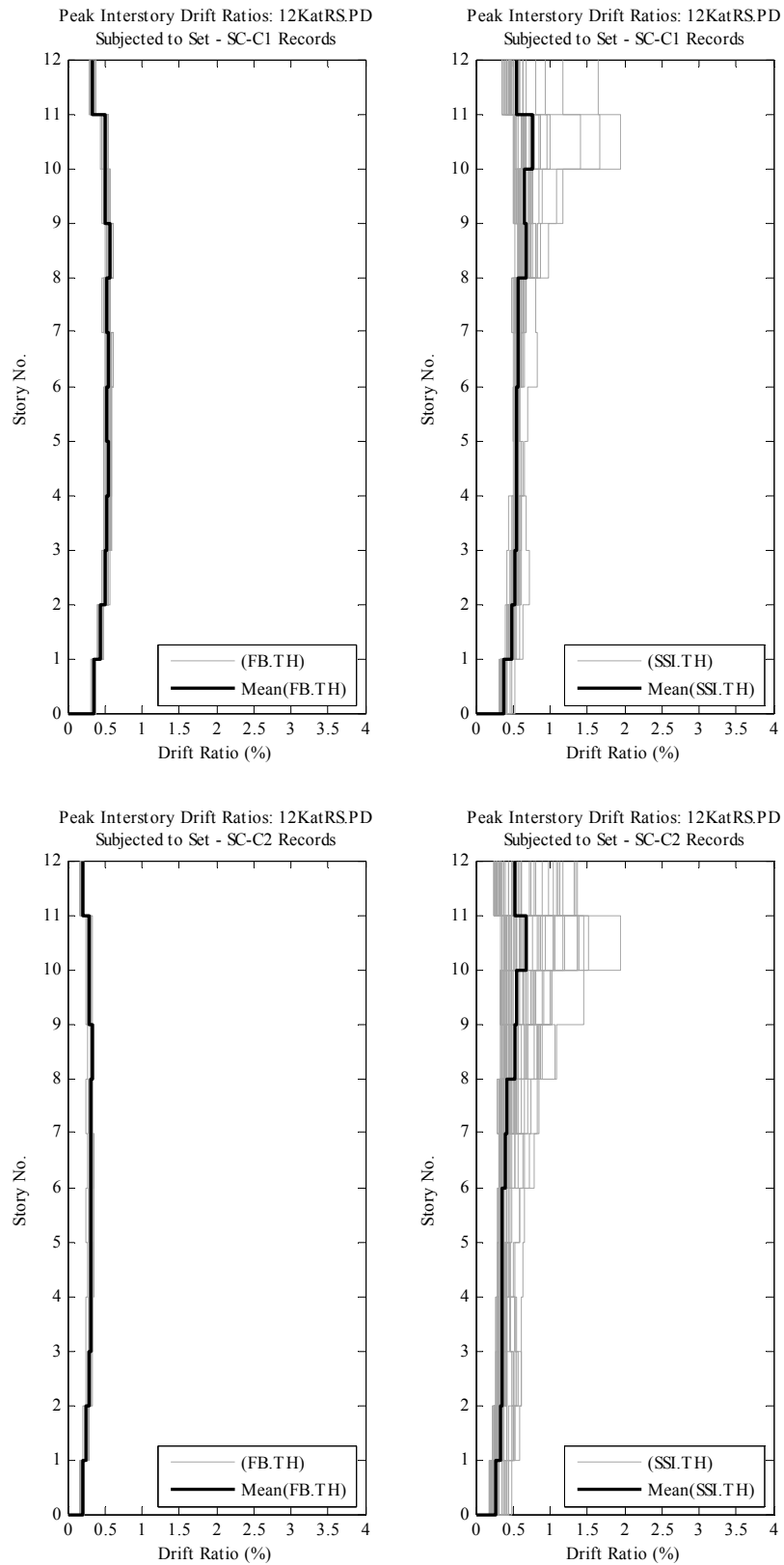


Figure F.20. Comparison of peak and mean interstory drift demands of Model 12KatRS subjected to Set SC-C1, C2, D1, D2 earthquake records.

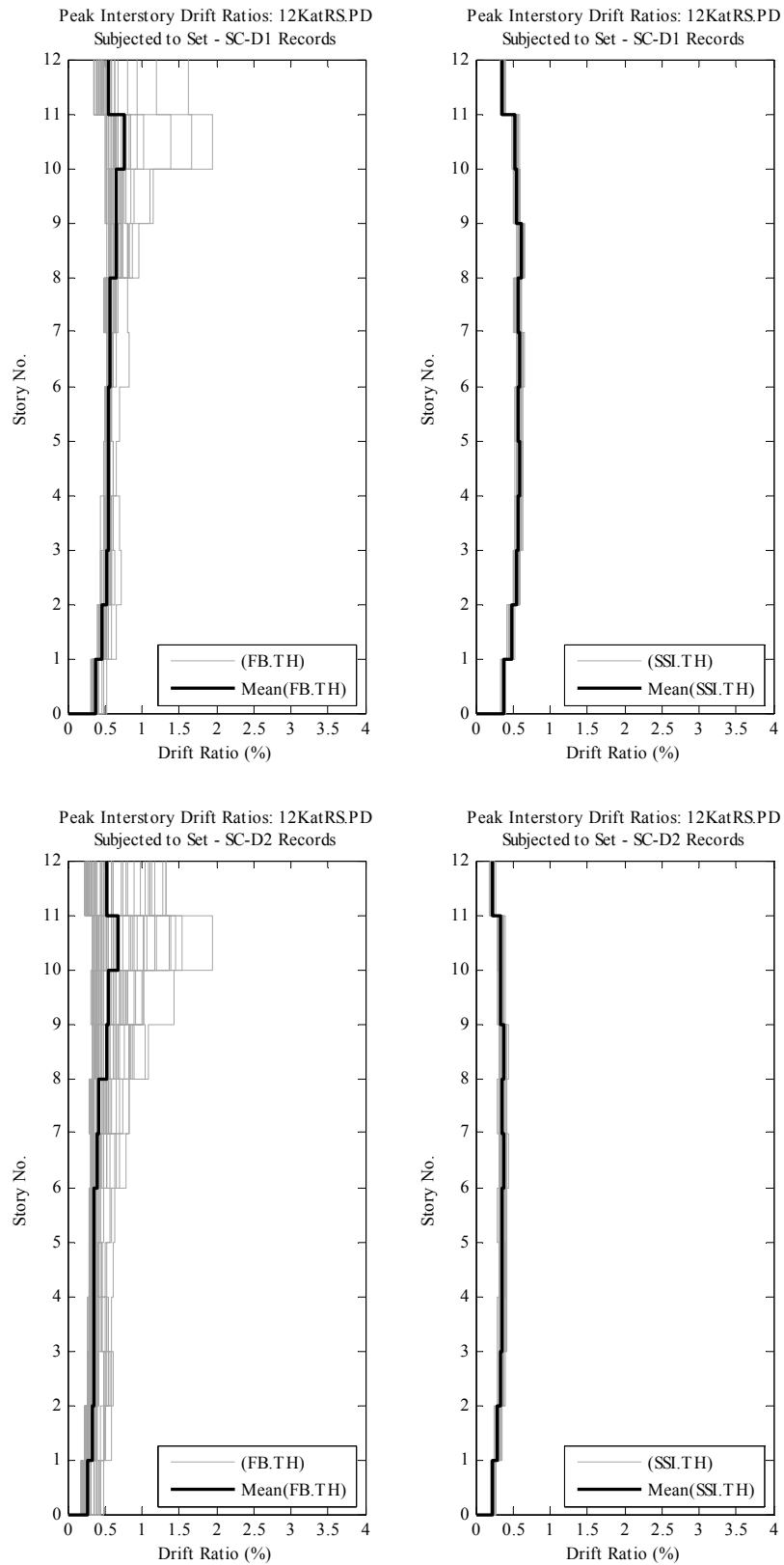


Figure F.20. (Cont'd)

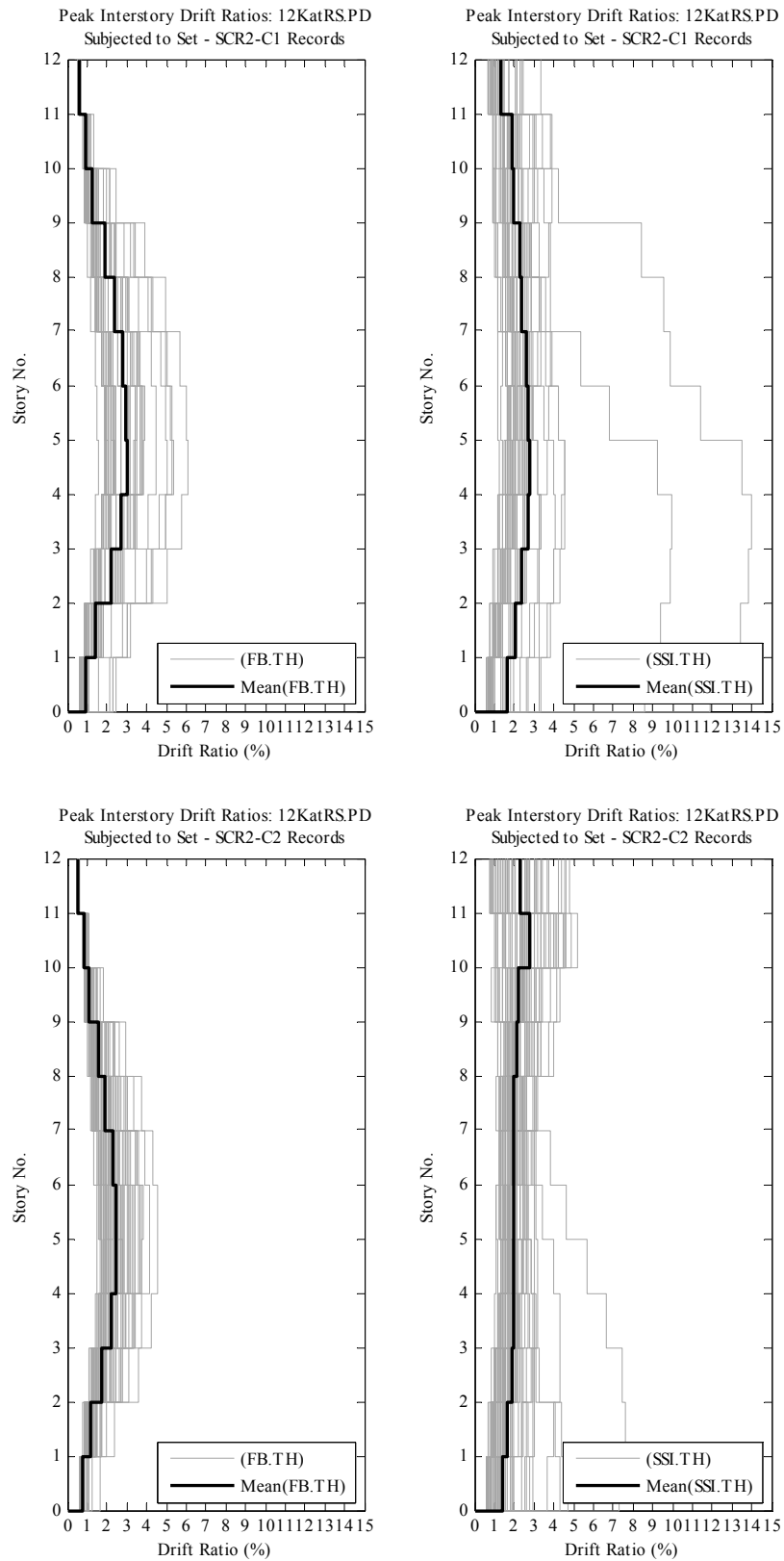


Figure F.21. Comparison of peak and mean interstory drift demands of Model 12KatRS subjected to Set SCR2-C1, C2, D1, D2 earthquake records.

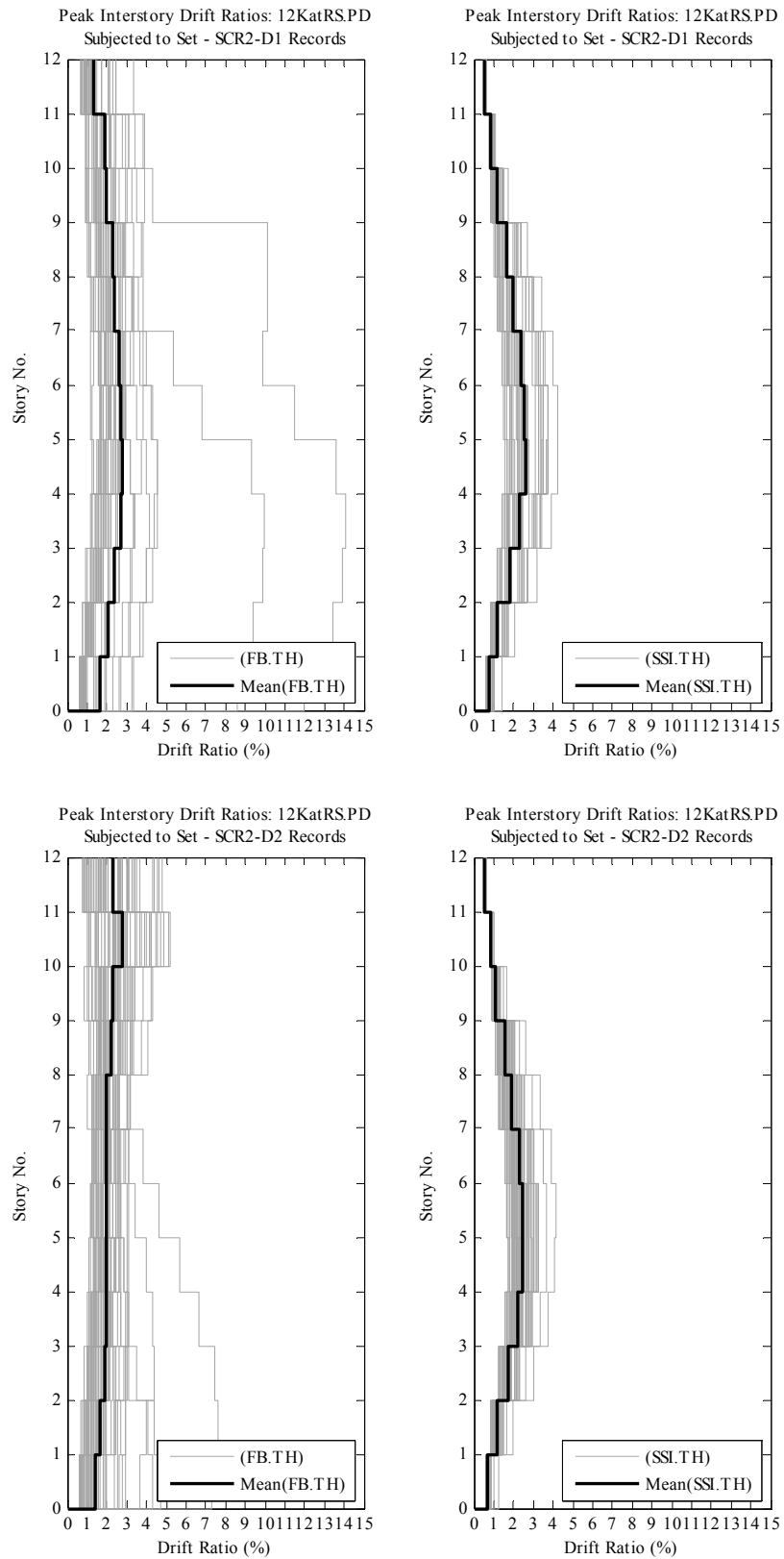


Figure F.21. (Cont'd)

DENİZ UTKUTUĞ

ARTI Architecture Engineering and Consulting Co. Ltd.
Cinnah Caddesi 72/5 06690 Çankaya, Ankara, Turkey.
www.artiproje.eu, dutkutug@artiproje.eu
Tel: +90 (312) 441 23 50
Fax: +90 (312) 441 09 93



ENGINEERING EXPERIENCE

- (2008-Present) Consultancy Services for Retrofitting Design of Selected Public Buildings in Istanbul (CB1.3/G) as a Part of Istanbul Seismic Risk Mitigation and Emergency Preparedness Project (ISMEP).
- (2008) Structural Engineering Design of Highway Toll Offices and Service and Park Area Buildings, Misuratah- Sirt & Sirt Ajdabia, Libya.
- (2008) Structural Engineering Design of General and Chemical Storage Buildings, Al-Fateh University, Tripoli, Libya.
- (2008) Structural Engineering Design of Mathematics and Statistics Faculty Building, Libya, Tripoli, Al-Fateh University.
- (2008) Preliminary Structural Engineering Design and Design Proposal for the Al U'rubah Street Ring Road One and Ring Road Three Bridges, Libya, Benghazi.
- (2008) Structural Engineering Design of EnerjiSA, Menge Dam Logistic Steel Bridge, Kozan, Adana, Turkey.
- (2008) Seismic Performance Assessment of Sanovel Headquarters Building Çankaya, Ankara, Turkey.
- (2008) Seismic Performance Assessment and Retrofitting Design of Residential and Office Buildings of Provincial Gendarmerie Headquarters, Malatya, Turkey.
- (2008) Training Seminars for Local Engineers on Seismic Performance Assessment of R/C Residential Buildings according to TEC2007.
- (2007) Structural Engineering Design of New Main Terminal Building of Republic of Turkey State Railways, Ankara, Turkey.
- (2007) Consultancy Services for Retrofitting Design of Selected Public Buildings in Istanbul (CB1.3/B) as a Part of Istanbul Seismic Risk Mitigation and Emergency Preparedness Project (ISMEP).
- (2006-2007) Bridges of Viaduct No.1 (R/C Arc Bridge), No.2, Underpass No.1, No.2, Overpass No.1, No.2 of North Ankara Urban Transformation Project.

WORK EXPERIENCE

- (2006-Present) Civil Engineer (Structure/Earthquake Engineering), ARTI Architecture Engineering and Consulting Co. Ltd., Ankara, Turkey.
- (1999-2005) Research Assistant, Civil Engineering Department, Middle East Technical University, Ankara, Turkey.
- (2004-2008) Web Administrator of Disaster Management Implementation and Research Center, Civil Engineering Department, Middle East Technical University, Ankara, Turkey: www.dmc.metu.edu.tr
- (1999-2005) Instructor of Civil Engineering Technical Drawing with AutoCAD, CE101, Civil Engineering Department, Middle East Technical University, Ankara, Turkey.

(1998-2005) Department Intranet and Server Administrator, Civil Engineering Department, Middle East Technical University, Ankara, Turkey.

EDUCATION

- (2002-2009) Doctor of Philosophy, Civil Engineering Department, Middle East Technical University, Ankara, Turkey. GPA: 3.71/4
(1998-2001) Master of Science, Civil Engineering Department, Middle East Technical University, Ankara, Turkey. GPA: 3.79/4
(1993-1997) Bachelor of Science, Civil Engineering Department, Middle East Technical University, Ankara, Turkey. GPA: 2.85/4
(1992-1993) High school, Özel Büyük Kolej, Ankara, Turkey (Graduation).
(1986-1992) High school, Özel Arı Lisesi, Ankara, Turkey.

PROFESSIONAL SKILLS

Computer Programming Skills Fortran, C++, VisualBasic, VBA (AutoCad, MS Excel), Tcl/Tk, Html, Php.
Engineering Software Skills AutoCad, Matlab, Sap2000, Etabs2000, Opensees, Ansys, ZeusNL, Nonlin.
Memberships Chamber of Civil Engineers, Union of Chambers of Turkish Engineers and Architects, Turkey (2006).
Languages Turkish (native), English (fluent)

PUBLISHED WORKS

- PhD Dissertation: A Parametric Study Investigating the Inertial Soil-Structure Interaction Effects on Global and Local Deformation Demands of Multistory Steel MRF Structures Resting on Surface Rigid Mat Foundations, METU, 2009. Supervisor: Prof. Dr. Polat Gülkan.
- Master's Thesis: Analysis of Earthquake Induced Hydrodynamic Effects in Cylindrical Container Tanks, METU, 2001. Supervisor: Prof. Dr. Çetin Yılmaz.
- NSolFEM , 3D Nonlinear Finite Element Analysis Software by Matlab, METU, 2005.
- P. Gülkan, D. Utkutuğ, "Okul Binalarının Deprem Güvenliği için Minimum Dizayn Kriterleri", Türkiye Mühendislik Haberleri, TMMOB İnşaat Mühendisleri Odası, 48/2003-3, No. 425.
- CE101-Technical Drawing Web Based Lecture Notes:
<http://www.ce.metu.edu.tr/~ce101/lecturenotes.htm>

PERSONAL

Date and Place of Birth November 10, 1975, Ankara, Turkey.
eMail Address dutkutug@gmail.com